FINAL REPORT
U.S. Department of Energy

Isolation of Metals from Liquid Wastes:
Reactive Scavenging in Turbulent Thermal Reactors

Principal Investigator: Jost O.L. Wendt
Department of Chemical and Environmental Engineering
The University of Arizona, Tucson Az.

Collaborators:

Alan R. Kerstein
Sandia Laboratories, Livermore, Ca.

Alexander Scheeline
Department of Chemistry
University of Illinois at Urbana-Champaign

Arne J. Pearlstein
Department of Mechanical and Industrial Engineering
University of Illinois at Urbana-Champaign

William P. Linak
Air Pollution Technology Branch
National Risk Management Research Laboratory
US Environmental Protection Agency

Table of Contents

Section 1
Executive Summary

This report describes results from a multi-institutional research project involving the University of Arizona (UA), the University of Illinois at Urbana Champaign (UIUC), the U.S. Environmental Protection Agency, National Risk Management Research Laboratory (EPA,NRMRL) and Sandia National Laboratories (Sandia). The objective was to provide the underlying scientific infrastructure behind the use of turbulent thermal reactors for the scavenging of cesium and strontium wastes. Thermal reactors allow these metals to be vaporized, and subsequently to react on kaolinite based substrates to form unleachable metal containing alumino-silicates. To this end, the project consisted of the following components. Chemistry of interaction was to be investigated at the UA by personal from both UA and UIUC. Theoretical models describing the motions of drops and particles in turbulent flow-fields were to be developed at UA working with Sandia and at UIUC. It was hoped that progress in both areas would allow:

1) modeling of the contacting of every last piece of metal waste with the kaolinite sorbent and;

2) prediction of the chemistry of interaction.

Finally, EPA, NRML was to conduct tests in a turbulent flow thermal reactor to confirm the findings of the more fundamental investigations. The goal was to develop a modeling tool that it can be used to help <u>guarantee</u> safe and effective operation of turbulent flow reactors (Wendt, 1992) that use kaolinite powders to scavenge and isolate radioactive cesium and strontium.

The overall project demonstrated that toxic metals (cesium Cs and strontium Sr) in aqueous and organic wastes can be isolated from the environment through reaction with kaolinite based sorbent substrates in high temperature reactor environments. In addition, a state-of-the-art laser diagnostic tool to measure droplet characteristic in practical 'dirty' laboratory environments was developed, and was featured on the cover of a recent edition of the scientific journal "*Applied Spectroscopy*" [Cabalo *et al.,* 2002]. Furthermore, great strides have been made in developing a theoretical model that has the potential to allow prediction of the position and life history of every

particle of waste in a high temperature, turbulent flow field, a very challenging problem involving as it does, the fundamentals of two phase turbulence and of particle drag physics.

1.1 Background

Metal-bearing solutions and slurries can pose environmental hazards. Among the most acute of these hazards is the accumulation of radioactive wastes, held in underground steel tanks at locations such as Hanford, WA and the Savannah River Site at Aiken, SC [Terrell, 1994; Zorpette, 1996; Stewart, 1997]. Vitrification of radioactive wastes, either as glass logs [Tollison & Finger 1997] or cement [Gougar et al. 1999] is the approach most actively being followed to sequester radionuclides over the millennia required for decay to negligible activity levels. An important step in preparation of vitrified material is removal of water and organic material, resulting in volume reduction. Among the ways to perform solvent removal, that simultaneously destroys organic matter, is thermal treatment. This process simply consists of spraying the waste into a high temperature (T>1800K) reactor and adding powdered sorbent material. Water is vaporized, organics are oxidized to water and carbon dioxide, and metallic species oxidized. Scavenging of metal ions by kaolinite [Davis et al. 1999; Davis et al. 1998; Davis and Wendt 2000A; Davis and Wendt 2000B] prior to cooling and oxide formation is a promising technology for high efficiency collection of gas-phase radionuclides. Under optimized conditions, Destruction/Recovery Efficiencies (DRE's) of up to 99.99% of metal ions in an entering waste stream can be scavenged.

It has been observed that in the incineration of liquid hazardous wastes there exist "rogue" droplets (>300 ?m diameter) which penetrate past the flame zone and burn as isolated droplets in the postflame gasses [Mulholland et al. 1991]. Detailed knowledge of the droplet burnout points are essential to keeping the destruction removal efficiency in excess of the 99.99% required by law. These drops avoid hot zones in the reactor, resulting in either incomplete vaporization or vaporization in a zone with insufficient temperature to vaporize the metal contents.

The processes considered all require the metal in question to be volatilized in a hot chamber and then to be reactively scavenged by inexpensive sorbents, which are introduced downstream. The metal is isolated within the molten like particles, which are subsequently collected. In order for this

process to be rendered effective and safe two issues must be resolved. First, the optimum application and choice of sorbents must be determined; second, there must be a method to guarantee that not one particle of radioactive waste (or, for that matter, any undesirable byproduct) can escape the system. The research performed in this project was designed to create the underlying knowledge that allows these issues to be addressed in practice so that the process can be realized in the field.

1.2 State of Knowledge before Initiation of Current Project

Prior to the current research grant, the nature of suitable sorbents for DOE relevant metals had yet to be identified, although, previous work on sodium capture by kaolinite suggested that sorbent to be a possible candidate for cesium sorption. No sorbent had been identified for strontium, another metal of interest to DOE. It was required to show that high temperature scavenging reactions between cesium and strontium metal vapors and dispersed kaolinite powders, were sufficiently rapid to allow isolation of both metals. Prediction of droplet trajectories and of contacting between metal vapor and dispersed kaolinite is also required to make this process viable. Available experimental results [Mulholland et al, 1991] showed that turbulence exerted a profound effect on the trajectories and final burnout points of identically injected droplets. A newly developed model framework, the One Dimensional Turbulence (ODT) model created by Kerstein, (1999) appeared to show promise of being able to predict this phenomenon, without requiring the unreasonable (in practice) computational effort of Direct Numerical Simulation (DNS) for the high level of turbulence which the waste would be exposed to during incineration. We believed this model could be extended to predict the individual trajectories of individual droplets and, for that matter, of fluid particles in hot turbulent flow-field. The development of a state-of-the-art Laser diagnostic apparatus was necessary to measure drop size as a function of position, drop and gas-phase temperature, and to observe speciation in the reactor including free atoms, small molecules, and soot. This would create the science supporting a future methodology that would be able to guarantee safe operation of the proposed process for metal scavenging in turbulent thermal reactors.

1.3 Accomplishments

1.3.1 Screening Studies on Cesium and Strontium Capture. Screening studies suggested that thermal treatment might be effective in capturing both cesium and strontium on dispersed kaolinite

powders, at high temperatures. Strontium required addition of chlorine to enable metal vaporization at moderately high temperatures, and it was shown that even under those conditions, significant capture was possible. These results are described in more detail in the Master's Thesis of Jonathon Amos [Amos, 1999], attached in its entirety as Appendix A. These results consist of:

    a)   theoretical equilibrium calculations;

    b)   experimental studies on cesium and strontium partitioning in the presence of kaolinite sorbent in a 17kW laminar flow reactor; and

    c)   inferences on pertinent mechanisms based on particle morphologies.

Fundamental kinetic rates and mechanisms of the sorption process were beyond the scope of these screening studies., but would properly be the subject of future work.

    1.3.2 *Theoretical Two-Phase Flow Model Development for ODT*. Results of this portion of the project are found in the University of Arizona Master's Thesis of John R. Schmidt [Schmidt, 2000], which is attached as Appendix B. The major accomplishments of this research are the development of a two-phase flow model, which is consistent with the phenomenology of ODT for predicting the particle trajectories of individual droplets and the implementation of many of these drops with burning to simulate individual evaporating droplet streams injected into a turbulent combustor. The spread in trajectory endpoints of these droplet streams was investigated numerically.   Results are in good agreement with the measurements and consisted of:

    a)   Theoretical development of a two-phase flow model which is consistent with the phenomenology of ODT

    b)   Implementation of a droplet burning model into ODT.

    c)   A parametric study of how burnout points are effected by initial droplet size, initial droplet velocity, interdroplet spacing, and droplet injection angle.

    1.3.3 *Laser Diagnostic apparatus*. It was desired to measure droplet trajectories in turbulent thermal reactors. To this end a laser diagnostic apparatus was designed, built, and tested. The major accomplishments of this portion of the work was to build a laser imaging instrument for emission, fluorescence, and scattering diagnostics of a 17 kW gas/air thermal reactor which consisted of:

a) Design of a laser apparatus using Z-pair parabolic (reflective) mirrors.

b) Building of this apparatus in a dirty lab environment.

c) Demonstration of the laser tool's imaging capabilities

Examples of data show non-axisymmetric flow in a nominally laminar flow system, drop shapes *in situ*, and Mie scattering from soot. Details of the state-of-the-art laser apparatus, which was also featured on the cover of the volume of the journal, are published in Cabalo *et al.* [2002],

Section 2
Research Objectives

2.1.   A Generic Technology for treatment of DOE Metal-Bearing Liquid Waste

The DOE metal-bearing liquid waste inventory is large and diverse, both with respect to the metals (heavy metals, transuranics, radionuclides) themselves, and the nature of the other species (annions, organics, etc.) present. Separation and concentration of metals is of interest from the standpoint of reducing the volume of waste that will require special treatment or isolation, as well as, potentially, from the standpoint of returning some materials to commerce by recycling.

The variety of metal-bearing liquid waste in the DOE complex is so great that it is unlikely that any one process (or class of processes) will be suitable for all material. However, processes capable of dealing with a wide variety of wastes will have major advantages in terms of process development, capital, and operating costs, as well as in environmental and safety permitting. Moreover, to the extent that a process operates well with a variety of metal-bearing liquid feedwastes, its performance is likely to be relatively robust with respect to the inevitable composition variations in each waste feed.

One such class of processes involves high-temperature treatment of atomized liquid waste to promote reactive capture of volatile metallic species on collectable particulate substrates injected downstream of a flame zone. Compared to low-temperature processes that remove metals from the original liquid phase by extraction, precipitation, ion exchange, etc., some of the attractive features of high-temperature reactive scavenging are:

- The organic constituents of some metal-bearing liquid wastes (in particular, some low-level mixed wastes) must be treated thermally in order to meet the requirements of the Resource Conservation and Recovery Act (RCRA) and Toxic Substances Control Act (TSCA), and the laws of various states.

- No species need be added to an already complex liquid system. This is especially important in light of the fact that DOE has already experienced problems with organic complexants added to precipitate radionuclides. For example, the Defense Nuclear Facilities Safety Board has expressed, in a formal Recommendation to the Secretary of Energy, its concern about the evolution of benzene vapor in concentrations greater then the lower flammability limit from tanks to which sodium tetraphenylborate has been added to precipitate ^{137}Cs in the "In-Tank Precipitation" (ITP) process at the Savannah River Site. Other species added to the waste in the ITP process are sodium titanate (to adsorb ^{90}Sr and Pu), and oxalic acid. Avoiding addition of organics to radioactive waste has the additional advantage that is likely to significantly reduce the rate of radiolytic and radiolytically- induced hydrogen generation (c.f. Meisel et al., [1993], in which it is shown that removal of oranics reduces the rate of hydrogen generation in simulated waste from Hanford tank 241-SY-101 by over 70%).

- Organic species already present are destroyed with very high efficiency. This attribute is especially attractive with respect to high-level tank waste at the Hanford Site, in which large amounts of citrate, glyoxylate, EDTA (ethylenediaminetetraacetic acid), and HEDTA [N-(2-hydroxyethyl)-ethylenediaminetriacetic acid] were added to precipitate radionuclides. These organic species are important in the thermal and radiolytic generation of methane, hydrogen, and nitrous oxide, flammable mixtures of which are episodically vented from 25 tanks on Hanford's Fammable Gas Watch List [Hopkins, 1994].

- The same basic approach can be used to treat a broad range of liquid wastes, in each case concentrating the metals (regardless of liquid-phase oxidation state or association with chelators or absorbents) using a collectable sorbent, and destroying any organic species present. In common with the Army's approach (see section 2.2) to the thermal destruction of a

range of chemical warfare agents (GB, VX, and two blister agents), this may drastically simplify process and plant design and facility permitting, and reduce capital costs, by avoiding development of a separate "wet" process for each type of liquid waste source.

- The expected robustness of the process with respect to gross feedwaste composition suggests a relatively high degree of tolerance with respect to inevitable variations in the composition of a given metal-bearing feedwaste.

For these reasons, high-temperature reactive scavenging is a potentially attractive approach to the removal of metals from liquid waste in the DOE complex.

2.2. Community Acceptability of High-Temperature Waste Processing

One of the issues affecting the viability of large-scale nuclear waste remediation processes is community (i.e. political) acceptability. If a process is not and cannot be made acceptable to a community, it will not operate there. In light of the financial and potential environmental costs of moving large quantities of liquid waste from sites at which a particular treatment process is unacceptable, it is fair to conclude that waste from such a site will not be destroyed by that process anywhere. If a process is unacceptable at all sites where treatable waste is stored, then the process is unusable. In this section, we discuss issues relevant to acceptability, with special emphasis on high temperature processing of extremely hazardous materials.

High-temperature treatment of non-nuclear hazardous waste has been plagued by problems of community acceptability for some time. In some cases, permitting of waste incinerators has been delayed so long that the would-be operators have abandoned the application process. As discussed below, there are, however, cases in which high-temperature treatment facilities have been successfully build and operated. The similarities of those cases to DOE's problems are important.

The primary public concern with regard to thermal treatment is emissions. Under proper conditions, the problem is both technically and politically solvable. This has been proven by the Army's Office of the Program Manager for Chemical Demilitarization (formally the Army Chemical Materiel Destruction Agency) which is successfully using incineration to destroy large volumes of liquid chemical warfare agents (nerve and blister agents). The technology underwent a four-stage Operational Verification Test at Johnston Atoll during 1990-1993. Since then, it has been successfully demonstrated on a production scale at Johnston Atoll Chemical Agent Disposal Facility (CADF) in the Pacific (over 1 million kg of agent destroyed), and since August 1996 at the Tooele CADF in Utah (over 380,000 kg of agent destroyed). These facilities have been designed, built, and permitted to meet all applicable civilian regulations (including RCRA, TSCA, the Clean Air Act, the clean Water Act, and the Occupational Safety and Health Act). In February 1997, a $586 million systems contract (for design, construction, operation, and closure) was awarded to Raytheon Demilitarization Company for a thermal treatment plant at Umatilla, Oregon.

With passage of the National Defense Authorization Act for Fiscal Year 1992 (Public Law 102-190), Congress prohibited the transport of stockpiled chemical warfare agents. After that date, the major factor in gaining community acceptance of incinerators in Utah, Oregon, Alabama, and Arkansas has been the realization that the alternatives are a) thermal destruction; b) further research on alternative technologies, followed by process development and testing, during which time munitions, canisters, and other containers would continue to degrade; or c) indefinite continued storage, again during this time munitions, canisters, and other containers would continue to degrade. The relative attractiveness of proven technology, coupled with diligence in operations and a concerted Army effort at community involvement and outreach, has led to the present state of affairs.

This project demonstrated how Cs and St could be captured by kaolinite. It also took large strides in developing a novel two-phase flow model able to predict <u>individual</u> droplet trajectories and environments in combustor turbulent flow fields. This was not merely a random process, since we

wished to capture the physics of turbulence and dominant turbulent mixing and eddy characteristics without DNS (direct numerical simulation). Kerstein's [1999] One Dimensional Turbulence (ODT) Model appeared to posses the correct attributes to do this. Like DNS, the ODT method requires multiple realizations. However, unlike DNS, ODT for droplet trajectories in a practical configuration, is currently "doable" for the turbulent intensities seen in turbulent combustors. We needed to produce a laser diagnostic apparatus to both give in-situ measurements of droplets in an actual combustor and capable of aiding the kinetic studies with in-situ gas phase species measurements. This requires the ability to generate drops, both as sprays and as monodisperse streams, to measure drop size as a function of position, to measure drop and gas-phase temperature, and to observe speciation in the reactor including free atoms, small molecules, and soot.

Section 3
Methods and Results

3.1   Metal Capture

3.1.1 Experimental methods: Screening Studies on Cesium and Strontium Capture.   Screening studies focused on capture of cesium and strontium (two important metallic wastes of interest to DOE) and consisted of:

a)   theoretical equilibrium calculations;
b)   experimental studies on cesium and strontium partitioning in the presence of kaolinite sorbent in a 17kW laminar flow reactor; and
c)   inferences on pertinent mechanisms based on particle morphologies.

Fundamental kinetic rates and mechanisms of the sorption process were beyond the scope of these screening studies.

Thermodynamic Predictions. Equilibrium calculations were performed to predict the metal dewpoints and speciation. Calculations were performed with the NASA Chemical Equilibrium and Applications (CEA) code. Calculations were performed to match experimental conditions {100 ppm metal, Stoichiometric Ratio (SR)=1.2, 1000 ppm of dopant gas}. Input thermodynamic data for cesium and strontium compounds were added to the database [Barin, 1994]. Twenty-three strontium and seventeen cesium compounds were considered [Amos, 1999 and Appendix A]. Cesium by itself has a dewpoint of 675 K, which categorizes it on the low end of semi-volatile. The presence of chlorine in the system raises the dewpoint to 900 K. This is slightly unusual, in that the presence of chlorine tends to lower the dewpoint of most metals. When sulfur is added to the system, it raises the dewpoint even higher, to 1300 K. On its own, strontium has a dewpoint of 2000 K. This classifies strontium as a refractory metal. In the presence of chlorine, strontium vaporizes with a dewpoint of 1400 K. This indicates that the presence of chlorine may be necessary in order to reactively capture strontium.

Experimental Studies.   Experiments were performed in the University of Arizona 17kW laminar, downflow furnace, operated a SR=1.2, with time-temperature profiles similar to those of practical combustors. Metals were injected into a natural gas flame as aqueous solutions of metal salts (cesium acetate and strontium nitrate). Flow rates were set to provide a metal concentration of 100 ppm in the furnace. The sorbent powder (kaolinite, lime) was injected below flame using a water-cooled probe. The sorbent was fed at a rate of 2 g/min. The furnace temperature at the sorbent injection point was 1400K. Dopant gases (Cl_2, SO_2) were mixed with the combustion air prior to entering the furnace. Samples were withdrawn from the furnace with a water-cooled isokinetic-sampling probe. The samples were withdrawn after a two second residence time in the furnace, and at a temperature of 1120K. The sampling rate was 1.3 liters per minute, and samples were collected for ten minutes. The sample stream was diluted with nitrogen at a ratio of 18:1 to quench reactions. Gas samples were passed through a Berner Low-Pressure Impactor (LPI) to segregate particles by size [Hillamo and Kauppinen, 1991], and particles were collected on greased polycarbonate substrates. The substrates were then digested in a strong acid solution prior to analysis. Strontium, aluminum, and calcium were analyzed by flame atomic adsorption spectroscopy, and cesium was analyzed by flame atomic emission spectroscopy.   Reactive capture on sorbents was determined by sampling above the

predicted metal dewpoint and by using the aerosol size fractionation methods described by Davis *et al.* [1998]. Strontium, aluminum, and calcium were analyzed by flame atomic adsorption spectroscopy, and cesium was analyzed by flame atomic emission spectroscopy.

3.1.2 <u>Screening Experimental Results</u>. Key results of the cesium tests are shown in Figures 1 and 2, which show the response of the cesium Particle Size Distribution (PSD) when kaolinite sorbent are added to the system. Without sorbent, the cesium alone forms a peak near 0.06 microns, indicating that the cesium is completely vaporized, and then nucleates to form a fume upon cooling in the probe [Davis et al, 1998]. The aerosol size fractionation method identifies the area under the curve, at approximately 1μm, as the fraction of cesium that is captured, and the area to the left of this, in the nano-particle size range, as that fraction of the cesium that remains uncaptured [Davis and Wendt, 2000A,B]. In Figure 1, when kaolinite is added to the system, the cesium peak shifts to near 1 micron because it has reacted with the substrate particles. Figure 2 shows that the presence of chlorine diminishes the Cs capture, probably because of the formation of the cesium chloride in the gas phase, although this must be confirmed through in-situ measurements. When lime is added to the system, which is indicated by the calcium peak, there is no shift in the cesium PSD, meaning the cesium does not react with the lime. Data were also obtained with sulfur present, the main effect of which is to raise the metal dewpoint and diminish the time available for reaction.
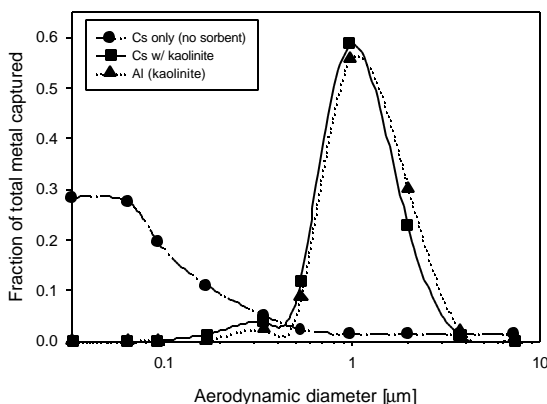
Figure 1. Cesium capture by kaolinite. No chlorine.
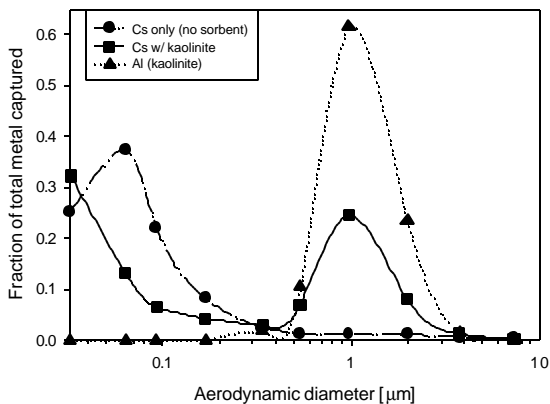
Figure 2 Diminished cesium capture by kaolinite in presence of chlorine.

The key strontium results are shown in Figure 3. Without chlorine present, the strontium does not volatilize and therefore cannot be captured by a sorbent. It forms large residual particles of unreacted strontium, as shown on the LHS of Figure 3. The presence of chlorine serves to volatilize strontium, as shown on the RHS of Figure 3, and this does allow capture, if not complete capture, as demonstrated by aerosol size fractionation and the narrow psd on the RHS of Figure 3. Lime as a sorbent showed no capture either with or without chlorine. Sulfur complicated the metal/sorbent interactions.

Figure 4 shows the morphological changes that occur upon reaction of cesium and strontium with kaolinite. In all cases where reaction occurs, a glass melt is formed (center and right), while very little (probably due to impurities) was formed when the kaolinite passed through the same temperature zone alone (left). These experimental screening results are very significant. First, they show that cesium and strontium can be scavenged by an inexpensive sorbent, kaolinite. Second, they show that chlorine is required to devolatilize strontium, but this can also diminish the reaction of cesium. Clearly, additional fundamental data on the pertinent kinetic mechanisms is required in order

to optimize the use of high temperature kaolinite to reactively scavenge both cesium and strontium in mixed wastes.
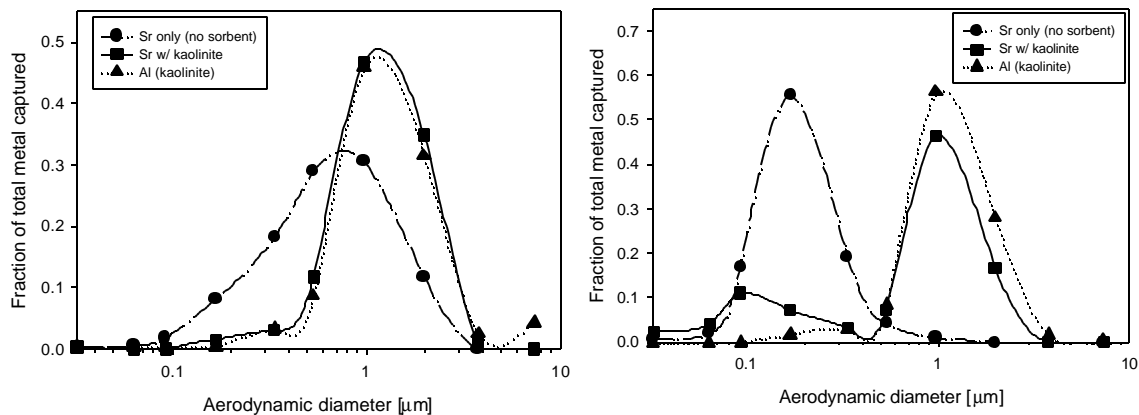
Figure 3. Strontium capture by kaolinite does *not* occur *without* chlorine (LHS) but *does* occur *with* chlorine (RHS)**.**
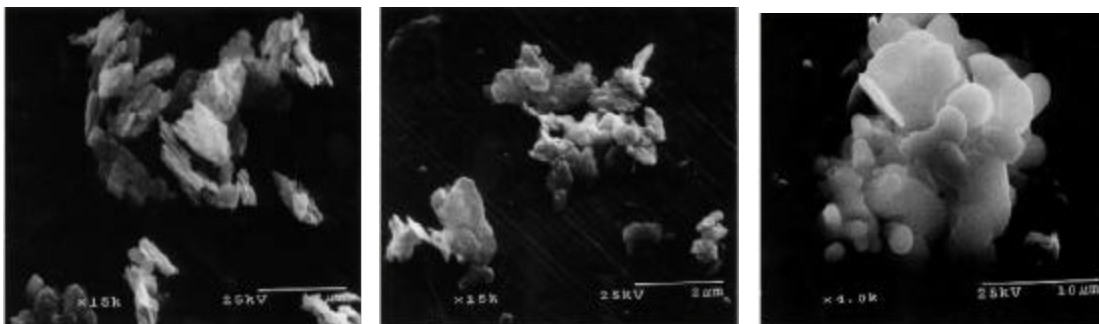
Figure 4. Morphology of unreacted kaolinite (left); product of scavenged cesium, no chlorine (center); product scavenged strontium with chlorine present (right).

3.3   Mathematical Modeling of Individual Droplet Trajectories.

3.2.1 Modeling Goals. We wished to determine whether it was possible to predict <u>individual</u> droplet trajectories and environments in combustor turbulent flow fields. This was not merely only a random process, since we wished to <u>capture </u>the <u>physics of turbulence</u> and dominant turbulent mixing and eddy characteristics without DNS (direct numerical simulation). Kerstein's [1999] One Dimensional Turbulence (ODT) Model appeared to posses the correct attributes to do this. Like DNS, the ODT method requires multiple realizations. However, unlike DNS, ODT for droplet trajectories in a practical configuration, is currently "doable."

The Problem. The following issues can be raised:
- Experimental data show wide range of droplet endpoints for identical initial conditions [Mulholland et al, 1991]
- We wished to predict *individual*, as distinct from *average*, droplet burnout points.

- We adapted Kerstein's [1999] One Dimensional Turbulence (ODT) model for droplet trajectories.
- We developed new two-phase flow model to be incorporated within ODT, consistent with phenomenology and assumptions in ODT.

There were three phases:

1. To confirm that ODT can adequately reproduce the axial evolution of *average* temperature and z velocity as measured by Mulholland. Calibration with experimental data occurred only through initial conditions. The model requires measured mean v_z and mean T at z=0, and then only one free parameter to be chosen to allow reasonable agreement between predicted and measured mean gas axial velocities and temperatures downstream. It is worth noting that, although a triplet map assumes a specific form of stretching and distortion due to turbulence, ODT is implemented such that turbulent energies and momenta are conserved. Triplet maps are modeled to occur instantaneously; yet there is a "turn over" time associated with them that is used to compute the transverse velocity component. ODT contains enough of the physics to replicate the downstream laminarization of the turbulent flow as measured also by Mulholland *et al* [1991].

2. To develop a droplet trajectory model which is consistent with the linearity of ODT. This consumed a major portion of the theoretical modeling effort of the current project, and required implementation of several innovative approaches. It is important to note that **NO** additional adjustable parameter was required.

3. To implement burning droplets into the ODT domain and track many realizations of the drop (of order 100) while keeping track of the burnout points.
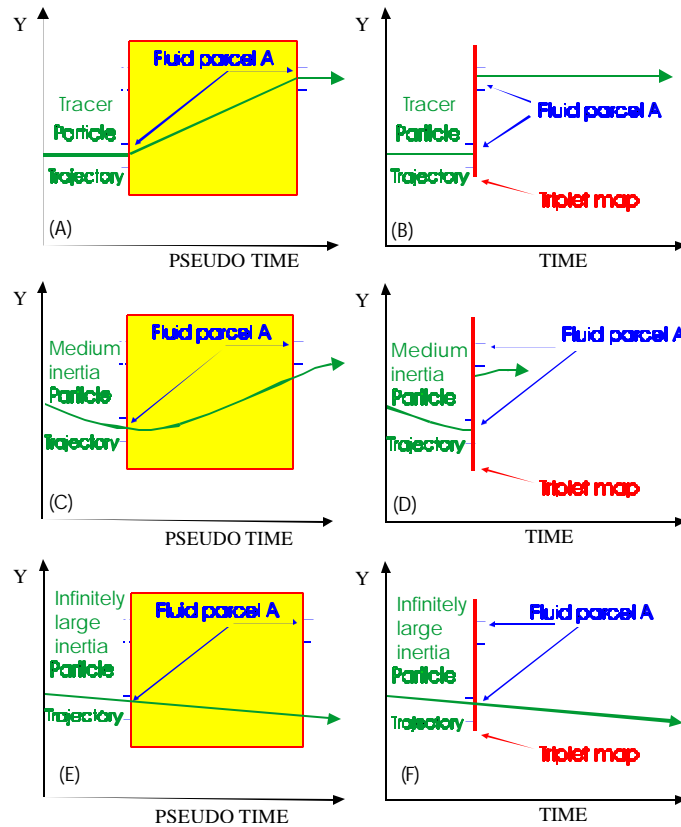
Figure 5. Implementation of two phase flow into ODT. Upper, middle and lower panels show interactions between triplet map and low, medium and high inertia droplets respectively.

3.2.2   Implementation of Droplet Trajectory Model in ODT.   Figure 5 depicts the major model development in this research. It schematically shows how droplet drag is implemented in the model. A particle traversing the ODT distance-time domain now can interact with areas (boxes, LHS of Figure 5) rather then lines (which are infinitesimally thin, RHS of Figure 5). Low inertia particles (top) follow the gas; medium inertia particles (center panel) do not, and are affected by the drag law, while high inertia droplets show no interaction with local turbulence (as postulated through the local triplet map). Another issue was to determine when and where a droplet actually did enter a triplet map. This was complex and is described by Schmidt [2000] and Schmidt, Wendt and Kerstein [2001A, B].

Conservation equations for the heat and mass transfer with burning were solved to predict the burning rates of the drop. The following approximations are used: spherical symmetry, infinitely fast chemical reaction at the flame sheet, pseudo steady state, adiabatic flame temperature. The authors direct you to Schmidt [2000] or Appendix B for further details on the burning model.

3.2.3   Results for ODT Model.   Results are shown on Figure 6. For an ensemble size of 350, experimental results depict the predicted axial spread for the four variations of initial stream conditions, namely diameter, velocity, droplet spacing, and injection angle. Analysis shows excellent agreement of the predicted spread with the measured spread for the variation in initial *diameter*. The agreement with the variation in initial *velocity* is also good with both the simulated and experimental data showing a downward trend as the initial velocity increases. The model shows a marked change in behavior of the spread as the initial *spacing/diameter* (s/D_o) changes. Above a value of s/D_o of 10, the particles behave independently. There is very good agreement in the second grouping (the last three cases) of the spread as compared to the measured data. The first grouping is not a good match.
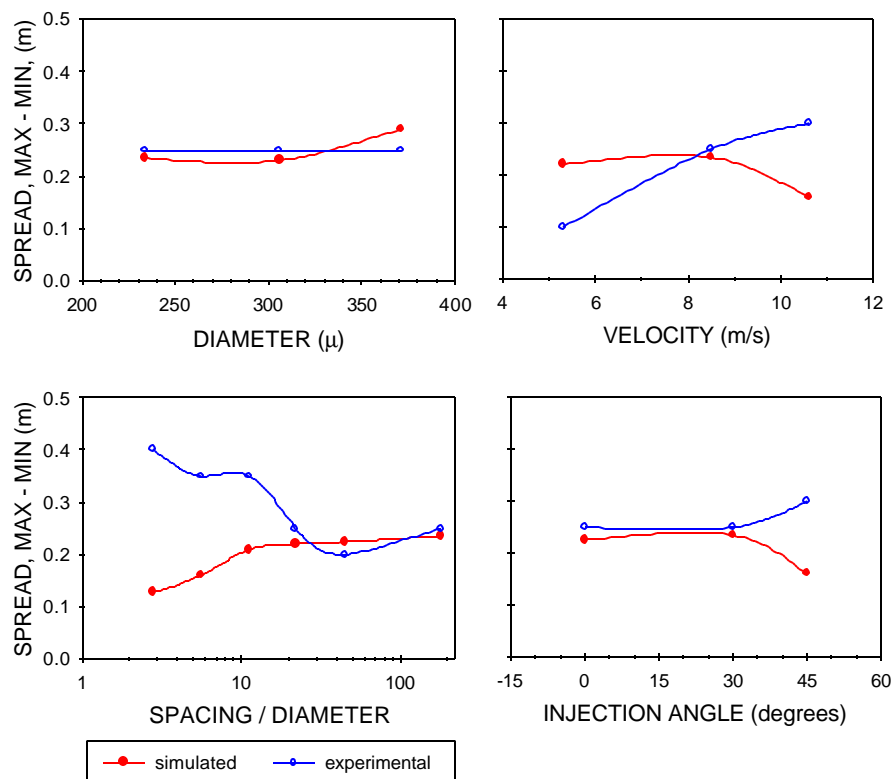
Figure 6: Results: comparison between the experimentally measured spread in burn out end points and the spread predicted by the simulation. This simulated data comes from an ensemble size of 350.

15

The lack of s/D_o parameterization in the ODT droplet submodel is probably the cause of this discrepancy. The agreement for the zero and thirty-degree *injection angles* is good. The trend of the simulated data is significantly different from the measured data. This is probably due to the artifact created in ODT by the assumption that eddies are instantaneous in time. As the injection angle increases the y-component of the particle velocity increases and the error due to this artifact becomes more pronounced.

3.3 Laser Diagnostic Equipment Methods

   3.3.1 <u>*Laser Diagnostic Goals*</u>. We needed to produce a laser diagnostic apparatus to test the rogue drop hypothesis. This required the ability to generate drops, both as sprays and as monodisperse streams, to measure drop size as a function of position, to measure drop and gas-phase temperature, and to observe speciation in the reactor including free atoms, small molecules, and soot. With the exception that a lack of a tunable laser prevented observation of free atoms, the apparatus reported here is capable of all these measurements. Drop generation is by use of an electronically-driven oscillating piezoelectric bimorph [Mulholland et al. 1991; Clampitt & Hieftje, 1972]. Temperature measurement within drops is based on exciplex fluorescence [Melton, 1983 and 1993; Murray & Melton, 1985; Gossage & Melton, 1987; Nickle & Melton, 1989; Bai & Melton, 1997; Lu & Melton, 2000]. While we had hoped to measure soot temperature via laser-induced incandescence (LII) [Melton, 1984; Wainner, 1999; Witze et al., 2001], the dispersion of the available spectrograph is more appropriate for atomic or molecular line/band emission rather than the LII continuum.
   3.3.2 <u>*Design Principles for Laser Diagnostic Tool*</u>. To have freedom from chromatic aberration and because of the success of all-reflective spatial and temporal resolution spectrometric systems in recent years, only reflective focusing elements were employed. The only transmissive components are windows in the sides of the reactor and one beam splitter.

   The excitation laser beam was focused to a sheet illuminating a plane passing through the axis of the cylindrical reactor (Figure 7). A cylindrical mirror, dielectric-coated for maximum reflectivity at 308 nm, converted the rectangular (24 mm by 6 mm) beam from the excimer excitation laser to a 50 mm high, 1.6 mm thick illumination sheet. The central plane of this sheet is the object plane for the observation optics.
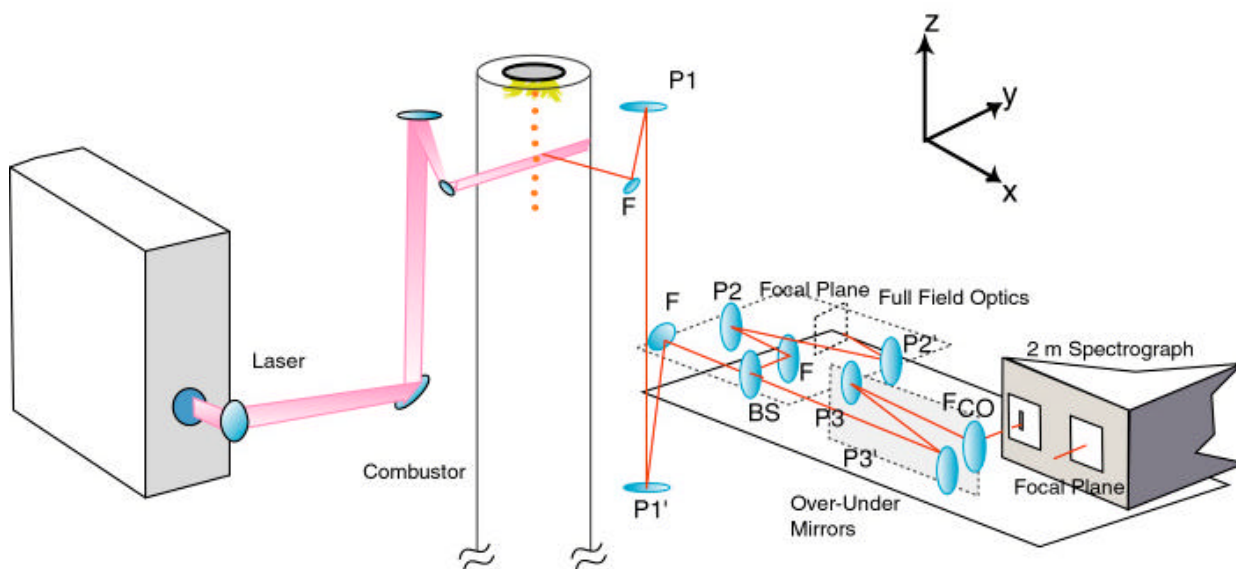
Figure 7. Optical Layout. Two planar folding mirrors direct the 308 nm, 25 ns 400 mJ beam to a cylindrical mirror that focuses the beam through a quartz window into the center of the reactor. The observation optics are orthogonal to the illumination optics, directing the fluoresced/emitted/scattered light to either a non-dispersed focal plane or to a 2 m spectrograph.

Stigmatic imaging was based on the work of Goldstein and Walters [1976] as later implemented by Klueppel *et al.* [1978], Hsu *et al.* [1989], Scheeline *et al.* [1984], and Scheeline *et al.* [1991]. In this arrangement, images are relayed from point to point using parabolic mirrors, illuminated off-axis. Mirrors of nearly identical focal length are used in Z-pairs, so that each pair has no third-order coma and a controlled amount of astigmatism. Parabolic figure guarantees freedom from first order spherical aberration. In contrast to most previous implementations of this design, closed-form approximations in the placement of optics have been supplemented by ray traces using *Zemax* (Focus Software, Tucson, AZ).

For some experiments, either wavelength-integrated measurements or measurements limited only by bandpass filters are desirable. For other measurements, sub-nanometer resolution as most conveniently provided by a scanning spectrograph is desirable. The optical system was designed with two focal planes (Figure 7), one of which used a 2 m Czerny-Turner spectrograph for dispersion (Minuteman Laboratories, Acton, MA), the other of which simply focused an image onto an intensified CCD camera. Because of the 10.92 mm astigmatism of the spectrograph, different astigmatism compensation optics were designed for the two focal planes. The initial image transfer was from a single Z-pair of mirrors; just beyond the astigmatic focal region for this pair was located a UV beam splitter.

In contrast to typical spectroscopic work, the optical system resided in a lab that can most succinctly be described as "dirty." Coal dust from experiments and infiltrating sand particles from the Arizona desert are frequent specimens in the reactor bay. UV laser optics are highly susceptible to damage from surface dust, yet dust was a concomitant of nearly all experiments. We thus covered the optical system with Lucite (which also served to enhance eye safety, as polymethylmethacrylate absorbs 308 nm laser light), and pumped dry HEPA-filtered air into the enclosure. Despite months of experiments on coal dust combustion taking place on both the reactor in which we observed drop dynamics and in an adjacent reactor, which together left a thick coating of dust on the outside of the spectrograph and Lucite box housings, the optical path remained free of detectable dust and the mirrors never suffered damage.

The only excitation yet employed on this apparatus is the 308 nm XeCl laser band (Lambda Physik COMPex 201, Ft. Lauderdale, FL). Ultraviolet wavelengths were chosen so that signals would be well away from the blackbody continuum emitted by the reactor walls. Pulsed illumination assisted in temporal selection against continuum while assisting in obtaining strong signals from single drops. Signal-to-noise ratio calculations suggested that illumination at over 10 mJ per pulse would be required to obtain adequate LIF, LII, and Mie scattering signals.

3.3.3 Laser Diagnostic Equiptment Results. To date, work has focused on the use of filtered full-field images to characterize drop trajectories and sooting behavior. Spectrographic/high resolution data have not been useful for single laser firings, as no atomic or diatomic molecular species present in the reactor absorb and efficiently fluoresce at 308 nm. Both the Al I and OH$^{\bullet}$ $X^2\Pi_i \rightarrow A^2\Sigma^+$ band overlaps with excimer emission, however, several conditions (see Cabalo et al., 2002) precluded observation.

We thus confine discussion to observations of drops, gas flows, and soot. Drops of either water or diesel fuel were used. Water had an acitone (5%) tracer added. No tracer was required with diesel drops because of naturally occurring aromatic hydrocarbons that are present in diesel fuel and are strongly pumped at 308 nm, fluorescing strongly as shown in Figure 8.

The drop sizing capability of the apparatus was investigated by comparing the size measured by the apparatus with known drop sizes. Results are shown in Table I. In all cases, optically determined sizes are less than those expected, typically by approximately 1 pixel or 5%. Considering that some evaporative loss is expected and that optical magnification is calculated to be 1.003, this is acceptable. In addition to drop sizing, drop imaging was quite effective in determining drop shapes. Smaller drops (d< 500 ?m) tended to be spherical, and larger drops tended to be slightly flattened. Drop shape and size are extremely important for determining drop drag coefficients that help predict
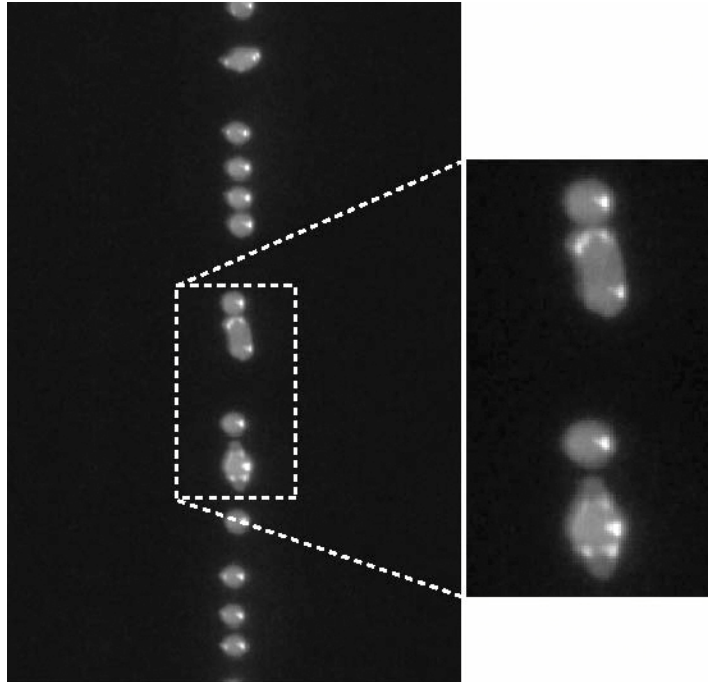
Figure 8 Drop stream showing agglomeration of adjacent drops.

the penetration of drops into the combustor. The drop size and shape also affect the transport of vapor material away from the drop.

At sufficiently high spray rates, drop collisions and coagulation can be seen (Figure 8). Drop growth as well as vaporization can thus be observed. The fate of diesel drop groups was observed at three points positioned along the centerline of the furnace 12.1 cm, 42.6 cm, and 73.0 cm downstream from the burner. At low gas flow rates, drop groups tended to remain intact even down to the third port, with no coagulation evident. However, as the gas flow was increased, the drop stream was broken up, the drops were observed to form clump like formations, and coagulation was observed at the second and third ports. Except at the highest flow rates, the drop groups were not broken up at the first port. We attribute the breakup of drop formations to turbulence. Except at the lowest flow rates, drops were rarely observed at the third port, and these drops no longer remained in linear formation.

Another issue of importance for thermal destruction of liquid waste is the gas phase transport of material originating from the liquid drops and possible uptake by sorbent particles. This was investigated by observing the transport of PAH from diesel drops, as shown in Figure 9. With the Schott BG-25 and WG-320 filters, the camera was optimized for imaging light in the range of 350 nm to 450 nm, the emission wavelength range for PAH. The most intense PAH signal arises from the liquid phase, where the strong attenuation of laser light through the thickness of the drops appears as the signal rapidly decays from the right to the left in Figure 9A. Fluorescence from the gas phase PAH in a gas phase concentration map clearly shows the transport of vapor away from the drop array.

Figure 10 shows the radial cross sections of PAH fluorescence from the middle of the drop stream to the edge of the observable volume. The lower curve is the signal through the saddle point between drops, and the upper curve is a cross section through the middle of a drop. The signal through the saddle point decreases in an exponential fashion until it reaches a cusp, which incidentally is where this curve intersects the cross section through the drop. The position of this intersection point does not change with respect to drop injection velocity. This can be explained by the fact that the decay in PAH signal is a combination of diffusive and convective transport away from
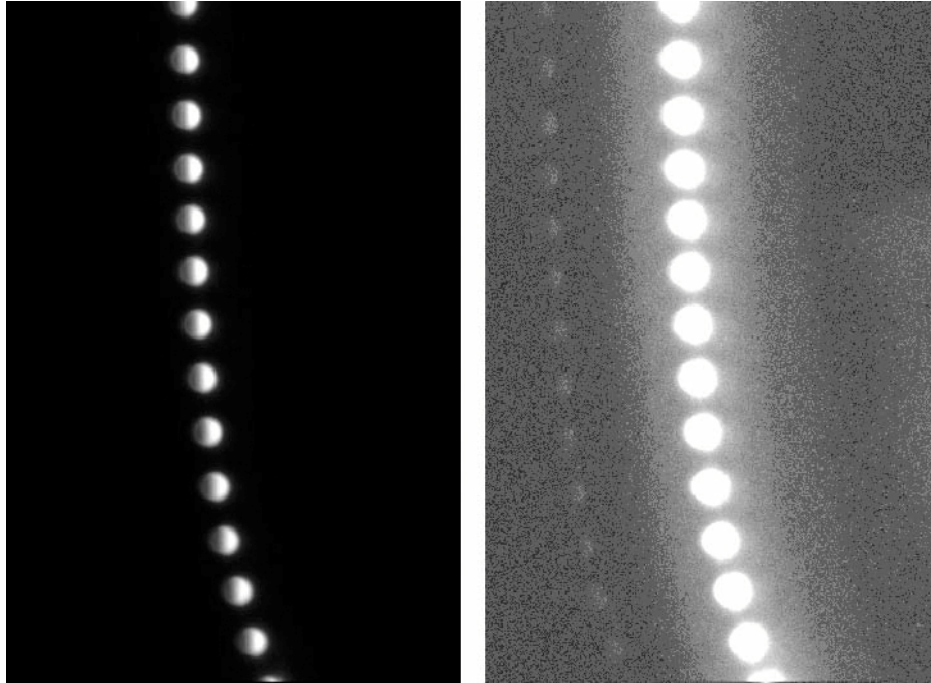
Figure 9   PAH fluorescence both in drops and in the atmosphere surrounding drop trajectories.

the drop stream and the thermal degradation of the PAH. Material vaporizing from the drop stream should experience rapid heating from the diesel wet bulb temperature to ~ 1700 K. Thus, thermal degradation should be a dominant factor in the decay of PAH signal.

In the case of combustion, soot formation is an important process. Thus, it is important that this system also have the capability of detecting small particles. Soot was imaged, as shown in Figure 11. Though the CCD camera does not have the resolution to image individual particles less than 25 ?m in size, the scattered light intensity was much more intense than the fluorescence signals. The apparatus is capable of detecting zones containing sufficient <u>concentrations</u> of particles.   Soot appeared in clouds surrounding the drop streams. Only for lean conditions did soot appear to be forming in the wake of individual drops. Otherwise, the soot appeared to be formed from the diesel vapor from previous drops. Some of the images showed clumping of the soot. Soot was also helpful in visualizing the motion of the gas surrounding the drop stream. At the second and third port, the soot also revealed turbulent eddies, as well as how diesel drops also interacted with the surrounding gas. It is clear from Figure 11 that even at port 2 the drops pulled soot material into their wakes when they were still traveling faster than the surrounding gas.

Table I. Observed vs. computed drop diameter.

Measured diameter (weighed drop stream)	Apparent diameter
405 µm	375 µm
511 µm	500 µm
606 µm	575 µm
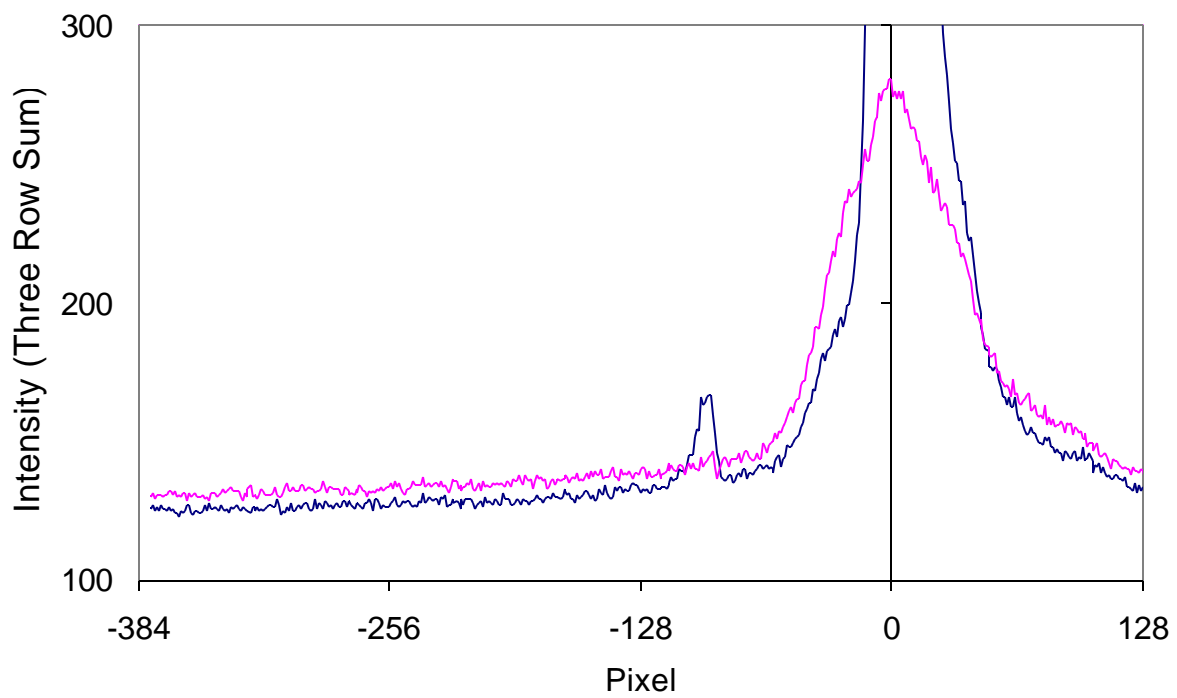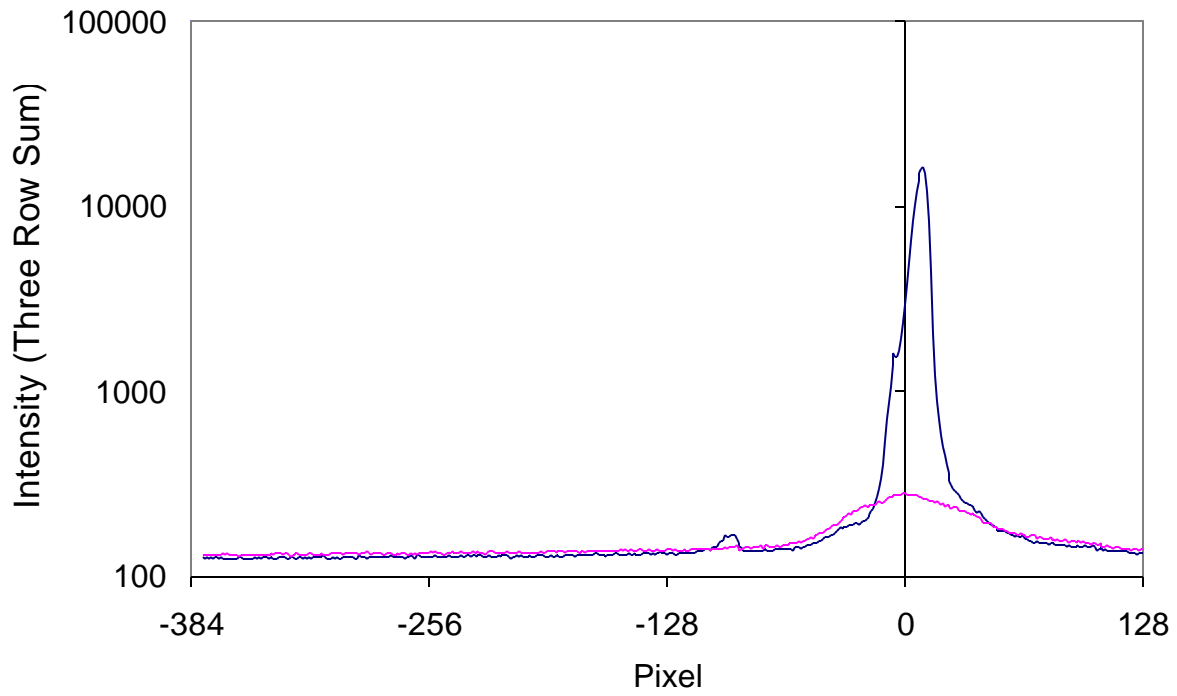
Figure 10   Cross sections of the PAH fluorescence in Figure 9. The ordinate axis position marks the midpoint of the drop array.
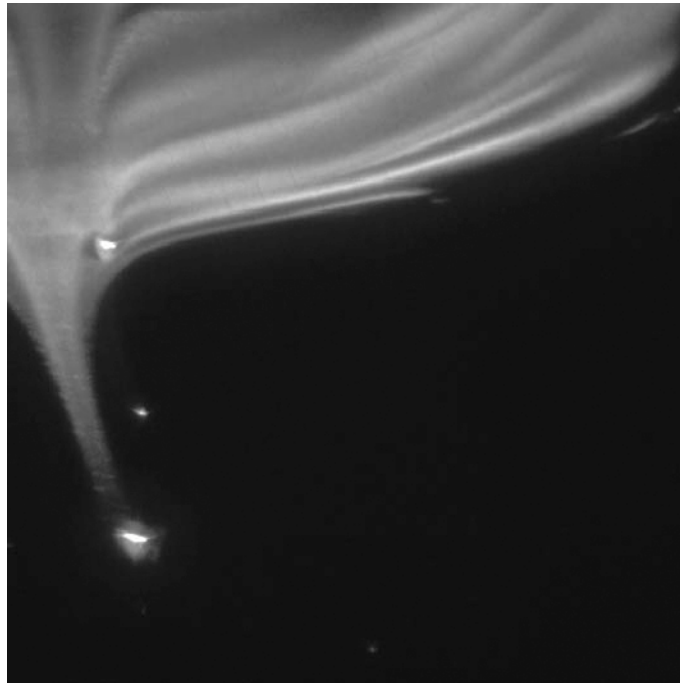
Figure 11   Image of scattered laser light from diesel drops passing through clouds of soot recorded at the second port. The soot material entrained in the drop wake indicates the high drop velocity with respect to the surrounding gases. Note that the drop acts as a lens and focuses laser light to a bright spot.

3.4 Summary of Accomplishments of Current Grant.

Research results from the current grant are encouraging. The experimental screening studies show that kaolinite will reactively capture cesium and strontium, to form glassy melts. The conditions under which this capture are complex, and for mixtures of cesium and strontium, require optimum levels of chlorine. The mechanism and kinetics of the process have not been delineated. To accomplish this will require *in-situ* measurements of metal species within the laminar flow combustor.

The One Dimensional Turbulence Model of Kerstein promises to make it possible one day to track every particle of waste, and every droplet injected into a hot turbulent flow reactor. A turbulent flow reactor would be the practical realization of this process. Public acceptance and process safety of this process would be greatly enhanced if the trajectories and instantaneous locations of all waste and sorbent particles were to be predicted, and the local chemistry known.

A new, high fidelity imaging apparatus has been constructed for the observation of drop dynamics and vapor transport properties in multi-kilowatt thermal reactors. The apparatus is capable of optically determining the size and shape of drops for the determination of drag coefficients. Important events such as drop coagulation can be observed. In addition, suspended and vapor phase material, such as soot and PAH vapor surrounding the drops that pertain to gas phase transport, have been imaged. Soot images showed the interaction between the drops and the surrounding combustion gases as the drops ploughed through. The instrument was also shown to be capable of recording emission spectra within the combustor.

Section 4
Relevance, Impact, and Technology Transfer

The relevance of this project lies in its relationship to providing solid scientific underpinnings required to make thermal treatment of radioactive metal wastes a viable and publicly acceptable technology. Two impediments to this technology must be addressed:
1. Lack of knowledge whether the chemistry of interaction between metal vapors and sorbent substrates is appropriate to make the process practical
2. Inability to quantitatively predict the physical processes of interactions between droplets, turbulent flows, metal vapors and dispersed particles, so that there is complete confidence that all the metal vapor is contacted by sorbent within the proper temperature regime.

This project was designed to surmount these two impediments, and to provide predictive tools that allow safety guarantees for thermal treatment processes.

The short term impact of this project is curtailed because, even though great progress has been made, further work was still required to meet these very ambitious goals, and thermal treatment of radioactive wastes remains an anathema both to the public and to practitioners in the field. The long term impact of this work may be substantial, because this work led to a basis for productive future research that may well make thermal treatment more acceptable. It also has led to advances in understanding the fundamentals of turbulent two phase flow.

Technology transfer to the scientific community is detailed below in Section 7. There has not been significant technology transfer to the field at this time, because application of the project results required further work.

Section 5
Project Productivity

This project was extremely ambitious and therefore fell somewhat short of meeting all its stated goals. Both the turbulence modeling and the laser diagnostics were at the cutting edge of their respective fields, and, not unexpectedly, very difficult problems in each area emerged, and were solved, but at the cost of time and money. They are described in detail in the appendices attached.

The successes of the project can be listed as follows:
1. Thermal scavenging of both cesium and strontium was shown to be a viable option for isolating those metals from the environment.
2. A new approach to model two phase turbulent flow was developed, and shown to be the only method currently available to predict individual droplet trajectories that have been measured in combusting turbulent flowfields.
3. A diagnostic tool was developed that allowed droplet positions to be observed non-intrusively. This work was featured on the cover of the October 2002 volume of the scientific journal "Applied Spectroscopy". With additional work, this tool could be improved to allow simultaneous measurement of droplet positions and species concentrations in a turbulent flow thermal reactor.

Details of all of the above are in the Appendices.

Section 6
Personnel Supported

Personnel who were supported with this research effort at the University of Arizona were:
- Dr. Jost O.L. Wendt, Professor and Head, Department of Chemical and Environmental Engineering, University of Arizona
- John R. Schmidt, Graduate Student, U of A

- Jonathon M. Amos, Graduate Student, U of A
- Dr. Sheldon B. Davis, Post-Doc, U of A
- Dr. Jerry Cabalo, Post-Doc (work completed at UA, funded through UIUC)

Section 7
Publications

7.1.   Published in peer-reviewed Journal.

"Spectrometric System for Characterizing Drop and Powder Trajectories and Chemistry in Reactive Flows," by Jerry C. Cabalo, John Schmidt, Jost O. L. Wendt, and Alexander Scheeline
Published in *Applied Spectroscopy*, January, 2002

7.2.   Published in unreviewed publications.

Preliminary results for this project were presented at the following symposia and published in the corresponding unreviewed proceeding.
- The First Joint Meeting of the US Sections of the Combustion Institute, George Washington University, Washington, DC March 1999 [Amos & Wendt, 1999].
- The Sixth International Congress on Toxic Combustion By-Products, Invited lecture, University of Karlsruhe, Germany, June 1999.[Wendt, 1999].
- The 4th International Syposium & Exhibition on Gas Cleaning at High Temperatures, University of Karlsruhe (TH),September 1999. [Davis et al. 1999].
- American Flame Research Council Semi-Annual Meeting, Tucson, Arizona, 1999.   Papers distributed at the meeting. [Amos & Wendt, 1999B].
- 2000 Spring Meeting Western States Section The combustion Institute, March 2000. [Schmidt et al., 2000 A].
- 2000 American Flame Research Committee International Symposium, September 2000. [Schmidt et al., 2000 B].
- The Second Joint Meeting of the US Section of the Combustion Institute, March 2001. [Schmidt et al., 2001].

7.2.   Submitted/in preparation for publication.

An article dealing with the numerical modeling portion of the completed project was submitted to the peer-reviewed journal.   It is entitled, "Trajectories of Evaporating Droplets in a Turbulent Combustor Using the One Dimensional Turbulence Model". The manuscript submitted for publication is reproduced in its entirety in Appendix C.

A second article dealing with the experimental portion of the completed project is in preparation. It will be submitted to the peer-reviewed journal Environmental Science and Technology [Amos et al., in preparation].

Section 8
Interactions

This project resulted in a close working relationship between UA and Sandia, to the extent that Dr. Alan Kerstein acted as a co-advisor to Schmidt's MS Thesis and Ph.D. Dissertation, and participated in all the exams. This collaboration is enduring.

This project also required close collaboration between UIUC where the laser diagnostic tool was constructed and UA where the tool was made to work and put to use. This collaboration will also continue.

Presentations of the preliminary results from this research were given at:
- ESMP workshop Chicago, July, 1998
- The First Joint Meeting of the US Section of the Combustion Institute, March 1999
- The Sixth International Congress on Toxic Combustion By-Products, Germany, June 1999.
- The 4th International Syposium & Exhibition on Gas Cleaning at High Temperatures, (TH), September 1999.
- ESMP workshop, Atlanta, April 2000
- Western States Section The combustion Institute, March 2000.
- American Flame Research Committee International Symposium, September 2000.
- The Second Joint Meeting of the US Section of the Combustion Institute, March 2001.

Section 9
Transitions

The results form this work need further refinement (see future work Section 11) in order to undergo the transition to a hazardous waste incineration technology.

Section 10
Patents

10.1 New Discoveries

Cesium alone vaporizes readily in the flame, and subsequently nucleates in the sampling probe to form sub-micron particles. Cesium is almost completely captured in the presence of kaolinite. It is not captured by lime. Chlorine raises the dewpoint of cesium. This is unusual, in that chlorine tends to lower the dewpoint of most metals. The presence of chlorine does appear to have some effect on the reactive capture of cesium by kaolinite. It does not appear to affect the capture of cesium by lime. The presence of sulfur also raises the dewpoint of cesium. However, this appears to have little effect on the capture by kaolinite. It does enhance the capture of cesium by lime. This is probably due to the speciation of the cesium compounds.

Strontium alone does not vaporize in the flame, and is only minimally captured on kaolinite and lime, probably by physical coagulation processes and not reactive scavenging. The presence of chlorine enhances the vaporization of strontium and subsequent capture by kaolinite. In this sense, strontium behaves similarly to nickel. However, this vaporization does not promote capture on lime. In contrast to the equilibrium predictions, sulfur enhances the volatilization of strontium. However, it does not aid in capture.

A novel two-phase flow model was added to the ODT turbulence model utilizing one-way coupling between gas flow and particle trajectories. Correlation between the spread in the burnout points and initial droplet size, droplet velocity, interdroplet spacing, and droplet injection angle are examined. The numerical investigation also includes a droplet heating/burning model. Results are in good agreement with the measurements of Mulholland et al. [1991].

An instrument for emission, fluorescence, and scattering diagnostics of a 17 kW gas/air thermal reactor was successfully designed buildt and tested. Z-pair parabolic mirrors provide diffraction-limited imaging in field center, with worst-case blur over a 12.8 mm field of view having a radius of 0.044 mm RMS. Either full-field filtered or transverse line dispersed viewing can occur simultaneously. Dispersion is achieved using a 2 m spectrograph f-matched to the feed optics. Examples of data show non-axisymmetric flow in a nominally laminar flow system, drop shapes *in situ*, and Mie scattering from soot.

10.2   Patents
None

Section 11
Future Work

11.1 Experimental

Given the continuing funding, the UA could conduct laminar flow reactor studies in the 17kW downflow reactor to determine the kinetic parameters that control the scavenging of cesium and strontium vapors by kaolinite. In situ diagnostics would be developed by UIUC. Obtaining a tunable dye laser in the future would do this. The only components that would have to be changed to accommodate a tunable operation are the mirrors that relay and focus the laser beam to the mid-plane of the reactor. With a tunable laser radiation source, the transport properties of various materials such as heavy metals and their oxides whose properties are not completely known can be directly measured under combustion conditions. The objective would be to elucidate the mechanism of interaction between cesium or strontium and kaolinite both in the absence and in the presence of chlorine. In-situ measurements would consist of elemental composition of particles, using LIBS, and also gas phase metal speciation, using PLIF.

11.2 Theoretical Modeling

Theoretical modeling will focus of further validation of the two phase ODT version. We have already shown that we can simulate accurately the spread in droplet trajectories that was measured by Mulholland *et al.* (1991). However, this was a rather unique experimental configuration and additional validation is essential, since the model does contain many assumptions. There is a paucity of experimental data analogous to Mulholland's, and so we propose to compare particle flow results from ODT with similar results from DNS (Direct Numerical Simulations). Then we shall incorporate the improved drag coefficients of Pearlstein into the model, and use them to determine maximum penetrations of large deformable droplets in a thermal reactor. Finally we may develop an ODT version that accounts for two separate streams of particles (droplets and sorbent particles) introduced at different locations, and determine the interactions between the two. As before, this work will be jointly supervised by Dr Alan Kerstein, who will co-advise Ph.D. students with Professor Wendt. These Ph.D. candidates will also spend time at Sandia, to learn from Dr. Kerstein. Finally, this model will be compared to experimental data to be obtained through yet another collaboration with Dr. William P. Linak of US EPA in North Carolina.

Section 12
Literature Cited

Amos, J, M., "High Temperature Reactive Capture of Cesium and Strontium by Sorbents", M.S. Thesis, University of Arizona, Department of Chemical and Environmental Engineering, 1999.

Amos J.M., Davis, S.B., and Wendt, J.O.L. " Evaluation of Sorbent to Reduce Radionuclide Emissions from Mixed Waste Incineration", In preparation, to be submitted to *Environmental Science and Technology*.

Amos, J.M. and Wendt J.O.L., "High Temperature Scavenging of Cesium and Strontium by Sorbents", Presented at Joint Meeting of the US Sections of the Combustion Institute, George Washington University, Washington, DC March 1999 A.

Amos, Jonathan and Wendt J.O.L. "High-Temperature Capture of Cesium and Strontium by Sorbents", American Flame Research Council Semi-Annual Meeting, Tucson, Arizona, 1999 B.

Bai, F. and Melton, L. A "High-temperature, Oxygen-resistant Molecular Fluorescence Thermometers," *Appl. Spectrosc.* **51**, 1276-1280 (1997).

Barin, I., Thermochemical Data of Pure Substances. Weinheim, FRG, VCH (1995).

Cabalo, J.C., Schmidt, J.R., Wendt, J.O.L., Scheeline, A., "Spectrometric System for Characterizing Drop and Powder Trajectories and Chemistry in Reactive Flows," Applied Spectroscopy **56**, 10, pp 1345 – 1353, 2002.

Clampitt, N.C., and Hieftje, G. M., "Mechanism of Desolvation of Sample Droplets in Flame Spectrometry," *Anal. Chem*. **44**, 1211-1219 (1972).

Davis, S.B., Amos, J.M., Gale, T.K., Wendt, J.O.L., Biermann, J.J.B. and Voogt, N., "Use of Sorbents from Paper recycling Wastes for the High Temperature Capture of Multiple Metals in the Presence of Chlorine" pp 784-796, Proceedings of 4th International Syposium & Exhibition on Gas Cleaning at High Temperatures, , University of Karlsruhe (TH),Sep 22-24, 1999.

Davis, S. B., Gale, T.K., Wendt, J.O.L. and Linak, W.P., "Multi-Component Coagulation and Condensation of Toxic Metals in Combustors" ,*Proceedings of the Combustion Institute*, Vol 27, pp1785-1791, The Combustion Institute, Pittsburgh, 1998.

Davis, S. B., Gale, T.K. and Wendt, J.O.L. "Competition for Sodium and Toxic Metals Capture on Sorbents," *Aerosol Sci. Technol.* **32**, 142-151 (2000).

Davis, S. B., Wendt, J.O.L. and Linak, W.P. "Interactions between Lead Vapor and Sorbents at High Temperatures," *Chem. Phys. Processes Combust.* 157-159 (1999).

Davis, S.B. and Wendt, J.O.L. "Mechanism and Kinetics of Lead Capture by Kaolinite in a Downflow Combustor", in press, *Proceedings of the Combustion Institute,* Vol 28(2000 A).

Davis, S.B. and Wendt, J.O.L. "Quantitative Analysis of High Temperature Toxic Metal Sorption Rates using Aerosol Fractionation", *Aerosol Sci. and Technol.,*33:536-543 *(*2000 B).

Goldstein, S. A., and Walters, J.P. "A Review of Considerations for High-fidelity Imaging of Laboratory Spectroscopic Sources. Part I," *Spectrochim. Acta*, **31B**, 201-220 (1976).

Gossage, H. E., and Melton, L.A. "Fluorescence Thermometers Using Intermolecular Exciplexes**."** *Appl. Opt.* **26**, 2256-2259 (1987).

Gougar, M. L. D., Scheetz, B.E. and Siemer, D.D. "A Novel Waste Form for Disposal of Spent-nuclear-fuel Reprocessing Waste: a Vitrifiable Cement," *Nucl Technol.* **125**, 93-103 (1999).

Hillamo, R. and Kauppinen, E. "On the Performance of the Berner Low Pressure Impactor. "Aerosol Science and Technology **14**: 33-47(1991).

Hopkins, J.D. (1994) "Criteria For Flammable Gas Watch List Tanks," WHC-EP-0702, Rev. 0, Westinghouse Hanford Company.

Hsu, W. H., Sainz, M.A. and Coleman, D.M., "An Aberration-Corrected Time- and Spatially-Resolved Spectrometer for Studies of Transient Discharges," *Spectrochim. Acta*, **44B**, 109-121 (1989).

Kerstein, Alan R., "One-dimensional turbulence: model formulation and application to homogeneous turbulence, shear flows, and buoyant stratified flows." J. Fluid Mech. **v392**,. pp. 277-334 (1999).

Klueppel, R. J., Coleman, D.M. Eaton, W.S., Goldstein, S.A., Sacks, R.D., and Walters, J.P., "A Spectrometer for Time-gated, Spatially-resolved Study of Repetitive Electrical Discharge," *Spectrochim. Acta*, **33B**, 1-30 (1978).

Lu, Q. –Z., and Melton, L.A., "Measurement of Transient Temperature Field within a Falling Droplet," *AIAA J*. **38**, 95-101 (2000).

Meisel, D., Jonah, C.D., Kapoor, S., Matheson, M.S., and Sauer, M.C., "Radiolytic and Radiolytically Induced Generation of Gates from Synthetic Wastes," ANL-93/43, Argonne National Laboratory (1993).

Melton, L. A., "Spectrally Separated Fluorescence Emissions for Diesel Fuel Droplets and Vapor," *Appl. Opt*. **22**, 2224-2226 (1983).

Melton, L. A., "Soot Diagnostics Based on Laser Heating," *Appl. Opt*. **23**, 2201-2208 (1984).

Melton, L. A. "Exciplex-based Vapor/Liquid Visualization Systems Appropriate for Automotive Gasolines," *Appl. Spectrosc*. **47**, 782-786 (1993).

Mulholland, J.A., Srivasta, R.K., Wendt, J.O.L., Agrawal, S.R., and Lanier, W.S., "Trajectory and Incineration of Rogue Droplets in a Turbulent Diffusion Flame." Combust. Flame, **v86**, pp. 297-310 (1991).

Murray, A. M., and Melton, L.A., "Fluorescence Methods for Determination of Temperature in Fuel Sprays," *Appl. Opt*. **24**, 2783-2787 (1985).

Nickle, S. K., and Melton, L.A., "Fluorescence Lifetime and Quenching Rates for N,N,N',N'-tetramethyl-p-phenylenediamine in the Vapor Phase," *Appl. Spectrosc*. **43**, 1406-1409 (1989).

Scheeline, A., Bye, C.A., Miller, D.L., Rynders, S.W., and Owen, R.C., "Design and Characterization of an Echelle Spectrometer for Fundamental and Applied Emission Spectrochemical Analysis," *Appl. Spectrosc*. **45**, 334-341 (1991).

Scheeline, A., Kamla, G.J., and Zoellner, M.J., "Electron Concentration Measurement in the High Voltage Spark Using Stark Broadening of H$_?$ Emission,'" *Spectrochim. Acta*, **39B**, 677-691 (1984).

Schmidt, J.R., *Trajectories of Evaporating Droplets in a Turbulent Combustor Using the One Dimensional Trubulence Model,* Masters Thesis, University of Arizona, 2000.

Schmidt, J.R., Wendt, J.O.L., and Kerstein, A.R., "Trajectories of Evaporating Droplets in Highly Turbulent Flows using the One Dimensional Turbulence Model", 2000 Spring Meeting Western States Section The combustion Institute, March 14 & 14, 2000 A.

Schmidt, J.R., Wendt, J.O.L., and Kerstein, A.R., "Capturing the Spatial Variation of Burning Droplets in Highly Turbulent Flows using the One Dimensional Turbulence Model", 2000 American Flame Research Committee International Symposium, September 18-21, 2000 B.

Schmidt, J.R., Wendt, J.O.L., and Kerstein, A.R., "Capturing the Spatial Variation of Burning Droplets in Highly Turbulent Flows using the One Dimensional Turbulence Model", The Proceeding of The Second Joint Meeting of the US Section of the Combustion Institute, March 25-28, 2001.

Schmidt, J.R., Wendt, J.O.L., and Kerstein, A.R., "Trajectories of Evaporating Droplets in a Turbulent Combustor Using the One Dimensional Turbulence Model", submitted for publication.

Stewart, T. L., "Overview of U. S. Radioactive Tank Problem, " Book of Abstracts, 214th ACS National Meeting, Las Vegas, NV I&EC-055 (1997).

Terrell, C.W., "High Level Waste Management, Processing, and Vitrification at the Savannah River Site," *Nucl. Mater. Manage.*, **23**, 233-237 (1994).

Tollison, S.A. and Finger, S.M., "Glass – the Ultimate Waste Form," *Radiat. Prot. Manage.* **14**, 45-49 (1997).

Wainner, R. T., *An Analytical and Quantitative Analysis of the Laser-Induced Incandescence of Soot*, Ph.D. Thesis, Georgia Institute of Technology (1999).

Wendt, J.O.L., Invited lecture "The Fate of Toxic Metals in High Temperature Combustion Systems", Invited Topical Review, The Sixth International Congress on Toxic Combustion By-Products, June 27-30, 1999, University of Karlsruhe, Germany.

Witze, P. O., Hochgreb, S., Kayes, D., Michelsen, H.A., and Shaddix, C.R., "Time-resolved Laser-induced Incandescence and Laser Elastic-scattering Measurements in a Propane Diffusion Flame," *Appl. Opt.* **40**, 2443-2452 (2001).

Zorpette, G., "Confronting the Nuclear Legacy – Part II. Hanford's Nuclear Wasteland," *Sci. Am.* **274**(5), 88-97 (1996).

Section 13
Feedback

There is no feedback at this time.

Appendix A

Manuscript of

"High Temperature Reactive Capture of Cesium and Strontium by Sorbents"

J. M. Amos

Department of Chemical and Environmental Engineering

The University of Arizona

1999

(Self paginated)

High Temperature Reactive Capture of Cesium

and Strontium by Sorbents

by

Jonathan Michael Amos

_____

A Thesis Submitted to the Faculty of the

DEPARTMENT OF CHEMICAL AND ENVIRONMENTAL ENGINEERING

In Partial Fulfillment of the Requirements
For the Degree of

MASTER OF SCIENCE
WITH A MAJOR IN CHEMICAL ENGINEERING

In the Graduate College

THE UNIVERSITY OF ARIZONA

1 9 9 9

APPROVAL BY THESIS DIRECTOR

This thesis has been approved on the date shown below:

_____   _____
         Jost O. L. Wendt   Date
Professor of Chemical Engineering

ACKNOWLEDGEMENTS

DEDICATION

This thesis is dedicated to my parents,

Candyce and Michael,

for all their love and support over the years.

TABLE OF CONTENTS

TABLE OF CONTENTS – *Continued*

LIST OF FIGURES

LIST OF TABLES

ABSTRACT

High-temperature reactive scavenging by sorbents is one possible treatment strategy for metal-bearing liquid wastes. The current work focuses on cesium and strontium, two metals that are present in the DOE waste inventory.

To explore the behavior of the metals and the expected speciation, equilibrium calculations were performed prior to the experimental work. Experiments were performed in an 18 kW laminar downflow furnace. Aqueous solutions of the metals were atomized and injected into the flame. Powdered sorbents were injected into the post-flame region of the furnace. The sorbents investigated were kaolinite, lime, a 50/50 mix of lime and kaolinite, and the CDEM product. Particles were sampled from the furnace isokinetically and passed through a Berner low-pressure impactor. The samples were then analyzed with flame atomic absorption spectroscopy and scanning electron microscopy. The effects of adding chlorine and sulfur to the waste stream were also explored.

Chapter 1

Introduction

1.1 Cesium and Strontium as Hazardous Waste

A significant portion of the U.S. Department of Energy's (DOE) hazardous waste

inventory is composed of metal-bearing liquid wastes (Serne et al. 1996). These wastes

are quite varied with respect to the hazardous constituents (metals, organics, anions, etc.).

Release of these wastes into the public domain, through air, water, or ground releases,

would have a large detrimental impact on public health. As such, it is very costly to

properly store and maintain the facilities for these wastes. A reduction in the volume of

these wastes is highly desirable.

Two of the metals present in these wastes are cesium and strontium (Serne et al.

1996). Cesium-137 and strontium-90 are both radioactive wastes that are produced from

fission reactions, with half-lives of 30 years and 28 years, respectively. They are often

found in reactor wastes, as well as fallout from nuclear accidents. The relatively long

half-lives (with respect to human lifetimes) mean these wastes can pose a significant

threat to human health over a long period. Any treatment method that is used with these

species must be able to immobilize the metals from all possible pathways (air, surface

water, ground water, etc.).

There are several different treatment methods available for reducing and

destroying these wastes. These include incineration, precipitation reactions, membrane

processes, biological processes, and ion-exchange processes. One of the more promising

methods is incineration. There are several advantages to this method of treatment. First, the organic portions of the wastes are destroyed with a very high efficiency. For some components of the organic waste, thermal destruction is required by current environmental legislation anyway. Second, no chemical species need to be added to the waste system. The DOE has experienced problems with some precipitation-type treatment methods producing additional hazardous components (benzene and hydrogen) after the addition of the complexing agents. A third advantage to this process is that the same basic approach can be used to treat a variety of wastes, with widely varying compositions. This will help keep costs low, and will simplify the design of any treatment facilities. Fourth, this treatment process is robust, being able to accommodate a large degree of variation in the feedwaste and operating parameters. Finally, incineration has existed for a long time, so the process and its limitations are much better understood than other treatment methods

There are some disadvantages to this treatment method. Metals cannot be destroyed by incineration. Either the metals remain with the non-combustible portion of the waste or they vaporize, depending on the volatility of the metals. Any gaseous metal constituents either condense onto larger particles in the waste stream which are removed by the air pollution control equipment, or nucleate and form sub-micron aerosols of their own. These particles can often penetrate standard air pollution control equipment. These sub-micron particles are enriched in the toxic species, and are easily inhaled into the lungs. They can also deposit into surface reservoirs or food crops. For these reasons,

incineration is often contested by the public as a viable treatment option (Costner and Thornton 1990).

Sorbent material can be injected into incineration systems to deal with the presence of metals. The metals react with the sorbent particles to form a metal/sorbent complex of some variety. The sorbent materials are inexpensive, readily available materials, such as kaolinite or lime, that have the potential to react with metals. The relatively large sorbent particles are easily removed from the exhaust stream with standard air pollution control equipment. The desire is to form a water insoluble product to prevent the metal from leaching into drinking water supplies after final disposal.

1.2 Metals in Combustion

Metals can occur in many different fuels and wastes, including coal, fuel oil, municipal wastes, hazardous wastes, etc. Extensive work has been performed to determine the behavior and fate of metals in combustion systems (Furr et al. 1977; Sill 1988; Fernandez et al. 1992; Ho et al. 1993; Linak and Wendt 1993; Linak et al. 1994; Rizeq et al. 1994; Bool et al. 1995; Gallagher et al. 1996; Karimanal and Hall 1996; Linak et al. 1996; Buckley et al. 1998; Davis et al. 1998; Linak and Wendt 1998; Yang et al. 1998). The review by Linak and Wendt provides a thorough overview of the issues encountered with metals in combustion systems (1993). Figure 1.1, which is adapted from their Figure 4, provides a summary of the possible mechanisms that may govern in a particular system. Based on the volatility of the metal, it will end up in either the supermicron fraction of the ash, which is easily collected and disposed of, or in the
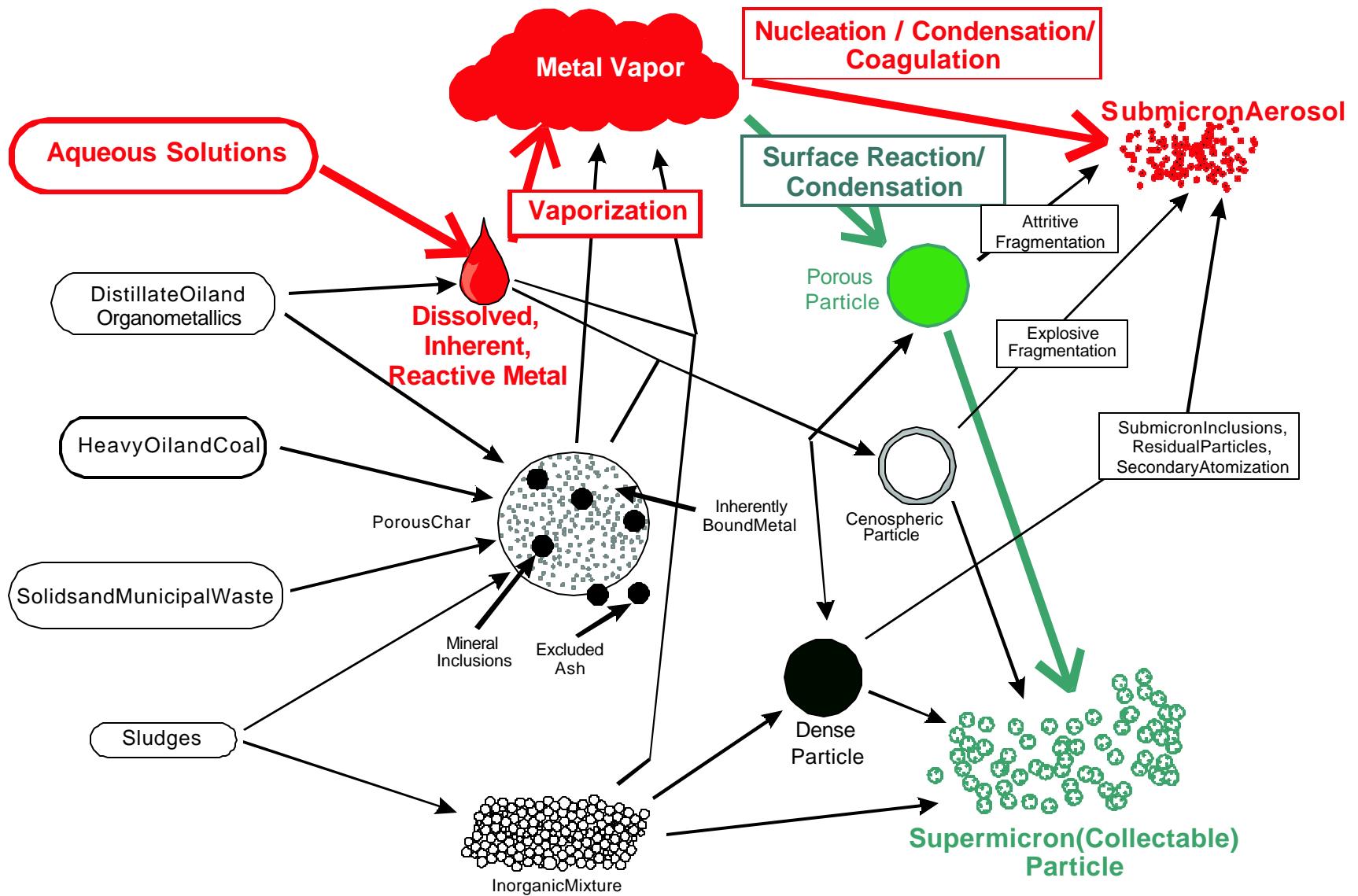
Figure 1.1 - Potential Metal Interactions in Combustion Systems

submicron aerosols, which are difficult to collect and can easily come in contact with the general population. The authors also discuss in some detail the aerosol mechanisms of coagulation, condensation, and nucleation, which determine the final form of the metals in the system. Finally, they discuss the use of sorbents to capture the metals and remove them from the combustion wastes. This topic will be discussed more in the next section.

The volatility of the metals plays an important role in determining the final form of the metal during combustion. Rizeq et. al. (1994) classified several metals into three categories: volatile, semi-volatile, and refractory. Each category exhibits certain characteristics when exposed to combustion environments. Volatile metals, like mercury and selenium, form vapors readily, and may remain in the gaseous state even when passed through the pollution control equipment. Semi-volatile metals partition in the furnace, with a portion of the metals vaporizing in the flame of the incinerator and then condensing further down the furnace to form a sub-micron fume. This fume may pass through air pollution control equipment, releasing an easily respirable aerosol that is concentrated in the metal. Refractory metals have low vapor pressures, even in the high temperature zone of the furnace. They tend not to vaporize and are generally found in the larger sized ash.

There has been little work with cesium or strontium in combustion systems. There has been no work with sorbent interactions of strontium and only some thermogravimetric studies of cesium and sorbents. Due to this dearth of prior experimental data, it would be useful to examine other metals that may have similar

characteristics to cesium and strontium. Here, strontium will be compared to nickel, and

sodium will be considered an analogue to cesium.

Strontium is considered a refractory metal. It has a dewpoint near 2000 K at a

metal vapor concentration of 100 ppm. The relevance of the dewpoint on metals

behavior will be discussed further in the next section. Some useful physical data for both

strontium and cesium are shown in Table 1.1.

Physical Property	Strontium	Cesium
Abbreviation	Sr	Cs
Atomic Number	38	55
Atomic Weight	87.6	132.9
Melting Point, °C at 1 atm	777	28.44
Boiling Point, °C at 1 atm	1382	671
Vapor Pressure, atm at 300 K	4.99E-23	2.4E-9
Vapor Pressure, atm at 1500 K	0.529	40.89
Density, g/cm^3	2.64	1.93
C_p, J/mol K	26.4	32.2
$\Delta_f H°$, kJ/mol (gas)	164.4	76.5
$\Delta_f G°$, kJ/mol (gas)	130.9	49.6
S°, J/mol K (gas)	164.6	175.6

Table 1.1 – Physical Properties of Cesium and Strontium (Data
from (Lide 1995))

There has been some work that has studied the behavior of nickel, another

refractory metal (Linak et al. 1994; Linak and Wendt 1998). In this work, the metal was

injected into a furnace, and the resulting aerosol was sampled and analyzed. It was found

that the nickel did not vaporize, and the nickel particle size distribution formed a peak

around one micron. When chlorine was added to the system, the nickel did vaporize and

formed smaller particles when cooled. The results of these previous works may be used

to help explain the behavior of strontium.

Cesium is considered a low-end semi-volatile metal, with a dewpoint near 700 K at 100 ppm of metal vapor. Cesium is in the same column of the periodic chart as sodium, so the chemical behavior of cesium should be similar to that of sodium. The chemical similarities between cesium and sodium will be explored further in Chapter 2. There has been some work on the fate of sodium from coal combustion (Gallagher et al. 1996). The ash aerosol from coal combustion was sampled and analyzed. The sodium was found to be rather volatile, with the majority of the sodium appearing on the sub-micron plates of the impactor. It was also found that the sodium tended to associate with the silica in the ash.

There has been some work to determine the partitioning behavior of cesium and strontium at high temperatures. There have been studies on species present in coal ash (Furr et al. 1977), but these have focused on the presence of a large number of elements, and have not focused on cesium and strontium in particular. Sill (1988) performed volatility experiments on cesium and strontium from synthetic basalt. The volatility of cesium increased linearly as the temperature increased, with some volatility evident even at low temperatures (400 °C). The strontium did not volatilize at any temperature studied.

Yang et. al. (1998) studied the behavior of several different metals. They performed both thermogravimetric studies and small-scale combustor tests. They used cesium chloride for their thermogravimetric tests, and found that the cesium did eventually vaporize (750 °C). This temperature is low for a combustion system. Their small-scale furnace results show that the majority of the strontium ends up in the bottom

ash of the incinerator. A larger portion of the cesium ended up downstream of the

incinerator. However, their experiments were performed at temperatures that are low

(850 °C) compared with practical incinerators (1200 °C).

Buckley et. al. (1998) studied the fate of cesium and strontium in the combustion

of a biomass fuel. Their experiments were performed on a 100 kW down flow

combustor. Samples were extracted isokinetically and passed through a multi-orifice

impactor (MOUDI). Filters were weighed to determine mass collected, and beta activity

was measured using an automated alpha/beta counter. The radionuclides tended to

concentrate in the sub-micron range (~0.4 microns) when the furnace was operated at

higher temperatures (1200 °C). At lower temperatures (800-1000 °C), the radioactivity

was spread over a large particle size range, with some concentration in the larger particle

sizes. Their analysis techniques did not allow them to separate the cesium and strontium

components of the beta radiation contribution. Therefore, the exact distributions of the

individual components cannot be determined.

1.3 Sorbent Technology

One of the major obstacles towards public acceptance of incineration technologies

is the presence of metals in the incinerated wastes, and the potential release of the metals

into the environment. Metal capture by sorbents is a promising method of metal control.

A lot of work has been done in this area (Ho et al. ; Lee and Johnson 1980; Shadman and

Punjak 1988; Punjak et al. 1989; Rizeq and Shadman 1989; Uberoi et al. 1990; Uberoi

and Shadman 1990; Uberoi and Shadman 1991; Crosley and Kedl 1992; Scotto 1992;

Scotto et al. 1992; Scotto et al. 1994; Jozewicz and Gullett 1995; Linak et al. 1995; Wu et al. 1995; Ghosh-Dastidar et al. 1996; Mwabe and Wendt 1996; Venkatesh et al. 1996; Aganihotri et al. 1998; Biswas and Wu 1998; Davis 1999). These studies include both thermogravimetric work and pilot-scale incinerator experiments.

Biswas and Wu (1998) wrote a review of sorbent control technology. The majority of the paper discusses general metals interactions in combustion environments. A small section does cover the use of sorbents introduced to the post-flame region of furnaces to control the metals. The majority of the sorbent discussion relates to sorbents formed in the furnace by gas-phase precursors, not the introduction of solid sorbents, which is explored in this work.

There has been a relatively larger body of work that has focused on thermogravimetric experiments to determine metals capture by sorbent (Lee and Johnson 1980; Punjak et al. 1989; Uberoi et al. 1990; Uberoi and Shadman 1990; Uberoi and Shadman 1991; Crosley and Kedl 1992; Wu et al. 1995; Ghosh-Dastidar et al. 1996; Aganihotri et al. 1998). Often, these tests are run at temperatures that are lower than typical combustion environments. The contact time between the metal vapors and the sorbents is also rather long, ranging from two to forty hours, compared to a few seconds in an incineration environment. Since these tests are often easier to set up and run than tests on laboratory-scale incinerators, they serve well as screening tests for further research. They are also useful for identifying possible reaction products that may form.

Crosley and Kedl (1992) performed thermogravimetric tests on cesium and silica. They heated a sample of CsCl and passed the cesium vapor over a bed of silica. The

silica was weighed before and after the experiments were performed, and weight gain by the sorbent was taken as a sign of reaction. They found that cesium does sorb on to silica. They used inductively coupled plasma atomic adsorption spectroscopy to verify the presence of cesium in the sorbent. However, they did not use any other technique to try and determine the final form of the cesium compounds. The authors did propose a method for making educated guesses about particular metal and sorbent combinations, based on finding a stable compound on the phase diagrams of the metal/sorbent systems. This method assumes the final compound is in an equilibrium state, however, and which may not be the case if a glass-like compound is formed. Therefore, this method can serve as a starting point for further investigation, but should not be relied upon for definitive conclusions.

There have also been several researchers who have studied sorbent capture technology in laboratory scale and semi-industrial scale incinerators (Scotto 1992; Scotto et al. 1992; Scotto et al. 1994; Linak et al. 1995; Mwabe and Wendt 1996; Venkatesh et al. 1996; Davis 1999 - not yet in print). Linak, et. al. investigated the capture of nickel onto kaolinite (1995). They found that the nickel would only capture when in the presence of chlorine. Without chlorine present, the nickel did not vaporize and capture. Mwabe and Wendt (1996) performed experiments to determine the capture of sodium onto kaolinite. Sodium was injected as an aqueous solution into a 17 kW laminar down flow reactor. The sorbent was injected as a disperse powder. Samples were collected isokinetically and passed through an Anderson cascade impactor. They found that sodium does capture onto kaolinite, and they determined a global rate constant for this

reaction. They also explored the effect of chlorine and sulfur on the capture of the sodium. Both dopants acted to decrease the amount of capture in the system. Chlorine was found to change the speciation of the reacting metal, effectively reducing the amount of metal available for capture. Sulfur was found to increase the dewpoint, which reduces the time the sodium has to react.

1.4 Scope of This Work

The purpose of the present work reported here is to explore the behavior of cesium and strontium in combustion systems. Experiments will be performed to determine the metal distribution when the cesium and strontium are injected as salts in aqueous solutions. Various sorbents will be added to attempt to capture the metals and force the metals into a larger particle size distribution. These sorbents are kaolinite, lime, a kaolinite/lime mix, and CDEM sorbent. CDEM sorbent is a paper recycling waste, and its characteristics will be discussed further in the experimental section. In addition, the effects of chlorine and sulfur on the experimental systems will be explored. These two elements are often found in waste streams, and they could have a significant effect on the behavior of the metals in these systems. These are first level screening tests to determine the reactions involved and to determine which combinations of metals, sorbents, and dopants warrant further study. No attempt has been made to optimize the operating conditions to maximize metal capture. Optimization of the process is a subject for future work.

Chapter 2

Thermodynamic Calculations

Prior to beginning experimental work, having some idea of the expected system behavior is useful. In order to accomplish this, thermodynamic calculations were performed. Other researchers have used this technique, both to predict the behavior of chemical species in their experimental systems and to develop a better understanding of the chemistry involved (Linak and Wendt 1993; Frandsen et al. 1994; Durlak et al. 1997; Davis et al. 1998; Linak and Wendt 1998). Buckley et. al. (1998) have performed equilibrium calculations for cesium and strontium species. Their results will be discussed later in this section.

This equilibrium approach does have several limitations that must be kept in mind. First, these calculations model the equilibrium condition of the system. It does not take into account the kinetics of the reactions involved. If the residence time in the real system is not long enough, the calculations will not match the experimental data. Second, this approach assumes that the reactor is thoroughly mixed. In real systems, turbulence and flow patterns may prevent this condition from existing. Finally, all the important chemical species must be included in the input data, or the final results will be misleading.

It is believed that the metal/ sorbent interactions that occur are between a gas phase metal and a solid sorbent (Scotto et al. 1992; Mwabe and Wendt 1996; Davis 1999). As such, it is useful to know when the metal exists in the furnace as a vapor. The dewpoint of the metals, or the point at which the first traces of metal begin to condense,

represents an ending point for the capture reaction. Below the dewpoint, condensation begins to occur, potentially competing with the capture reaction. Once the temperature drops below the bubble point of the metal, the metal is no longer in a form that will react with the sorbent. The dewpoint of the metals is one of the essential pieces of information that can be obtained from the thermodynamic calculations.

Metals may be considered to fall into three basic categories, based on their volatility (Rizeq et al. 1994). Refractory metals have high dewpoints, and will not exist as vapor in practical combustors under normal circumstances. The dewpoints of refractory metals are usually around 2000 K or higher at concentrations of approximately 100 ppm of metal vapor in the gaseous mixture. This category includes nickel, chromium, barium, and beryllium. Semi-volatile metals are those metals that will normally vaporize in the flame zone of a furnace, but return to a solid form at the cooler end of the combustor. This category includes lead, cadmium, arsenic, and antimony. The dewpoints of these metals, at a concentration of 100 ppm of metal vapor, range between 1800 K and 1000 K. Volatile metals are those metals that exist as gases, even in the relatively cool exhaust sections of the combustor. This category includes mercury and selenium, and exhibit dewpoints of less than 1000 K at 100 ppm of metal.

The computer code used to perform the current calculations was the NASA Chemical Equilibrium and Applications (CEA) code (Gordon and McBride 1994). The numerical algorithm used by CEA is based on the minimization of Gibbs free energy. This allows the use of temperature and pressure as the primary thermodynamic variables, and it permits the chemical species to be treated independently, without specifying the

chemical reactions beforehand. Some important assumptions are made by CEA. The code considers all gaseous species ideal, and the gaseous mixture is considered ideal as well. All condensed species are treated as pure. It is also important to note that the results obtained from these calculations are the results as they would occur if given infinite time to react. Kinetic and transport limitations may be present in the actual furnace that would prevent the system from achieving thermodynamic equilibrium.

Cesium compounds considered	Strontium compounds considered
Cs, CsCl, CsO, CsOH, Cs_2, Cs_2Cl_2, Cs_2O, $Cs_2(OH)_2$, Cs_2SO_4, Cs(cr), Cs(L), CsCl(s), CsCl(L),CsOH(s), CsOH(L), Cs_2SO_4(s), Cs_2SO_4(L)	Sr, SrCl, $SrCl_2$, SrO, SrOH, $Sr(OH)_2$, SrS, Sr(s), Sr(L), $SrCl_2$(s), $SrCl_2$(L), SrO(s), SrO(L), $Sr(OH)_2$(s), $Sr(OH)_2$(L), SrS(s), SrO_2(s), Sr_3N_2(s), SrC_2(s), SrH_2(s), $SrSO_4$, $SrCO_3$(s), $SrSO_4$(s)

Table 2.1 – Compounds considered in equilibrium calculations

Thermodynamic data must be supplied to CEA in order to perform the calculations. These data are the specific heat, the enthalpy, and the entropy of each species, as functions of temperature. These data are supplied to the program as a set of least-squares coefficients. These coefficients are placed in a seven-term polynomial for specific heat, with corresponding equations for enthalpy and entropy. The quality of the calculations performed by CEA is a result of the input data supplied. For example, if an important chemical specie is excluded from the input data, CEA will give erroneous results. In addition to the standard database, seventeen cesium compounds and twenty-three strontium compounds were added to the input data (Barin 1995). These compounds

26

are shown in Table 2.1. The actual input data for the cesium, strontium, and sodium

species considered here, are included in Appendix A.1.

The equilibrium calculations were set up to match experimental feed conditions.

Methane and air were used as the fuel and oxidizer, with a stoichiometric ratio of 1.2.

The pressure was set to one atmosphere, and the temperature was varied. The metal

concentration in each case was set to 100 ppm. The remainder of the calculation input

conditions are shown in Table 2.2.

Metal	Dopant	Figure
Cs	None	2.2
Cs	1000 ppm Cl	2.3
Cs	1000 ppm S	2.4
Na	None	2.6
Na	1000 ppm Cl	2.7
Na	1000 ppm S	2.8
Sr	None	2.10
Sr	1000 ppm Cl	2.11
Sr	1000 ppm S	2.12

Table 2.2 - CEA input conditions

The cesium results are shown in Figure 2.1 through 2.4. Figure 2.1 shows an

overview of the dewpoint of the cesium species. Cesium alone has a relatively low

dewpoint, approximately 675 K, which classifies it as a low-end semi-volatile metal. The

addition of chlorine tends to raise the dewpoint to around 900 K. This is slightly unusual,

as the addition of chlorine tends to decrease the dewpoint of most metals (Scotto et al.

1992; Mwabe and Wendt 1996). This is important for two reasons. First, in the case of

sodium, it is believed that the capture reaction that occurs is between NaOH and the
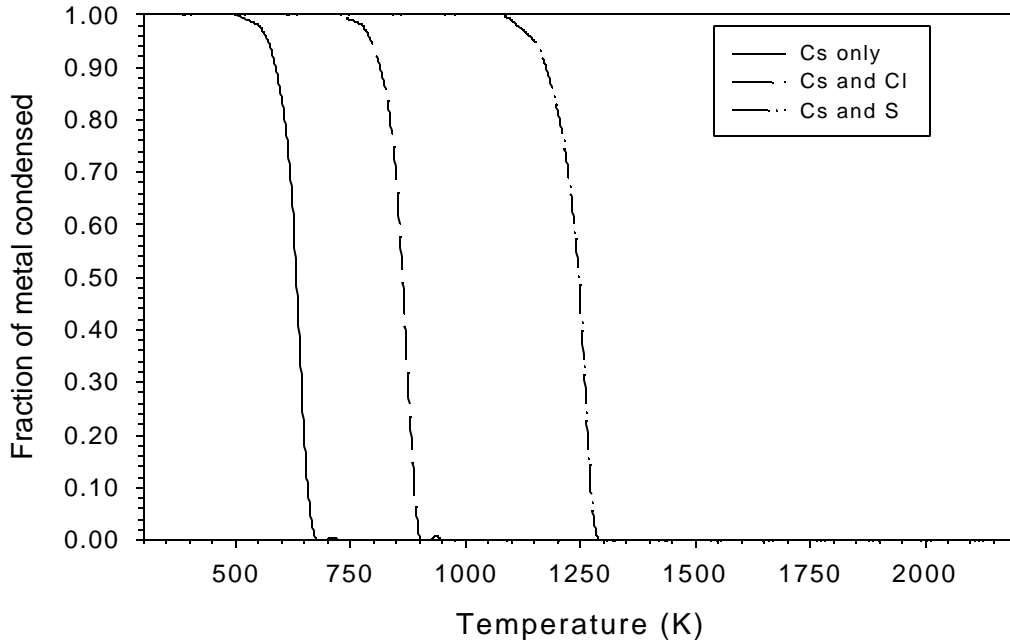
Figure 2.1 – Cesium dewpoint calculations
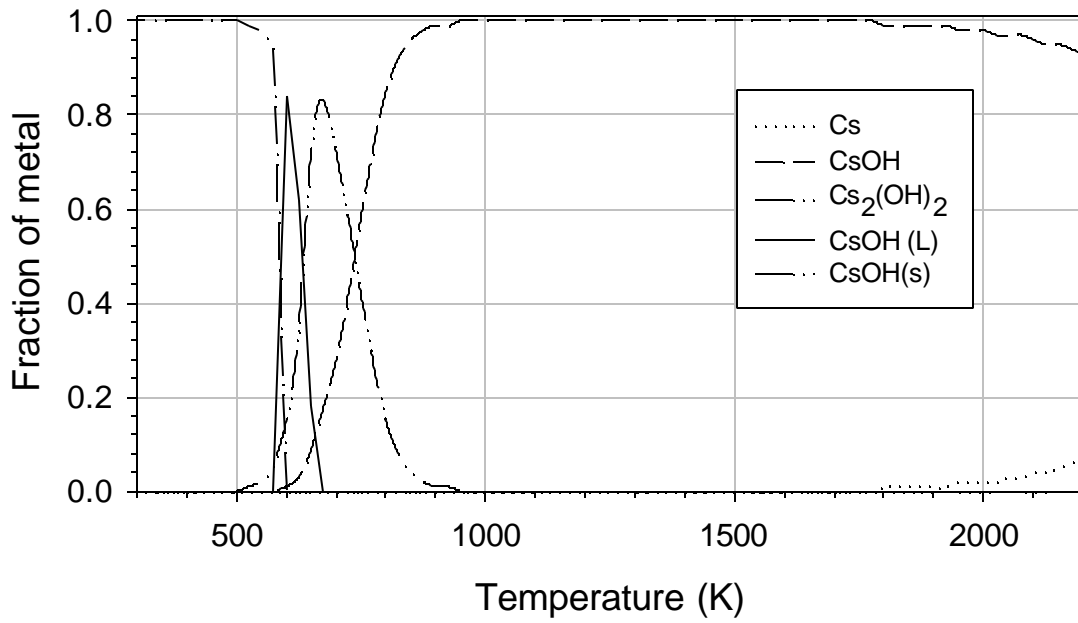
Figure 2.2 – Cesium speciation, no dopant

kaolinite particle. Since sodium and cesium are in the same period of the periodic table, it might be expected that the two metals will show similar chemical behavior. Comparison calculations for sodium will be presented later. The presence of chlorine reduces the NaOH concentration in the furnace, decreasing the overall rate of the capture reaction. Second, since the dewpoint of the sodium is reduced, the time for reaction to occur has increased, which helps offset the lower NaOH concentration. In the case of cesium, however, the dewpoint increases, reducing the time to react as well as the CsOH concentration in the furnace. The combination of these two factors could have a large impact on the capture of cesium. The addition of sulfur raises the dewpoint of cesium even further, to around 1300 K. This increase in dewpoint can significantly reduce the time the metal and sorbent have to react.

Figures 2.2, 2.3, and 2.4 show the speciation of cesium for each of the three cases examined. With no dopant present, the cesium exists in the gas phase as CsOH. As the temperature decreases, the CsOH condenses to first liquid, then solid form. When chlorine is present in the system, the cesium exists primarily as CsCl in the gas phase. The condensed phase is predicted to be CsCl, as well. When sulfur is added to the system, the cesium is present as CsOH at higher temperatures. As the temperature drops, the equilibrium shifts to Cs_2SO_4 as the gaseous specie. The Cs_2SO_4 then condenses and forms the prevalent specie in the solid phase. This indicates that cesium in the presence of sulfur may be captured at high temperatures, but the favorable capture conditions do not last for long.
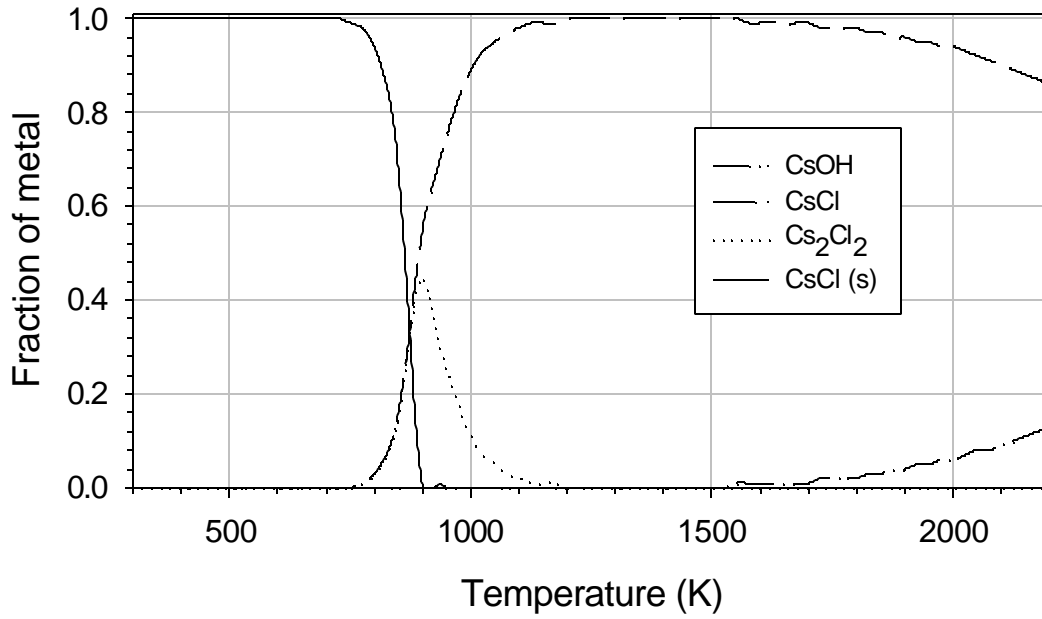
Figure 2.3 – Cesium speciation, in presence of chlorine
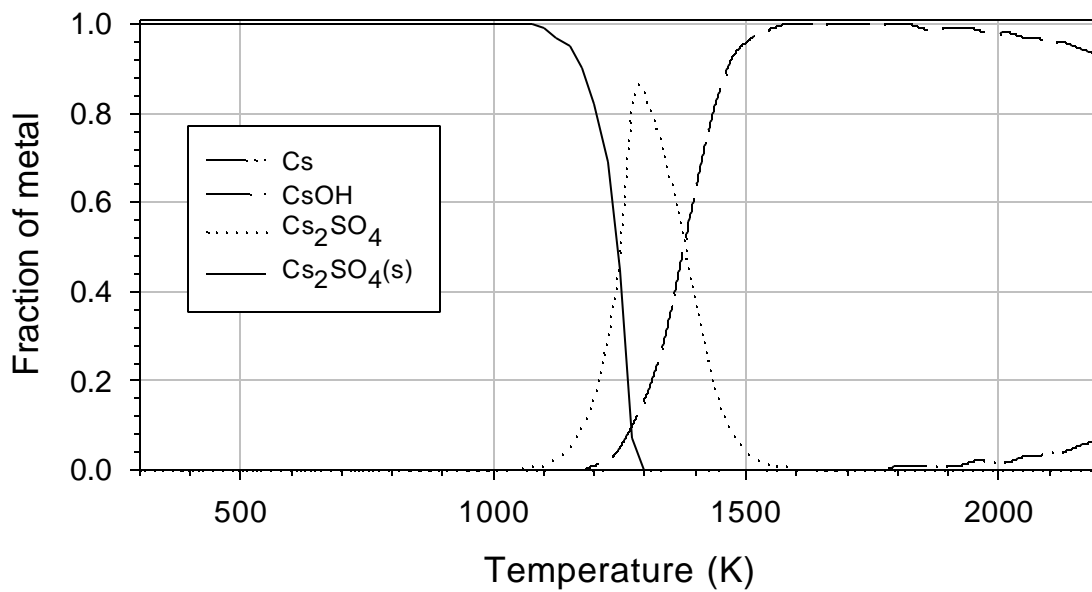
Figure 2.4 – Cesium speciation, in presence of sulfur

For comparison, sodium calculations were performed to match the cesium

conditions. These results are shown in Figures 2.5 through 2.8. Figure 2.5 illustrates the

dewpoint behavior of sodium. With no dopant gases present, sodium has a dewpoint near

1200 K. This is higher than the dewpoint of cesium. When chlorine is added to the

system, the sodium dewpoint drops, which is similar to the behavior of most metals, to

around 1000 K. This number is within 100 K of the value for cesium. With sulfur

present, the dewpoint of sodium jumps to near 1500 K, which is about 200 K higher than

in the case of cesium.

The sodium speciation plots are shown in Figures 2.6, 2.7, and 2.8. Without

chlorine or sulfur present, sodium exists primarily as NaOH in the gas phase. When the

sodium condenses, it forms liquid Na_2CO_3, which then quickly solidifies. This varies

from the cesium results. The condensed cesium tends to form the solid hydroxide, and

not the carbonate. However, it should be noted that Cs_2CO_3 is not included in the input

data for cesium. The addition of this specie could change the results of the equilibrium

calculation. When chlorine is added to the system, the majority of the sodium exists as

NaCl in the gas phase. As the temperature drops, the sodium shifts briefly towards

Na_2Cl_2 before it condenses into solid NaCl. This behavior mirrors the cesium results

almost exactly. Therefore, we can expect cesium to behave similarly to sodium when

chlorine is present. When sulfur is added to the system, the sodium exists chiefly as

NaOH in the gas phase. The equilibrium shifts towards Na_2SO_4 as the temperature drops.

When the temperature drops further, the sodium condenses to liquid Na_2SO_4 and finally

solidifies. This is also similar to the behavior exhibited by cesium, except the cesium
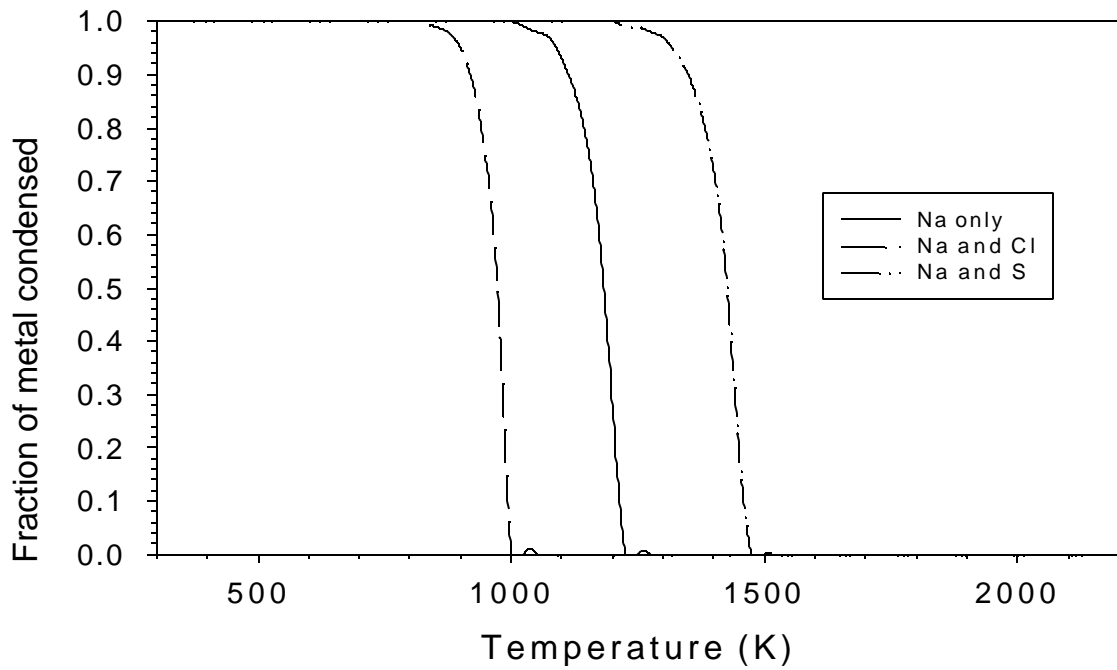
Figure 2.5 – Sodium dewpoint calculations
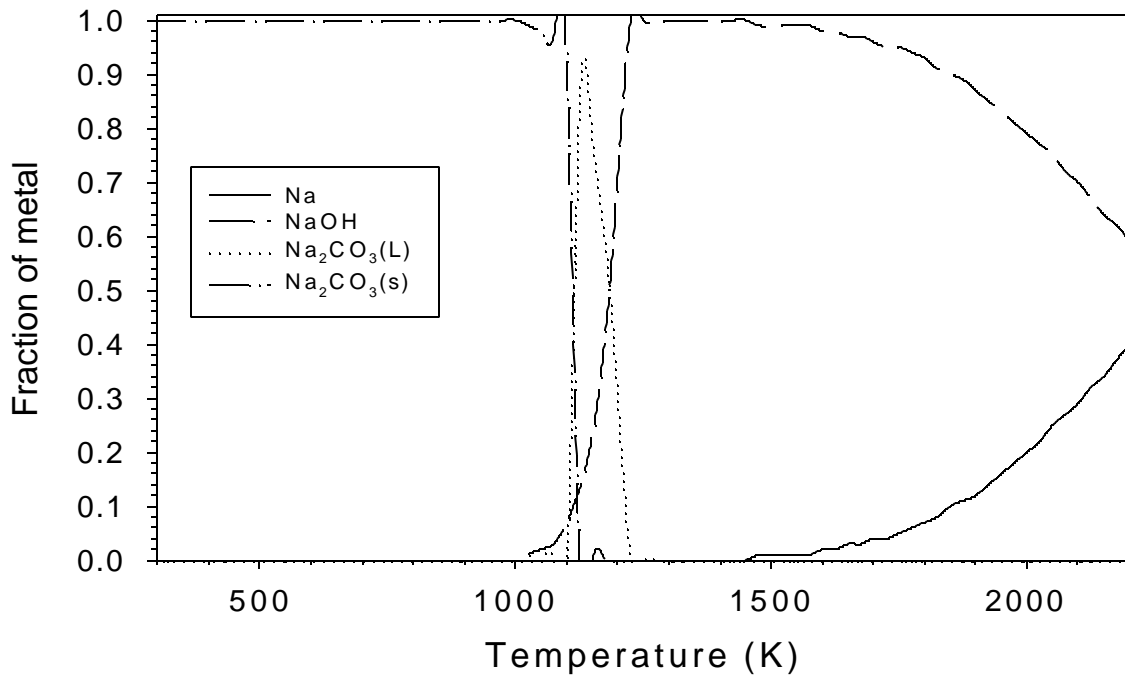
Figure 2.6 – Sodium speciation, no dopant
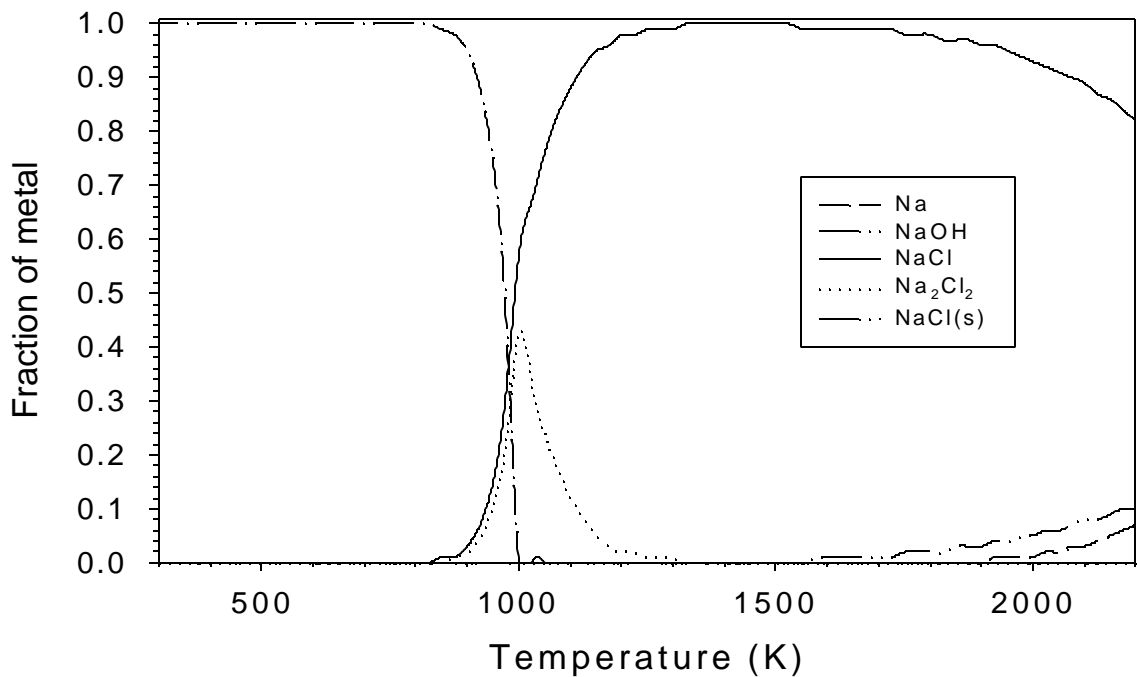
Figure 2.7 – Sodium speciation, in presence of chlorine
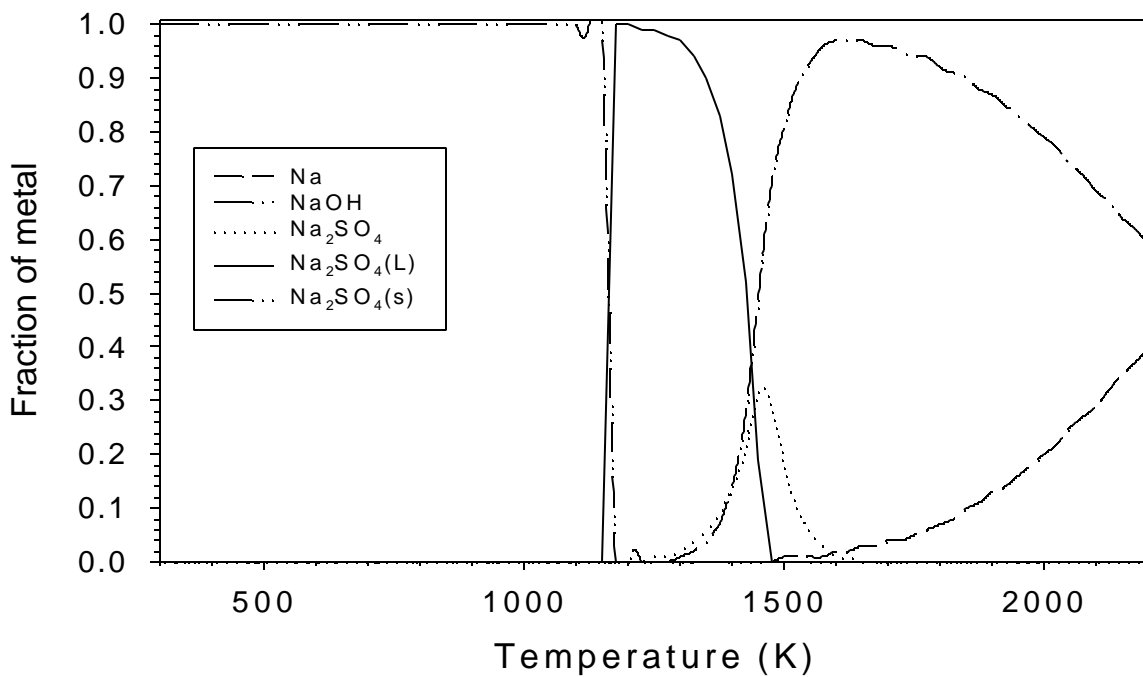
Figure 2.8 – Sodium speciation, in presence of sulfur

condenses directly to the solid phase, and does not form a liquid. These results suggest that cesium may indeed behave similarly to sodium when reacted with kaolinite sorbent.

The strontium calculations are shown in Figures 2.9 through 2.12. Figure 2.9 is an overview of the dewpoint calculations. With no dopant gas present, strontium has a high dewpoint at 2000 K. This classifies strontium as a refractory metal. Temperatures this high are seldom seen in practical combustors. This suggests that the water in the droplets of the injected strontium solution will evaporate, leaving a residual strontium particle behind. Since it is believed that the capture reactions occur between a gaseous metal and a solid sorbent, no reaction will occur if the strontium does not vaporize. When chlorine is added to the system, the dewpoint is reduced to around 1400 K. This suggests that strontium will be vaporized and may be captured by sorbents when chlorine is present in the system. This behavior is similar to that seen in nickel, another refractory metal (Linak and Wendt 1998). There appears to be little change in the dewpoint when sulfur is added to the system, which again would suggest that no capture will occur.

The speciation plots for strontium are shown in Figures 2.10, 2.11, and 2.12. $Sr(OH)_2$ is the primary gaseous specie present when no dopant is added to the system. The strontium then condenses as SrO. As the temperature continues to drop, the equilibrium shifts to condensed $SrCO_3$. When chlorine is present, the primary gaseous strontium specie is $SrCl_2$. This then condenses to a liquid, and as the temperature continues to drop, solid SrCl is formed. With sulfur present in the system, the strontium exists as $Sr(OH)_2$ in the gas phase, which then condenses to form solid SrO. This is the
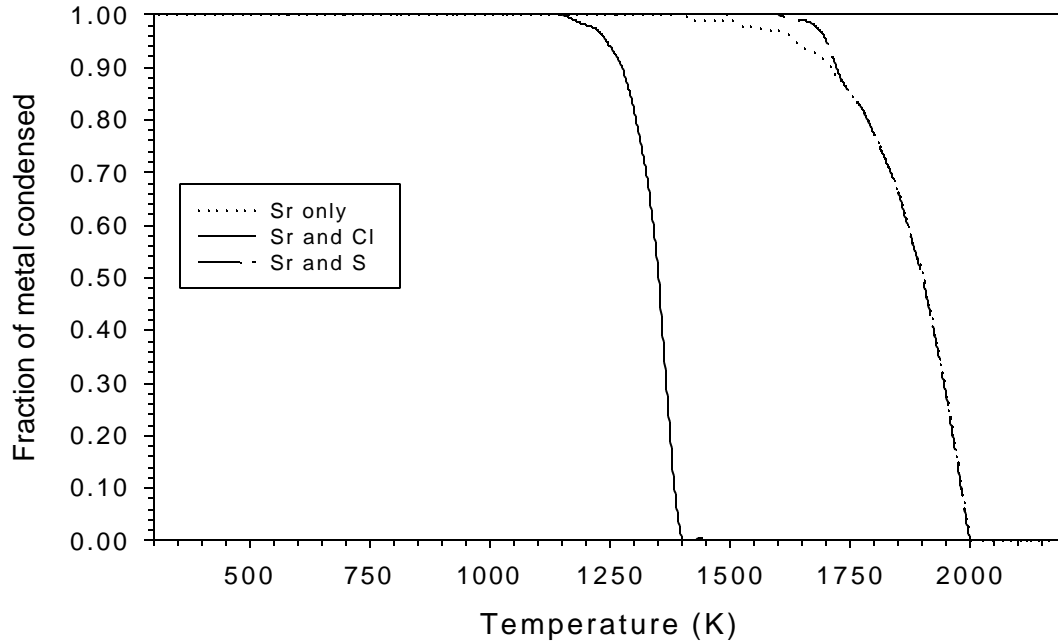
Figure 2.9 – Strontium dewpoint calculations
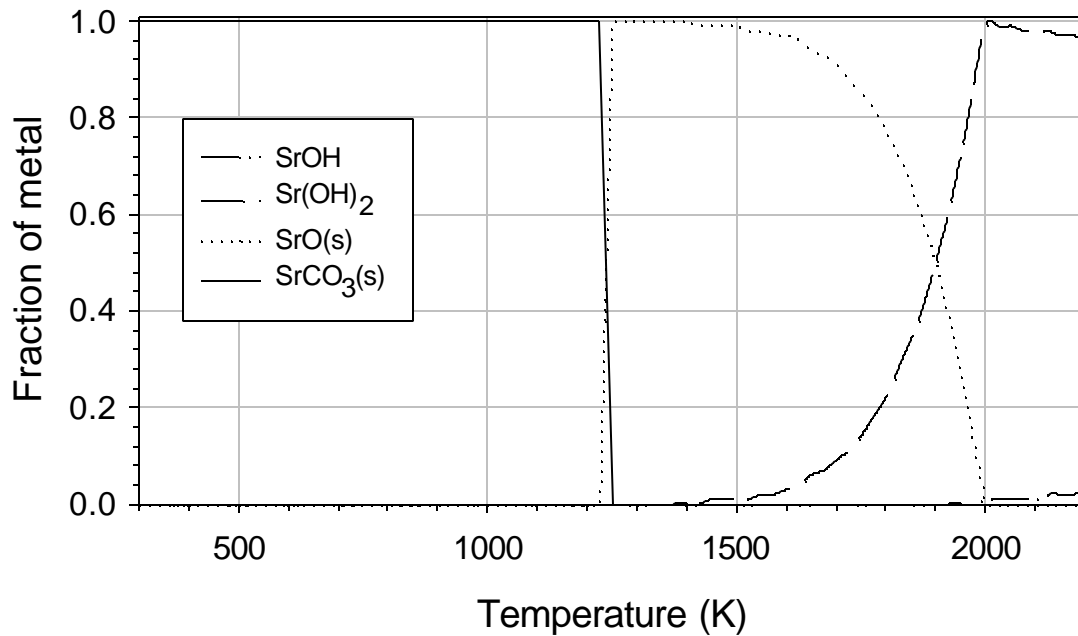
Figure 2.10 – Strontium speciation, no dopant
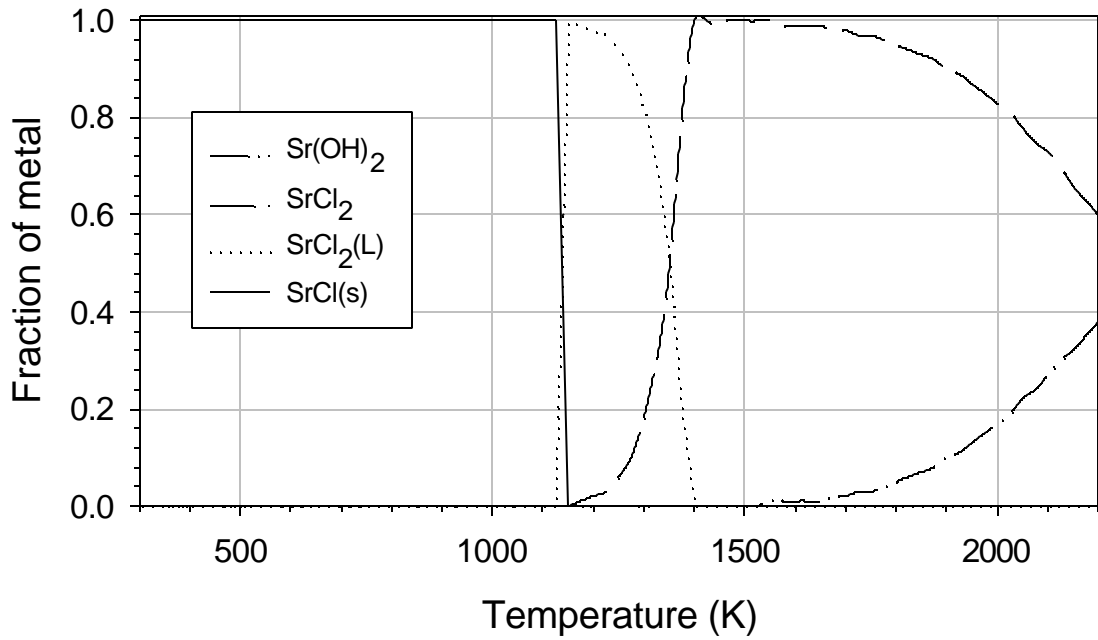
Figure 2.11 – Strontium speciation, in presence of chlorine
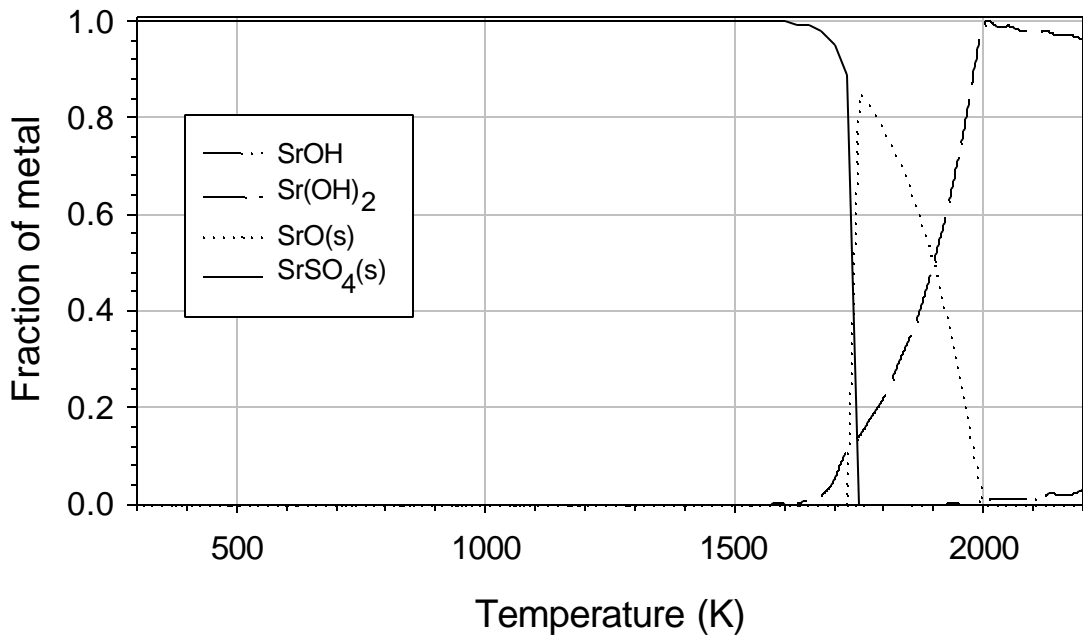
Figure 2.12 – Strontium speciation, in presence of sulfur

same behavior as when no dopant gas is present in the system. However, as the temperature decreases, the equilibrium shifts so that $SrSO_4$ is the prevalent solid specie.

These results provide some insight into the behavior that can be expected from the experimental research. Cesium should be present in the furnace in a gaseous form over the entire length of the furnace. Only when sulfur is added to the system will conditions be such that solid cesium will exist in the furnace. In addition, the chemical speciation of the cesium should be similar to that of sodium, and hence its capture characteristics should be similar as well. The strontium, on the other hand, will probably never vaporize in the furnace, except when chlorine is added. It is believed that in order for metal to react with sorbents, the metal must be present in the gas phase. If the metal never vaporizes in the furnace, it will not react with the sorbents. This suggests that in order to obtain reactive capture of strontium, chlorine must be present in the system.

Buckley, et. al. (1998) performed similar equilibrium calculations for cesium and strontium. There are some substantial differences between their results and the present work. Their calculations were performed using the Stanjan equilibrium code, and their input data was taken from the JANAF tables. The list of cesium and strontium species corresponds well, except their work lacks several of the sulfate species. Also, they were attempting to model a more complex situation, a biomass fuel with trace amounts of cesium and strontium present. As such, the presence of other chemical species, such as sodium, probably affected the behavior of the various species. These are effects that would not necessarily be seen in the simple situations modeled here. The results they obtained for strontium closely match those calculated in this work. The cesium results,

however, show some differences. They predict that the cesium primarily exists as CsOH in the gaseous phase, and then condenses as liquid CsCl. The temperature at which this occurs is significantly higher than the temperature predicted in this work. It is likely that these differences are due to two different factors: the presence of other chemical species in the system and the difference in the concentrations of the metals between the two studies. Sodium, potassium, and possibly magnesium are species that would compete, chemically, with cesium and strontium to bind with chlorine, sulfur, and other elements. This would lead to differences in the dewpoints and speciation of the various chemical species. Also, the dewpoint of the metal is dependent on the concentration of the metal present.

Chapter 3

Experimental Approach

3.1 Furnace Description

Experiments were performed on the University of Arizona 18 kW laminar, down-flow, swirl-flame combustor. This furnace was designed to have a time/temperature profile similar to those found in practical boilers and incinerators. This furnace was originally described by Scotto (1992). However, due to a catastrophic failure in the furnace wall, major portions of the furnace had to be rebuilt. The terminal crack was discovered in early July of 1998, and the rebuild occurred over the next four months. The furnace was operational again in November of 1998.

A diagram of the furnace and its support apparatus is shown in Figure 3.1. A variable swirl burner is mounted to the top of the furnace. The furnace is approximately seven meters tall and has an inner diameter of 0.15 meters. Seventeen sampling ports are spaced down the front of the furnace at approximately 30 centimeters intervals. The ports have a five-centimeter inner diameter and are capped by two-inch ball valves. A removable ash trap is attached to the bottom. A baghouse removes the particulate matter from the exhaust stream. The exhaust then passes through a condenser and a mist eliminator to remove any water from the gas and to protect the exhaust fan.

The upper section of the furnace is the portion that needed to be rebuilt. This encompasses the top three meters of the furnace structure, reaching from the burner to below the upper-level floor. A schematic of the new furnace construction, as well as the

Liquid:
H_2O / MetalSalt

AtomizingAir

Natural
Gas

CombustionAir/Dopant Gas

VariableSwirlBurner
w/ CenterlineAirBlastAtomizer

Exhaust

Mist
Eliminator

Bypass to
Exhaust

Primary
Condenser

Baghouse

Ash Trap

Water Capture
System
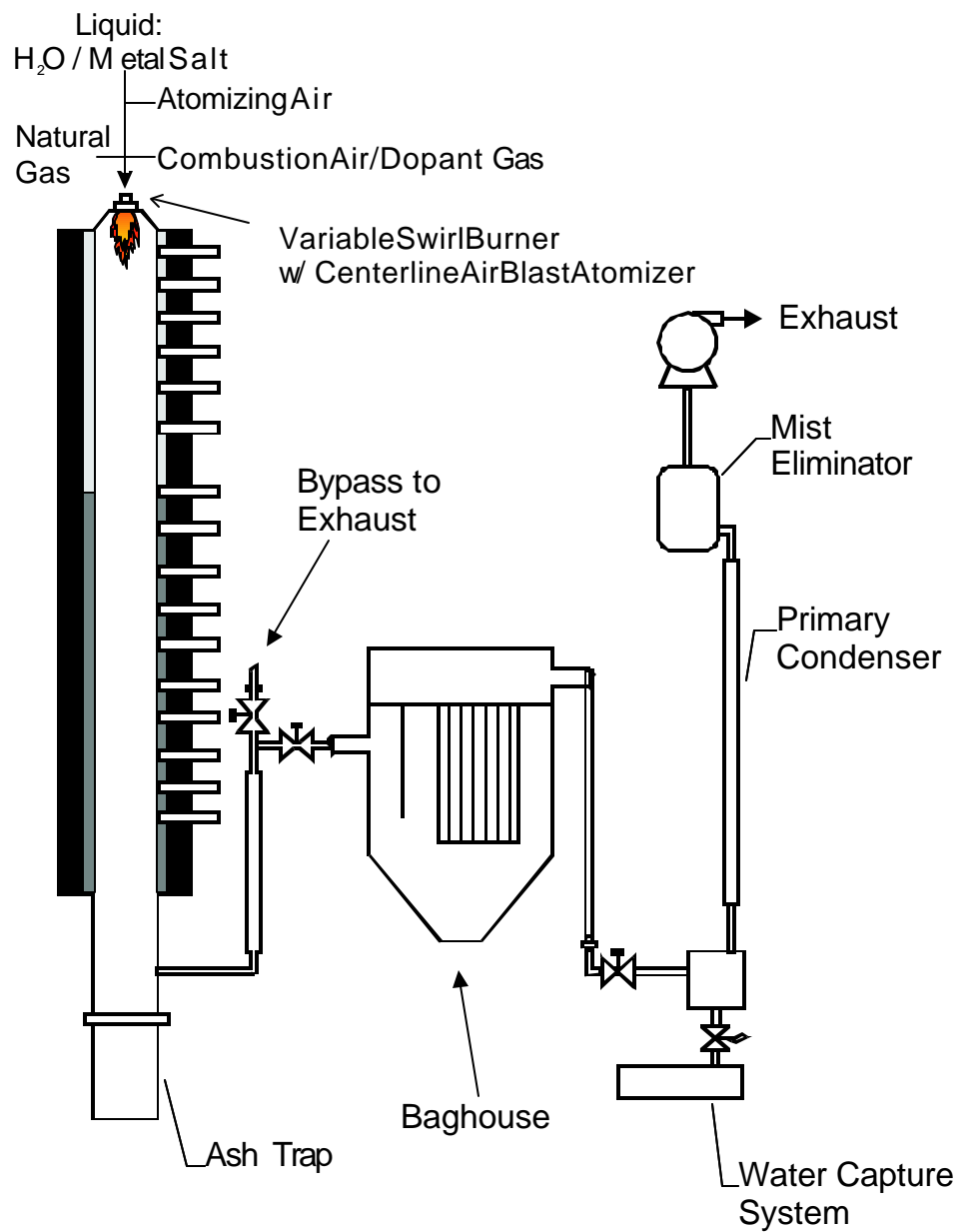
Figure 3.1 - Laboratory downflow combustor and
support apparatus

materials used, is shown in Figure 3.2. The main portion of the upper furnace is cast of

Thermal Ceramics HPM-95, a high-density slag resistant castable refractory. The upper

two feet of this block has an inner diameter of six inches and an outer diameter of

fourteen inches. The bottom foot of the block has an outer diameter of eighteen inches,

which allows the block to rest on the stainless steel support structure. Three ports are

cast into this section. The upper cone section of the furnace is cast of Thermal Ceramics

2800-LI insulating refractory cement. An insulating cement was used for this section in

order to protect the various pieces of support equipment (burner, atomizer, UV flame

detector, etc.) that are attached to the top of the furnace. The two refractory cement

sections are joined together with a thin layer of Zircar type SALI moldable alumina

insulation.

The upper furnace structure rests on a frame made from 2" x 4" hollow

rectangular stainless steel beam, with a ¼" wall thickness. The stainless steel beams are

attached to the existing furnace frame and support the upper four feet of the new furnace.

Placed on top of the stainless steel beams are lengths of 2" x 2" Zircar RS-100 coil post.

This is a high-density fiber reinforced alumina composite. This material has a high

compressive strength and is able to withstand the temperatures produced by the furnace.

This layer helps protect the stainless steel supports from the high temperatures seen at the

outer surface of the upper furnace section. Layers of Fiberfrax felt are placed on top of

the RS-100 post to help protect the post surfaces from abrasion and to level the top

section of the furnace.

Figure 3 .2 - Schematic of furnace materials
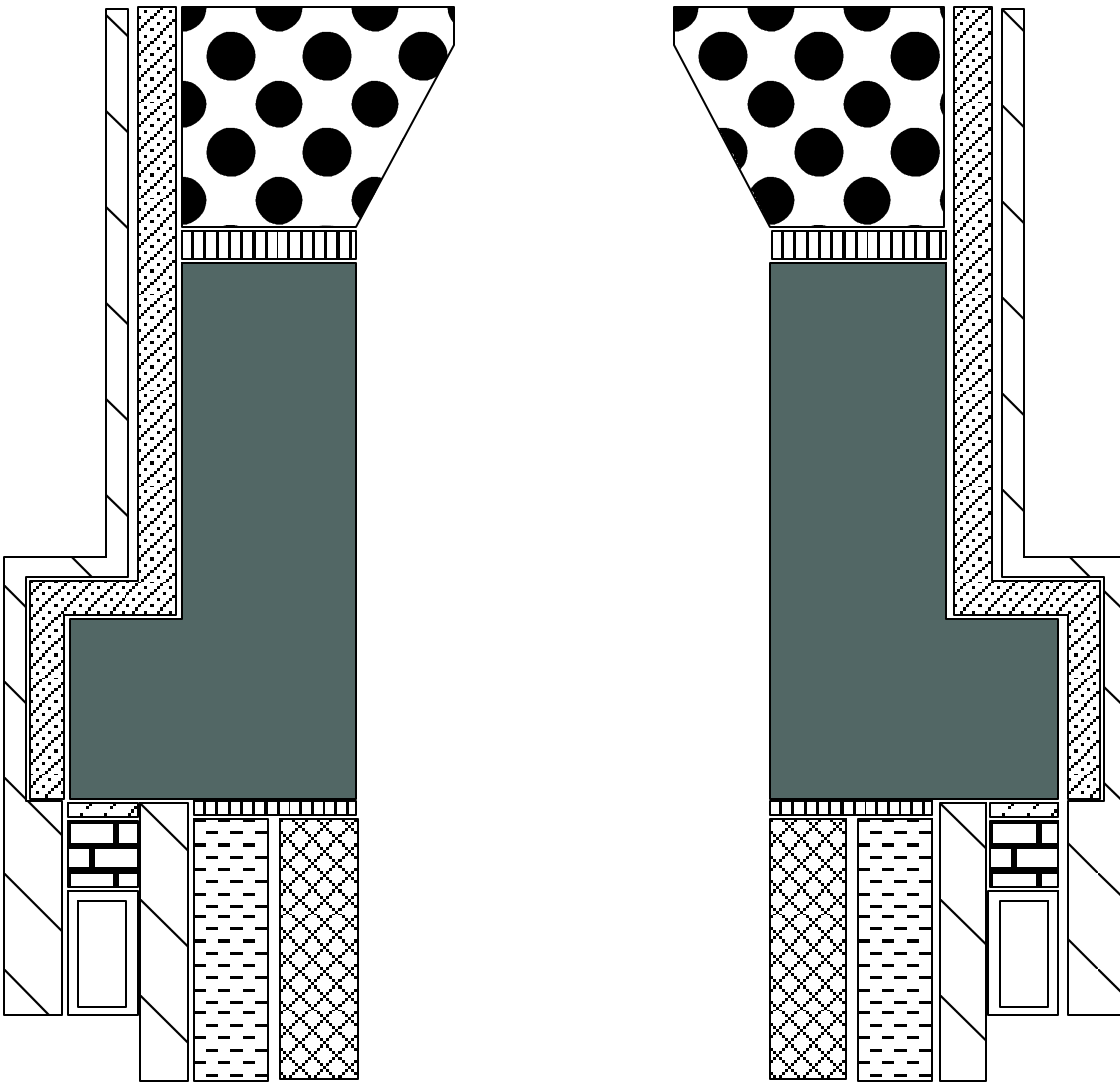
Legend:
- 2800-LI
- SALI moldable
- HPM-95
- RS-100 post
- Fiberfrax f elt
- TypeALC-AA alumina-silica
- Type A S H alumina-silica
- Kaowool insulation
- Cerachem insulation
- Stainless steel beam

The first furnace section above the floor and the first section below the floor were also rebuilt. This section is constructed from Zircar alumina insulating cylinders. The inner cylinders are made of Zircar type ALC "AA" high-purity alumina bond in order to withstand the inner furnace temperatures. These cylinders have an inner diameter of six inches and an outer diameter of eight inches. The outer cylinders, which have an inner diameter of eight inches and an outer diameter of ten inches, are made of Zircar type ASH alumina-silica insulation. This material is significantly less expensive than the type ALC "AA" insulation, but cannot withstand the temperatures on the inner wall of the furnace. All the cylinders are in one-foot sections and are joined together with the type SALI moldable alumina, with the cylinder seams offset to prevent leaks. The alumina cylinders are sealed to the HPM-95 refractory block by a layer of type SALI moldable.

The port cylinders are constructed of the type SALI moldable alumina that has been coated with Zircar alumina rigidizer/hardener, which provides additional rigidity to the material. The port cylinders are sealed into the furnace body with additional SALI moldable.

The upper four feet of the furnace is insulated with a two-inch thick layer of Thermal Ceramics Cerachem blanket. This is a high temperature insulation composed of alumina-silica-zirconia fiber. Around this layer is a two-inch thick layer of Thermal Ceramics Kaowool insulation. This is a lower cost insulation, but cannot withstand the temperatures generated at the outside of the HPM-95 block. The lower sections of the furnace are insulated with a four-inch layer of the Kaowool insulation. The insulation is held in place by steel wire and wire mesh.

43

The baghouse has also been rebuilt. A schematic of the new baghouse is shown in Figure 3.3. This baghouse is constructed of carbon steel, rather than stainless steel, which is what the old baghouse was made of. The carbon steel was less expensive and easier to work with than stainless steel. The exhaust enters the baghouse and flows around a baffle. This attempts to distribute the airflow over the entire surface area of the bags. The exhaust then passes through woven Teflon fiber bags with a surface air velocity of nine feet per minute. The bags are manufactured by GoreTex and can withstand temperatures up to 250 degrees C. The particulate matter is retained on the bags, and the gas passes out through the exhaust.

In order to remove the particles from the bags, the baghouse is equipped with an air pulse line. This provides a pressurized pulse of air that flows counter to the exhaust gases. This air pulse cleans the bags and knocks the particulate material into the base of the baghouse. Each pulse has a pressure of 30 psi and lasts for 0.1 seconds. An access port allows for periodic emptying of the baghouse. A magnehelic gauge monitors the pressure drop across the bags, which provides an indication of plugging in the bags. When the pressured drop across the bags has increased by 0.5" H_2O, the baghouse is pulsed. The baghouse is also equipped with electric heaters, which prevent water from condensing in the baghouse during furnace warm-up. If water were to condense on the bags, it would mix with the sorbent particles collected by the cartridges, forming a cement-like mixture that would foul the bags. Two K-type thermocouples are used to monitor the inlet and outlet temperatures in the baghouse.
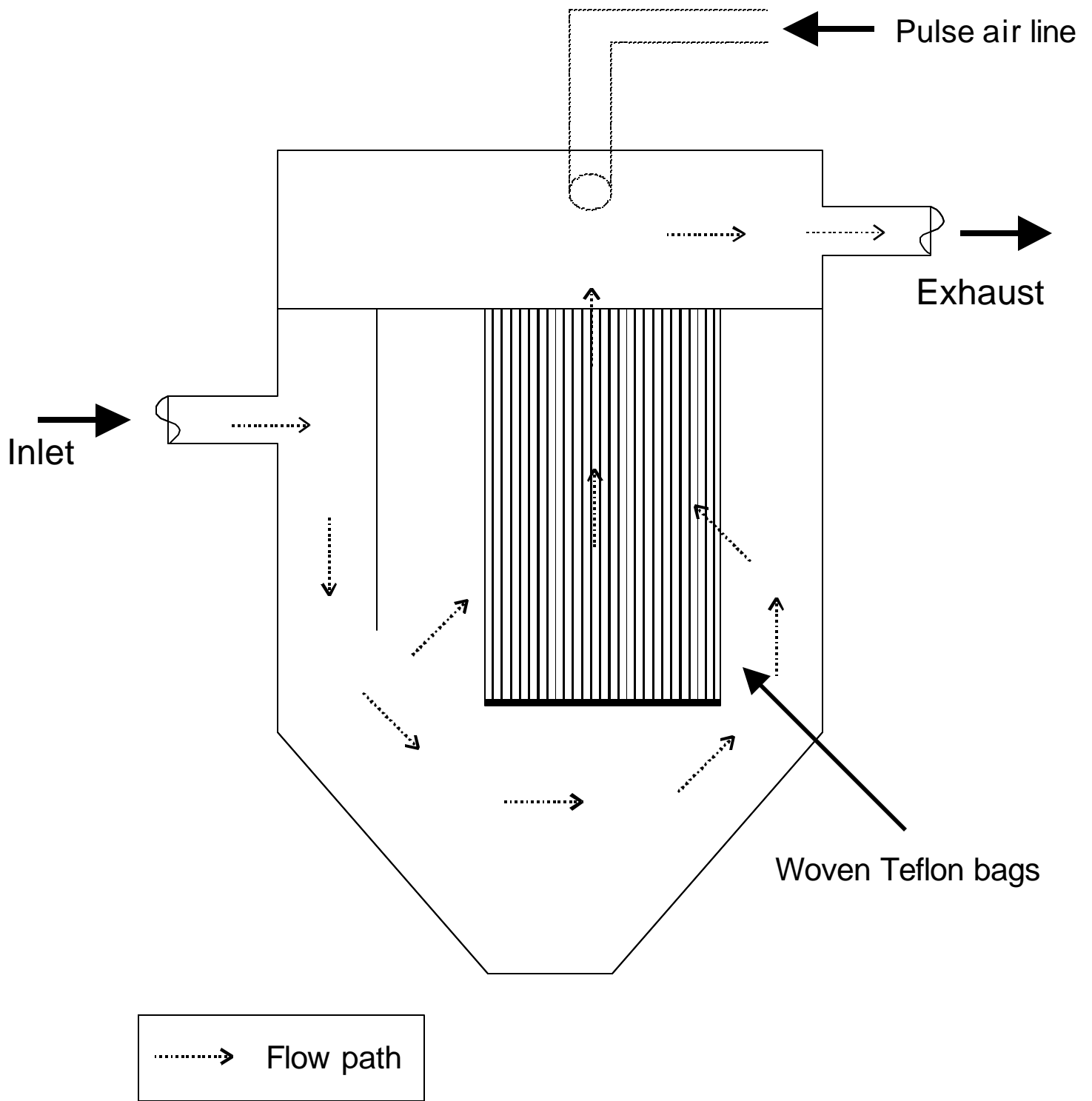
Figure 3.3 - Baghouse schematic

3.2 Auxiliary Systems

Metals were injected into the furnace as aqueous solutions. All metals used in these experiments were non-radioactive isotopes. This fact should not significantly affect the results of these experiments, as the chemical kinetics and transport properties of the metals are not a function of the radioactivity of the species. Cesium solutions were prepared from cesium acetate salt, $CsCH_3CO_2$, and strontium solutions were prepared with strontium nitrate, $Sr(NO_3)_2$, both of which were obtained from Aldrich Chemical Company. These salts were chosen because they are sufficiently soluble in water, yet are free of chemical species that may interfere with the reactions of interest (Cl, S, etc.). The salts were added to distilled water and mixed thoroughly. The solution was then injected into the furnace using a Fluid Metering, Inc. FM-100 positive-displacement pump with a QVC pump head. The solution traveled to a plain-jet air-blast atomizer located at the furnace through the center of the burner, with the tip extending ¼" from the methane nozzle.

Several sorbents were used for these experiments. The physical properties of the sorbents are listed in Table 3.1. The first was a kaolinite powder. The primary kaolinite used was called Burgess No. 40, and is referred to as kaolinite throughout the rest of this report. For some experiments, other kaolinite powders were used. The Burgess No. 80 and the 6104-B have different characteristics than the kaolinite. The third sorbent used was a pulverized hydrated lime. The next sorbent used is called CDEM. Four Dutch paper manufacturers founded CDEM Holland B. V. in order to address environmental concerns of the paper recycling industries. A de-inking residue is passed through a

fluidized bed combustor. This process destroys the organic portion of the residue, drives

off the water, and leaves the mineral fraction in a cement-like form. For further

information on the CDEM sorbent, see Biermann et. al. (1997). Experiments involving

the "mixed" sorbent used a 50/50 mechanical mixture of the kaolinite and lime described

above. This mixture simulated the CDEM sorbent, and provided some insight into the

role of the individual constituents of the CDEM. For further information on the physical

characteristics of the sorbent, such as particle and pore size distributions, see Davis

(1999).

Sorbent	Supplier	Composition	d_{ave} (mm)
Kaolinite (B-40)	Burgess Pigment Company	$Al_2O_3 \bullet 2SiO_2 \bullet 2H_2O$	1.4
B-80	Burgess Pigment Company	$Al_2O_3 \bullet 2SiO_2 \bullet 2H_2O$	0.6
6104-B	Burgess Pigment Company	$Al_2O_3 \bullet 2SiO_2 \bullet 2H_2O$	27
Hydrated Lime	Global Stone, Inc.	$Ca(OH)_2$	6
CDEM	CDEM Holland B. V.	$CaCO_3$ 33% CaO 21% SiO_2 30% Al_2O_3 15% Other 1%	10
Mixed Sorbent	As above	50% kaolinite 50% lime	As above

Table 3.1 – Sorbent characteristics

The sorbents were pneumatically injected into the furnace by a water-cooled

probe. A K-Tron twin-screw feeder was calibrated, and the rotation rate was set to

deliver a set sorbent flow rate to the probe. Due to the different handling characteristics

of each sorbent, a calibration curve was produced for each. The feeder dropped the

sorbent into a pneumatic transfer device, where a high velocity air stream intercepted the

sorbent and carried it through the probe.

Dopant gases, Cl_2 and SO_2, were used to explore the effects of sulfur and chlorine

on the metal/sorbent systems. Cl_2 and SO_2 were metered out through a Matheson 602

rotameter. The gaseous dopants were then mixed with the combustion air prior to

entering the furnace.

The typical furnace settings, as well as a listing of the experimental conditions for

each experimental run, are listed in Appendix A.2 and A.3, respectively.

3.3 Sampling Systems

Two systems were used to characterize the furnace. A probe composed of an R-

type bare wire thermocouple encased in a ceramic sheath measured the temperature along

the centerline of the furnace. These measurements were not corrected for radiation. An

average temperature profile is shown in Figure 3.4. The error bars denote the 99%

confidence interval. Also shown are the sorbent injection and sampling points that were

used for the majority of the experiments. The furnace was allowed to achieve thermal

equilibrium prior to each set of experimental runs. Equilibrium was achieved when the

temperature of the furnace varied by no more than two degrees in an hour.

The second system used to classify the furnace was the gas sampling system. A

water-cooled stainless steel probe withdrew the gas samples from the furnace ports. The

gas stream then passed through a refrigerated knock-out pot and a coalescing filter to

48
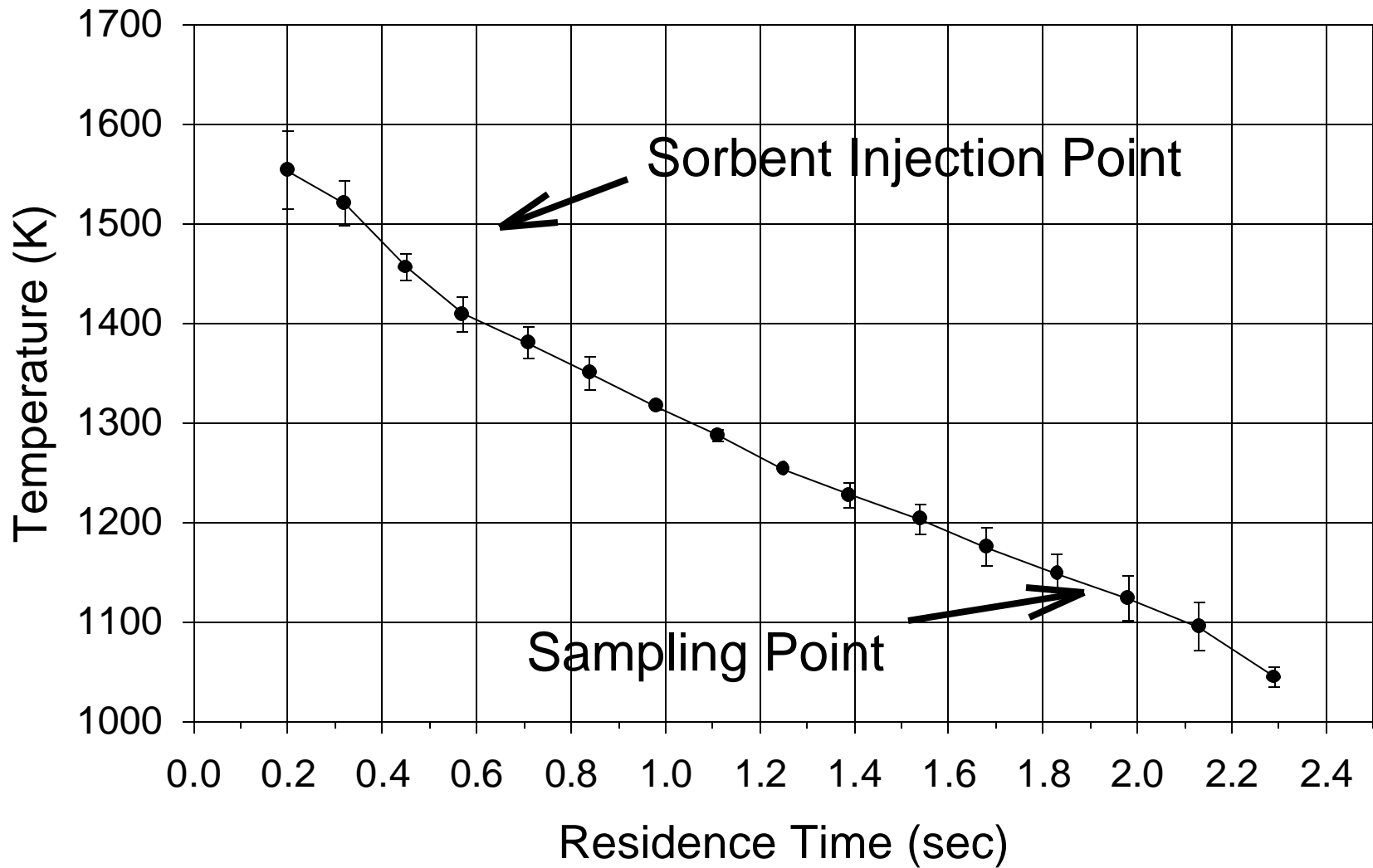
Figure 3.4 - Average temperature profile at 18 kW load

remove the water from the sample. The gas sample then entered a bank of continuous emissions monitors (CEMs) that were used to determine the gas concentrations. The CEMs were calibrated with certified calibration gases of known concentrations. CO and CO_2 were measured with a California Analytical ZRH infrared gas analyzer. A Rosemont Analytical Model 755D paramagnetic oxygen analyzer measured the O_2 in the sample. A typical gas profile can be found in Appendix A.4.

A schematic of the particulate sampling system is shown in Figure 3.5. Samples were withdrawn from the appropriate sampling port using a water-cooled sampling probe and a large vacuum pump. Nitrogen was injected into the probe at a ratio of about 20:1 to dilute and cool the sample. This method provides a rapid cooling rate that should freeze any chemical reactions at the point of sampling and prevent water from condensing in the sampling system. A mass flow controller maintained the nitrogen flow rate. The sampling flow rate was determined by calculating the isokinetic sampling rate based on the current furnace conditions. The sampling rate was monitored by a mass flow meter.

After being removed from the furnace, the sample passed through a Berner low-pressure impactor (LPI) (Hillamo and Kauppinen 1991). A diagram of the impactor showing the general arrangement and the cut diameter of each stage is shown in Figure 3.6. This cascade impactor was designed so that several of the stages operate at pressures below atmospheric, allowing the segregation of particles down to 0.032 microns. There were ten stages in the set-up used, with the Plate 11 data disregarded due to poor collection ability. A Nucleopore polycarbonate filter, obtained from Osmonics, was
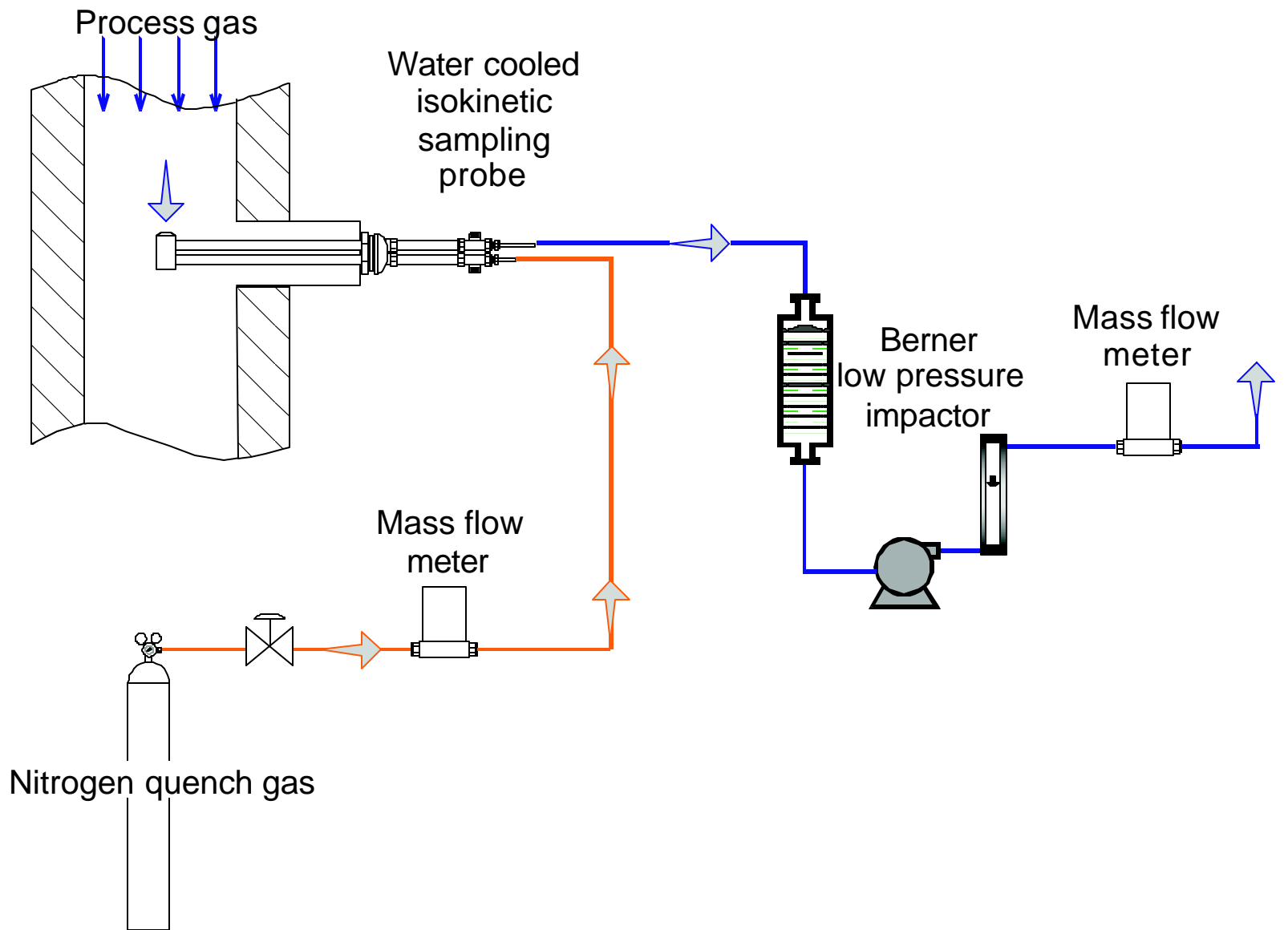
Figure 3.5 - Sampling system

Aerodynamic 50% Cut-Off Diameter [µm]	
Plate 11	15.7
Plate 10	7.33
Plate 9	3.77
Plate 8	1.98
Plate 7	0.973
Plate 6	0.535
Plate 5	0.337
Plate 4	0.168
Plate 3	0.0926
Plate 2	0.0636
Plate 1	0.0324

Orifice Plate

Substrate

Atmospheric section

Low pressure section

Final plate acts as a sonic orifice
Downstream Pressure
8 kPa (abs.)
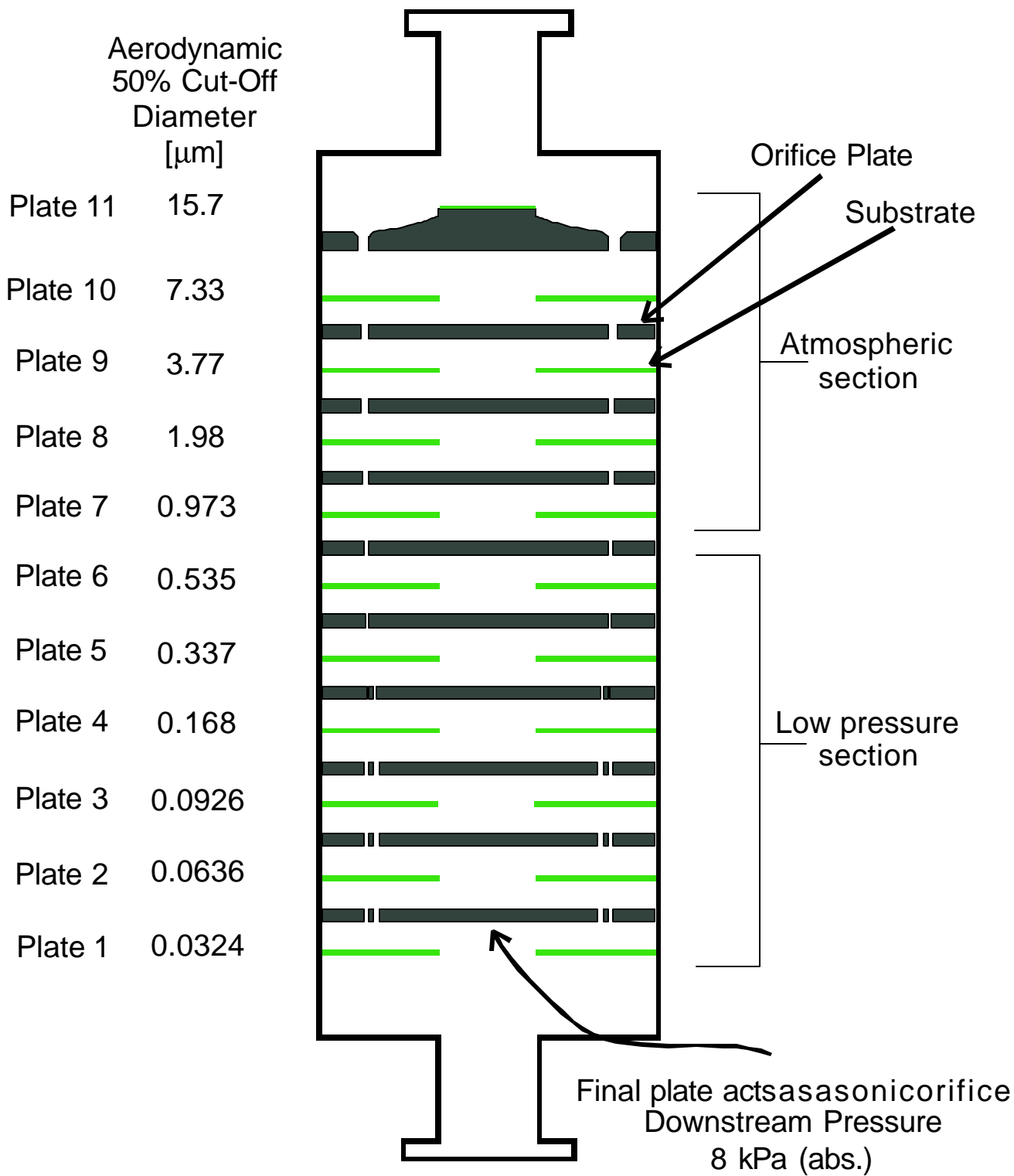
Figure 3.6 - Berner low pressure cascade impactor

52

placed on each impaction stage. Each filter was lightly airbrushed with a mixture of Apiezon-L vacuum grease and toluene, to prevent particle bounce-off. The substrates were then vacuum desiccated for 24 hours prior to use, in order to remove the solvent.

A full discussion of the particle sampling method can be found elsewhere (Davis et al. 1998).

3.4 AA/AE Analysis

Once the samples were collected, the substrates were removed from the LPI and placed in polyethylene vials. A 15 mL aliquot of digestion acid was then added to each vial. The digestion acid was composed of a 5:3:1:1 mixture of ultrapure water, hydrofluoric acid, nitric acid, and hydrochloric acid. The samples were placed in a ultrasonic cleaner for ten minutes, and the samples were allowed to sit for a period of 24 hours. After the 24 hour waiting period, a 15 mL aliquot of a boric acid solution was added. The boric acid binds with the excess fluorine in the samples, helping to protect the components of the atomic adsorption system. The composition of the boric acid solution was dependent upon the contents of the samples. The boric acid solution added to the samples containing strontium was composed of 56.6 g of boric acid crystals, one liter of ultrapure water, and 0.78 g of $CsNO_3$, added to reduce ionization interferences. The boric acid solution added to those samples containing cesium was the same, except the $CsNO_3$ was replaced with 0.6 g of KCl. The KCl was substituted for the $CsNO_3$ into those runs that contain cesium because the amount of cesium added in the digestion step

cannot be measured precisely enough to correct for. The samples were again sonicated for ten minutes, after which the samples were ready for analysis.

The majority of the elements of interest were analyzed for using flame atomic absorption spectroscopy (AAS). This was performed on a Perkin-Elmer Model 2380 Atomic Absorption Spectrophotometer. Hollow cathode lamps were used for the light sources. The spectral lines examined were: 309.3 nm for aluminum, 422.7 nm for calcium, 251.6 nm for silica, and 460.7 nm for strontium. Cesium was analyzed using flame atomic emission spectroscopy (AES). The same instrument was used as before, except no lamp was used. An optical filter was installed on the spectrometer prior to use. The spectral line of 852.1 nm was examined. For all analysis, standards were prepared from purchased standard metal solutions. To prevent matrix errors, the preparation solutions were matched to the dissolving acid used on the samples. More information on the theory of atomic absorption spectroscopy, atomic emission spectroscopy, and the specific settings used for the Perkin-Elmer machine can be found elsewhere (Siemer 1986) (1982).

3.5 SEM/EDS Procedures

Samples generated for scanning electron microscopy and energy dispersive spectroscopy (SEM/EDS) analysis were collected using the same sampling equipment. Instead of the polycarbonate substrates used for AAS, ungreased aluminum foil substrates were used. Samples were collected for one minute. After collection, a small piece of the substrate was cut and mounted on an aluminum pin mount using a carbon-based glue tab.

The samples were then coated with an approximately 200-angstrom layer of gold/palladium using an Anatech Ltd. Hummer VI sputter coater. The samples were stored in a dessicator when not in use.

The microscope used was a Hitachi Model S-2460N scanning electron microscope equipped with a Noran Instruments SiLi x-ray detector. The SEM was operated such that high-magnification images of the samples were obtained. For more information, consult the appropriate equipment manuals (Hitachi 1992), (1995). No attempt was made to perform quantitative EDS on the particles.

4.1 Introductory Comments

The results are presented in the following series of graphs. The raw data from which these figures are constructed are presented in Appendix A.5. Each of the curves presented is plotted based on the average of two separate experimental runs. The variation between each of the experimental runs was no greater than 15%. For the sake of clarity, error bars were not included in the figures.

Each of the results figures is constructed in a similar manner. The x-axis presents the aerodynamic diameter of the particles in microns. Since this characteristic spans four orders of magnitude, this axis is presented in a logarithmic scale. The aerodynamic diameter assumes a particle density of one, so the actual size of particles on a plate may vary based on the density. The y-axis is the fraction of total metal captured. Thus, each point represents the mass of metal on a stage, divided by the sum of the masses found on all stages. This graphic presentation gives an indication of the distribution of the metals of interest over the range of the impactor. Shifts in the shape and position of these curves indicate the activity of the metals present.

In each of these figures, the particle size distribution (PSD) of the metal of interest is plotted without the presence of sorbent. This gives a baseline indication to compare with, in order to determine the effect of sorbent on the system. The second curve on the graphs is the metal in the presence of the particular sorbent. The sorbent

56

size distribution is shown on these graphs by plotting the major element of each of the sorbents: aluminum for kaolinite and calcium for lime. For the mixed sorbent and the CDEM sorbent, both aluminum and calcium curves are shown, as the chemical behavior of the two constituents can be significantly different.

4.2 Cesium Results

The results of the cesium experiments are shown in Figures 4.1 through 4.19. The first of these figures shows the behavior of cesium with the sorbents but with no dopant gases added.

Figure 4.1 shows the behavior of cesium with kaolinite. The cesium alone exhibits a curve with a peak near 0.05 microns. This indicates that the cesium metal vaporizes in the flame. When the gaseous cesium is withdrawn from the furnace, it quickly nucleates in the probe to form a fume of fine metal particles. These results coincide well with the behavior predicted by the thermodynamic calculations. When kaolinite is injected into the furnace, the cesium peak shifts to near one micron. This peak almost perfectly overlaps the aluminum peak from the sorbent. This shift and overlap of the cesium peak indicates that the cesium is reacting with the kaolinite in the furnace, forming larger particles.

Figures 4.2 and 4.3 are SEM micrographs of kaolinite and cesium with kaolinite. Unless noted otherwise, all SEM images are taken from samples on Plate 6 of the impactor. The morphology of kaolinite is seen in Figure 4.2. This kaolinite was injected in the furnace and collected with the particulate sampling system, but no metals were
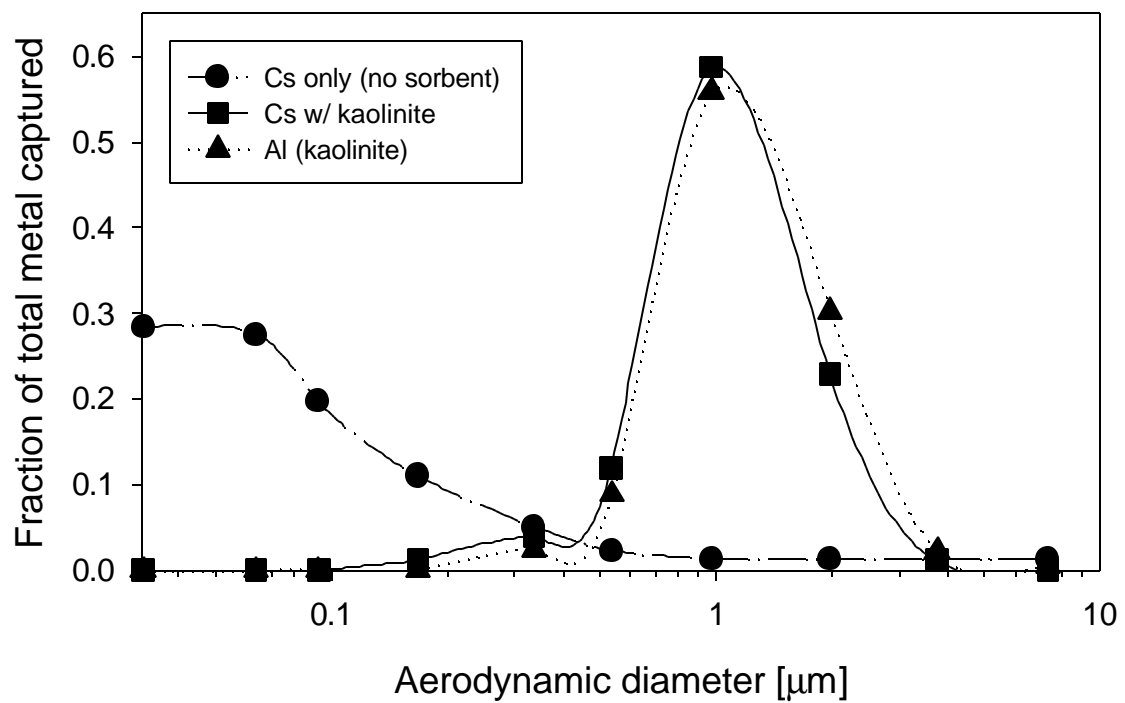
Figure 4.1 - Cesium and kaolinite, no dopant
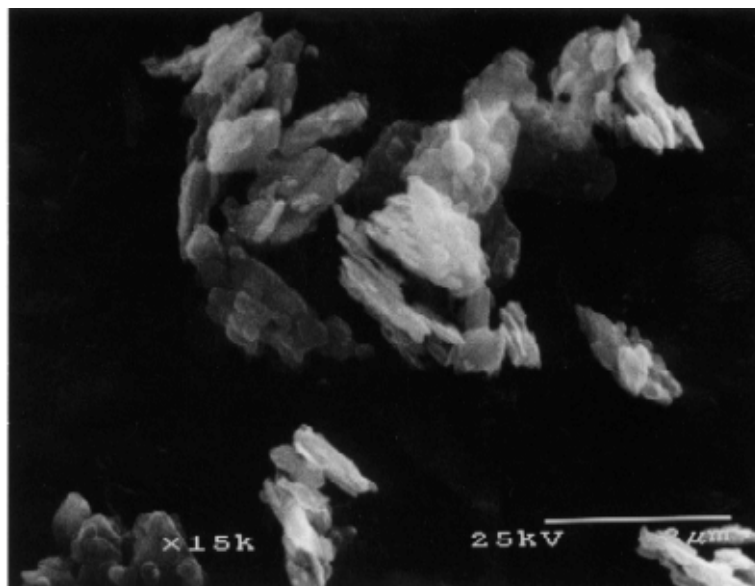
Figure 4.2 – SEM micrograph of unreacted kaolinite
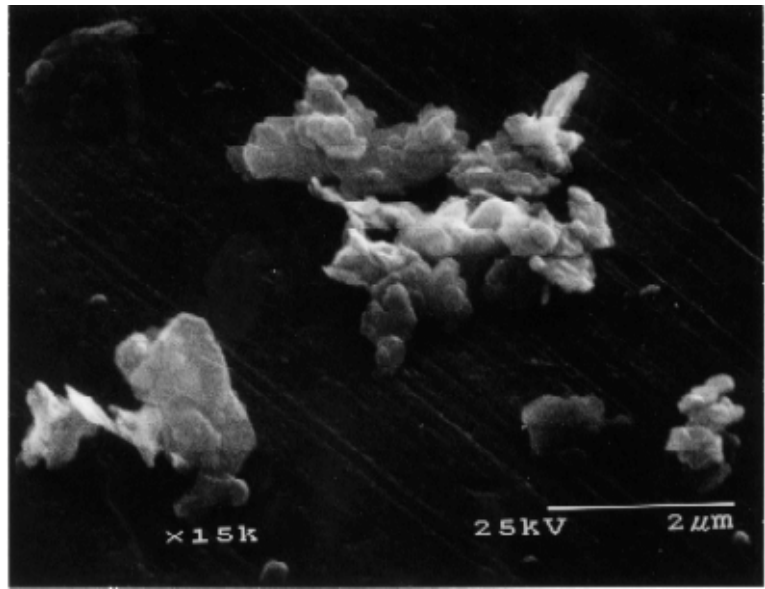
Figure 4.3 – SEM micrograph of cesium and kaolinite particles
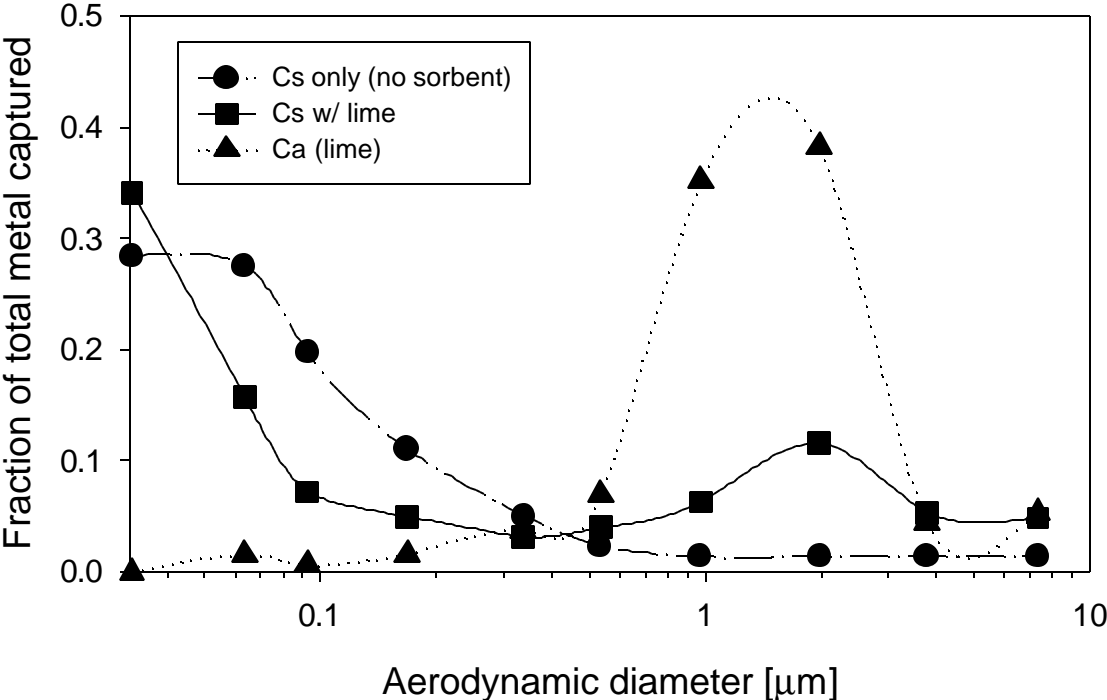
Figure 4.4 - Cesium and lime, no dopant

added with the sorbent. The kaolinite particles show a jagged and angular morphology. A sample from the cesium and kaolinite system is shown in Figure 4.3. The PSD analysis indicated that the cesium reacts with the kaolinite, so some evidence of this reaction might be expected in the SEM image. The particles again have a jagged and angular appearance. Very little difference in the morphology can be seen between the two samples.

The results of cesium with lime are shown in Figure 4.4. Here, the cesium exhibits a large peak near the small end of the impactor, and a short peak at around two microns. This suggests that there may be some reaction of the cesium with the lime. However, the rate of the reaction is probably very slow, preventing a significant fraction of the cesium from reacting. The majority of the metal ends up as a fume in the probe, similar to what is seen when there is no sorbent present.

The results of experiments in the presence of the mixed sorbent are shown in Figure 4.5. The cesium shows a peak near one micron, similar to that seen in the presence of kaolinite. This implies that the cesium is reacting with the kaolinite in the mixture, and not with the lime. Since the degree of reaction with kaolinite was much greater than with lime, this result is not surprising.

Figure 4.6 shows the results of injecting cesium and CDEM together in the furnace. The cesium forms a double peak, with a large peak near 0.07 microns, and a shorter peak near 1.5 micron. This result is similar to that seen in the lime experiments. This could indicate the cesium is reacting only with the calcium products in the sorbent
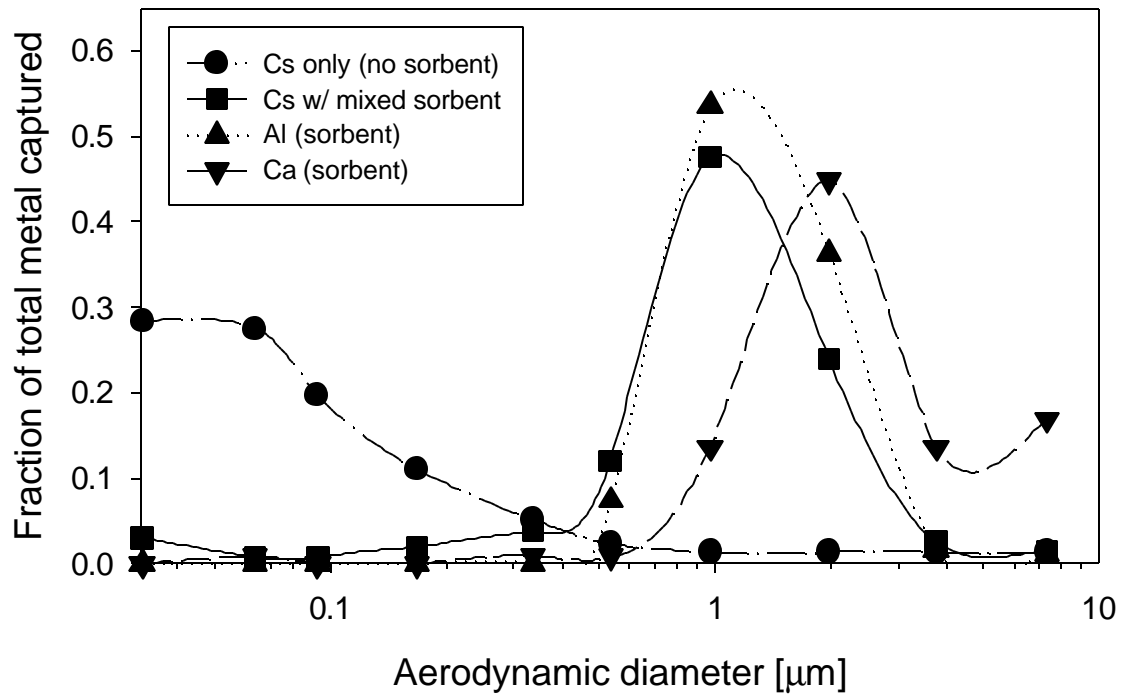
Figure 4.5 - Cesium and mixed sorbent, no dopant
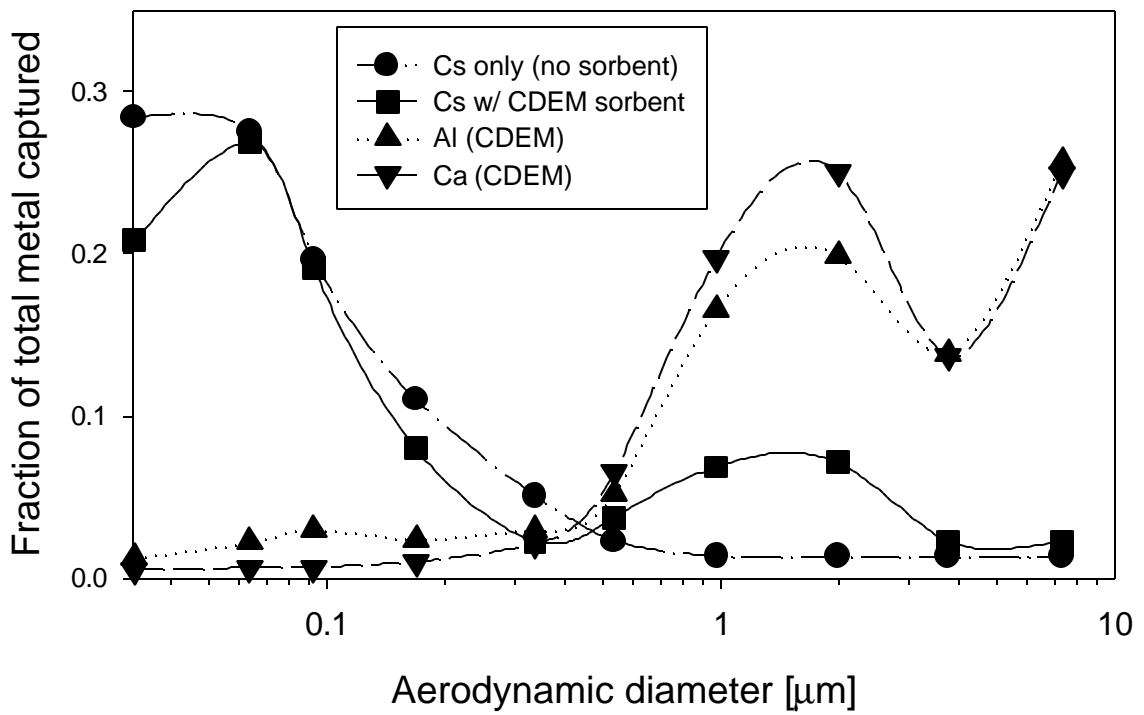
Figure 4.6 - Cesium and CDEM, no dopant

or that the cesium is blocked in some manner from reacting with the alumino-silicate portion of the sorbent.

The next set of figures display the results of the experiments with cesium in the presence of chlorine gas. Figure 4.7 displays the results of cesium with kaolinite in the presence of chlorine. Cesium and chlorine alone, with no sorbent present, exhibits a peak near 0.09 microns. This peak is slightly different from that seen when there was no chlorine in the system. The cesium peak with no chlorine was butted right up to the small end of the impactor, indicating that the fume that formed was composed of relatively undeveloped particles. With the chlorine present, the peak was fully within the impactor, suggesting a slightly more mature aerosol. This is consistent with the thermodynamic calculations, which indicated that the dewpoint of the cesium would rise.

When the kaolinite was added to the cesium/chlorine system, a double peak formed. The first peak trails off the small end of the impactor, and the second peak forms around one micron. This indicates that the cesium is still reacting with the kaolinite, but to a lesser extent. The remaining cesium forms a sub-micron fume. This could be explained by the gaseous cesium species present. It is suspected that CsOH is the product that reacts with the kaolinite. When an excess amount of chlorine is present, a large fraction of the cesium is present in the form of CsCl, which does not react with the sorbent. Equilibrium is established between the gaseous CsOH and CsCl. As the CsOH reacts with the sorbent, some of the CsCl forms CsOH to replace that lost to the sorbent. So, the cesium is still reacting with the kaolinite, but at a much slower rate.
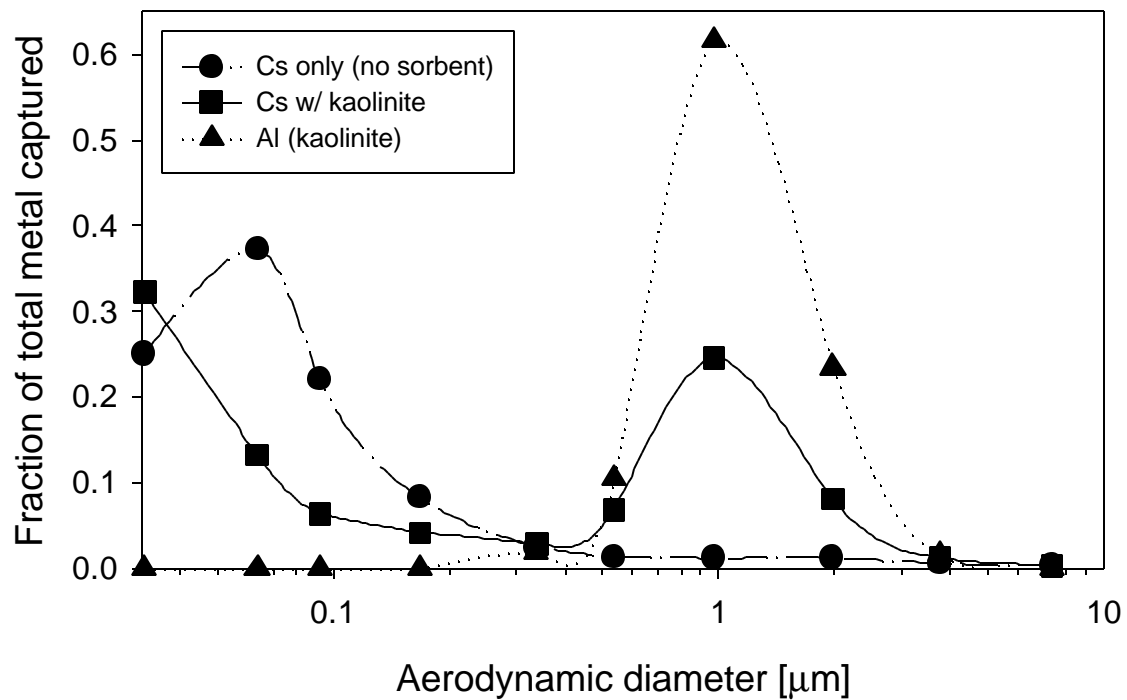
Figure 4.7 - Cesium and kaolinite, with chlorine
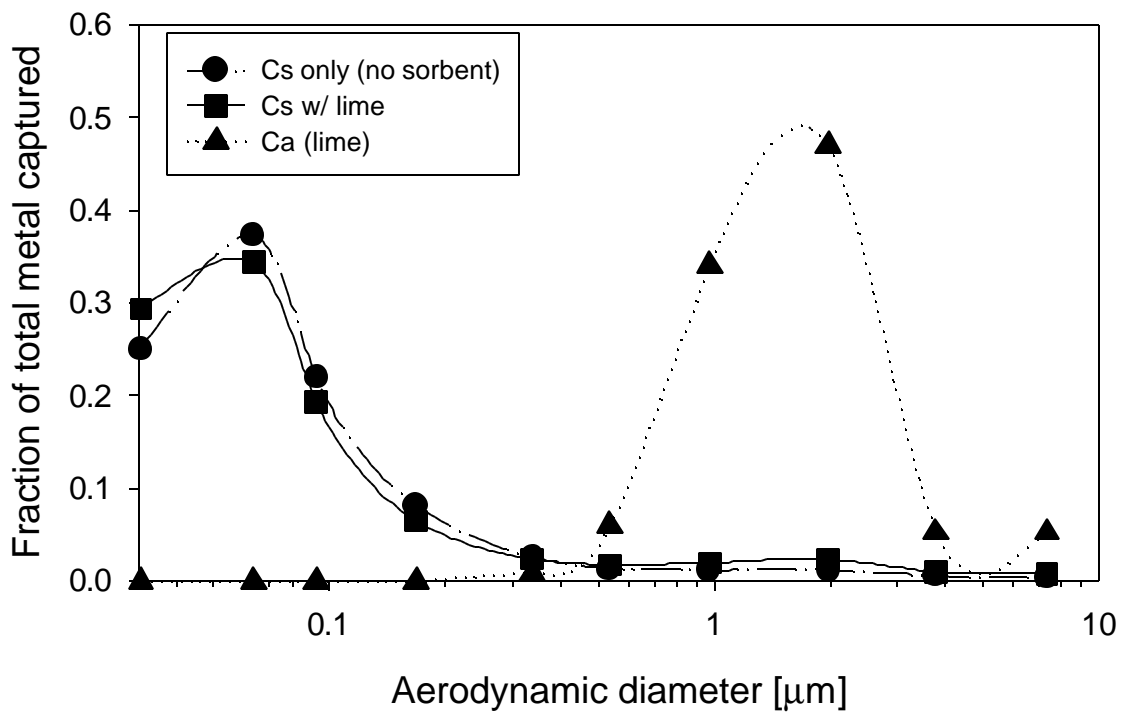
Figure 4.8 - Cesium and lime, with chlorine

The results of the cesium/chlorine system experiments with injected lime are shown in Figure 4.8. The cesium in this case forms only a single peak near 0.08 microns. This peak exactly matches the peak formed with no sorbent present. This means that the cesium does not react with lime when chlorine is present in the system.

Figure 4.9 shows the cesium/chlorine/mixed sorbent experiment results. The cesium again forms a double peak. The first peak trails out the small end of the impactor, suggesting the formation of a fume, and the second peak is around one micron. The second peak forms near the aluminum peak from the kaolinite. These results indicate that the cesium is reacting with the kaolinite in the sorbent and not with the lime. This is consistent based on the results from the previous two figures.

The results in Figure 4.10 are from the cesium/chlorine/CDEM test system. The cesium in this case forms a single peak near 0.08 microns, matching the peak that forms without sorbent present. This indicates that the cesium is not reacting with the sorbent. In addition, there was a change in the appearance of the sorbent after being exposed to the chlorine. The sorbent started as a beige/white powder, prior to injection in the furnace. After being exposed to the chlorine, the sorbent appeared more yellowish, with some evidence of crystallization. Thus, the chlorine appears to react with the sorbent, changing its chemical characteristics.

The results from the cesium and sulfur tests are depicted in the next group of figures. Shown in Figure 4.11 are the data that demonstrate the effect of sulfur on cesium particulate formation. The one curve shows the results when cesium in the presence of sulfur is sampled from the furnace at Port 14, which is where all the previous samples
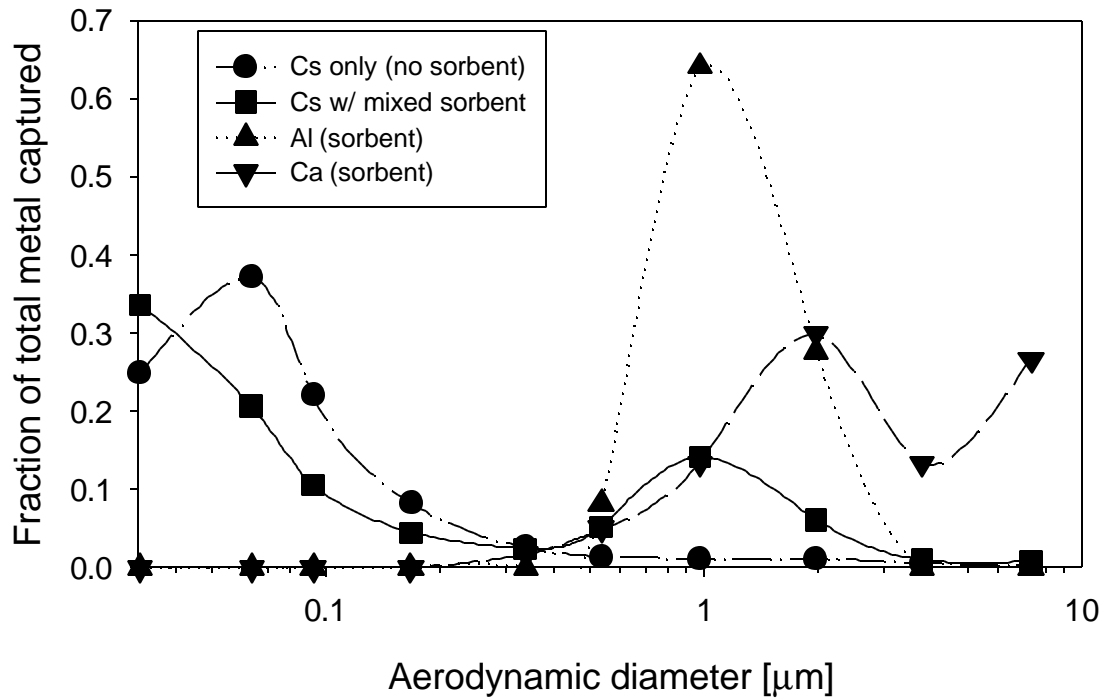
Figure 4.9 - Cesium and mixed sorbent, with chlorine
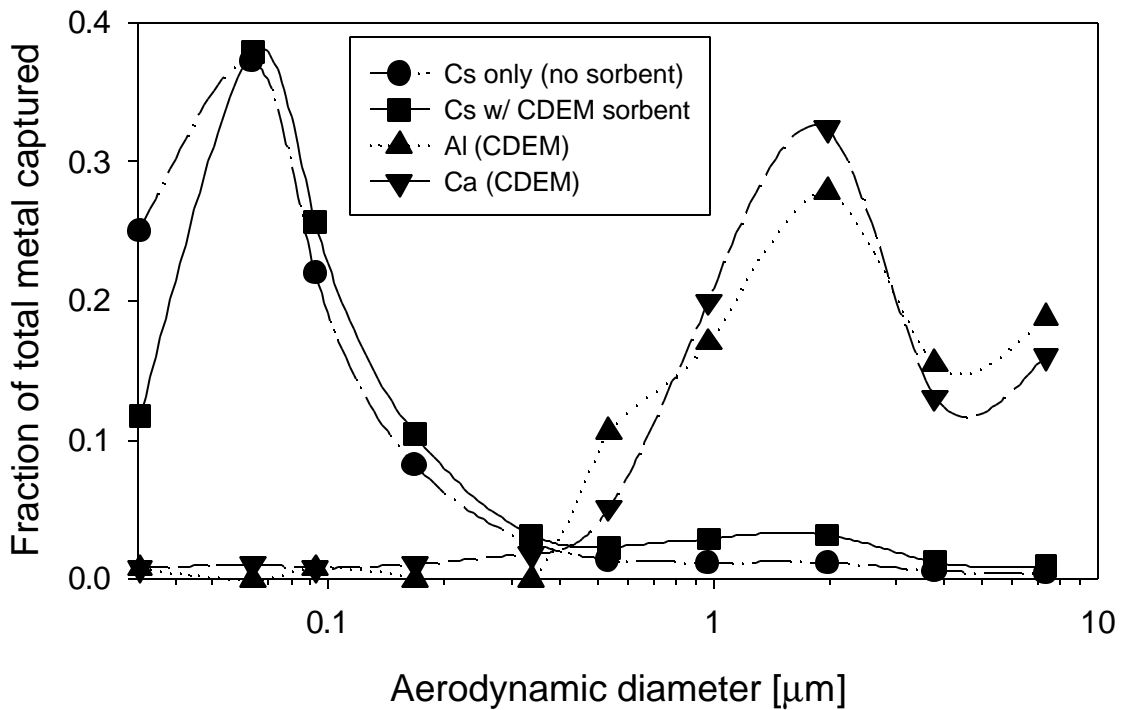
Figure 4.10 - Cesium and CDEM, with chlorine
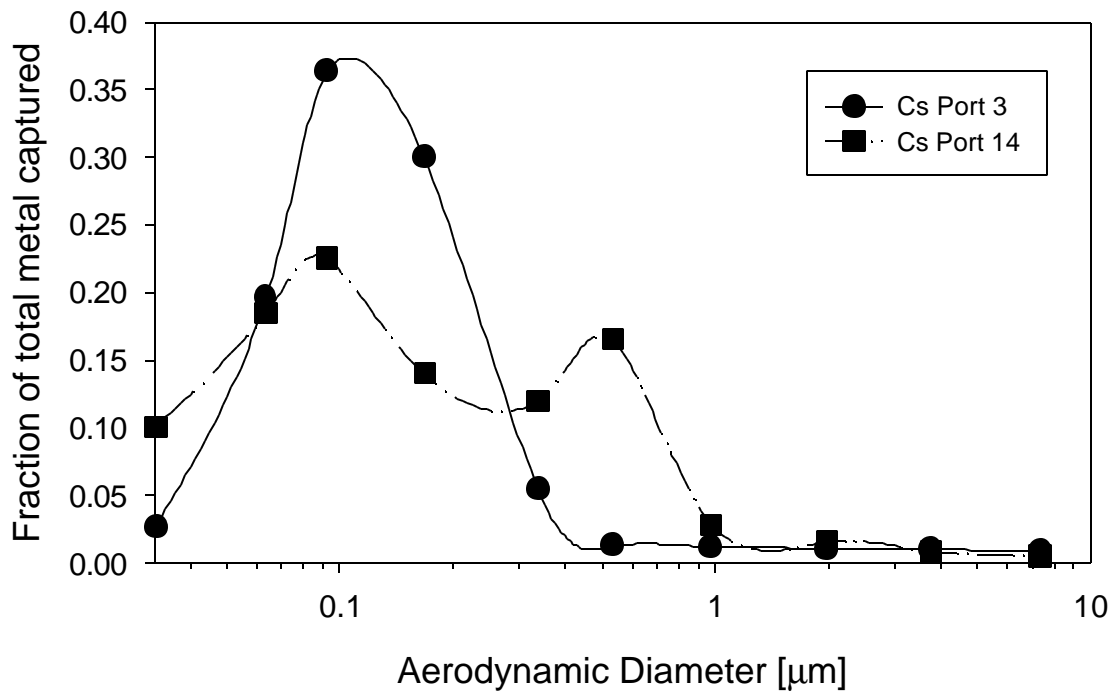
Figure 4.11 - Time evolution of cesium/sulfur particles
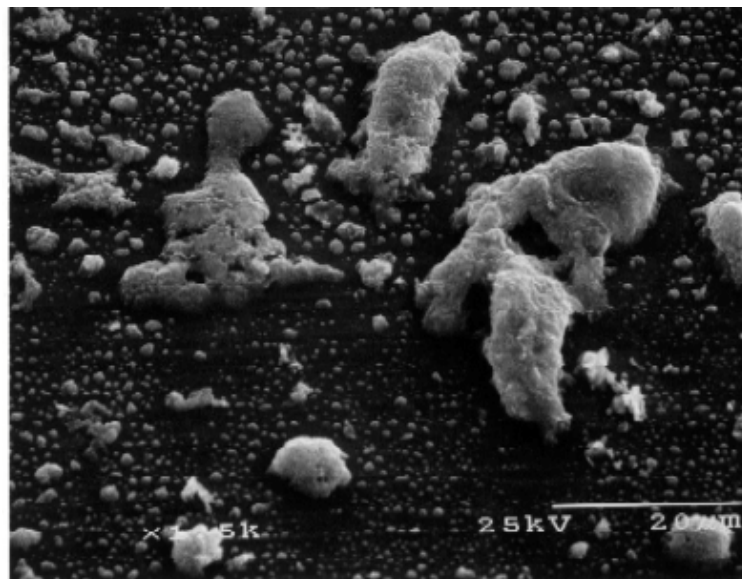
Figure 4.12 – SEM micrograph of cesium particles with sulfur

have been collected. This point in the furnace has a temperature of about 1125 K and a residence time of about two seconds. The cesium shows a double peaked curve, with the peaks forming at 0.1 and 0.5 microns. To better understand the nature of these results, a second sample was taken at exactly the same conditions, except the aerosol was sampled at Port 3. This port has a temperature of 1450 K and a residence time of about 0.4 seconds. This sample exhibits a curve with a single peak at 0.1 microns. This suggests that when the cesium enters the furnace, it is completely vaporized. As the cesium passes down the length of the furnace, the temperature drops and the cesium starts to nucleate and form particles. As time progresses, additional cesium condenses onto the existing cesium particles. Therefore, the first peak seen at Port 14 is due to nucleation, and the second peak is due to condensation.

SEM images of the cesium/sulfur tests are shown in Figures 4.12 and 4.13. Figure 4.12 is an image taken at a relatively low magnification. Very large (~20 micron) particle clusters are evident. This size of particle, had it existed in the sample stream, would have been collected on a higher plate, most likely Plate 10. These particles appear to be agglomerations of smaller particles that formed due to impaction in the impactor. Figure 4.13 is a close-up of some of the smaller particles on the plate. These particles also appear to be built-up and show some agglomeration. These particles represent the second peak of the PSD curve. This morphologic evidence supports the theory that these particles are formed by nucleation of the gas phase cesium, followed by condensation.

The results when kaolinite is added to the system are shown in Figure 4.14. The cesium shows a strong peak near one micron. This peak follows the aluminum peak from
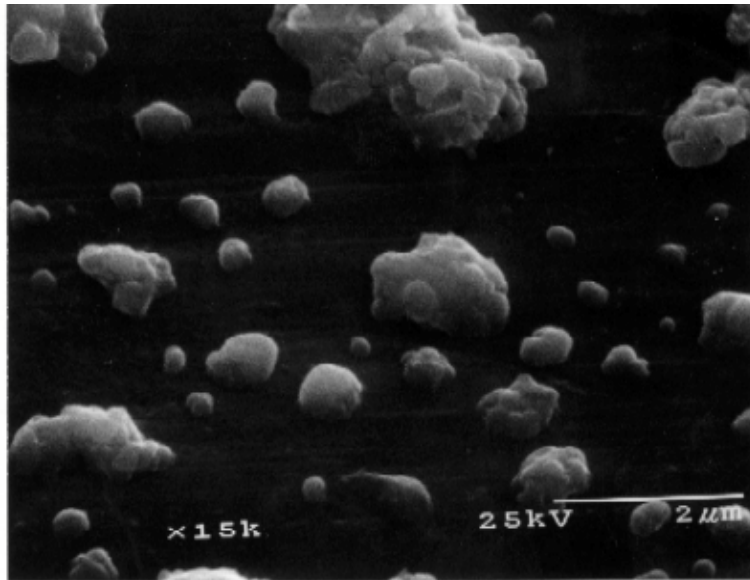
Figure 4.13 – SEM micrograph of cesium particles with sulfur

Aerodynamic diameter [μm]
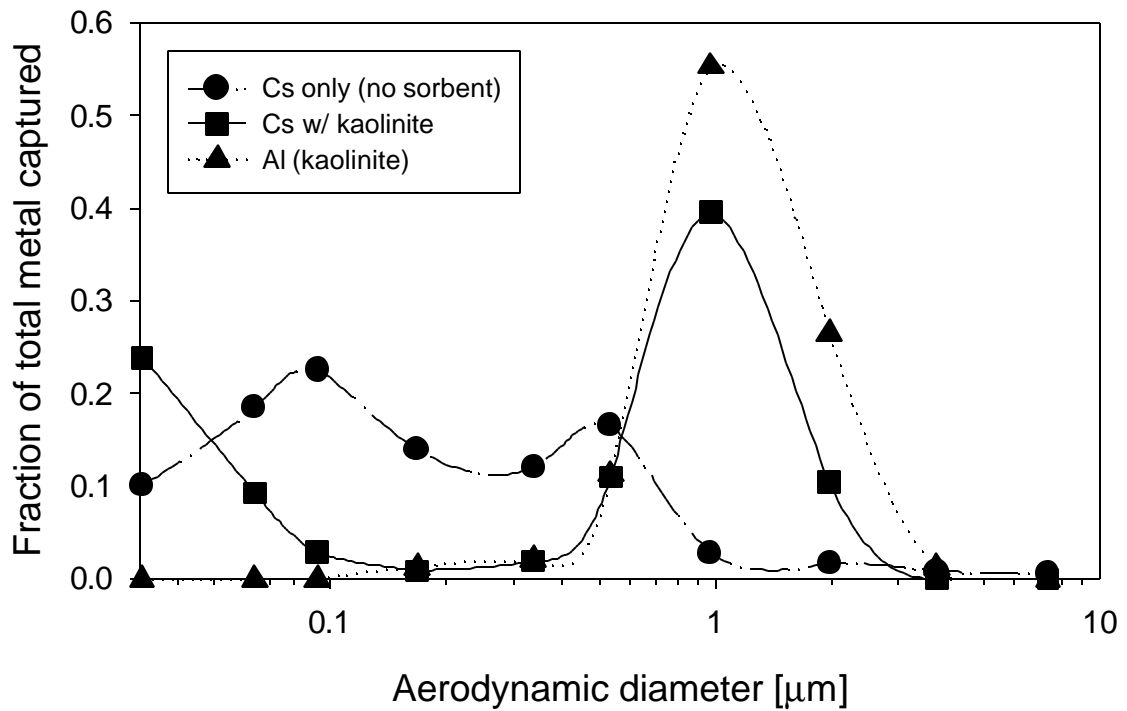
Figure 4.14 - Cesium and kaolinite, with sulfur

the sorbent. This suggests that the cesium is reactively captured. There is also a trailing peak at the low end of the impactor, indicating that not all of the cesium has reacted. This coincides with the thermodynamic predictions. The presence of sulfur increased the dewpoint of the cesium. This allowed less time in the reactor for the cesium to react with the sorbent, hence reducing the total capture of the cesium.

The results of the cesium/sulfur/lime experiments are shown in Figure 4.15. A double peak is formed, with peaks at the trailing end and at two microns. This indicates that the cesium is reacting with the lime, but at a finite rate, leaving a portion of the metal unreacted. Thus, it appears that the presence of sulfur enhances the ability of lime to capture cesium.

Figures 4.16 and 4.17 are micrographs that show the cesium/sulfur/lime samples. Figure 4.16 is a sample of lime, with no metal or dopant present. The particles in this picture have a chunky appearance, with some degree of angularity. The edges are a little more rounded than those seen in the kaolinite. Figure 4.17 shows the cesium/sulfur/lime sample, which was taken from Plate 7 of the impactor. There are two different particle morphologies present in this sample. Particles in the upper left and lower left corners have an angular shape. These are lime particles that show little evidence of melting or reaction. The particles in the lower center of the picture have a rounded appearance. These appear to be cesium particles that have agglomerated onto the sorbent particles, but that have not reacted with the lime.

In Figure 4.18 are the results of cesium and sulfur with the mixed sorbent. Again, the double peak is formed, with one peak trailing out the bottom of the impactor and the
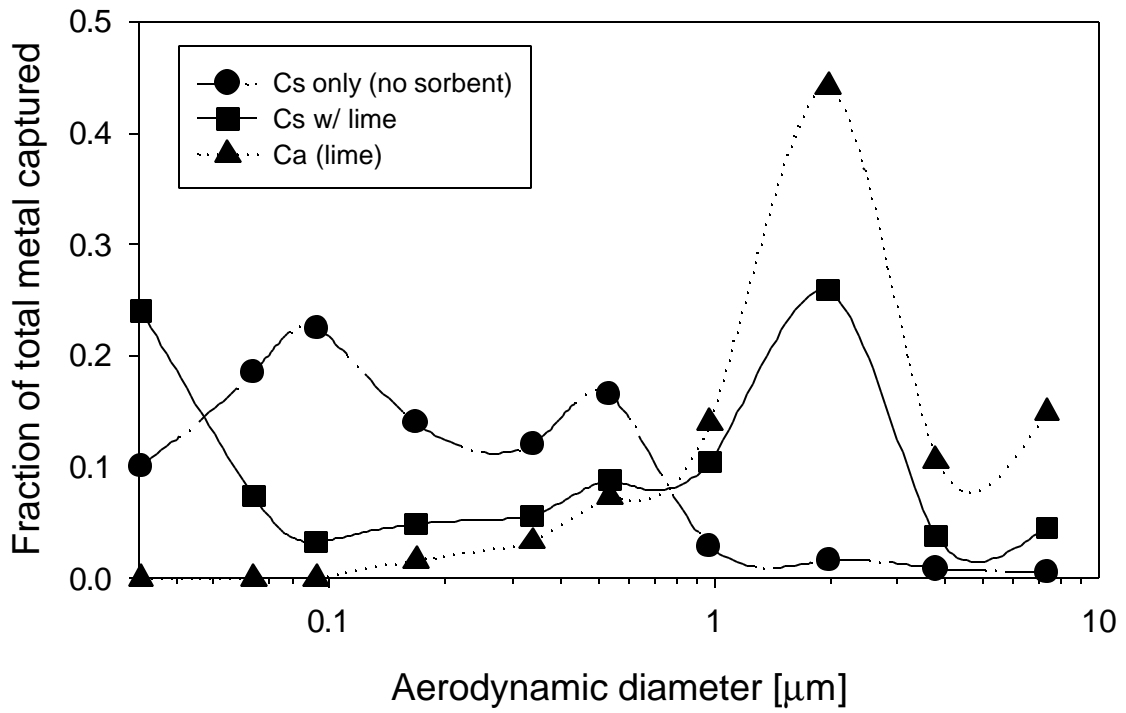
Figure 4.15 - Cesium and lime, with sulfur
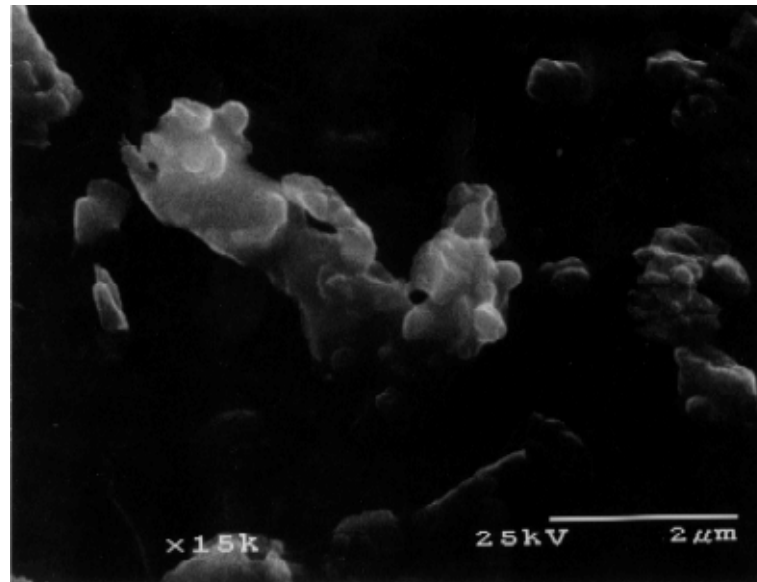
Figure 4.16 – SEM micrograph of unreacted lime
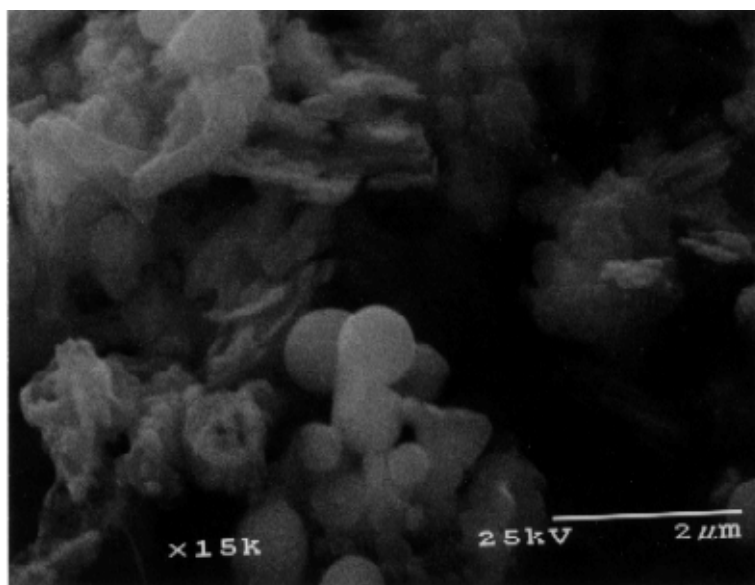
Figure 4.17 – SEM micrograph of cesium and lime particles, with sulfur
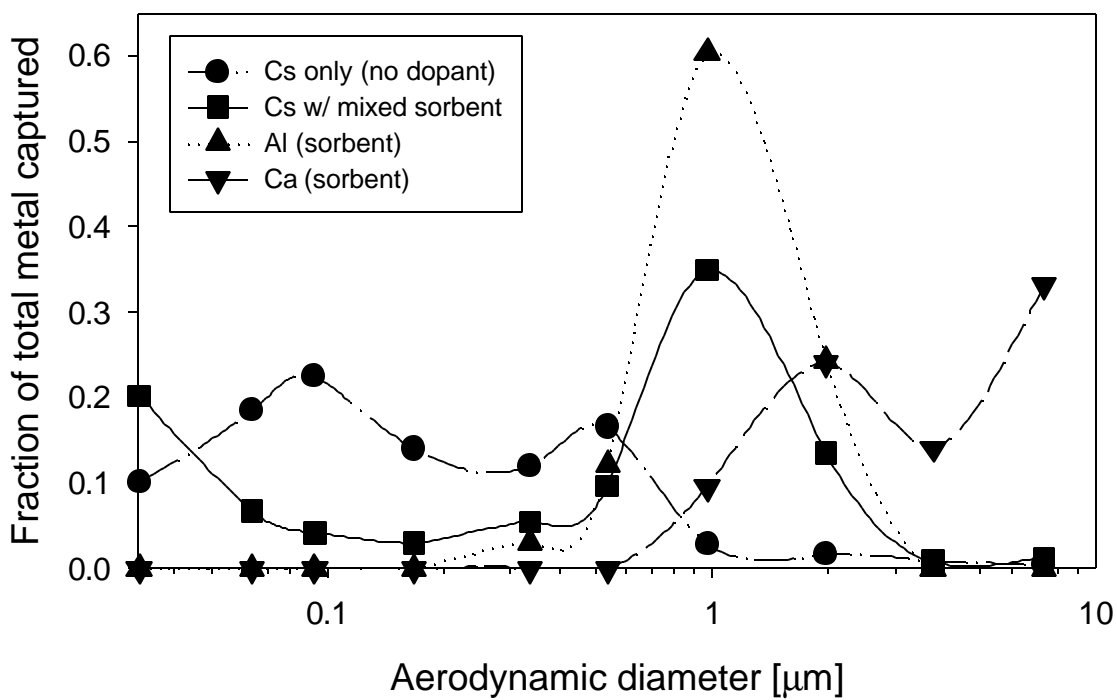
Figure 4.18 - Cesium and mixed sorbent, with sulfur

other forming at one micron. This shows that the cesium is preferentially reacting with the kaolinite in the system, but is still being captured.

Figure 4.19 shows the results from the cesium/sulfur/CDEM tests. There is a large peak formed near two microns, indicating that the CDEM sorbent is fairly effective in capturing cesium in the presence of sulfur. There is also a small peak at the trailing end, showing that the reaction is occurring at some finite rate.

4.3 Strontium Results

The results of the strontium tests are shown in Figures 4.20 through 4.39. The first of these figures represent the results of the tests with strontium only, without the addition of dopants.

Figure 4.20 displays the results of the strontium and kaolinite system, with no dopant gas. Strontium on its own forms a broad peak at 0.8 microns, with a long tail extending to the smaller particle size. This most likely represents residual strontium from the aqueous solution. The water from the droplets evaporates, leaving the strontium behind. When kaolinite is added to the system, the peak shifts to a slightly larger (one micron) particle diameter and the long trailing tail disappears. This might represent capture, but the other evidence suggests that the strontium does not vaporize, preventing it from reacting. The strontium is probably collected on the kaolinite particles by some physical mechanism, such as coagulation or impaction.

The particles shown in Figure 4.21 are strontium particles collected without sorbent present. These particles show a very rounded morphology. This shape is

72
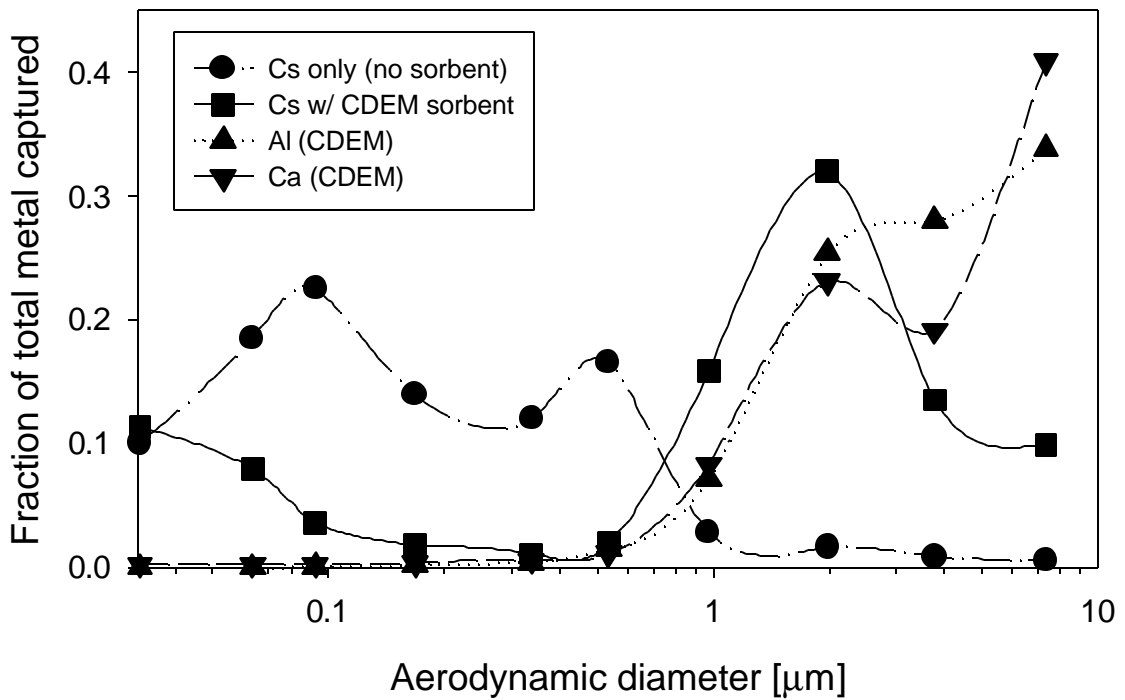
Figure 4.19 - Cesium and CDEM, with sulfur
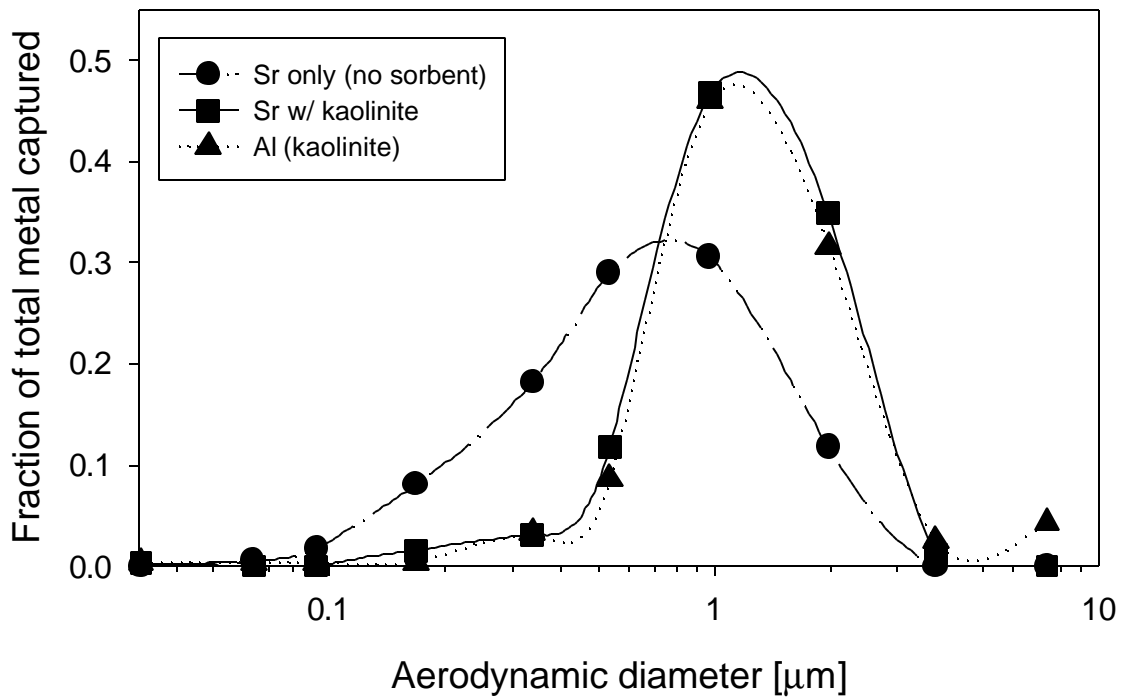
Figure 4.20 - Strontium and kaolinite, no dopant

Figure 4.21 – SEM micrograph of residual strontium particles
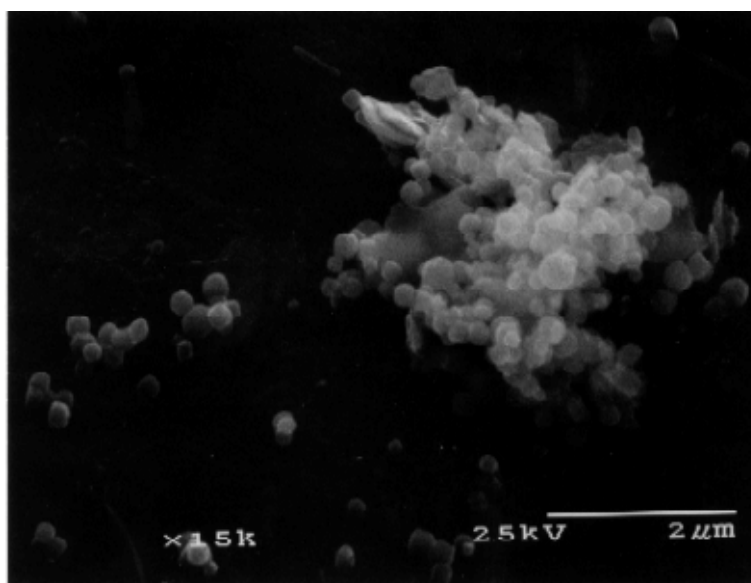
Figure 4.22 – SEM micrograph of strontium and kaolinite particles

consistent with the idea that the water from the spray droplets evaporates, leaving the strontium behind. The results when kaolinite is added to the system are shown in Figure 4.22. The residual strontium particles are quite evident. In addition, obscured by the strontium particles clinging to their surface, are kaolinite particles that show the jagged, angular appearance of unreacted kaolinite. Thus, it appears that no reaction occurs between the strontium and kaolinite.

The results of the strontium and lime experiments are shown in Figure 4.23. The strontium forms a peak at around one micron, with some evidence of a tail in the smaller size range. Again, the strontium appears to be collected by some physical mechanism. This is supported by the fact that the strontium peak does not exactly follow the lime peak. Figure 4.24 is a micrograph of this system. As in the case of strontium and kaolinite, the residual strontium particles are seen clinging to the sorbent particles, which show no evidence of chemical reaction.

The strontium and mixed sorbent results are depicted in Figure 4.25. The strontium again forms a peak at around one micron, with the smaller sized tail significantly reduced. Again, this appears to be a physical mechanism shifting the PSD. This is supported by the fact that the strontium does not exactly match the distribution of either of the components of the sorbent.

Shown in Figure 4.26 are the results of the strontium and CDEM tests. The peak in this case appears similar to that in the other sorbent cases. However, there is a small tail that appears on the larger end of the distribution. Because the size of the CDEM
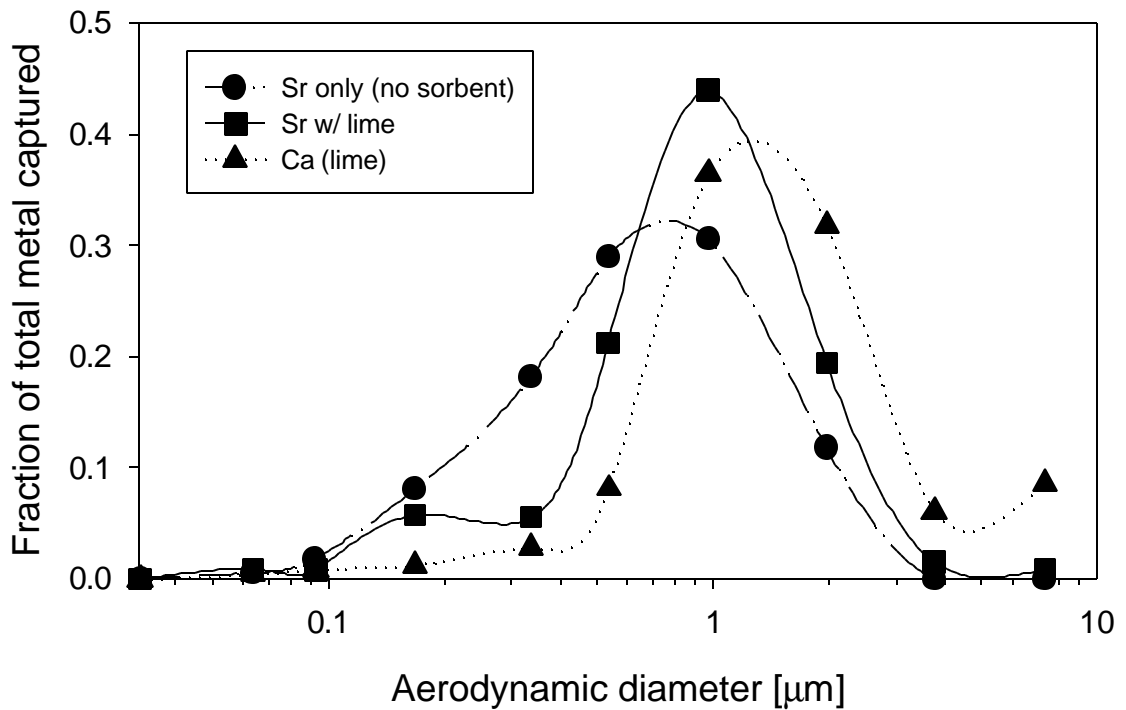
Figure 4.23 - Strontium and lime, no dopant
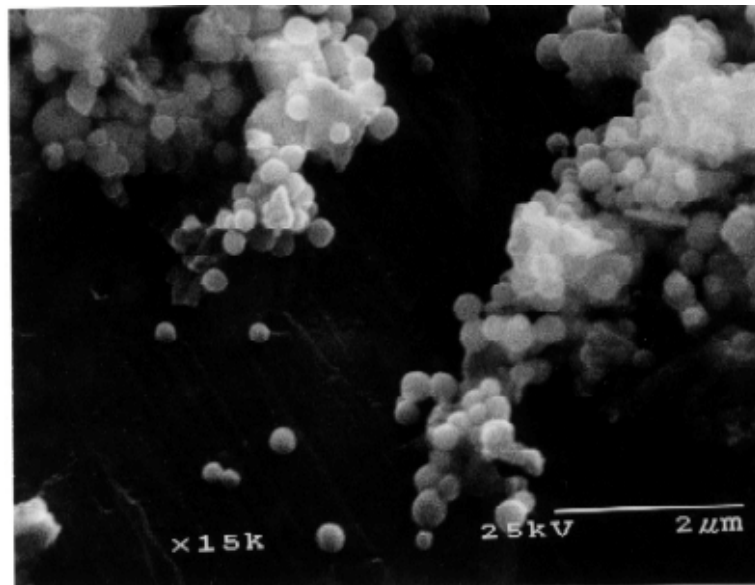
Figure 4.24 – SEM micrograph of strontium and lime particles
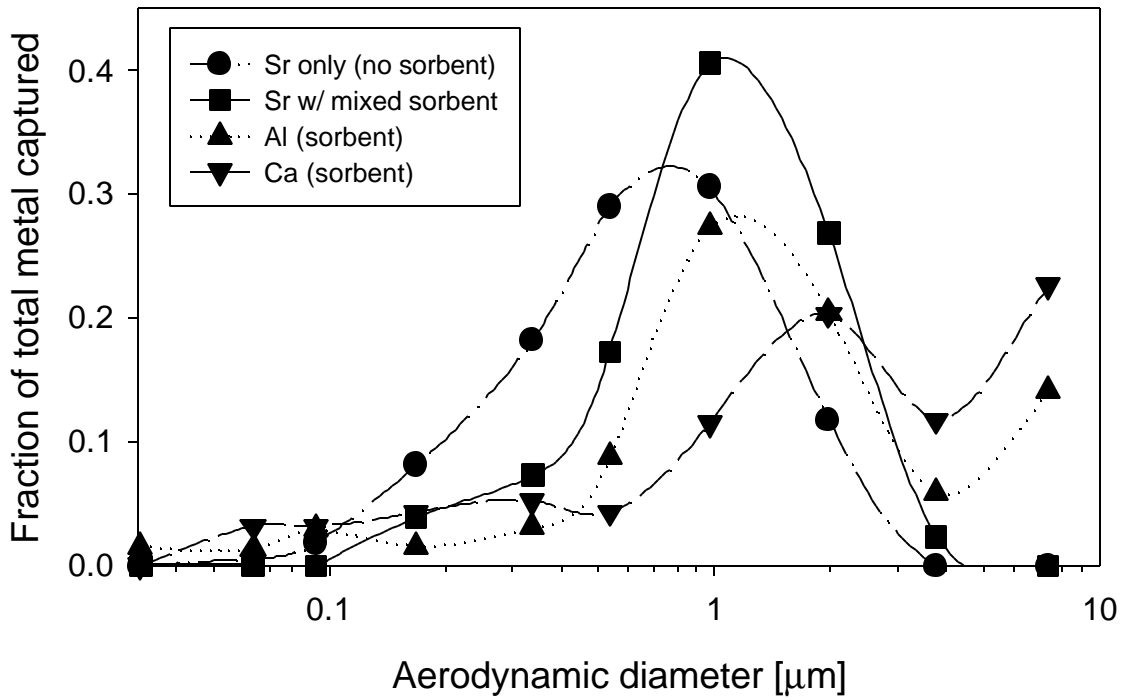
Figure 4.25 - Strontium and mixed sorbent, no dopant
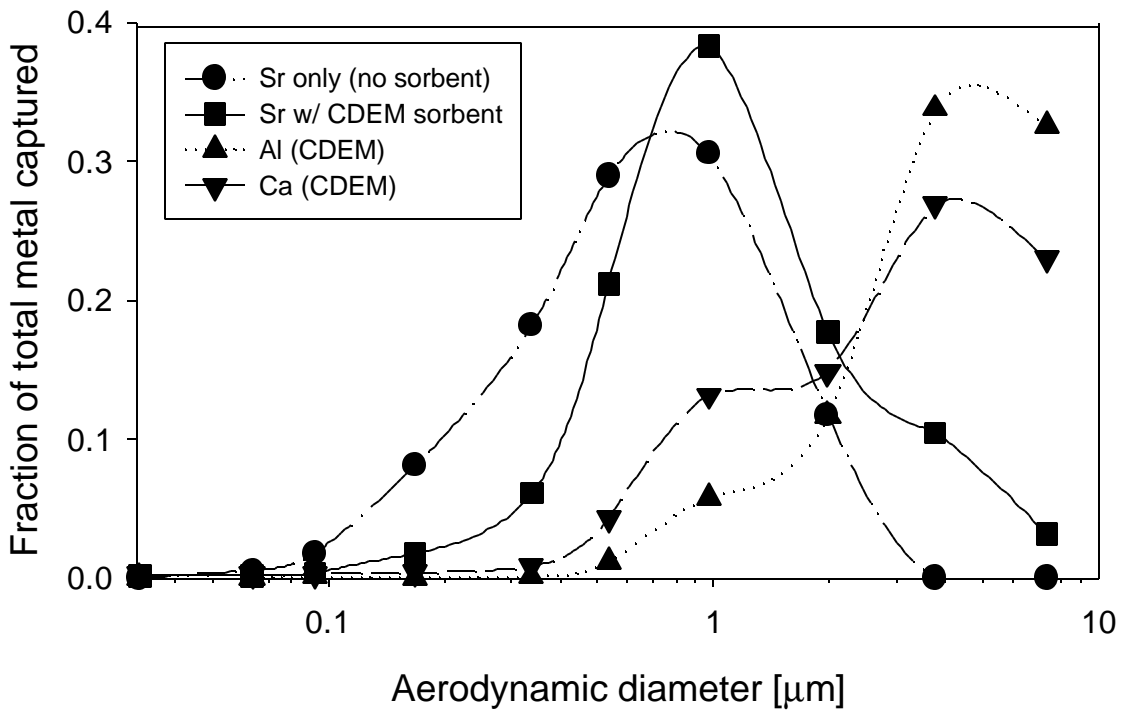
Figure 4.26 - Strontium and CDEM, no dopant

sorbent is larger, this tail is not unexpected. This is also consistent with the physical mechanism explanation.

The results for the strontium and kaolinite tests with chlorine present in the system are shown in Figure 4.27. The strontium with no sorbent present forms a curve with the peak around 0.2 microns. This indicates that the sorbent is actually vaporizing in the furnace. This was predicted by the thermodynamic calculations. When kaolinite is added to the system, the strontium peak shifts to around one micron. This peak closely matches the aluminum peak from the kaolinite. This shows that reactive capture is occurring with chlorine present.

SEM images of this situation are seen in Figures 4.28 and 4.29. Figure 4.28 is an image of the particles at a relatively low magnification. The metal and sorbent mix appears to be a fairly large (~15 microns) agglomeration, with significant melting of the sorbent particles. This agglomeration must have occurred on the impactor plate, as a particle of that size would have been separated from the impactor earlier had it formed in the furnace or probe. Figure 4.29 is an image taken at higher magnification. This image also shows significant melting.

The strontium/lime/chlorine results are shown in Figure 4.30. The strontium peak remains near 0.2 microns and closely follows the strontium peak when no sorbent is present. This demonstrates that no reaction occurs between the strontium and lime, even in the presence of chlorine.

Figure 4.31 shows the results of the strontium and mixed sorbent results, in the presence of chlorine. The strontium displays a double peaked curve, with peaks at 0.2
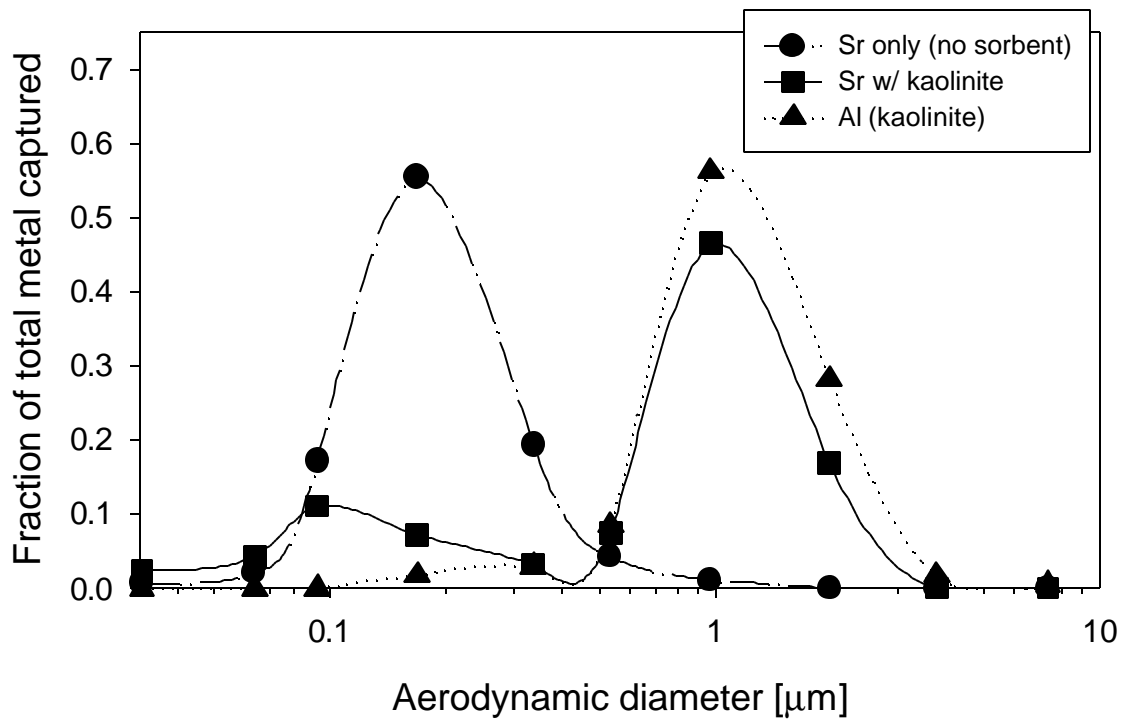
Figure 4.27 - Strontium and kaolinite, with chlorine
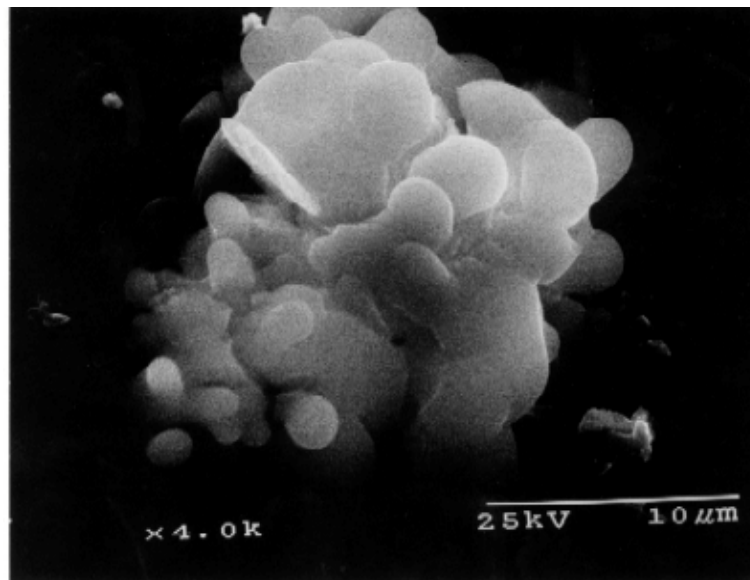
Figure 4.28 – SEM micrograph of strontium and kaolinite, with chlorine
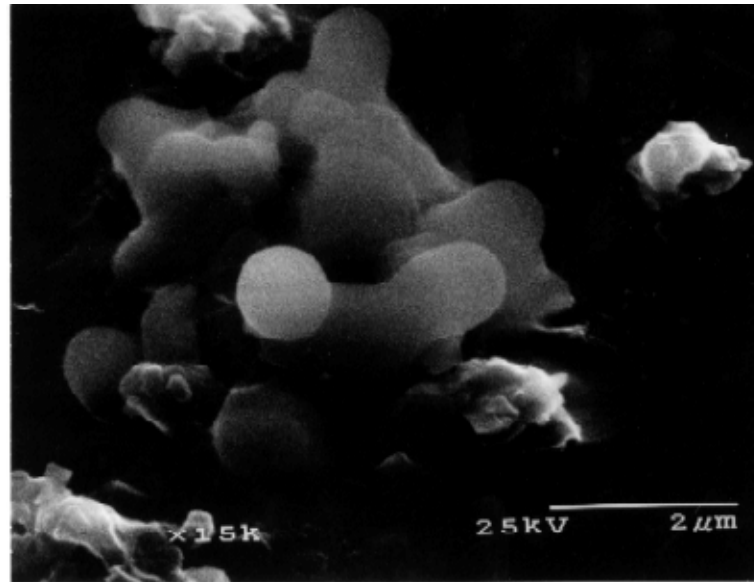
Figure 4.29 – SEM micrograph of strontium and kaolinite, with chlorine
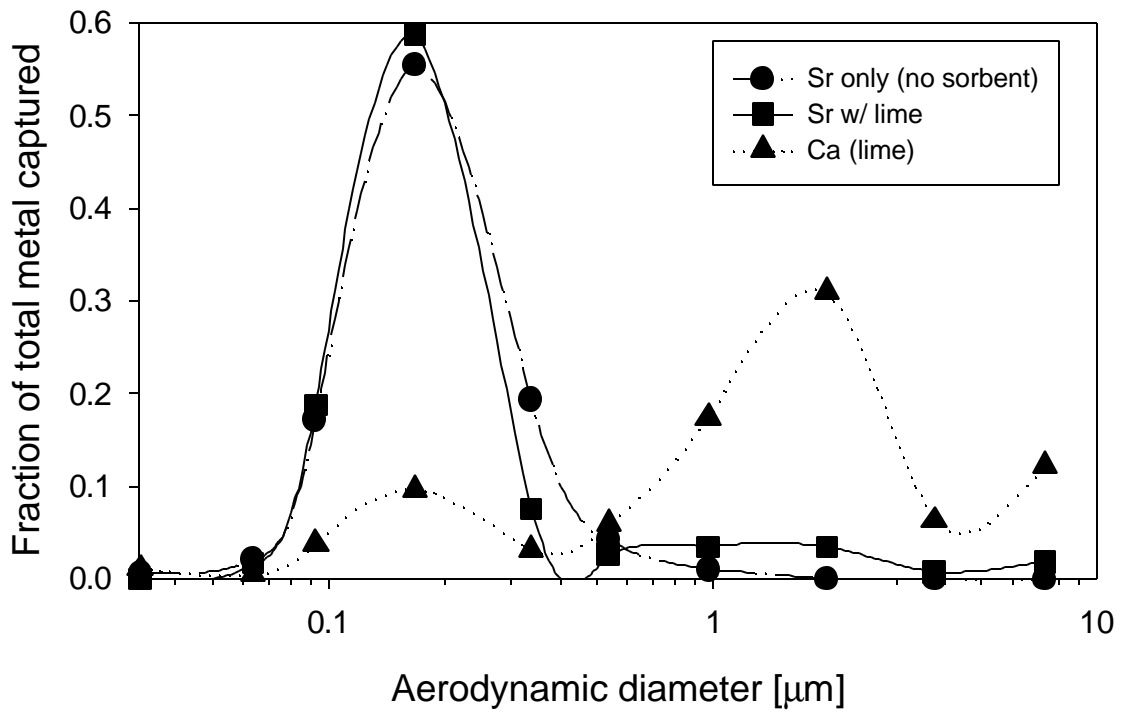
Figure 4.30 - Strontium and lime, with chlorine

microns and one micron. This change in the strontium peak represents partial reaction with the sorbent. The strontium is reacting with the kaolinite portion of the sorbent, and not reacting with the lime. Higher sorbent feed rates would probably lead to increased capture, but only on the kaolinite fraction.

The CDEM and strontium results with chlorine present are shown in Figure 4.32. The strontium peak is formed near 0.2 microns, with a little bit of tail on the larger size end. This indicates that the strontium may be reacting to a small extent with the sorbent, but the majority of the metal is unreacted. This may be related to the changes in the sorbent due to the presence of chlorine. Some of the strontium may be showing reaction with the alumino-silicate portion of the sorbent even after it has been affected by the chlorine, which would explain the tail of the curve.

Figure 4.33 presents the results of strontium when exposed to sulfur. The strontium, when sampled at Port 14, displays a double peaked curve, with the peaks forming at 0.2 microns and 0.7 microns. To further explore this situation, a sample was taken from Port 3. This curve shows a large peak at around one micron, and a small peak near 0.1 microns. This would suggest that the strontium enters the furnace as residual strontium from the aqueous spray. As the strontium comes in contact with the sulfur in the combustion air, the residual strontium particles are etched or decomposed in some way by the sulfur. Smaller strontium particles result. The residence time in the furnace is not sufficient to allow a complete decomposition of the particles, hence the double peaked curve seen at the base of the furnace.
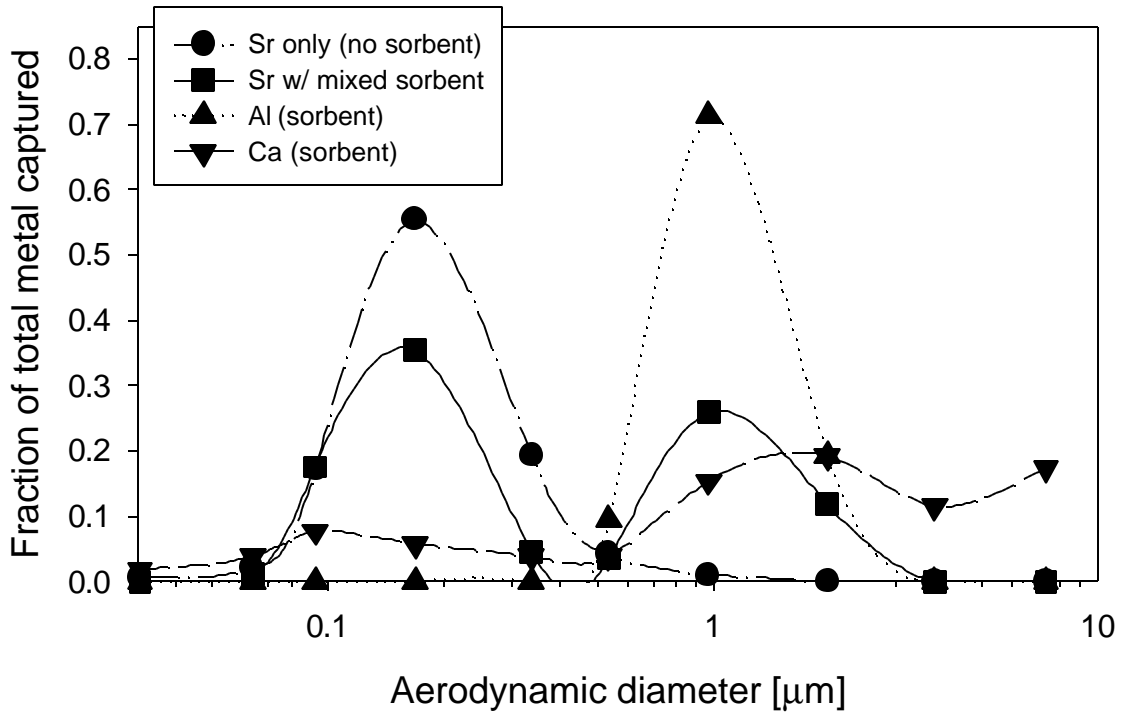
Figure 4.31 - Strontium and mixed sorbent, with chlorine
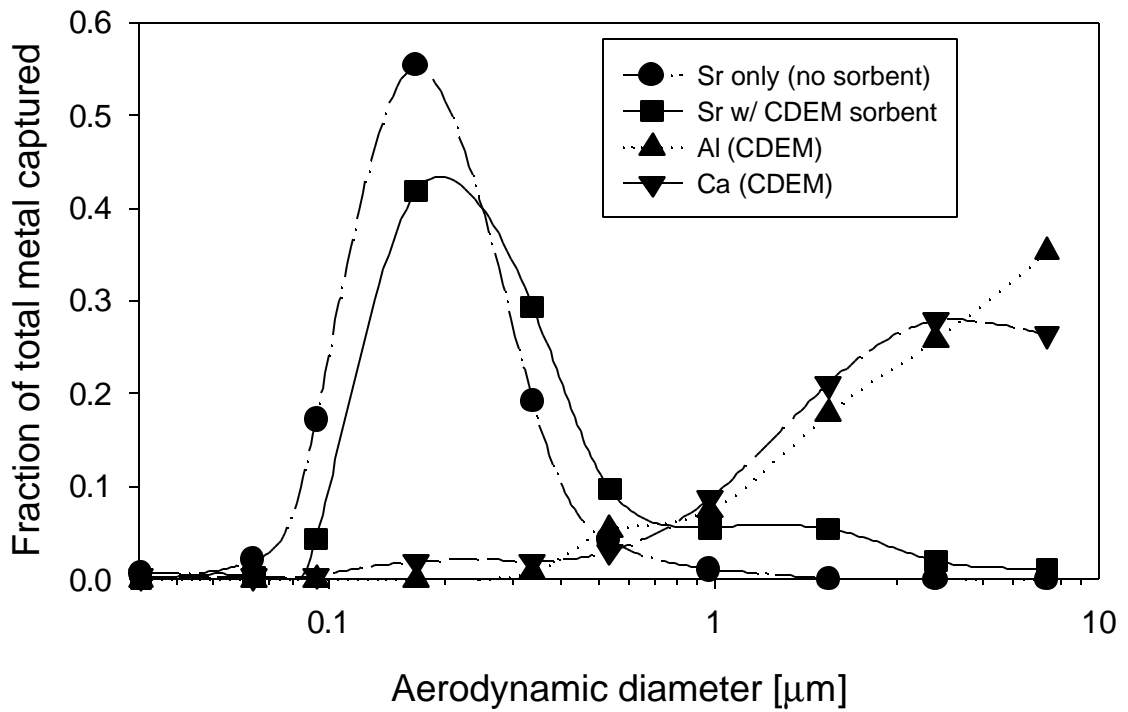
Figure 4.32 - Strontium and CDEM, with chlorine
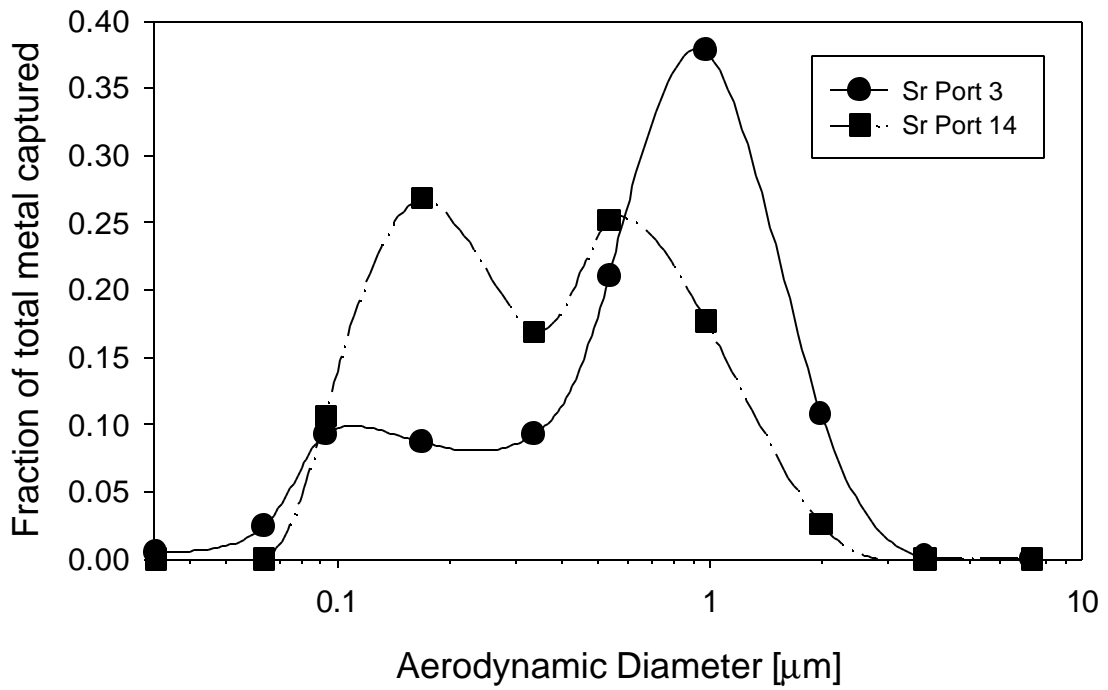
Figure 4.33 - Time evolution of strontium/sulfur particles
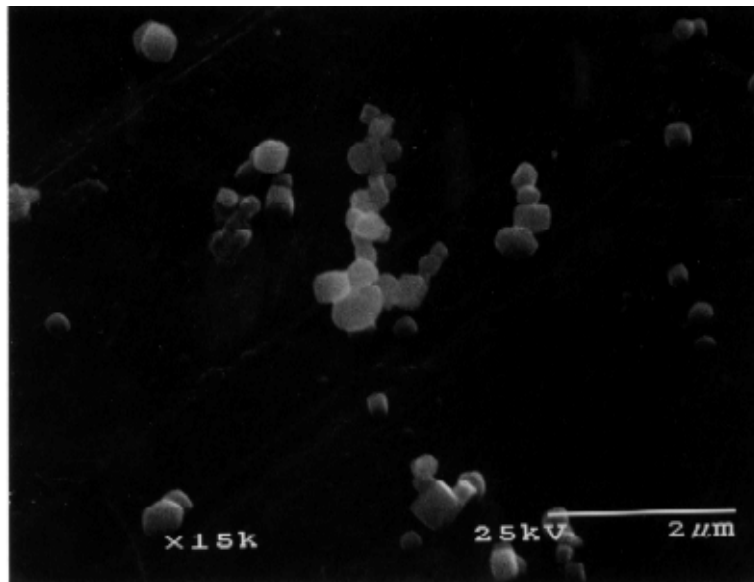
Figure 4.34 – SEM micrograph of strontium particles, with sulfur

A SEM image of the strontium/sulfur experiments is shown in Figure 4.34. The particles are similar in appearance to the strontium only particles seen in Figure 4.21. However, the particles in this case do show some signs of angularity. Some of the particles almost appear to be cubical, as if some degree of crystallization of the metal is occurring.

When kaolinite is added to the system, the curve in Figure 4.35 is the result. The strontium still shows the double peaked curve, but the peaks are slightly shifted. The peak on the smaller end of the curve is only slightly larger than 0.2 microns, and the peak on the upper end is shifted closer to one micron. This is most likely due to some physical interaction, similar to that exhibited when sulfur was not present in the system. Figure 4.36 is a micrograph of this condition. The smaller strontium particles are seen clinging to the large angular sorbent particles. This also supports the theory that the metal is not reacting with the sorbent, and is only being gathered by some physical mechanism.

The results of the strontium/lime/sulfur system, shown in Figure 4.37, are similar to those of the strontium/kaolinite sulfur system. The peak at the larger end of the size distribution is shifted to a slightly larger peak, near two microns. The other peak has not shifted in this case. Once again, this shift is probably due to some physical mechanism, and is not the result of reactive capture of the metal.

The results of the strontium and mixed sorbent tests with sulfur are shown in Figure 4.38. The strontium again shows the double peaked curve that is shifted slightly by the presence of the sorbent. The upper peak is formed near one micron, and the lower peak has not moved. This shift matches the shift seen by the kaolinite and the lime
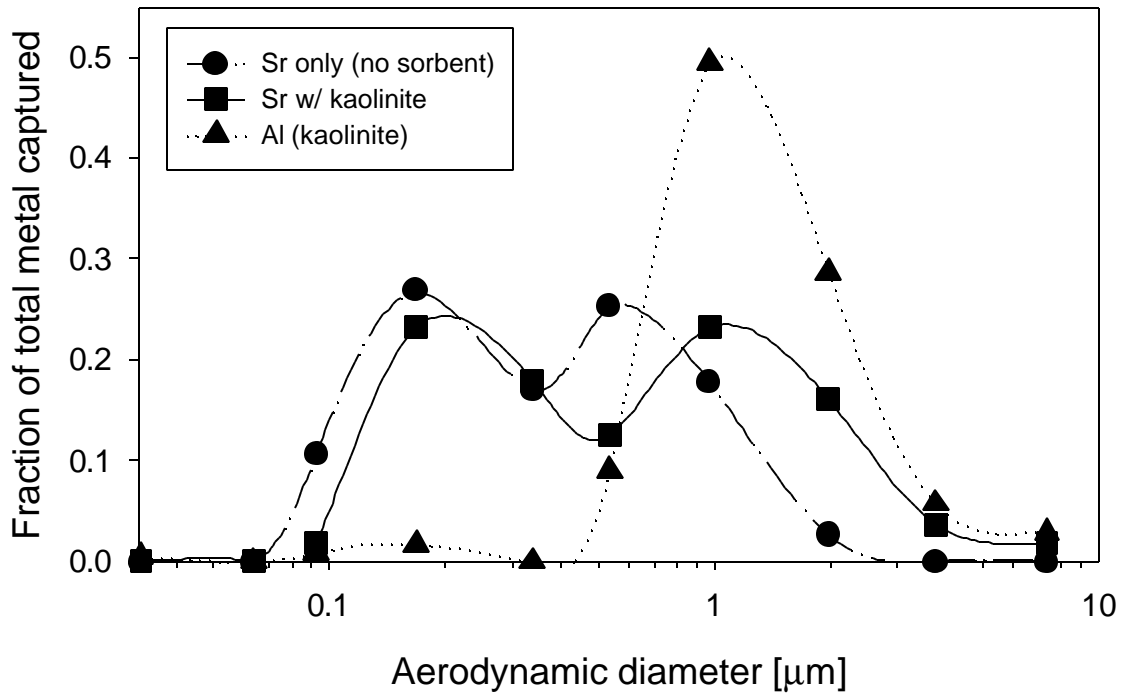
Figure 4.35 - Strontium and kaolinite, with sulfur
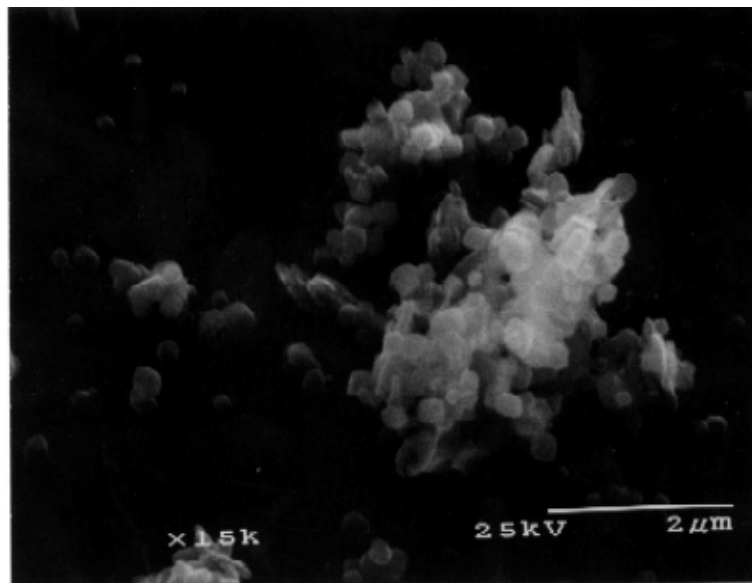
Figure 4.36 – SEM micrograph of strontium and kaolinite, with sulfur
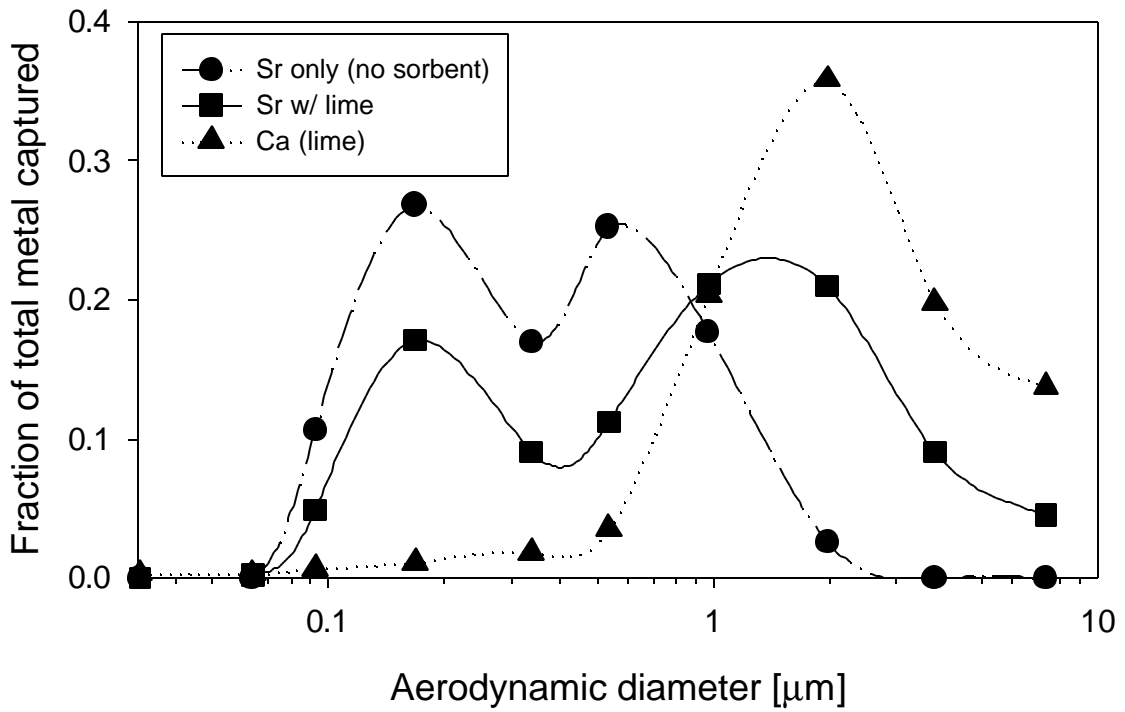
Figure 4.37 - Strontium and lime, with sulfur
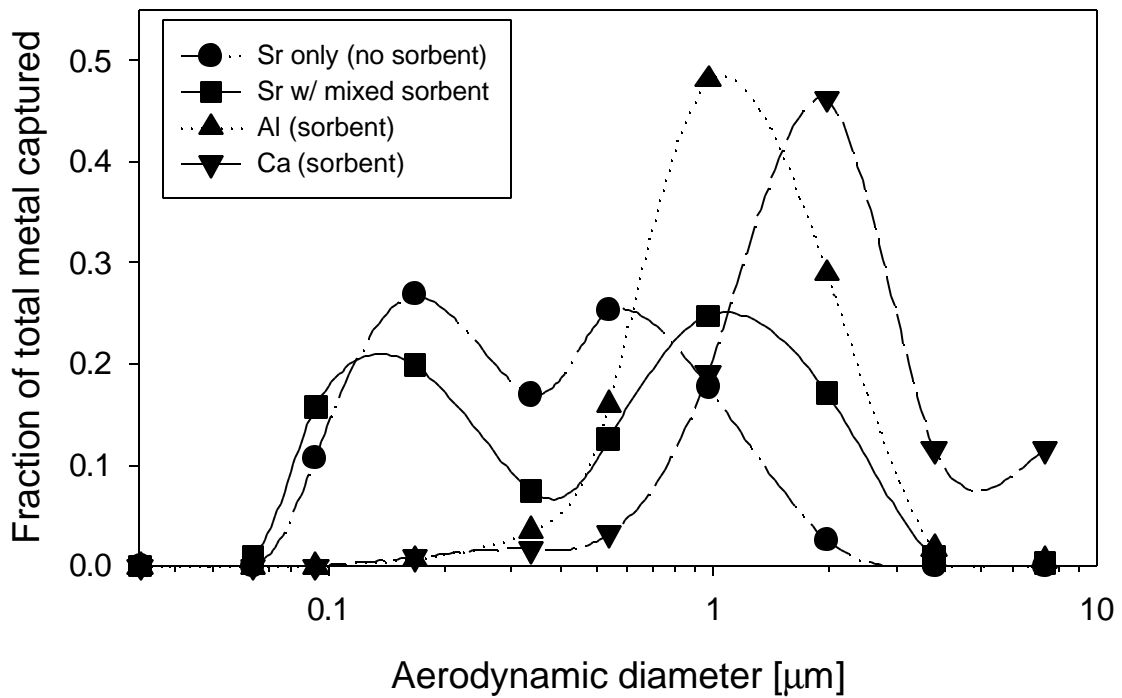
Figure 4.38 - Strontium and mixed sorbent, with sulfur

separately. The effect of the two sorbents on the strontium is not additive, which lends additional support to the idea that the shift in the curve is due to some physical mechanism, and not due to some form of chemical reaction.

Figure 4.39 shows the results of the strontium and sulfur system when CDEM is the added sorbent. There is a double peak formed, but it is different in shape than those seen previously. The larger of the two peaks is centered around one micron, and has more of a tail towards the larger particle sizes. The second peak is substantially smaller, and is centered near 0.1 microns. It is possible that the smaller strontium particles are reacting with the CDEM sorbent, which would explain the diminished lower peak. The larger strontium particles are probably only being shifted by the same physical mechanisms seen previously.
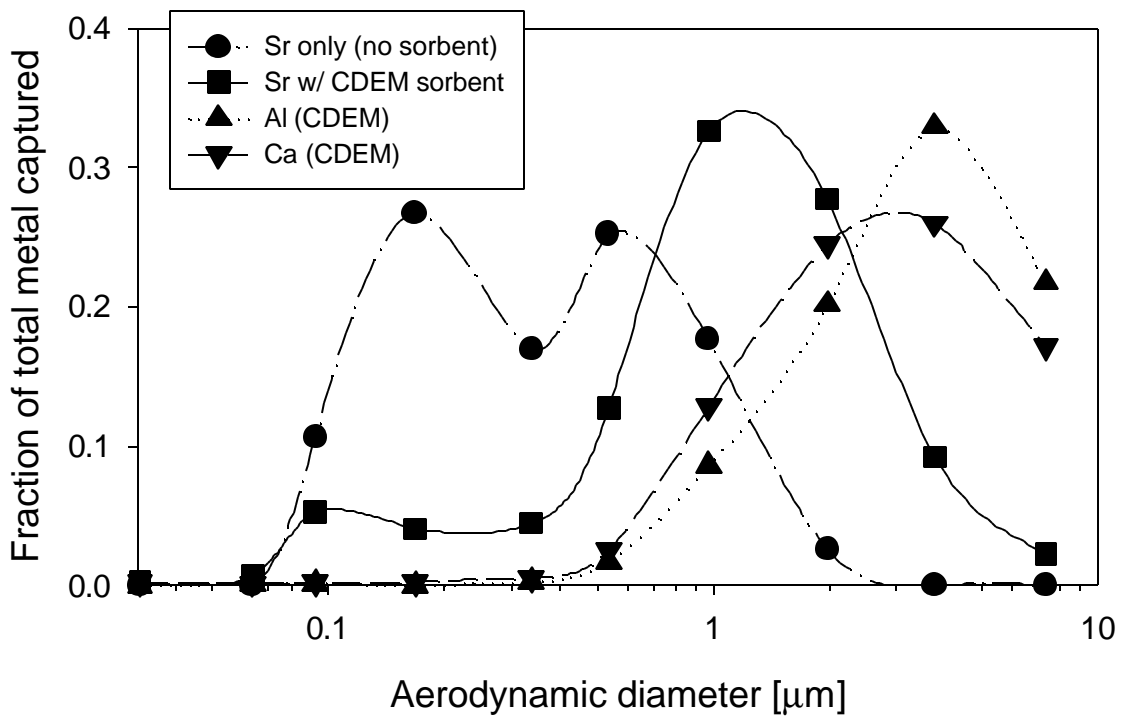
Figure 4.39 - Strontium and CDEM, with sulfur

Chapter 5

Conclusions

This work has explored the reactions of two metal species, cesium and strontium, with several different sorbents in a combustion system. The effects produced by adding other chemical species, chlorine and sulfur, were also explored. Several conclusions can be drawn from this work. A summary of the results is presented in Table 5.1.

Metal	Dopant	Sorbent	Interaction
Cesium	None	Kaolinite	Capture
Cesium	None	Lime	Slight Capture
Cesium	None	Mixed	Capture
Cesium	None	CDEM	Slight Capture
Cesium	Chlorine	Kaolinite	Some Capture
Cesium	Chlorine	Lime	None
Cesium	Chlorine	Mixed	Slight Capture
Cesium	Chlorine	CDEM	None
Cesium	Sulfur	Kaolinite	Capture
Cesium	Sulfur	Lime	Capture
Cesium	Sulfur	Mixed	Capture
Cesium	Sulfur	CDEM	Capture
Strontium	None	Kaolinite	Coagulation
Strontium	None	Lime	Coagulation
Strontium	None	Mixed	Coagulation
Strontium	None	CDEM	Coagulation
Strontium	Chlorine	Kaolinite	Capture
Strontium	Chlorine	Lime	None
Strontium	Chlorine	Mixed	Some Capture
Strontium	Chlorine	CDEM	None
Strontium	Sulfur	Kaolinite	Coagulation
Strontium	Sulfur	Lime	Coagulation
Strontium	Sulfur	Mixed	Coagulation
Strontium	Sulfur	CDEM	Possible Capture

Table 5.1 - Summary of Results

5.1 Cesium

In order to gain a fuller understanding of the possible metal transformation mechanisms that may be occurring, the data were analyzed according to Figures 5.1 through 5.4. For those cases where capture appeared to occur, the weight percent metal oxide on a plate was plotted against the aerodynamic diameter of the particle. Only those plates where sorbent was found were included on the plots. If the data shows a $1/d_p$ dependence, as indicated by a line with a slope of -1 on the logarithmic plots, the capture mechanism is surface reaction or pore diffusion controlled in the continuum regime ($d_p > 0.5$ μm). If the line on the logarithmic plots has a slope of -2, due to a $1/d_p^2$ dependence, then the mechanism is film diffusion controlled, probably an indication of rapid condensation. A thorough explanation of this methodology can be found elsewhere (Linak and Wendt 1993).

The data for cesium on kaolinite are shown in Figure 5.1 It appeared that kaolinite would capture cesium in all instances. The capture appeared to be reduced with the addition of chlorine or sulfur. The data in Figure 5.1 indicate there is a weak (less than $1/d_p$) diameter dependence for the cesium/kaolinite and the cesium/kaolinite/chlorine cases. This suggests that the mechanism is not surface reaction or pore diffusion controlled. The data for the cesium/kaolinite/sulfur case might indicate a $1/d_p$ dependence, although the data are too sparse to draw a definitive conclusion.

Figure 5.2 illustrates similar data for the cesium and lime cases. Lime appeared to capture cesium with no dopant and with sulfur present, but not with chlorine added. The cesium/lime case shows no diameter dependence. The cesium/lime/sulfur case does

90
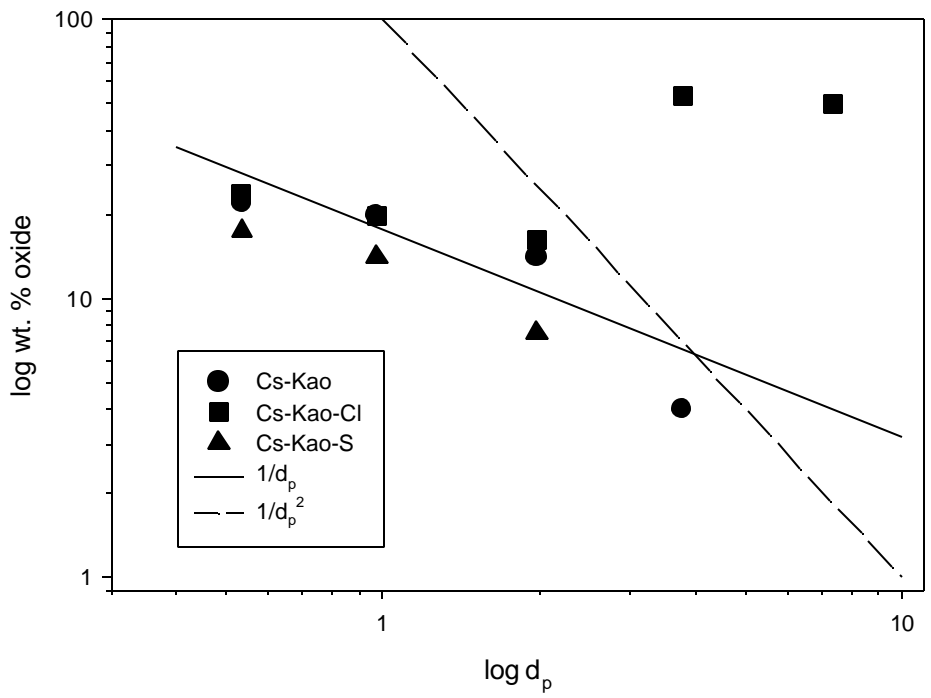
Figure 5.1 - Weight Percent Oxide versus Diameter
for Cesium on Kaolinite
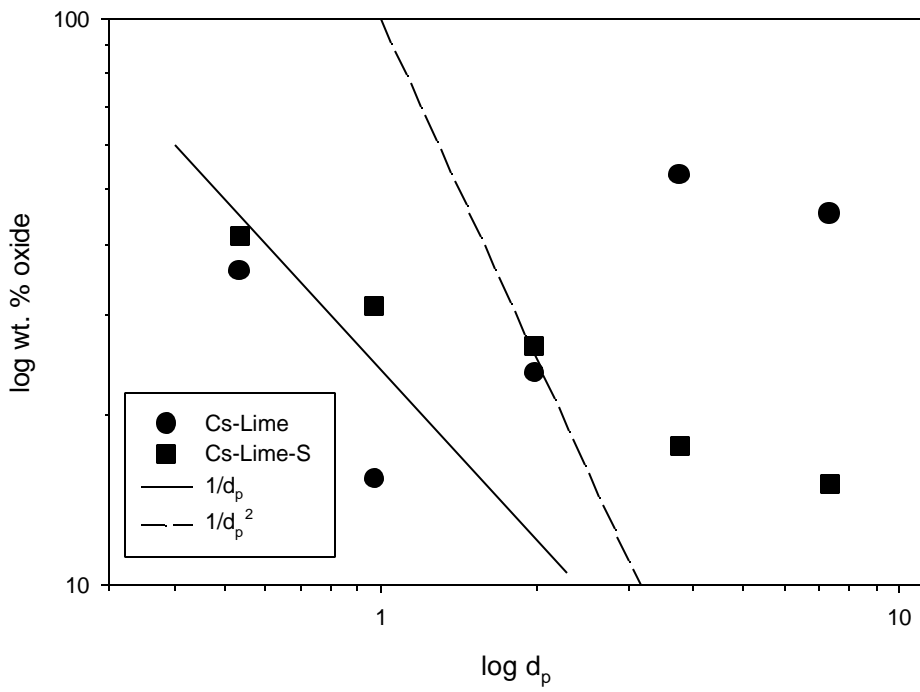
Figure 5.2 - Weight Percent Oxide versus Diameter
for Cesium on Lime

appear to have some diameter dependence. However, the slope of the line indicates a dependence on d_p less than $1/d_p$, the ramifications of which are not clear.

The data for the cesium and mixed sorbent is shown in Figure 5.3. Capture appeared to occur under all three dopant conditions. The cesium/mixed/sulfur case does not appear to have a clear diameter dependence. The cesium/mixed and cesium/mixed/chlorine cases appear to have a diameter dependence that is very close to $1/d_p$. This indicates that the mechanism is surface reaction or pore diffusion controlled.

For CDEM and cesium, capture only appeared to occur with the cesium/CDEM and cesium/CDEM/sulfur cases. These data are plotted in Figure 5.4. In both cases, there appears to be a $1/d_p$ dependence of the data. This dependence is very good for the cesium/CDEM/sulfur case. Again, this suggests that the mechanism is controlled by surface reaction or pore diffusion.

Thermodynamic calculations were performed prior to beginning experimental work. This was done in order to gain some understanding of the potential behavior of the metals in the combustion system. Cesium was predicted to behave as a semi-volatile metal. The dewpoint of the cesium with no dopants present was predicted to be fairly low. The addition of chlorine to the system was expected to push the dewpoint of cesium to a higher temperature, and the addition of sulfur was predicted to push the dewpoint even higher. The experimental evidence suggests that the thermodynamic calculations were fairly accurate. Cesium alone exhibited a fairly low dewpoint, forming a sub-micron fume in the probe when extracted from the bottom of the furnace. Chlorine did appear to increase the dewpoint of the metal. The addition of sulfur appeared to push the
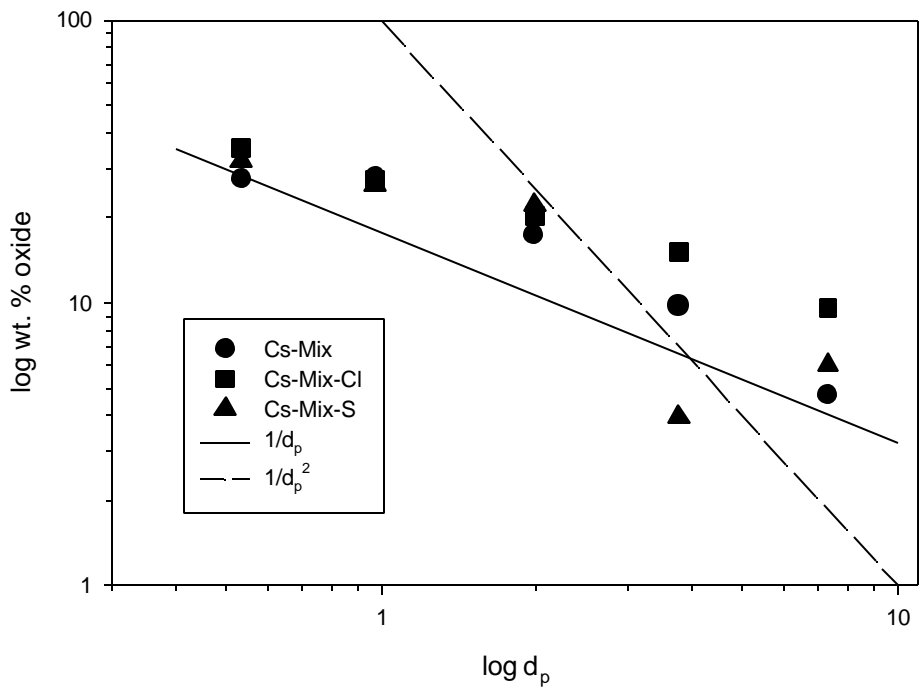
Figure 5.3 - Weight Percent Oxide versus Diameter
for Cesium on Mixed Sorbent
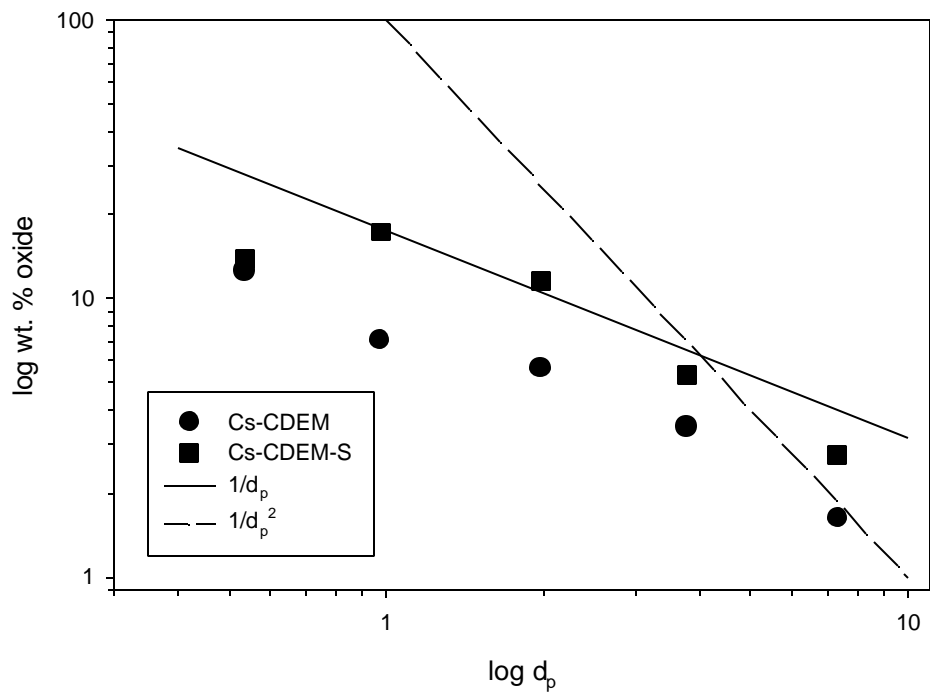
Figure 5.4 - Weight Percent Oxide versus Diameter
for Cesium on CDEM

dewpoint even higher, which can be inferred from the change in the curves in Figure 4.11. Overall, the thermodynamic predictions for cesium appeared to match the experimental data fairly well.

Earlier in this work, sodium was introduced as an analogue to cesium. Little work had been done with cesium up to this point. Sodium is in the same period of the periodic table as cesium, and there has been some work that has examined the capture of sodium by sorbents (Mwabe and Wendt 1996). Therefore, in order to gain some idea of the possible behavior of cesium, the existing sodium results were examined.

The thermodynamic calculations showed some difference between the two metals. Sodium has a higher dewpoint when no dopant gases are present. There is some difference in the speciation of the two metals, particularly in the solid phase, which may account for the difference in the dewpoint temperatures.. With the dopants added, the cesium and sodium behavior was very similar, both in terms of speciation and dewpoint temperatures. The thermodynamic database for sodium is slightly larger, so some of the variation may be due to deficiencies in the cesium data.

The experimental results also appear to match fairly well. Cesium, like sodium appears to be reactively captured by kaolinite. When chlorine is added to the furnace, the capture of both metals is reduced. For sodium, this is due to the reduction in gas phase NaOH due to the presence of the chlorine. This is slightly offset by the decreased dewpoint temperature. For cesium, not only is the gas phase CsOH reduced, but the dewpoint is also increased, which reduces the time for capture. With the addition of

sulfur, capture is reduced for sodium due to the increased dewpoint of the metal. This also appears to be the case with cesium.

It appears that kaolinite is the best choice of sorbent to capture cesium. It has the highest capture capacity over all conditions explored. The lime only captured cesium when sulfur was present, and then only moderately. The CDEM sorbent worked well when sulfur was added, but performed poorly in the other conditions.

5.2 Strontium

The thermodynamic calculations that were performed for strontium appeared to match the experimental results fairly well. When no dopant was present, the strontium did not vaporize in the furnace, forming residual particles, as was predicted. When chlorine was added, the strontium did vaporize and was able to react with kaolinite, which was suggested by the thermodynamic results. However, when sulfur was added as the dopant, the results did not match as closely. The thermodynamic calculations predicted that sulfur would have no effect on the strontium dewpoint, and it would form the residual particles as were seen in the no dopant case. The experimental results suggest that there is some vaporization of the strontium occurring, as seen in Figure 4.33. This discrepancy is most likely due to an important missing specie in the thermodynamic database.

There were only a few cases where capture of strontium appeared to occur. These cases are illustrated in Figure 5.5. Strontium did appear to be captured by kaolinite in the presence of chlorine. The capture that occurred in the strontium/mixed/chlorine case is
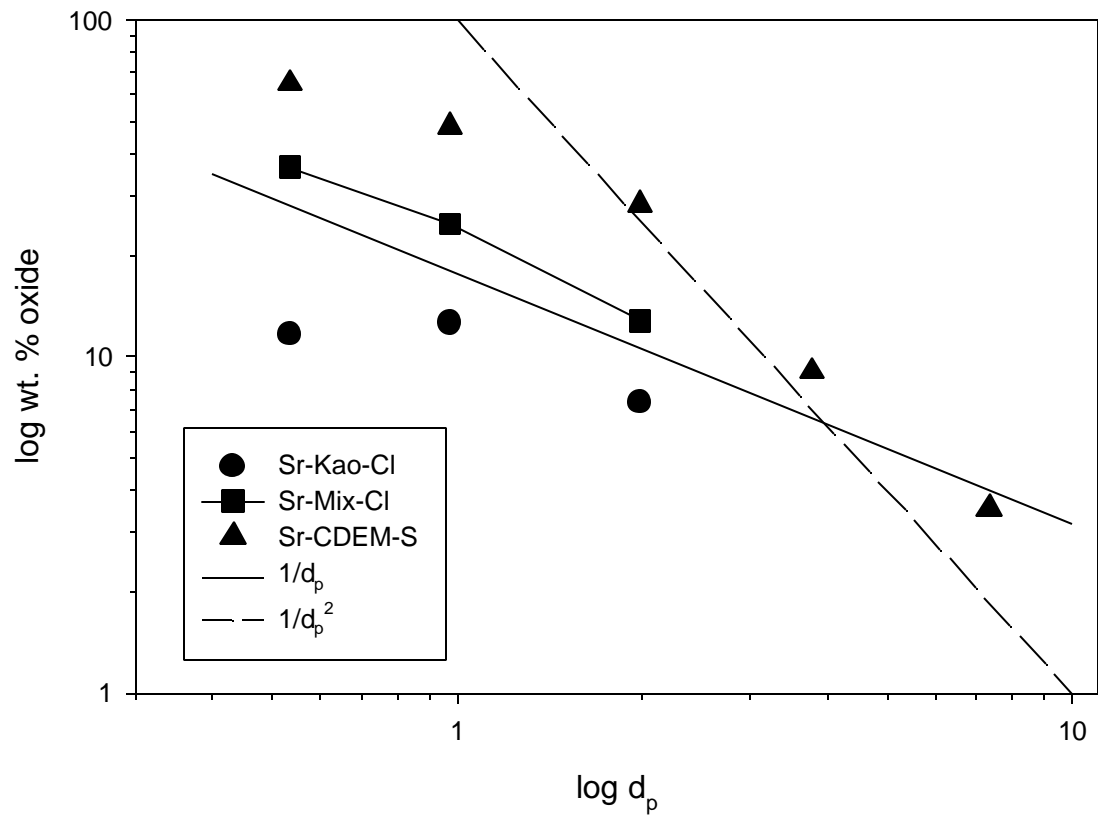
Figure 5.5 - Weight Percent Oxide versus Diameter
for Strontium Capture Cases

most likely due to the kaolinite, with no contribution from the lime. There may be some capture in the strontium/CDEM/sulfur case, so its data were included here. There may be a strong contribution from a physical mechanism in this case, however. The strontium/kaolinite/chlorine and strontium/CDEM/sulfur cases do not appear to have any diameter dependence. The strontium/mixed/chlorine case may have a $1/d_p$ dependence. This result may be skewed, however, due to the presence of the non-reactive lime.

In several cases with the strontium, it appears that coagulation may play a role in the final metal distribution. These include the cases where no dopant was used, and where the dopant was sulfur. The thermodynamic predictions and the SEM images support this conclusion. In order to better understand the mechanisms that are important, further aerosol modeling and experimental work may need to be performed.

Strontium and nickel were compared earlier to gain some idea of the behavior of strontium in the combustion system. Very little work had been done on strontium, but there had been some work using nickel (Linak et al. 1994; Linak et al. 1995; Linak and Wendt 1998).

The thermodynamic calculations performed for strontium for this work will be compared to the nickel calculations in Linak and Wendt (1998). There is fairly good agreement between the two metals. Both have a high dewpoint with no dopant gases present. When chlorine is introduced to the system, the dewpoints of both nickel and strontium drop considerably. This reduction in dewpoint may enable the capture of these metals in a real system. When sulfur is added to the system, there is no change in the dewpoint from the initial values. However, experimental evidence suggests that there is

some volatilization of strontium in the presence of sulfur that was not identified in the thermodynamic calculations. This is probably due to the lack of an important specie in the thermodynamic data base. For nickel, no experiments were performed with the addition of sulfur. Therefore, it is possible that nickel may exhibit the same behavior as strontium.

Kaolinite may be the best choice of sorbent for strontium capture. This reaction only occurs when chlorine is present in the system. Lime remains non-reactive in all cases, and the mixed sorbent only exhibits capture when chlorine is present. There may be some reaction with the CDEM sorbent, but only when sulfur is present, and only to a small extent.

5.3 Areas for Future Work

Based on this work, several areas for future exploration suggest themselves. First, now that particular capture situations have been identified, further experiments can be performed to determine the kinetics of these reactions. In particular, the cesium reactions with kaolinite, both with and without dopants, and the strontium/chlorine/kaolinite reactions should be examined further. Second, the partitioning of the metals should be determined based on the form the metal takes in the feed. The final partitioning could depend upon whether the metals start as aqueous solutions, chelated complexes, or organo-metallic species bound in the fuel. Third, leaching tests can be performed with identified capture situations to determine whether the metals are bound in an insoluble form in the sorbent. This could have an impact on the acceptance of this methodology as

a form of treatment technology. Fourth, aerosol modeling, using an algorithm like

MAEROS, should be done in order to more fully understand the behavior of strontium

with the sorbents. In particular, the issue of whether coagulation is a realistic possibility

to explain the shift in the strontium curves. Finally, it appears that the dopant gases may

react with the CDEM sorbent. Chlorine appears to destroy the capture capability of the

sorbent, while sulfur may enhance this ability in some situations. These relationships

warrant further exploration.

Appendix A.1 : CEA INPUT DATA

Cesium Species

```
Cs
 2 L 3/93 CS  1.00  .00   .00   .00   .00 0   132.90540   76500.002
    200.000  1000.000 5   .0  1.0   2.0   3.0   4.0   5.0   .0    .0
  2.50004600D+00 -4.66833400D-07  1.68005100D-09 -2.48218000D-12
                 1.27712200D-15  8.45540400D+03  6.87573500D+00
   1000.000  6000.000 5   .0  1.0   2.0   3.0   4.0   5.0   .0    .0
  2.82023300D+00 -3.34840300D-04 -9.82915700D-08  1.27564400D-10
                -1.46119300D-14  8.30639400D+03  5.00894000D+00


Cs+
 2 J12/83 CS  1.00E  -1.00  .00   .00   .00 0   132.90490  458401.967
    298.150  1000.000 5   .0  1.0   2.0   3.0   4.0   5.0   .0    .0
  2.50000000D+00  0.00000000D+00  0.00000000D+00  0.00000000D+00
                 0.00000000D+00  5.43874000D+04  6.18275700D+00
   1000.000  6000.000 5   .0  1.0   2.0   3.0   4.0   5.0   .0    .0
  2.50000000D+00  0.00000000D+00  0.00000000D+00  0.00000000D+00
                 0.00000000D+00  5.43874000D+04  6.18275700D+00


CsCL
 2 J 6/68 CS  1.00CL  1.00  .00   .00   .00 0   168.35810  -240166.783
    300.000  1000.000 5   .0  1.0   2.0   3.0   4.0   5.0   .0    .0
  4.18230300D+00  1.37595500D-03 -2.05869300D-06  1.48364700D-09
                -3.97645500D-13 -3.01779300D+04  6.63848800D+00
   1000.000  5000.000 5   .0  1.0   2.0   3.0   4.0   5.0   .0    .0
  4.47984600D+00  1.09491600D-04 -3.99899100D-09  2.06420000D-13
                 2.21846400D-17 -3.02358100D+04  5.21731700D+00


CsO
 2 J12/68 CS  1.00O  1.00  .00   .00   .00 0   148.90480   62763.052
    300.000  1000.000 5   .0  1.0   2.0   3.0   4.0   5.0   .0    .0
  3.98574200D+00  2.12792500D-03 -3.21702600D-06  2.27642900D-09
                -5.97219800D-13  6.28989400D+03  7.51602300D+00
   1000.000  5000.000 5   .0  1.0   2.0   3.0   4.0   5.0   .0    .0
  4.46602800D+00  1.15632300D-04 -5.99891900D-09  1.31767000D-13
                 5.76397500D-17  6.19503100D+03  5.21454900D+00


CsOH
 2 J 6/71 CS  1.00O  1.00H  1.00  .00   .00 0   149.91280  -259409.386
    300.000  1000.000 5   .0  1.0   2.0   3.0   4.0   5.0   .0    .0
  4.54860000D+00  7.96123300D-03 -1.33265000D-05  1.03142300D-08
                -2.89737800D-12 -3.28108900D+04  2.86188000D+00
   1000.000  5000.000 5   .0  1.0   2.0   3.0   4.0   5.0   .0    .0
  5.70056500D+00  1.18203800D-03 -3.19390900D-07  3.86429200D-11
                -1.66356400D-15 -3.29192000D+04 -2.11870000D+00


CsOH+
 2 J12/71 CS  1.00O  1.00H  1.00E  -1.00  .00 0   149.91220  443519.577
    300.000  1000.000 5   .0  1.0   2.0   3.0   4.0   5.0   .0    .0
  4.84871600D+00  6.89083500D-03 -1.18393300D-05  9.43353800D-09
```

```
                              -2.72226900D-12  5.16781700D+04  3.08484800D+00
    1000.000  5000.000 5    .0  1.0  2.0  3.0  4.0  5.0    .0    .0
   5.72925600D+00  1.15713200D-03 -3.10444300D-07  3.70962900D-11
                              -1.55094600D-15  5.16264800D+04 -5.76482200D-01


Cs2
 2 J12/83 CS  2.00   .00   .00   .00   .00 0  265.81090  107377.157
     200.000  1000.000 5    .0  1.0  2.0  3.0  4.0  5.0    .0    .0
   4.74588200D+00 -2.63862800D-03  1.14139300D-05 -1.60430500D-08
                   6.56112300D-12  1.15444900D+04  7.60679300D+00
    1000.000  6000.000 5    .0  1.0  2.0  3.0  4.0  5.0    .0    .0
   6.86645200D+00 -3.99014300D-03  1.31948100D-06 -1.63413200D-10
                   6.88125900D-15  1.08054300D+04 -4.29749500D+00


Cs2CL2
 2 J 6/68 CS  2.00CL  2.00   .00   .00   .00 0  336.71620  -659831.365
     300.000  1000.000 5    .0  1.0  2.0  3.0  4.0  5.0    .0    .0
   9.29526400D+00  2.85056000D-03 -4.55760200D-06  3.25577300D-09
                  -8.60673600D-13 -8.22228600D+04 -7.51835300D+00
    1000.000  5000.000 5    .0  1.0  2.0  3.0  4.0  5.0    .0    .0
   9.94243700D+00  6.26593000D-05 -2.63311000D-08  4.89121400D-12
                  -3.35541500D-16 -8.23458500D+04 -1.05980600D+01


Cs2O
 2 J12/68 CS  2.00O  1.00   .00   .00   .00 0  281.81030  -92046.781
     300.000  1000.000 5    .0  1.0  2.0  3.0  4.0  5.0    .0    .0
   5.75536400D+00  4.91160700D-03 -7.70725200D-06  5.41569600D-09
                  -1.40809000D-12 -1.29468300D+04  4.30015500D+00
    1000.000  5000.000 5    .0  1.0  2.0  3.0  4.0  5.0    .0    .0
   6.89794700D+00  1.01651000D-04 -3.80620600D-08  6.14663900D-12
                  -3.57582200D-16 -1.31699900D+04 -1.16591700D+00


Cs2O2H2
 2 J 6/71 CS  2.00O  2.00H  2.00   .00   .00 0  299.82550  -687868.558
     300.000  1000.000 5    .0  1.0  2.0  3.0  4.0  5.0    .0    .0
   7.52281900D+00  7.90783800D-03  3.54303000D-06 -1.04563300D-08
                   4.80140300D-12 -8.53384100D+04 -1.90663300D+00
    1000.000  5000.000 5    .0  1.0  2.0  3.0  4.0  5.0    .0    .0
   9.58093600D+00  5.32605100D-03 -1.87805400D-06  3.09259300D-10
                  -1.94295300D-14 -8.60258400D+04 -1.32145900D+01


Cs2SO4
 2 J 6/79 CS  2.00S  1.00O  4.00   .00   .00 0  361.87450  -1122581.073
     300.000  1000.000 5    .0  1.0  2.0  3.0  4.0  5.0    .0    .0
   4.29653800D+00  4.48543000D-02 -6.09879200D-05  4.05163900D-08
                  -1.06735000D-11 -1.37825600D+05  1.34096400D+01
    1000.000  5000.000 5    .0  1.0  2.0  3.0  4.0  5.0    .0    .0
   1.54190500D+01  4.05276500D-03 -1.79103400D-06  3.50246500D-10
                  -2.52157400D-14 -1.40367800D+05 -4.14921800D+01


Cs(cr)
 1 CODA89 CS  1.00   .00   .00   .00   .00 1  132.90540       .000
     100.000   301.590 5    .0  1.0  2.0  3.0  4.0  5.0    .0    .0
   3.31157200D+00 -9.67974800D-03  1.19926600D-04 -5.20608100D-07
```

```
                        8.33415900D-10  -9.80844400D+02  -8.10866800D+00

Cs(L)
 2 CODA89 CS  1.00  .00   .00   .00   .00 2  132.90540        .000
    301.590  1000.000 5   .0  1.0  2.0  3.0  4.0  5.0   .0   .0
  3.20358100D+00  6.53560200D-03 -1.88609300D-05  1.88262500D-08
                 -6.10371800D-12 -8.61341900D+02 -8.43100400D+00
   1000.000  2000.000 5   .0  1.0  2.0  3.0  4.0  5.0   .0   .0
  5.11512900D+00 -3.83970300D-03  2.01555300D-06  3.64202600D-10
                 -5.43974500D-14 -1.13841800D+03 -1.70567600D+01

CsCL(a)
 1 J 6/68 CS  1.00CL  1.00  .00   .00   .00 1  168.35810  -442845.686
    300.000   743.000 5   .0  1.0  2.0  3.0  4.0  5.0   .0   .0
  5.54534000D+00  2.38058300D-03  8.35703300D-07 -9.95716400D-10
                  3.80548000D-13 -5.50265400D+04 -2.01642600D+01

CsCL(b)
 1 J 6/68 CS  1.00CL  1.00  .00   .00   .00 2  168.35810        .000
    743.000   918.000 5   .0  1.0  2.0  3.0  4.0  5.0   .0   .0
  8.16107400D+00 -1.76235700D-03 -2.25085200D-07  3.93073200D-09
                 -2.34523400D-12 -5.54804300D+04 -3.39413900D+01

CsCL(L)
 2 J 6/68 CS  1.00CL  1.00  .00   .00   .00 3  168.35810        .000
    918.000  1000.000 5   .0  1.0  2.0  3.0  4.0  5.0   .0   .0
  9.30974500D+00  0.00000000D+00  0.00000000D+00  0.00000000D+00
                  0.00000000D+00 -5.50311600D+04 -4.08101300D+01
   1000.000  5000.000 5   .0  1.0  2.0  3.0  4.0  5.0   .0   .0
  9.30974500D+00  0.00000000D+00  0.00000000D+00  0.00000000D+00
                  0.00000000D+00 -5.50311600D+04 -4.08101300D+01

CsOH(a)
 1 J 6/71 CS  1.00O  1.00H  1.00   .00   .00 1  149.91280  -416725.985
    298.150   410.000 5   .0  1.0  2.0  3.0  4.0  5.0   .0   .0
  5.88946100D+00  6.13190000D-03  8.60764000D-06 -1.20614700D-08
                  0.00000000D+00 -5.22010400D+04 -2.37840100D+01

CsOH(b)
 1 J 6/71 CS  1.00O  1.00H  1.00   .00   .00 2  149.91280  -416725.985
    410.000   493.000 5   .0  1.0  2.0  3.0  4.0  5.0   .0   .0
  4.92104600D+00  1.00655100D-02  0.00000000D+00  0.00000000D+00
                  0.00000000D+00 -5.18660700D+04 -1.87438100D+01

CsOH(c)
 1 J 6/71 CS  1.00O  1.00H  1.00   .00   .00 3  149.91280  -416725.985
    493.000   588.000 5   .0  1.0  2.0  3.0  4.0  5.0   .0   .0
  1.00644500D+01  0.00000000D+00  0.00000000D+00  0.00000000D+00
                  0.00000000D+00 -5.24488600D+04 -4.41931500D+01

CsOH(L)
 2 J 6/71 CS  1.00O  1.00H  1.00   .00   .00 4  149.91280  -416725.985
    588.000  1000.000 5   .0  1.0  2.0  3.0  4.0  5.0   .0   .0
  9.81284300D+00  0.00000000D+00  0.00000000D+00  0.00000000D+00
```

```
                          0.00000000D+00  -5.17524700D+04 -4.16559600D+01
   1000.000  6000.000 5    .0  1.0  2.0  3.0  4.0  5.0    .0    .0
 9.81284300D+00  0.00000000D+00  0.00000000D+00  0.00000000D+00
                          0.00000000D+00  -5.17524700D+04 -4.16559600D+01


Cs2SO4(II)
 1 J 6/79 CS  2.00S  1.00O  4.00  .00  .00 1 361.87450  -1442695.528
    300.000   940.000 5    .0  1.0  2.0  3.0  4.0  5.0    .0    .0
-2.97893100D+00  1.26508800D-01 -2.95532100D-04  3.32073100D-07
                         -1.31049900D-10  -1.76233500D+05  1.51857500D+01


Cs2SO4(I)
 2 J 6/79 CS  2.00S  1.00O  4.00  .00  .00 2 361.87450       .000
    940.000  1000.000 5    .0  1.0  2.0  3.0  4.0  5.0    .0    .0
 4.73498300D+00  1.86196000D-02  0.00000000D+00  0.00000000D+00
                          0.00000000D+00  -1.71541400D+05  1.37370500D-01
   1000.000  1278.000 5    .0  1.0  2.0  3.0  4.0  5.0    .0    .0
-2.72327200D-02  3.13540400D-02 -1.13005300D-05  3.32831100D-09
                          0.00000000D+00  -1.70211600D+05  2.48399900D+01


Cs2SO4(L)
 1 J 6/79 CS  2.00S  1.00O  4.00  .00  .00 3 361.87450       .000
   1278.000  5000.000 5    .0  1.0  2.0  3.0  4.0  5.0    .0    .0
 2.48592000D+01  0.00000000D+00  0.00000000D+00  0.00000000D+00
                          0.00000000D+00  -1.77762000D+05 -1.16657400D+02
```

Sodium Species

```
Na
 2 L 4/93 NA  1.00  .00  .00  .00  .00 0  22.98977   107299.999
    200.000  1000.000 5    .0  1.0  2.0  3.0  4.0  5.0    .0    .0
 2.50000000D+00 -4.98492300D-10  1.76034100D-12 -2.54461600D-15
                          1.27603900D-18  1.21597800D+04  4.24402800D+00
   1000.000  6000.000 5    .0  1.0  2.0  3.0  4.0  5.0    .0    .0
 2.39858900D+00  2.15467000D-04 -1.49077600D-07  3.66821800D-11
                         -1.66036000D-15  1.21943100D+04  4.79181100D+00


Na+
 2 J12/83 NA  1.00E  -1.00  .00  .00  .00 0  22.98922   609343.000
    298.150  1000.000 5    .0  1.0  2.0  3.0  4.0  5.0    .0    .0
 2.50000000D+00  0.00000000D+00  0.00000000D+00  0.00000000D+00
                          0.00000000D+00  7.25413300D+04  3.55084500D+00
   1000.000  6000.000 5    .0  1.0  2.0  3.0  4.0  5.0    .0    .0
 2.50000000D+00  0.00000000D+00  0.00000000D+00  0.00000000D+00
                          0.00000000D+00  7.25413300D+04  3.55084500D+00


NaCN
 2 J3/66  NA  1.00C  1.00N  1.00  .00  .00 0  49.00751   94271.660
    300.000  1000.000 5    .0  1.0  2.0  3.0  4.0  5.0    .0    .0
 4.97725600D+00  5.32259400D-03 -7.55524400D-06  6.18398000D-09
                         -2.00714300D-12  9.67314900D+03 -3.88207300D-01
   1000.000  5000.000 5    .0  1.0  2.0  3.0  4.0  5.0    .0    .0
 5.79897700D+00  1.68279500D-03 -6.74379200D-07  1.22345000D-10
```

```
                         -8.29660900D-15  9.49334500D+03 -4.34426000D+00

     NaCL
      2 J12/64 NA  1.00CL  1.00   .00   .00   .00 0  58.44247  -181412.215
         300.000  1000.000 5    .0  1.0  2.0  3.0  4.0  5.0    .0    .0
       3.70322900D+00  3.19976100D-03 -4.89245000D-06  3.46392200D-09
                        -9.13575200D-13 -2.30282800D+04  5.77347900D+00
        1000.000  5000.000 5    .0  1.0  2.0  3.0  4.0  5.0    .0    .0
       4.42829300D+00  1.56272400D-04 -2.81083800D-08  4.71635700D-12
                        -2.88325600D-16 -2.31709000D+04  2.30097500D+00

     NaH
      2 J 3/63 NA  1.00H  1.00   .00   .00   .00 0  23.99771   124261.017
         300.000  1000.000 5    .0  1.0  2.0  3.0  4.0  5.0    .0    .0
       3.12039500D+00  1.39962200D-03  2.21412300D-06 -3.99507900D-09
                         1.67261800D-12  1.39400700D+04  4.39456100D+00
        1000.000  5000.000 5    .0  1.0  2.0  3.0  4.0  5.0    .0    .0
       3.81305800D+00  8.56438000D-04 -3.12268200D-07  5.85024700D-11
                        -4.05139200D-15  1.36830600D+04  4.84168100D-01

     NaO
      2 J12/67 NA  1.00O  1.00   .00   .00   .00 0  38.98917    83684.379
         300.000  1000.000 5    .0  1.0  2.0  3.0  4.0  5.0    .0    .0
       3.44210100D+00  4.16172400D-03 -6.31183700D-06  4.44792000D-09
                        -1.17204900D-12  8.90114700D+03  6.95032500D+00
        1000.000  5000.000 5    .0  1.0  2.0  3.0  4.0  5.0    .0    .0
       4.39241600D+00  2.13205700D-04 -4.52206000D-08  7.97518200D-12
                        -5.17359900D-16  8.71189900D+03  2.38809000D+00

     NaO-
      2 J12/67 NA  1.00O  1.00E  1.00   .00   .00 0  38.98972  -121336.721
         300.000  1000.000 5    .0  1.0  2.0  3.0  4.0  5.0    .0    .0
       3.41868500D+00  4.21173800D-03 -6.31046400D-06  4.38735100D-09
                        -1.13726400D-12 -1.57522300D+04  5.66855600D+00
        1000.000  5000.000 5    .0  1.0  2.0  3.0  4.0  5.0    .0    .0
       4.38680100D+00  2.23446700D-04 -4.82124700D-08  8.57208700D-12
                        -5.60943300D-16 -1.59462700D+04  1.01363500D+00

     NaOH
      2 J12/70 NA  1.00O  1.00H  1.00   .00   .00 0  39.99711  -197755.798
         300.000  1000.000 5    .0  1.0  2.0  3.0  4.0  5.0    .0    .0
       4.00503900D+00  9.99220500D-03 -1.64342100D-05  1.24765900D-08
                        -3.46376100D-12 -2.53004700D+04  2.30643600D+00
        1000.000  5000.000 5    .0  1.0  2.0  3.0  4.0  5.0    .0    .0
       5.64693800D+00  1.22273900D-03 -3.32710400D-07  4.06663000D-11
                        -1.77906900D-15 -2.55082200D+04 -5.03687500D+00

     NaOH+
      2 J12/71 NA  1.00O  1.00H  1.00E  -1.00   .00 0  39.99656   677830.533
         300.000  1000.000 5    .0  1.0  2.0  3.0  4.0  5.0    .0    .0
       4.35052100D+00  8.74650100D-03 -1.46426700D-05  1.13515000D-08
                        -3.21100300D-12  7.99464000D+04  2.34484100D+00
        1000.000  5000.000 5    .0  1.0  2.0  3.0  4.0  5.0    .0    .0
       5.66885500D+00  1.22539300D-03 -3.40295600D-07  4.28532700D-11
```

```
                              -1.95937600D-15   7.98065200D+04 -3.42468300D+00

          Na2
           2 J12/83 NA   2.00   .00   .00   .00   .00 0   45.97954    142043.093
              200.000   1000.000 5   .0  1.0  2.0  3.0  4.0  5.0    .0    .0
           4.11568300D+00   2.52904000D-03 -5.62168600D-06   6.46171600D-09
                            -2.75128300D-12   1.57824600D+04   3.68672400D+00
            1000.000   6000.000 5   .0  1.0  2.0  3.0  4.0  5.0    .0    .0
           5.96201900D+00  -1.06049500D-03 -4.39279800D-07   3.05174800D-10
                            -3.39488800D-14   1.49990900D+04 -6.69613600D+00

          Na2C2N2
           2 J 3/66 NA   2.00C   2.00N   2.00   .00   .00 0   98.01502   -8776.980
              300.000   1000.000 5   .0  1.0  2.0  3.0  4.0  5.0    .0    .0
           1.03680300D+01   1.33485500D-02 -1.99103300D-05   1.61564800D-08
                            -5.12645500D-12  -4.59375300D+03 -2.05494400D+01
            1000.000   5000.000 5   .0  1.0  2.0  3.0  4.0  5.0    .0    .0
           1.25727900D+01   3.39473200D-03 -1.36169300D-06   2.47209600D-10
                            -1.67732500D-14  -5.04910200D+03 -3.10742000D+01

          Na2CL2
           2 J12/64 NA   2.00CL   2.00   .00   .00   .00 0  116.88490  -566077.366
              300.000   1000.000 5   .0  1.0  2.0  3.0  4.0  5.0    .0    .0
           7.95839500D+00   8.39623600D-03 -1.38171200D-05   1.02776700D-08
                            -2.86449900D-12  -7.07259400D+04 -8.17532400D+00
            1000.000   5000.000 5   .0  1.0  2.0  3.0  4.0  5.0    .0    .0
           9.82620000D+00   1.91847600D-04 -8.16087500D-08   1.52981800D-11
                            -1.05589900D-15  -7.10771500D+04 -1.70361000D+01

          Na2O
           2 L10/74 NA   2.00O   1.00   .00   .00   .00 0   61.97894  -41417.543
              300.000   1000.000 5   .0  1.0  2.0  3.0  4.0  5.0    .0    .0
           4.77871800D+00   9.94877100D-03 -1.48144600D-05   1.00032400D-08
                            -2.51378700D-12  -6.73602100D+03   1.79947600D+00
            1000.000   5000.000 5   .0  1.0  2.0  3.0  4.0  5.0    .0    .0
           7.14705800D+00   3.98331000D-04 -1.74089100D-07   3.35651600D-11
                            -2.38108000D-15  -7.21912600D+03 -9.63481000D+00

          Na2O2H2
           2 J12/70 NA   2.00O   2.00H   2.00   .00   .00 0   79.99422  -607530.104
              300.000   1000.000 5   .0  1.0  2.0  3.0  4.0  5.0    .0    .0
           5.97129300D+00   1.40492700D-02 -6.24451400D-06 -3.39357500D-09
                             2.89337700D-12  -7.54129400D+04 -9.37386500D-01
            1000.000   5000.000 5   .0  1.0  2.0  3.0  4.0  5.0    .0    .0
           9.41607500D+00   5.51965200D-03 -1.96596100D-06   3.26803400D-10
                            -2.07124800D-14  -7.63663700D+04 -1.88543500D+01

          Na2SO4
           2 J 6/78 NA   2.00S   1.00O   4.00   .00   .00 0  142.04310 -1033641.591
              300.000   1000.000 5   .0  1.0  2.0  3.0  4.0  5.0    .0    .0
           2.07275000D+00   5.45820500D-02 -7.85435300D-05   5.51042200D-08
                            -1.52666800D-11  -1.26769500D+05   1.66688300D+01
            1000.000   5000.000 5   .0  1.0  2.0  3.0  4.0  5.0    .0    .0
           1.52061300D+01   4.29842600D-03 -1.90084100D-06   3.71875300D-10
```

```
                         -2.67804600D-14  -1.29673600D+05 -4.76569200D+01

      Na(cr)
       1 CODA89 NA  1.00  .00  .00  .00  .00 1  22.98977        .000
          200.000   371.010 5   .0  1.0  2.0  3.0  4.0  5.0   .0   .0
        1.23954200D+00  2.00562200D-02 -7.36418200D-05  1.02712100D-07
                         0.00000000D+00  -8.13320900D+02 -4.50651400D+00

      Na(L)
       2 CODA89 NA  1.00  .00  .00  .00  .00 2  22.98977        .000
          371.010  1000.000 5   .0  1.0  2.0  3.0  4.0  5.0   .0   .0
        4.32382400D+00 -1.41145500D-03 -1.31068800D-07  9.17457700D-10
                        -2.35065100D-13  -9.36522300D+02 -1.72722600D+01
         1000.000  2300.000 5   .0  1.0  2.0  3.0  4.0  5.0   .0   .0
        4.59858600D+00 -2.42459400D-03  1.32453800D-06 -4.12375300D-11
                         6.40167100D-15  -9.98535500D+02 -1.86257100D+01

      NaCN(s)
       1 J 3/66 NA  1.00C  1.00N  1.00  .00  .00 1  49.00751  -90679.210
          300.000   835.000 5   .0  1.0  2.0  3.0  4.0  5.0   .0   .0
        7.99677300D+00  1.91545500D-03 -5.34215900D-06  6.80916400D-09
                        -3.14149100D-12  -1.33402900D+04 -3.17039300D+01

      NaCN(L)
       2 J 3/66 NA  1.00C  1.00N  1.00  .00  .00 2  49.00751        .000
          835.000  1000.000 5   .0  1.0  2.0  3.0  4.0  5.0   .0   .0
        9.56136000D+00  0.00000000D+00  0.00000000D+00  0.00000000D+00
                         0.00000000D+00  -1.33864100D+04 -4.02873100D+01
         1000.000  5000.000 5   .0  1.0  2.0  3.0  4.0  5.0   .0   .0
        9.56136000D+00  0.00000000D+00  0.00000000D+00  0.00000000D+00
                         0.00000000D+00  -1.33864100D+04 -4.02873100D+01

      NaCL(s)
       2 J 9/64 NA  1.00CL  1.00  .00  .00  .00 1  58.44247  -411131.151
          300.000  1000.000 5   .0  1.0  2.0  3.0  4.0  5.0   .0   .0
        5.02407800D+00  5.19490700D-03 -7.28337300D-06  6.06719800D-09
                        -1.20134200D-12  -5.11233400D+04 -2.12272000D+01
         1000.000  1073.800 5   .0  1.0  2.0  3.0  4.0  5.0   .0   .0
        2.21349300D+00  1.58599000D-03  5.04863800D-06  2.60205500D-09
                        -3.64871000D-12  -4.92632000D+04 -2.60256600D+00

      NaCL(L)
       1 J 9/64 NA  1.00CL  1.00  .00  .00  .00 2  58.44247        .000
         1073.800  5000.000 5   .0  1.0  2.0  3.0  4.0  5.0   .0   .0
        1.23584900D+01 -6.30712000D-03  3.20047200D-06 -6.77173600D-10
                         5.10156100D-14  -5.14232700D+04 -6.05855300D+01

      NaOH(a)
       1 J12/70 NA  1.00O  1.00H  1.00  .00  .00 1  39.99711  -425851.742
          300.000   596.000 5   .0  1.0  2.0  3.0  4.0  5.0   .0   .0
        8.58795000D+00 -3.54060100D-03 -4.55333900D-05  1.84184800D-07
                        -1.50189700D-10  -5.35118500D+04 -3.94075900D+01

      NaOH(L)
```

```
    2 J12/70 NA  1.00O  1.00H  1.00   .00   .00 2  39.99711      .000
       596.000  1000.000 5   .0  1.0  2.0  3.0  4.0  5.0   .0   .0
     9.05567700D+00  4.30250400D-03 -2.42591300D-06 -3.54796600D-09
                    2.68894200D-12  -5.29424500D+04 -4.35151400D+01
     1000.000  2500.000 5   .0  1.0  2.0  3.0  4.0  5.0   .0   .0
     9.49723200D+00  2.27179700D-03 -2.39779300D-06  7.83984800D-10
                   -8.19764700D-14  -5.29068200D+04 -4.52999000D+01

NaO2(s)
    2 J 6/63 NA  1.00O  2.00   .00   .00   .00 1  54.98857  -260669.367
       300.000  1000.000 5   .0  1.0  2.0  3.0  4.0  5.0   .0   .0
     7.27988800D+00  4.41607200D-03  1.24139200D-06 -1.29211700D-09
                    4.82594800D-13  -3.37265600D+04 -2.88998100D+01
     1000.000  2000.000 5   .0  1.0  2.0  3.0  4.0  5.0   .0   .0
     6.67531800D+00  6.42345100D-03 -1.54377700D-06  6.83577700D-10
                   -1.10739200D-13  -3.35725500D+04 -2.58486100D+01

Na2CO3(I)
    1 J 3/66 NA  2.00C  1.00O  3.00   .00   .00 1 105.98870 -1130792.483
       300.000   723.150 5   .0  1.0  2.0  3.0  4.0  5.0   .0   .0
     6.78356600D+00  3.88297000D-02 -9.82624600D-05  1.65430800D-07
                   -8.32945200D-11  -1.39170100D+05 -3.04632900D+01

Na2CO3(II)
    2 J 3/66 NA  2.00C  1.00O  3.00   .00   .00 2 105.98870      .000
       723.150  1000.000 5   .0  1.0  2.0  3.0  4.0  5.0   .0   .0
     1.18483400D+01 -3.51389900D-03  2.06155700D-05 -7.39651800D-09
                    0.00000000D+00  -1.38141900D+05 -4.80643700D+01
     1000.000  1123.150 5   .0  1.0  2.0  3.0  4.0  5.0   .0   .0
     8.28177500D+00  1.12753900D-02  1.99633000D-06  0.00000000D+00
                    0.00000000D+00  -1.37612700D+05 -3.13725800D+01

Na2CO3(L)
    1 J 3/66 NA  2.00C  1.00O  3.00   .00   .00 3 105.98870      .000
      1123.150  5000.000 5   .0  1.0  2.0  3.0  4.0  5.0   .0   .0
     2.27963000D+01  0.00000000D+00  0.00000000D+00  0.00000000D+00
                    0.00000000D+00  -1.42292200D+05 -1.16221200D+02

Na2O(c)
    2 J 6/68 NA  2.00O  1.00   .00   .00   .00 1  61.97894  -417992.119
       300.000  1000.000 5   .0  1.0  2.0  3.0  4.0  5.0   .0   .0
     5.26545800D+00  1.11168700D-02 -6.38753800D-07 -9.69932000D-09
                    5.37200700D-12  -5.23143400D+04 -2.41870200D+01
     1000.000  1243.200 5   .0  1.0  2.0  3.0  4.0  5.0   .0   .0
     2.41689600D+01 -2.52797400D-02 -4.73906600D-06  3.18363900D-08
                   -1.45702700D-11  -5.80482300D+04 -1.25180600D+02

Na2O(a)
    1 J 6/68 NA  2.00O  1.00   .00   .00   .00 2  61.97894      .000
      1243.200  1405.200 5   .0  1.0  2.0  3.0  4.0  5.0   .0   .0
    -1.49065900D+02  2.27990400D-01  3.83912700D-05 -1.70999200D-07
                    6.13959200D-11  1.16147900D+04  8.46892700D+02

Na2O(L)
```

```
      1 J 6/68 NA   2.00O  1.00   .00   .00   .00 3  61.97894          .000
        1405.200  5000.000 5    .0  1.0  2.0  3.0  4.0  5.0    .0    .0
        1.25807400D+01  0.00000000D+00  0.00000000D+00  0.00000000D+00
                        0.00000000D+00  -4.85948600D+04 -6.06615500D+01


    Na2O2(a)
      1 J 6/68 NA   2.00O  2.00   .00   .00   .00 1  77.97834  -513227.680
         300.000   785.000 5    .0  1.0  2.0  3.0  4.0  5.0    .0    .0
        4.58152800D+00  3.24559100D-02 -5.11542000D-05  4.26639800D-08
                       -1.39916400D-11  -6.41610500D+04 -2.24554500D+01


    Na2O2(b)
      2 J 6/68 NA   2.00O  2.00   .00   .00   .00 2  77.97834          .000
         785.000  1000.000 5    .0  1.0  2.0  3.0  4.0  5.0    .0    .0
        1.36626800D+01  0.00000000D+00  0.00000000D+00  0.00000000D+00
                        0.00000000D+00  -6.56325700D+04 -6.68415500D+01
        1000.000  5000.000 5    .0  1.0  2.0  3.0  4.0  5.0    .0    .0
        1.36626800D+01  0.00000000D+00  0.00000000D+00  0.00000000D+00
                        0.00000000D+00  -6.56325700D+04 -6.68415500D+01


    Na2S(1)
      2 J 3/78 NA   2.00S  1.00   .00   .00   .00 1  78.04554  -366105.003
         300.000  1000.000 5    .0  1.0  2.0  3.0  4.0  5.0    .0    .0
        9.70756000D+00 -3.11261800D-04  5.51211600D-06 -6.04350700D-09
                        2.30175500D-12  -4.69503800D+04 -4.38376100D+01
        1000.000  1276.000 5    .0  1.0  2.0  3.0  4.0  5.0    .0    .0
        4.46755600D+02 -1.05851100D+00  8.11700900D-04 -1.88778800D-07
                        0.00000000D+00  -1.77483900D+05 -2.34626600D+03


    Na2S(2)
      1 J 3/78 NA   2.00S  1.00   .00   .00   .00 2  78.04554          .000
        1276.000  1445.000 5    .0  1.0  2.0  3.0  4.0  5.0    .0    .0
       -5.67935500D+05  1.68041200D+03 -1.86226800D+00  9.16205900D-04
                       -1.68848800D-07  1.53328000D+08  2.91086900D+06


    Na2S(L)
      1 J 3/78 NA   2.00S  1.00   .00   .00   .00 3  78.04554          .000
        1445.000  5000.000 5    .0  1.0  2.0  3.0  4.0  5.0    .0    .0
        1.10710500D+01  0.00000000D+00  0.00000000D+00  0.00000000D+00
                        0.00000000D+00  -4.27909300D+04 -4.86158900D+01


    Na2SO4(V)
      1 J 6/78 NA   2.00S  1.00O  4.00   .00   .00 1 142.04310 -1387816.437
         200.000   458.000 5    .0  1.0  2.0  3.0  4.0  5.0    .0    .0
        5.83393200D+00  3.08202000D-02  5.97986400D-05 -2.59779100D-07
                        2.47854000D-10  -1.70156100D+05 -2.52886400D+01


    Na2SO4(IV)
      1 J 6/78 NA   2.00S  1.00O  4.00   .00   .00 2 142.04310 -1387816.437
         458.000   514.000 5    .0  1.0  2.0  3.0  4.0  5.0    .0    .0
        9.71967800D+00  2.18820400D-02 -6.19770800D-06  0.00000000D+00
                        0.00000000D+00  -1.70712800D+05 -4.36063400D+01


    Na2SO4(I)
```

```
   2 J 6/78 NA  2.00S  1.00O  4.00   .00   .00 3  142.04310  -1387816.437
      514.000  1000.000 5   .0  1.0  2.0  3.0  4.0  5.0   .0   .0
   1.54854400D+01  1.92613800D-02 -3.32257300D-05  3.56283300D-08
                  -1.30577200D-11 -1.71322900D+05 -7.35127000D+01
   1000.000  1157.000 5   .0  1.0  2.0  3.0  4.0  5.0   .0   .0
   1.61157400D+01  8.20925900D-03 -2.33305500D-07  0.00000000D+00
                   0.00000000D+00 -1.71129100D+05 -7.46990700D+01


Na2SO4(L)
   1 J 6/78 NA  2.00S  1.00O  4.00   .00   .00 4  142.04310  -1387816.437
    1157.000  6000.000 5   .0  1.0  2.0  3.0  4.0  5.0   .0   .0
   2.36977700D+01  0.00000000D+00  0.00000000D+00  0.00000000D+00
                   0.00000000D+00 -1.71658900D+05 -1.16358500D+02


Na2SO3(S)
   2 IB1993 NA  2.00S  1.00O  3.00   .00   .00 1  126.04400  -2187.573
     300.000  1000.000 5   .0  1.0  2.0  3.0  4.0  5.0   .0   .0
   1.29308100D+01  5.05243600D-03  4.39577300D-07 -4.54161200D-10
                   1.69408200D-13 -1.36495200D+05 -5.76433100D+01
   1000.000  1184.000 5   .0  1.0  2.0  3.0  4.0  5.0   .0   .0
  -1.20010500D+03  4.55784100D+00 -6.39711800D-03  3.98843700D-06
                  -9.30917500D-10  1.21659700D+05  5.87084200D+03


Na2SO3(L)
   1 IB1993 NA  2.00S  1.00O  3.00   .00   .00 2  126.04400  -2187.573
    1184.000  2000.000 5   .0  1.0  2.0  3.0  4.0  5.0   .0   .0
   2.18928000D+01  0.00000000D+00  0.00000000D+00  0.00000000D+00
                   0.00000000D+00 -1.40356300D+05 -1.12315000D+02
```

Strontium Species

```
Sr
   2 L 4/93 SR  1.00   .00   .00   .00   .00 0   87.62000   163999.968
     200.000  1000.000 5   .0  1.0  2.0  3.0  4.0  5.0   .0   .0
   2.50000000D+00  0.00000000D+00  0.00000000D+00  0.00000000D+00
                   0.00000000D+00  1.89791800D+04  5.55782100D+00
   1000.000  6000.000 5   .0  1.0  2.0  3.0  4.0  5.0   .0   .0
   2.05240000D+00  1.19516500D-03 -1.07453400D-06  3.57531000D-10
                  -3.05613300D-14  1.91041000D+04  7.88029900D+00


SrO
   2 J 6/74 SR  1.00O  1.00   .00   .00   .00 0  103.61940   -13389.038
     300.000  1000.000 5   .0  1.0  2.0  3.0  4.0  5.0   .0   .0
   2.73300000D+00  6.73994200D-03 -1.08004900D-05  8.17679300D-09
                  -2.36198700D-12 -2.64435700D+03  1.05012900D+01
   1000.000  5000.000 5   .0  1.0  2.0  3.0  4.0  5.0   .0   .0
   9.64030300D+00 -1.12851500D-02  7.88423200D-06 -1.90358800D-09
                   1.51465500D-13 -4.74994900D+03 -2.57981700D+01


SrOH+
   2 J 6/76 SR  1.00O  1.00H  1.00E  -1.00   .00 0  104.62680   320809.299
     300.000  1000.000 5   .0  1.0  2.0  3.0  4.0  5.0   .0   .0
   2.61018100D+00  1.70676800D-02 -3.12755500D-05  2.65708500D-08
```

```
                        -8.43013900D-12  3.72752300D+04  1.02040900D+01
     1000.000  5000.000 5   .0  1.0  2.0  3.0  4.0  5.0   .0   .0
   5.49519800D+00  1.42140700D-03 -4.32450200D-07  6.23424300D-11
                        -3.47974800D-15  3.68741100D+04 -2.77068400D+00


Sr(OH)2
 2 IB1993 SR  1.00O  2.00H  2.00  .00  .00 0  121.63500  -1184.019
      300.000  1000.000 5   .0  1.0  2.0  3.0  4.0  5.0   .0   .0
   3.80093900D+00  3.04115700D-02 -5.32503400D-05  4.30919700D-08
                        -1.29541000D-11 -7.36600200D+04  7.99448500D+00
     1000.000  3000.000 5   .0  1.0  2.0  3.0  4.0  5.0   .0   .0
   9.45464000D+00  1.82868500D-03 -6.65686200D-08 -1.41706000D-10
                         2.49844400D-14 -7.46376000D+04 -1.79024500D+01


SrS
 2 IB1993 SR  1.00S  1.00  .00  .00  .00 0  119.68600   215.022
      300.000  1000.000 5   .0  1.0  2.0  3.0  4.0  5.0   .0   .0
   2.67162600D+00  1.05732400D-02 -2.39330900D-05  2.39977900D-08
                        -8.75468000D-12  1.19164900D+04  1.17357200D+01
     1000.000  3000.000 5   .0  1.0  2.0  3.0  4.0  5.0   .0   .0
   9.98606000D+00 -1.21444300D-02  8.38752400D-06 -1.74814200D-09
                         7.38802000D-14  9.85813000D+03 -2.58584000D+01


SrCl
 2 IB1993 SR  1.00CL 1.00  .00  .00  .00 0  123.07300   -246.118
      300.000  1000.000 5   .0  1.0  2.0  3.0  4.0  5.0   .0   .0
   3.85903800D+00  2.76846700D-03 -4.59415800D-06  3.52594900D-09
                        -1.01211900D-12 -1.62574800D+04  7.70847700D+00
     1000.000  3000.000 5   .0  1.0  2.0  3.0  4.0  5.0   .0   .0
   4.29647600D+00  4.61254800D-04 -2.86582200D-07  8.26862700D-11
                        -6.65729500D-15 -1.63174400D+04  5.73657200D+00


SrCl2
 2 IB1993 SR  1.00CL 2.00  .00  .00  .00 0  158.52500   -944.478
      300.000  1000.000 5   .0  1.0  2.0  3.0  4.0  5.0   .0   .0
   5.74237900D+00  5.54972700D-03 -9.90483400D-06  8.04247200D-09
                        -2.45631100D-12 -5.90542400D+04  4.05769700D+00
     1000.000  3000.000 5   .0  1.0  2.0  3.0  4.0  5.0   .0   .0
   6.88595900D+00  1.47557800D-04 -7.65094900D-08  1.80194000D-11
                        -1.59413900D-15 -5.92576800D+04 -1.29272500D+00


SrOH
 2 IB1993 SR  1.00O  1.00H  1.00  .00  .00 0  104.62700   -408.400
      300.000  1000.000 5   .0  1.0  2.0  3.0  4.0  5.0   .0   .0
   2.25609000D+00  1.93675800D-02 -3.68307900D-05  3.22364200D-08
                        -1.04593000D-11 -2.59918900D+04  1.23912100D+01
     1000.000  3000.000 5   .0  1.0  2.0  3.0  4.0  5.0   .0   .0
   6.07768100D+00  2.61819700D-04  4.04240300D-07 -2.02704000D-10
                         2.89666400D-14 -2.66601400D+04 -5.32818000D+00


Sr(a)
 1 SRD 93 SR  1.00  .00  .00  .00  .00 1  87.62000     .000
      298.150   820.000 5   .0  1.0  2.0  3.0  4.0  5.0   .0   .0
   2.61121800D+00  3.06923900D-03 -4.43980800D-06  4.03524800D-09
```

```
                    -1.48087800D-12  -8.83002700D+02 -9.01331100D+00

Sr(b)
 2 SRD 93 SR  1.00  .00  .00  .00  .00 2  87.62000         .000
    820.000  1000.000 5   .0  1.0  2.0  3.0  4.0  5.0   .0   .0
  3.19032600D+00  4.83732600D-04  0.00000000D+00  0.00000000D+00
                    0.00000000D+00  -8.56080600D+02 -1.15723500D+01
   1000.000  1041.000 5   .0  1.0  2.0  3.0  4.0  5.0   .0   .0
  3.19032600D+00  4.83732600D-04  0.00000000D+00  0.00000000D+00
                    0.00000000D+00  -8.56080600D+02 -1.15723500D+01

Sr(L)
 1 SRD 93 SR  1.00  .00  .00  .00  .00 3  87.62000         .000
   1041.000  6000.000 5   .0  1.0  2.0  3.0  4.0  5.0   .0   .0
  4.45005200D+00  0.00000000D+00  0.00000000D+00  0.00000000D+00
                    0.00000000D+00  -9.43175500D+02 -1.88970000D+01

Sr(OH)2(L)
 2 IB1993 SR  1.00O  2.00H  2.00  .00  .00 1  121.63500  -1925.424
    783.150  1000.000 5   .0  1.0  2.0  3.0  4.0  5.0   .0   .0
  1.89738300D+01  0.00000000D+00  0.00000000D+00  0.00000000D+00
                    0.00000000D+00  -1.22624900D+05 -9.96716500D+01
   1000.000  1500.000 5   .0  1.0  2.0  3.0  4.0  5.0   .0   .0
  1.89738300D+01  0.00000000D+00  0.00000000D+00  0.00000000D+00
                    0.00000000D+00  -1.22624900D+05 -9.96716500D+01

SrCO3(S-A)
 2 IB1993 SR  1.00C  1.00O  3.00  .00  .00 1  147.62900  -2424.137
    300.000  1000.000 5   .0  1.0  2.0  3.0  4.0  5.0   .0   .0
  1.68103200D+00  4.70123200D-02 -8.07549400D-05  6.94034400D-08
                   -2.24189100D-11  -1.48736800D+05 -8.89308100D+00
   1000.000  1197.000 5   .0  1.0  2.0  3.0  4.0  5.0   .0   .0
  2.22031400D+04 -8.30613100D+01  1.16381800D-01 -7.23366400D-05
                    1.68279000D-08  -4.88544700D+06 -1.08571300D+05

Sr(OH)2(S)
 1 IB1993 SR  1.00O  2.00H  2.00  .00  .00 1  121.63500  -1925.424
    300.000   783.150 5   .0  1.0  2.0  3.0  4.0  5.0   .0   .0
  4.24632900D+00  1.59500500D-02  1.15752600D-07 -1.26170800D-10
                    5.04093800D-14  -1.18520300D+05 -1.72774200D+01

SrS(S)
 2 IB1993 SR  1.00S  1.00  .00  .00  .00 1  119.68600   -931.242
    300.000  1000.000 5   .0  1.0  2.0  3.0  4.0  5.0   .0   .0
  5.35220100D+00  9.34821000D-04  4.08559200D-06 -6.10693700D-09
                    2.49096800D-12  -5.81669600D+04 -2.27073600D+01
   1000.000  2500.000 5   .0  1.0  2.0  3.0  4.0  5.0   .0   .0
  5.48896100D+00  2.10174600D-03 -1.20463100D-06  4.25698000D-10
                   -5.51285200D-14  -5.82477200D+04 -2.37148900D+01

SrSO4(S-2)
 1 IB1993 SR  1.00S  1.00O  4.00  .00  .00 1  183.68400  -2971.456
   1429.000  1878.000 5   .0  1.0  2.0  3.0  4.0  5.0   .0   .0
  2.05339700D+01  0.00000000D+00  0.00000000D+00  0.00000000D+00
```

```
                              0.00000000D+00  -1.89885000D+05 -1.10075200D+02

     SrO2(S)
      1 IB1993 SR  1.00O   2.00   .00   .00   .00 1  119.61900   -1258.842
         300.000   600.000 5   .0  1.0  2.0  3.0  4.0  5.0   .0   .0
       6.46467400D+00  5.83817700D-03  1.72861200D-06 -2.43966600D-09
                      1.26201500D-12  -7.83947800D+04 -3.15352800D+01

     SrSO4(S-1)
      2 IB1993 SR  1.00S   1.00O   4.00   .00   .00 1  183.68400   -2971.456
         300.000  1000.000 5   .0  1.0  2.0  3.0  4.0  5.0   .0   .0
       1.02316500D+01  6.70759100D-03 -2.47856200D-08  1.64938000D-11
                     -2.89411500D-15  -1.83208600D+05 -4.56492700D+01
        1000.000  1429.000 5   .0  1.0  2.0  3.0  4.0  5.0   .0   .0
       9.72983600D+00  8.42666300D-03 -2.22039900D-06  1.25774700D-09
                     -2.65795100D-13  -1.83092200D+05 -4.31521600D+01

     SrSO4(L)
      1 IB1993 SR  1.00S   1.00O   4.00   .00   .00 1  183.68400   -2971.456
        1878.000  2000.000 5   .0  1.0  2.0  3.0  4.0  5.0   .0   .0
       2.18928000D+01  0.00000000D+00  0.00000000D+00  0.00000000D+00
                      0.00000000D+00  -1.88108700D+05 -1.18013500D+02

     Sr3N2(S)
      2 IB1993 SR  3.00N   2.00   .00   .00   .00 1  290.87300    -777.423
         300.000  1000.000 5   .0  1.0  2.0  3.0  4.0  5.0   .0   .0
       1.46205700D+01  3.27101200D-03  6.08461700D-10 -6.36035100D-13
                      2.41706800D-16  -5.15614700D+04 -6.94308200D+01
        1000.000  1300.000 5   .0  1.0  2.0  3.0  4.0  5.0   .0   .0
       1.46043000D+01  3.32962900D-03 -7.84031500D-08  4.66284900D-11
                     -1.03607600D-14  -5.15578700D+04 -6.93506500D+01

     SrC2(S)
      1 IB1993 SR  1.00C   2.00   .00   .00   .00 1  111.64200    -149.038
         300.000  1000.000 5   .0  1.0  2.0  3.0  4.0  5.0   .0   .0
       3.05005700D+00  2.58310000D-02 -4.63152900D-05  3.98061800D-08
                     -1.28572700D-11  -1.07411700D+04 -1.47887900D+01

     SrCl2(S)
      2 IB1993 SR  1.00CL  2.00   .00   .00   .00 1  158.52500   -1647.129
         300.000  1000.000 5   .0  1.0  2.0  3.0  4.0  5.0   .0   .0
       6.56115600D+00  1.35459200D-02 -2.09403300D-05  1.33740100D-08
                      1.90203100D-13  -1.02097600D+05 -2.69065500D+01
        1000.000  1147.000 5   .0  1.0  2.0  3.0  4.0  5.0   .0   .0
       3.04442300D+03 -1.08245900D+01  1.44096200D-02 -8.48479200D-06
                      1.86806700D-09  -7.80114000D+05 -1.50231100D+04

     SrCl2(L)
      1 IB1993 SR  1.00CL  2.00   .00   .00   .00 2  158.52500   -1647.129
        1147.000  2329.000 5   .0  1.0  2.0  3.0  4.0  5.0   .0   .0
       1.25817800D+01  0.00000000D+00  0.00000000D+00  0.00000000D+00
                      0.00000000D+00  -1.02748400D+05 -5.88816900D+01

     SrCO3(S-B)
```

```
 1 IB1993 SR  1.00C  1.00O  3.00   .00   .00 1  147.62900   -2424.137
   1197.000  1400.000 5   .0  1.0  2.0  3.0  4.0  5.0   .0   .0
 1.71117300D+01  0.00000000D+00  0.00000000D+00  0.00000000D+00
                 0.00000000D+00  -1.52694300D+05 -8.96734500D+01


SrH2(S)
 1 IB1993 SR  1.00H  2.00   .00   .00   .00 1   89.63600     -358.364
    300.000  1000.000 5   .0  1.0  2.0  3.0  4.0  5.0   .0   .0
 4.02619300D+00  2.71750800D-03  3.81507400D-10 -3.93011400D-13
                 1.46533600D-16  -2.30125900D+04 -1.77606700D+01


SrO(S)
 2 IB1993 SR  1.00O  1.00   .00   .00   .00 1  103.61900   -1176.528
    300.000  1000.000 5   .0  1.0  2.0  3.0  4.0  5.0   .0   .0
 3.23059000D+00  1.16841800D-02 -1.77643200D-05  1.35763800D-08
                -3.98072400D-12  -7.25643300D+04 -1.45336400D+01
   1000.000  2938.000 5   .0  1.0  2.0  3.0  4.0  5.0   .0   .0
 5.53593800D+00  1.55753900D-03 -4.59282400D-07  1.24833900D-10
                -1.29241300D-14  -7.30053700D+04 -2.54924000D+01


SrO(L)
 1 IB1993 SR  1.00O  1.00   .00   .00   .00 2  103.61900   -1176.528
   2938.000  3500.000 5   .0  1.0  2.0  3.0  4.0  5.0   .0   .0
 8.05234100D+00  0.00000000D+00  0.00000000D+00  0.00000000D+00
                 0.00000000D+00  -6.67408100D+04 -3.90953600D+01
```

APPENDIX A.2 : FURNACE SETTINGS

Furnace Parameters	
Stoichiometric Ratio	1.2
Air Temperature	78 deg F
Primary Air Pressure	50 psig
Methane Rotameter	18 units
UV Sweep Air	110 units
Draft Fan Frequency	45 Hz
Secondary Air Pressure	20 psig
Lower Air Monometer	1.85 in H20
Metal Injection Parameters	
Atomizer Pressure	50 psig
Atomizer Flow	95 units
Solution CsAct	15.5 g/L
SrNit	17.1 g/L
Injection Rate	20 mL/min
Sorbent Parameters	
Transport Air Pressure	50 psig
Transport Air Flow	125 units GB
Injection Rate	2 g/min
Feeder Rotation Reading	
Kaolinite	1150 rpm
Lime	775 rpm
Mixture	1000 rpm
CDEM	610 rpm
B-80	1800 rpm
6104-B	750 rpm
Dopant Parameters	
Flowrate SO2	420 mL/min
Cl2	210 mL/min
Sampling Port	14
Target Sampling Rate	1.25 Lpm
LPI Backside Pressure	27 in Hg
LPI Flowrate	22 Lpm
Sampling Time	10 min
Impactor	EPA-LPI, UA-LPI, PSI-LPI

APPENDIX A.3 : EXPERIMENTAL CONDITIONS

Run #	Fluid [ppm in gas] Cs	Sr	Sorbent	Sorbent Flowrate [g/min]	Dopant	Time [min]	Substrate	Sorbent Injection Port	Sample Port	Date Completed
C2-1	100	-	-	-	-	10	PC	-	14	01/05/1999
C2-2	100	-	-	-	-	10	PC	-	14	01/05/1999
C2-3	100	-	-	-	Cl - 1000 ppm	10	PC	-	14	01/05/1999
C2-4	100	-	-	-	Cl - 1000 ppm	10	PC	-	14	01/05/1999
C2-5	100	-	-	-	S - 1000 ppm	10	PC	-	14	01/05/1999
C2-6	100	-	-	-	S - 1000 ppm	10	PC	-	14	01/06/1999
C2-7	100	-	KAO	2	-	10	PC	4	14	01/05/1999
C2-8	100	-	KAO	2	-	10	PC	4	14	01/05/1999
C2-9	100	-	KAO	2	Cl - 1000 ppm	10	PC	4	14	01/05/1999
C2-10	100	-	KAO	2	Cl - 1000 ppm	10	PC	4	14	01/05/1999
C2-11	100	-	KAO	2	S - 1000 ppm	10	PC	4	14	01/05/1999
C2-12	100	-	KAO	2	S - 1000 ppm	10	PC	4	14	01/05/1999
C2-13	100	-	Lime	2	-	10	PC	4	14	01/06/1999
C2-14	100	-	Lime	2	-	10	PC	4	14	01/06/1999
C2-15	100	-	Lime	2	Cl - 1000 ppm	10	PC	4	14	01/06/1999
C2-16	100	-	Lime	2	Cl - 1000 ppm	10	PC	4	14	01/06/1999
C2-17	100	-	Lime	2	S - 1000 ppm	10	PC	4	14	01/06/1999
C2-18	100	-	Lime	2	S - 1000 ppm	10	PC	4	14	01/06/1999
C2-19	100	-	CDEM	2	-	10	PC	4	14	02/03/1999
C2-20	100	-	CDEM	2	-	10	PC	4	14	02/03/1999
C2-21	100	-	CDEM	2	Cl - 1000 ppm	10	PC	4	14	02/03/1999
C2-22	100	-	CDEM	2	Cl - 1000 ppm	10	PC	4	14	02/03/1999
C2-23	100	-	CDEM	2	S - 1000 ppm	10	PC	4	14	-
C2-24	100	-	CDEM	2	S - 1000 ppm	10	PC	4	14	-
C2-25	100	-	Mixture	2	-	10	PC	4	14	01/07/1999
C2-26	100	-	Mixture	2	-	10	PC	4	14	01/07/1999
C2-27	100	-	Mixture	2	Cl - 1000 ppm	10	PC	4	14	01/07/1999
C2-28	100	-	Mixture	2	Cl - 1000 ppm	10	PC	4	14	01/07/1999
C2-29	100	-	Mixture	2	S - 1000 ppm	10	PC	4	14	01/07/1999
C2-30	100	-	Mixture	2	S - 1000 ppm	10	PC	4	14	01/07/1999

APPENDIX A.3 : EXPERIMENTAL CONDITIONS - *Continued*

Run #	Fluid [ppm in gas] Cs	Sr	Sorbent	Sorbent Flowrate [g/min]	Dopant	Time [min]	Substrate	Sorbent Injection Port	Sample Port	Date Completed
S2-1	-	100	-	-	-	10	PC	-	14	12/31/1998
S2-2	-	100	-	-	-	10	PC	-	14	12/31/1998
S2-3	-	100	-	-	Cl - 1000 ppm	10	PC	-	14	12/31/1998
S2-4	-	100	-	-	Cl - 1000 ppm	10	PC	-	14	12/31/1998
S2-5	-	100	-	-	S - 1000 ppm	10	PC	-	14	12/31/1998
S2-6	-	100	-	-	S - 1000 ppm	10	PC	-	14	12/31/1998
S2-7	-	100	KAO	2	-	10	PC	4	14	01/02/1999
S2-8	-	100	KAO	2	-	10	PC	4	14	01/02/1999
S2-9	-	100	KAO	2	Cl - 1000 ppm	10	PC	4	14	01/02/1999
S2-10	-	100	KAO	2	Cl - 1000 ppm	10	PC	4	14	01/02/1999
S2-11	-	100	KAO	2	S - 1000 ppm	10	PC	4	14	01/02/1999
S2-12	-	100	KAO	2	S - 1000 ppm	10	PC	4	14	01/02/1999
S2-13	-	100	Lime	2	-	10	PC	4	14	01/06/1999
S2-14	-	100	Lime	2	-	10	PC	4	14	01/06/1999
S2-15	-	100	Lime	2	Cl - 1000 ppm	10	PC	4	14	01/06/1999
S2-16	-	100	Lime	2	Cl - 1000 ppm	10	PC	4	14	01/06/1999
S2-17	-	100	Lime	2	S - 1000 ppm	10	PC	4	14	01/06/1999
S2-18	-	100	Lime	2	S - 1000 ppm	10	PC	4	14	01/06/1999
S2-19	-	100	CDEM	2	-	10	PC	4	14	02/03/1999
S2-20	-	100	CDEM	2	-	10	PC	4	14	02/03/1999
S2-21	-	100	CDEM	2	Cl - 1000 ppm	10	PC	4	14	02/03/1999
S2-22	-	100	CDEM	2	Cl - 1000 ppm	10	PC	4	14	02/03/1999
S2-23	-	100	CDEM	2	S - 1000 ppm	10	PC	4	14	-
S2-24	-	100	CDEM	2	S - 1000 ppm	10	PC	4	14	-
S2-25	-	100	Mixture	2	-	10	PC	4	14	01/06/1999
S2-26	-	100	Mixture	2	-	10	PC	4	14	01/06/1999
S2-27	-	100	Mixture	2	Cl - 1000 ppm	10	PC	4	14	01/06/1999
S2-28	-	100	Mixture	2	Cl - 1000 ppm	10	PC	4	14	01/07/1999
S2-29	-	100	Mixture	2	S - 1000 ppm	10	PC	4	14	01/07/1999
S2-30	-	100	Mixture	2	S - 1000 ppm	10	PC	4	14	01/07/1999

APPENDIX A.3 : EXPERIMENTAL CONDITIONS - *Continued*

Run #	Fluid [ppm in gas] Cs	Sr	Sorbent	Sorbent Flowrate [g/min]	Dopant	Time [min]	Substrate	Sorbent Injection Port	Sample Port	Date Completed
C2-23	100	-	CDEM	2	S - 1000 ppm	10	PC	4	14	05/10/1999
C2-24	100	-	CDEM	2	S - 1000 ppm	10	PC	4	14	05/10/1999
C3-1	100	-	-	-	S - 1000 ppm	10	PC	-	3	05/10/1999
C3-2	100	-	-	-	S - 1000 ppm	10	PC	-	3	05/10/1999
S2-19	-	100	CDEM	2	-	10	PC	4	14	05/10/1999
S2-20	-	100	CDEM	2	-	10	PC	4	14	05/10/1999
S2-23	-	100	CDEM	2	S - 1000 ppm	10	PC	4	14	05/10/1999
S2-24	-	100	CDEM	2	S - 1000 ppm	10	PC	4	14	05/10/1999
S3-3	-	100	-	-	S - 1000 ppm	10	PC	-	3	05/10/1999
S3-4	-	100	-	-	S - 1000 ppm	10	PC	-	3	05/10/1999
S3-5	-	100	B-80	2	Cl - 1000 ppm	10	PC	4	14	05/10/1999
S3-6	-	100	B-80	2	Cl - 1000 ppm	10	PC	4	14	05/10/1999
C3-3	100	-	B-80	2	-	10	PC	4	14	05/10/1999
C3-4	100	-	B-80	2	-	10	PC	4	14	05/10/1999
C3-5	100	-	1040	2	-	10	PC	4	14	05/12/1999
C3-6	100	-	1040	2	-	10	PC	4	14	05/12/1999
S3-7	-	100	1040	2	Cl - 1000 ppm	10	PC	4	14	05/12/1999
S3-8	-	100	1040	2	Cl - 1000 ppm	10	PC	4	14	05/12/1999
S3-1	-	100	Kao	2	S - 1000 ppm	10	PC	4	14	05/12/1999
S3-2	-	100	Kao	2	S - 1000 ppm	10	PC	4	14	05/12/1999

Appedix A.4 - GAS PROFILE
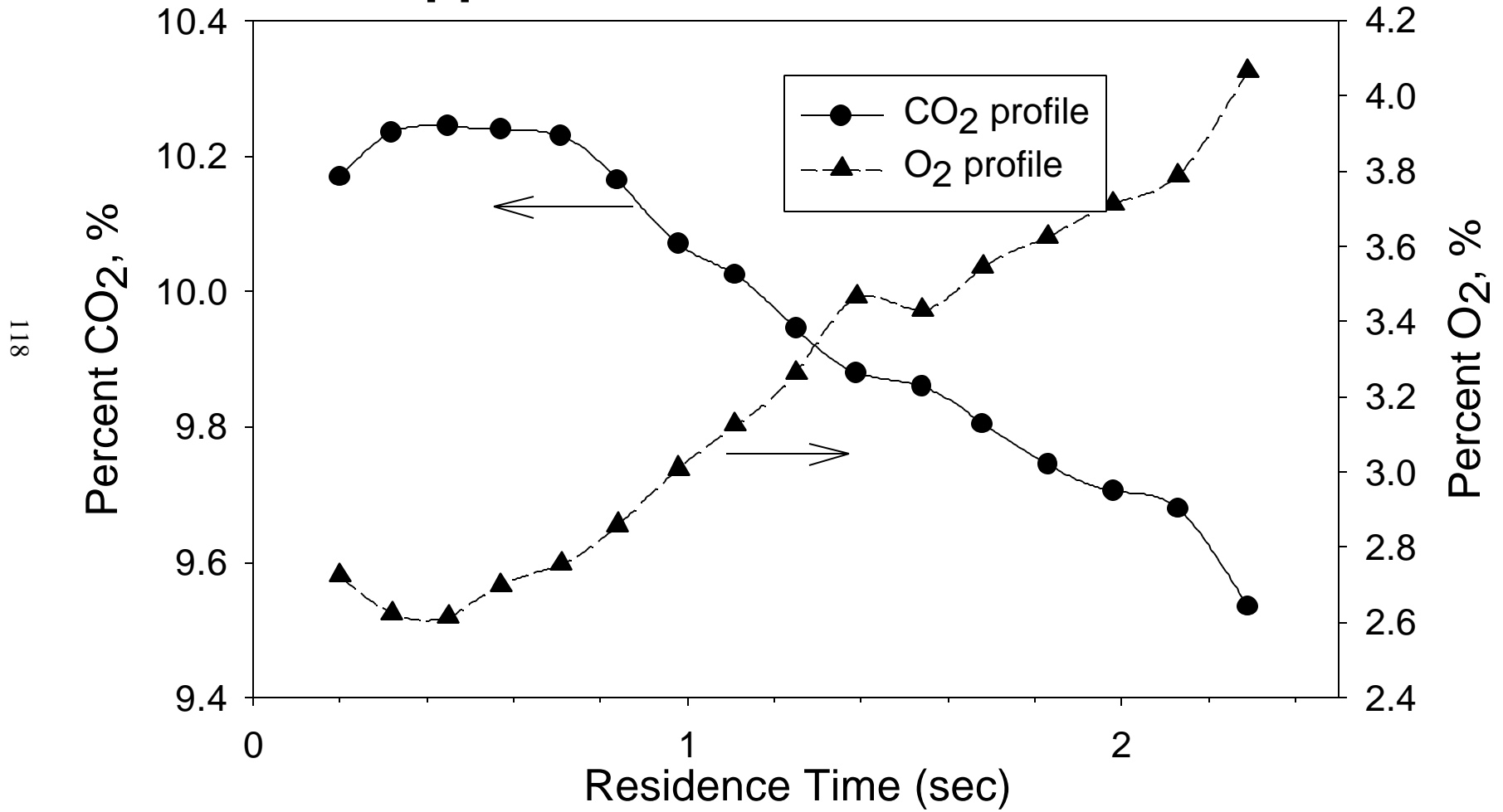
Figure A.4 - Average furnace gas profile

APPENDIX A.5 : RAW EXPERIMENTAL DATA

Run   C2-1   Figures where data appears: 4.1, 4.4, 4.5, 4.6

	Cs		Si		Al		Ca	
Date	#######							
Initials	JMA							
	conc.	s.d.	conc.	s.d.	conc.	s.d.	conc.	s.d.
Plate 1	2.9	0.14						
Plate 2	3	0.16						
Plate 3	2	0.1						
Plate 4	1.3	0.07						
Plate 5	0.7	0.14						
Plate 6	0.3	0.09						
Plate 7	0.1	0.08						
Plate 8	0.1	0.05						
Plate 9	0.1	0.04						
Plate 10	0.1	0.06						
Plate 11	0	0.07						

Run   C2-2   Figures where data appears: 4.1, 4.4, 4.5, 4.6

	Cs		Si		Al		Ca	
Date	#######							
Initials	JMA							
	conc.	s.d.	conc.	s.d.	conc.	s.d.	conc.	s.d.
Plate 1	3.3	0.11						
Plate 2	3	0.12						
Plate 3	2.3	0.12						
Plate 4	1.1	0.12						
Plate 5	0.4	0.09						
Plate 6	0.2	0.05						
Plate 7	0.2	0.07						
Plate 8	0.2	0.06						
Plate 9	0.2	0.05						
Plate 10	0.2	0.04						
Plate 11	0.1	0.04						

Run   C2-3   Figures where data appears: 4.7, 4.8, 4.9, 4.10

	Cs		Si		Al		Ca	
Date	#######							
Initials	JMA							
	conc.	s.d.	conc.	s.d.	conc.	s.d.	conc.	s.d.
Plate 1	7.7	0.14						
Plate 2	9.3	0.15						
Plate 3	4.9	0.17						
Plate 4	2	0.09						
Plate 5	0.6	0.06						
Plate 6	0.3	0.08						
Plate 7	0.3	0.07						
Plate 8	0.3	0.08						
Plate 9	0.2	0.08						

	Cs		Si		Al		Ca	
Plate 10	0.1	0.08						
Plate 11	0.1	0.05						

Run C2-4   Figures where data appears: 4.7, 4.8, 4.9, 4.10

	Cs		Si		Al		Ca	
	Cs		Si		Al		Ca	
Date	#######							
Initials	JMA							
	conc.	s.d.	conc.	s.d.	conc.	s.d.	conc.	s.d.
Plate 1	5.1	0.06						
Plate 2	9.7	0.18						
Plate 3	6.3	0.07						
Plate 4	2.2	0.05						
Plate 5	0.7	0.11						
Plate 6	0.4	0.03						
Plate 7	0.3	0.05						
Plate 8	0.3	0.07						
Plate 9	0.1	0.03						
Plate 10	0.1	0.06						
Plate 11	0	0.06						

Run C2-5   Figures where data appears: 4.11, 4.14, 4.15, 4.18, 4.19

	Cs		Si		Al		Ca	
Date	#######							
Initials	JMA							
	conc.	s.d.	conc.	s.d.	conc.	s.d.	conc.	s.d.
Plate 1	1.6	0.09						
Plate 2	3	0.09						
Plate 3	4.2	0.05						
Plate 4	2.6	0.12						
Plate 5	2.1	0.06						
Plate 6	2.6	0.1						
Plate 7	0.2	0.03						
Plate 8	0.3	0.07						
Plate 9	0.2	0.06						
Plate 10	0.1	0.06						
Plate 11	0.1	0.06						

Run C2-6   Figures where data appears: 4.11, 4.14, 4.15, 4.18, 4.19

	Cs		Si		Al		Ca	
Date	#######							
Initials	JMA							
	conc.	s.d.	conc.	s.d.	conc.	s.d.	conc.	s.d.
Plate 1	2.1	0.07						
Plate 2	3.8	0.09						
Plate 3	4	0.09						
Plate 4	2.5	0.05						
Plate 5	2.3	0.08						
Plate 6	3.5	0.11						
Plate 7	0.9	0.09						

	conc.	s.d.				
Plate 8	0.3	0.13				
Plate 9	0.1	0.05				
Plate 10	0.1	0.04				
Plate 11	0	0.03				

Run	C2-7		Figures where data appears:		4.1		
	Cs		Si		Al		Ca
Date	#######		#######		#######		
Initials	JMA		DS		JMA		
	conc.	s.d.	conc.	s.d.	conc.	s.d.	conc.	s.d.
Plate 1	0	0.04	0.3	0.59	0	0.06		
Plate 2	0	0.05	0.4	0.86	0	0.04		
Plate 3	0	0.05	0	0.75	0	0.05		
Plate 4	0.1	0.03	0.7	0.87	0	0.07		
Plate 5	0.3	0.07	1	0.75	0.2	0.07		
Plate 6	1	0.07	1.7	0.62	0.9	0.06		
Plate 7	4.7	0.04	6.5	0.75	4.8	0.07		
Plate 8	1.9	0.07	4.5	0.5	2.9	0.12		
Plate 9	0.1	0.05	1.1	0.59	0.4	0.06		
Plate 10	0	0.03	1.6	0.47	0.1	0.08		
Plate 11	0	0.07	0.9	0.55	0	0.05		

Run	C2-8		Figures where data appears:		4.1		
	Cs		Si		Al		Ca
Date	#######		#######		#######		
Initials	JMA		DS		JMA		
	conc.	s.d.	conc.	s.d.	conc.	s.d.	conc.	s.d.
Plate 1	0	0.03	0.6	0.34	0	0.05		
Plate 2	0	0.06	0.7	0.65	0	0.08		
Plate 3	0	0.03	0.6	0.66	0	0.05		
Plate 4	0.1	0.07	1.2	0.27	0	0.09		
Plate 5	0.4	0.05	0	0.64	0.2	0.06		
Plate 6	1.1	0.04	0.9	0.7	0.6	0.09		
Plate 7	5.6	0.09	5.8	0.57	4.5	0.09		
Plate 8	2.1	0.09	3.4	0.48	2.2	0.07		
Plate 9	0.1	0.04	1	0.52	0	0.07		
Plate 10	0	0.04	0.9	0.33	0	0.04		
Plate 11	0	0.07	1.3	0.49	0	0.05		

Run	C2-9		Figures where data appears:		4.7		
	Cs		Si		Al		Ca
Date	#######		#######		#######		
Initials	JMA		DS		JMA		
	conc.	s.d.	conc.	s.d.	conc.	s.d.	conc.	s.d.
Plate 1	5.1	0.07	0.5	0.63	0	0.05		
Plate 2	2.2	0.07	0	0.65	0	0.06		
Plate 3	1.3	0.07	0	0.54	0	0.05		
Plate 4	0.8	0.06	0.5	0.78	0	0.06		
Plate 5	0.5	0.08	0.8	0.42	0	0.07		

	Cs		Si		Al		Ca	
Plate 6	1	0.05	0.9	0.44	0.5	0.1		
Plate 7	3.6	0.11	3	0.87	3.2	0.08		
Plate 8	1.2	0.04	1.5	0.64	1.2	0.06		
Plate 9	0.2	0.06	0	0.82	0.1	0.08		
Plate 10	0	0.04	0	0.7	0	0.04		
Plate 11	0	0.09	0	0.68	0.1	0.06		

Run	C2-10		Figures where data appears:		4.7			
	Cs		Si		Al		Ca	
Date	#######		#######		#######			
Initials	JMA		DS		JMA			
	conc.	s.d.	conc.	s.d.	conc.	s.d.	conc.	s.d.
Plate 1	4.9	0.06	0.6	0.74	0	0.04		
Plate 2	1.9	0.07	0.4	0.59	0	0.04		
Plate 3	0.7	0.07	0.7	0.76	0	0.05		
Plate 4	0.5	0.05	1	0.95	0	0.07		
Plate 5	0.4	0.04	0.8	0.56	0.3	0.05		
Plate 6	1.1	0.06	1.3	0.79	0.9	0.06		
Plate 7	4	0.11	6	0.83	4.9	0.09		
Plate 8	1.3	0.07	2.4	0.65	1.9	0.09		
Plate 9	0.2	0.03	0	0.59	0.1	0.06		
Plate 10	0.1	0.05	0	0.61	0	0.05		
Plate 11	0	0.05	0	0.46	0	0.03		

Run	C2-11		Figures where data appears:		4.14			
	Cs		Si		Al		Ca	
Date	#######		#######		#######			
Initials	JMA		JMA		JMA			
	conc.	s.d.	conc.	s.d.	conc.	s.d.	conc.	s.d.
Plate 1	0.8	0.03	0.2	0.25	0	0.04		
Plate 2	0.2	0.06	0	0.29	0	0.07		
Plate 3	0.1	0.04	0.2	0.23	0	0.08		
Plate 4	0	0.04	0.2	0.36	0	0.06		
Plate 5	0.1	0.07	0.7	0.25	0.1	0.07		
Plate 6	0.6	0.04	0.9	0.16	0.6	0.05		
Plate 7	2	0.06	4.6	0.27	3.3	0.05		
Plate 8	0.8	0.06	2.7	0.26	1.8	0.08		
Plate 9	0	0.05	0.3	0.31	0	0.06		
Plate 10	0	0.04	0.4	0.09	0	0.05		
Plate 11	0	0.04	0.2	0.36	0	0.06		

Run	C2-12		Figures where data appears:		4.14			
	Cs		Si		Al		Ca	
Date	#######		#######		#######			
Initials	JMA		JMA		JMA			
	conc.	s.d.	conc.	s.d.	conc.	s.d.	conc.	s.d.
Plate 1	1.7	0.06	0.3	0.3	0	0.06		
Plate 2	0.8	0.06	0.3	0.32	0	0.04		
Plate 3	0.2	0.06	0.4	0.22	0	0.06		

Plate 4	0.1	0.03	0.3	0.33	0.1	0.06
Plate 5	0.1	0.03	0.5	0.27	0.1	0.05
Plate 6	0.5	0.04	0.7	0.21	0.5	0.05
Plate 7	2	0.07	3	0.24	2.2	0.07
Plate 8	0.2	0.04	0.6	0.29	0.9	0.04
Plate 9	0	0.03	0	0.19	0.1	0.1
Plate 10	0	0.04	0	0.31	0	0.04
Plate 11	0	0.03	0	0.33	0.2	0.05

Run	C2-13		Figures where data appears:				4.4		
	Cs		Si		Al		Ca	
Date	#######						#######	
Initials	JMA						DS	
	conc.	s.d.	conc.	s.d.	conc.	s.d.	conc.	s.d.
Plate 1	3.7	0.11					0	0.01
Plate 2	1.4	0.06					0.1	0.01
Plate 3	0.6	0.06					0	0.01
Plate 4	0.5	0.04					0.1	0.01
Plate 5	0.4	0.03					0.2	0.01
Plate 6	0.6	0.09					0.4	0.01
Plate 7	0.8	0.05					1.9	0.02
Plate 8	1.4	0.05					1.9	0.02
Plate 9	0.8	0.06					0.2	0.01
Plate 10	0.8	0.06					0.3	0.01
Plate 11	0.4	0.08					0.1	0.01

Run	C2-14		Figures where data appears:				4.4		
	Cs		Si		Al		Ca	
Date	#######						#######	
Initials	JMA						DS	
	conc.	s.d.	conc.	s.d.	conc.	s.d.	conc.	s.d.
Plate 1	3.9	0.1					0	0.01
Plate 2	2.1	0.06					0.1	0.01
Plate 3	1	0.05					0.1	0.01
Plate 4	0.6	0.07					0.1	0.01
Plate 5	0.3	0.06					0.3	0.01
Plate 6	0.3	0.05					0.5	0.01
Plate 7	0.6	0.03					2.7	0.02
Plate 8	1.2	0.09					3.2	0.04
Plate 9	0.4	0.09					0.4	0.01
Plate 10	0.3	0.04					0.4	0.01
Plate 11	0.2	0.07					0.2	0.01

Run	C2-15		Figures where data appears:				4.8		
	Cs		Si		Al		Ca	
Date	#######						#######	
Initials	JMA						DS	
	conc.	s.d.	conc.	s.d.	conc.	s.d.	conc.	s.d.
Plate 1	5.8	0.11					0	0
Plate 2	10.9	0.09					0	0.01
Plate 3	6.3	0.1					0	0.01
Plate 4	2.1	0.06					0	0.01
Plate 5	0.6	0.04					0.1	0.01
Plate 6	0.5	0.05					0.4	0.01
Plate 7	0.5	0.04					2	0.02
Plate 8	0.6	0.04					2.9	0.03
Plate 9	0.2	0.06					0.3	0.01

	Cs conc.	Cs s.d.	Si conc.	Si s.d.	Al conc.	Al s.d.	Ca conc.	Ca s.d.
Plate 10	0.1	0.04					0.3	0.01
Plate 11	0	0.06					0.1	0.01

Run	C2-16		Figures where data appears:			4.8		
	Cs		Si		Al		Ca	
Date	#######						#######	
Initials	JMA						DS	
	conc.	s.d.	conc.	s.d.	conc.	s.d.	conc.	s.d.
Plate 1	9	0.17					0	0.01
Plate 2	7	0.11					0	0.01
Plate 3	3.8	0.08					0	0.01
Plate 4	1.3	0.08					0	0.01
Plate 5	0.6	0.04					0	0.01
Plate 6	0.4	0.05					0.3	0.01
Plate 7	0.5	0.04					1.9	0.02
Plate 8	0.6	0.05					2.5	0.02
Plate 9	0.3	0.06					0.3	0.01
Plate 10	0.3	0.04					0.3	0.01
Plate 11	0.1	0.04					0.1	0.01

Run	C2-17		Figures where data appears:			4.15		
	Cs		Si		Al		Ca	
Date	#######						#######	
Initials	JMA						DS	
	conc.	s.d.	conc.	s.d.	conc.	s.d.	conc.	s.d.
Plate 1	1.8	0.07					0	0.01
Plate 2	0.5	0.06					0	0.01
Plate 3	0.2	0.03					0	0.01
Plate 4	0.3	0.04					0.1	0.01
Plate 5	0.3	0.04					0.2	0.01
Plate 6	0.5	0.05					0.5	0.01
Plate 7	0.6	0.08					1.2	0.02
Plate 8	1.2	0.05					3.5	0.02
Plate 9	0.1	0.03					0.7	0.01
Plate 10	0.1	0.03					0.9	0.01
Plate 11	0	0.02					0.3	0.01

Run	C2-18		Figures where data appears:			4.15		
	Cs		Si		Al		Ca	
Date	#######						#######	
Initials	JMA						DS	
	conc.	s.d.	conc.	s.d.	conc.	s.d.	conc.	s.d.
Plate 1	1.1	0.05					0	0.01
Plate 2	0.4	0.03					0	0.01
Plate 3	0.2	0.02					0	0.01
Plate 4	0.3	0.04					0.1	0.01
Plate 5	0.4	0.03					0.2	0.01
Plate 6	0.6	0.03					0.4	0.01
Plate 7	0.7	0.03					0.6	0.01

	Cs						Ca	
Plate 8	2.1	0.05					2.1	0.02
Plate 9	0.4	0.07					0.6	0.01
Plate 10	0.5	0.01					0.9	0.01
Plate 11	0.2	0.03					0.2	0.01

Run C2-19   Figures where data appears: 4.6

	Cs		Si		Al		Ca	
Date	#######		#######		#######		#######	
Initials	JS		JS		SF		JS	
	conc.	s.d.	conc.	s.d.	conc.	s.d.	conc.	s.d.
Plate 1	3.8	0.06	0	0.31	0.1	0.18	0.1	0.01
Plate 2	5.2	0.08	0	0.45	0.4	0.14	0.2	0.01
Plate 3	3.1	0.06	0	0.32	0.4	0.32	0.2	0.01
Plate 4	1.4	0.04	0.3	0.3	0.3	0.25	0.3	0.02
Plate 5	0.4	0.02	0	0.68	0.4	0.26	0.7	0.01
Plate 6	0.6	0.02	0	0.41	0.3	0.25	1.9	0.03
Plate 7	1.2	0.03	1.2	0.33	1.3	0.28	6.3	0.08
Plate 8	1.1	0.04	1.9	0.49	1.5	0.2	7.9	0.14
Plate 9	0.4	0.03	1.7	0.38	1.2	0.22	5.1	0.08
Plate 10	0.4	0.02	4.1	0.43	2.4	0.24	8.8	0.2
Plate 11	0.1	0.02	0.2	0.39	0.6	0.16	1.8	0.05

Run C2-20   Figures where data appears: 4.6

	Cs		Si		Al		Ca	
Date	#######		#######		#######		#######	
Initials	JS		JS		SF		JS	
	conc.	s.d.	conc.	s.d.	conc.	s.d.	conc.	s.d.
Plate 1	3.5	0.07	0	0.38	0.1	0.28	0.2	0.01
Plate 2	4.2	0.09	0.1	0.33	0	0.21	0.2	0.01
Plate 3	3.6	0.05	0.3	0.33	0.1	0.23	0.2	0.02
Plate 4	1.4	0.04	0.4	0.41	0.1	0.19	0.3	0.01
Plate 5	0.4	0.02	0.4	0.39	0.1	0.14	0.6	0.02
Plate 6	0.7	0.02	0	0.6	0.5	0.15	2	0.02
Plate 7	1.2	0.02	0.6	0.51	1.3	0.18	5.6	0.08
Plate 8	1.4	0.03	1.5	0.68	1.6	0.23	7.2	0.14
Plate 9	0.4	0.02	0.2	0.49	1	0.35	3.3	0.07
Plate 10	0.4	0.02	2.3	0.42	1.7	0.16	6.4	0.13
Plate 11	0.1	0.02	0	0.39	0.5	0.18	1.3	0.03

Run C2-21   Figures where data appears: 4.10

	Cs		Si		Al		Ca	
Date	#######		#######		#######		#######	
Initials	JS		JS		SF		JS	
	conc.	s.d.	conc.	s.d.	conc.	s.d.	conc.	s.d.
Plate 1	4.5	0.08	0	0.32	0.1	0.13	0.1	0.01
Plate 2	12.6	0.11	0.1	0.4	0	0.12	0.2	0.02
Plate 3	7.5	0.1	0	0.44	0.1	0.3	0.2	0.01
Plate 4	2.7	0.06	0.3	0.34	0	0.24	0.2	0.02
Plate 5	1	0.02	0	0.27	0	0.17	0.4	0.02

	conc.	s.d.	conc.	s.d.	conc.	s.d.	conc.	s.d.
Plate 6	0.7	0.03	0.4	0.55	0.8	0.25	1	0.02
Plate 7	1	0.05	0.7	0.47	1.2	0.24	4.4	0.09
Plate 8	1	0.02	1.3	0.4	1.6	0.23	6.4	0.06
Plate 9	0.4	0.04	0.7	0.59	1	0.19	2.8	0.04
Plate 10	0.3	0.04	1.1	0.55	1	0.22	2.9	0.04
Plate 11	0.2	0.02	0.4	0.31	0.7	0.26	1.5	0.03

Run	C2-22		Figures where data appears:			4.10		
	Cs		Si		Al		Ca	
Date	#######		#######		#######		#######	
Initials	JS		JS		SF		JS	
	conc.	s.d.	conc.	s.d.	conc.	s.d.	conc.	s.d.
Plate 1	3.2	0.06	0	0.38	0	0.25	0.2	0.01
Plate 2	12.5	0.07	0	0.33	0	0.24	0.2	0.01
Plate 3	9.6	0.1	0.2	0.64	0	0.18	0.1	0.01
Plate 4	4.3	0.1	0.1	0.57	0	0.19	0.2	0.02
Plate 5	1.1	0.04	0.1	0.62	0	0.16	0.3	0.01
Plate 6	0.8	0.08	0.7	0.36	0.4	0.2	1	0.03
Plate 7	0.9	0.03	0.6	0.34	0.7	0.26	3.4	0.07
Plate 8	1.1	0.04	1.3	0.63	1.4	0.14	6.2	0.11
Plate 9	0.4	0.02	0.4	0.62	0.7	0.16	2.3	0.05
Plate 10	0.3	0.02	1.6	0.49	1	0.14	3.3	0.05
Plate 11	0.2	0.03	0.5	0.46	0.3	0.23	1.6	0.03

Run	C2-23		Figures where data appears:			4.19		
	Cs		Si		Al		Ca	
Date	#######		#######		#######		#######	
Initials	JS		JS		SF		JS	
	conc.	s.d.	conc.	s.d.	conc.	s.d.	conc.	s.d.
Plate 1	3.3	0.06	0	0.37	0	0.16	0.1	0.01
Plate 2	2.2	0.07	0.1	0.43	0	0.17	0.1	0.01
Plate 3	1	0.06	0.1	0.48	0.1	0.26	0.1	0.01
Plate 4	0.5	0.03	0.2	0.57	0.2	0.17	0.1	0.01
Plate 5	0.3	0.02	0.3	0.48	0.4	0.19	0.3	0.01
Plate 6	0.5	0.07	0.3	0.75	1	0.21	0.5	0.02
Plate 7	3.6	0.03	2.6	0.64	3.4	0.26	3.4	0.06
Plate 8	7	0.08	11.1	0.49	12.6	0.35	9.3	0.14
Plate 9	2.6	0.06	12.6	0.33	14.1	0.29	7.5	0.14
Plate 10	1.4	0.04	14.1	0.63	15.3	0.3	19.8	0.67
Plate 11	0.2	0.01	1.4	0.63	2	0.22	3.3	0.04

Run	C2-24		Figures where data appears:			4.19		
	Cs		Si		Al		Ca	
Date	#######		#######		#######		#######	
Initials	JS		JS		SF		JS	
	conc.	s.d.	conc.	s.d.	conc.	s.d.	conc.	s.d.
Plate 1	2.9	0.05	0	0.41	0	0.12	0.2	0.01
Plate 2	2.2	0.04	0	0.46	0	0.1	0.2	0.01
Plate 3	1	0.04	0.1	0.4	0	0.23	0.2	0.02

Plate 4	0.5	0.02	0	0.35	0	0.26	0.3	0.02
Plate 5	0.3	0.02	0.2	0.49	0	0.19	0.3	0.01
Plate 6	0.6	0.02	0.7	0.42	0.4	0.29	0.7	0.03
Plate 7	5.6	0.09	4	0.3	3.6	0.18	5.6	0.07
Plate 8	11.7	0.11	11.8	0.62	12.1	0.36	15.7	0.25
Plate 9	5.5	0.12	13.1	0.43	13.1	0.25	13.3	0.14
Plate 10	4.8	0.08	18.3	0.51	17.6	0.26	23.1	0.26
Plate 11	0.3	0.03	1.4	0.45	1.3	0.21	2.3	0.04

Run	C2-25		Figures where data appears:					4.5	
	Cs		Si		Al		Ca		
Date	#######		#######		#######		#######		
Initials	JMA		BN		JMA		DS		
	conc.	s.d.	conc.	s.d.	conc.	s.d.	conc.	s.d.	
Plate 1	0.5	0.03	0.5	0.87	0	0.02	0	0.02	
Plate 2	0.1	0.03	0.5	0.85	0	0.04	0	0.01	
Plate 3	0.1	0.02	2.4	0.62	0	0.06	0	0.01	
Plate 4	0.3	0.04	2.7	0.78	0	0.09	0	0.01	
Plate 5	0.5	0.03	3.2	0.67	0	0.07	0	0.01	
Plate 6	1.5	0.07	1.9	0.75	0.3	0.06	0	0.01	
Plate 7	5.8	0.07	5.1	1.01	2.5	0.03	0.5	0.01	
Plate 8	2.9	0.12	4	0.73	1.6	0.05	1.7	0.02	
Plate 9	0.3	0.02	0.8	0.79	0	0.06	0.5	0.01	
Plate 10	0.2	0.02	2	0.83	0.1	0.06	0.7	0.01	
Plate 11	0.3	0.03	3.5	0.72	0	0.06	0.7	0.01	

Run	C2-26		Figures where data appears:					4.5	
	Cs		Si		Al		Ca		
Date	#######		#######		#######		#######		
Initials	JMA		JMA		JMA		DS		
	conc.	s.d.	conc.	s.d.	conc.	s.d.	conc.	s.d.	
Plate 1	0.3	0.03	0.4	0.21	0	0.06	0	0.01	
Plate 2	0.1	0.02	0.6	0.26	0	0.06	0.1	0.01	
Plate 3	0.1	0.02	0.5	0.13	0	0.08	0	0.01	
Plate 4	0.2	0.02	0.1	0.26	0	0.07	0	0.01	
Plate 5	0.5	0.03	0.4	0.33	0	0.04	0.1	0.01	
Plate 6	1.7	0.05	1.5	0.35	0.5	0.07	0.1	0.01	
Plate 7	6.9	0.1	4.9	0.25	3.2	0.04	0.9	0.01	
Plate 8	3.5	0.06	3.6	0.13	2.3	0.08	2.9	0.03	
Plate 9	0.4	0.04	1.1	0.22	0.2	0.06	0.9	0.01	
Plate 10	0.2	0.02	0.7	0.22	0	0.06	1	0.01	
Plate 11	0.2	0.02	0.7	0.32	0	0.04	0.5	0.01	

Run	C2-27		Figures where data appears:					4.9	
	Cs		Si		Al		Ca		
Date	#######		#######		#######		#######		
Initials	JMA		JMA		JMA		DS		
	conc.	s.d.	conc.	s.d.	conc.	s.d.	conc.	s.d.	
Plate 1	6.5	0.14	0	0.32	0	0.04	0	0.01	
Plate 2	4.1	0.08	0.1	0.26	0	0.07	0	0.01	
Plate 3	2	0.07	0.2	0.18	0	0.09	0	0.01	
Plate 4	0.7	0.03	0	0.29	0	0.05	0	0.01	
Plate 5	0.5	0.06	0.2	0.15	0	0.07	0.1	0.01	
Plate 6	1	0.04	0.7	0.3	0.1	0.07	0.1	0.01	
Plate 7	3	0.09	2.5	0.21	1.4	0.06	0.4	0.01	
Plate 8	1.6	0.05	1.8	0.28	0.7	0.04	1	0.02	
Plate 9	0.3	0.08	0.5	0.21	0	0.05	0.4	0.01	

Plate 10	0.2	0.02	0.7	0.27	0	0.04	0.8	0.01
Plate 11	0.1	0.02	0.4	0.19	0	0.05	0.2	0.01

Run	C2-28		Figures where data appears:			4.9		
	Cs		Si		Al		Ca	
Date	#######		#######		#######		#######	
Initials	JMA		JMA		JMA		DS	
	conc.	s.d.	conc.	s.d.	conc.	s.d.	conc.	s.d.
Plate 1	5.7	0.11	0.4	0.24	0	0.06	0	0.01
Plate 2	3.4	0.1	0.1	0.36	0	0.06	0	0.01
Plate 3	1.8	0.05	0.1	0.26	0	0.06	0	0.01
Plate 4	0.9	0.03	0.2	0.29	0	0.05	0	0.01
Plate 5	0.4	0.02	0.4	0.27	0	0.04	0	0.01
Plate 6	0.9	0.05	0.6	0.3	0.2	0.06	0.1	0.01
Plate 7	2.2	0.07	1.7	0.29	1.1	0.07	0.2	0.01
Plate 8	0.7	0.04	0.6	0.14	0.4	0.07	0.4	0.01
Plate 9	0.1	0.03	0.1	0.35	0	0.06	0.2	0.01
Plate 10	0.1	0.02	0	0.33	0	0.06	0.4	0.01
Plate 11	0.1	0.02	0	0.31	0	0.04	0.2	0.01

Run	C2-29		Figures where data appears:			4.18		
	Cs		Si		Al		Ca	
Date	#######		#######		#######		#######	
Initials	JMA		JMA		JMA		DS	
	conc.	s.d.	conc.	s.d.	conc.	s.d.	conc.	s.d.
Plate 1	0.8	0.05	0	0.25	0	0.06	0	0.01
Plate 2	0.2	0.02	0	0.3	0	0.06	0	0.01
Plate 3	0.2	0.03	0	0.27	0	0.08	0	0.01
Plate 4	0.1	0.02	0	0.19	0	0.04	0	0.01
Plate 5	0.3	0.02	0	0.32	0	0.06	0	0
Plate 6	0.3	0.03	0.1	0.29	0.2	0.06	0	0.01
Plate 7	1.3	0.07	1.1	0.32	1.1	0.05	0.1	0.02
Plate 8	0.6	0.03	0.4	0.31	0.4	0.03	0.3	0.01
Plate 9	0	0.02	0	0.29	0	0.05	0.1	0.01
Plate 10	0.1	0.02	0.1	0.2	0	0.06	0.3	0.01
Plate 11	0	0.01	0.1	0.29	0	0.08	0.2	0.01

Run	C2-30		Figures where data appears:			4.18		
	Cs		Si		Al		Ca	
Date	#######		#######		#######		#######	
Initials	JMA		JMA		JMA		DS	
	conc.	s.d.	conc.	s.d.	conc.	s.d.	conc.	s.d.
Plate 1	1.2	0.05	0	0.23	0	0.07	0	0.01
Plate 2	0.5	0.02	0	0.27	0	0.08	0	0.01
Plate 3	0.2	0.02	0.1	0.26	0	0.04	0	0.01
Plate 4	0.2	0.04	0.2	0.24	0	0.06	0	0.01
Plate 5	0.2	0.03	0.1	0.27	0.1	0.06	0	0.01
Plate 6	0.7	0.03	0.7	0.38	0.2	0.05	0	0.01
Plate 7	2.2	0.05	1.7	0.24	0.9	0.06	0.1	0.01

	Cs		Si		Al		Ca	
Plate 8	0.7	0.03	0.7	0.15	0.4	0.04	0.2	0.01
Plate 9	0.1	0.01	0.4	0.31	0	0.07	0.2	0.01
Plate 10	0	0.03	0.2	0.27	0	0.05	0.4	0.01
Plate 11	0	0.03	0.4	0.2	0	0.06	0.2	0.01

Run	C3-1		Figures where data appears:		4.11			
	Cs		Si		Al		Ca	
Date	#######							
Initials	JS							
	conc.	s.d.	conc.	s.d.	conc.	s.d.	conc.	s.d.
Plate 1	1.2	0.03						
Plate 2	9.1	0.07						
Plate 3	18	0.14						
Plate 4	18.7	0.19						
Plate 5	3.5	0.08						
Plate 6	0.8	0.03						
Plate 7	0.7	0.04						
Plate 8	0.7	0.03						
Plate 9	0.8	0.03						
Plate 10	0.6	0.03						
Plate 11	0.2	0.02						

Run	C3-2		Figures where data appears:		4.11			
	Cs		Si		Al		Ca	
Date	#######							
Initials	JS							
	conc.	s.d.	conc.	s.d.	conc.	s.d.	conc.	s.d.
Plate 1	1.6	0.04						
Plate 2	11.1	0.19						
Plate 3	19.5	0.24						
Plate 4	12.6	0.14						
Plate 5	2.2	0.03						
Plate 6	0.6	0.02						
Plate 7	0.5	0.02						
Plate 8	0.4	0.03						
Plate 9	0.3	0.02						
Plate 10	0.3	0.02						
Plate 11	0.1	0.01						

Run	C3-3		Figures where data appears:					
	Cs		Si		Al		Ca	
Date	#######		#######		#######			
Initials	JS		JS		SF			
	conc.	s.d.	conc.	s.d.	conc.	s.d.	conc.	s.d.
Plate 1	0.4	0.02	0	0.35	0	0.19		
Plate 2	0.2	0.01	0	0.48	0	0.18		
Plate 3	0.2	0.02	0.1	0.46	0.1	0.18		
Plate 4	0.2	0.01	0.2	0.44	0.3	0.2		
Plate 5	0.7	0.03	1	0.4	1	0.16		

	Cs		Si		Al		Ca	
Plate 6	5.2	0.06	6.5	0.55	6.9	0.35		
Plate 7	11.9	0.17	14	0.36	16.5	0.38		
Plate 8	4.4	0.06	7	0.46	7.9	0.21		
Plate 9	0.7	0.02	1	0.54	2.1	0.24		
Plate 10	0.2	0.02	0.2	0.43	1.3	0.25		
Plate 11	0.1	0.01	0	0.59	0.8	0.24		

Run	C3-4		Figures where data appears:					
	Cs		Si		Al		Ca	
Date	#######		#######		#######			
Initials	JS		JS		SF			
	conc.	s.d.	conc.	s.d.	conc.	s.d.	conc.	s.d.
Plate 1	0.3	0.02	0.1	0.52	0.2	0.24		
Plate 2	0.1	0.02	0	0.52	0.1	0.22		
Plate 3	0.1	0.01	0.1	0.51	0	0.21		
Plate 4	0.2	0.02	0	0.5	0.2	0.22		
Plate 5	0.9	0.03	0.5	0.58	1.1	0.23		
Plate 6	4.4	0.05	6.8	0.51	6.5	0.19		
Plate 7	8.8	0.07	10.9	0.37	10.8	0.16		
Plate 8	4.2	0.08	7.4	0.37	7.1	0.25		
Plate 9	0.8	0.04	2	0.41	1.8	0.27		
Plate 10	0.2	0.02	1.5	0.5	1.1	0.19		
Plate 11	0.1	0.01	0.3	0.42	0.2	0.16		

Run	C3-5		Figures where data appears:					
	Cs		Si		Al		Ca	
Date	#######		#######		#######			
Initials	JS		JS		SF			
	conc.	s.d.	conc.	s.d.	conc.	s.d.	conc.	s.d.
Plate 1	0.3	0.02	0	0.38	0	0.2		
Plate 2	0.7	0.03	0	0.48	0	0.12		
Plate 3	0.7	0.02	0	0.47	0.1	0.29		
Plate 4	0.5	0.03	0	0.58	0.1	0.13		
Plate 5	0.7	0.02	0.3	0.37	0.7	0.2		
Plate 6	3	0.03	3.9	0.27	3.3	0.18		
Plate 7	9.5	0.14	12	0.68	12	0.26		
Plate 8	8.9	0.1	16	0.51	17.2	0.39		
Plate 9	6.1	0.1	15	0.37	15.8	0.35		
Plate 10	5.3	0.07	18.7	0.5	20.3	0.36		
Plate 11	0.4	0.02	2.6	0.53	2	0.27		

Run	C3-6		Figures where data appears:					
	Cs		Si		Al		Ca	
Date	#######		#######		#######			
Initials	JS		JS		SF			
	conc.	s.d.	conc.	s.d.	conc.	s.d.	conc.	s.d.
Plate 1	3.3	0.06	0.3	0.27	0	0.25		
Plate 2	2.1	0.06	0.2	0.54	0	0.21		
Plate 3	0.8	0.02	0.1	0.35	0	0.17		

Plate 4	0.6	0.02	0	0.41	0	0.1
Plate 5	0.8	0.02	1.1	0.37	0.3	0.19
Plate 6	2.8	0.04	3.1	0.38	2.2	0.22
Plate 7	7.3	0.11	7.8	0.57	6.3	0.25
Plate 8	7.3	0.06	11	0.68	10.1	0.29
Plate 9	3.8	0.06	9.9	0.39	9.2	0.24
Plate 10	3.3	0.05	15	0.52	15.4	0.29
Plate 11	0.3	0.02	2.2	0.54	1.1	0.26

Run S2-1 Figures where data appears: 4.20, 4.23, 4.25, 4.26

	Sr		Si		Al		Ca	
Date	#######							
Initials	JMA							
	conc.	s.d.	conc.	s.d.	conc.	s.d.	conc.	s.d.
Plate 1	0	0						
Plate 2	0	0.01						
Plate 3	0.2	0.02						
Plate 4	0.9	0.04						
Plate 5	2.2	0.05						
Plate 6	3.8	0.07						
Plate 7	4.5	0.1						
Plate 8	1.6	0.06						
Plate 9	0	0.02						
Plate 10	0	0.01						
Plate 11	0	0.04						

Run S2-2 Figures where data appears: 4.20, 4.23, 4.25, 4.26

	Sr		Si		Al		Ca	
Date	#######							
Initials	JMA							
	conc.	s.d.	conc.	s.d.	conc.	s.d.	conc.	s.d.
Plate 1	0	0.01						
Plate 2	0.1	0.01						
Plate 3	0.2	0.01						
Plate 4	0.9	0.02						
Plate 5	1.9	0.11						
Plate 6	2.8	0.06						
Plate 7	2.6	0.07						
Plate 8	1.1	0.02						
Plate 9	0	0.01						
Plate 10	0	0.01						
Plate 11	0	0.01						

Run S2-3 Figures where data appears: 4.27, 4.30, 4.31, 4.32

	Sr		Si		Al		Ca	
Date	#######							
Initials	JMA							
	conc.	s.d.	conc.	s.d.	conc.	s.d.	conc.	s.d.
Plate 1	0.1	0.01						
Plate 2	0.2	0.02						
Plate 3	2.4	0.06						
Plate 4	9.7	0.2						
Plate 5	3.7	0.09						
Plate 6	0.9	0.04						
Plate 7	0.2	0.01						
Plate 8	0	0.02						
Plate 9	0	0.02						
Plate 10	0	0.01						

	Sr		Si		Al		Ca	
Plate 11	0	0.01						

Run	S2-4		Figures where data appears: 4.27, 4.30, 4.31, 4.32					
	Sr		Si		Al		Ca	
Date	#######							
Initials	JMA							
	conc.	s.d.	conc.	s.d.	conc.	s.d.	conc.	s.d.
Plate 1	0.1	0.01						
Plate 2	0.4	0.03						
Plate 3	2.5	0.05						
Plate 4	6.7	0.14						
Plate 5	2.1	0.07						
Plate 6	0.4	0.03						
Plate 7	0.1	0.03						
Plate 8	0	0.02						
Plate 9	0	0.01						
Plate 10	0	0.01						
Plate 11	0	0.02						

Run	S2-5		Figures where data appears: 4.33, 4.35, 4.37, 4.38, 4.39					
	Sr		Si		Al		Ca	
Date	#######							
Initials	JMA							
	conc.	s.d.	conc.	s.d.	conc.	s.d.	conc.	s.d.
Plate 1	0	0.01						
Plate 2	0	0.04						
Plate 3	0.7	0.02						
Plate 4	1.7	0.06						
Plate 5	1.1	0.02						
Plate 6	1.5	0.03						
Plate 7	1.2	0.04						
Plate 8	0.2	0.02						
Plate 9	0	0.01						
Plate 10	0	0.01						
Plate 11	0	0.02						

Run	S2-6		Figures where data appears: 4.33, 4.35, 4.37, 4.38, 4.39					
	Sr		Si		Al		Ca	
Date	#######							
Initials	JMA							
	conc.	s.d.	conc.	s.d.	conc.	s.d.	conc.	s.d.
Plate 1	0	0.01						
Plate 2	0	0.01						
Plate 3	0.5	0.02						
Plate 4	1.3	0.04						
Plate 5	0.8	0.02						
Plate 6	1.3	0.04						
Plate 7	0.8	0.04						
Plate 8	0.1	0.02						
Plate 9	0	0.01						

	Plate 10	0	0.01						
	Plate 11	0	0.01						

Run	S2-7		Figures where data appears:			4.20			
		Sr		Si		Al		Ca	
Date	#######		#######		#######				
Initials	BN		DS		JS				
	conc.	s.d.	conc.	s.d.	conc.	s.d.	conc.	s.d.
Plate 1	0.1	0.05	0.5	0.4	0.1	0.08		
Plate 2	0	0.07	2.4	0.39	0	0.1		
Plate 3	0	0.04	2.4	0.67	0	0.08		
Plate 4	0.3	0.05	2	0.5	0	0.09		
Plate 5	0.8	0.04	2.6	0.51	0.3	0.06		
Plate 6	2	0.08	0	0.52	0.9	0.11		
Plate 7	7.1	0.12	5.5	0.51	5.1	0.1		
Plate 8	4.6	0.08	4.1	0.61	3.3	0.11		
Plate 9	0.2	0.04	1	0.39	0.5	0.08		
Plate 10	0	0.04	1.9	0.47	1	0.09		
Plate 11	0.1	0.06	1.2	0.38	0.5	0.09		

Run	S2-8		Figures where data appears:			4.20			
		Sr		Si		Al		Ca	
Date	#######		#######		#######				
Initials	BN		DS		JS				
	conc.	s.d.	conc.	s.d.	conc.	s.d.	conc.	s.d.
Plate 1	0	0.05	0.7	0.45	0	0.07		
Plate 2	0	0.05	1.5	0.35	0.1	0.06		
Plate 3	0	0.04	2.3	0.48	0.1	0.09		
Plate 4	0.1	0.04	2.2	0.71	0.1	0.07		
Plate 5	0.1	0.05	3	0.46	0.5	0.12		
Plate 6	1	0.04	1.6	0.63	1.2	0.08		
Plate 7	4.5	0.06	6.7	0.3	6.1	0.12		
Plate 8	3.8	0.05	6.1	0.46	4.4	0.06		
Plate 9	0.1	0.05	2.6	0.36	0.1	0.11		
Plate 10	0	0.06	2.5	0.49	0	0.1		
Plate 11	0	0.05	2.6	0.39	0	0.06		

Run	S2-9		Figures where data appears:			4.27			
		Sr		Si		Al		Ca	
Date	#######		#######		#######				
Initials	BN		DS		JS				
	conc.	s.d.	conc.	s.d.	conc.	s.d.	conc.	s.d.
Plate 1	0	0.06	0.3	0.45	0	0.1		
Plate 2	0.1	0.04	1.2	0.48	0	0.11		
Plate 3	0.6	0.05	1.6	0.55	0	0.08		
Plate 4	0.3	0.07	2	0.3	0.1	0.1		
Plate 5	0	0.06	2.4	0.65	0.2	0.07		
Plate 6	0.4	0.05	1	0.54	0.7	0.11		
Plate 7	2.3	0.06	4.9	0.53	4.7	0.07		
Plate 8	1	0.07	3.9	0.5	2.7	0.08		

	Plate 9	0	0.03	1.3	0.3	0.2	0.07		
	Plate 10	0	0.06	1.9	0.44	0.1	0.11		
	Plate 11	0.1	0.08	0.8	0.5	0.1	0.1		

Run	S2-10		Figures where data appears:		4.27				
	Sr		Si		Al		Ca		
Date	#######		#######		#######				
Initials	BN		DS		JS				
	conc.	s.d.	conc.	s.d.	conc.	s.d.	conc.	s.d.	
Plate 1	0.3	0.06	8.3	0.43	0	0.1			
Plate 2	0.4	0.06	0.5	0.61	0	0.1			
Plate 3	0.6	0.05	1.3	0.35	0	0.07			
Plate 4	0.5	0.03	1.6	0.34	0.2	0.07			
Plate 5	0.4	0.06	1.6	0.45	0.3	0.09			
Plate 6	0.4	0.1	1	0.39	0.8	0.09			
Plate 7	2.8	0.04	5.8	0.51	5.3	0.13			
Plate 8	0.8	0.05	4.2	0.97	2.3	0.1			
Plate 9	0	0.04	1.1	0.42	0.1	0.1			
Plate 10	0	0.07	1.3	0.32	0	0.09			
Plate 11	0	0.05	1.6	0.58	0	0.08			

Run	S2-11		Figures where data appears:		4.35				
	Sr		Si		Al		Ca		
Date	#######		#######		#######				
Initials	BN		DS		JS				
	conc.	s.d.	conc.	s.d.	conc.	s.d.	conc.	s.d.	
Plate 1	0	0.03	0.2	0.57	0	0.08			
Plate 2	0	0.07	0.8	0.37	0.1	0.08			
Plate 3	0.9	0.05	1	0.29	0	0.08			
Plate 4	3.3	0.09	1.2	0.3	0	0.08			
Plate 5	0.4	0.06	1.6	0.5	0.2	0.05			
Plate 6	0.2	0.12	1.6	0.54	1.3	0.07			
Plate 7	0.2	0.06	5.9	0.44	5.2	0.08			
Plate 8	0.2	0.06	3.3	0.54	2.4	0.1			
Plate 9	0.2	0.05	0.8	0.39	0.3	0.05			
Plate 10	0.2	0.06	1	0.32	0.2	0.1			
Plate 11	0	0.1	1	0.62	0.3	0.11			

Run	S2-12		Figures where data appears:		4.35				
	Sr		Si		Al		Ca		
Date	#######		#######		#######				
Initials	BN		DS		JS				
	conc.	s.d.	conc.	s.d.	conc.	s.d.	conc.	s.d.	
Plate 1	0	0.1	0	0.52	0	0.06			
Plate 2	0	0.06	0.5	0.61	0.1	0.08			
Plate 3	0	0.05	0.8	0.47	0.1	0.1			
Plate 4	0.2	0.06	1.3	0.34	0.1	0.07			
Plate 5	0.6	0.05	1.7	0.44	0.3	0.1			
Plate 6	0.9	0.08	0.8	0.58	1.2	0.12			
Plate 7	2.2	0.04	4.7	0.59	4.5	0.14			

Plate 8	0.9	0.09	2.9	0.46	1.7	0.09
Plate 9	0	0.08	1.8	0.4	0.1	0.11
Plate 10	0	0.07	1.9	0.41	0.1	0.09
Plate 11	0	0.07	1.2	0.49	0.1	0.1

Run	S2-13		Figures where data appears:				4.23		
	Sr		**Si**		**Al**		**Ca**		
Date	#######						#######		
Initials	BN						JS		
	conc.	s.d.	conc.	s.d.	conc.	s.d.	conc.	s.d.	
Plate 1	0	0.16					0	0.05	
Plate 2	0	0.04					0.1	0.09	
Plate 3	0.1	0.03					0.1	0.1	
Plate 4	0.5	0.06					0.2	0.03	
Plate 5	0	0.08					0.4	0.06	
Plate 6	1.3	0.11					1.1	0.09	
Plate 7	2.9	0.09					4.6	0.11	
Plate 8	1.3	0.11					4.3	0.15	
Plate 9	0.2	0.07					0.9	0.13	
Plate 10	0.1	0.07					1.1	0.1	
Plate 11	0	0.05					0.4	0.11	

Run	S2-14		Figures where data appears:				4.23		
	Sr		**Si**		**Al**		**Ca**		
Date	#######						#######		
Initials	BN						JS		
	conc.	s.d.	conc.	s.d.	conc.	s.d.	conc.	s.d.	
Plate 1	0	0.07					0	0.11	
Plate 2	0.1	0.05					0	0.11	
Plate 3	0	0.05					0.1	0.09	
Plate 4	0.2	0.07					0.1	0.08	
Plate 5	0.6	0.05					0.3	0.08	
Plate 6	1.2	0.06					0.9	0.07	
Plate 7	2.3	0.05					4.3	0.13	
Plate 8	1	0.08					3.5	0.15	
Plate 9	0	0.09					0.6	0.1	
Plate 10	0	0.04					1	0.07	
Plate 11	0	0.04					0.5	0.1	

Run	S2-15		Figures where data appears:				4.30		
	Sr		**Si**		**Al**		**Ca**		
Date	#######						#######		
Initials	BN						JS		
	conc.	s.d.	conc.	s.d.	conc.	s.d.	conc.	s.d.	
Plate 1	0	0.06					0.1	0.07	
Plate 2	0.1	0.07					0.1	0.1	
Plate 3	0.9	0.07					0.4	0.06	
Plate 4	3.3	0.06					1.1	0.08	
Plate 5	0.3	0.07					0.4	0.15	
Plate 6	0.2	0.05					0.6	0.17	
Plate 7	0.2	0.06					1.8	0.1	
Plate 8	0.2	0.08					3.3	0.12	
Plate 9	0	0.07					0.8	0.05	
Plate 10	0.2	0.05					1.5	0.08	

	Sr		Si		Al		Ca	
Plate 11	0	0.05					0.5	0.09

Run	S2-16		Figures where data appears:		4.30			
	Sr		Si		Al		Ca	
Date	#######						#######	
Initials	BN						JS	
	conc.	s.d.	conc.	s.d.	conc.	s.d.	conc.	s.d.
Plate 1	0	0.06					0.1	0.06
Plate 2	0.1	0.06					0	0.1
Plate 3	1.3	0.07					0.3	0.08
Plate 4	3.5	0.04					0.7	0.06
Plate 5	0.6	0.05					0.2	0.14
Plate 6	0.1	0.04					0.5	0.09
Plate 7	0.2	0.05					1.4	0.1
Plate 8	0.2	0.07					2.4	0.17
Plate 9	0.1	0.06					0.4	0.07
Plate 10	0	0.08					0.8	0.13
Plate 11	0.1	0.07					1	0.14

Run	S2-17		Figures where data appears:		4.37			
	Sr		Si		Al		Ca	
Date	#######						#######	
Initials	JS						JS	
	conc.	s.d.	conc.	s.d.	conc.	s.d.	conc.	s.d.
Plate 1	0	0.05					0.1	0.11
Plate 2	0.1	0.07					0.1	0.12
Plate 3	0.8	0.09					0.2	0.12
Plate 4	2.8	0.05					0.5	0.15
Plate 5	1.5	0.04					1	0.1
Plate 6	1.8	0.08					2.5	0.15
Plate 7	4.1	0.04					15.8	0.37
Plate 8	5.1	0.07					24.3	0.24
Plate 9	3.2	0.06					25.6	0.31
Plate 10	1.5	0.08					13.9	0.35
Plate 11	0.3	0.06					1.2	0.12

Run	S2-18		Figures where data appears:		4.37			
	Sr		Si		Al		Ca	
Date	#######						#######	
Initials	JS						JS	
	conc.	s.d.	conc.	s.d.	conc.	s.d.	conc.	s.d.
Plate 1	0	0.08					0.1	0.11
Plate 2	0	0.05					0.1	0.07
Plate 3	0.6	0.06					0.2	0.08
Plate 4	2.1	0.07					0.3	0.08
Plate 5	1.1	0.07					0.5	0.09
Plate 6	1.4	0.06					0.8	0.15
Plate 7	2.3	0.06					4.4	0.13
Plate 8	1.8	0.05					8.5	0.12
Plate 9	0.3	0.06					1.9	0.1

	Sr conc.	Sr s.d.	Si conc.	Si s.d.	Al conc.	Al s.d.	Ca conc.	Ca s.d.
Plate 10	0.2	0.06					2.2	0.15
Plate 11	0.2	0.05					0.7	0.1

Run	S2-19		Figures where data appears:			4.26		
	Sr		Si		Al		Ca	
Date	#######		#######		#######		#######	
Initials	JS		JS		SF		JS	
	conc.	s.d.	conc.	s.d.	conc.	s.d.	conc.	s.d.
Plate 1	0.1	0.01	0	0.31	0	0.35	0.3	0.01
Plate 2	0.1	0.01	0	0.62	0	0.24	0.3	0.01
Plate 3	0.4	0.02	0.1	0.57	0.1	0.41	0.4	0.02
Plate 4	1.7	0.04	0.2	0.48	0	0.28	0.5	0.01
Plate 5	5.9	0.13	0.8	0.38	0.1	0.26	1.3	0.02
Plate 6	21.2	0.37	0.8	0.48	0.6	0.32	6.7	0.07
Plate 7	45.6	0.71	5.8	0.32	3.6	0.23	23.4	0.24
Plate 8	27.7	1.06	12.1	0.55	8.1	0.37	30.2	0.39
Plate 9	10.7	0.28	24.9	0.68	16.8	0.33	43.7	0.61
Plate 10	3.8	0.11	29.4	0.87	18.5	0.47	42	0.7
Plate 11	0.5	0.06	8.6	0.48	5.7	0.39	20.3	0.17

Run	S2-20		Figures where data appears:			4.26		
	Sr		Si		Al		Ca	
Date	#######		#######		#######		#######	
Initials	JS		JS		SF		JS	
	conc.	s.d.	conc.	s.d.	conc.	s.d.	conc.	s.d.
Plate 1	0.2	0.02	0.1	0.42	0	0.25	0.5	0.02
Plate 2	0.2	0.01	0.1	0.41	0	0.28	0.4	0.01
Plate 3	0.3	0.03	0.1	0.42	0	0.31	0.5	0.02
Plate 4	1.7	0.04	0.1	0.28	0	0.29	0.6	0.01
Plate 5	5.9	0.21	0	0.31	0	0.25	1.4	0.02
Plate 6	19.9	0.45	0.9	0.5	0.5	0.22	6.7	0.07
Plate 7	31	0.8	2.9	0.54	2.1	0.27	18.2	0.21
Plate 8	9.7	0.37	4.5	0.52	3.5	0.3	17.2	0.36
Plate 9	9.7	0.26	22.7	0.64	15.5	0.26	40.7	0.55
Plate 10	2.6	0.1	19.6	0.89	13.1	0.41	31	0.2
Plate 11	0.6	0.02	11.1	0.3	8	0.4	28.1	0.43

Run	S2-21		Figures where data appears:			4.32		
	Sr		Si		Al		Ca	
Date	#######		#######		#######		#######	
Initials	JS		JS		SF		JS	
	conc.	s.d.	conc.	s.d.	conc.	s.d.	conc.	s.d.
Plate 1	0	0.01	0	0.31	0	0.26	0.1	0.01
Plate 2	0	0.01	0.2	0.41	0	0.16	0.1	0.01
Plate 3	1	0.03	0.3	0.57	0	0.23	0.2	0.01
Plate 4	9	0.26	0	0.51	0	0.36	0.7	0.02
Plate 5	7.7	0.82	0	0.62	0	0.26	0.8	0.02
Plate 6	2.1	0.06	0	0.41	0.3	0.41	1	0.03
Plate 7	1.6	0.06	0	0.31	0.5	0.18	3.3	0.04
Plate 8	1.6	0.05	0.9	0.35	1	0.24	8	0.13

	Sr		Si		Al		Ca	
	conc.	s.d.	conc.	s.d.	conc.	s.d.	conc.	s.d.
Plate 9	0.5	0.02	0.9	0.55	1.4	0.38	10.1	0.13
Plate 10	0.2	0.02	1.8	0.46	1.5	0.17	8.2	0.13
Plate 11	0.1	0.01	0.2	0.45	0.2	0.28	1.9	0.02

Run	S2-22		Figures where data appears:		4.32			
	Sr		Si		Al		Ca	
Date	#######		#######		#######		#######	
Initials	JS		JS		SF		JS	
	conc.	s.d.	conc.	s.d.	conc.	s.d.	conc.	s.d.
Plate 1	0	0.01	0.6	0.48	0	0.25	0.1	0.01
Plate 2	0.1	0.01	0.5	0.3	0	0.33	0.1	0.02
Plate 3	1	0.04	0.1	0.35	0	0.25	0.1	0.02
Plate 4	10.3	0.3	0.4	0.23	0	0.19	0.7	0.02
Plate 5	5.9	0.2	0.7	0.4	0.1	0.4	0.6	0.02
Plate 6	2.4	0.07	0.9	0.4	0.3	0.29	1.2	0.02
Plate 7	1	0.02	1.2	0.33	0.3	0.29	3	0.03
Plate 8	0.9	0.04	2	0.48	1	0.32	7.3	0.09
Plate 9	0.4	0.02	2.6	0.52	1.5	0.33	10.2	0.62
Plate 10	0.3	0.02	6	0.43	2.6	0.26	11.2	0.21
Plate 11	0.1	0.02	1.2	0.35	0.7	0.28	4.1	0.07

Run	S2-23		Figures where data appears:		4.39			
	Sr		Si		Al		Ca	
Date	#######		#######		#######		#######	
Initials	JS		JS		SF		JS	
	conc.	s.d.	conc.	s.d.	conc.	s.d.	conc.	s.d.
Plate 1	0.3	0.01	0.8	0.46	0	0.31	0.2	0.02
Plate 2	0.9	0.02	0.5	0.34	0.1	0.31	0.1	0.01
Plate 3	6.4	0.17	1	0.55	0.1	0.23	0.2	0.01
Plate 4	5	0.16	0.8	0.58	0	0.28	0.2	0.02
Plate 5	5.4	0.2	0.9	0.38	0	0.26	0.5	0.01
Plate 6	15.6	0.58	1.2	0.34	0.5	0.36	2.6	0.05
Plate 7	37.2	0.92	4.5	0.53	3	0.24	13.2	0.03
Plate 8	30.1	0.99	9	0.48	6.8	0.21	22	0.26
Plate 9	9.3	0.27	15.2	0.98	11.6	0.26	24	0.34
Plate 10	2.8	0.1	12.7	0.7	9.3	0.32	20.6	0.32
Plate 11	1	0.02	7.4	0.52	5.3	0.33	17.6	0.25

Run	S2-24		Figures where data appears:		4.39			
	Sr		Si		Al		Ca	
Date	#######		#######		#######		#######	
Initials	JS		JS		SF		JS	
	conc.	s.d.	conc.	s.d.	conc.	s.d.	conc.	s.d.
Plate 1	0.2	0.02	0.1	0.48	0	0.37	0.2	0.02
Plate 2	0.7	0.03	0	0.26	0	0.27	0.2	0.02
Plate 3	5.8	0.23	0.2	0.46	0	0.37	0.2	0.01
Plate 4	4.4	0.14	0	0.38	0	0.39	0.3	0.01
Plate 5	5	0.23	0.4	0.53	0.2	0.32	0.7	0.02
Plate 6	14	0.45	0.7	0.6	0.9	0.41	3.3	0.03
Plate 7	38.9	0.93	4.8	0.26	4.2	0.29	17.2	0.22

Plate 8	34.7	0.91	12.4	0.48	10.1	0.25	37	0.48
Plate 9	12.2	0.35	21.1	0.39	15.9	0.38	38.5	0.43
Plate 10	2.4	0.08	11.4	0.45	8.4	0.22	19.1	0.21
Plate 11	0.6	0.02	9.8	0.62	6.6	0.39	19.3	0.41

Run	S2-25		Figures where data appears:				4.25	
	Sr		**Si**		**Al**		**Ca**	
Date	#######		#######		#######		#######	
Initials	JS		BN		JS		JS	
	conc.	s.d.	conc.	s.d.	conc.	s.d.	conc.	s.d.
Plate 1	0	0.07	0.2	0.43	0.1	0.07	0	0.2
Plate 2	0	0.06	0.3	0.24	0	0.11	0.4	0.06
Plate 3	0	0.06	1	0.39	0.1	0.08	0.4	0.05
Plate 4	0.2	0.04	2.1	0.35	0.1	0.07	0.5	0.11
Plate 5	0.3	0.06	3.7	0.42	0.2	0.08	0.7	0.07
Plate 6	0.7	0.05	0.9	0.39	0.3	0.09	0.5	0.07
Plate 7	1.6	0.07	2	0.52	0.8	0.06	1.2	0.08
Plate 8	1.2	0.08	1.1	0.6	0.7	0.07	2.4	0.09
Plate 9	0.2	0.05	1.3	0.4	0.2	0.1	1.4	0.09
Plate 10	0	0.04	1.7	0.6	0.3	0.09	1.8	0.1
Plate 11	0.1	0.03	2.1	0.73	0.4	0.11	1.3	0.12

Run	S2-26		Figures where data appears:				4.25	
	Sr		**Si**		**Al**		**Ca**	
Date	#######		#######		#######		#######	
Initials	JMA		BN		JS		JS	
	conc.	s.d.	conc.	s.d.	conc.	s.d.	conc.	s.d.
Plate 1	0	0.01	0	0.61	0	0.09	0	0.09
Plate 2	0	0.03	0.7	0.42	0.1	0.08	0.2	0.08
Plate 3	0	0.02	0.7	0.44	0.1	0.1	0.2	0.04
Plate 4	0.2	0.01	1	0.58	0	0.04	0.3	0.1
Plate 5	0.5	0.03	1.4	0.52	0	0.1	0.3	0.1
Plate 6	1.2	0.04	0.5	0.55	0.3	0.1	0.3	0.07
Plate 7	2.9	0.07	2.2	0.48	1.1	0.06	0.9	0.1
Plate 8	1.7	0.07	2	0.38	0.7	0.11	1.4	0.09
Plate 9	0	0.03	1.2	0.48	0.2	0.04	0.8	0.1
Plate 10	0	0.01	2.6	0.45	0.7	0.01	2.2	0.13
Plate 11	0.1	0.01	1.8	0.36	0.5	0.07	1.2	0.13

Run	S2-27		Figures where data appears:				4.31	
	Sr		**Si**		**Al**		**Ca**	
Date	#######		#######		#######		#######	
Initials	JMA		BN		JS		JS	
	conc.	s.d.	conc.	s.d.	conc.	s.d.	conc.	s.d.
Plate 1	0	0.03	0	0.42	0	0.11	0.1	0.08
Plate 2	0	0.01	0.2	0.23	0	0.13	0.1	0.09
Plate 3	0.7	0.04	0.7	0.49	0	0.08	0.3	0.08
Plate 4	1.5	0.03	0.6	0.32	0	0.06	0.1	0.08
Plate 5	0.1	0.01	1	0.37	0	0.07	0	0.06
Plate 6	0.1	0.01	0	0.4	0.1	0.09	0.2	0.11
Plate 7	1.1	0.03	0.6	0.5	0.8	0.13	0.4	0.05
Plate 8	0.5	0.02	1.2	0.48	0	0.1	0.4	0.09
Plate 9	0	0.02	0.3	0.46	0	0.12	0.3	0.09
Plate 10	0	0.01	0.8	0.31	0	0.09	0.5	0.07

Plate 11	0	0.01	1.1	0.4	0	0.1	0.2	0.11

Run	S2-28		Figures where data appears:			4.31		
	Sr		Si		Al		Ca	
Date	#######		#######		#######		#######	
Initials	JMA		BN		JS		JS	
	conc.	s.d.	conc.	s.d.	conc.	s.d.	conc.	s.d.
Plate 1	0	0.02	0	0.43	0	0.09	0	0.1
Plate 2	0.1	0.01	0	0.47	0	0.11	0.1	0.08
Plate 3	0.8	0.01	0	0.32	0	0.08	0.1	0.11
Plate 4	1.5	0.05	0.7	0.41	0	0.07	0.2	0.04
Plate 5	0.3	0.01	1.4	0.61	0	0.05	0.2	0.09
Plate 6	0.2	0.02	0	0.51	0.1	0.08	0	0.11
Plate 7	1.1	0.05	1.1	0.5	0.7	0.08	0.4	0.1
Plate 8	0.5	0.02	1.4	0.53	0.5	0.08	0.6	0.06
Plate 9	0	0.01	1.3	0.46	0	0.08	0.3	0.07
Plate 10	0	0.01	1.9	0.31	0	0.11	0.4	0.15
Plate 11	0	0.02	1.9	0.23	0	0.1	0.3	0.06

Run	S2-29		Figures where data appears:			4.38		
	Sr		Si		Al		Ca	
Date	#######		#######		#######		#######	
Initials	JMA		BN		JS		JS	
	conc.	s.d.	conc.	s.d.	conc.	s.d.	conc.	s.d.
Plate 1	0	0.01	0.1	0.3	0	0.1	0	0.08
Plate 2	0.2	0.02	0	0.34	0	0.08	0	0.08
Plate 3	2.8	0.05	0.2	0.39	0	0.06	0	0.06
Plate 4	2.8	0.08	0.2	0.42	0.1	0.09	0.1	0.12
Plate 5	1.1	0.05	0.3	0.22	0.3	0.08	0.1	0.09
Plate 6	1.9	0.04	0.9	0.36	1.3	0.09	0.2	0.11
Plate 7	3.8	0.07	4	0.42	4.1	0.12	1.2	0.09
Plate 8	2.4	0.06	1.9	0.51	2.2	0.17	2.6	0.17
Plate 9	0.1	0.02	0	0.3	0	0.09	0.6	0.11
Plate 10	0.1	0.01	0	0.21	0	0.07	0.8	0.12
Plate 11	0.1	0.02	0	0.47	0	0.1	0.4	0.11

Run	S2-30		Figures where data appears:			4.38		
	Sr		Si		Al		Ca	
Date	#######		#######		#######		#######	
Initials	JMA		BN		JS		JS	
	conc.	s.d.	conc.	s.d.	conc.	s.d.	conc.	s.d.
Plate 1	0	0.02	0	0.32	0	0.09	0	0.1
Plate 2	0.1	0.01	0	0.44	0	0.14	0	0.07
Plate 3	2.4	0.08	0	0.34	0	0.05	0	0.09
Plate 4	3.9	0.16	0	0.38	0	0.1	0	0.12
Plate 5	1.4	0.06	0.2	0.59	0.3	0.08	0.1	0.11
Plate 6	2.3	0.07	1	0.5	1.4	0.11	0.2	0.07
Plate 7	4.5	0.07	3.4	0.35	4	0.11	1.1	0.1
Plate 8	3.4	0.08	2.3	0.4	2.7	0.1	3	0.13
Plate 9	0.2	0.02	0.6	0.53	0.3	0.1	0.8	0.1

	Sr		Si		Al		Ca	
	conc.	s.d.	conc.	s.d.	conc.	s.d.	conc.	s.d.
Plate 10	0	0.01	0	0.25	0.1	0.09	0.6	0.1
Plate 11	0	0.01	0	0.31	0.1	0.07	0.3	0.1

Run	S3-1		Figures where data appears:		4.35			
	Sr		Si		Al		Ca	
Date	#######		#######		#######			
Initials	JS		JS		SF			
	conc.	s.d.	conc.	s.d.	conc.	s.d.	conc.	s.d.
Plate 1	0.5	0.02	0	0.53	0.4	0.27		
Plate 2	2.4	0.07	0.1	0.64	0.2	0.21		
Plate 3	2.7	0.06	0	0.56	0	0.2		
Plate 4	1.6	0.03	0.3	0.64	0.4	0.17		
Plate 5	2.1	0.05	0.1	0.68	0.4	0.23		
Plate 6	6.7	0.18	1.2	0.41	1.8	0.26		
Plate 7	8.7	0.18	8.3	0.82	8.6	0.39		
Plate 8	2.6	0.07	4.6	0.7	4.5	0.22		
Plate 9	0.5	0.02	0.4	0.58	1.5	0.3		
Plate 10	0.3	0.01	1.2	0.51	1.3	0.25		
Plate 11	0	0.06	0	0.45	0.5	0.35		

Run	S3-2		Figures where data appears:		4.35			
	Sr		Si		Al		Ca	
Date	#######		#######		#######			
Initials	JS		JS		SF			
	conc.	s.d.	conc.	s.d.	conc.	s.d.	conc.	s.d.
Plate 1	0.5	0.01	0	0.38	0.2	0.27		
Plate 2	2.6	0.1	0	0.45	0.1	0.26		
Plate 3	3.1	0.12	0	0.48	0.2	0.27		
Plate 4	1.7	0.06	0.3	0.59	0.3	0.41		
Plate 5	2.2	0.06	0.4	0.49	0.3	0.32		
Plate 6	4.3	0.2	2	0.47	1.9	0.26		
Plate 7	11	0.27	15.7	0.74	13.7	0.44		
Plate 8	3.3	0.11	9.1	0.68	7.6	0.31		
Plate 9	0.6	0.02	2.9	0.8	2.4	0.27		
Plate 10	0.5	0.02	2.4	0.67	2	0.26		
Plate 11	0.1	0.01	0.5	0.69	0.5	0.22		

Run	S3-3		Figures where data appears:		4.33			
	Sr		Si		Al		Ca	
Date	#######							
Initials	JS							
	conc.	s.d.	conc.	s.d.	conc.	s.d.	conc.	s.d.
Plate 1	0.3	0.02						
Plate 2	1.3	0.06						
Plate 3	5.2	0.1						
Plate 4	5.2	0.14						
Plate 5	5.5	0.2						
Plate 6	10.9	0.33						
Plate 7	22	0.88						
Plate 8	6.1	0.16						

	Sr		Si		Al		Ca	
Plate 9	0.1	0.02						
Plate 10	0	0.01						
Plate 11	0	0.02						

Run	S3-4		Figures where data appears:		4.33			
	Sr		Si		Al		Ca	
Date	#######							
Initials	JS							
	conc.	s.d.	conc.	s.d.	conc.	s.d.	conc.	s.d.
Plate 1	0.3	0.02						
Plate 2	1.5	0.04						
Plate 3	5.6	0.21						
Plate 4	4.8	0.15						
Plate 5	5.3	0.22						
Plate 6	13.5	0.58						
Plate 7	21.9	0.5						
Plate 8	6.4	0.22						
Plate 9	0.1	0.02						
Plate 10	0	0.02						
Plate 11	0	0.01						

Run	S3-5		Figures where data appears:					
	Sr		Si		Al		Ca	
Date	#######		#######		#######			
Initials	JS		JS		SF			
	conc.	s.d.	conc.	s.d.	conc.	s.d.	conc.	s.d.
Plate 1	0.1	0.01	0.4	0.77	0.5	0.24		
Plate 2	0.1	0.01	0.6	0.34	0.5	0.19		
Plate 3	0.2	0.02	0.1	0.68	0.5	0.37		
Plate 4	0.5	0.02	0.2	0.5	0.6	0.17		
Plate 5	0.9	0.03	0.7	0.51	0.6	0.19		
Plate 6	2.6	0.09	7.5	0.6	5.8	0.33		
Plate 7	6.1	0.18	16.9	0.96	14.3	0.39		
Plate 8	5	0.2	16	0.6	13.6	0.28		
Plate 9	0.3	0.02	2.4	0.46	1.3	0.28		
Plate 10	0.1	0.02	1	0.48	0.4	0.24		
Plate 11	0.1	0.02	0.3	0.55	0.2	0.32		

Run	S3-6		Figures where data appears:					
	Sr		Si		Al		Ca	
Date	#######		#######		#######			
Initials	JS		JS		SF			
	conc.	s.d.	conc.	s.d.	conc.	s.d.	conc.	s.d.
Plate 1	0	0.02	0	0.56	0.1	0.46		
Plate 2	0.1	0.01	0	0.58	0.1	0.25		
Plate 3	0.2	0.01	0	0.67	0	0.31		
Plate 4	0.4	0.02	0.3	0.6	0.3	0.25		
Plate 5	0.6	0.02	0.5	0.56	0.8	0.26		
Plate 6	2.4	0.04	7.2	0.54	5.8	0.42		
Plate 7	8.5	0.28	18	0.66	16.2	0.31		

Plate 8	6.2	0.16	17.7	0.4	15.8	0.35
Plate 9	0.8	0.05	2.8	0.45	2.6	0.36
Plate 10	0.2	0.02	1.4	0.57	0.9	0.31
Plate 11	1.8	0.08	4.3	0.66	3.4	0.27

Run	S3-7		Figures where data appears:					
	Sr		Si		Al		Ca	
Date	#######		#######		#######			
Initials	JS		JS		SF			
	conc.	s.d.	conc.	s.d.	conc.	s.d.	conc.	s.d.
Plate 1	0.1	0.01	0	0.44	0	0.34		
Plate 2	0.5	0.01	0.9	0.28	0	0.28		
Plate 3	1.6	0.07	0.2	0.6	0	0.24		
Plate 4	3.5	0.11	0	0.52	0	0.27		
Plate 5	4.7	0.13	0.6	0.52	0.1	0.25		
Plate 6	5.7	0.15	2	0.67	1.5	0.33		
Plate 7	6.1	0.2	11.8	0.71	10.3	0.39		
Plate 8	5.1	0.17	12.4	0.53	11.2	0.32		
Plate 9	0.9	0.03	5.3	0.6	4.8	0.2		
Plate 10	0.7	0.03	11.1	0.51	9.7	0.42		
Plate 11	0.2	0.01	4.5	0.74	4.1	0.35		

Run	S3-8		Figures where data appears:					
	Sr		Si		Al		Ca	
Date	#######		#######		#######			
Initials	JS		JS		SF			
	conc.	s.d.	conc.	s.d.	conc.	s.d.	conc.	s.d.
Plate 1	0.1	0.01	0	0.74	0.1	0.32		
Plate 2	0.4	0.02	0.1	0.51	0	0.28		
Plate 3	2.3	0.11	0	0.39	0	0.31		
Plate 4	4.4	0.1	0	0.56	0	0.24		
Plate 5	4.8	0.1	0	0.53	0.1	0.3		
Plate 6	8.5	0.31	1.6	0.55	1.7	0.32		
Plate 7	7.1	0.27	11.4	0.69	10.7	0.33		
Plate 8	5.6	0.19	12.7	0.57	11	0.29		
Plate 9	0.7	0.04	2.7	0.6	3	0.24		
Plate 10	0.6	0.03	7.7	0.51	6.9	0.16		
Plate 11	0.2	0.02	5.6	0.7	5.5	0.22		

REFERENCES

Aganihotri, R., et al. (1998). "Selenium Removal Using Ca-Based Sorbents: Reaction Kinetics." Environmental Science and Technology **32**: 1841-1846.

Barin, I. (1995). Thermochemical Data of Pure Substances. Weinheim, FRG, VCH.

Biermann, J. J. P., et al. (1997). Thermal Conversion of Deinking Residue to Produce Valuable Cement Products. 18th VDI German/Dutch Engineering meeting.

Biswas, P. and C. Y. Wu (1998). "Control of Toxic Metal Emissions from Combustors Using Sorbents: A Review." Journal of the Air and Waste Management Association **48**(February): 113-127.

Bool, L. E., et al. (1995). "The Partitioning of Iron during the Combustion of Pulverized Coal." Combustion and Flame **100**: 262-270.

Buckley, S. G., et al. (1998). Fate of Sr and Cs in Biomass Combustion. 1998 Spring Technical Meeting of the Western States Section of the Combustion Institute, U.C. Berkeley, Berkeley, CA.

Costner, P. and J. Thornton (1990). Playing with Fire: Hazardous Waste Incineration. A Greenpeace Report, Washington D.C., Greenpeace U.S.A.

Crosley, S. M. and R. J. Kedl (1992). Laboratory Measurements of Metal Adsorption from Simulated Incinerator Flue Gases: Sorbent Selection for Cesium Capture. 1992 Incineration Conference, Albuquerque, NM.

Davis, S. B. (1999 - not yet in print). Interactions Between Semi-Volatile Toxic Metals and Sorbents in Combustors. Chemical and Environmental Engineering, Tucson, AZ, University of Arizona.

Davis, S. B., et al. (1998). Multi-Component Coagulation and Condensation of Toxic Metals in Combustors. 27th Symposium (International) on Combustion, University of Colorado at Boulder.

Durlak, S. K., et al. (1997). "Equilibrium Analysis of the Affect of Temperature, Moisture, and Sodium Content on Heavy Metal Emissions from Municipal Solid Waste Incinerators." Journal of Hazardous Materials **56**: 1-20.

Fernandez, M. A., et al. (1992). "Behavior of Heavy Metals in the Combustion Gases of Urban Waste Incinerators." Environmental Science and Technology **26**: 1040-1047.

Frandsen, F., et al. (1994). "Trace Elements From Combustion and Gasification of Coal - An Equilibrium Approach." Progress in Energy and Combustion Science **20**: 115-138.

Furr, A. K., et al. (1977). "National Survey of Elements and Radioactivity in Fly Ashes: Absorption of Elements by Cabbage Grown in Fly Ash-Soil Mixtures." Environmental Science and Technology **11**(13): 1194-1201.

Gallagher, N. B., et al. (1996). Sodium Partitioning in a Pulverized Coal Combustion Environment. Twenty-Sixth Symposium (International) on Combustion.

Ghosh-Dastidar, A., et al. (1996). "Selenium Capture Using Sorbent Powders: Mechanism of Sorption by Hydrated Lime." Environmental Science and Technology **30**: 447-452.

Gordon, S. and B. J. McBride (1994). Computer Program for Calculation of Complex Chemical Equilibrium Compositions and Applications, Cleveland, Ohio, National Aeronautics and Space Administration.

Hillamo, R. and E. Kauppinen (1991). "On the Performance of the Berner Low Pressure Impactor." Aerosol Science and Technology **14**: 33-47.

Hitachi (1992). Instrument Manual for Model S-2460N, Hitachi.

Ho, T. C., et al. (1993). "Metal Volatilization and Separation During Incineration." Waste Management **13**: 455-466.

Ho, T. C., et al. "Characteristics of Metal Capture during Fluidized Bed Incineration." AIChE Symposium Series **87**(281): 118-126.

Noran Instruments. (1995). Voyager Handbook, Noran Instruments.

Jozewicz, W. and B. K. Gullett (1995). "Reaction Mechanisms of Dry Ca-Based Sorbents with Gaseous HCl." Industrial and Engineering Chemistry Research **34**: 607-612.

Karimanal, K. V. and M. J. Hall (1996). "Effect of Temperature and Flow on the Volatilization of Elemental Lead and Cadmium." Hazardous Waste and Hazardous Materials **13**(1): 63-71.

Lee, S. H. D. and I. Johnson (1980). "Removal of Gaseous Alkali Metal Compounds from Hot Flue Gas by Particulate Sorbents." Journal of Engineering for Power **102**(April): 397-402.

Lide, D. R. (1995). CRC Handbook of Chemistry and Physics. Boca Raton, FL, CRC Press.

Linak, W. P., et al. (1996). "Formation and Destruction of Hexavalent Chromium in a Laboratory Swirl Flame Incinerator." <u>Combustion Science and Technology</u> **116-117**: 479-498.

Linak, W. P., et al. (1994). "Metal Aerosol Formation in a Laboratory Swirl Flame Incinerator." <u>Combustion Science and Technology</u> **101**: 7-27.

Linak, W. P., et al. (1995). "Sorbent Capture of Nickel, Lead, and Cadmium in a Laboratory Swirl Flame Incinerator." <u>Combustion and Flame</u> **100**: 241-250.

Linak, W. P. and J. O. L. Wendt (1993). "Toxic Metal Emissions From Incineration: Mechanisms and Control." <u>Progress in Energy and Combustion Science</u> **19**: 145-185.

Linak, W. P. and J. O. L. Wendt (1998). "Partitioning of the Refractory Metals, Nickel and Chromium, in Combustion Systems." <u>Combustion Science and Technology</u>: 29.

Mwabe, P. O. and J. O. L. Wendt (1996). <u>Mechanisms Governing Trace Sodium Capture by Kaolinite in a Downflow Combustor</u>. Twenty-Sixth Symposium (International) on Combustion, Naples, Italy.

Perkin-Elmer (1982). <u>User's Manual for the Model 2380 Atomic Absorption Spectrophotometer</u>, Perkin-Elmer.

Punjak, W. A., et al. (1989). "High-Temperature Adsorption of Alkali Vapors on Solid Sorbents." <u>AIChE Journal</u> **35**(7, July): 1186-1194.

Rizeq, R. G., et al. (1994). "Predictions of metals emissions and partitioning in coal-fired combustion systems." <u>Fuel Processing Technology</u> **39**: 219-236.

Rizeq, R. G. and F. Shadman (1989). "Alkali-Induced Agglomeration of Solid Particles in Coal Combustors and Gasifiers." <u>Chemical Engineering Communication</u> **81**: 83-96.

Scotto, M. V. (1992). Mechanisms Governing the Abatement of Metal Emissions From Waste Incineration. <u>Chemical Engineering</u>, Tucson, University of Arizona**:** 360.

Scotto, M. V., et al. (1992). <u>Hazardous Waste Incineration: The In-situ Capture of Lead by Sorbents in a Laboratory Down-Flow Combustor</u>. Twenty-Fourth Symposium (International) on Combustion.

Scotto, M. V., et al. (1994). "Metal Capture by sorbents in combustion processes." <u>Fuel Processing Technology</u> **39**: 357-372.

Serne, R. J., et al. (1996). Characterization of Radionuclide-Chelating Agent Complexes Found in Low-Level Radioactive Decontamination Waste, Richland, WA, Pacific Northwest National Laboratory**:** 147.

Shadman, F. and W. A. Punjak (1988). "Thermochemistry of Alkali Interactions with Refractory Adsorbents." <u>Thermochimica Acta</u>: 141-152.

Siemer, D. D. (1986). Atomic Absorption Spectroscopy. <u>Materials Characterization</u>. R. E. Whan, ASM International. **10:** 43-59.

Sill, C. W. (1988). "Volatility of Cesium and Strontium from a Synthetic Basalt." <u>Nuclear and Chemical Waste Management</u> **8**: 97-105.

Uberoi, M., et al. (1990). "The Kinetics and Mechanism of Alkali Removal from Flue Gases by Solid Sorbents." <u>Progress in Energy and Combustion Science</u> **16**: 205-211.

Uberoi, M. and F. Shadman (1990). "Sorbents for Removal of Lead Compounds from Hot Flue Gases." <u>AIChE Journal</u> **36**(2): 307-309.

Uberoi, M. and F. Shadman (1991). "High-Temperature Removal of Cadmium Compounds Using Solid Sorbents." <u>Environmental Science and Technology</u> **25**(7): 1285-1289.

Venkatesh, S., et al. (1996). "Evaluation of Mineral-Based Additives as Sorbents for Hazardous Trace Metal Capture and Immobilization in Incineration Processes." <u>Hazardous Waste and Hazardous Materials</u> **13**(1): 73-94.

Wu, B., et al. (1995). "Multi-Functional Sorbents for the Removal of Sulfur and Metallic Contaminants from High-Temperature Gases." <u>Environmental Science and Technology</u> **29**: 1660-1665.

Yang, H. C., et al. (1998). "Behavior of Hazardous and Radioactive Metals in a Laboratory Furnace and a Demonstration-Scale Incinerator." <u>Environmental Engineering Science</u> **15**(4): 299-311.

Appendix B

Manuscript of

"Trajectories of Evaporating Droplets in a Turbulent Combustor Using the One Dimensional Turbulence Model"

J. R. Schmidt

Department of Chemical and Environmental Engineering

The University of Arizona

2000

(Self paginated)

TRAJECTORIES OF EVAPORATING DROPLETS IN A TURBULENT

COMBUSTOR USING THE ONE DIMENSIONAL TURBULENCE MODEL

by

John Richard Schmidt

_____

A Thesis Submitted to the Faculty of the

DEPARTMENT OF CHEMICAL AND ENVIRONMENTAL ENGINEERING

In Partial Fulfillment of the Requirements
For the Degree of

MASTER OF SCIENCE
WITH A MAJOR IN CHEMICAL ENGINEERING

In the Graduate College

THE UNIVERSITY OF ARIZONA

2 0 0 0

STATEMENT BY THE AUTHOR

This thesis has been submitted in partial fulfillment of requirements for an advanced degree at the University of Arizona and is deposited in the University Library to be made available to borrowers under rules of the Library.

Brief quotations from this thesis are allowable without special permission, provided that accurate acknowledgment of source is made. Requests for permission for extended quotation from or reproduction of this manuscript in whole or in part may be granted by the head of the major department or the Dean of the Graduate College when in his or her judgement the proposed use of the material is in the interest of scholarship. In all other instances, however, permission must be obtained from the author.

SIGNED: _____

APPROVAL BY THESIS DIRECTOR
This thesis has been approved on the date shown below:

_____   _____
Jost Otto Lutz Wendt, Ph D   Date
Professor and Head
Department of Chemical and
Environmental Engineering

ACKNOWLEDGEMENTS

It is with much gratitude that I acknowledge professor Jost Wendt for his support, guidance and help. Most of all for allowing me the opportunity to return to my studies after a long absence in industry. Returning to the rigors and discipline of the academic life was not easy, but Dr. Wendt remained patient and understanding.

Also, the completion of this work would have never come about in a timely manner, if it were not for the advice and guidance of Dr. Alan Kerstein of Sandia National Laboratories. His keen interest in this project and the sharing of his technical brilliance were of great help.

Funding from the Department of Energy under project number DEFG0797ER14831 was greatly appreciated.

Dr. Tom Dreeben was kind enough to give me a highly developed ODT proper FORTRAN code which was the starting point for the two-phase flow modeling I did. I also thank him for his patience as I learned his code. Many people offered up valuable advice and help at various stages of my research. While I cannot possibly thank everyone by name, I would like to name Marvin Landis, Dr. Sheldon Davis, Scot Wunsch, Vebjorn Nilsen, Tereck Echekki, Art Fernandez, John Hewson, Tom Gale, Greg Ogden and Wayne Seams.

I thank my mother, Aida Villagran Schmidt, for her love faith and encouragement were essential in bringing this work to completion. The kindness, love and encouragement of my brother (Henry) and sisters (Frances, Aida, Anne, and Maria [niece]) were of great comfort in times of distress.

I thank my many friends, both recent and lifelong for their help and encouragement.

Most importantly I thank God, the source of life, for the plethora of gifts which he has bestowed on me. Both the natural gifts which allowed me to do the engineering portion of this work and the everyday gifts (e.g. food, clothing, …). His church has also brought me much support, encouragement, and consolation over the many years of my studies. Also the patronage of Mary has been instrumental in my studies, for which I am very grateful.

"Burn from my brain and from my breast

Sloth, and the cowardice that clings,

And stiffness and the soul's arrest:

And feed my brain with better things."

- Gilbert Keith Chesterton

TABLE OF CONTENTS

TABLE OF CONTENTS -- continued

TABLE OF CONTENTS -- continued

List of Figures

List of Figures -- continued

List of Figures -- continued

List of Figures -- continued

List of Tables

ABSTRACT

In the incineration of liquid hazardous wastes there exist "rogue" droplets (>300 μm diameter) which penetrate past the flame zone and burn as isolated droplets in the postflame gasses. Detailed knowledge of the droplet burnout points are essential to keeping the destruction removal efficiency in excess of the 99.99% required. The spread in trajectory endpoints of individual evaporating droplet streams injected into a turbulent combustor was investigated numerically. Results are in good agreement with the measurements. Correlation between the spread in the burnout points and initial droplet size, initial droplet velocity, interdroplet spacing, and droplet injection angle were investigated. The numerical investigation utilizes the novel One Dimensional Turbulence (ODT) {Kerstein (1999)} for the time developing fluid velocity and temperature fields with a new two phase flow model for predicting particle trajectories. The droplet heating/burning model used by Mulholland et al. (1991) is modified for application to this thesis.

Chapter 1

Research Goals and Approach

Two-phase flows are designated as flows in which there are two distinct phases [Sirignano (1999)]. Gas-liquid and solid-gas are the two most common. Examples include bubbles rising in a liquid; liquid being sprayed into a gas phase, such as a fuel into a combustor; and a dusty gas, solid particles dispersed in a gas phase. Most two-phase flow applications involve one of the phases occupying a relatively small volume fraction. The phase with the largest volume fraction is referred to as the continuous phase. The other phase is referred to as the discrete phase. The example of bubbly flow given above would have the gas phase as the discrete phase, and the liquid phase as the continuous phase. However, the example of fuel being sprayed into a combustor would be arranged in the opposite order. The liquid phase is the discrete phase and the gas phase is the continuous phase.

The modeling of two-phase flow systems accurately is of economic importance because of the multitude of industrial manufacturing world-wide which uses this technology (Sirignano, 1999; Stock, 1996). Just a few examples are, spray drying, spray coating, pulverized coal combustion, and even such obscure applications as the entrainment of prescription drugs as an

aerosol so that patients may ingest the drugs through their lungs rather then through the stomach. Using this method enables the drug to get into the blood stream much more quickly and lessens the possibility of destructive reactions with the gastric fluids.

Another area of two-phase flow modeling which is of major importance is in the area of combustion. Here the challenge of turbulence modeling is added to the already difficult modeling of two phase flows.

The motivation of the present work lies in the existence of a large volume of liquid hazardous waste in virtually perpetual storage by the Department of Energy (DOE). Some of the storage containers housing these hazardous wastes have leaked and contaminated the surrounding soil. This has motivated the DOE to look at other ways to handle, perhaps dispose of these liquid hazardous wastes. A good method of disposing of these wastes is thermal reaction or incineration. Specifically the incineration of metal containing liquid hazardous wastes provided the funding for this project. The United States law in many cases (such as for principal organic hazardous constituents) requires a 99.99 % destruction of the organic hazardous material (Wendt, 1994). In a few cases (e.g. polychlorobiphenyls) a destruction level of 99.9999 % is required by law.

Even though this destruction level must only be demonstrated during test burns, this places a tremendous burden on the proper design and implementation of these incineration systems to assure the safety of those working in the incineration plant and those people living in the area. Typically the incineration system consists of an ignited gas fired combustor into which the liquid hazardous waste is sprayed through a relatively large bore spray nozzle. Since these are wastes, there are large variations in the composition and viscosity of these wastes. It is this wide range of viscosity that requires the use of a large bore spray nozzle so the spray nozzle does not clog up and cause a furnace shutdown and cleaning out of the nozzle by a HazMat team (Kramlich, et al., 1984).

Studies of the incineration systems showed the existence of large "rogue" droplets which penetrated the flame zone and burn as individual droplets (Wendt, 1994). The existence of rogue droplets, which are approximately 10X the size of the mean droplet, causes a legitimate concern for the safety of those who may come in contact with the exhaust fumes of the furnace, if the droplets traverse the hot zone of the furnace with out being combusted. One rogue droplet (10X the mean radius) which is only 80% converted out of two million mean size droplets is enough to fail the 99.99% conversion

requirement. The systematic study and modeling of rogue droplets is essential to the safe design of these systems. Motivated by this, Mulholland et al. (1991) performed a number of systematic experiments and some numerical modeling with the intention of improving the state-of-the-art design technology.

Mulholland et al. took great pains in the experimental arrangement to be able to reproduce droplet streams of nearly identical initial diameter, velocity, inter-droplet spacing, and injection angle into a 100 kW (lab scale) turbulent combustor. A fuel oil was used as the hazardous waste surrogate. The droplets themselves were designed to be representative of the rogue droplets with an initial diameter greater than 300 μ. The stream was injected through an opening ~14 cm above the centerline. The centerline of the reactor is also the position of the gas burner. The burner was set to produce a type C flame. A type C flame uses a high combustion air swirl (swirl number = 1.3 in this case) therefore the flame is stabilized close to the burner. The injected droplet stream proceeded in a straight line trajectory until it reached the high shear layer of the combustion gas flow, at which point the droplet stream broke into what appeared to be random individual drops. The droplets passed through the flame zone and subsequently ignited

and burned out. Mulholland et al. performed careful position measurements of the droplet ignition and burnout. They found a surprising large spread (maximum axial distance traveled before complete burning minus the minimum axial distance traveled before complete burning) in the burnout points for all cases. A schematic of the experimental apparatus used by Mulholland et al. is reproduced in Figure 1.1. It shows a drawing of the 100 kW combustor and relevant equipment. Figure 1.2 shows the observed range of trajectory endpoints (location at which burn out was completed) for one specific test case (the nominal case). The authors were surprised because of the droplet streams themselves were highly reproducible and in the absence of turbulence one would expect the spread in the burnout to be small. Hence, the large spread was properly attributed to the highly turbulent nature of the fluid flow in the lab scale kiln. Attempts by the authors to model the mean trajectory of the droplets were of limited success They could not hope to predict the spread in the endpoints because of the failure of their model to capture properly the turbulent flow in the reactor.

What is needed in order to render incineration completely safe, is a tool that can predict the time/temperature/environment history of every single fragment of waste that is introduced into the reactor. In turbulent flows,
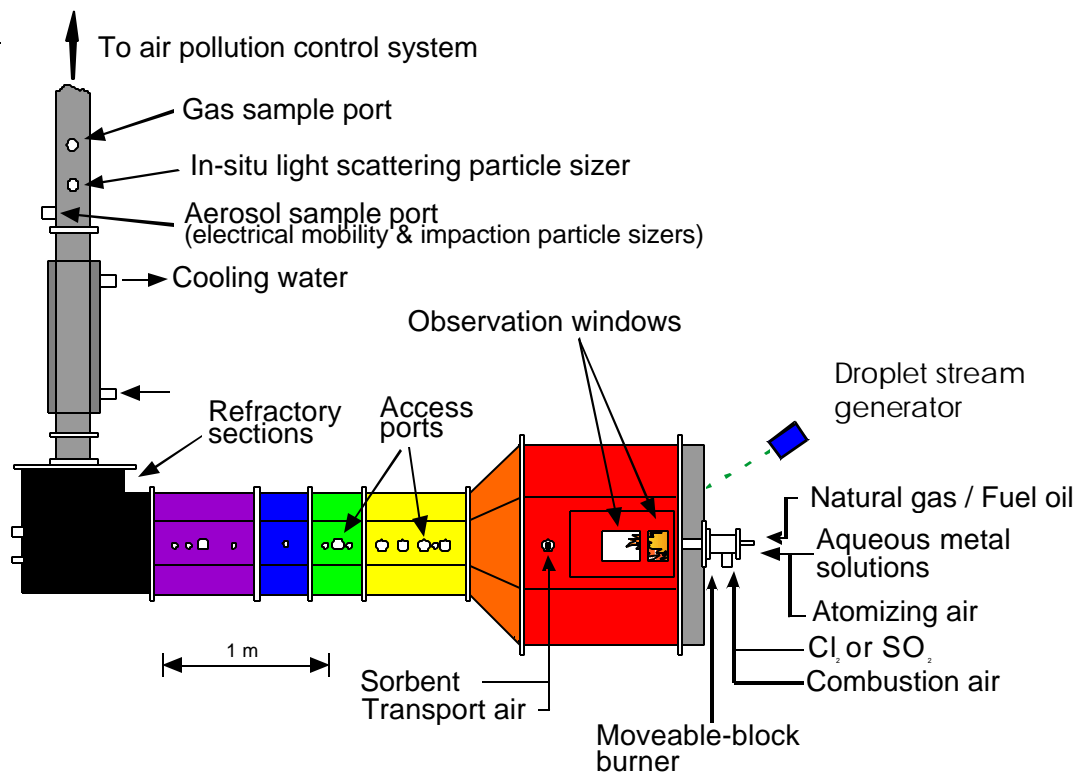
Figure 1.1: Drawing of the 100 kW furnace. Modular furnace for turbulent diffusion flame study, with monodisperse droplet stream generator.

different fragments of waste that are introduced in an identical manner have different time/temperature/environment histories. See Figure 1.2 These are not completely random. A description of the mean or median time/temperature/environment history is not adequate. Rather it is required to find a modeling method which captures the relevant physics of the turbulent fluid flow and the two-phase flow, in as simple a formulation as possible. Also a model for predicting the droplet heating and evaporation is necessary
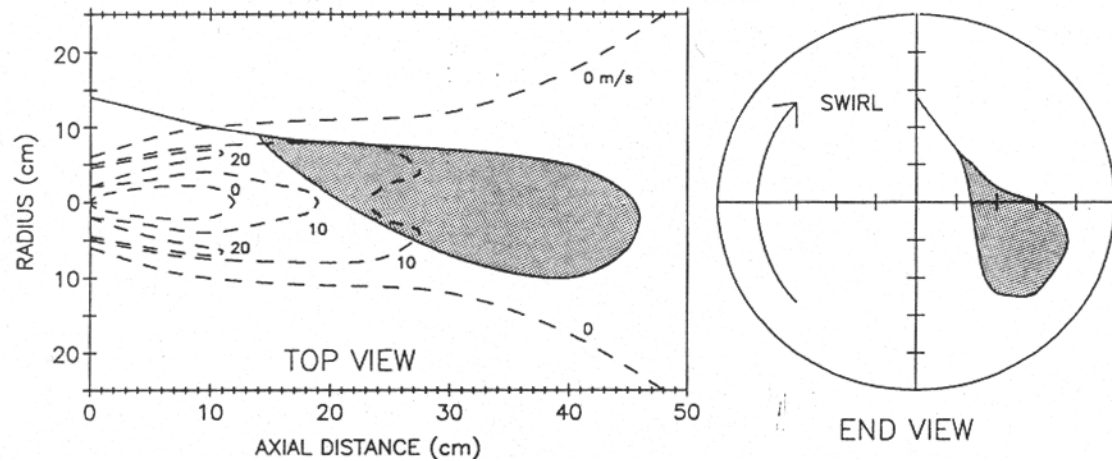
Figure 1.2: Measured trajectories for the nominal stream condition (Case 1) in a Type C turbulent flame. The shaded area represents the range of trajectory endpoints. The gas phase axial velocity profile is superimposed on the top view (dashed lines).

to capture the spread in the burn out points is needed. The successful modeling of the spread of these rogue droplets would provide a significant contribution to further the design of incineration facilities to assure the wastes be disposed of in a safe and efficient manner.

The novel One Dimensional Turbulence model (ODT) developed by Kerstein (1999) seemed uniquely suited to fulfilling the need to predict accurately and simply this turbulent gas flow. (ODT is described in detail in Chapter 2.) The kiln has the requisite one homogeneous dimension (θ) and the gas flow is predominantly down the axis of the reactor yet the flow is

highly turbulent. The Reynolds number (Re) based on the gas fuel nozzle diameter is of order 10,000.

Other methods such as Large Eddy Simulation (LES) and Direct Numerical Simulation (DNS) could probably be applied successfully to solve this problem. Unlike LES, ODT would resolve the scales necessary to capture the smallest eddies. Albeit only in the one dimension (transverse to the flow) which ODT keeps track of. In addition LES needs a subgrid model to account for energy losses due to such things as viscosity. Since ODT keeps track of the smallest eddy scales, the standard viscous dissipation equation takes care of this. An additional consideration is that the LES method would need a subgrid model to account properly for the two-phase flow portion of the model. Because ODT captures the smallest scales, no additional assumptions are needed for implementation into ODT.

The state-of-the-art DNS modeling of turbulent flows is restricted by the maximum Re allowable due to the memory and speed of the fastest computers available. The memory requirement for DNS goes as the number of grid points needed to resolve fully the turbulent (Kolmogorov) scale raised to the third power. Since ODT keeps track of only one dimension, the required memory scales directly with the number of grid points needed to

resolve the turbulent scale. Though progress to bring DNS to the high Re regime continues on all fronts, there is still much work to be done in order to use DNS for practical industrial applications. Since the ODT model capitalizes on the symmetry of the flow and utilizes innovative methods to model three-dimensional turbulent behavior on a one-dimensional domain, it is the model of choice for this highly turbulent flow configuration.

The existing ODT formulations did not have the option for two-phase flow computations already built in. Consequently a two-phase flow submodel to ODT needed to be developed for this work.

The development of two-phase flow models with a turbulent gas phase is traditionally broken into three categories, 1-way coupling, 2-way coupling, and 4-way coupling. The simplest is 1-way coupling, in this case the turbulent contribution of the dispersed phase is negligible. The turbulent field is much more likely to gain kinetic energy from the gas flow rather than from the flow of the dispersed phase (the liquid droplets in this case). Here, the fluid affects the particle, but the particle does not affect the fluid. This is often symbolized as: fluid → particle (one arrow).

The 2-way coupling flows are the next complicated. In this case the volume fraction of the dispersed phase is high enough that the mean flow of

the particles can induce turbulent motion in the fluid. (Also as in the 1-way coupling the turbulent fluid motion induces motion in the particles. Hence the title, 2-way coupling.) This is symbolized as fluid ← → particle (two arrows).

The most complicated of the flows is referred to as 4-way coupling. In this case, the volume fraction of the dispersed phase is so large, that the dispersed phase particles not only affect the fluid flow, but also affect each other by way of collisions or near collisions (wake or boundary layer interactions). This is symbolized as fluid ← → particle ← → particle (four arrows). Elghobashi (1991, 1994) shows the range in which the three types of coupling are of importance.

This model utilizes the 1-way coupling assumption. A Lagrangian framework for the particle is used with the key forces on the particle considered to be a modified Stokes drag and gravity. Sirignano (1999) states that good engineering analysis can be performed using only modified stokes drag and the gravitational force. A majority of the state-of-the-art publications in the area of two-phase flow use the 1-way coupling assumption along with a drag force to compute the equation of motion of particles.

In this thesis, the salient features of Kerstein's one-dimensional turbulence model are described in Chapter2. This is followed by a description of how two-phase flow can be added to the ODT model. Chapter 4 designates the droplet burning model also necessary to describe experimental droplet trajectory endpoints. While the following chapter the results and comparisons with Mulholland et al.'s data. Chapter 6 shows additional results showing the effects of the empirical parameter β, which appears in the formulation of the ODT two-phase flow submodel. The conclusions are presented in Chapter 7.

Chapter 2

One Dimensional Turbulence Model (ODT)

2.1   Introduction

Kerstein (1999) developed a one-dimensional Monte Carlo modeling technique for turbulent mixing of velocity and scalar fields. He develops both time developing and spatially developing models, but only the time developing model will be discussed here since that is what was used in this application. The ODT approach represents turbulent advection by a random sequence of "eddy" maps applied to a one-dimensional computational domain. Profiles of the advected velocity component (u) and the advected scalars evolve on this domain. Equations for the turbulent flow field are not solved explicitly, rather the viscous and diffusive equations are solved,

$$\frac{\partial u}{\partial t} = \boldsymbol{u}\frac{\partial^2 u}{\partial y^2} - \frac{1}{\boldsymbol{r}}\frac{\partial p}{\partial x} \qquad (2-1)$$

$$\frac{\partial \boldsymbol{q}}{\partial t} = \boldsymbol{k}\frac{\partial^2 \boldsymbol{q}}{\partial y^2} \qquad (2-2)$$

where θ can be any advected scalar (e.g. temperature, species concentration, etc.) and κ is the corresponding diffusion coefficient. In this thesis the last term in Equation 2-1 was set to zero, see Section 2.9 for a discussion of this.

In order for ODT to be used there must be a minimum of one homogeneous direction.   There should be a predominantly streamwise direction. The one dimension in the One Dimensional Turbulence model is transverse to the mean flow.   See Figure 2.1 for an example flow configuration. It is informative to note that the application of Equation 2-1 under the given conditions would yield the well known laminar fluid flow solution without the intervention of triplet maps.   The ODT model implements triplet maps or eddies as instantaneous rearrangements of the velocity $u(y,t)$ field.

2.2   Definition of the triplet map

The triplet map has a starting point y_o and a length l which is sampled randomly from an eddy distribution rate. The mapping y $\rightarrow$ $\overline{y}$ rule for a triplet map is given by:

$$
\overline{y} = \begin{cases} y_o + \tfrac{1}{3}(y - y_o) & y_o < \overline{y} < y_o + \tfrac{1}{3}l \\ y_o + \tfrac{2}{3}l - \tfrac{1}{3}(y - y_o) & y_o + \tfrac{1}{3}l < \overline{y} < y_o + \tfrac{2}{3}l \\ y_o + \tfrac{2}{3}l + \tfrac{1}{3}(y - y_o) & y_o + \tfrac{2}{3}l < \overline{y} < y_o + l \\ y & otherwise \end{cases} \qquad (2-3)
$$

Where $\overline{y}$ is the y profile after the instantaneous rearrangement.
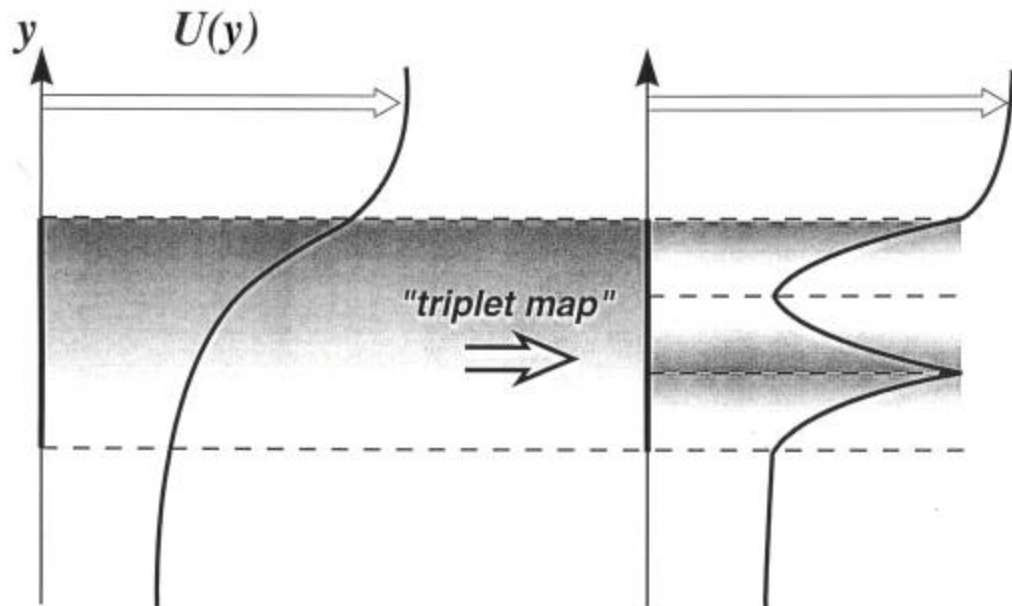
Figure 2.1: A sample velocity profile undergoing a triplet map "eddy".

The desired attribute of the triplet map is to provide a means of mimicking the increase in strain intensity, the decrease in strain length scale and the increase in mixing due to eddies in actual turbulent flow. This mapping rule assures that closest neighbors after the mapping event were no more then 3 cells apart before the mapping event. Hence the increased strain rate and shortening length scale is attained without undue introduction of discontinuities. As a matter of fact, in the limit as the discretized cell size

becomes infinitesimally small, so that the velocity field becomes continuous, the resulting velocity profile $u(y,t)$ has no discontinuities, only discontinuous derivatives. This can be seen in Figure 2.1 as well as Figure 2.2 (A) and (B). Using the continuous analog to describe the triplet map: the original u profile is reduced by a factor of three, and a copy is placed on both the top third and the bottom third of the eddy domain. For the middle third, the reduced image is inverted. The added benefit of the triplet map can be seen in Figure 2.2 (C) where neighboring cells (or fluid elements) before a triplet map can be separated by more than one half the eddy size after the mapping, thereby achieving the desired increase in mixing which is evidenced in real-life eddies.

Fluid parcels or elements are moved instantaneously during the triplet map from one y location to another. The momentum and passive scalar properties of each fluid particle or cell is preserved and remains unaffected by the instantaneous rearrangement. Though this may seem counterintuitive, this method is also used in Prandtl's Mixing Length theory for turbulent transport. Also Monin and Yaglom (1971) note that all mixing length theories transfer momentum as a passive scalar, neglecting pressure-induced momentum changes within the fluid element during exchange. A recent
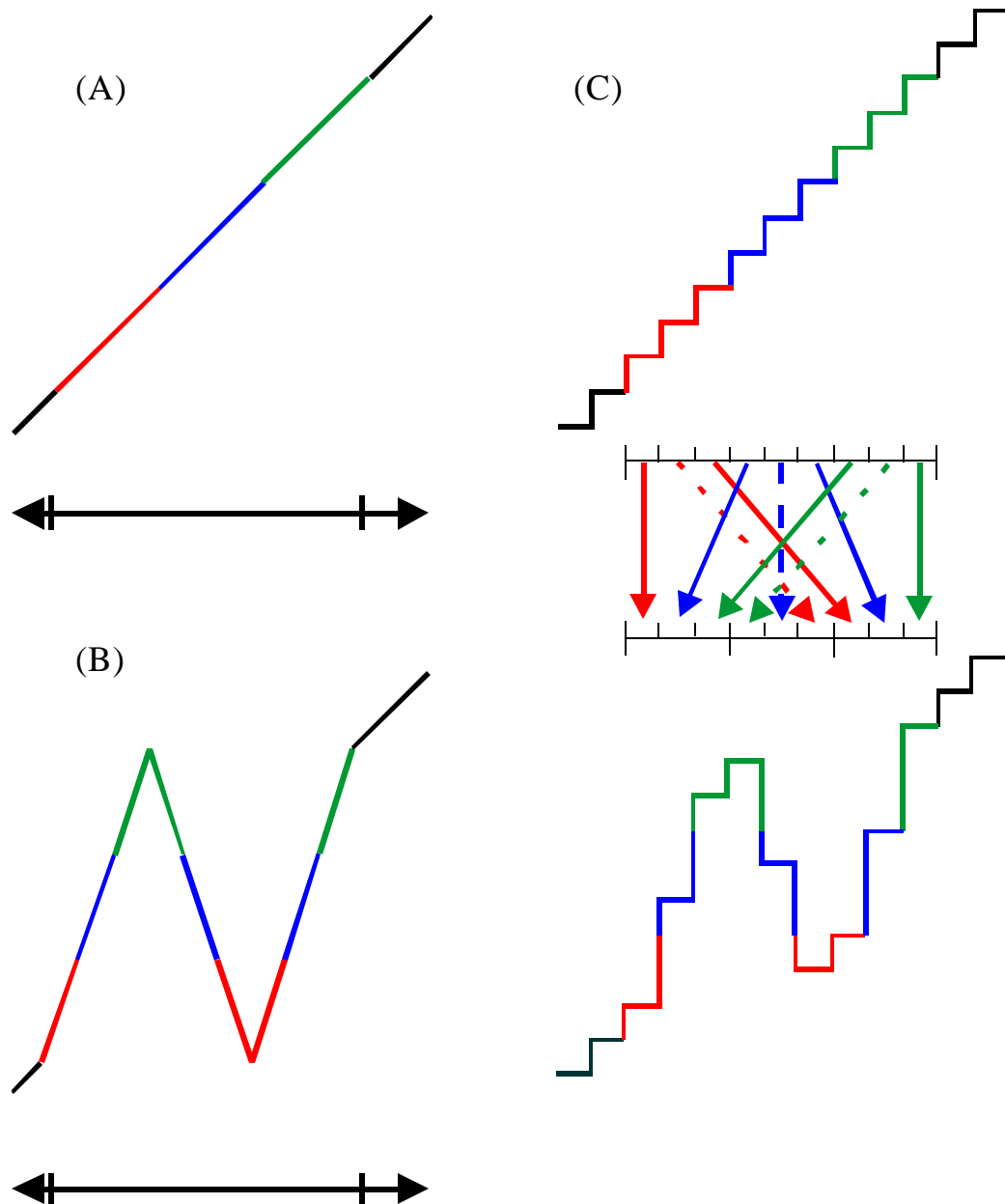
Figure 2.2: Effect of the triplet map on an initially linear velocity profile $u(y,t)$. (A) Initial profile. (B) Velocity profile after applying the triplet map to the interval denoted by ticks. (C) Discrete representation of the initial profile and illustration of the effect of a triplet map on an interval consisting of nine cells. For clarity, arrows indicating formation of the central of the three images of the original interval are dashed. Redrawn from Kerstein (1999).

development in ODT keeps three velocity components, this in turn allows

pressure scrambling (Kerstein et al., 2000)

2.3   Eddy rate distribution

The next challenge in the ODT model is deciding how to compute the eddy

rate distribution $\lambda(l; y, t)$, where $\lambda(l)$ dl dy is the frequency of events in the

size range $[l, l+\mathrm{d}l]$ per unit length along the y coordinate in the range $[y,$

$y+\mathrm{d}y]$, which gives λ units of (length^2 $\times$ time)$^{-1}$. It is defined such that the

total event rate R(t) (the total number of events per second) is given by

$$R(t) = \int_{l_{\min}}^{Y} \int_{y_{\min}}^{y_{\max}} \boldsymbol{I}(l; y_o, t) \, dy \, dl \quad . \qquad (2-4A)$$

An event is taken to be the occurrence of a triplet map. It describes the

idealization of an eddy on the ODT domain. By dimensional arguments,

$$\boldsymbol{I}(l) = \frac{1}{l^2 \boldsymbol{t}(l)} \qquad (2-4B)$$

where $\tau(l)$ is an eddy time scale. Kerstein (1999) treats $\tau(l)$ as a local

instantaneous time scale denoted $\tau(l; y, t)$ whose evaluation is based on $u(y,t)$,

$$\boldsymbol{t}(l; y_o, t) = \frac{l}{A \Delta u(y_o, l)} \qquad (2-5)$$

where $\Delta u(y_o, l)$ represents the velocity difference across the interval

$[y_o, y_o+l]$ and A is a free parameter. Specifically

$$\Delta u(y_o, l) = 2\left| u_l\left(y_o + \frac{l}{2}, t\right) - u_l(y_o, t) \right| \qquad (2-6)$$

where

$$u_l(y, t) = \frac{2}{l} \int_y^{y+\frac{l}{2}} u(y', t) dy' \quad . \qquad (2-7)$$

Hence the Δu in Equation 2-5 is based on the mixing cup average velocity

(Equation 2-7) of each half of the eddy. If these averages are shown to

differ greatly (hence there is a large strain rate across the eddy) then $\tau(l;y_o,t)$

is small and $\lambda(l; y_o, t)$ is large. Equations (2-4) – (2-6) give

$$\mathbf{1}(l; y_o, t) = \frac{2A \left| u_l(y_o, t) - u_l\left(y_o + \frac{l}{2}, t\right) \right|}{l^3} \quad . \qquad (2-8)$$

The free parameter A is the only free parameter in the ODT model proper.

The free parameter A was introduced to compensate for the fact that

$\Delta u(y_o, l)$ was chosen as a matter of preference. This arbitrary choice of

Equation 2-6 may in turn affect the numerical results, hence A allows fine

adjustments to the eddy rate distribution. The upshot is that A becomes a

turbulence intensity knob. Decreasing A decreases the level of turbulent intensity, and increasing A increases the turbulent intensity.

2.4 Dynamic feedback

At this point the eddy rate distribution is completely defined by the local position [y_o, y_o+l] and velocity distribution $u(y, t)$. Areas of high strain rate will have a higher $\lambda(l; y_o, t)$ therefore becoming more likely to have an eddy event (triplet map) than an identical area with a low strain rate. The onset of a triplet map increases the strain rate locally and hence increases the probability of spawning other eddies. Experiments have shown that this phenomenon of an eddy spawning other eddies occurs in physical flows. Kerstein (1999) has demonstrated in a number of flow simulations that a large triplet map will spawn a family of smaller triplet maps.

This is a powerful advantage of the ODT model. Flow properties (e.g. velocity variations) effect the eddy rate distribution through Equation 2-8 and the successful eddy events affect the velocity distribution (and passive scalars). This creates a feedback by increasing the strain rate which allows more triplet maps to occur.

2.5   Computing the eddy rate

With the eddy rate distribution, $\lambda(l; y_o, t)$ fully defined it would be possible to form the event rate,

$$R(t) = \int_{l_{min}}^{Y} \int_{y_{min}}^{y_{max}} \boldsymbol{1}(l; y_o, t) \, dy \, dl \quad . \qquad (2-9)$$

From this, one could then obtain the time between stirring events (or eddies) by inverting the rate,

$$\Delta t_{stir} = [R(t)]^{-1} = \left[\iint \boldsymbol{1}(l; y_o, t) \, dy \, dl \right]^{-1} \quad . \qquad (2-10)$$

However since λ is a function of starting position of the eddy, y_o, the length of the eddy, l, and the instant in time, t, this calculation is very expensive. As an alternative Kerstein (1999) proposes the following equivalent method based on the probability theory of a Poisson process.

At successive time increments Δt, sample the eddy parameters y_o and l from specified pdfs g(y_o) and f(l). respectively. Compute the corresponding value of $\lambda(l; y_o, t)$ based on the current $u(y, t)$ profile. Then apply a triplet map to [y_o, y_o+l] with probability

$$P(l; y_o, t, \Delta t) = \frac{\textbf{1}(l; y_o, t)\Delta t}{f(l)g(y_o)} \quad , \qquad (2-11)$$

Which is the probability that the eddy at y_o with length l will occur. Provided that f and g are nonzero for all allowed values of y_o and l, Kerstein (1999) showed that this procedure is equivalent to direct sampling of the eddy rate distribution $\lambda(l; y_o, t)$ in the limit as $\Delta t \rightarrow 0$.

Here $g(y_o)$ is chosen to be a pdf which gives a uniform probability of the entire y domain [0,Y], because, there is no reason to assume there would be a preference in the eddy location. Similarly, f(l) is the pdf which gives the eddy length or domain. The form f(l) = Bl^{-2} is used where B is the pdf normalization constant when l^{-2} is integrated over all possible eddy sizes. Kerstein (1991) defines the minimum triplet map as six discretized cells. The maximum allowable eddy size is taken to be any eddy which fits into the physical domain [0,Y]. Theoretically the largest possible eddy would start at $y_o = 0$ and have a length of $l = Y$. Any triplet map whose domain y_o + l exceeds Y is suppressed on physical grounds. An eddy cannot pass through the chamber walls.

2.6   Small eddy suppression

In real physical flows, the presence of viscosity dampens small scale u fluctuations. This phenomenon is captured in the viscous evolution equation (Equation 2-1). However, no mechanism exists for preventing a small triplet mapping event from being driven by a large scale fluctuation. One of the very purposes of the triplet map is to increase the strain intensity (Section 2.2). The possibility exists of another (random) eddy event just after a large scale eddy, in which the smaller eddy is entirely or largely contained in just one of the previously defined eddies reduced images (the top third, the middle third, or the bottom third). Left to its own accord, this scenario would produce a plethora of small scale eddies. Note that this dynamic feedback is similar to that discussed in section 2.4 and is one of the real strengths of ODT over previous methods like LEM [Kerstein (1988)]

The small scale eddies do little to enhance advection because of their small scale. Kerstein (1999) has demonstrated this numerically, by allowing $\Delta y \rightarrow 0$ and confirming that the results became independent of Δy. This multiplication of small scale eddies is recognised as an artifact of the ODT phenomenology. (Separating eddies out as random events.) As an artifact of the model with little effect on the resulting u profiles, small scale eddies

are suppressed in order to save computaional time and mimic the role of viscosity in eddy events. Kerstein (1999) laboriously derives a relation for a viscous suppression time scale τ_d.

$$t_d = {l^2}/{16n} \qquad (2-12)$$

This is achieved by an analogy to the energy dissipation rate of a real eddy in ODT. He provides an analogy and not a derivation. As such there could be another free parameter inserted into Equation 2-12, but this is not done in order to keep empiricism down to a minimum. Using the model developed thus far, any eddy in which $\tau(l;y_o,t) > \tau_d$ is suppressed.

However, further development by Kerstein and Dreeben (2000) provides an energy relationship in which the square of l/τ_d is taken to represent the viscous damping of eddy turnovers. The time scale $\tau(l;y_o,t)$ can now be derived from this new relationship,

$$\left(\frac{l}{t(l;y_o,t)}\right)^2 = \left[A\left|u_l(y_o,t) - u_l(y_o + \tfrac{l}{2},t)\right|\right]^2 - \left(\frac{l}{t_d}\right)^2 \quad . \qquad (2-13)$$

The left-hand side is a representation, based on dimensional reasoning, of the kinetic energy per unit mass of a size l eddy. While the first term on the

right-hand side is taken to be the total amount of shear kinetic energy per unit mass which is available to drive the eddy. Under the improved energy formulation (which is used in this work) any event in which the viscous dampening estimate (the square of l/τ_d) exceeds the available shear kinetic energy, the negative right-hand side is interpreted as reflecting the suppression of small, dissipation-range, eddies and is therefore forbidden.

2.7   Numerical implementation

ODT requires the running of an ensemble of individual realizations. Using the ergodic hypothesis, the statistical averaging of the ensemble yields the mean flow properties of the turbulent flow. Consequently an individual realization can be viewed as a numerical experiment. All such realizations have identical initial conditions, but because of the randomness of triplet map implementation each realization develops in time uniquely under a variety of different processes. These processes include, but are not restricted to, turbulent motion and diffusion. This is pictorially represented in Figure 2.3 where the processes of diffusion, eddies, statistics, and droplet motion (which is discussed in Chapter 3) are given their own time lines with discrete tick marks representing events on that time line. A clock sweeps from left to right dictating the ordering of the process tasks.
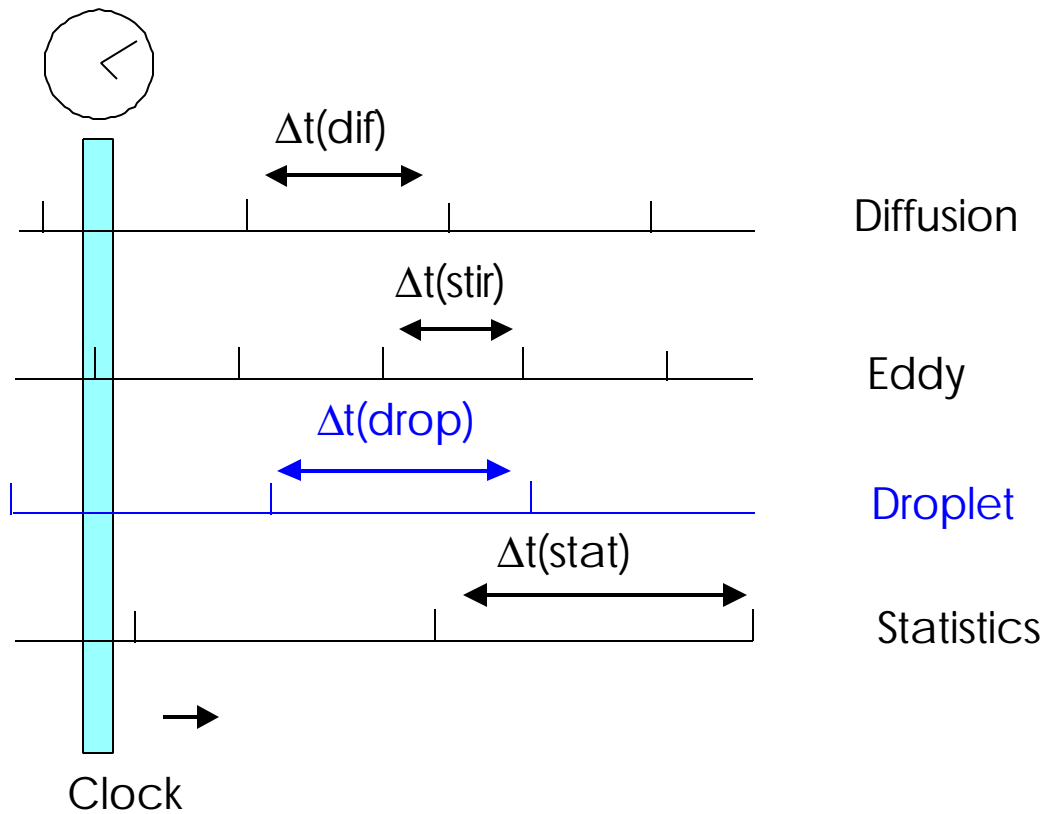
Figure 2.3: Illustration of a pointer, "clock" choosing the next logical process code to execute. Here the eddy process is chosen.

When the clock pointer reaches a tick mark on the stirring time line (as depicted in Figure 2.3) the program checks the possibility of an eddy event. The pdfs g and f are sampled by drawing one random number each. With y_o and l chosen, $\lambda(l; y_o, t)$ can be computed for that particular choice of eddy, and with a Δt given from the turbulent motion time line (Δt_{stir}) the probability of that particular eddy at that particular time can be computed

from Equation 2-11. This probability has two important uses. The first deals with whether or not the eddy is implemented. This process is executed by selecting another random number. If the probability, P(l; y_o, t, Δt), computed from Equation 2-11 is less than or equal to this random number then the triplet map is implemented.

Second, the basis for using this technique (a Poison process) to determine the occurrence of triplet maps is valid only for a Δt_{stir} small enough so that the probability P(l; y_o, t, Δt) is much less then 1. This leads to the requirement that there be many more attempts at eddies than actual triplet map implementations. At first glance this may seem wasteful. However, it is still much cheaper to evaluate P(l; y_o, t, Δt), with λ(l; y_o, t) at one pair of y_o, l values, many times without an eddy event taking place than evaluating Equation 2-9 over all possible combinations of y_o and l.

There is however one complication since Δt_{stir} is chosen in advance of the actual calculations. The possibility exists of choosing a Δt_{stir} too long and thereby generating a multitude of large P(l; y_o, t, Δt) values. A large P(l; y_o, t, Δt) value indicates that more then one stirring event should have occurred in that particular Δt_{stir}. This can be catastrophic since the

probability argument which allows the use of P(l; y_o, t, Δt) (Equation 2-11) to determine eddy events rather than the computing of costly pdf reconstruction (Equation 2-9) insists that the probability be small. To insure this, records are kept of the percentage of high P(l; y_o, t, Δt) values. If this percentage goes above a certain acceptance level then Δt_{stir} must be decreased and the simulation re-run.

Typically the time between possible eddy events is shorter than the time between diffusion events. However the triplet maps are not always implemented, but the diffusion rate occurs predictably and therefore the diffusion events have ample opportunity to begin smoothing out the velocity and passive scalar profiles before the next eddy event. Since diffusion processes are often the most time consuming a brief discussion of the numerical method needed to solve Equations 2-1 and 2-2 is in order.

These equations were discretized using the forward Euler difference method in time (t) and the central difference method in space (y). A stability analysis readily shows, {Carnahan et al. (1969)}

$$\Delta t_{dif} = \frac{a(\Delta y)^2}{D} \quad , \qquad (2-14)$$

where D is either ν or κ from Equations 2-1 or 2-2, and α must be $<= 0.5$.

Intuitively one would suspect that going to an implicit method in time, such as backward Euler or the trapezoidal rule, would be beneficial since the rather stringent condition of $\alpha <= 0.5$ would be relaxed and much larger time steps could be taken for the diffusion processes (which are the most time consuming calculations of the code). However, stability is not the dominant constraint on α, but rather α is constrained by the frequency of the triplet map implementations. As mentioned earlier, the Δt_{dif} should be chosen so that diffusion occurs often enough to start smoothing the velocity profiles between actual eddy implementations. Therefore the ease of programming the forward Euler method and the speed of computation of that method as compared to the implicit methods make the explicit formulation the form of choice.

A general logic flow diagram for a basic ODT sub program (with a droplet model timeline included) is given in Figure 2.4. Modifications to the eddy event time line (Δt_{stir}) are indicated by a " * " in the diagram. The droplet model is the subject of chapter 3. The subprogram shown in Figure 2.4 would be executed once for each realization desired.
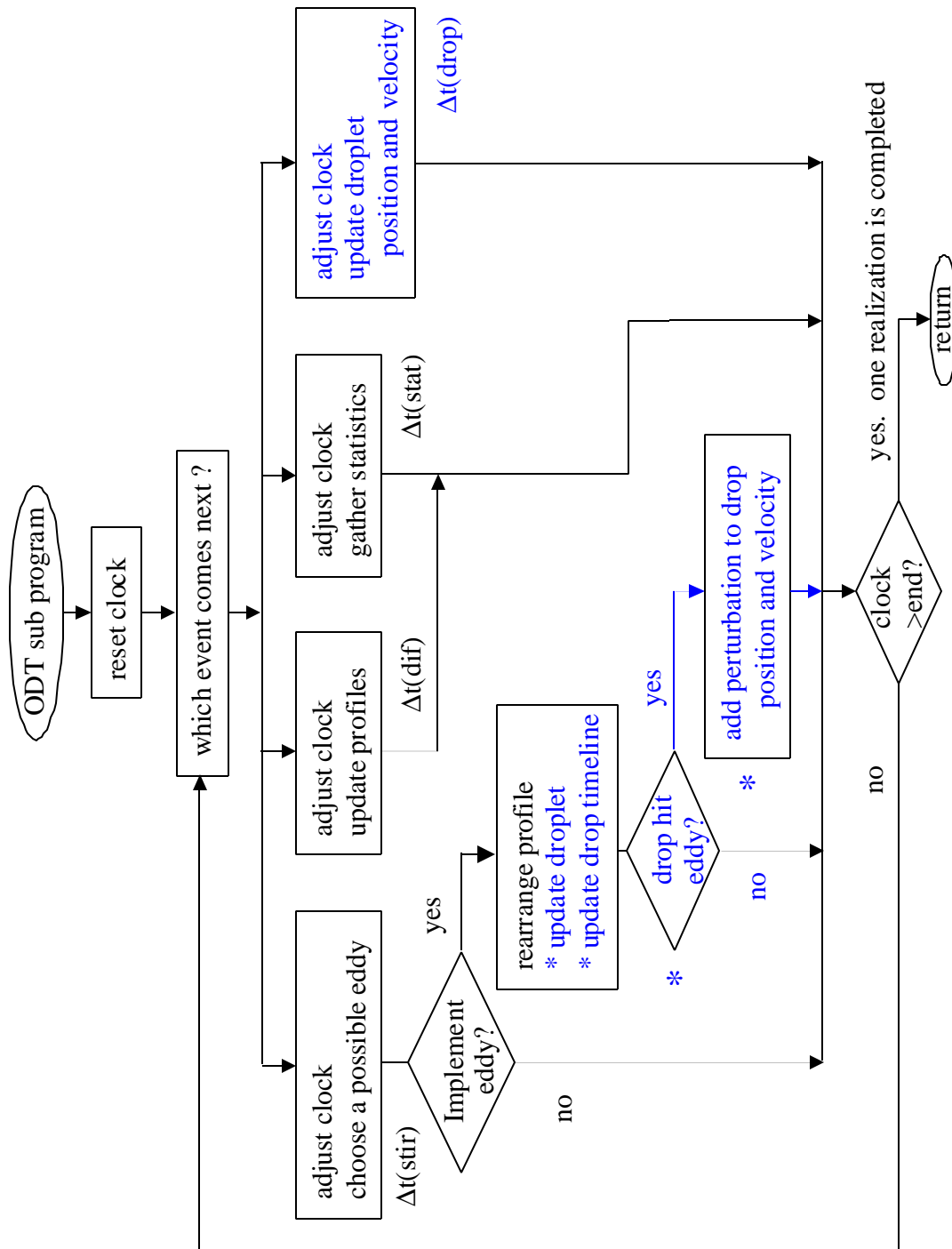
Figure 2.4: General logic flow for an ODT sub program with the droplet sub model added. This flow accounts for a single realization.

2.8   Space-time eddy history

A pictorial rendering of the triplet maps, which will prove instrumental in understanding the development of the droplet sub model for ODT, is given in Figure 2.5. In this diagram the vertical spatial axis is the ODT y domain and the abscissa is time. At each instant in time (each vertical line) there exists a complete (instantaneous) velocity profile and complete profiles for all the passive scalars, none of which are shown in the diagram. Whenever a triplet map is implemented at a certain point in time, the domain of the eddy event $[y_o, y_o+l]$ is recorded by placing a darkened line segment over said domain. Therefore the figure gives an overview of the eddy event history. One can see the time evolution of eddy events. This includes the spawning of smaller eddies from larger eddies. The pictorial in Figure 2.5 is an actual space-time history diagram from the first member of the ensemble used to generate the data presented in this paper.

2.9   Specific Application of ODT

In the time developing version of ODT, the flow develops at the rate of the bulk mean fluid velocity. To convert ODT time development to distance traveled downstream use

$$\Delta x_{ODT} = \Delta t_{ODT} \; \overline{u}_b \quad . \qquad (2-15)$$

In order to have ODT generate the time developing fluid velocity and temperature fields, the mean velocity and temperature profile as reported in Mulholland et al. (1991) were input as an initial condition into the ODT program. This ODT program is a constant density flow between two infinite parallel plates, so a point had to be chosen for the initial condition far enough downstream from the burner such that the constant density velocity profiles would match up well with those measured in the paper. Yet the desire was to have it as close to the burner as possible. Several initial conditions were tried, with the one decided upon being five cm down the *x*-coordinate (axial distance). With these initial conditions and a value of the one free parameter A equal to 0.169, ODT was able to match the published velocity and temperature profiles well using a decaying turbulence assumption. (That is dp/dx was set to zero.) With this value of A, the ending time of Figure 2.5 (0.4 seconds) is equivalent to 0.32 meters down the *x*-axis of the reactor. The ODT simulation was run for a maximum of 0.7 seconds, this is equivalent to one channel height down the reactor. The approximation of using decaying turbulence rather than a non-zero dp/dx

Space-Time History of Events:
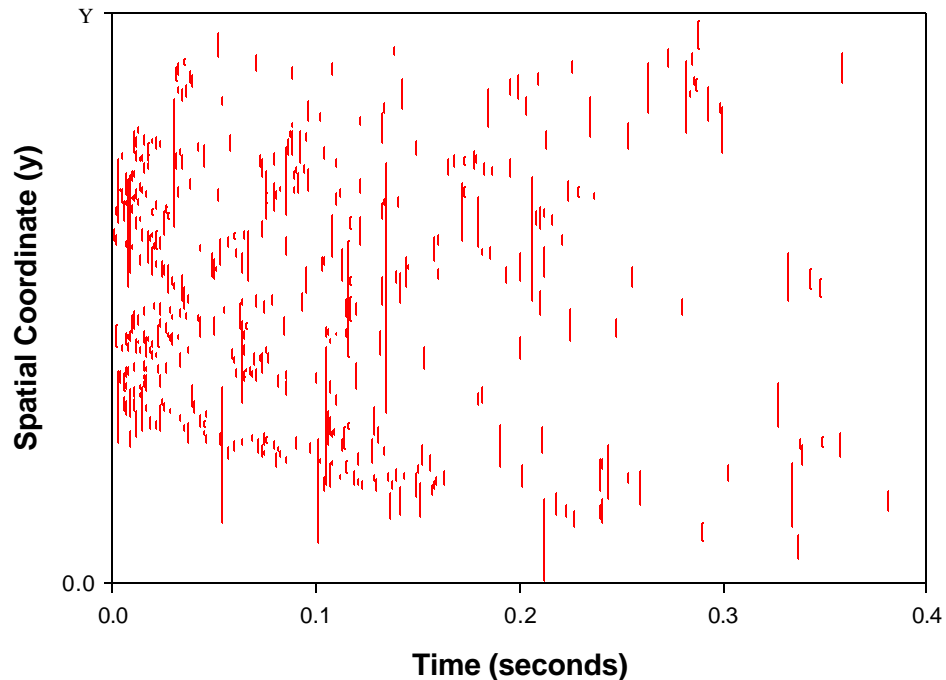
Figure 2.5: Pictorial representing the triplet maps in space-time coordinates. Darkened vertical lines represent eddies. Presented here is the space-time history of an actual realization used in this paper.

causes only a negligible error. Also, a numerical investigation with a non-zero dp/dx was tried. The resultant eddy distribution was not significantly different for the time period in question. Hence for one channel length, the decaying turbulence resembles pressure driven flow.

For comparison, the contour plots showing axial velocity and temperature profiles given in Srivastava et al. (1988) are reproduced in Figure 2.6. They state that due to the turbulent nature of the flow, standard deviations of the velocity ranged from 1 to 5 m/s, often exceeding 50% of the mean velocity. Figure 2.7 shows selected plots with the computed mean axial velocity (u) at selected distances from the burner. Keeping in mind the large standard deviation in the values of Mulholland et al., the comparison of the computed velocities, based on the model input of the mean measured velocity and temperature profiles at 5 cm downstream, shows good agreement. Figure 2.8 shows selected plots of the computed mean temperature profiles, the agreement is good. Figure 2.9 show a sample mean velocity profile (smooth curve) superimposed on an instantaneous velocity profile. Figure 2.10 shows a sample mean temperature profile (smooth curve) superimposed on an instantaneous temperature profile.

2.10   Conclusion

The ODT model is able to capture the relevant physics in this application of a highly turbulent bench scale furnace despite seemingly gross simplifications. The meticulous derivation of ODT in translating the three-dimensional physical effects of a streamwise turbulent flow into a one-

dimensional analogy with random rearrangements adequately matches the

tubular reactor's velocity and temperature profile.
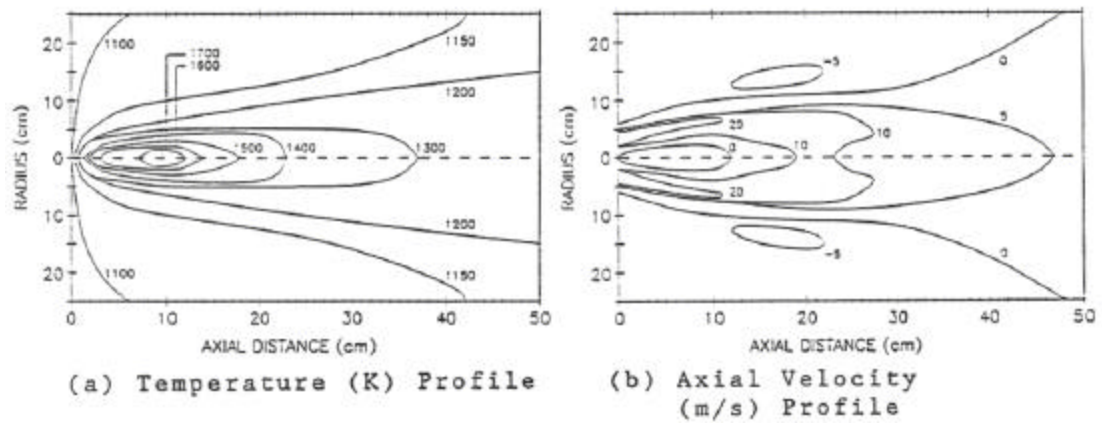
Figure 2.6: Measured mean temperature and axial velocity profiles. These are the near burner proflies for the Type C flame condition. Taken from mulholland et al. (1988)
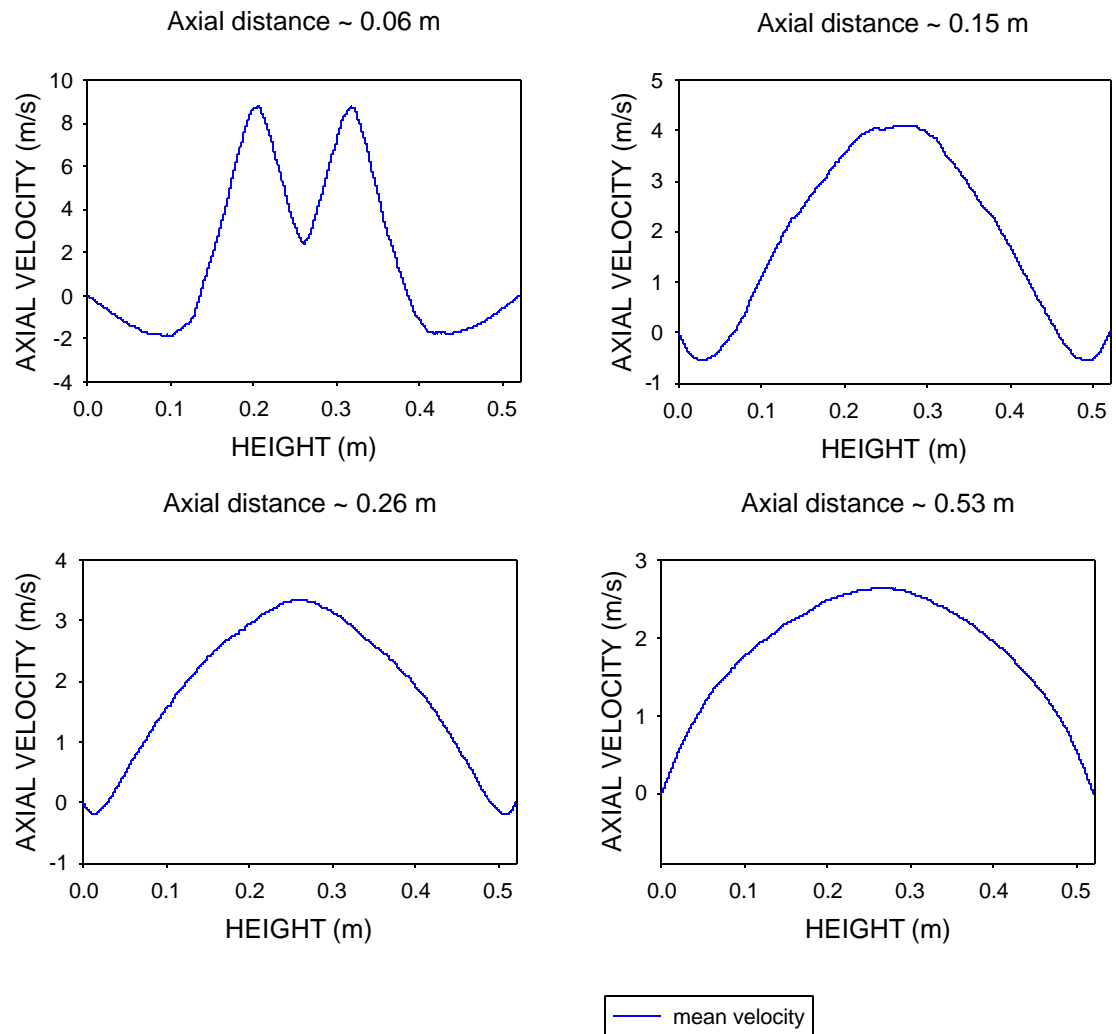
Figure 2.7: Selected mean velocity profiles. Four mean velocity profiles were chosen to show the mean axial velocity development over the range of the axial distance. These can be compared to Figure 2.6 to confirm agreement between the ODT model and the measured mean velocities.
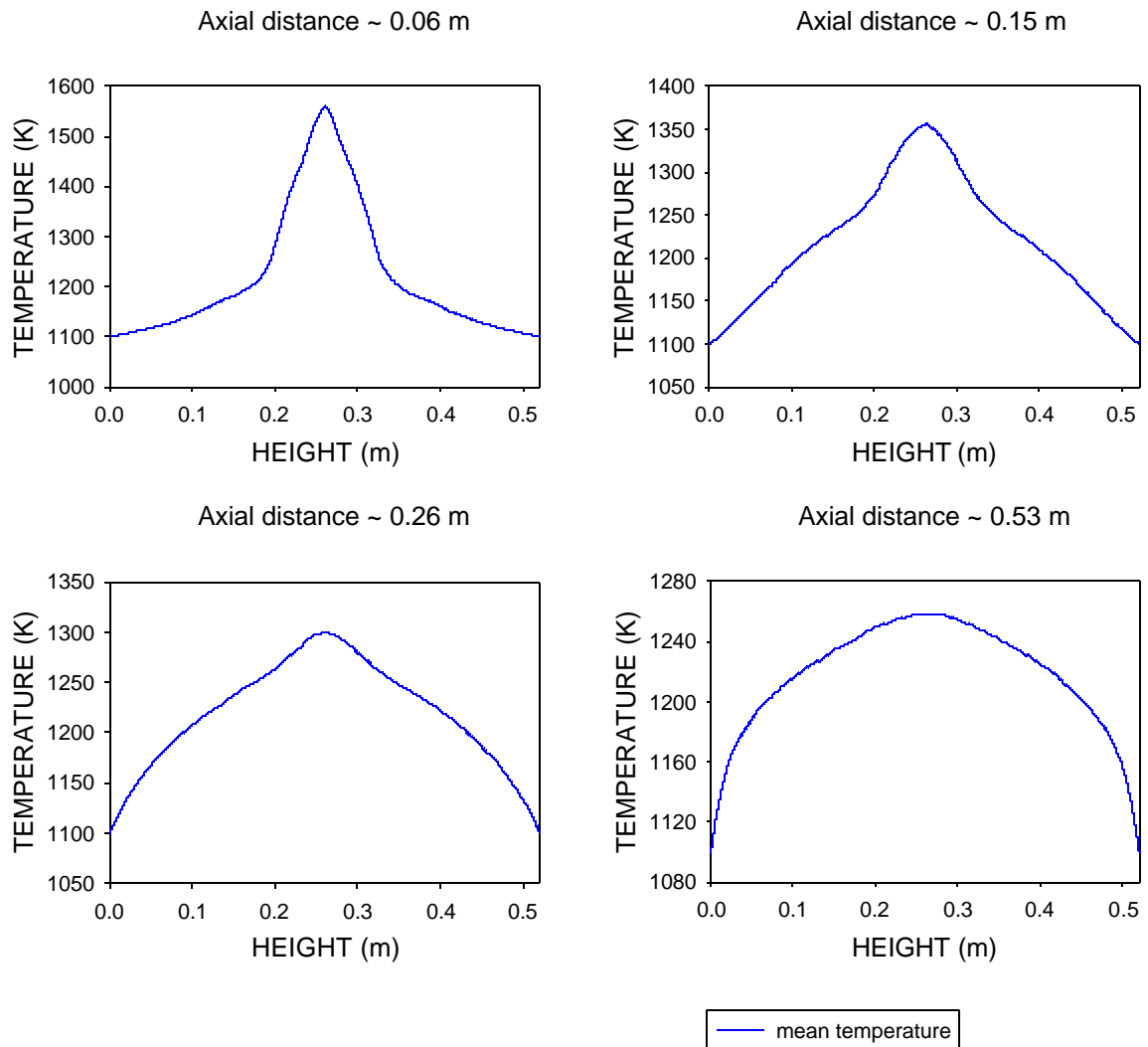
Figure 2.8: Selected mean temperature profiles. Four mean temperature profiles were chosen to show the mean temperature development over the range of the axial distance. These can be compared to Figure 2.6 to confirm agreement between the ODT model and the measured mean temperatures.

Axial distance ~ 0.19 m
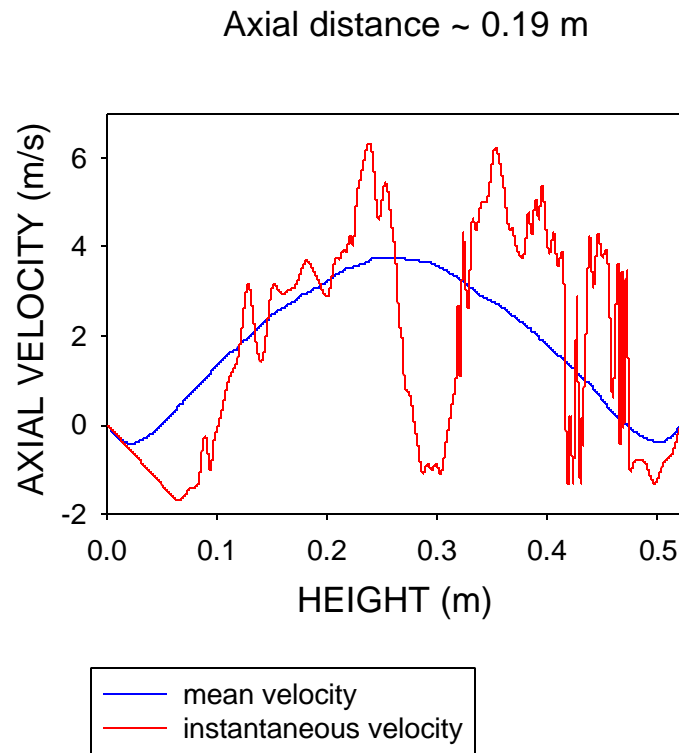
Figure 2.9: Mean and instantaneous velocity profiles. The data shown was randomly picked to demonstrate the difference between the mean velocity, computed for an ensemble size of 2000, and an arbitrary instantaneous velocity profile for an axial distance of ~0.19 m. The mean velocity is the smooth one.
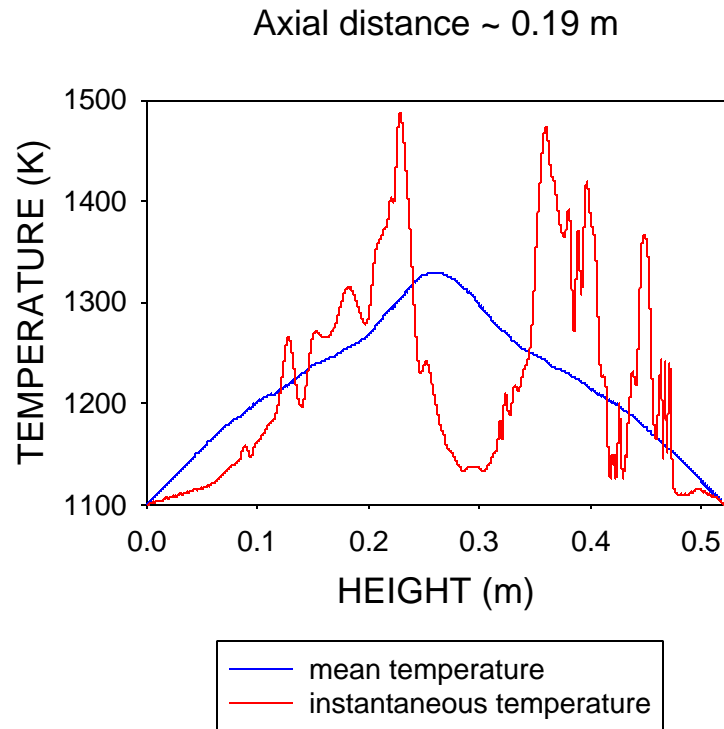
Figure 2.10: Mean and instantaneous temperature profiles. The data show was randomly picked to demonstrate the difference between the mean temperature, computed for an ensemble size of 2000, and an arbitrary instantaneous temperature profile for an axial distance of ~0.19 m. The mean temperature is the smooth one.

Chapter 3

Two-Phase Flow Addition to the ODT Model

3.1   Introduction

An area of ongoing research is particle trajectories in turbulent flows. The development and validation of a two-phase flow submodel for ODT would prove advantageous for the advancement of one-dimensional (inexpensive) modeling. As a submodel to ODT, the particle-drag law must be in the same spirit as ODT. That is to say that the particle drag law should be linear, or better yet linearized in its application. As a linear equation it can easily be broken into x- and y-components.   The y-component is identified with the spatial coordinate y in the ODT formulation and the x-component is identified with the streamwise spatial development. In this derivation, the flow will affect the particle trajectory, but the particle will not affect the fluid flow.

The modeling approach is exemplified by the special case of a tracer particle (zero inertia) traversing the ODT space-time domain. Since ODT idealizes the transverse velocity v to be zero everywhere except at the triplet maps, the tracer particle will have a zero y velocity ($V = 0$) everywhere in the ODT space-time where $u(y, t)$ is undergoing continuous time evolution.

In ODT, when *y* fluid motion occurs, it is an instantaneous jump induced by a triplet map, hence a tracer particle must jump also. (See Figure 3.1 tracer path 2.) The goal of this chapter is to modify this picture to include particle inertia greater than zero.

The interaction between a particle and an eddy event is here defined as both the particle and the triplet map occupying the same space-time. Figure 3.1 shows a space-time history diagram similar to that introduced in Chapter 2, Figure 2.4, in which the representation of triplet maps are darkened vertical lines on the space-time domain. In Figure 3.1 we see an imagined representative detail of the eddy event history diagram (Figure 2.4). Only a magnified portion is chosen to simplify the chart so that particle trajectories can be seen in detail. Tracer particle path (1) transverses the eddy event history diagram without once encountering a triplet map. The challenge, then, is to develop a particle-drag interaction scheme for particle-eddy interactions consistent with the ODT phenomenology. When tracer particle path (2) intersects a triplet map it undergoes a position and velocity adjustment. The specifics of this adjustment are to be discussed in section 3.5 and following.

A particle with finite inertia would experience the net effects of its own
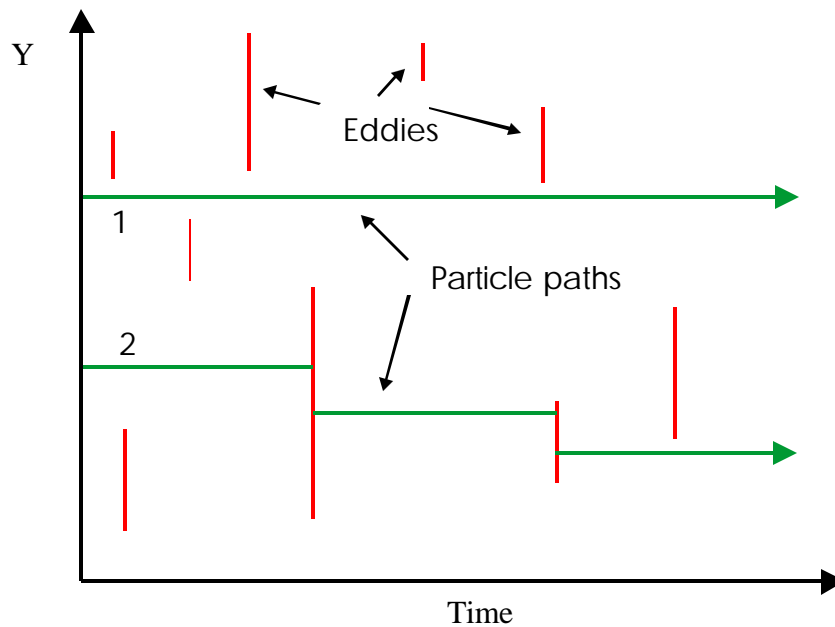
Figure 3.1: Tracer particle paths, 1 and 2, are represented as horizontal lines with arrowheads. Triplet maps are represented as darkened vertical lines. Areas of the plot without triplet maps are referred to as continuous time. Path 1 has no interactions with any triplet map. Path 2 interacts with two eddies.

inertia, the gravitational force, and the drag force. Any combination of these could give a curved trajectory to the particle path. The burden of this chapter is to derive the equations of motion to predict the particle trajectory in continuous time and to devise a model to correctly handle particle interactions with the instantaneous eddy events.

To derive the equation of motion of a particle of mass m_p, a force balance is performed on the particle, which in vector form can be written as

$$m_p \frac{d\tilde{V}}{dt} = \sum_i \tilde{F}_i \quad , \qquad (3-1)$$

where "~" denotes a vector quantity, and the sum, i, is over all the forces acting on the particle. For this application, the only forces on the particle are gravity and the drag force. Hence Equations 3.2 and 3.3 give the equation of motion of the particle in vector form.

$$m_p \frac{d\tilde{V}}{dt} = m_p \tilde{F}_G + \frac{3\pmb{p}\,\pmb{m}\,D_p}{C_c} \left(\tilde{v} - \tilde{V} \right) \qquad (3-2)$$

$$\frac{d\tilde{X}}{dt} = \tilde{V} \quad . \qquad\qquad (3-3)$$

These equations are correct only for linear (Stokes) drag force. Nonlinear drag laws do not decompose exactly into x and y components, however, a non-linear drag force results for a Reynolds number greater than one. This requires an empirical drag law for our application. The empirical nonlinear drag law (f) of Rowe (1961) is used:

$$\frac{d\tilde{V}}{dt} = \tilde{F}_G + \left(\tilde{v} - \tilde{V}\right)\frac{f}{t_p} \qquad (3-4)$$

where the aerodynamic response time, τ_p, the nonlinear correction factor, f, and the particle Reynolds number are given by:

$$t_p = \frac{r_p C_c D_p^2}{18m} \qquad (3-5)$$

$$f = \begin{cases} 1 & \text{Re} \leq 1 \\ 1 + 0.15\,\text{Re}^{0.687} & 1 \leq \text{Re} \leq 1000 \end{cases} \qquad (3-6)$$

$$\text{Re} = \frac{r_g\, r_d \left|\tilde{V}_d - \tilde{v}_g\right|}{m_g} \qquad . \qquad (3-7)$$

Derivation of this two-phase flow model is necessarily complicated by its attention to detail. This must be done to adequately capture the relevant physics of particle-eddy interactions. In order to assist the reader, the derivation is broken into several levels of complexity. First will come a discussion of the decomposing of the equation of motion (Equation 3-4) into y and x components for "conventional" fluid flow. Conventional fluid flow would be that ODT fluid flow which is not reshuffled by triplet maps. (See

Chapter 2, specifically section 2.2 for a discussion on triplet maps.) This is followed in the later part of the chapter by a discussion of implementation of the equation of motion for fluid flow which undergoes triplet map rearrangements. Next a summary of the two-phase flow model is presented. Finally sections on two-phase flow model extensions and numerical implementation strategies are presented. For each component, levels of complexity are developed from simplest to most difficult, with the more complicated levels building on the concepts of the previous levels. Liberal use of diagrams and equations illustrates the points made in the various sections.

3.2   Y component of the particle-drag law

First a detailed look at the *y* component. With the particle *y*-velocity denoted V and the fluid *y*-velocity by *v*, the linearized particle-drag law in the *y* direction is

$$\frac{dV}{dt} = -\frac{(V-v)}{t_p}f + F_G \quad , \qquad (3-8)$$

where τ_p and f are as defined above. When f = 1, the first term on the right

hand side Equation 3-8 reduces to the well known Stokes drag force on a

particle.

Examination of Equation 3-8 shows that the effect of the particle-drag

law is to relax the velocity of the particle to the velocity of the fluid parcel

which surrounds it with a particle time constant τ_p corrected by a factor f

which is a function of the Reynolds number.

This particle-drag law fits well into the framework of ODT's time

developing formulation (see Chapter 2). In the ODT idealized flow, $v = 0$

outside of eddy events. Hence the equation of motion (3-8) in continuous

time is

$$\frac{dV}{dt} = -\left(V\right)\frac{f}{t_p} + F_G \quad . \qquad (3-9)$$

Two important opposite limits must be considered in the two-phase flow

submodel. One is a particle with low inertia (small τ_p) and the other is a

particle with high inertia (large τ_p). Emphasis here is on small inertia. The

large inertia particles remain mostly unaffected by the forces of drag or

gravity.

In the limit of vanishing inertia, a particle would act in an identical manner as a fluid tracer particle. This can be seen by letting $\tau_p \rightarrow 0$ in Equation 3-9. That is, it would conform instantaneously in velocity and position to its host fluid parcel. A fluid tracer particle in the idealized turbulent flow of ODT must not undergo translation in the *y* direction unless it interacts with a triplet map. Indeed, Equation 3-9 readily reproduces the desired particle path behavior during times in which the particle does not interact with an eddy event.

3.3 X component of the drag law

By direct analogy, the particle-drag law (Equation 3-4) can be decomposed in the *x* direction with U denoting the *x* velocity of the particle and *u* denoting the *x* velocity of the fluid element containing the particle.

$$\frac{dU}{dt} = \frac{-(U-u)f}{t_p} \quad , \qquad (3-10)$$

where τ_p and f are as defined in Equations 3-5 and 3-6. Here, the force of gravity is perpendicular to the *x* direction and there are no additional body forces. However, the model is readily adapted to situations in which there is a streamwise body-force component. In an identical manner to that noted

previously, with f = 1, the right hand side of Equation 3-10 reduces to the well known Stokes drag force on a particle.

Taking the limit of Equation 3-10 for vanishing inertia ($\tau_p \rightarrow 0$) requires that U = u. Tracer particles always match the local velocity of the fluid. Looking at the other extreme, the limit of Equation 3-10 as τ_p tends to infinity, is U = U_o. The infinite inertia particle x velocity is unaffected by the particle drag.

Since the ODT x direction develops in time with the mean u velocity of the fluid, denoted $\overline{u_b}$, there is a problem when computing the particle trajectory in the x direction. The particle proceeds with its own x velocity this is generally different from the gas u velocity. The particle is subject to time-varying u velocity both because u evolves in time and because particle motion in the y direction induces time variation of u in the particle reference frame. Due to finite inertia, U generally differs from u at the particle location, and both these quantities differ from $\overline{u_b}$. Thus, there is typically a difference between the speed at which the particle traverses the x direction and that at which the bulk mean velocity $\overline{u_b}$ traverses the x direction. This inconsistency can best be fixed by computing the time, Δt_p it would take that

particle surrounded by that fluid parcel to traverse the distance which the mean bulk flow traverses in a given time Δt_{ODT}.

$$\Delta t_p = \frac{\overline{u_b}\,\Delta t_{ODT}}{U(t_p)} \qquad (3-11)$$

This equation becomes complicated because U is a function of t_p due to the equation of motion. The introduction of t_p defines a particle time coordinate for integrating the drag law. Now the continuous time process, as modified to give the correct particle time, gives the means to faithfully represent the particles streamwise trajectory evolution.

3.4   Particle-eddy interactions in ODT

The discussion and the particle equation of motion up until this point reflect conventional approaches to drag law implementation in laminar flow, subject to two major caveats: (1) only the u component of gas velocity is nonzero, and (2) interpretation of time evolution in ODT as streamwise spatial evolution required the introduction of a particle time coordinate, t_p, distinct from the fluid time coordinate. Particle interaction with a triplet map requires a novel approach. As defined in Section 3.1, this interaction occurs when the particle and triplet map occupy the same space-time. The

particle drag law as written is not applicable to ODT particle-eddy interactions because triplet maps are instantaneous in time yet the particle-drag law requires an interaction time to cause a change in the particle velocity or position.

Before discussing in detail possible solutions to this type of particle-eddy interaction (when they occupy the same space-time), there is yet another problem which arises due to the ODT formulation of eddies as instantaneous in time.

To understand this, first recall that in Figure 3.1 the particle path was that of a tracer particle and as such had no y velocity, reflecting the corresponding feature of ODT gas-phase evolution. However, particles with finite inertia will generally have a finite, nonzero, y velocity. Figure 3.2 depicts an eddy event history diagram consisting of four particle trajectories with varying initial y velocities (V). Particle trajectory 1 has no initial y velocity component. After the particle interacts with eddy A, it obtains a positive y velocity and a positive y displacement, as explained shortly (Section 3.4.2). Trajectories 2, 3, and 4 have increasing (in magnitude) negative y velocity components. Trajectory 2, shows the effect of the gravitational force, (curved line) on the drag law, prior to the eddy
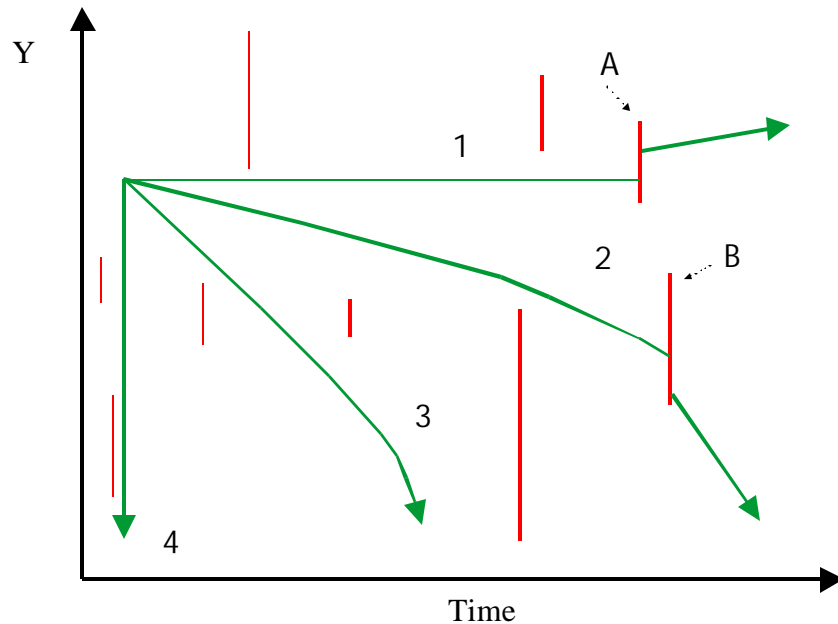
Figure 3.2: Particles with an initial velocity may transverse the ODT space-time domain without interacting with an eddy.

interaction. This particle-eddy interaction with eddy B gives the particle an negative *y* displacement and increases the negative *y* velocity of the particle. In the scenario set forth in Figure 3.2 both particle trajectories 1 and 2 eventually intersect an eddy event. At the intersection points the particle positions and velocities are changed instantaneously. (This process will be discussed in detail in the following section.) However the larger (in magnitude) the *y* velocity becomes, the less likely a particle is to intersect an eddy event. In the limit (Figure 3.2, path 4) as the *y* velocity component becomes infinite, the probability of an eddy interaction becomes zero

because both the triplet maps and the particle trajectories are vertical lines. This phenomenon is an artifact of the ODT formulation since particles with large y velocities should interact with eddies. There needs to be a way for particles to interact with eddies even if the particles do not intersect the triplet map. This can be achieved by allowing the eddies to exist for an as yet undefined length of time. The essence of this would be to "pretend" that the ODT instantaneous eddies existed for a finite time. This would be represented as a box (not just a line) in the eddy event history diagram. Interactions of the type in which a particle enters the space time box associated with an eddy event through either of the two horizontal edges are referred to as type-C interactions because the particle is acted upon in a continuous manner by the eddy event as long as the particle is inside the box.

Type-C interactions are not developed further in this model application since the overwhelming majority of the Mulholland et al. data falls into the category of low *y* velocity data. The low *y* velocity data leads to mostly particle-eddy interactions in which the particle enters the space time box through the left vertical edge (i.e., the vertical line that represents an eddy in Figure 3.2), so there exists little need for type-C interactions in this model

application. However, the concept of Type-C interactions is explained in detail in Section 3.11, entitled Model Extensions, type-C interactions. There are therefore, only two possibilities in this model for particle-eddy interactions. Either the particle path misses the vertical surface (representing the triplet map) of the eddy and therefore there is no interaction, or the particle path strikes the vertical surface and the particle undergoes an interaction of the type to be discussed next. These will be called type-I interactions.

Since this application of the two-phase flow submodel to ODT is mainly concerned with particle-eddy interactions occurring when particles intersect triplet maps, a major effort was put into capturing as much of the physics of this interaction onto the ODT model framework.

A zeroth order approximation of this interaction might be to simply adjust the *y* position of the particle (y_p) by an amount equal to the mapping-induced displacement of the fluid element containing the particle just prior to the eddy event. {A detailed description of triplet maps and their instantaneous jumps are given in Chapter 2 section 2.2.} Even though this approximation will yield the desired solution for one special limiting case

(zero inertia limit, illustrated in Figure 3.1), it fails for all other cases. Hence it is abandoned.

3.5   Particle-eddy interaction model

The logical solution to the difficulty of applying the particle drag law to particle-eddy interactions (due to the instantaneous nature of the triplet map) is to assign an interaction time to the particle-eddy interaction. For now, we will denote the interaction time coordinate as T, and the duration of the interaction as T_1. The latter quantity is specified in Section 3.9. The interaction time coordinate will be referred to as pseudotime because it is not a real time, just a time made up so that the particle drag law can have an effect on the particle. Another way to say this is since T has units of time, but is not interpreted as real time due to the fact that eddy events are instantaneous in real time, it is referred to as pseudo (or fictitious) time. The latter quantity will be developed and defined later in the discussion. Particle evolution during this interaction is governed by the y and x components of the particle drag law (Equations 3-8 and 3-10) adjusted for the pseudotime coordinate.

$$\frac{dV}{dT} = -\frac{(V-v)}{t_p}f + F_G \qquad (3-12)$$

$$\frac{dU}{dT} = \frac{-(U-u)f}{t_p} \qquad (3-13)$$

where v (defined later) is the fluid y component velocity induced by the triplet map, T is the interaction time coordinate, u is the velocity of the fluid cell which surrounds the particle, and all other terms are as previously defined. In this formulation tracer particles behave correctly, that is, they mimic the u and v velocities of the fluid cell which surrounds it during pseudotime. This can be verified by taking the limit of Equations 3-12 and 3-13 as $\tau_p \rightarrow 0$.

3.6   Effect of pseudotime integration in the particle time domain

A problem arises when comparing the integration done in pseudotime over a time period T_1 (Equation 3-12) and the conventional continuous-time integration of the particle-drag law (Equation 3-9, both duplicated here for clarity) subsequent to the particle-eddy interaction, over a comparable time interval $\Delta t = T_1$ and $\Delta T = T_1$.

$$\frac{dV}{dt} = -(V)\frac{f}{t_p} + F_G \qquad (3-9)$$

$$\frac{dV}{dT} = -\frac{(V - v)}{t_p} f + F_G \qquad (3-12)$$

Comparison of Equations 3-12 and 3-9 indicates that the equations contain similar terms and therefore the resultant actions of integrating them over the same time period are in fact double counting the effect of the gravitational force, once during the pseudotime integration from $T = 0$ to $T = T_1$ and once during the real time integration from the birth time of the eddy to a time increment of T_1. The particle experiences the gravitational force first for a period of T_1 in pseudotime and again for a period of T_1 in continuous time. This method represents a double counting of the effects of gravity and could lead to erroneous results.

To overcome this problem, which occurs when the particle and the triplet map occupy the same space-time, the particle trajectories with and without the effect of the eddy are computed. This is achieved by integrating (first to get velocity and then again to get position) both Equations 3-12 and 3-9 concurrently over the period T_1, and determining the difference in the ending y_p position (defined in Equation 3-14). Similarly, the difference in the ending V velocities (defined in Equation 3-15) is also computed. These computations define the perturbations felt by the particle due to the eddy,

$$\Delta y_p = y_p^e(T_1) - y_p^c(T_1) \qquad (3-14)$$

$$\Delta V = V^e(T_1) - V^c(T_1) \quad , \qquad (3-15)$$

where the superscript e (for eddy) denotes the results based on Equation 3-12 and the superscript c (for continuous) denotes using Equation 3-9.

This procedure is pictorially represented in Figure 3.3 (A). The perturbation distance, Δy_p, [demarcated with a "}" in Figure 3.3] and the perturbation velocity, ΔV, are then added to the particle's original position and velocity (respectively) at the instant it first encounters the triplet map. The particle is then allowed to proceed in continuous time without the worry of double counting the gravity effects. The results of this procedure are shown in Figure 3.3 (B) as they would appear in Figure 2.4, a space-time history diagram.

In Figure 3.3 (A), the trajectory with the eddy interaction is based on pseudotime integration. It is convenient to define the shaded region as an eddy interaction box, whose vertical span is the y range of the eddy and whose horizontal span is the time duration T_1 of the interaction.

With the eddy interaction box so defined in space (y) and time, the duration of a particle-eddy interaction is now idealized as the overlap of the
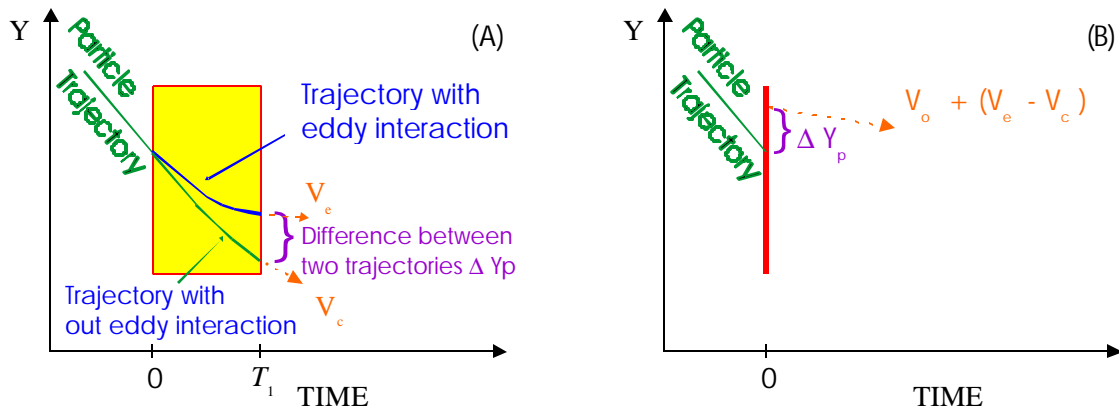
Figure 3.3: The procedure for implementing particle-eddy interactions which avoids double counting. Find Δy_p and ΔV then add them to the original position and velocity. The resultant position and velocity are shown in B.

particle trajectory {under the influence of the eddy (Equation 3-12)} and the

eddy interaction box. The right hand side of the interaction box marks the

end of the eddy lifetime. A particle with an initial y velocity, under the

effect of gravity, under the effect of drag, or any combination of these can

exit the eddy interaction box from either of the two horizontal surfaces. This

is visualized by understanding that the particle has left the space in which

the eddy occupies before the eddy lifetime has expired.

The intended goal of introducing the particle-eddy interaction box and

defining a position and velocity perturbation, which do not double count the

gravitational effects, was to try to accommodate the particle-eddy interaction

model to accurately fit variations in eddy size, particle speed and entry point

into the eddy. As long as the correct interaction time, T_1, can be determined, this perturbation technique will give velocity and position jumps commensurate with the orientation of the particle trajectory and the eddy size.

A non-zero fluid velocity imposed by the eddy event (Equation 3-17) may act in the same direction as the particle's initial *trajectory* or in an opposing direction. The resultant particle path will either be bent upwards or downwards from the trajectory the particle would have taken if it did not interact with the eddy. For an example see Figure 3.4. A (the dotted line) is the path with no eddy interaction. All other trajectories (B, C, D) include an imposed v velocity from the eddy event. The particle-drag law, Equation 3-12, is used to define the path from the moment the particle first encounters the eddy ($T = 0$) to the end of the eddy lifetime ($T = t_e$, where t_e is defined in Section 3.7). For path B, the v component due to the triplet map is negative. For this particular case, the particle leaves the eddy interaction box by the bottom horizontal surface before time $t = T_1$ has elapsed. For comparison, Path C has a positive v, the particle trajectory curves upward and exits the eddy interaction box through the back vertical surface. This path exits precisely at $T = t_e$. A larger positive v component is used in the calculation
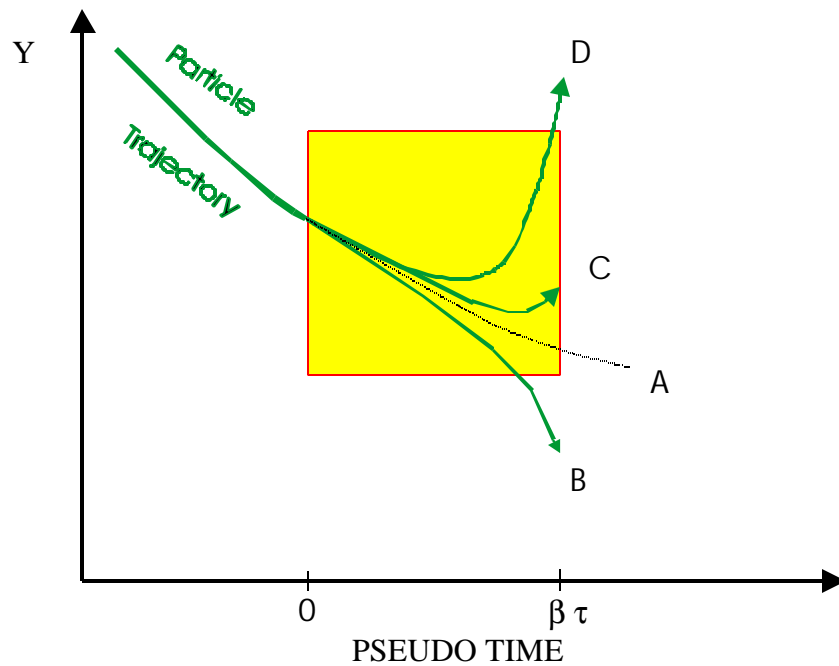
Figure 3.4: Particle-eddy interactions cause the path to deviate and may exit the interaction box by one of the horizontal surfaces before the eddy lifetime has expired

of path D. Note that there is an extremum (minimum) in the trajectory (as well as case C) and in a manner similar to path B, path D leaves the eddy interaction box by the horizontal (top) surface before the pseudotime interval t_e has elapsed.   Care must be taken when computing particle-eddy interactions that these interactions stop the when a trajectory leaves the interaction box for the first time. This is because the eddy is "seen" by the particle as occupying that particular space-pseudotime and a particle path which leaves the box should no longer "feel" that eddy.

Finding the correct interaction time T_1 is no easy matter, so we begin by considering only particles which interact with the eddy for the entire eddy lifetime. This will give insight into the behavior of particles while they interact with eddies without the added concern of computing the correct interaction time. This motivates the qualitative illustration of interaction regimes shown in Figure 3.5.

Figure 3.5 (A) shows the trajectory of a *particle tracer* as it enters an eddy interaction box (from the left of the box) to after it leaves (from the right of the box) in pseudotime. Figure 3.5 (B) presents the equivalent diagram as it appears in real space-time coordinates, just as it would if the trajectory were rendered in Figure 2.4. The particle is displaced in the *y* direction the identical amount which the fluid parcel surrounding it is displaced in the *y* direction by the triplet map. Figure 3.5 (C) represents the trajectory of a particle with medium inertia (neither low nor high) in pseudo time. Figure 3.5 (D) gives the same trajectory in real space-time coordinates. One can readily see that the particle is displaced upwards by the eddy event but only a fraction of the distance the fluid cell travels. Note carefully that the velocity vector in Figure 3.5 (D) is adjusted instantaneously in the manner defined by Equation 3-15. For completeness
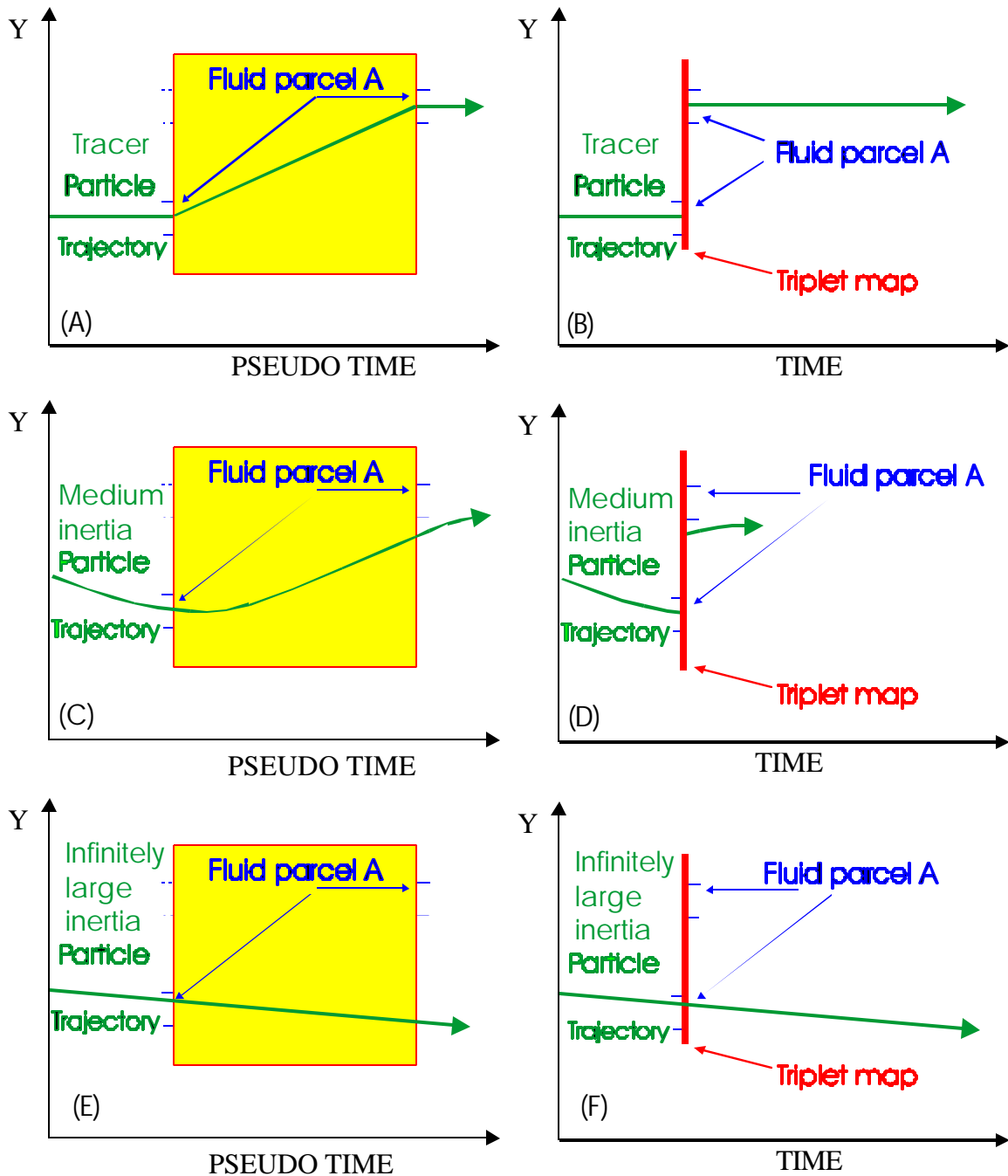
Figure 3.5: The trajectories of particles with varying inertia (low to high) are shown in pseudo time during particle-eddy interactions (A), (C), and (E). The paths in real time are shown for comparison, paths (B), (D), and (F) respectively.

Figure 3.5 (E) shows the trajectory of a particle with infinitely large inertia in pseudotime. The corresponding trajectory in real space-time coordinates is shown in Figure 3.5 (F). As expected the particle-eddy interaction has no effect on the particle trajectory of an infinitely large inertia particle.

3.7 Alternative representations of particle-eddy interactions

There exist other possibilities for the design of a particle-eddy interaction model which include time, in other words procedures other than inventing pseudotime, computing the particle path, then projecting this difference back to the initial time. The most worthy of consideration is simply to allow the triplet map induced velocity profile (v) to act upon the particle for an amount of real time equivalent to the amount of pseudotime T which is the eddy lifetime t. This has the effect of reproducing the particle trajectories of Figure 3.5 (A), (C), and (E) with the pseudo time axis (abscissa) replaced with real time. This is indeed a simplification in model design and implementation, so some justification needs to be made for choosing the more complicated model. Three arguments present themselves. The first and weakest argument is the heuristic argument that since the eddy events are instantaneous in time, so their effects (particle velocity/position changes) should be instantaneous also. The reason this argument is weak is that the

instantaneous triplet maps are an artifact of the ODT model and are only an idealization of the physical reality in which eddies have a finite lifetime. This argument by itself cannot justify choosing the more complicated model.

The second argument relies on the physical principle that a particle with low enough inertia will exactly mimic a fluid tracer parcel. As is depicted (for example) in Figure 3.5 (B, D, and F) the fluid parcel has a discontinuous jump in the y axis (the ordinate) so a particle would need to have a discontinuous jump in order to mimic the fluid particle. Here the counter argument can be made that this discontinuous jump is also an artifact of the ODT model and that using the simpler model the particle path does not deviate from the fluid parcel for a very long time. After that "short" time period, the particle and the fluid parcel which surrounded it are reunited. So the simpler model still reasonably mimics a tracer particle and deserves consideration.

This leads to the final argument. In order to follow the logic, the following representative scenario is proposed, see Figure 3.6. A tracer particle is traveling along with its fluid parcel (denoted fluid parcel A). It encounters an eddy event denoted 1. Assuming the simple model, Figure 3.6 (A) results in: the particle's adjustment to the eddy interaction occurs over a
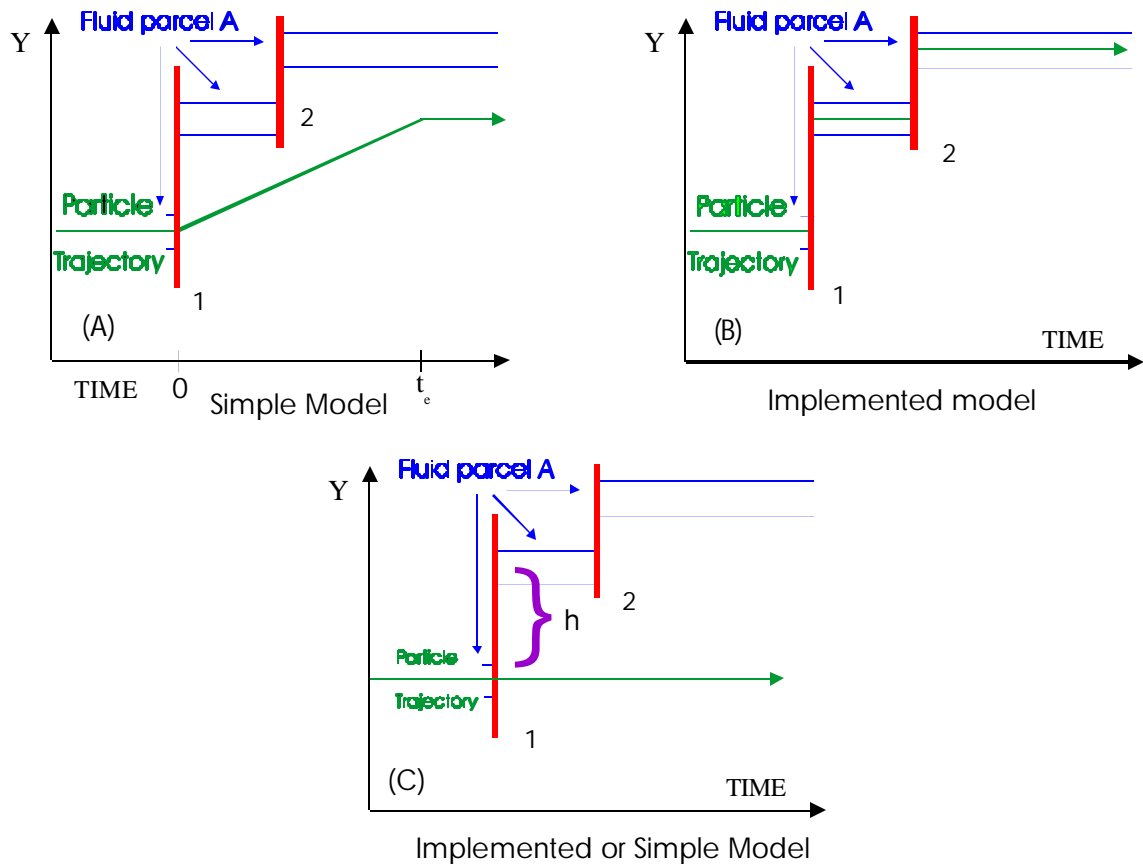
Figure 3.6: Diagram A shows the trajectory of a tracer particle for a particle-eddy interaction using the simple model. B shows the implemented model for a tracer particle. Diagram C shows the path for a particle with very large inertia. Diagram C is the same for either the simple or the implemented model. In this example, there is no continuous time v velocity.

time period t_{e1}, while the fluid parcel A undergoes the discontinuous jump h.

Before the particle has time to rejoin the fluid parcel A another eddy event

(denoted 2) occurs and fluid parcel A is displaced farther away on the y axis.

At this point any correlation between the fluid parcel A and the tracer

particle is lost. The simpler model does not reproduce the small inertia limit for this scenario. Even though this is only a plausible scenario and does not have to occur, the dynamic feedback property of ODT makes this scenario likely. Only the implemented (more complicated) particle-eddy interaction model {see Figure 3.6 (B)} correctly matches the fluid parcel A with its tracer particle.

It is interesting to note that for the other extreme, a particle of infinitely high inertia, both the simple and implemented particle-eddy interaction models give the correct result {see Figures 3.6 (C)}. In both formulations, the eddy has no effect on the particle.

Even though it is impossible to precisely capture the particle-eddy interactions for the entire inertia range in a one-dimensional model, it is our goal to be as accurate as possible. The implemented model fits exactly for the two extremes and therefore should do a reasonable job fitting the values in between. Because the implemented model redirects the particles instantaneously when a particle-eddy interaction occurs, this type of particle-eddy interaction is referred to as a type-I interaction, where I is for Instantaneous effect.

3.8   Eddy lifetime

As will be shown in Section 3.8, determination of the particle-eddy interaction time, T_1, requires a definition of the lifetime t_e of an ODT eddy. The eddy lifetime is also used to determine v in Equation 3-17.

The ODT local instantaneous time scale, $\tau(l; y_o, t)$, is discussed in detail in Chapter 2. $\tau(l; y_o, t)$ is best interpreted as the characteristic time of the eddy event if it were to happen over a time period and not instantaneously. $\tau(l; y_o, t)$ is however an artifact of the ODT model development and not an actual or physical time. Even though parameter dependencies of $\tau(l; y_o, t)$ are based on solid reasoning there is no compelling reason to believe that it actually corresponds to the eddy lifetime.   Therefore it is justifiable to introduce a particle model free parameter called β. The eddy lifetime is now given by Equation 3-16

$$t_e = \boldsymbol{b}\, \boldsymbol{t}\!\left(l; y_o, t\right) \quad . \qquad (3-16)$$

Ideally β is a number close to unity since $\tau(l; y_o, t)$ was based on good reasoning and logically should not be too far off. $\beta = 1$ was used for all runs reported in this paper, except for a set of sensitivity runs designed to investigate the model's response to changes in β. The additional runs were

for $\beta = 0.5$ and $\beta = 2.0$. Decreasing β causes the particle trajectory to deviate more from its original path due to the particle-eddy interaction. Increasing β causes less of a disturbance. This may seem counterintuitive, but a detailed discussion on the subject can be found in Chapter 6, along with the results from the sensitivity runs on burning droplets.

Now that we have a suitable choice for an eddy lifetime, $t_e = \beta\tau$, it follows that the velocity v of a fluid cell as it travels in pseudotime from its starting position (the one it occupied before the triplet map) to its ending position (that which it occupies after the eddy event) is the y distance traveled by the cell (h) divided by t_e,

$$v = h \Big/ t_e \qquad . \qquad (3-17)$$

It is interesting to note that Kerstein (1999) uses this definition, with $\beta = 1$, to define v' in order to compute the ODT "Reynolds stress" profile $<u'v'>$.

With v thus defined, Equation 3-9 governing the particle-eddy interaction is fully defined, though the time duration T_1 of the interaction is as yet undetermined.

3.9 Duration of the particle-eddy interaction

A real-life eddy would exist in a defined space (three-dimensional) and exist for a defined (measurable) lifetime. Particle-eddy interactions would occur while the particle occupies the same space-time (x, y, z, t) as the real life eddy. It is the goal of this part of the two-phase flow submodel to discuss in detail the analysis required to assure that the particle-eddy interaction ceases the first time the particle leaves the ODT space time (x, y, t) which the eddy is idealized to occupy in this model.

3.9.1 Particle-eddy interactions in the *y* direction

For clarity in discussion, Figure 3.5 purposefully omitted instances in which the particle exited the eddy interaction box by one of the horizontal surfaces. Here we revisit type-I interactions with particles which do exit by the top or bottom of the space-pseudotime interaction box.

As long as the particle exits the interaction box and remains outside of the interaction box for the duration of the eddy lifetime, no added complications occur in determining the eddy interaction time T_1. Any number of root finding techniques can be implemented to determine the correct interaction time to for a given accuracy.

However, not all particle trajectories will remain out side of the eddy interaction box once it has exited. Figure 3.7 shows a trajectory in which the particle path (as calculated for the complete lifetime of the eddy) shows an extremum occurring outside of the eddy interaction box and the particle re-enters the box. In cases like these checking particle y location only the end point t_e of the particle path would give the false impression that the particle first leaves the box by the back side at time $T = t_e$, when actually the particle first leaves the box on the bottom at time $T = T_1$. Here the particle-eddy interaction should cease at $T = T_1$.

3.9.2 Particle-eddy interactions in the x direction

No adjustments are made to the x position, x_p, or the x velocity, U, of the particle due to a particle-eddy interaction. The nature of the time developing ODT model does not lend itself readily to sudden jumps in the x domain which is related to the ODT time by Equation 2-14. So no reasonable method to account for instantaneous movement backward or forward in time could be developed. A jump in x for this time developing flow is equivalent to a jump in time. There would have to be some provision for allowing movement backward in time, which seems more trouble than it is worth. However, in the analysis of the particle-eddy interactions it is

X

Particle
Trajectory

(A)

0 T₁   t_e
PSEUDO TIME
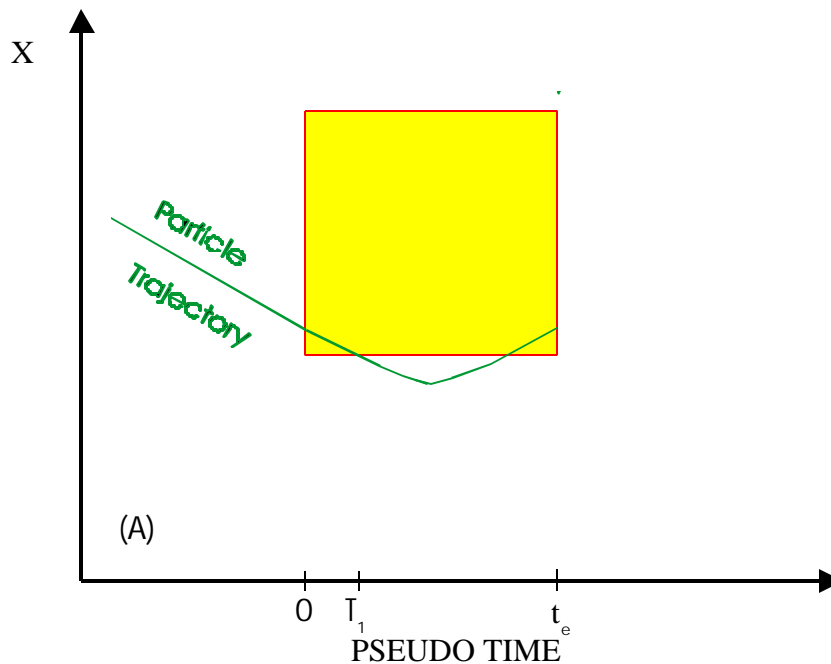
Figure 3.7: Particle paths can exit the interaction box
and reenter the box due to particle eddy interactions. The
particle-eddy interaction should cease when the path exits
the box for the first time at T1.

important to determine whether and when the particle leaves the eddy ODT

space-time in the x dimension in order to correctly determine the duration of

the interaction.

The lifetime of the eddy in the x direction is identical to the lifetime t_e for

an eddy as viewed in the y direction. (There is no reason why the lifetime

should change for the different directions.)

$$0 \leq T \leq t_e \qquad (3-18)$$

The y direction has a characteristic length, l, associated with the eddy in the ODT formulation, however, the x direction does not have any special length dimension associated with it. The logical choice then would be to use the distance of order l in the x direction. Since there is no connection between l and the x direction, there is nopredetermined relation between the position of the particle, x_p, and the eddy interval l on the x coordinate. The formulation used to define the eddy in the x direction is given in Equation 3-19, in which x_o is defined as the x position of the particle, x_p, at the moment the particle-eddy interaction begins:

$$x_o + u_{eddy}T - l \leq x_e \leq x_o + u_{eddy}T + l \qquad (3-19)$$

defines the range of x values, x_e , contained within the eddy, where u_{eddy} is defined shortly.

Even though the parameter, l, is based on solid reasoning there is no compelling reason to believe that it actually corresponds to the eddy length. Therefore it would be possible to introduce another particle model free parameter called δ. The length of the particle-eddy interaction box would be given by Equation 3-20.

$$x_o + u_{eddy}T - \boldsymbol{d}\, l \leq x_e \leq x_o + u_{eddy}T + \boldsymbol{d}\, l \quad . \qquad (3-20)$$

The use of δ as a free parameter is not implemented in the model. The author wishes to keep empiricism down to a minimum, that is, to keep the number of two-phase flow model free parameters to the one, β. There is a sound argument to implement the model with $\delta = \frac{1}{2}$. This would allow the total length of the eddy interaction box in the x direction to be identical to the total length of the eddy interaction box in the y direction. This is aesthetically pleasing to those who view real life eddies as circles, circles having the same height as width. The author however resisted this argument and refused to add yet another free parameter.

Particle-eddy interactions are more complicated in the x direction because the fluid parcels usually have a u velocity. This can clearly be seen for the particular case depicted in Figure 2.1, where these particular fluid parcels all have a positive u velocity. One would naturally expect that the eddy in that figure would have a net positive u velocity since all of its elements have a positive u. A logical definition for the average u velocity of

an eddy event is the average of the u velocities of the individual cells in the domain of the triplet map, [y_o, y_o+l], at the time, t_{eo}, of the eddy event.

$$u_{eddy} = \langle u_{cells} \rangle = \frac{\int_{y_o}^{y_o+l} u(y, t_{eo})dy}{l} \quad . \qquad (3-21)$$

Since turbulent eddies have a wide variation in their eddy velocities, u_{eddy}, one would expect a wide variety of interaction times between eddies and particles due to this relative motion.

The effect of a non-zero x component eddy velocity (u_{eddy}) on the particle-eddy interaction time can be seen in Figure 3.8. This figure is a different rendering of the space-pseudotime eddy interaction box already introduced in Figure 3.4. Figure 3.8 has the x direction associated with the ordinate (rather than the y direction). The height of the interaction box is as defined in Equation 3-19 ($2l$), but the particle is centered in the height at the moment the particle eddy interaction begins. In all other ways, the new x-pseudotime eddy interaction box is the same as the previously defined interaction box. In Figure 3.8 diagram A, the eddy velocity is zero, the eddy does not move in time, and this particular particle trajectory is contained in the eddy for the duration of the eddy lifetime, t_e. In diagram B, the eddy has
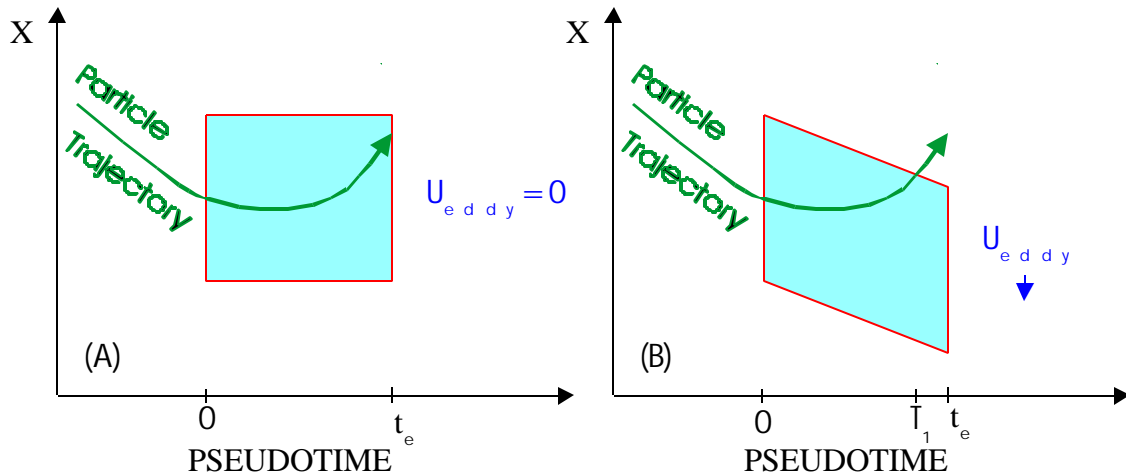
Figure 3.8: Effect of non-zero *x* component eddy velocity on the particle-eddy interaction time. In figure A, the eddy velocity (U_{eddy}) is zero, and the particle trajectory is contained in the eddy for the duration of the eddy lifetime. In figure B, the eddy has a negative velocity hence the eddy moves down as the particle curves up. This causes the particle to leave the eddy interaction box before t_e at time = T_1.

a negative velocity hence the eddy moves down as the particle curves up. This causes the particle to leave the eddy interaction box at time equal to T_1, before the eddy lifetime expires at time t_e, which it would not do if the eddy were not moving (diagram A). Therefore the correct end point for the particle eddy interaction is at time T_1 not time t_e.

The proper ending time for the eddy-particle interaction must be the first time the particle leaves the eddy in either the *x* or the *y* direction, or the eddy lifetime , whichever comes first. The space-time eddy interaction box has

been very useful in understanding the interaction time based on one spatial dimension (for example y) and one time dimension (pseudotime). The duration of the particle-eddy space-time overlap is governed by two spatial dimensions and time. The flipping between x and y on the ordinate tends to be confusing so that the intuitive understanding of the diagrams can easily be lost. Hence the introduction of a new diagram.

3.9.3   Spatial (x and y) particle-eddy interaction box

A more intuitive two-dimensional pictorial would be to place the spatial dimensions on the same graph. This would be equivalent to seeing a snapshot of the eddy and the particle at an instant in time. Subsequent times could be viewed in a series of snapshots. The new pictorial for the particle-eddy interaction box in two spatial dimensions (x and y) is given in Figure 3.9 (B), with the x direction used as the abscissa. Consequently the length (x dimension) is twice the height (y dimension) of the spatial eddy interaction box. Figure 3.9 (A) depicts the particle trajectory in x-y space just prior to a particle-eddy event. Figure 3.9 (B) depicts the instant in time when the particle intersects the triplet map. The newly defined "spatial eddy interaction box" is demarcated as a box, that horizontally extends a distance l in each direction from the particle x location, x_o, at the instant of the type-I

interaction. (This is consistent with Equation 3-19.) The box extends vertically with a starting point and length as defined by the eddy parameters:

$$y_o \leq y_e \leq y_o + l \quad . \qquad (3-22)$$

The y position of the particle in relation to the spatial eddy interaction box is the actual y_p of the particle. The box itself has its own u velocity, u_{eddy}, which may be positive, negative, or zero. The relative motion of the particle and the eddy, U - u_{eddy} , can cause a drastic shortening of the interaction time as discussed in Section 3.8.2 for the x dimension only. In order to better understand these variations in (x, y, t) space, three particular test cases will be explored using the new pictorial. The three test cases shall consist of a particle with finite inertia and modest U velocity interacting with three different eddies. All the eddies will have the same eddy interaction box, but the mean eddy velocities will vary as follows: $u_{eddy} \gg$ U, $u_{eddy} =$ U, and $u_{eddy} \ll$ U. All three cases will therefore share the same initial conditions, as shown in Figure 3.9 A and B. In diagram A, the particle trajectory just prior to the type-I interaction is shown. Diagram B shows the moment the type I interaction begins. This corresponding to $T = 0$. Also, x_o is defined as the particle x position at this instant. This is used to define the

horizontal center of the eddy as defined in Equation 3-19. The u_{eddy} depicted by an arrow is as yet undefined. (It can be positive, negative or zero.) In the first case ($u_{\text{eddy}} \gg U$) the mean velocity of the eddy will carry the eddy much faster in the x direction than the particle can travel (because the particle has finite inertia) so the eddy leaves the particle behind. This can be visualized in time by viewing Figure 3.9 in the sequence diagram A, B, and then C. For diagram C, a characteristic time increment, t_{ch}, was chosen such that u_{eddy} travels a distance just a little bit more than l. Implicit in the discussion of all three cases is the assumption that the eddy lifetime t_e is greater then t_{ch}. There is little effect of the eddy on the particle trajectory in case C (its U velocity is increased slightly) because of the short interaction time.

In the second case ($u_{\text{eddy}} = U$) the particle and eddy travel in unison. This can be visualized in time by viewing Figure 3.9 in the sequence diagram A, B, and then D. The characteristic time is significantly longer then either of the other two cases, since t_{ch} is defined as the amount of time for the eddy to travel l plus a little more. Note that we are still assuming that the eddy lifetime. t_e, is greater than the characteristic time shown in D. However the mean eddy velocity in this case is much smaller than the mean eddy velocity
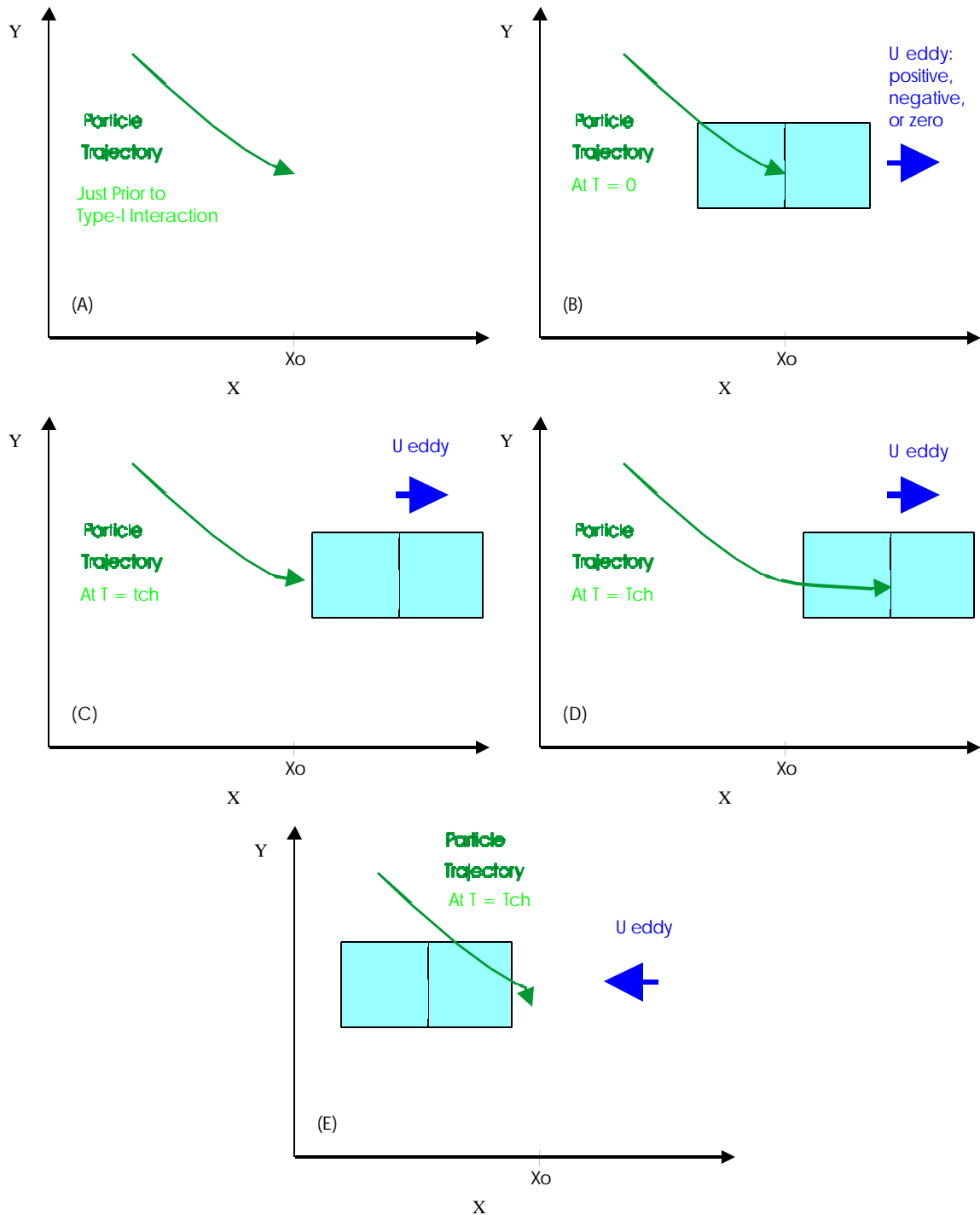
Figure 3.9: Time series qualitatively demonstrating the various affects of eddy velocities on particle trajectories. Diagram A and B show the initial conditions and are common to all trajectories. $U_{eddy} \gg U_p$ is shown in C, $U_{eddy} = U_p$ is shown in D, and $U_{eddy} \ll U_p$ is shown in E.

for either of the other two cases, hence the time is much longer. Analysis of Figure 3.9 (D) shows the particle-eddy interaction has had time to significantly change the particle trajectory. In this case, the eddy and particle travel together to the right a distance slightly larger than l, and the particle's U velocity is increased slightly.

In the third case ($u_{\text{eddy}} \ll$ U) the particle leaves the eddy behind. This can be visualized in time by viewing Figure 3.9 in the sequence diagram A, B, and then E. The characteristic time is the same as case 1 since u_{eddy} for case 1 is equal to the negative of u_{eddy} for case 3. Analysis of Figure 3.9 (E) shows the same trend as the particle-eddy interaction depicted in diagram C, that is the interaction time was too short to change significantly the particle trajectory. In diagram E, the eddy passes to the left of the particle and the particle velocity, U, is decreased slightly.   In order to handle all combinations of U and u_{eddy} correctly, the model must keep track of the relative positions of the particle and the eddy and must end the type-I interaction at the first instant the particle leaves the eddy.

The particle trajectory, under the influence of the eddy, has the possibility of leaving the eddy and then re-entering the eddy in either the x or y direction. This event is not easily depicted in this particular rendering of the

spatial eddy interaction box since both the particle and the eddy move in time but the representation is at a given instant in time. This problem is solved by a simple coordinate transform. A switch from the fixed reference frame to the moving reference frame of the eddy provides a simple and informative pictorial of the particle trajectory as compared to the stationary spatial interaction box. To achieve this new reference frame only one transformation is needed, that is for the abscissa.

$$x^* = x - u_{eddy} T \qquad (3-23)$$

With U* and X* denoting the resulting transformed particle velocity and position respectively, the resulting drag law equation is:

$$\frac{dU^*}{dT} = -\frac{f}{t_p}\left(U^* - u + u_{eddy}\right) \qquad (3-24)$$

The horizontal dimension of the spatial eddy interaction box in the moving reference frame is defined in Equation 3-25. The vertical dimension is unchanged in this transformed reference frame and is still given by Equation 3-22,

$$x_o - l \leq x_e^* \leq x_o + l \quad . \qquad (3-25)$$

Figure 3.10 shows two particle trajectories in the reference frame of the eddy. In these particular examples there are extrema in both the x^* and y directions. In these representations the particle trajectory is traced in x^*-y space from the time of birth of the eddy until the lifetime of the eddy, t_e, elapses. As can be seen in Figure 3.10 (A), during that time period (t_e) the particle exits and reenters the eddy twice. The first time it leaves the vertical (right) face of the box. The second time it exits the bottom surface. Lastly the particle leaves the spatial interaction box for the last time by the left vertical surface. The particle equation of motion (based on the particle-drag laws Equations 3-12 and 3-24) evaluated in the x^* and y direction allow for a maximum of one extremum in each direction. Hence Figure 3.10 (A) is a worst case scenario which exits the interaction box three times. Figure 3.10 (B) also has two extrema, but only exits the interaction box once and that is well after both extrema are achieved. Not all particles will exit the spatial interaction box before the lifetime of the eddy expires. As explained in the beginning of Section 3.9 the actual particle interaction time, T_1, is taken to be the first time the particle leaves the spatial interaction box or the eddy lifetime, t_e, whichever is sooner. This value of T_1 is plugged into Equations 3-14 and 3-15 to obtain the perturbations caused by the particle eddy
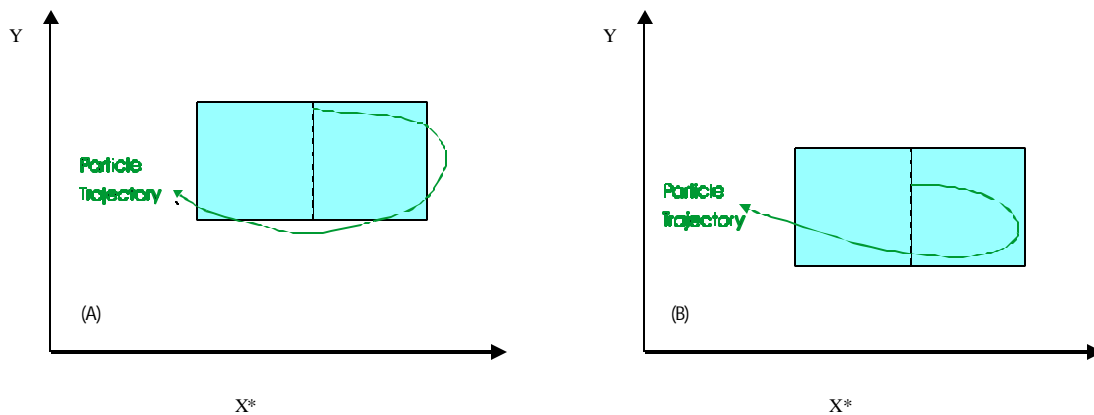
Figure 3.10: Particle trajectories in the moving reference frame of the eddy. This provides a clear view for the ending point of the particle-eddy interaction. The ending time of the interaction should be the first moment it leaves the spatial interaction box.

interaction. The particle position, y_p, and velocity, V, are adjusted instantaneously and the particle is allowed to proceed under the particle-drag law (Equations 3-9 and 3-10) in continuous time until the particle encounters another eddy. There are no adjustments made to the x position, x_p, or the x velocity, U, of the particle due to the particle-eddy interaction. The nature of the time developing ODT model does not lend itself readily to sudden jumps in the x domain. As noted in Section 3.3, the continuous-time process provides an adequate representation of streamwise particle evolution.

3.10   Conclusion and summary

The two phase flow submodel for ODT is now complete. It reflects the key (Stokes) particle-drag interactions for regimes in which the fluid motion affects the particle but the particle does not effect the fluid flow. This model does so in a manner which captures the relevant physics in terms of the ODT phenomenology.

This derivation started with the basics and worked up to the final two-phase flow submodel for ODT. There were many places in which the reader could have lost track of which equations were actually used in the submodel and which were used to derive the model or to illustrate a point. The model equations are summarized here to help clarify the two-phase flow model.

A particle is born into the ODT domain with an initial position (x_p and y_p) and velocity (U and V). The particle moves in "particle time" during which it follows the equations of motion defined by the particle-drag laws in x and y components given in Equations 3-9 and 3-10 modified to reflect the introduction of the particle time, t_p, with τ_p, f, and Re defined in Equations 3-5, 3-6, and 3.7:

$$\frac{dV}{dt_p} = -\left(V\right)\frac{f}{t_p} + F_G \quad , \qquad (3-9^*)$$

$$\frac{dU}{dt_p} = \frac{-(U-u)f}{t_p} \quad , \qquad (3-10^*)$$

with the particle time, Δt_{p} , computed by Equation 3-11. Pseudotime is not adjusted for the difference in particle and gas velocities since it is a fictitious time.

The particle follows the empirical nonlinear drag law until it occupies the same space-time as a triplet map, at which time it undergoes a type-I interaction. Type-I interactions are realized by the integrating the particle drag law components (Equations 3-12 and 3-24) in pseudotime, T, for a duration in pseudotime not exceeding t_{e} as defined in Equation 3-18. There is no adjustment of U for the particle-eddy interaction. The x component of the particle-drag law has been transformed to the constant velocity, u_{eddy}, coordinate system of the moving eddy as defined in Equation 3-23. The transformed coordinate is indicated by a *.

$$\frac{dV}{dT} = -\frac{(V-v)}{t_p} f + F_G \qquad\qquad (3-12)$$

$$v = {h}\big/{t_e} \qquad\qquad (3-17)$$

$$\frac{dU^*}{dT} = -\frac{f}{t_p}\left(U^* - u + u_{eddy}\right) \qquad\qquad (3-24)$$

with u_{eddy} defined in Equation 3-21. The initial conditions y_{To}, X_o, V_{To}, and $U_o{}^*$ are given by the particle position and velocity at the moment the particle intersects the eddy event. The form of the pseudotime equation of motion shows that the particle may exit and re-enter the eddy interaction box in either the x^* or y direction. The box is defined in the y direction by Equation 3-22 and in the x^* direction by Equation 3-25. Hence, merely evaluating the equation of motion at the end of pseudotime (letting $T_1 = t_e$) and verifying the particle is still in the eddy interaction box is not sufficient to assure that the particle-eddy interaction ceases the moment the particle first leaves the eddy interaction box. To overcome this added complication, one merely needs to evaluate the extrema in x_p and y_p. If both extrema reside in the eddy interaction box, and the position of the particle, evaluated at $T = t_e$ also resides in the eddy interaction box then the particle assuredly has remained inside the eddy interaction box for the entire time t_e. If any one of these evaluations the particle exists outside of the eddy interaction box then a search of the x^*, y, t space is necessary in order to find the first time in which the particle leaves the eddy. Care must be taken to ensure that T_1 is the first time at which the particle leaves the box, or if it does not leave the box, that T_1 is set to t_e.

The instantaneous change in the particle velocity, Δy, and position, ΔV can then be calculated from Equations 3-14 and 3-15. These changes are then added to the particle's position and velocity at the instant of the eddy, y_{To} and V_{To}. The particle is then allowed to continue on in continuous time with the new values of y_p and V.

3.11   Two-phase Flow Model Extension – type-C interactions

As explained in Section 3.4.1, the idealization of eddy events as instantaneous in time causes a model artifact. The larger (in magnitude) the y velocity becomes, the less likely a particle is to intersect an eddy event. In the limit as the y velocity component becomes infinite, the probability of an eddy interaction becomes zero because both the triplet maps and the particle trajectories are vertical lines. Since particles with large y velocities should interact with eddies in some way, the concept was put forward to allow the eddies to exist for a set length of time, this time would be the adjusted eddy lifetime t_e. The essence of this would be to "pretend" that the ODT instantaneous eddies existed for a finite time. This would be represented as a box (not just a line) in the eddy event history diagram. Interactions of the type in which a particle enters the space time box associated with an eddy event through either of the two horizontal edges are referred to as type-C

interactions because the particle is acted upon in a continuous manner by the eddy event as long as the particle is inside the box. This particular application did not require the added complication of type-C interactions. However, a brief outline of the conceptual design of type-C interactions is in order.

In contrast to type-I interactions, there are no instantaneous jumps from a type-C interaction. Type-C interactions can only occur in the y direction, hence, the pictorial with the most insight is the y space-time diagram. In this case the eddy is allowed exist in real time for the duration of the eddy lifetime t_e. (See Figure 3.11)

Any particle which enters an eddy by the left vertical surface interacts with the eddy event in a type-I fashion and is not allowed to interact with the same eddy in a type-C fashion even if the particle leaves the eddy interaction box and comes back into the box by one of the horizontal surfaces. This is because the type-I interaction already takes into account the entire lifetime of the eddy. Conversely a particle which first enters an eddy interaction box from one of the horizontal surfaces may not undergo a type-I interaction with that eddy, but may interact with that eddy in a type-C manner as long as it is in the interaction box and may interact with that same eddy as many

times as it re-enters the box. As soon as the particle exits the box by either one of the horizontal or the right vertical side the particle-eddy interaction ceases. Because of the random nature of the ODT triplet maps, virtually any conceivable combination of eddies may occur in a turbulent flow simulation. Once eddies are allowed to exist in time for the eddy lifetime, t_e, it is quite probable that a particle trajectory may intersect in a type-C fashion with two or more eddies at the same time. While undergoing a type-C interaction a particle may interact with a different eddy in a type-I fashion. There is no possibility that two type-I interactions can occur simultaneously because of the ODT formulation implements triplet maps only one at a time.

One scenario is presented in Figure 3.11. Here a particle intersects a large eddy event denoted 1, the particle continues to interact in a type-C fashion as long as the particle is inside of the eddy interaction box. While in the box, it also enters the interaction box of the eddy denoted 2. The particle feels both eddies # 1 and # 2 in a type-C manner until the particle leaves the interaction box of eddy number 2. The particle continues feeling eddy # 1 only, until it also enters eddy number 3. At this point, it feels both # 1 and # 3. While still in eddy number 3, the particle leaves the interaction box of
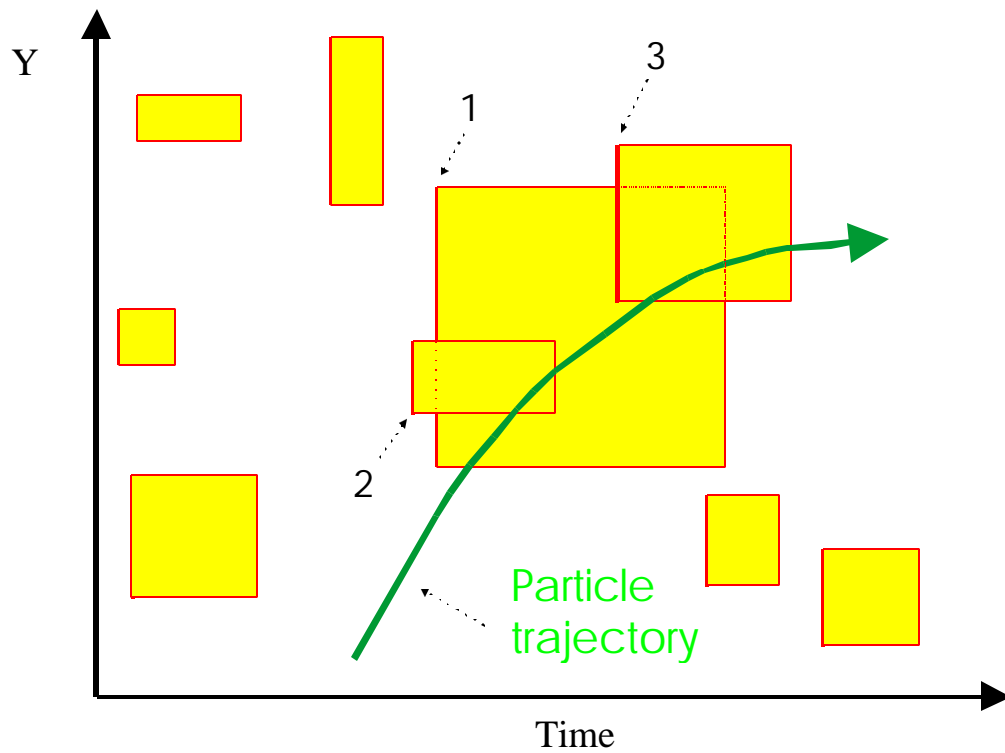
Figure 3.11: Multiple type-C interactions may occur at the same time. Here the particle interacts in a type-C fashion first with eddy number 1, then with both eddies 1 and 2, then with eddy 1 only, the with eddy 1 and 3, and finally with eddy number 3 only.

eddy number one. After this, the particle continues in a type-C interaction with eddy # 3 only, until the particle leaves the last interaction box.

Figure 3.12 gives a space-time history diagram with two possible particle paths in the same eddy sequence. In Figure 3.12 (A) the particle undergoes a type-I interaction with eddy number 1, this is demarcated on the abscissa with a tick mark and is labeled I1 (for type-I interaction with eddy #1).
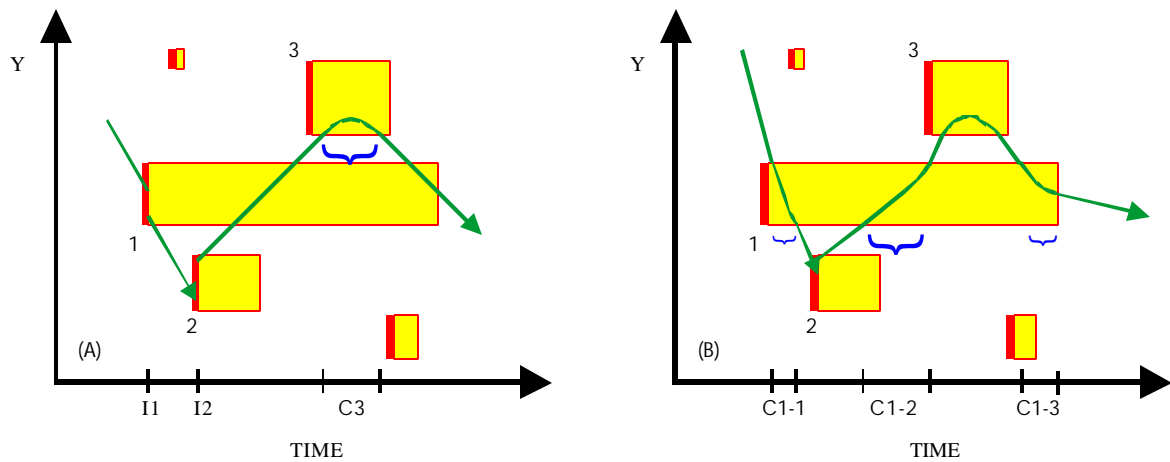
Figure 3.12: Possible type-I and type-C interactions for two different initial velocities. In (A) the particle re-enters eddy #1 twice, but there is no additional interaction. In (B) the particle interacts with eddy #1 three distinct times labeled C1-1, C1-2, and C1-3.

Then the particle undergoes a type-I interaction with eddy #2, labeled I2. Finally it undergoes a type-C interaction with eddy #3, this is demarcated with " { " and the time interval on the abscissa is marked with a C3 (for a Continuous interaction with eddy #3). Even though the particle crosses the eddy #1 interaction box two more times it does not interact with the eddy since it first experienced a type-I interaction. Figure 3.12 (B) depicts a different particle which enters eddy #1 from the top and undergoes a type-C interaction for a time interval labeled C1-1 (for Continuous interaction with eddy #1 - 1st occurrence). It then experiences a type-I interaction with eddy #2. It changes course and re-enters eddy #1 and again experiences a type-C

interaction labeled C1-2. It then undergoes a type-C interaction with eddy #3 (not marked on the abscissa) and gets turned around once more where it re-enters eddy #1's interaction box a third and final time. The particle then experiences a type-C interaction labeled C1-3.

Implementation of type-C interactions onto the ODT domain requires keeping track of the positions of all eddies from the time each eddy is born until that individual eddy's lifetime has expired. Any particle entering any of these y positions during that particular eddy's lifetime would interact continuously with that eddy as long as it had not undergone a type-I interaction with that same eddy previously. The result of allowing eddies to exist in the time domain is that for the duration of t_e the y domain of the eddy [y_o, y_o+l] is allowed to have a nonzero gas phase velocity v. Recall that in the ODT formulation turbulent flows are idealized as having a zero v component, and the instantaneous triplet maps implement the eddy caused phenomena. Though the ODT program proper would be unaffected by the addition of the nonzero v velocities, they would effect the particle time evolution as defined by the particle-drag law. Equation 3-9* would now have a gas phase component only in the y interval [y_o, y_o+l] and from the instant of the triplet map until the ODT time increment t_e elapsed.

$$\frac{dV}{dt}_p = -\left(V - \sum_j v\right)\frac{f}{t_p} + F_G \quad , \qquad (3-9**)$$

Here the summation over j includes only the eddy events whose interaction box occupy the same space-time as the particle trajectory. There exists latitude in the specific mechanics to the type-C implementation, but the eddies would have either a positive or negative v velocity (this could be chosen randomly). As such, the summation in Equation 3-9** would have to be a vector sum over all overlapping eddy events. Hence the affects of eddies could cancel each other out. There is also latitude in the definition of what the correct gas velocity is of the eddy. Some type of weighted average displacement of all the cells in the triplet map could be used as the distance, that with the eddy lifetime, t_e, would then define the gas phase velocity of that particular eddy.

3.12   Numerical implementation

At this point the two-phase flow model is complete and a discussion of assumptions, simplifications, and numerical implementation techniques is in order.

Rather than computing the Reynolds number as defined in Equation 3-7, the following numerical implementation simplifications were made for the x and y direction.

$$\text{Re}_x = \frac{\mathbf{r}_g\, r_d\, \left| U - u_g \right|}{\mathbf{m}_g} \qquad (3-26)$$

$$\text{Re}_y = \frac{\mathbf{r}_g\, r_d\, \left| V - v \right|}{\mathbf{m}_g} \qquad (3-27)$$

These Reynolds numbers were then plugged into the Equation 3-6 (the empirical nonlinear drag law, f) to predict the variation from Stokes drag for the respective particle-drag laws (in particle time, Equations 3-10* and 3-9*; in pseudotime modified to the moving coordinate system, Equations 3-24 and 3-12).

Integration of the 4 particle-drag laws (x and y components for particle time and pseudo time) is a key issue in efficient numerical implementation of the two-phase flow submodel. As discussed in detail in Section 2.7, the design of ODT is such that the greater the turbulence intensity (the larger the free parameter A) the shorter the eddy time step, Δt_{stir}, and hence a shorter the diffusion time step, Δt_{dif}, is required to start smoothing the velocity

profiles between implemented eddies. For highly turbulent flows, the values of eddy time-step and the diffusion time-step are constrained to be small.

Letting the droplet time step, Δt_{drop}, be approximately equal to the diffusion time step, allows the assumption that the coefficients in the particle-drag laws, τ_{p} and f, are constant or nearly constant over the time period of integration of Equations 3-10* and 3-9*. An added benefit is that Δt_{drop} is in ODT time and must be adjusted to particle time, Δt_{p}, by equation 3-11. On average the particle U velocity is greater then the bulk mean gas u velocity hence the particle time increment is smaller then the prescribed ODT time difference, Δt_{drop}. This gives more of a comfort zone to the assurance that the particle time increment is small enough to assure that the coefficients of the particle-drag law components are constant. An added level of comfort comes from the way in which the droplet submodel is implemented into the ODT structure. (See the general logic flow chart Figure 2.4, the pointer "clock" in Figure 2.3 and the corresponding discussion in Section 2.7.) The model implementation uses a fixed Δt_{drop}. Hence in the absence of an implementation of an eddy event the particle time is updated in proportion to the fixed Δt_{drop}. However, whenever an eddy is implemented in the ODT time domain, the position of all particles at

that instant must be computed in order to be assured that the particle and the triplet map occupy the same space time. This changes the time interval for the calculations from the maximum Δt_{drop} to only some fraction of the maximum time interval. The time interval for the next update for the droplet is then adjusted to be Δt_{drop}. This corresponds to a shift in the droplet time line shown Figure 2.3. In the absence of another implementation of an eddy event during that time interval, Δt_{drop}, the particle position and velocity is not updated until the end of that time interval. If however, another eddy event is implemented, the particle is udated at the time of the eddy implementation and the time line is again adjusted as before.

Figure 3.13 is a pictorial continuation of Figure 2.3. The eddy event in Figure 2.3 was implemented hence the droplet position was computed at the identical time (using the much shorter particle time interval) and the droplet time line is adjusted (shifted left) so that the maximum time interval for integration of the particle-drag law is never more then the maximum Δt_{drop}.

Assuming a small enough time interval such that the coefficients of Equation 3-9* (τ_{p} and f) are considered constant, integrating yields first the velocity, V, (Equation 3-28) and then integrating gives the position y_{p}
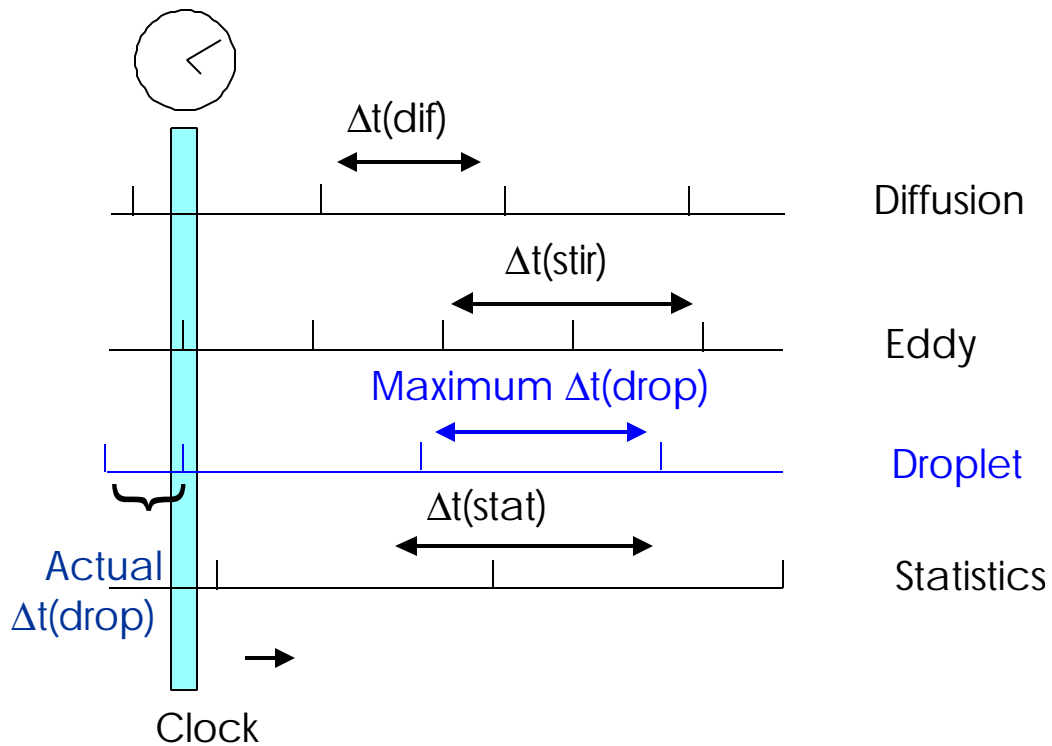
Figure 3.13: Actual Δt_{drop} is only a fraction of the maximum Δt_{drop} due to the implementation strategy of the two-phase flow submodel. The droplet time line is shifted in order to assure that the maximum time between droplet updates does not exceed the time interval Δt_{drop}.

(Equation 3-29) in continuous time. The standard boundary conditions were used: at $t_p = 0$, $V = V_o$ and $y_p = y_o$.

$$V = \frac{t_p}{f} F_G + \left(V_o - \frac{t_p}{f} F_G \right) \exp\left(-\frac{f}{t_p} t_p \right) \qquad (3-28)$$

$$y_p = y_o + \frac{t_p}{f} F_G t_p + \frac{t_p}{f} \left(V_o - \frac{t_p}{f} F_G \right) \left(1 - \exp\left[-\frac{f}{t_p} t_p \right] \right) \qquad (3-29)$$

As discussed earlier, in continuous time there is no fluid y velocity component, so, a fluid tracer particle (zero inertia) must not undergo translation in the y direction. This can be verified easily by taking the limit as the particle inertia tends to zero of either Equation 3-28 or 3-29.

$$\lim_{t_p \to 0} y_p = y_o \qquad (3-31)$$

$$\lim_{t_p \to 0} V = 0 \qquad (3-30)$$

The infinite inertia limit of Equation 3-28 shows that the particle continues to proceed unaffected by the particle drag law.

$$\lim_{t_p \to \infty} V = V_o \qquad (3-32)$$

The continuous time particle trajectory in the x direction is achieved by integrating Equation 3-10* twice with the standard initial conditions (at $t_p = 0$; $x_p = x_o$, and $U = U_o$). Again, assuming a small enough time interval such that the coefficients (u, τ_p) of Equation 3-10* are considered constant,

$$U = u + \left(U_o - u\right) \exp\left[-\frac{f}{t_p} t_p\right] \qquad (3-33)$$

$$x_p = x_o + u\,t_p + \frac{t_p}{f}\left(U_o - u\right)\left\{1 - \exp\left[-\frac{f}{t_p} t_p\right]\right\} \qquad . \quad (3-34)$$

As expected in the vanishing inertia limit, the particle matches the fluid parcel which surrounds it,

$$\lim_{t_p \to 0} U = u \qquad (3-35)$$

$$\lim_{t_p \to 0} x_p = x_o + u\,t \qquad . \quad (3-36)$$

In the limit of infinite inertia Equation 3-33 gives the expected result that the velocity is unaffected by the particle drag,

$$\lim_{t_p \to \infty} U = U_o \qquad . \qquad (3-37)$$

The analytical solutions (Equations 3-33 and 3-34) had the added assumption that the particle does not leave the fluid parcel it is in during the particle time interval. This is an assumption since during continuous

(particle) time the particles are allowed to move from one cell to another. This is a good assumption only for short time periods.

We now have a closed form solution for the particle velocity $U(t_p)$ for short times. With this the particle time can be computed using Equation 3-11 assuming the Re and diameter are constant and the particle does not leave the particular fluid cell it is in. This is only an approximation but gives the best estimate for the actual time the particle sees during the time the ODT streamwise evolution (at the mean u velocity of the fluid). An alternate method to compute the time the particle actually experiences while the ODT time develops would be to actually iterate on the whole variable coefficient Equation (3-34) until convergence. This however would be very costly.

To compute the change in time, Δt_p, which the particle experiences as the ODT time domain develops, Δt_{ODT}, the ODT time is multiplied by at the mean u velocity of the fluid, $\overline{u}_b$, to get the distance traveled. This resulting distance, given in Equation 3-38, is assigned to the difference in which the particle travels in Equation 3-34.

$$x_p - x_o = \Delta x_p = \Delta t_{ODT}\, \overline{u}_b \qquad (3-38)$$

The resulting transcendental equation is

$$0 = \Delta x_p + u\,\Delta t_p + \frac{t_p}{f}\,(U_o - u)\left\{1 - \exp\left[-\frac{f}{t_p}\Delta t_p\right]\right\} \qquad . \qquad (3-39)$$

Equation 3-39 could be solved, using any root finding technique, for the time the particle would take to traverse the distance Δx_p while experiencing drag. However, since the equation is only approximate, the exponential term in Equation 3-39 is expanded in a series with Δt_p and only the terms up to $\Delta t_p^{\,2}$ are kept, giving

$$HOT + \frac{(U - u)f}{2t_p}\left(\Delta t_p\right)^2 - U\,\Delta t_p + \Delta x_p = 0 \qquad . \qquad (3-40)$$

All Higher Order Terms (HOT) are thrown out since Δt_p is small, and the resulting equation is solved using the standard equation to find the roots of a constant coefficient quadratic equation, where the particle time increment used is taken to be the smallest in magnitude, real root of the quadratic equation given in Equation 3-40. The ending particle position and velocity for the current step are taken as the initial conditions for the next step. Once the best estimate of the Δt_p for the particle is obtained, application of the continuous time particle-drag law is straightforward. This time increment is used to calculate actual variations in the particle position (x_p and y_p); particle

velocity (U and V); and adjustments to the particle properties, e.g. diameter and temperature as discussed in detail in Chapter 4.

The next challenge is implementing the particle-drag laws for pseudotime. {In pseudotime, there are no adjustments made to the particle properties (diameter, temperature, etc.) since this would cause double counting once the particle re-enters particle time. The cause of this double counting is the analogous to the cause explained in Section 3.6. A brief discussion on alternative ways to take into account changing droplet properties during particle-eddy interactions is given in Chapter 4.} In a manner similar to the particle time, it is assumed that during the pseudotime interval, T_1: the eddy imposed v velocity is constant (true in the limit for tracer particles) and the coefficients τ_p and f are constants, resulting in the ability to analytically integrate Equation 3-12. Integrating yields first the y velocity (Equation 3-41) and then integrating again gives the position y_{Tp} (Equation 3-42) as a function of T. The particle's velocity and position at the instant of the particular particle-eddy interaction are taken as the boundary conditions: at $T = 0$, $V_T = V_{To}$ and $y_{Tp} = y_{To}$. Pseudotime integration gives

$$V_T = v + \frac{t_p}{f} F_G + \left(V_{To} - v - \frac{t_p}{f} F_G \right) \exp\left(-\frac{f}{t_p} T \right) \qquad (3-41)$$

$$y_{Tp} = y_{To} + \left(v + \frac{t_p}{f} F_G \right) T + \frac{t_p}{f} \left(V_{To} - v - \frac{t_p}{f} F_G \right) \left(1 - \exp\left[-\frac{f}{t_p} T \right] \right) \qquad . \qquad (3-42)$$

Note that a tracer particle behaves as it should (Equations 3-43 and 3-44).

$$\lim_{t_p \to 0} V_T = v \qquad (3-43)$$

$$\lim_{t_p \to 0} y_{Tp} = y_{To} + v T \qquad (3-44)$$

Also, an infinitely large inertia particle is unaffected by the particle-eddy interaction (Equation 3-45).

$$\lim_{t_p \to \infty} V_T = V_o \qquad (3-45)$$

In the x^* direction, we also make the assumptions that during the pseudotime interval, T_1: the fluid imposed u velocity is a constant equal to the u value of the cell initially containing the particle, (true in the limit for tracer particles) and the coefficients τ_p and f are constants, resulting in the ability to analytically integrate Equation 3-24. Integrating yields first the x^* velocity (Equation 3-46) and then integrating again gives the position X^* (Equation 3-47) as a function of T. The particle velocity and position at the

instant of the particular particle-eddy interaction are taken as the boundary conditions: at $T = 0$, $U^* = U^*_o$ and $X^* = X_o$. Pseudotime integration gives

$$U^* = u - u_{eddy} + \left(U^*_o - u + u_{eddy}\right)\exp\left\{-\frac{f}{t_p}T\right\} \qquad (3-46)$$

$$X^* = X_o + \left(u - u_{eddy}\right)T - \frac{t_p}{f}\left(U^*_o - u + u_{eddy}\right)\exp\left[-\frac{f}{t_p}T\right] \qquad . \quad (3-47)$$

The infinitesimally small and infinitely large limits of particle inertia behave properly:

$$\lim_{t_p \to 0} U^* = u - u_{eddy} \qquad (3-48)$$

$$\lim_{t_p \to 0} X^* = X_o + \left(u - u_{eddy}\right)T \qquad (3-49)$$

$$\lim_{t_p \to \infty} U^* = U^*_o \qquad . \qquad (3-50)$$

With the pseudotime particle position X^* and y_{Tp} known analytically, determining the correct particle-eddy interaction time T_1, is quite easy. First. set Equation 3-41 to zero and solve for the time, if any, at which the y extrema, T_{ey}, exists. Second, checking to see if this time, T_{ey}, is less than the eddy lifetime t_e. If the extremum occurs during the eddy lifetime then the particle position y_{Tp}, is evaluated using Equation 3-42. If this value is

between y_o and $y_o + l$ then there is no danger of the particle exiting the interaction box and reentering as depicted in Figure 3.7. In this case where the extremum is not outside the interaction box, T_1 is set equal to t_e. If the particle exits the interaction box, for example, from the bottom, $y_{Tp}(T_{ey})$ is less than y_o, then in Equation 3-42 y_{Tp} is set equal to y_o and this is solved by a root finding technique to determine the time T_{1y} at which the particle first leaves in the y direction. For a particle which exits the top surface, y_p is set equal to $y_o + l$, and the first exit time is determined in the same fashion as above, after which T_1 is set to T_{1y}.

The next step in finding the correct particle-eddy interaction time is analogous to the procedure in determining T_{1y}. To determine whether and when the particle leaves the interaction box in the x^* direction, Equation 3-46 is set to zero and the time T_{ex} of the occurrence of an extremum (if any) is calculated. If T_{ex} is less than T_1 then $X^*(T_{ex})$ is evaluated using Equation 3-47. If X^* is inside the range $[-l, + l]$ then the particle does not leave the interaction box in the x direction. There is no danger of the particle exiting the interaction box in the x^* direction and returning as shown in Figure 3.10.

However, if a particle leaves the interaction box by one of the vertical sides (say the right), X^* in Equation 3-47 is set equal to l, {if the particle

exits on the left hand side of the box, X* is set equal to $-l$}. Equation 3-47 is then solved for the time T_{1x} at which the particle exits the interaction box. The interaction time T_1 is then set to T_{1x}. If the extrema of the particle trajectory exited the interaction box by either the y or x^* directions before the eddy lifetime expired, then T_1 is set to the correct interaction time at this point.

However, if neither the y nor x^* direction extrema exited the interaction box before the eddy lifetime expired, then y_{Tp} and X* are evaluated at t_e. If $y_{Tp}(t_e)$ and X*(t_e) are inside the interaction box, then the correct value of T_1 is t_e. If the particle trajectory endpoint (X*(t_e), $y_{Tp}(t_e)$) falls outside the interaction box, then one or both of Equations 3-47 and 3-42 has to be solved in an analogous manner to the technique explained above for finding the first time that the particle exits the eddy. This is the correct value for T_1.

This completes the major simplification (Re), the assumptions (constant coefficients, etc.), and the numerical implementation techniques necessary to fully implement the two-phase flow submodel in an analogous manner used by the author to produce the numerical data which are presented in this paper.

Chapter 4

Droplet Burning Model

4.1 Introduction

In order to understand the model for vaporization of the droplets, the reader requires a discussion of the principal physical phenomena which the droplets experienced during the experiment. Great effort was made to inject streams of droplets with uniform size, D_o; uniform spacing, s/D_o; injection velocity, V_o; and injection angle, θ. Droplets were injected by way of a vibrating orifice device from a reservoir at room temperature into a 100 kW furnace. Sirignano (1999) states that a significant amount of the lifetime of this type of burning droplet is used in heating the droplet from room temperature to its dew point. This is accompanied by a significant ignition delay time, after which the droplet will ignite, provided there is an ignition source. After the droplet is burning, the heat release from the surrounding flame is a significant added heat source for the evaporating droplet. These phenomena were also observed by Mulholland et al. Hence a droplet heating/burning model is needed which includes the significant variables and predicts the heating rate is necessary. The flame is hot enough (maximum mean temperature is 1750 K) to serve as an ignition source for the droplets.

The ignition delay time was measured for each case. This measured ignition delay was used in the model to determine the onset of droplet ignition.

Another significant variable is the initial droplet spacing s/D_o. A droplet that is part of a stream of droplets travels farther into a turbulent reactor than it would if it were injected alone. The droplet travels in the wake of the droplets in front of it. Therefore the drop experiences less drag and less evaporation and can travel farther into the reactor. Mulholland et al. (1991) observed that the measured droplet stream, once injected into the reactor, travels in a straight line until the droplets reach the high shear layer of the gas flow, at which point the droplet stream breaks up into random droplets.

Unfortunately the ODT model with its two-phase flow sub model does not lend itself to modeling droplet streams. The idea of a stream of droplets traveling in unison along a trajectory is hard to conceive of in a one-dimensional turbulence model which develops in time and treats eddies as instantaneous mappings of the velocity and scalar fields. The main difficulty arises when one tries to model what happens to a droplet in the stream which is suddenly tossed about by an eddy. Does it leave the stream and go off by itself leaving the other droplets in the stream continuing in a linear manner? What effects would this one missing droplet out of a stream

of droplets have on the drag and evaporation of the rest of the stream? No logically consistent model presents itself for a one-dimensional time developing flow.

Besides the conceptual difficulty of having a stream of droplets in ODT and the many complications any model would have to have in order to handle suddenly allowing a single droplet to leave instantaneously the droplet line, this type of behavior was not observed experimentally in the reactor. Hence a different approach to modeling the initial linear droplet trajectory is in order.

One of the main objectives of this work was to see whether the ODT model could reproduce the spread in the burn out points of the burning droplets observed in Mulholland et al. (1991). A reasonable plan then would be to reproduce the droplet burning model and droplet trajectory model used in the original paper as closely as possible for the initial linear trajectory of the droplets. Once the droplet stream reached the high shear layer of the fluid flow the droplet position, diameter, velocity and temperature computed from that model would be used as initial conditions for the ODT two-phase flow model. The only remaining addition needed for the ODT two-phase flow model would be that of a heating/burning model, for which the same

model used for the initial conditions is utilized with the exception that the correction factor (η_s) for inter droplet spacing is assumed unity. In the ODT simulations, the droplets were assumed to act independently of each other. In the spirit of ODT each case would be modeled as an ensemble of droplets all having the same initial conditions. The computed spread of the droplet burnout points would be compared to the experiment.

4.2 Droplet heating model used by Mulholland et al.

A brief recapitulation of the droplet transient heating/burning model given in Mulholland et al. follows. The reader is referred to that publication for more details. The liquid droplet is assumed to be spherically symmetric with infinite heat diffusivity ("rapid mixing limit"). Therefore the droplet temperature is allowed to change with time, but there is no need to solve any of the fluid flow equations inside the droplet since the temperature is assumed constant across the droplet. The liquid phase properties (e.g. density and heat capacity) are constant. The heating time of the droplet is slow compared to the gas diffusion time. Mulholland et al. idealizes the droplet fuel mixture to be one representative (unnamed) chemical component. They give a table with mean properties of the liquid density, liquid heat capacity, boiling temperature, the heat of vaporization, the heat

of combustion and the stoichiometric fuel-to-oxygen mass ratio for this idealized one component fuel. The concentration of this component in the gas phase (assuming equilibrium) is determined by the Clausius-Clapeyron equation:

$$X_{fs} = \frac{1}{p} \exp\left[\frac{L}{R}\left(\frac{1}{T_b} - \frac{1}{T}\right)\right] \qquad (4-1)$$

where X_{fs} is the gas phase mole fraction of the fuel species, f, at the interface. The mass fraction, Y, and mole fraction, X, are related by the standard equations

$$Y_n = \frac{X_n W_n}{\sum_i X_i W_i} \qquad (4-2)$$

$$X_n = \frac{Y_n / W_n}{\sum_i Y_i / W_i} \qquad (4-3)$$

with the sum i being over all the species in the gas phase.

The gas phase is assumed to be in a quasi-steady state, with heat and mass diffusion rate controlling. With the assumption of Le = 1, the Sherwood number is equal to the Nusselt number. Ambient gas phase conditions are sub critical and the gas phase mixture is assumed to behave as an ideal gas mixture. Infinitely fast kinetics are assumed, so the flame sheet surrounds the burning droplet. (In other

words, the reaction time is shorter than the diffusion time and a flame surrounds the droplet after it has ignited.) This was experimentally verified by Mulholland et al.. The droplets would ignite (glow) a short time before they would completely burn out.

The authors derive [following Law (1976)] the following set of equations. An energy balance around the drop results in

$$m\,c_{pl}\left(\frac{dT_d}{dt}\right) = \left(H - \Delta H_v\right)\frac{dm}{dt} \qquad (4-4)$$

where H is the total heat transfer from the gas to the droplet. A mass balance yields

$$\frac{dm}{dt}\left[=-\left(\mathbf{p}\,\mathbf{r}\,D^2/2\right)\left(dD/dt\right)\right]=\mathbf{p}\,\overline{\mathbf{r}}\,\overline{D}_{AB}\,D\,Sh^*\ln\left(1+B\right)\mathbf{h}_s \qquad (4-5)$$

with η_s, representing the effect of the interaction of the droplets in a linear array on vaporization. This has been quantified by Labowsky [(1980)] as

$$\mathbf{h}_s = 1 - \left(2\frac{s}{D}\right)^{-1} + \left(2\frac{s}{D}\right)^{-2} \qquad , \qquad (4-6)$$

The Spalding mass transfer number, B, is given by

$$B = \left\{ \bar{c}_p \left(T_\infty - T_d \right) + Y_{0\infty} f \, \Delta H_c \right\} / H \qquad (4-7)$$

and the total heat transfer from the gas to the droplet, H, is given by

$$H = \left(1 - Y_{Fs} \right) \left\{ c_p \left(T_\infty - T_d \right) + Y_{0\infty} f \, \Delta H_c \right\} \left(Y_{Fs} + Y_{0\infty} f \right)^{-1} \quad . \qquad (4-8)$$

The gas-phase density and other mean gas properties in the film layer are evaluated at the 'one-third law' temperature [Hubbard et al. (1975)]. Hence, the gas phase components of the Re, Pr, and the Sc are computed at the representative temperature:

$$\bar{T} = T_d + \frac{1}{3} \left(T_f - T_d \right) \quad . \qquad (4-9)$$

Assuming the adiabatic flame temperature for the flame sheet temperature, T_f becomes:

$$T_f = T_\infty + Y_{0\infty} f \left\{ \Delta H_c - H - \bar{c}_p \left(T_f - T_d \right) \right\} / c_p \qquad (4-10)$$

where $\bar{c}_p$ is the heat capacity of the fuel in the gas phase.

Clift et al. [1978] gives the following correlation for the Sherwood number without any vaporization:

$$Sh_0 = 1 + \left(1 + \mathrm{Re}\ Sc\right)^{1\!/\!3} f\left(\mathrm{Re}\right) \qquad (4-11)$$

$$f\left(\mathrm{Re}\right) = \begin{cases} 1 & \mathrm{Re} \leq 1 \\ \mathrm{Re}^{0.077} & 1 < \mathrm{Re} \leq 400 \end{cases} \qquad (4-12)$$

The droplet Re,).

$$\mathrm{Re} = \frac{\pmb{r}_g\, r_d \left| \tilde{V}_d - \tilde{v}_g \right|}{\pmb{m}_g} \quad , \qquad\qquad (3-7)$$

is based on the relative velocity between the droplet and the fluid, droplet radius, and gas properties (the same as in Chapter 3

They use the analysis of Abramzon and Sirignano [(1987)] to account for forced convection and vaporization effects on convective heat and mass transfer. They consider a spherical vaporizing droplet inducing a radial Stefan flow. The vapor convects radially outward while the heat conducts radially inward against the flow of the vapor toward the liquid-gas interface. The energy of the heat conducted in is divided between heating the liquid and the phase change of the liquid at the surface into the gas phase. This newly evaporated fluid in turn convects radially outward. The Sherwood number with Stefan type flow vaporization becomes

$$Sh^* = 2 + (Sh_0 - 2)\left\{(1+B)^{0.7} \ln(1+B)/B\right\}^{-1} \qquad (4-14)$$

4.3 Introduction of the burning rate parameter

The phenomenon of droplet burning is very complex and the many simplifying assumptions used in the preceding analysis caused Mulholland et al. to introduce a measured parameter λ for the burning rate. They chose a parameter that could be measured in a laboratory-scale reactor. They defined λ as

$$\frac{dD}{dt} = -\lambda \left(\frac{Sh^*}{2}\right) h_s / 2D \qquad (4-15)$$

By the integration of Equation 4-15 for a constant λ and both Sh* equal to two and η_s equal to unity, the familiar d^2 law is reproduced

$$D_o^2 - D^2 = \lambda t. \qquad (4-16)$$

The Spalding mass transfer number is easily calculated from λ from Equation 4-17 or 4-18.

$$l = \left\{ 8\overline{rD}_{AB} \middle/ r_l \right\} \ln(1+B) \qquad (4-17)$$

$$= \left\{ 8\overline{k} \middle/ (\overline{c_P} r_l) \right\} \ln(1+B) \qquad (4-18)$$

B is calculated independently, using Equation 4-7, from the point of injection until the droplet reaches its wet bulb temperature. This constitutes the major portion of the droplet lifetime. The wet bulb temperature is achieved as dT_d/dt approaches zero and simultaneously the total heat transfer H is used to cause a phase change in the liquid at the surface. After this, the measured burning rate, λ, is utilized in the model to compute B for the remainder of the droplet lifetime.

4.4 Review of droplet-drag law used in Mulholland et al.

As mentioned previously, the ideal initial conditions for the ODT two-phase flow submodel would be to reproduce the droplet trajectory model from Mulholland et al. They develop a three-dimensional model which allows them to compute the x, y, and z variations of the drop. They use the mean measured gas velocity and temperature profiles to compute droplet trajectories. Mulholland et al. (1988) relate the drag of nonvaporizing droplets to interdroplet spacing as follows

$$\left\{ C_D \left(\mathrm{Re}, \frac{s}{D} \right) \right\}^{-0.678} = \left\{ C_D^0 \left(\mathrm{Re}, \frac{s}{D} \right) \right\}^{-0.678} + \left\{ C_D^\infty (\mathrm{Re}) \right\}^{-0.678} \qquad (4-19)$$

$$C_D^0 \left(\mathrm{Re}, \frac{s}{D} \right) = C_D^{00} (\mathrm{Re}) + 43\,\mathrm{Re}^{-1} \left\{ \frac{s}{D} - 1 \right\} \qquad (4-20)$$

$$C_D^{00} = 0.755/\mathrm{Re} \qquad (4-21)$$

$$C_D^\infty (\mathrm{Re}) = \left\{ 24 \Big/ \mathrm{Re} \right\} \left\{ 1 + 0.11\,\mathrm{Re}^{0.687} \right\} \qquad (4-22)$$

They use the model of Ayers et al. (1980) for the prediction of isolated droplets and modify it to include effects of droplet interaction on drag. Drag and gravitation are assumed the only external forces and they come up with

$$|F_{D1}| = C_D^* \, r \, A v_{r1}^2 / 2 \qquad (4-23)$$

$$|F_{D2}| = C_D^{\infty*} \, r \, A v_{r2}^2 / 2 \qquad (4-24)$$

where the * denotes mass transfer droplet drag coefficient with evaporation, they define, v_g is the gas velocity, V is the droplet velocity, v_{r1} is the relative droplet-gas velocity aligned in the direction in which the droplet is proceeding and v_{r2} is the resultant vector of the difference of v_r and v_{r1}.

$$\tilde{v}_r = \tilde{V} - \tilde{v}_g \qquad (4-25)$$

$$\tilde{v}_{r2} = \tilde{v}_r - \tilde{v}_{r1} \qquad (4-26)$$

Eisenklam et al. (1967) found a correlation between the mass transfer droplet drag coefficient with and without evaporation

$$C_D^* = h_e C_D \qquad (4-27)$$

$$h_e = \frac{1}{(1+B)} \qquad (4-28)$$

They (Mulholland et al.) do a force balance and get:

$$\sum F_x = ma_x = F_{D1x} + F_{D2x} \qquad (4-29)$$

$$\sum F_y = ma_y = F_{D1y} + F_{D2y} + F_G \left(=-mg\right) \qquad (4-30)$$

$$\sum F_z = ma_z = F_{D1z} + F_{D2z} \qquad . \qquad (4-31)$$

4.5   Modification of trajectory model for this application

This three-dimensional model is unnecessary for this particular application since they mentioned that the droplets travel in a straight line during the initial "droplet stream" phase of the trajectory. Also, an initial three-dimensional trajectory model would not make much sense feeding a

one-dimensional model. Therefore the three-dimensional model is simply projected onto the straight linear path expressed in Equation 4-32.

$$\sum F_{D1} = m\frac{dV_{D1}}{dt} = F_{GD1} + C_D^* \, \boldsymbol{r} \, A \left(v_{D1} - V_{D1}\right)^2 \qquad (4-32)$$

where V_{D1} is the (scalar) velocity of the droplet in the D1 direction and v_{D1} is the component of the velocity of the gas in the direction the drop is traveling. The D1 direction is defined as the direction the droplet is traveling, so this is precisely the injection angle, θ, measured down from the horizon, so

$$F_{GD1} = -\, m \, g \, \sin\left(\boldsymbol{q}\right) \ . \qquad (4-33)$$

Equation 4-32 is the non-linear droplet-drag law. When Equations 4-19, 4-20, 4-21, 4-22, 4-27, 4-28, 4-32 and 4-33 are used in conjunction with

$$\text{Re} = \frac{\boldsymbol{r}_g \, r_d \left|V - v_{D1}\right|}{\boldsymbol{m}_g} \qquad (4-34)$$

and Equations 4-1, 4-4, 4-5, 4-6, 4-8, 4-9, 4-10, 4-11, 4-12, 4-14, and 4-7 the total set of equations determine the model to compute the boundary

conditions for the ODT two-phase submodel, from initial droplet injection up until the point that the droplet appears in ODT space.

Since the initial conditions are only required to be computed once for each of the 12 cases (and are identical for all the ensembles) in this specific application of these equations the time steps were taken to be very small, of order 10^{-5} seconds. Hence the coefficients in Equation 4-32 are considered constant over that short time and the non-linear droplet-drag law is solved analytically over a given Δt. Then the droplet diameter is adjusted for that time period as per the droplet transient heating model.

Equations 4-1; 4-4; 4-5; 4-6; 4-8; 4-9; 4-10; 4-11; 4-12; 4-14; and 4-7 are used to determine the transient droplet heating/evaporation model for use in ODT space except that η_s is set equal to one, hence, there is no droplet-droplet interaction or to put it another way the s/D effect becomes nonexistent for the lone drop. After ignition has been achieved, the last equation (4-7) is replaced by Equations 4-15 and 4-17 or 4-18 to give the transient droplet heating/evaporation model used, until complete burnout is achieved. In a manner similar to Mulholland et al. the published gas mean velocities and temperature profiles were used for calculating the drag.

Once in the ODT space the simplifications of the Re number as given in Equations 3-26 and 3-27 are implemented (where needed) for all calculations of the transient heating/evaporation model.

No droplet diameter adjustments are made during a type-I eddy event no matter how long the droplet-eddy interaction event persists in pseudotime. This is because eddy events in ODT are considered instantaneous events and would lead to double counting the evaporation (loss in mass) and particle heating (increase in temperature) during the time T_1 of the droplet-eddy interaction once the droplet returned to particle time. There is the possibility of doing a subtraction method directly analogous to that used to avoid double counting of the gravitational force, as explained in Section 3.6. That is to compute the particle trajectories and corresponding mass and temperature changes with and without the presence of the eddy induced velocity v. After computing the loss in mass and the increase in temperature both ways, subtract the differences in mass and temperature in the same manner as the velocity and position of the particle are changed in Equations 3-14 and 315. This was not done in this thesis because of the added complexity involved.

4.6   Conclusion

The end result is that the initial conditions used for the droplets in the ODT two-phase flow model are as close as possible to the droplet diameter, temperature, and position used in the numerical model of Mulholland et al. Only access to the original droplet trajectory code used by them would yield a more precise initial condition for the ODT droplet sub model. Application of their droplet heating/evaporation model to the ODT droplet sub model provided consistency between their work and this work and more importantly consistency between the initial conditions to this model and the model itself. This method has proved to provide insight into the prediction of the spread in end points for the burning of rogue droplets. (See Chapter 5.)

Chapter 5

Numerical Simulation Results

5.1   Introduction

The results discussed in this chapter use the existing ODT model to predict turbulent fluid flow behavior (Chapter 2) along with the two-phase flow submodel developed in Chapter 3 and the droplet heating/evaporation model given in Chapter 4. Simulations were done to mimic the 12 cases (See Table 5.1) done by Mulholland et al. (1991) in which they varied the initial diameter, initial velocity, initial droplet spacing and the injection angle of a stream of droplets into a 100 kW combustor. According to Mulholland (2000) the amount of data used to compute the statistics in the 1991 paper was on the order of 100 droplets. Consequently, three cases of ensemble sizes are investigated for comparisons with the published experimental data. They are 200, 750, 2000 in number respectively. We believe that this is a wide enough range to capture any variation due to ensemble size. Pertinent figures will be given in all three ensemble sizes so the reader may compare them at his/her leisure.

As mentioned earlier, experimental observation revealed that the droplets traveled in a straight line trajectory until they reached the high fluid shear

layer. After this point the droplet stream appeared to break up into individual droplets. This point is taken to be the point at which the individual droplets are born into the ODT simulation. In order to properly account for droplet heating and vaporization from the point of droplet injection to the point in which the droplets are born into ODT, the droplet drag law and droplet heating/vaporization scheme put forth in Chapter 4 were calculated for each case to determine the best possible estimate of the droplet diameter, and temperature. These Initial Conditions (ICs) were used for each case for all 2000 realizations. The computer code was modified such that all twelve cases (maximum of 15 cases possible) were computed simultaneously. Hence all twelve cases saw the same flow realization. Another way to say this is that a single ODT realization contained within it twelve different droplets of varying diameter, velocity, position, and temperature, which represented the twelve different cases being simulated. This was repeated 2000 times in order to get the total data set. The 200 realization set was taken to be the first 200 realizations, and the 750 realization set was taken to be the first 750 realizations.

5.2   Droplet trajectories

As discussed in Chapter 3, the two-phase flow model allows instantaneous jumps in the y position of the droplet to account for eddy-particle interactions. To demonstrate this visually, a thorough (but not exhaustive) search was done of Case 1 (the baseline case used in investigating variations in initial diameter, initial velocity, initial droplet spacing and the injection angle of a stream of droplets) for trajectories which would exemplify the extremes in the spread (x and y) in the burn out points of the 2000 size ensemble. The burn out point is taken to be the point at which the last amount of liquid is vaporized. This occurs after the droplet has been ignited, therefore the vapor is assumed combusted in the surrounding flame sheet.

Figure 5.1 shows twenty-one individual trajectories chosen from Case 1. The random nature of the submodel can be seen by examining the different trajectories. Individual trajectories can proceed to the end of their paths (the burn out point) without much visible effect of the eddy interaction. (See the center trajectory.)   Trajectories may also jump up or down (or both) randomly as demonstrated in Figure 5.1. These instantaneous jumps cause variation in the y position of the burn out point. Note also that the ODT

imposed variations in fluid velocity and temperature cause a wide variation in the *x* burn out position. Recall that these trajectories were purposefully chosen to show extremes and are not typical trajectories (nor are they a random sample).

5.3   Burn out scatter plots

To provide a clearer understanding of the simulated effects of the different varied parameters (i.e. initial diameter, initial velocity, initial droplet spacing and the injection angle) scatter plots of the burn out points are grouped together. (Scatter plots are *x-y* plots where *x* is the axial distance penetrated by the droplet and y is the height. The *y* = 0 datum plane is defined as 0.25 meters below the burner. The burner is on the central axis of the tubular combustor.)

In Figure 5.2 the scatter plots for the variations in initial diameter: Case 1 (base case with $D_o = 234$ μ) diagram (A), Case 2 ($D_o = 306$ μ) diagram (B), and Case 3 ($D_o = 371$ μ) diagram (C) are grouped together for easy comparison of the 200 realization. Figure 5.3 gives the same grouping for the 750 realization and Figure 5.4 gives the variation in initial diameter for the 2000 realization.   Analysis of the scatter plots in each of the figures, gives the conclusion that the model predicts that larger droplets (more mass)

travel farther down the reactor. This is exemplified in both the onset of burnout (leftmost points) and in the completion of burnout (rightmost points). Analysis also shows that the larger the droplet (greater inertia) the less scatter (in the y direction) from the mean droplet trajectory. The mean axial penetration of the droplets increase as the diameter increases. This is evident from the plots, however, the calculated mean values are presented in Figures 5.14, 5.15, and 5.16 (to be discussed later).

Figure 5.5 gives the scatter plots which account for the model's prediction of the variation due to the initial velocity: Case 4 (V_o = 5.3 m/s) diagram (A), Case 1 (V_o = 8.5 m/s) diagram (B), and Case 5 (V_o = 10.6 m/s) diagram (C) for an ensemble size of 200. Figure 5.6 gives the same grouping for an ensemble size of 750. Figure 5.7 gives the grouping for an ensemble size of 2000. The trend, visible in all three figures, is that the simulation predicts the onset of burnout (leftmost points) occurs at shorter axial distances as the initial velocity decreases. Figures 5.6 and 5.7 readily show that the simulation predicts the completion of burnout that penetrates farther axially as the initial velocity increases. The 200 ensemble size comparison however does not exemplify this trend everywhere. Figure 5.5 (A) shows a single droplet which penetrates just a little bit farther axially

than the right most point of the faster initial velocity case shown in Figure

5.5 (B). This anomaly is taken to be a function of the sample size because

both the 750 and 2000 ensemble size comparisons give the correct trend, and

that the mean penetration in all three ensemble sizes increase as the initial

velocity increases.

Figure 5.8 gives the scatter plots which account for the model's

prediction of the variation due to the initial droplet spacing: Case 6 (s/D =

2.8) diagram (A), Case 7 (s/D = 5.6) diagram (B), Case 8 (s/D = 11.2)

diagram (C), Case 9 (s/D = 22) diagram (D), Case 10 (s/D = 45) diagram

(E), and Case 1 (s/D = 180) diagram (F) for an ensemble size of 200. Figure

5.9 gives the same grouping for an ensemble size of 750. Figure 5.10 gives

the grouping for an ensemble size of 2000. The model predict a marked

difference in the behavior of the burn out points below s/D = 11.2 and the

behavior of s/D at 11.2 and above. The first two s/D cases travel farther

axially before burn out than any of the other 4 cases. This is consistent with

the expected behavior.

There is no detectable trend inside of either of these two groupings (small

s/D, large s/D). The model does not seem to be able to differentiate the

effects of initial droplet spacing other than to say that a spacing of 11.2 or

greater causes the droplets to behave independently. This result is consistent with that published by Mulholland et al. The failure of this model to predict a trend for the variation in initial droplet spacing occurs because the ODT droplet model does not have any s/D affects in it. The s/D affects are confined to the initial conditions and once the droplets are born into ODT space they are assumed to be independent of each other. In implementation of the simulation, all six cases for studying variations in initial droplet spacing, were assumed to enter the ODT domain at the same point. This reflects that the point at which the droplet stream is assumed to break into individual droplets is when the stream trajectory reaches the high shear layer of the gas phase. This was the only assumption possible given the statements by Mulholland et al. Hence s/D effects were investigated by variations in the droplet initial conditions only (diameter, velocity, and temperature). The lack of an overall trend would indicate that the point at which the droplets break free of the stream as a function of the initial spacing is not constant for all six cases. No avenue based on published experimental observation was available to adjust the position of the droplet stream break up. Any adjustment to the birth time into ODT would have been only a guess and therefore this avenue was not pursued.

Figure 5.11 gives the scatter plots which account for the model's prediction of the variation due to the injection angle: Case 10 ($\theta = 0$ degrees) diagram (A), Case 1 ($\theta = 30$ degrees) diagram (B), and Case 12 ($\theta = 45$ degrees) diagram (C) for an ensemble size of 200. Figure 5.12 gives the same grouping for an ensemble size of 750. Figure 5.13 gives the grouping for an ensemble size of 2000. The trend, visible in all three figures, is that the model predicts that smaller injection angles travel farther down the reactor. This is exemplified in both the onset of burn out (leftmost points) and in the completion of burn out (rightmost points). Also, the model predicts that the y scatter is reduced as the injection angle increases. Based on physical grounds, the model predictions seem reasonable. The hottest part of the furnace (mean temperature of 1750 K) occurs at a height of .25 meters and an axial distance of 0.05 meters. As the mean droplet path travels closer to the mean highest gas phase temperatures (as it does as the injection angle increases) the lifetime of the droplets gets shorter. The zero degree injection angle on average sees a less defined gas phase u velocity which leads to more y scatter. The gas phase velocity is less defined in the sense that the u velocity tends to be smaller in magnitude and changing in direction. There is a re-circulation zone directly in the path of the zero

degree droplet stream. The ODT representation of this recirculation zone is achieved by imputing negative axial velocities as the initial condition. These were the actual negative velocities measured.

Therefore the model predictions for injection angle variation are consistent with the physics captured in the model. However, the experimental observations of Mulholland et al do not agree with the model. The probable cause for the observed discrepancy is the lack of type-C interactions in the two-phase flow submodel. Type-C interactions were introduced in Chapter 3 to account for the ODT artifact that as the particle y velocity increases (in magnitude) the probability of interacting with a triplet map becomes zero. As the injection angle increases the y velocity increases and the number of eddy interactions decrease. Using a rough estimate (viewing eddy events as boxes, the 45 degree injected droplet would be just as likely to strike the eddy event on the horizontal surface as on the front surface) the number of eddy interactions for a particle injected at 45 degrees is approximately half as many as it would be if type-C interactions were included in the model. This could cause more variation in the y scatter and might lead to longer droplet lifetimes. Another contributing factor is that the 45 degree stream will hit the high shear layer of the gas phase the earliest of

all the cases. As such, the particle Re will be the largest, and the assumptions used to derive the equations in Chapter 4 are therefore the weakest. There would be a tendency for the droplets not to be spherical and drops are more likely to spin, causing lift forces, which are not accounted for in this model.

5.4   Summary of burn out points by method varied

Figure 5.14 (shows for an ensemble size of 200) in condensed form the maximum, average, and minimum axial burn out points for the four variations on initial conditions, namely diameter, velocity, droplet spacing, and injection angle. Also shown in open symbols are the published experimental data for maximum, average, and minimum axial burn out points. Figure 5.15 gives the same form for an ensemble size of 750. Figure 5.16 gives the same form for an ensemble size of 2000. Analysis reveals that for all ensemble sizes and for all cases the model tends to under predict the axial penetration for the maximum, average and minimum distance traveled. The cause for this discrepancy is probably due to the idealization of the droplet fuel [which is a combination of hydrocarbons, predominantly aliphatic C_7 hydrocarbons (40%); Aromatic solvents {xylene} (29%); and

fuel distillate {consisting of C_{10} – C_{23} hydrocarbons} (31%)] as a single component unnamed pure fuel and the use of the burning rate parameter λ.

Variations in initial diameter and velocity show trends that match the observed experimental data. Variation in initial droplet spacing shows only a qualitative agreement with the first grouping (the two smallest s/D trials) penetrating significantly farther than the second grouping. Variation of the injection angle predicts a trend which is counter to the observed experimental trend. The model predicts that the penetration of the droplets decreases as the injection angle increases. The observed experimental data indicates that it remains the same for the zero and 30 degree trials. For the 45 degree trial it penetration distance increases. These observations can be found true for all ensemble sizes.

A major objective in this paper was to try to predict the spread in the burn out points due to the turbulent fluctuations. The spread was considered key since there were numerous simplifying assumptions in the model development. Figure 5.17 shows, for an ensemble size of 200, the predicted axial spread for the four variations on initial conditions, namely diameter, velocity, droplet spacing and injection angle. Analysis of Figure 5.18 shows excellent agreement of the predicted spread to the measured spread for the

variation in initial diameter. The agreement with the variation in initial velocity is also very good with both the simulated and experimental data showing a downward trend as the initial velocity increases. There is also very good agreement in the second grouping (the last four cases) of the spread as function of the initial droplet spacing. The first grouping is not a good fit. As mentioned previously, the lack of s/D parameterization in the droplet submodel and the choice of the birth point into ODT is probably the cause of this discrepancy. The agreement for the zero and thirty degree injection angles is excellent. The forty-five degree case is significantly different from the measured data. This is probably due to the lack of type-C interactions and the larger particle Re.

The figures also show the experimental spread using open circles. Figure 5.18 gives the same form for an ensemble size of 750. Figure 5.19 gives the same form for an ensemble size of 2000. Analysis of Figure 5.17 reveals a good agreement with spread over the entire range. The agreement for velocity is good, but the predicted trend is opposite that of the experimental trend. The predicted spread for the s/D variation is virtually constant. The measured spread approaches the predicted spread for the last three cases. This would indicate that the s/D effects were not important for these cases.

Hence the modeling approach, for these last three cases, of confining the s/D affects to the boundary conditions was successful. The predicted spread for variation in injection angle was good for the zero and thirty degree case. It was contrary to the experimental results for the 45 degree case.

Analysis of Figure 5.18 shows excellent agreement of the predicted spread to the measured spread for the variation in initial diameter. The agreement with the variation in initial velocity is also very good with both the simulated and experimental data showing a downward trend as the initial velocity increases. There is also very good agreement in the second grouping (the last four cases) of the spread as function of the initial droplet spacing. Qualitatively the shape of the curve even matches. The first grouping is not a good fit. As mentioned previously, the lack of s/D parameterization in the droplet submodel and the choice of the birth point into ODT is probably the cause of this discrepancy. The agreement for the zero and thirty degree injection angles is excellent. The forty-five degree case is significantly different from the measured data. This is probably due to the lack of type-C interactions and the larger particle Re.

Analysis of Figure 5.19 shows good agreement of the predicted spread with the measured spread for the variation in initial diameter. Both the size

200 and the size 750 ensembles are a better match however. The agreement with the variation in initial velocity is also very good with both the simulated and experimental data showing a downward trend as the initial velocity increases. The size 2000 ensemble set is a slight improvement to the agreement in the size 750 ensemble set. There is also good agreement in the second grouping (the last four cases) of the spread as function of the initial droplet spacing. However, the qualitative agreement found in the size 750 ensemble set is no longer seen. The predicted spread for last grouping has become a horizontal line, meaning that the model cannot tell them apart at 2000 iterations. The first grouping is a poor fit. As mentioned previously, the lack of s/D parameterization in the droplet submodel and the choice of the birth point into ODT is probably the cause of this discrepancy. The agreement for the zero and thirty degree injection angles is not as good as for the size 750 set, but better than the size 200 ensemble set. The forty-five degree case is significantly different from the measured data. This is probably due to the lack of type-C interactions and the larger particle Re.

Based on Figures 5.17, 5.18 and 5.19, the closest match to the experimental data of order 100 droplets is the size 750 ensemble set. The size 200 ensemble set seems to be too small. Random variations are playing

too much of a role in the outcome of the model. With a sample size of order 100, the ensemble size of 2000 seems to be overkill. The results from the experiment may have shifted if the data set were order 1000 so it is best not to use an ensemble size of 2000.

Mulholland et al. published only one set (maximum and minimum) of data points concerning the spread in the y direction of all the data collected (the twelve cases). This one set of data points was for the base case which occurs in all the variations of initial conditions. Strictly for closure, the y variation (height in the reactor) of each case is plotted. The form of the plot shows variations based on initial diameter, velocity, droplet spacing, and injection angle. The plots show the simulated maximum, average, minimum y value for the burn out point along with the predicted standard deviation. These are all shown in closed symbols. The one set of experimental data points are shown in open symbols, an open circle for the maximum experimental data point and an open square for the minimum experimental data point. Figure 5.20 gives the results for the size 200 ensemble. Figure 5.21 gives the results for the 750 ensemble set. Figure 5.22 gives the results for the size 2000 ensemble.

Certain trends can be correctly gleaned from the plots in Figures 5.20,

Selected droplet trajectories for Case 1
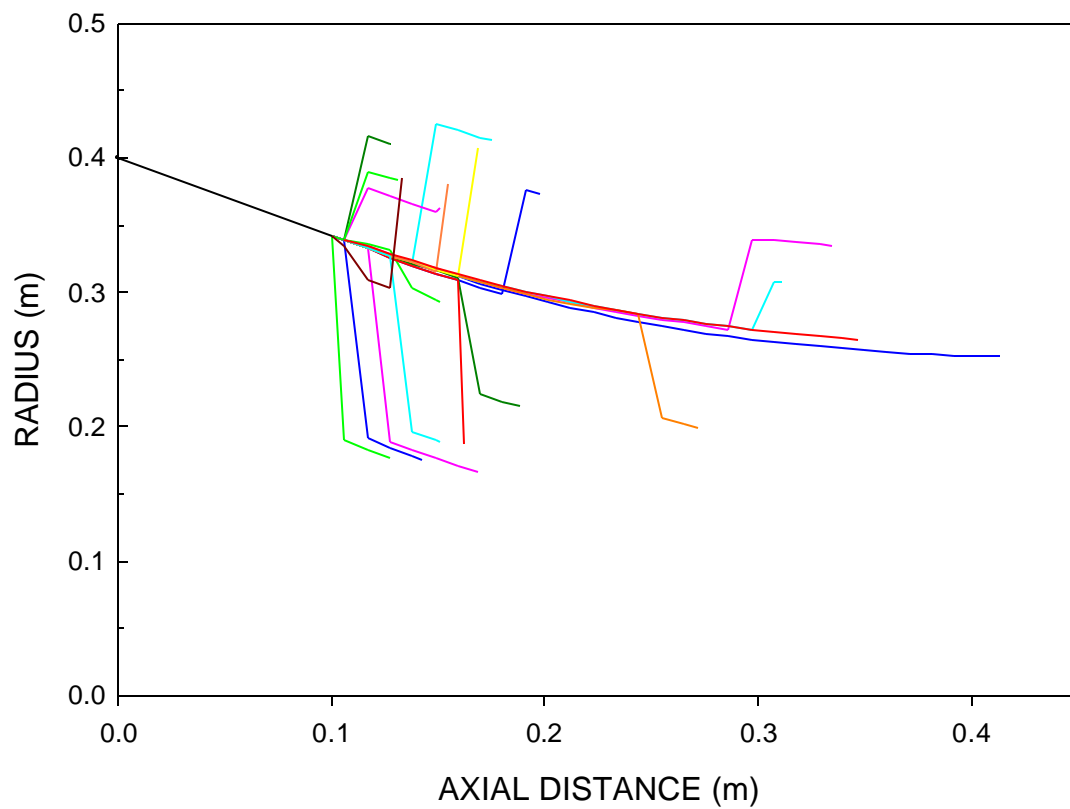
Figure 5.1: Trajectories from Case 1 chosen to exemplify the extremes of spread in the *x* and *y* directions of the burn out points.

5.21, and 5.22, such as the decrease in the *y* scatter due to an increase in initial diameter. However, other properties are not so easily recognized. The scatter plots Figures 5.2 – 5.13 give a better feeling for trends.

Table 5.1   Droplet Stream Test Conditions*

Title	Parameter Varied	D^0 (microns)	V_d^0 (m/s)	s^0/D^0	q^0 (deg)
Case 1	Nominal	234	8.5	180	30
Case 2	Size	306	8.5	140	30
Case 3		371	8.5	115	30
Case 4	Velocity	216	5.3	120	30
Case 5		250	10.6	210	30
Case 6	Spacing	234	8.5	2.8	30
Case 7		234	8.5	5.6	30
Case 8		234	8.5	11.2	30
Case 9		234	8.5	22	30
Case 10		234	8.5	45	30
Case 11	Angle	234	8.5	180	0
Case 12		234	8.5	180	45

* taken from Mulholland et al. (1991)
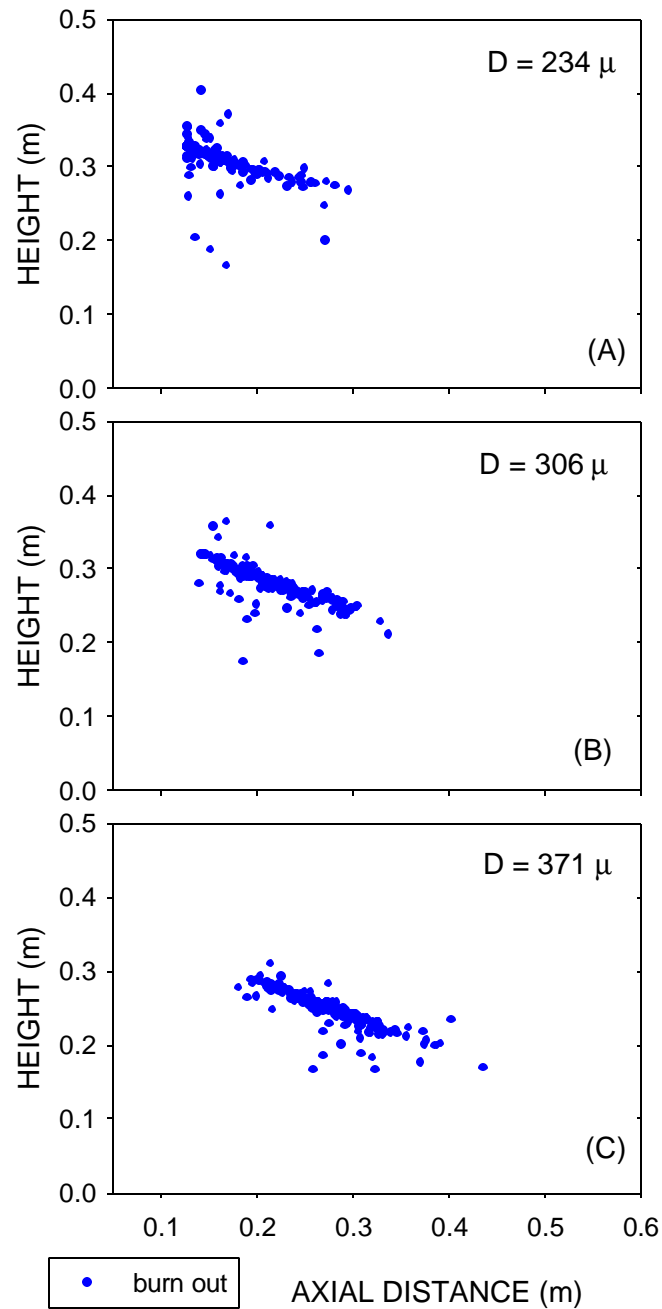
Figure 5.2: Burn out points for variation in initial diameter, D. Various scatter plots of the burn out points for different initial diameter are shown in increasing order. An ensemble size of 200 was used to generate these plots. Larger droplets travel further down stream and resist being jostled around as much in the y direction (height).
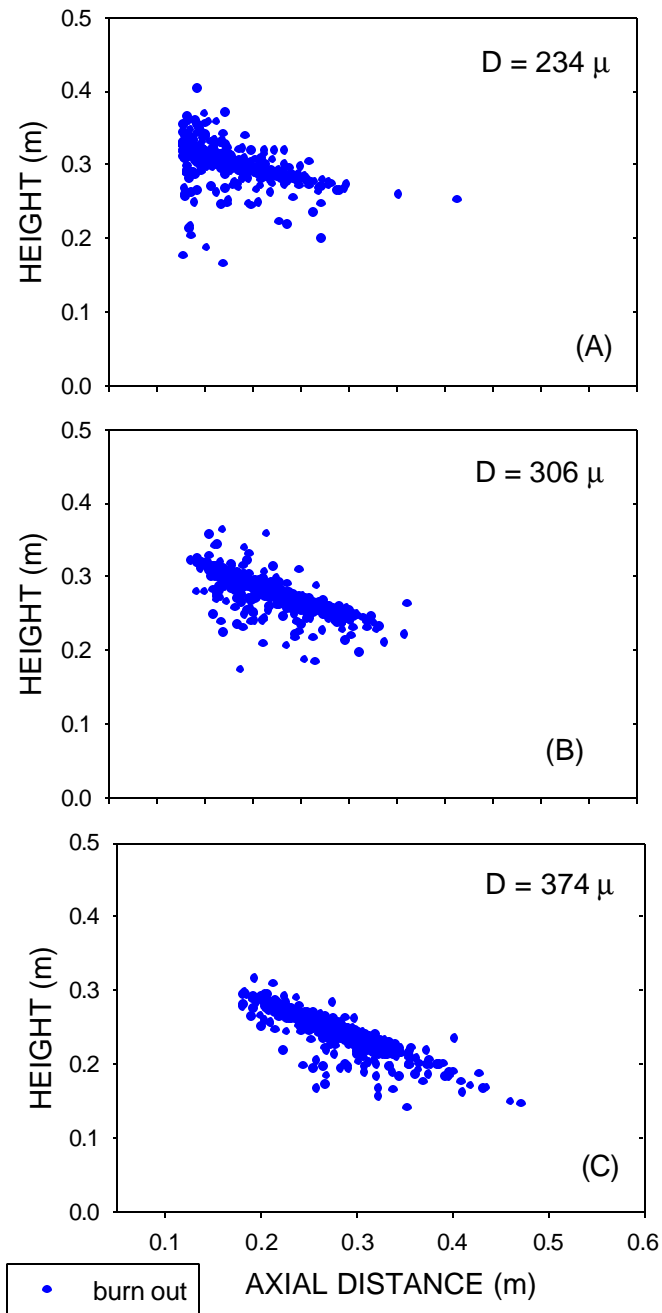
Figure 5.3: Burn out points for variation in initial diameter, D. Various scatter plots of the burn out points for different initial diameter are shown in increasing order. An ensemble size of 750 was used to generate these plots. Larger droplets travel further down stream and resist being jostled around as much in the y direction (height).
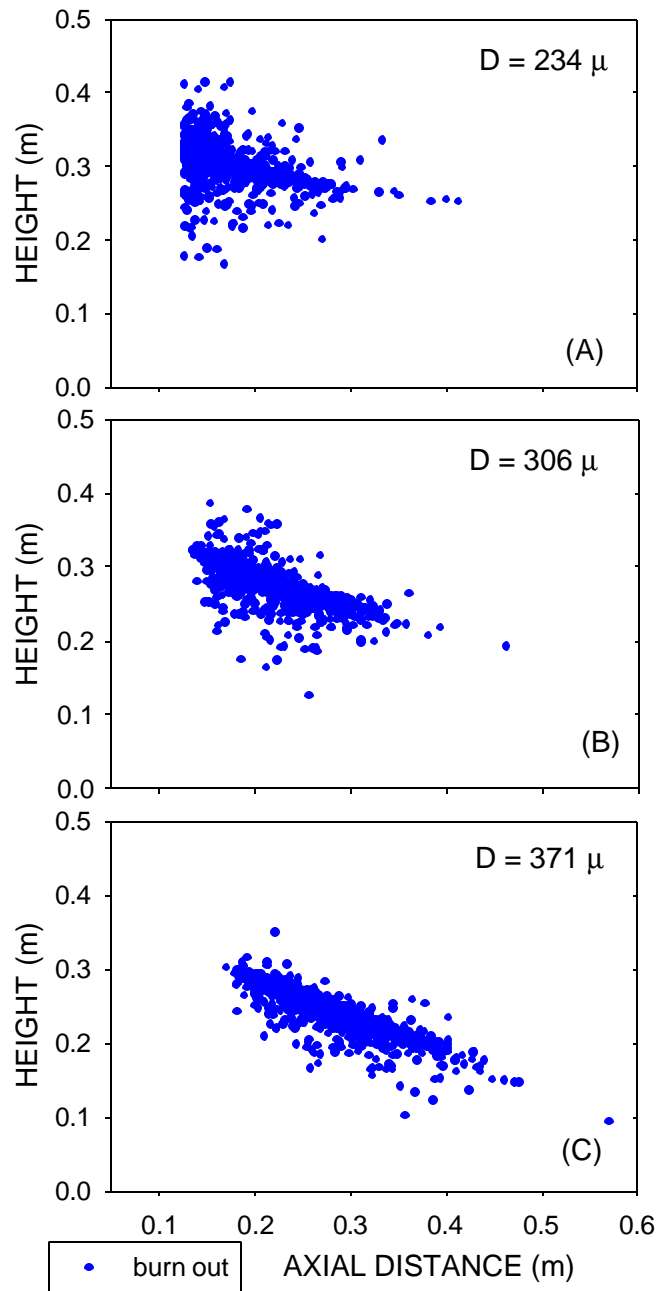
Figure 5.4: Burn out points for variation in initial diameter, D. Various scatter plots of the burn out points for different initial diameter are shown in increasing order. An ensemble size of 2000 was used to generate these plots. Larger droplets travel further down stream and resist being jostled around as much in the y direction (height).
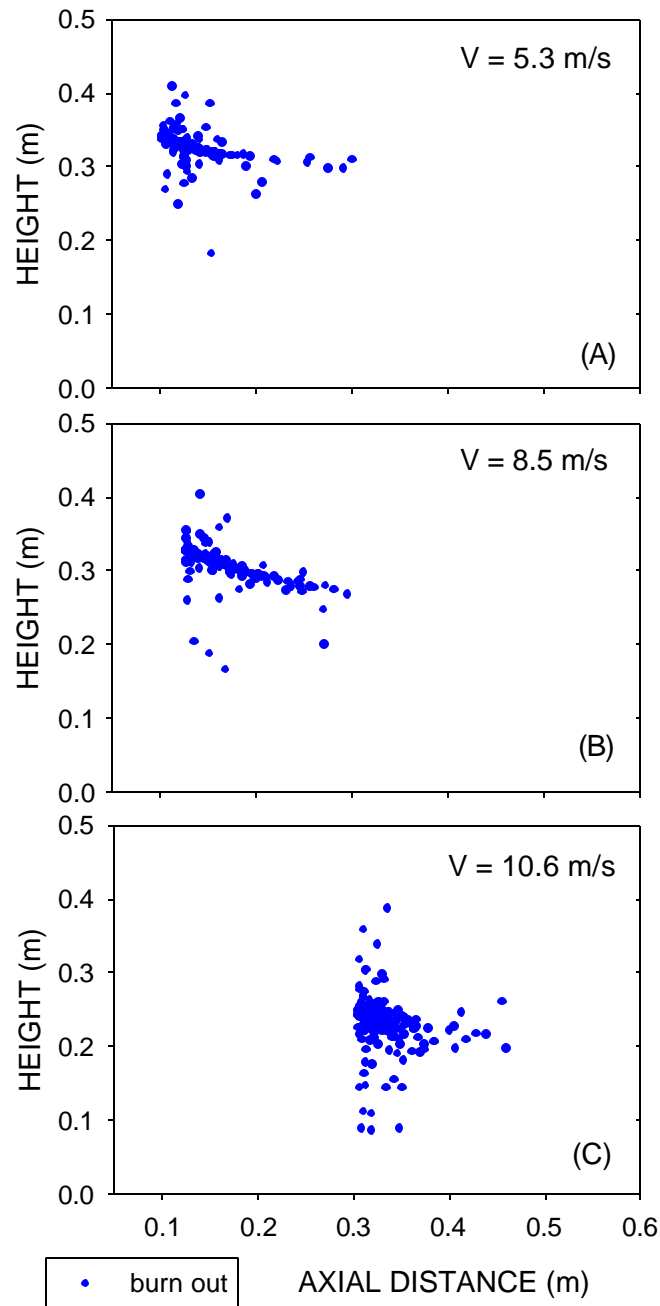
Figure 5.5: Burn out points for variation in initial velocity, V. Various scatter plots of the burn out points for different initial velocities are shown in increasing order. An ensemble size of 200 was used to generate these plots. Faster droplets travel further down stream and resist being jostled around as much in the y direction (height). However the further the particles travel downstream the more they are jostled.
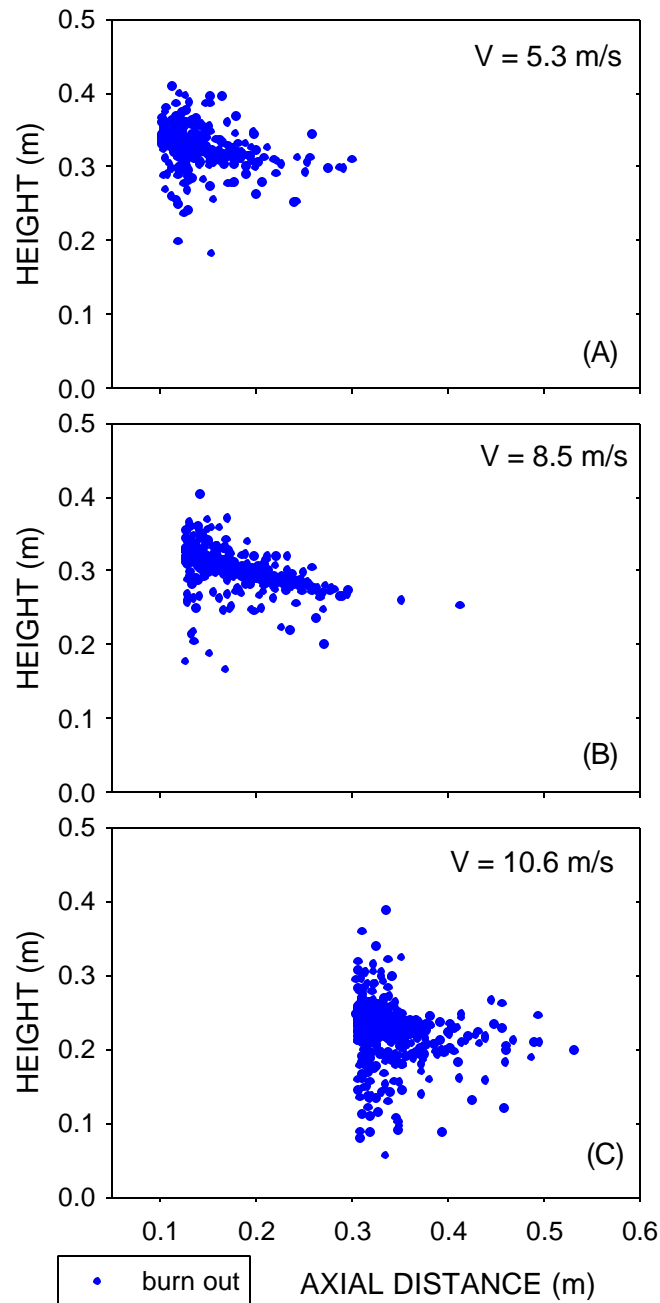
Figure 5.6: Burn out points for variation in initial velocity, V. Various scatter plots of the burn out points for different initial velocities are shown in increasing order. An ensemble size of 750 was used to generate these plots. Faster droplets travel further down stream and resist being jostled around as much in the y direction (height). However the further the particles travel downstream the more they are jostled.
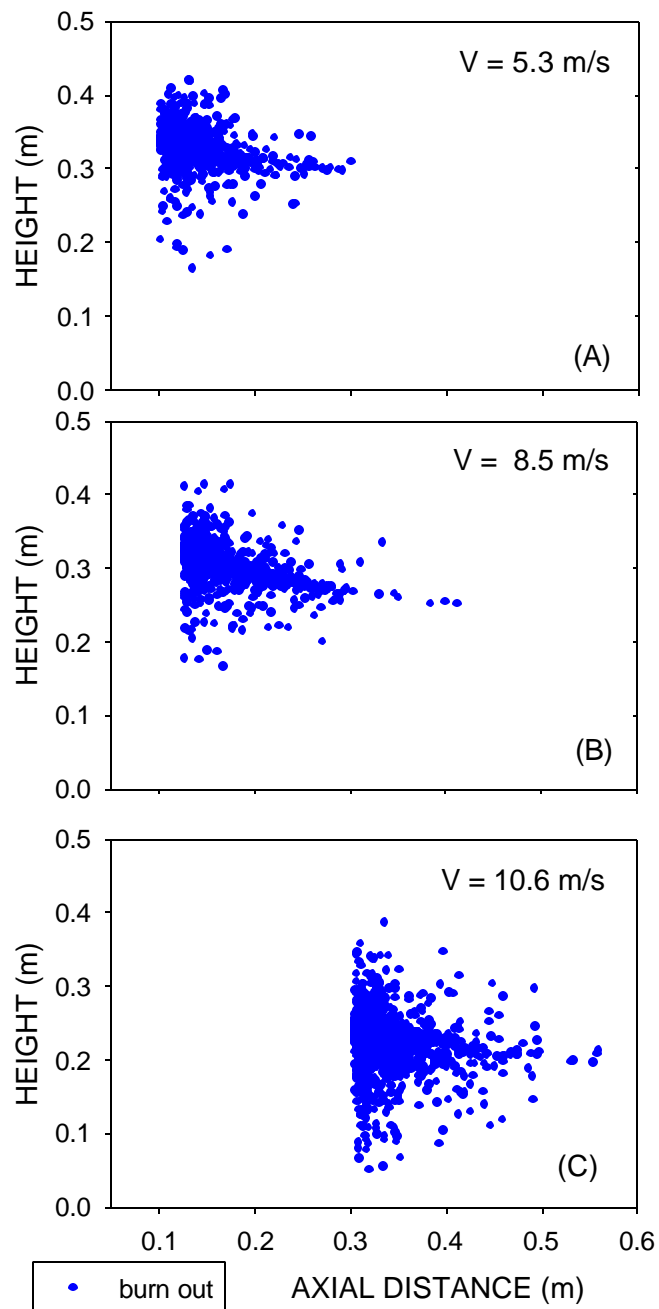
Figure 5.7: Burn out points for variation in initial velocity, V. Various scatter plots of the burn out points for different initial velocities are shown in increasing order. An ensemble size of 2000 was used to generate these plots. Faster droplets travel further down stream and resist being jostled around as much in the y direction (height). However the further the particles travel downstream the more they are jostled.
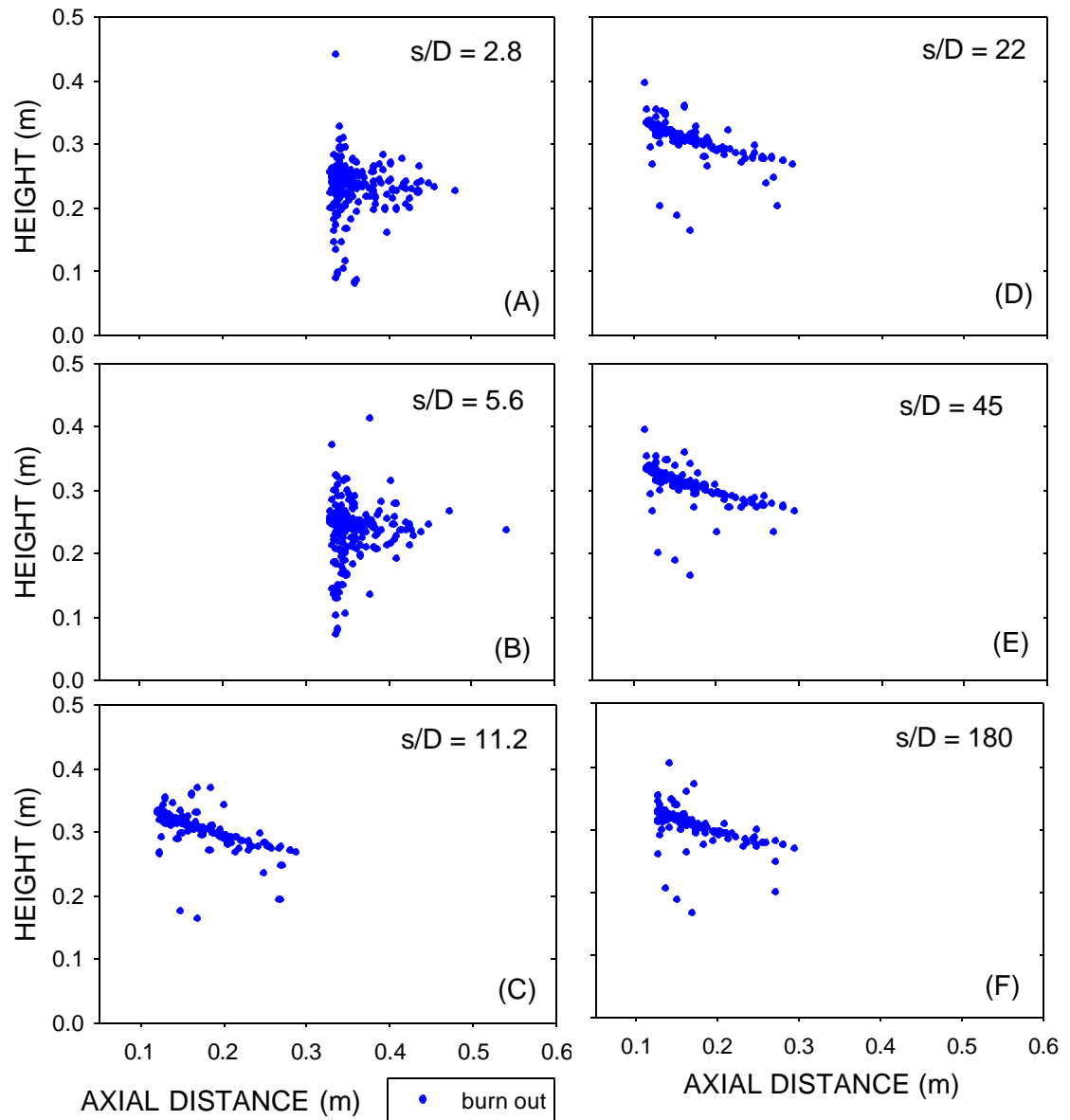
Figure 5.8: Burn out points for variation in initial droplet spacing, s/D. Various scatter plots of the burn out points for different initial droplet spacing are shown in increasing order. An ensemble size of 200 was used to generate these plots. A marked difference exists between the small s/D group (diagrams a and b) and the large s/D group (diagrams c, d, e, and f). No significant differences occur within either group.
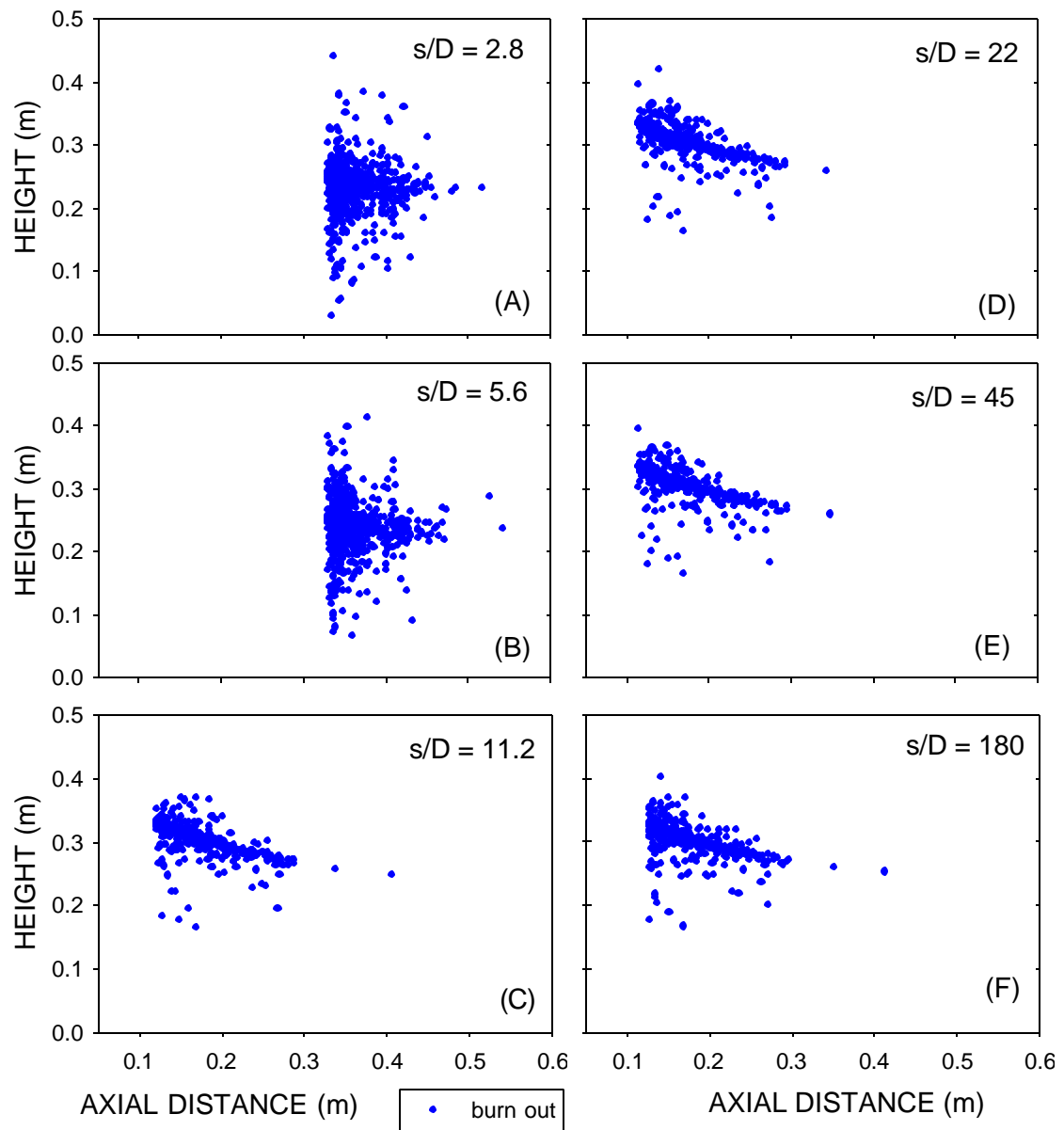
Figure 5.9: Burn out points for variation in initial droplet spacing, s/D. Various scatter plots of the burn out points for different initial droplet spacing are shown in increasing order. An ensemble size of 750 was used to generate these plots. A marked difference exists between the small s/D group (diagrams a and b) and the large s/D group (diagrams c, d, e, and f). No significant differences occur within either group.
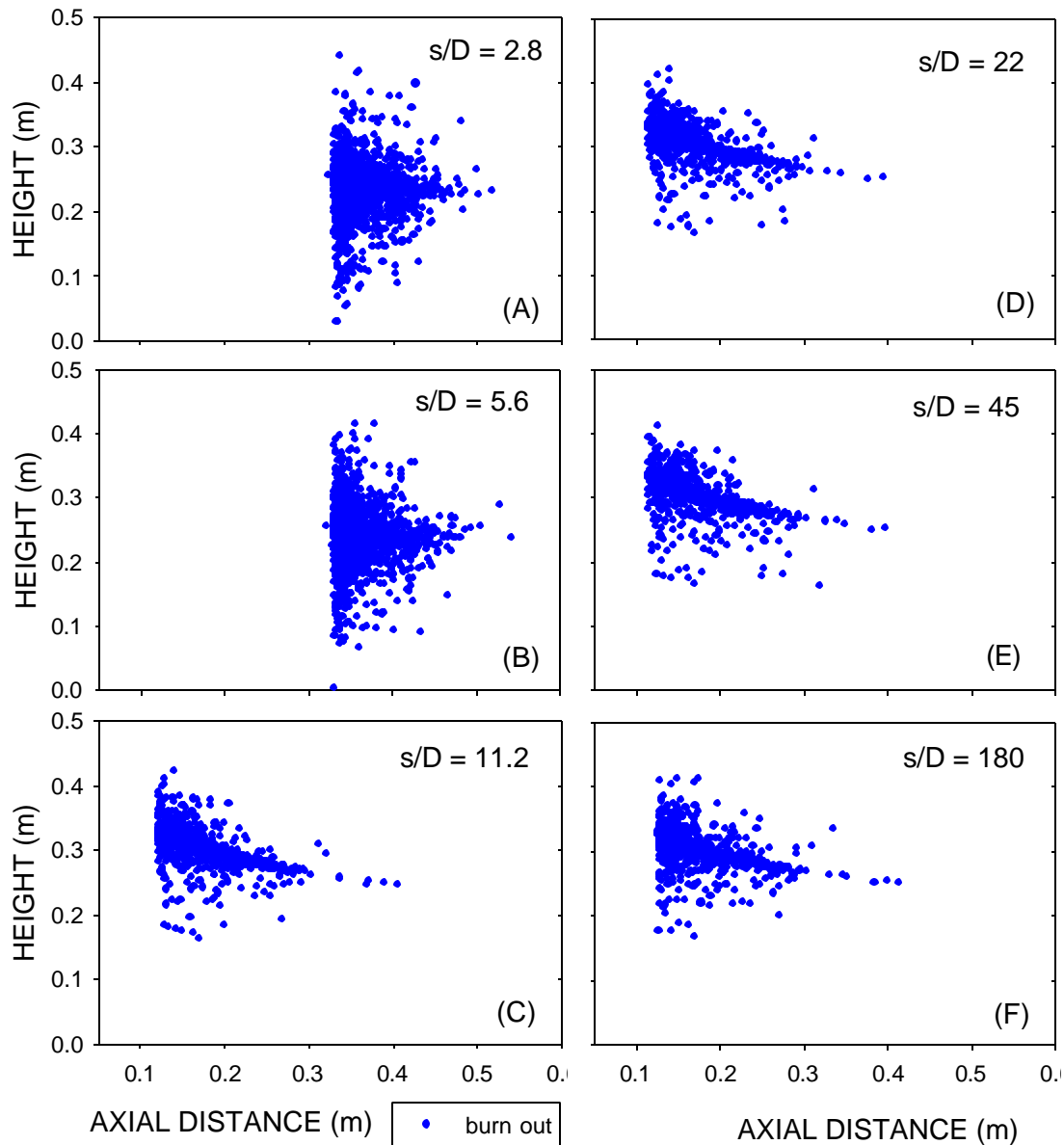
Figure 5.10: Burn out points for variation in initial droplet spacing, s/D. Various scatter plots of the burn out points for different initial droplet spacing are shown in increasing order. An ensemble size of 2000 was used to generate these plots. A marked difference exists between the small s/D group (diagrams a and b) and the large s/D group (diagrams c, d, e, and f). No significant differences occur within either group.
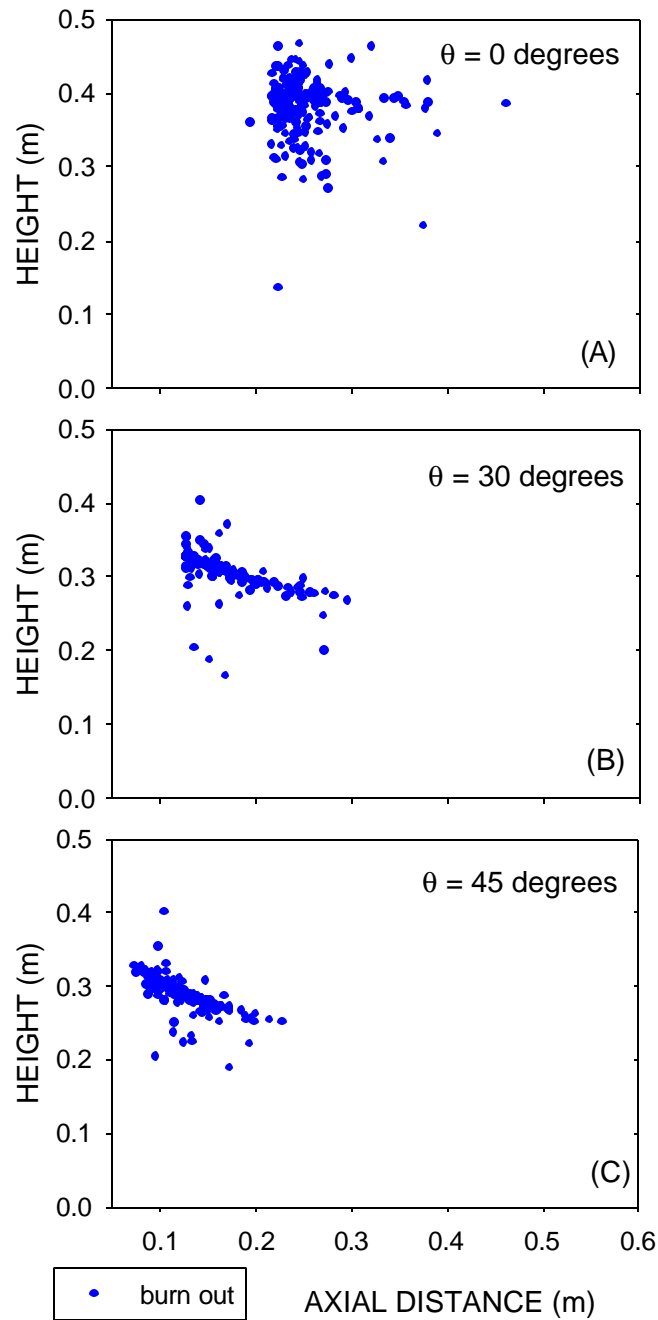
Figure 5.11: Burn out points for variation in initial injection angle, θ. Various scatter plots of the burn out points for different initial injection angles are shown in increasing order. An ensemble size of 200 was used to generate these plots. Higher injection angles cause the droplets to travel closer to the flame and experience higher mean temperatures and larger mean down stream velocities.
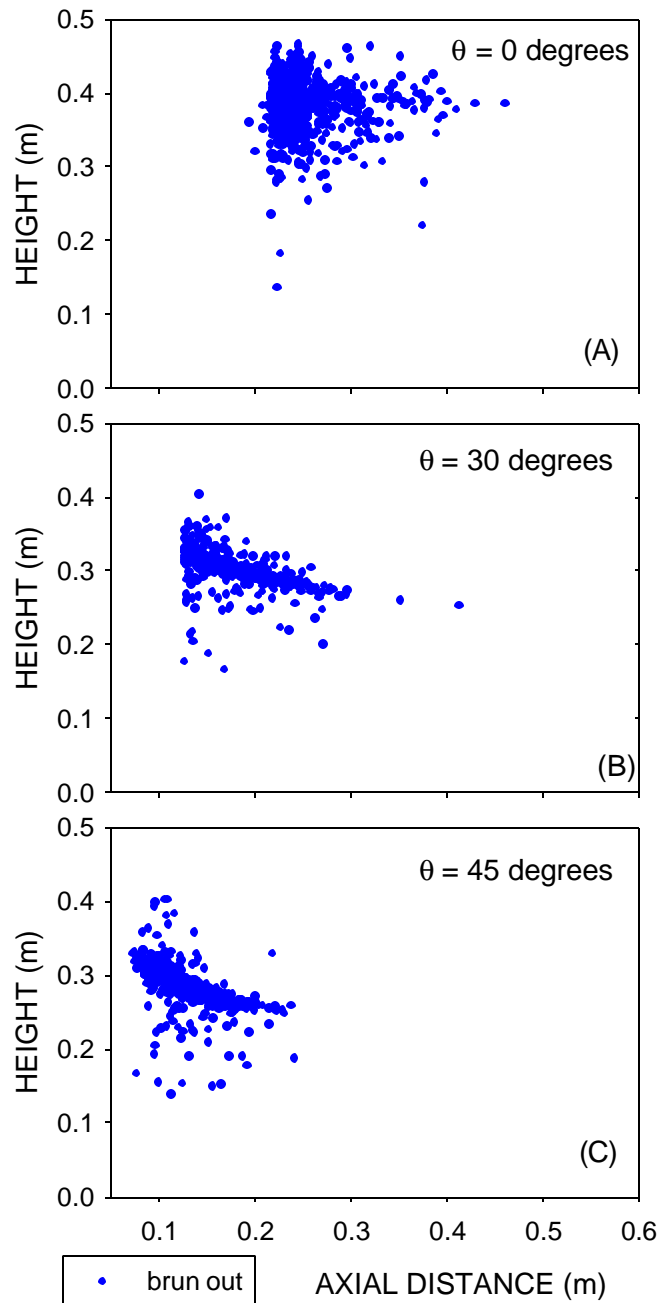
Figure 5.12: Burn out points for variation in initial injection angle, θ. Various scatter plots of the burn out points for different initial injection angles are shown in increasing order. An ensemble size of 750 was used to generate these plots. Higher injection angles cause the droplets to travel closer to the flame and experience higher mean temperatures and .larger mean down stream velocities.
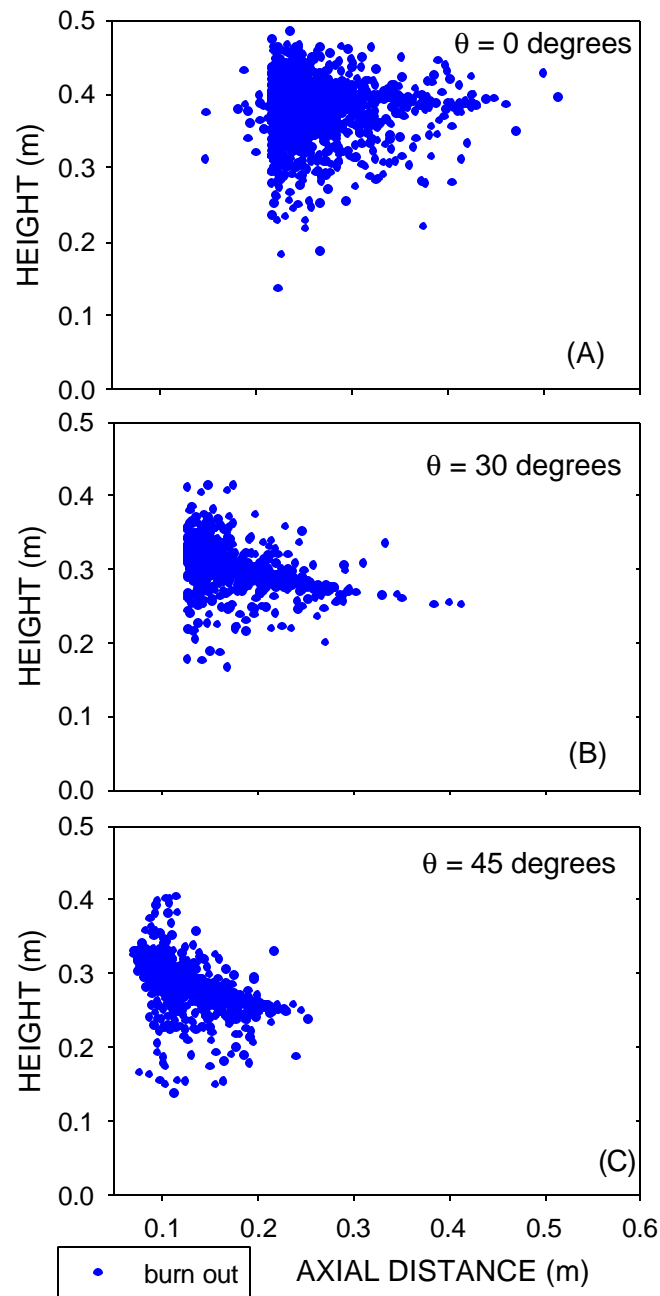
Figure 5.13: Burn out points for variation in initial injection angle, θ. Various scatter plots of the burn out points for different initial injection angles are shown in increasing order. An ensemble size of 2000 was used to generate these plots. Higher injection angles cause the droplets to travel closer to the flame and experience higher mean temperatures and larger mean down stream velocities.
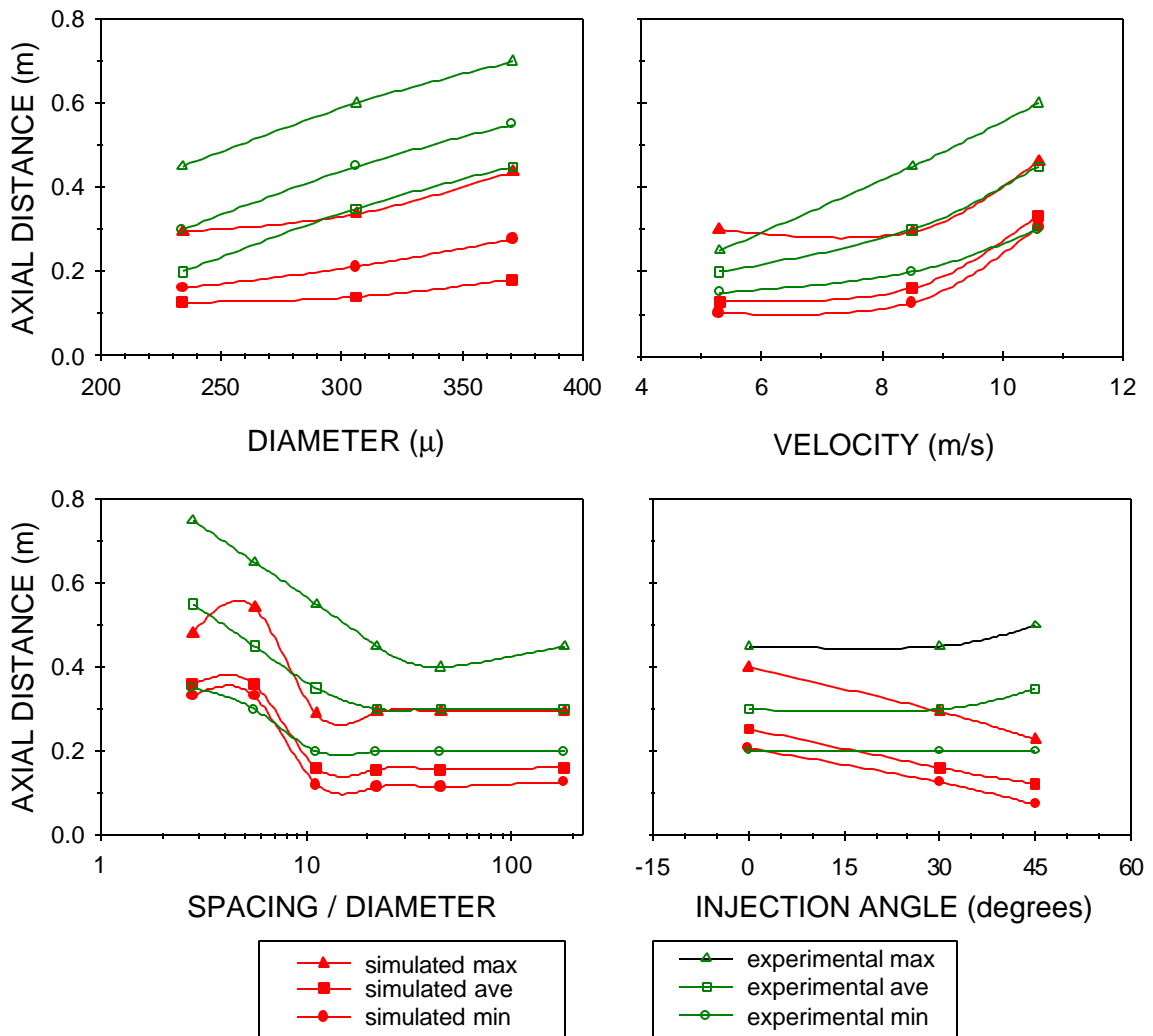
Figure 5.14: Comparison of experimental measurements and simulated burning droplets. The closed symbols represent the predicted maximum (triangle) average (square) and minimum (circle). The experimental data are shown in open symbols. An ensemble size of 200 was used to generate these plots.
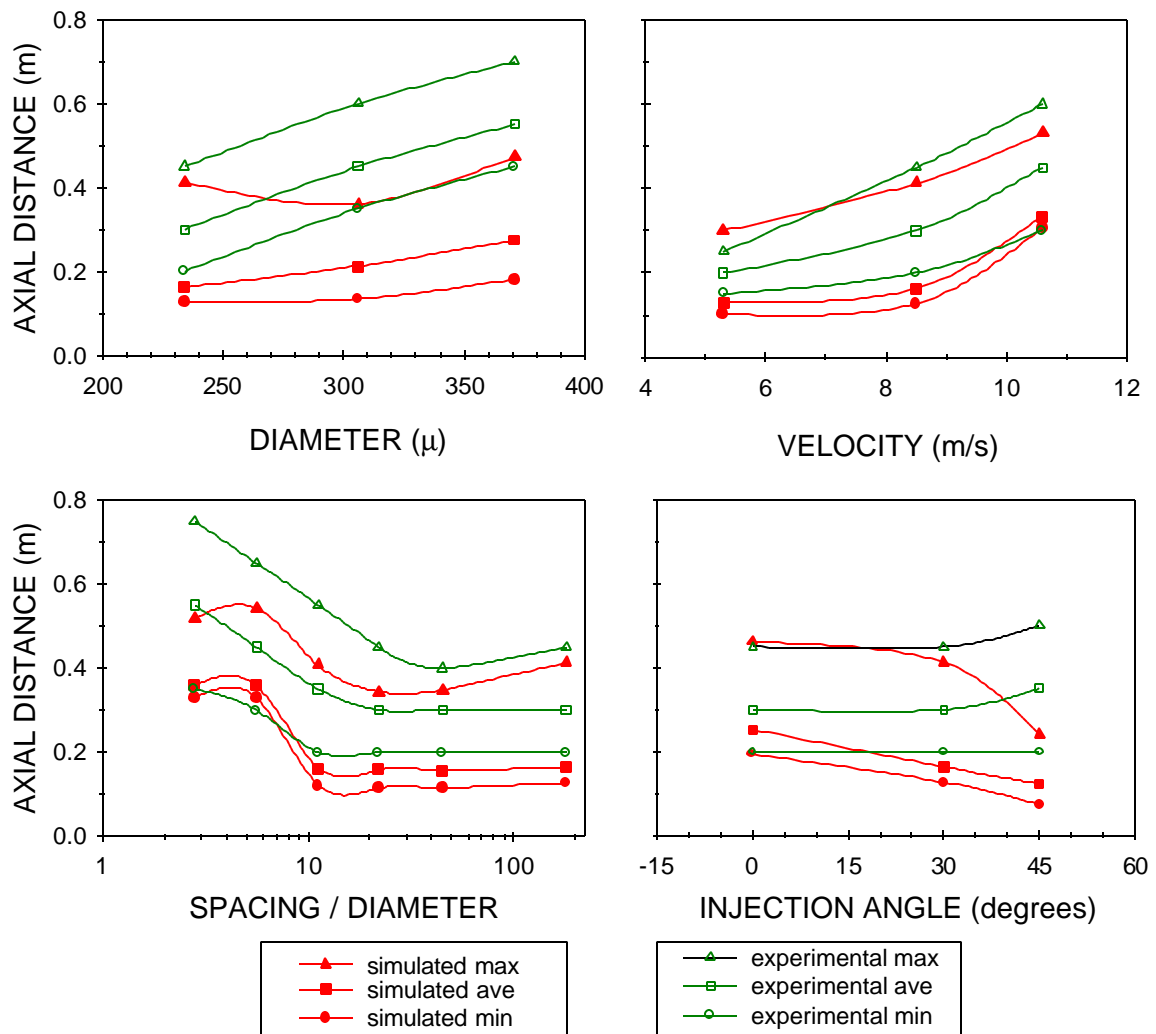
Figure 5.15: Comparison of experimental measurements and simulated burning droplets. The closed symbols represent the predicted maximum (triangle) average (square) and minimum (circle). The experimental data are shown in open symbols. An ensemble size of 750 was used to generate these plots.
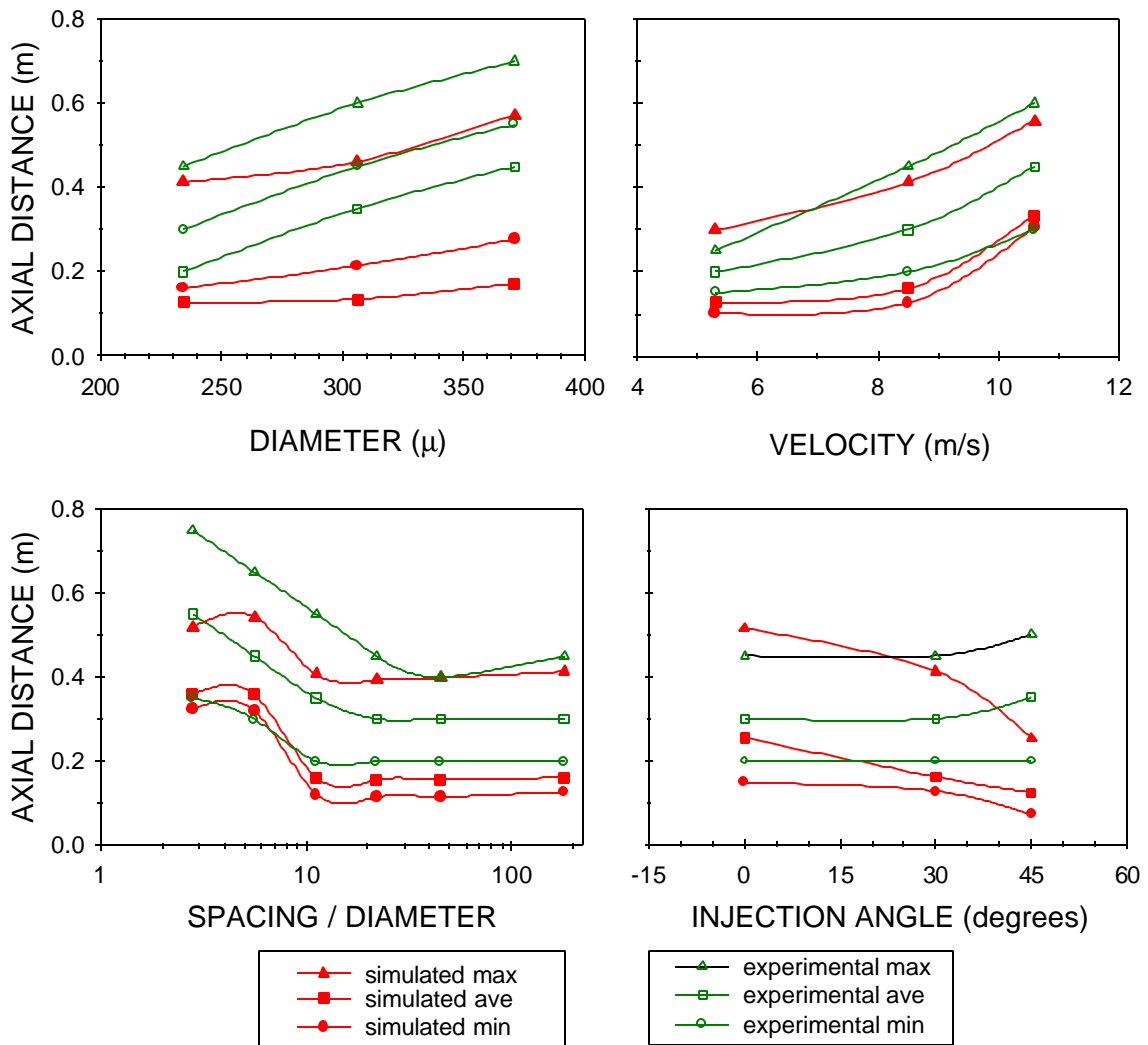
Figure 5.16: Comparison of experimental measurements and simulated burning droplets. The closed symbols represent the predicted maximum (triangle) average (square) and minimum (circle). The experimental data are shown in open symbols. An ensemble size of 2000 was used to generate these plots.
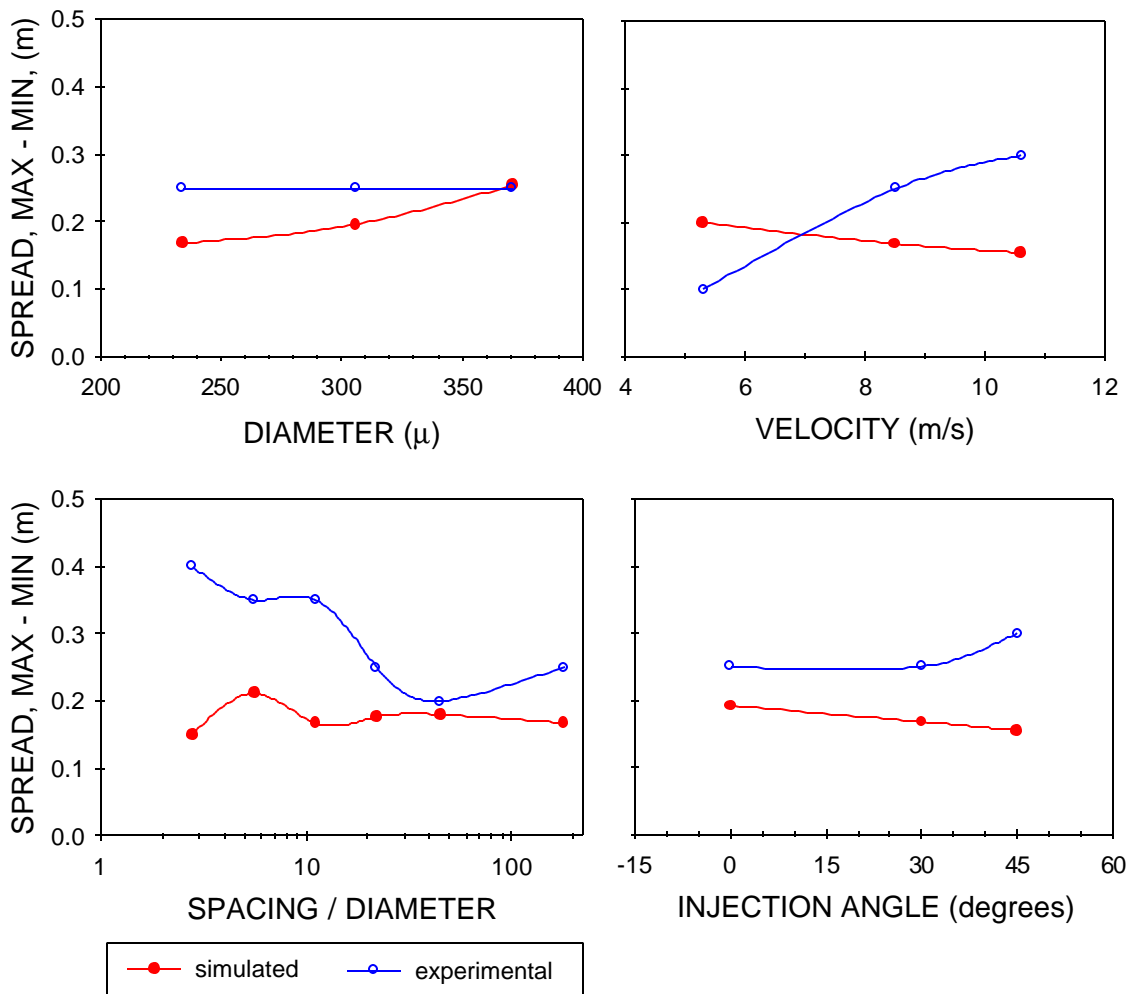
Figure 5.17: Comparison between the experimentally measured spread in burn out end points and the spread predicted by the simulation. This simulated data comes from an ensemble size of 200.
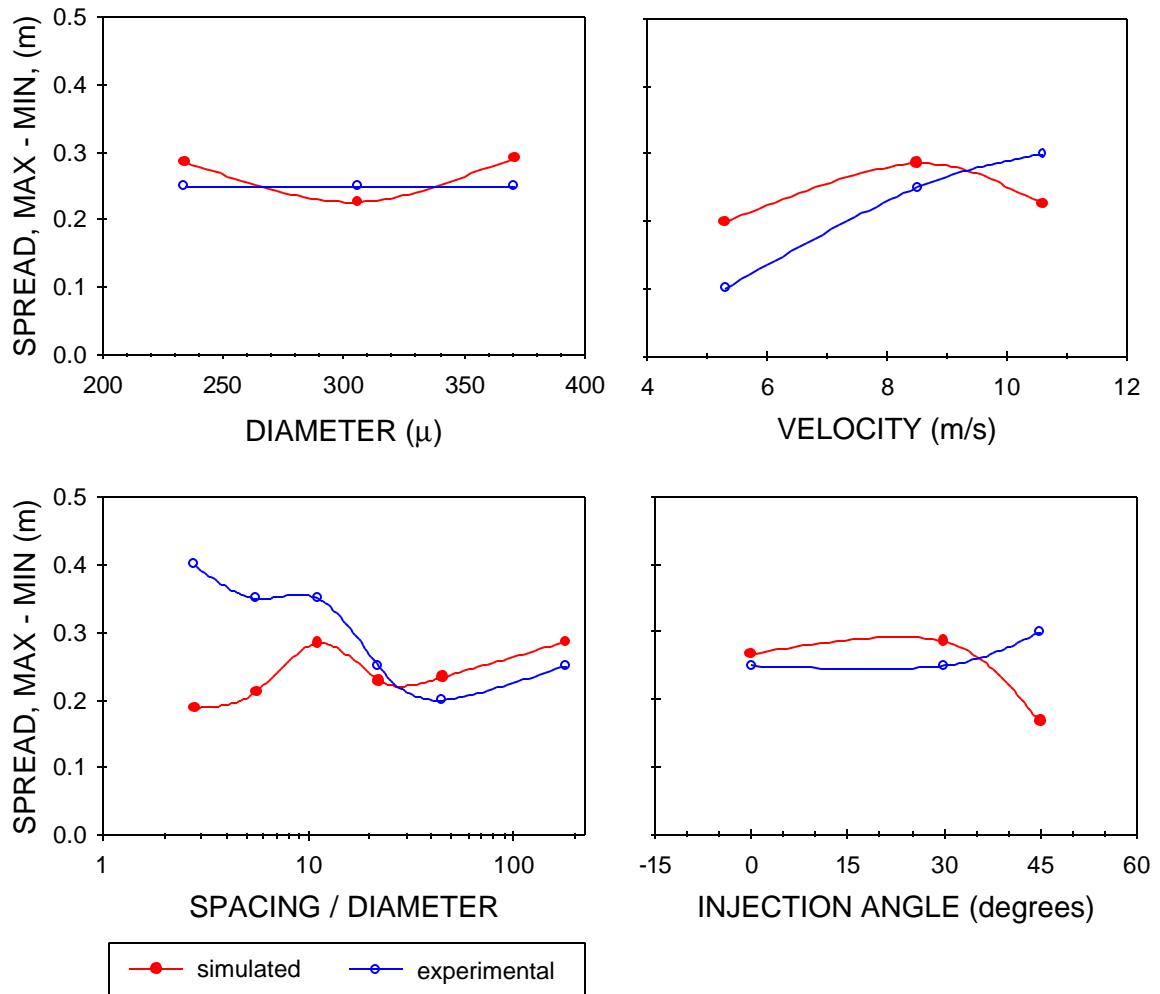
Figure 5.18: Comparison between the experimentally measured spread in burn out end points and the spread predicted by the simulation. This simulated data comes from an ensemble size of 750.
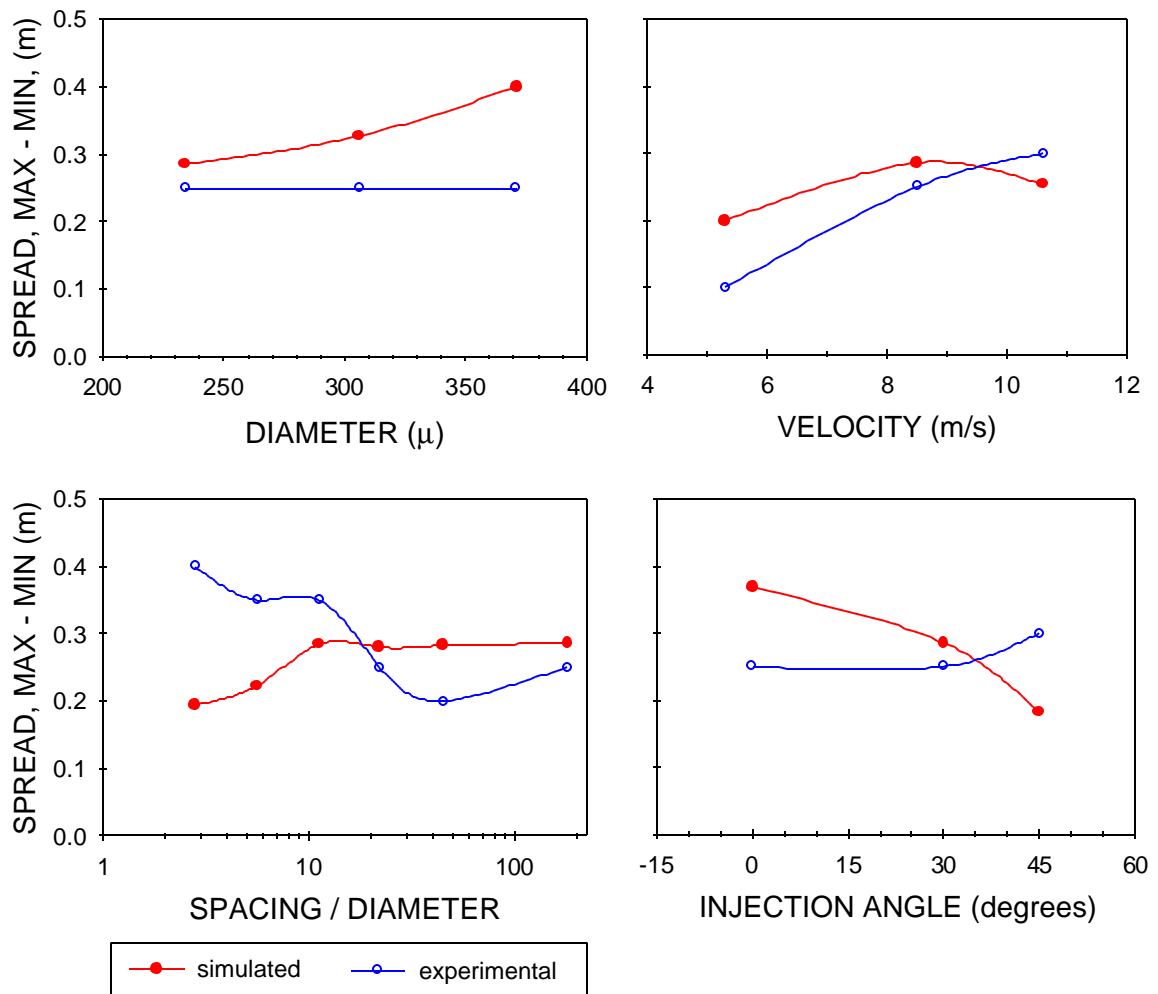
Figure 5.19: Comparison between the experimentally measured spread in burn out end points and the spread predicted by the simulation. This simulated data comes from an ensemble size of 2000.
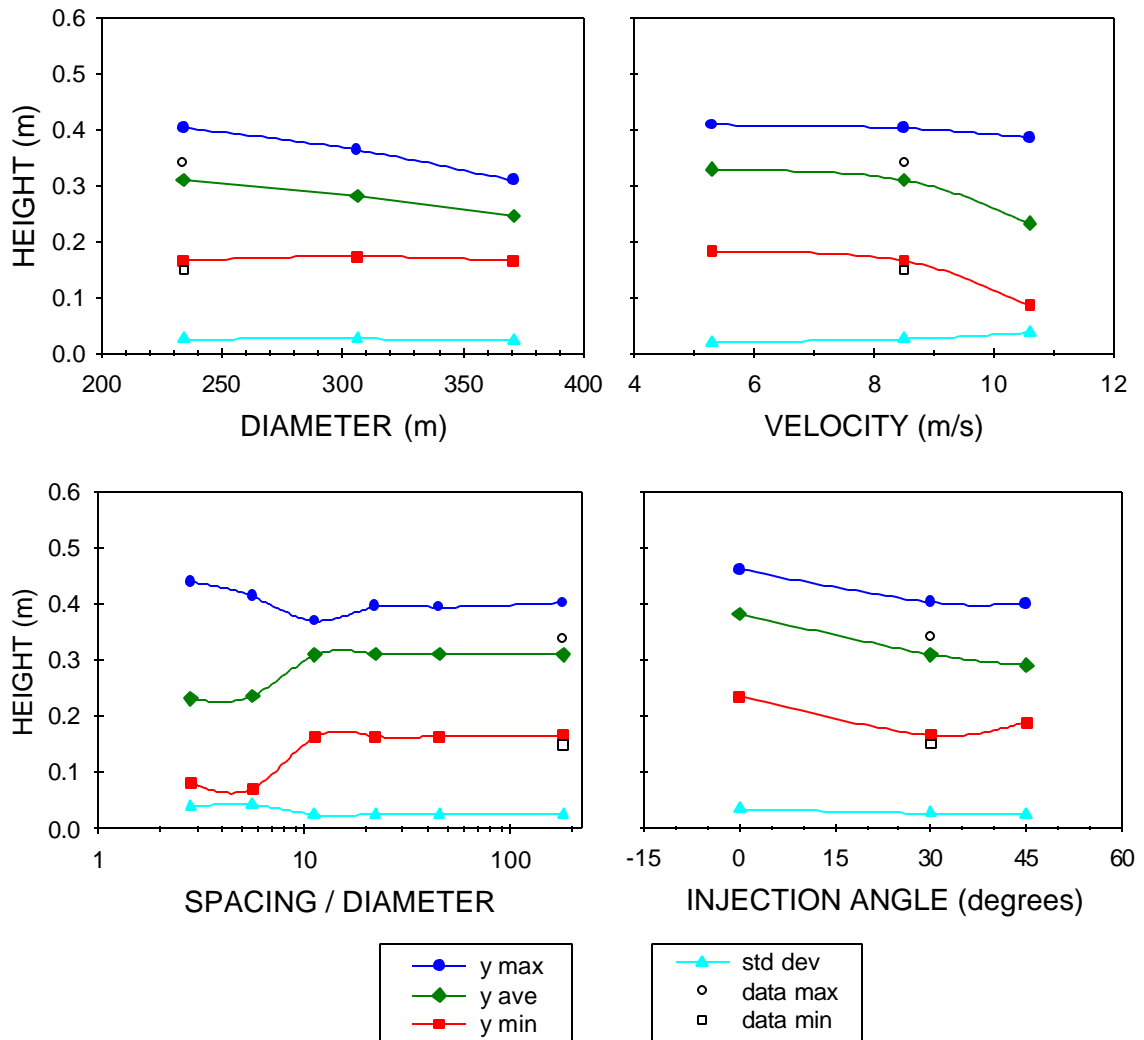
Figure 5.20: Variation in the Y component of the droplet position as a function of the input conditions. The only pair of measured variation in the Y position available is shown with an open circle for the maximum and an open square for the minimum. An ensemble size of 200 was used to generate these plots.
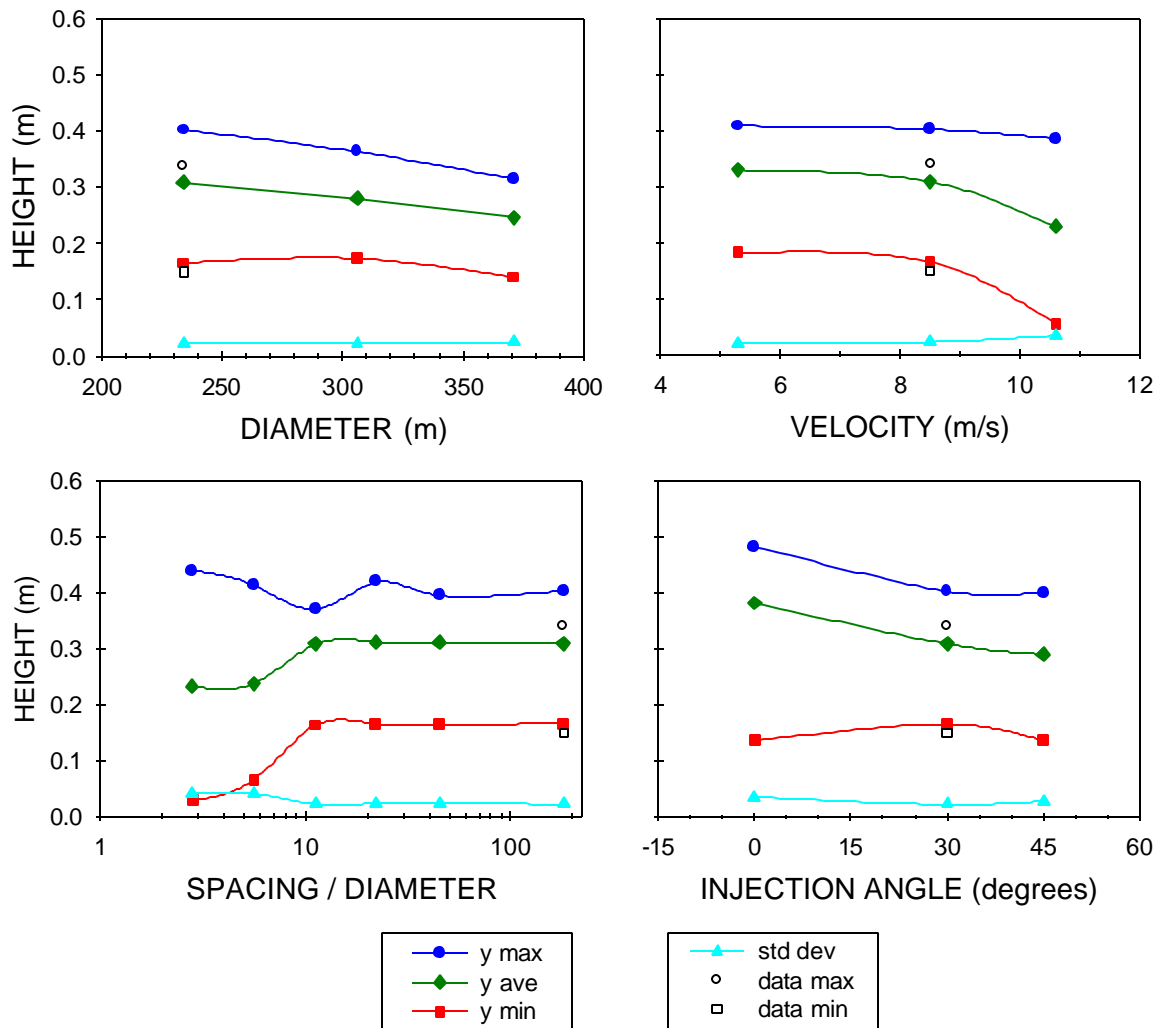
Figure 5.21: Variation in the Y component of the droplet position as a function of the input conditions. The only pair of measured variation in the Y position available is shown with an open circle for the maximum and an open square for the minimum. An ensemble size of 750 was used to generate these plots.
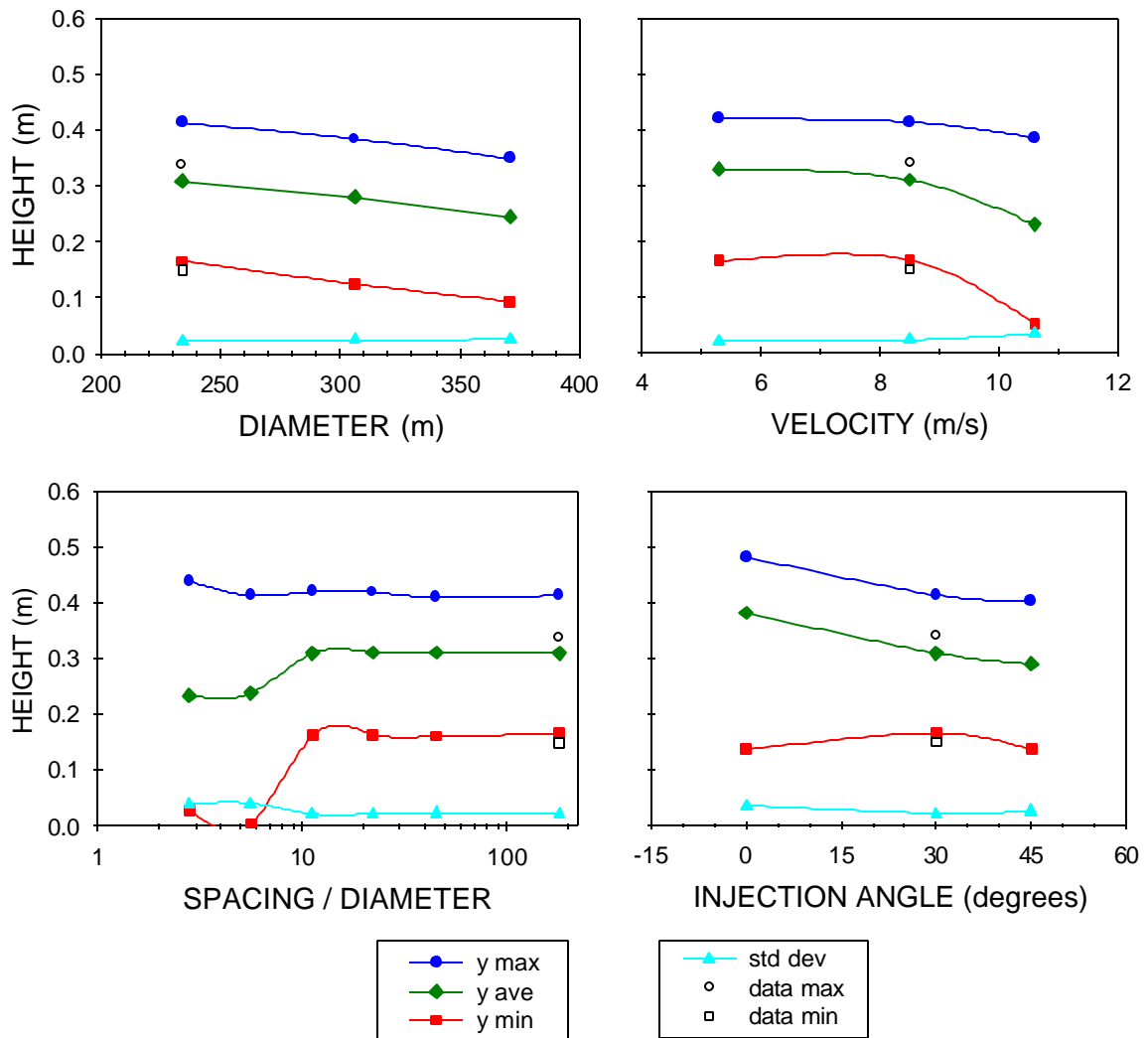
Figure 5.22: Variation in the Y component of the droplet position as a function of the input conditions. The only pair of measured variation in the Y position available is shown with an open circle for the maximum and an open square for the minimum. An ensemble size of 2000 was used to generate these plots.

Chapter 6

Effects of the Two-phase Flow Parameter **b**

6.1   Droplet model free parameter **b**

As discussed in Section 3.7, the internal ODT local instantaneous time scale $\tau(l; y_o, t)$ is not a real physical time and therefore a droplet model free parameter called β was introduced into the model to account for discrepancies between the actual eddy lifetime and the ODT instantaneous time scale $\tau(l; y_o, t)$. This free parameter should ideally be a number close to unity since $\tau(l; y_o, t)$ was based on good reasoning and logically should not be too far off. $\beta = 1$ was used for all runs reported in this paper outside of this chapter. Here additional runs were made with $\beta = 0.5$ and $\beta = 2.0$. The eddy lifetime, t_e, was defined in Chapter 3 as:

$$t_e = \boldsymbol{b}\, \boldsymbol{t}(l; y_o, t) \quad . \qquad (3-16)$$

t_e has two important and somewhat competing effects on the droplet-eddy interaction. The first effect is that it adjusts the end time of the eddy interaction box which either lengthens or shortens the maximum amount of time during which the droplet relaxes to the fluid velocity. The second is that it adjusts the fluid phase y velocity, Equation 3-17:

$$v = h \Big/ t_e \qquad . \qquad (3-17)$$

A value of $\beta < 1$ increases v, as compared to v computed with $\beta = 1$. A $\beta > 1$ decreases v. The burden of the droplet-drag law (Equation 3-25) is to relax the particle to the surrounding gas flow v. With $\beta > 1$, the maximum relaxation time t_e increases, but the velocity v, to which the particle is being relaxed to, is being decreased.

6.2 Effect of **b** on a tracer particle, $\mathbf{t_p} \rightarrow \mathbf{0}$

For the limit of infinitely low inertia, the net y displacement caused by the particle-eddy interaction with $\beta > 1$ is identical to the y displacement which would be achieved with $\beta = 1$ or $\beta < 1$. However, the y velocity of the particle, V, at the end of the pseudo time calculations are all different. The particle velocity, V, for $\beta > 1$ would be the smallest in Magnitude, followed by V for $\beta = 1$ and ending with the largest magnitude velocity V for $\beta < 1$.

The tracer particle paths for the three cases $\beta = 2$, $\beta = 1$, $\beta = 1/2$, are shown in Figure 6.1 with the arrows as shown in (B) now indicating velocity
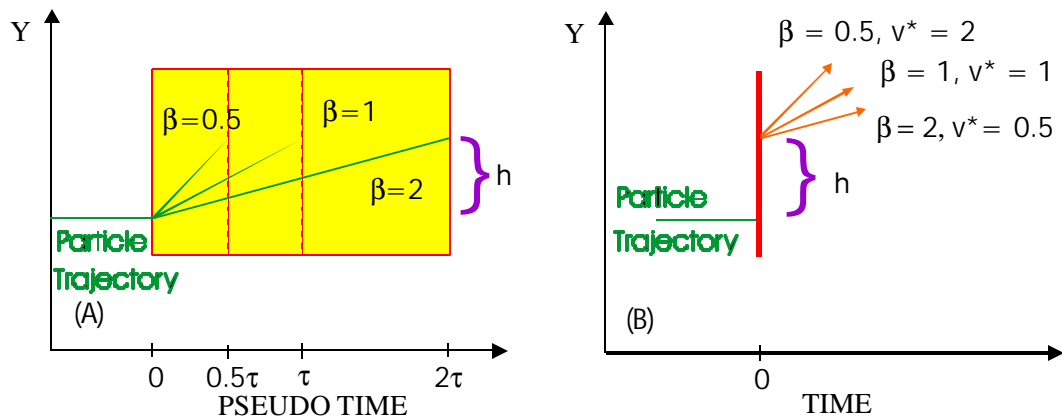
Figure 6.1: Effects of the free parameter β on the eddy interaction box (A) and on the particle velocity (B) at the moment of the eddy interaction.

vectors, rather than trajectories as in previous diagrams. The velocity of the particle relative to the velocity of the particle with β = 1 is given by:

$$v* = {v(\boldsymbol{b})}\big/{v(\boldsymbol{b} = 1)} \qquad (6-1)$$

The velocity of the particle path with β = ½ will wish to deviate (by virtue of its velocity vector) the furthest from the particles original path. Conversely the path with β = 2 will wish to deviate the least. Even though this analysis holds exactly only for the infinite drag droplet-eddy interaction ($\tau_p \rightarrow 0$) at the instant of the interaction, the trend is identical for particles with finite drag in both the particle-eddy interaction and afterwards. The smaller the β

the greater the tendency of a real particle to deviate from its original course after the particle-eddy interaction is completed.

6.3 Effect on a finite inertia particle exiting the eddy event early

An additional complication is encountered when a particle leaves the eddy interaction box by one of the horizontal surfaces. The particular situation varies depending on the relative sign of the particle velocity, V, and the gas velocity, v, but suffice it to say that: if the particle eddy interaction times $t_{\beta=2}$, $t_{\beta=1}$, and $t_{\beta=0.5}$ do not vary much (are similar in duration) then the interaction with the largest relative velocity, $v^*(\beta = 1/2)$, will produce the largest y deviation from the original trajectory. One particular case where this is true is shown in Figure 6.2.
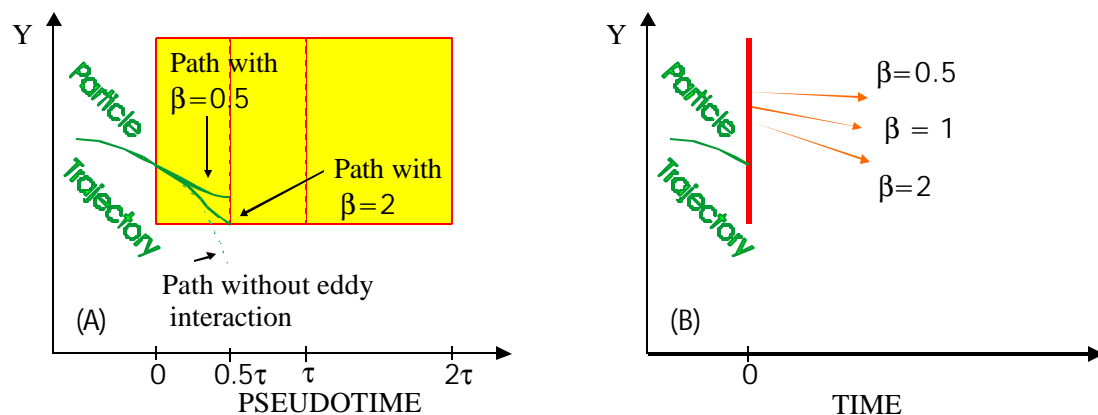
Figure 6.2: Effects of β on one real particle with an initial y velocity. The smaller value of β tends to cause a greater deviation from the particles original path. Path for $\beta = 1$ is not shown. The arrows in (B) are velocities at the time just after the eddy event, not particle paths.

In Figure 6.2 (A) the dotted line represents the path the particle would take if it did not interact with the illustrated eddy. The fluid cell which surrounds the particle at the point of the particle-triplet map interaction has an upward velocity (a positive v). This positive velocity will have varying effects depending on the value of β used. Careful examination of the illustration shows that for all values of β, the velocity adjustment is positive since the v velocity is positive. The smaller the value of beta used the greater the velocity difference compared to the velocity just before (0^-) the particle-eddy interaction. Refer to Section 3.6 for details on how the change in position and velocity is computed.

6.4   Particles with infinitely large inertia

A brief discussion of the effects of β on the other limiting case, infinite particle inertia is added for completeness. There is no scatter from the original path whatsoever for any value of β. No matter what the choice of β the infinite inertia particle is not deflected by it, with the possible exception of $\beta = 0$, in which v^* tends to infinity and might than deflect the infinite inertia particle. However, since in the introduction of β was made with the supposition that β be a number close to one, no provision was added to account for a vanishing β.

6.5   Numerical results for 12 cases studied

Figures 6.3 – 6.14 give the variations in β for each of the 12 cases studied, 1 – 12 respectively, using an ensemble size of 750. See Table 5.1 for details on the initial diameter, initial velocity, initial droplet spacing and the injection angle of the stream of droplets for each particular case. All cases show the same trend, the smaller β (0.5) causes more of a scatter in the y direction than the unity β and there is even less scatter on average for the large β (2.0). There are however outliers in all of cases even the large β due to the random nature of the ODT formulation. For the cases shown in this chapter (an ensemble size of 750) there is no appreciable change in the scatter in the x direction due to changes in β. Though not shown in this thesis, the results for the ensemble size of 2000 yielded the same results as that of the 750 size. That is there was no appreciable change in the scatter in the x direction due to β and the scatter in the y direction increased as β decreased. The reason β has an effect in the y direction is that the idealized eddy events cause instantaneous displacements in the y direction and adjustments to the y velocity of the particle. No adjustments are made to the x direction, see Section 3.9.2 for a discussion on this point. Since there is no direct effect of β on motion in the x direction the only influence that β can

have in the scatter in the x direction is a secondary affect. For example, a smaller value of β may cause the droplet to deviate from its path to a fluid zone which is significantly hotter (or colder) which in turn would cause the droplet to vaporize quicker (or more slowly). This change in vaporization rate of the droplet would result in more scatter in the x direction. Hence this is only a secondary influence on the x scatter.

This same (secondary) influence can be achieved by allowing the ODT program to run more realizations. That is the random nature of the ODT program (with a value of $\beta = 1$) will, after a sufficient number of realizations, jostle the droplets enough to sample the range of temperature variations which influence the scatter in the x direction. The runs with ensemble sizes of 750 and 2000 are large enough so that the x direction scatter is not influenced by adjustments to β.

The results for an ensemble size of 200 (not shown in this thesis) show variation in the x scatter due to changes in β, however, these variations are attributed to the small number of realizations and not to any physical phenomenon.

Figure 6.15 gives the variation as a function of β (top, middle , bottom diagrams) of the variation in height (the y direction) of the numerical data as

a function of the initial diameter D_o based on an ensemble size of 750. The only available data points, for the variation in the y direction, from the Mulholland et al. paper are shown as open symbols (circle for the maximum and a square for the minimum). This data is also included in Figures 6-16 – 6-18. The trend of larger β giving less of a spread is detectable from these diagrams. However, the scatter plots given in Figures 6.3 – 6.14 give a much more intuitive feeling for this conclusion since even for large β there are outliers.

Figure 6.16 gives the variation in the y direction as both a function of β and initial velocity based on an ensemble size of 750. The trend of larger β producing less y spread is also evident here. Figure 6.17 gives the variation in the y direction as a function of β and the initial s/D based on an ensemble size of 750. Figure 6.18 gives the variation in the y direction as a function of β and the initial injection angle based on an ensemble size of 750.

Also included here are comparisons between the variation in the x direction as a function of β and initial diameter for an ensemble size of 750 in Figure 6.19. Figures 6.20 gives the variations in the x direction variation as a function of initial velocity and β. Figures 6.21 gives the x direction

spread as a function of initial droplet spacing and β. Figure 6.22 gives the x direction variation as function of injection angle and β. No definite trends could be derived from the variations in the axial direction burn out points as a function of β.

6.6   Conclusions

Consistent in all 12 cases, which included variations in initial diameter, initial velocity, initial droplet spacing and injection angle, the smaller value of β, produced the larger variation in the y (transverse direction) from the droplets original trajectory. The larger value of β produced less scatter in the y direction. There were no detectable trends in the variation in the axial (x) direction due to variation in β in runs with an ensemble size of 750.
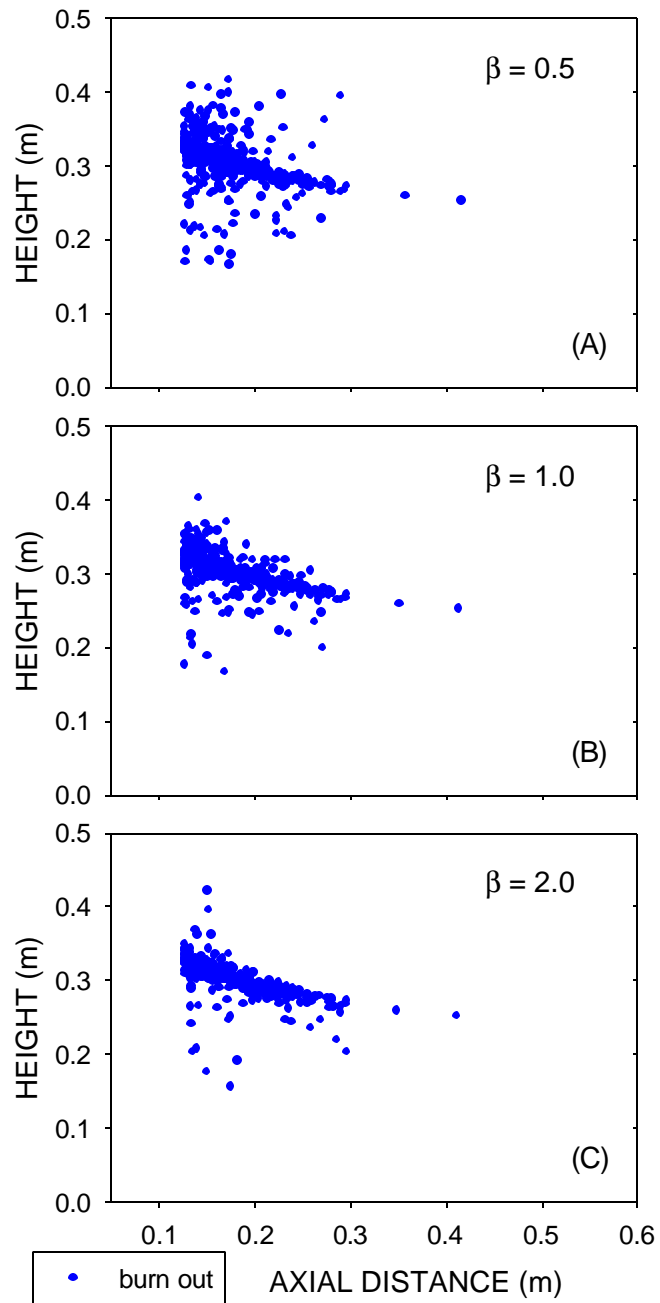
Figure 6.3: Variation of case 1 as a function of β. As beta decreases from a value of 1.0 the vertical *y* spread increases. As beta increases from a value of 1.0, the vertical spread decreases.
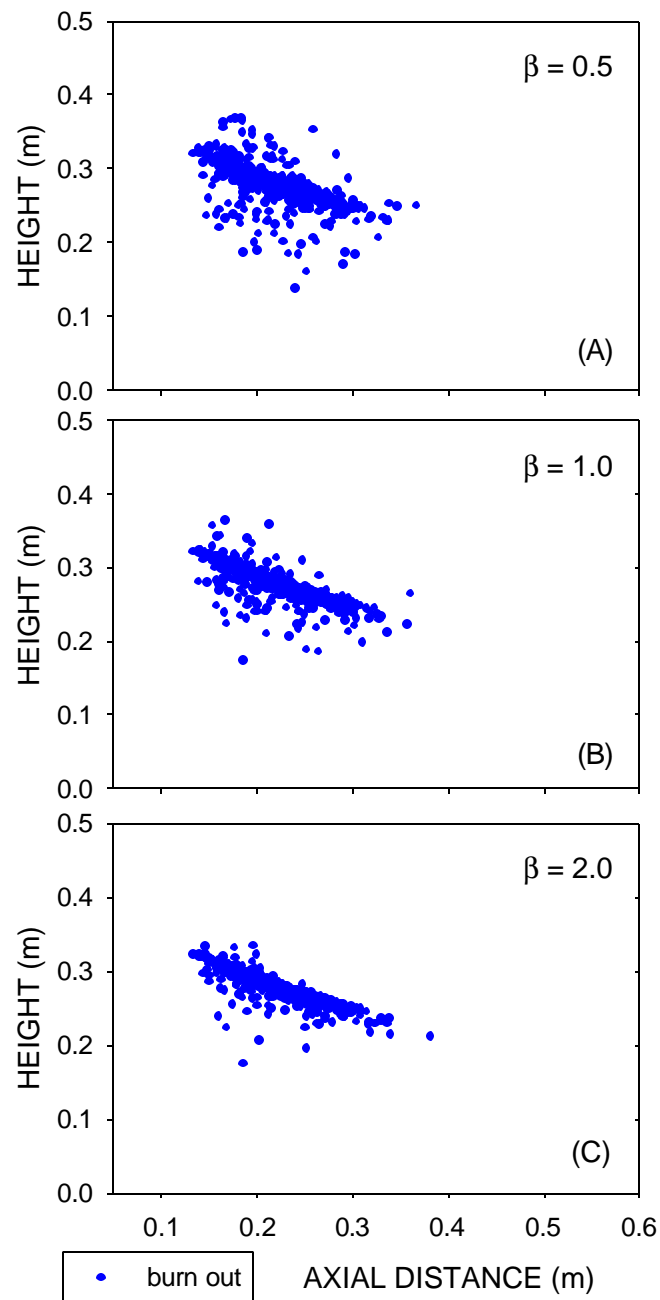
Figure 6.4: Variation of case 2 as a function of β. As beta decreases from a value of 1.0 the vertical *y* spread increases. As beta increases from a value of 1.0, the vertical spread decreases.
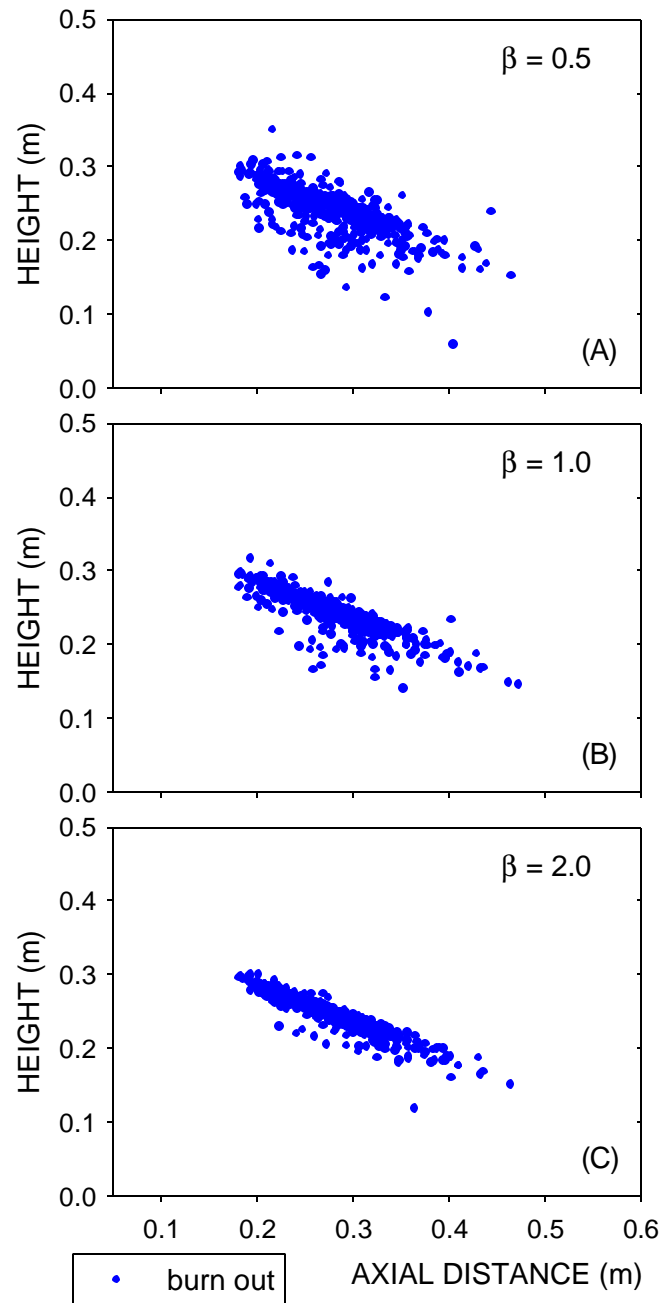
Figure 6.5: Variation of case 3 as a function of β. As beta decreases from a value of 1.0 the vertical *y* spread increases. As beta increases from a value of 1.0, the vertical spread decreases.
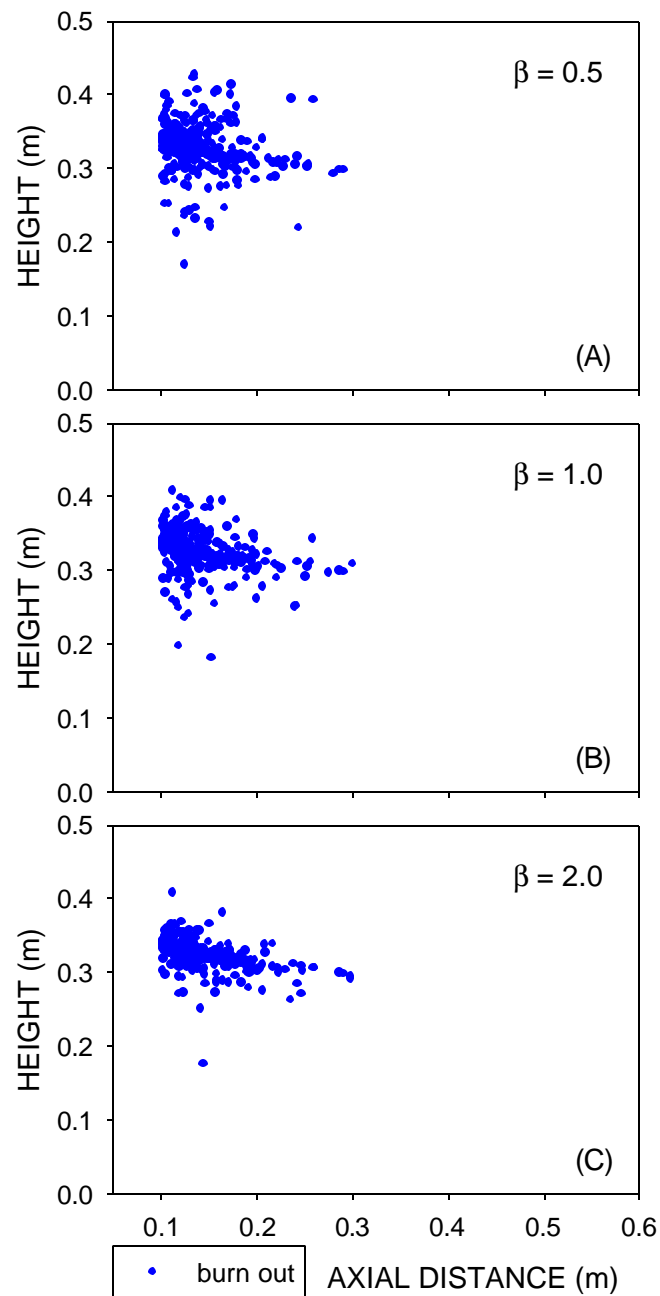
Figure 6.6: Variation of case 4 as a function of β. As beta decreases from a value of 1.0 the vertical *y* spread increases. As beta increases from a value of 1.0, the vertical spread decreases.
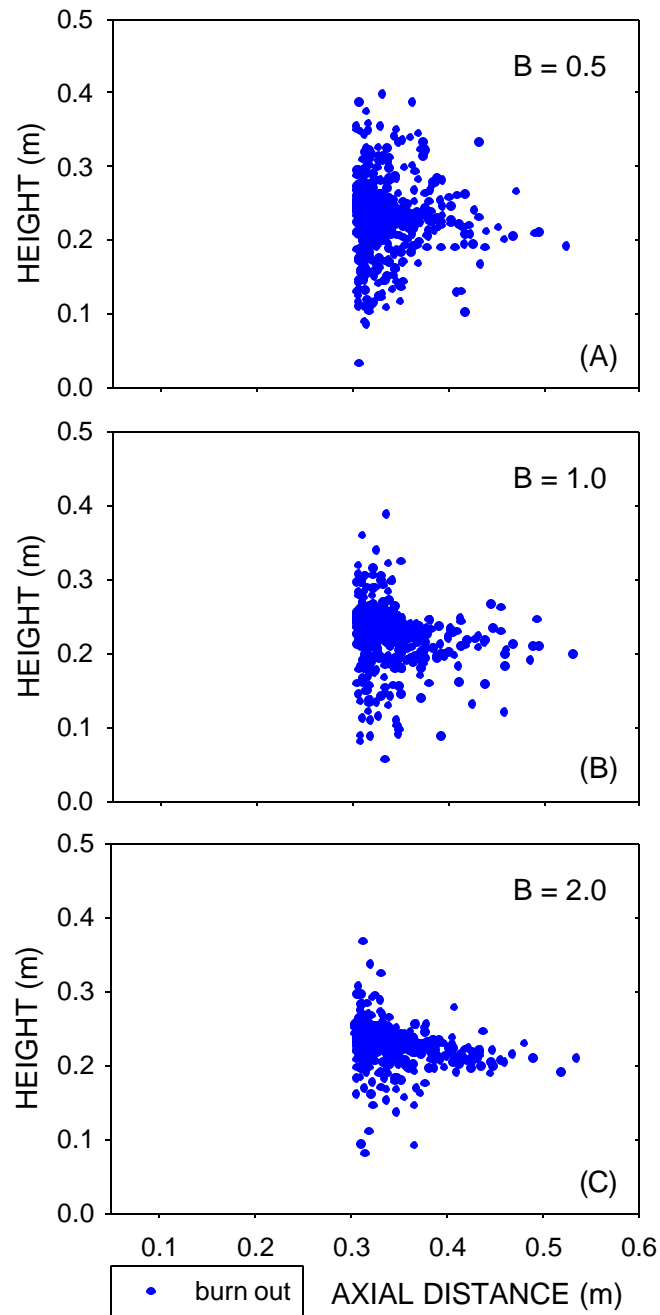
Figure 6.7: Variation of case 5 as a function of β. As beta decreases from a value of 1.0 the vertical *y* spread increases. As beta increases from a value of 1.0, the vertical spread decreases.
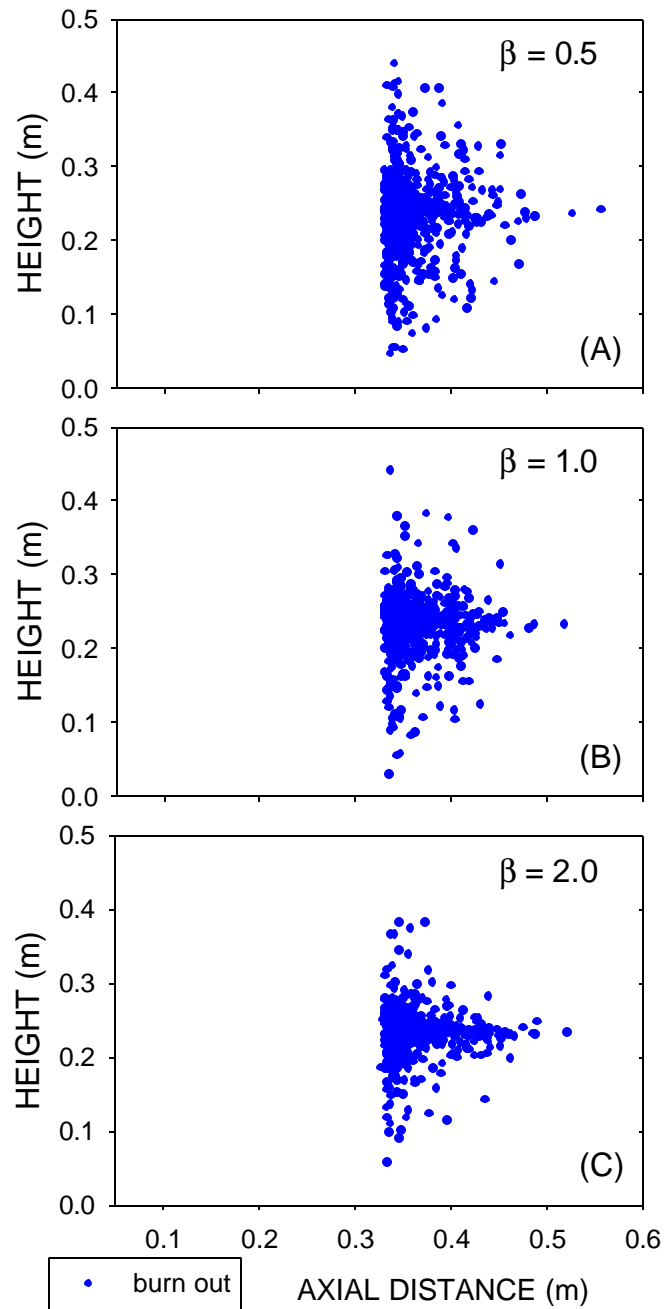
Figure 6.8: Variation of case 6 as a function of β. As beta decreases from a value of 1.0 the vertical *y* spread increases. As beta increases from a value of 1.0, the vertical spread decreases.
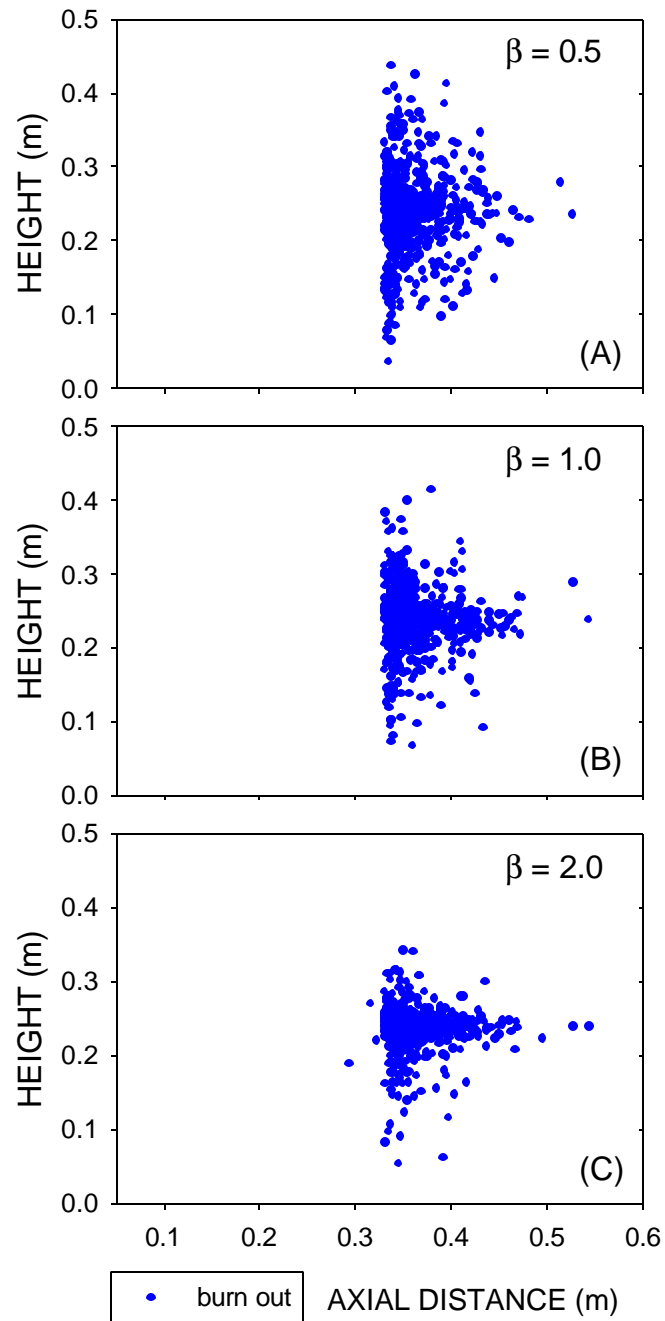
Figure 6.9: Variation of case 7 as a function of β. As beta decreases from a value of 1.0 the vertical *y* spread increases. As beta increases from a value of 1.0, the vertical spread decreases.
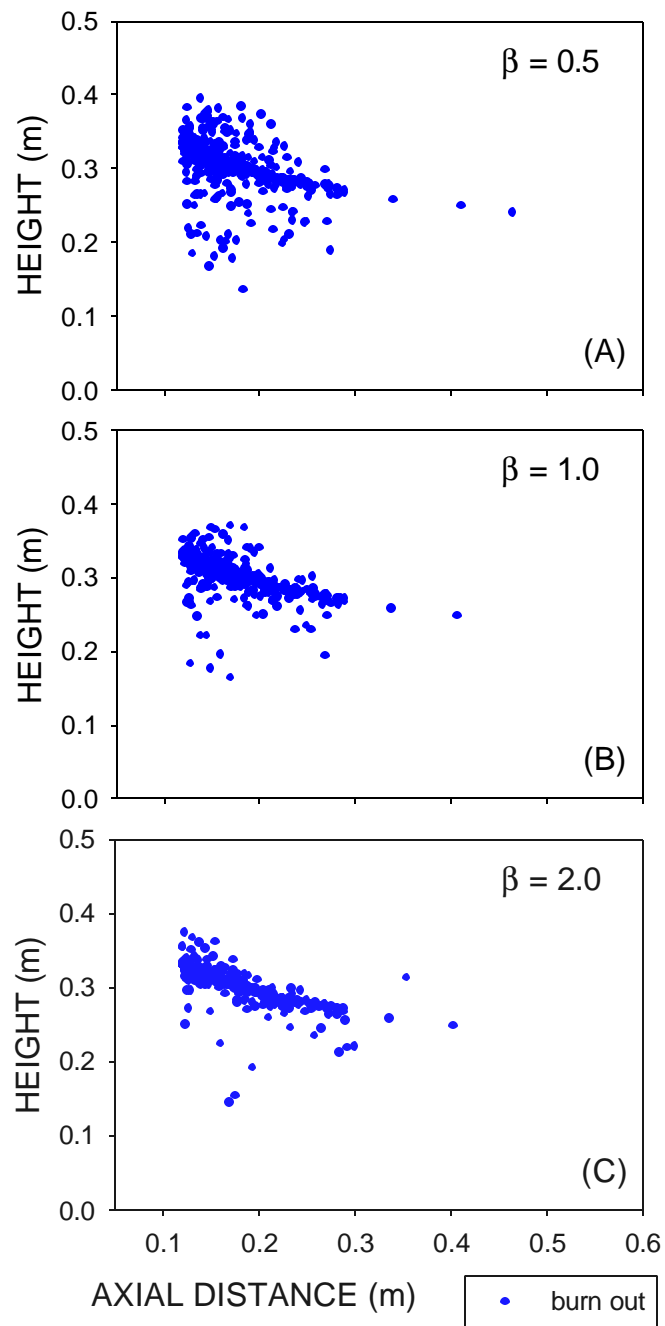
Figure 6.10: Variation of case 8 as a function of β. As beta decreases from a value of 1.0 the vertical *y* spread increases. As beta increases from a value of 1.0, the vertical spread decreases.
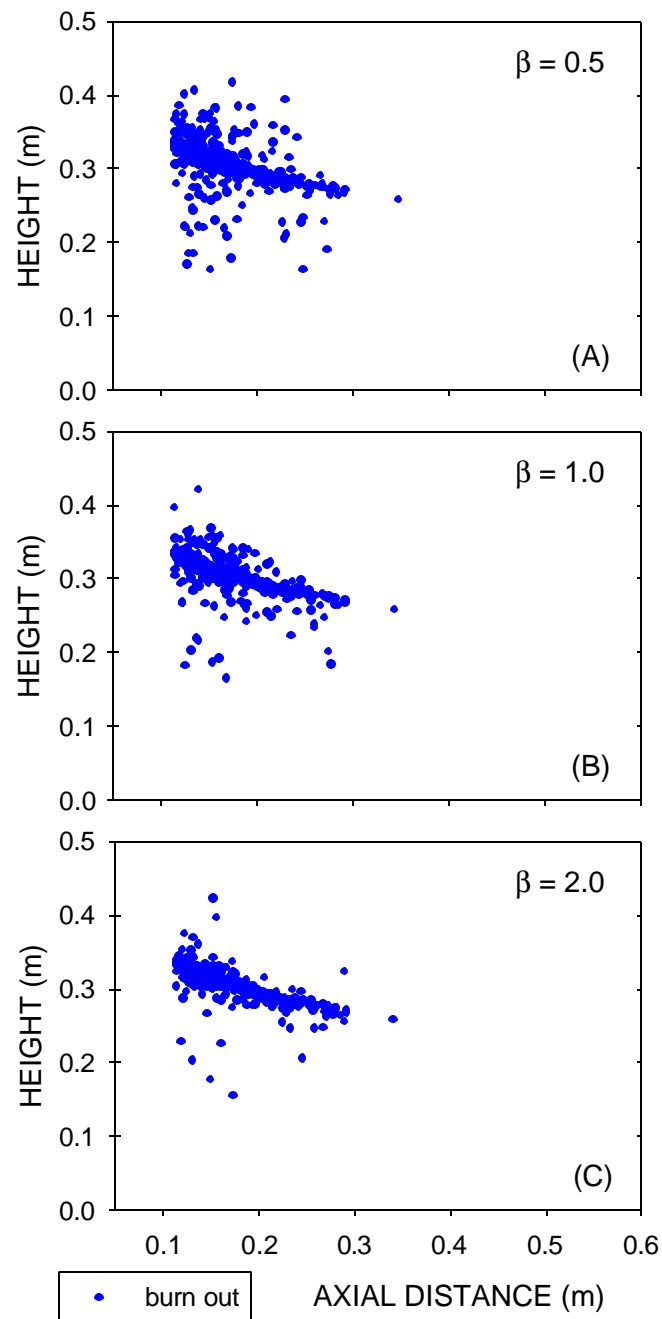
Figure 6.11: Variation of case 9 as a function of β. As beta decreases from a value of 1.0 the vertical *y* spread increases. As beta increases from a value of 1.0, the vertical spread decreases.
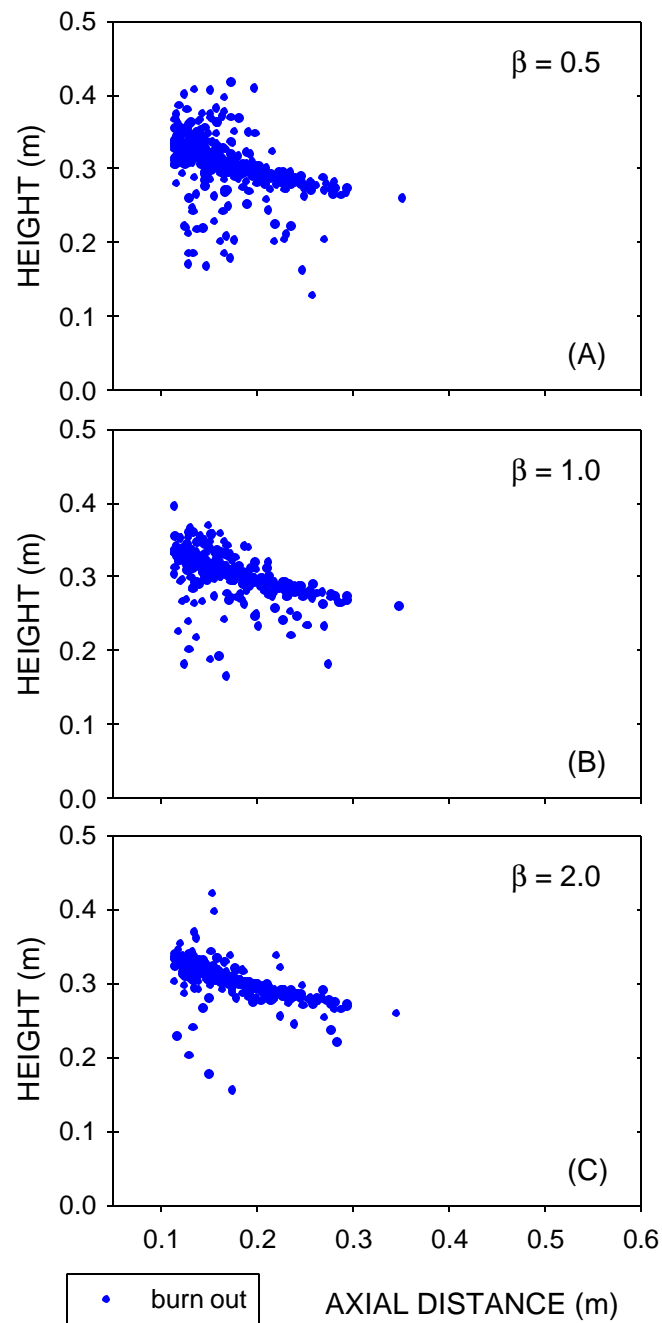
Figure 6.12: Variation of case 10 as a function of β. As beta decreases from a value of 1.0 the vertical *y* spread increases. As beta increases from a value of 1.0, the vertical spread decreases.
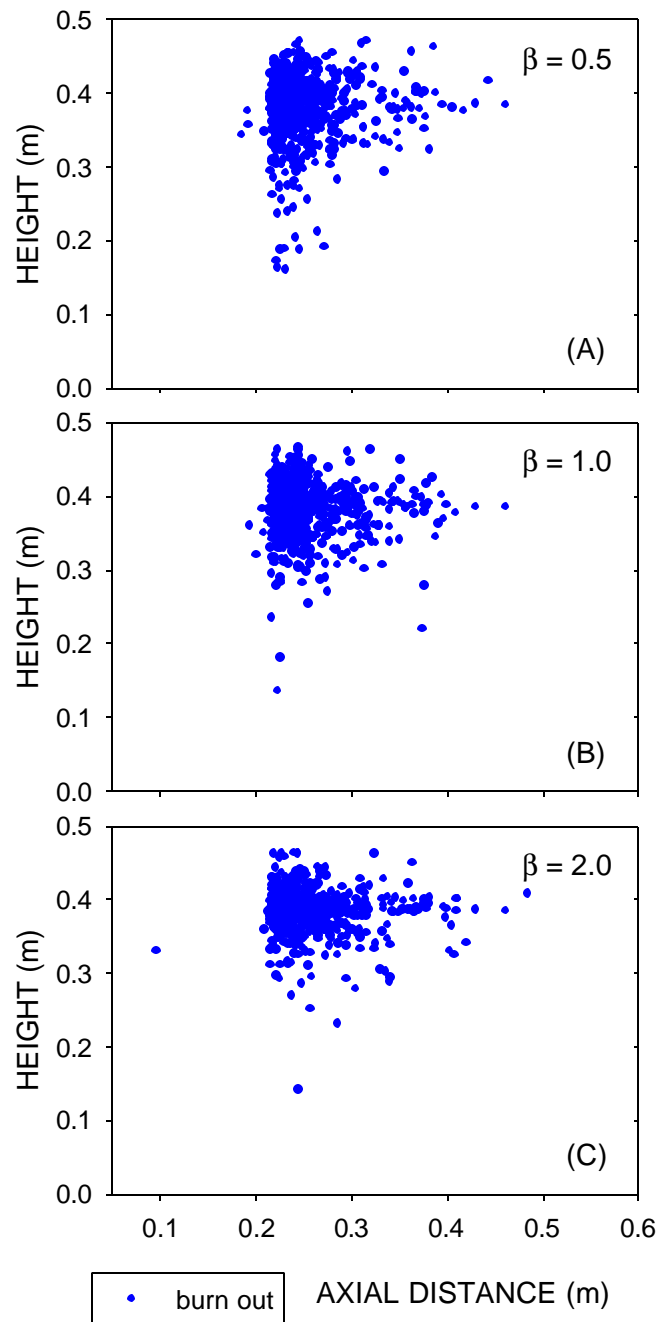
Figure 6.13: Variation of case 11 as a function of β. As beta decreases from a value of 1.0 the vertical *y* spread increases. As beta increases from a value of 1.0, the vertical spread decreases.
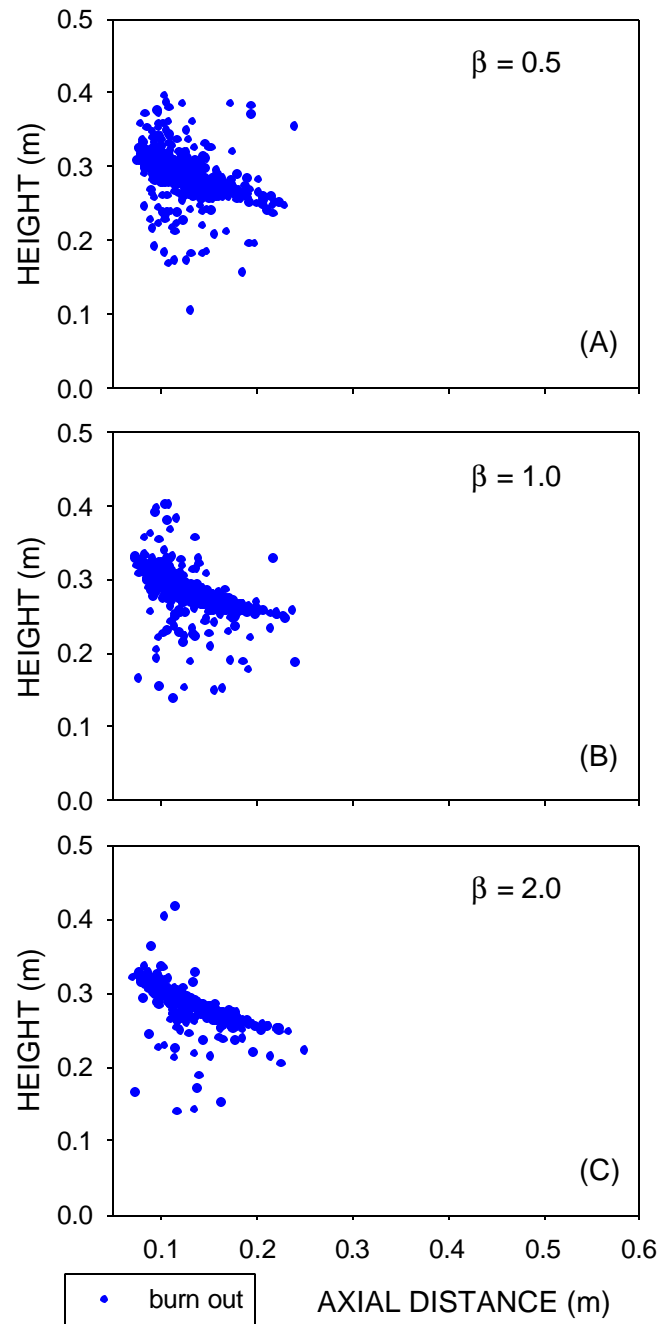
Figure 6.14: Variation of case 12 as a function of β. As beta decreases from a value of 1.0 the vertical *y* spread increases. As beta increases from a value of 1.0, the vertical spread decreases.
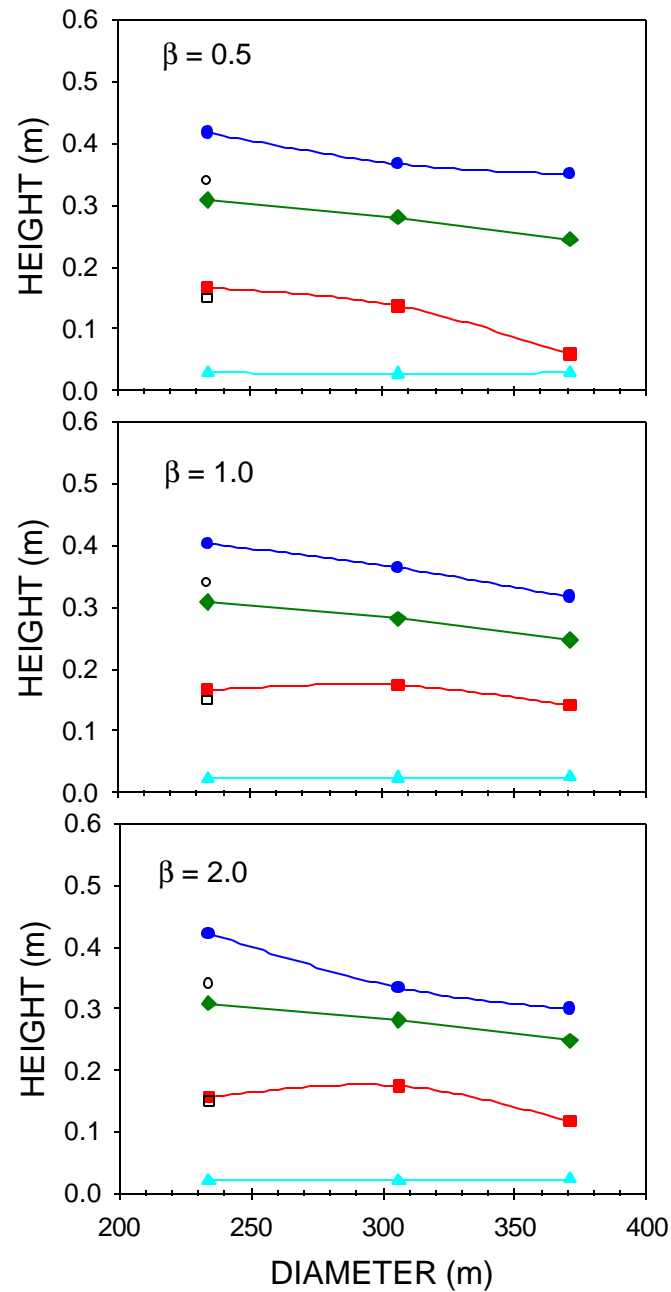
Figure 6.15: Variation in the Y direction as a function of Diameter and β. As beta decreases from a value of 1.0 the vertical *y* spread increases. As beta increases from a value of 1.0, the vertical spread decreases.
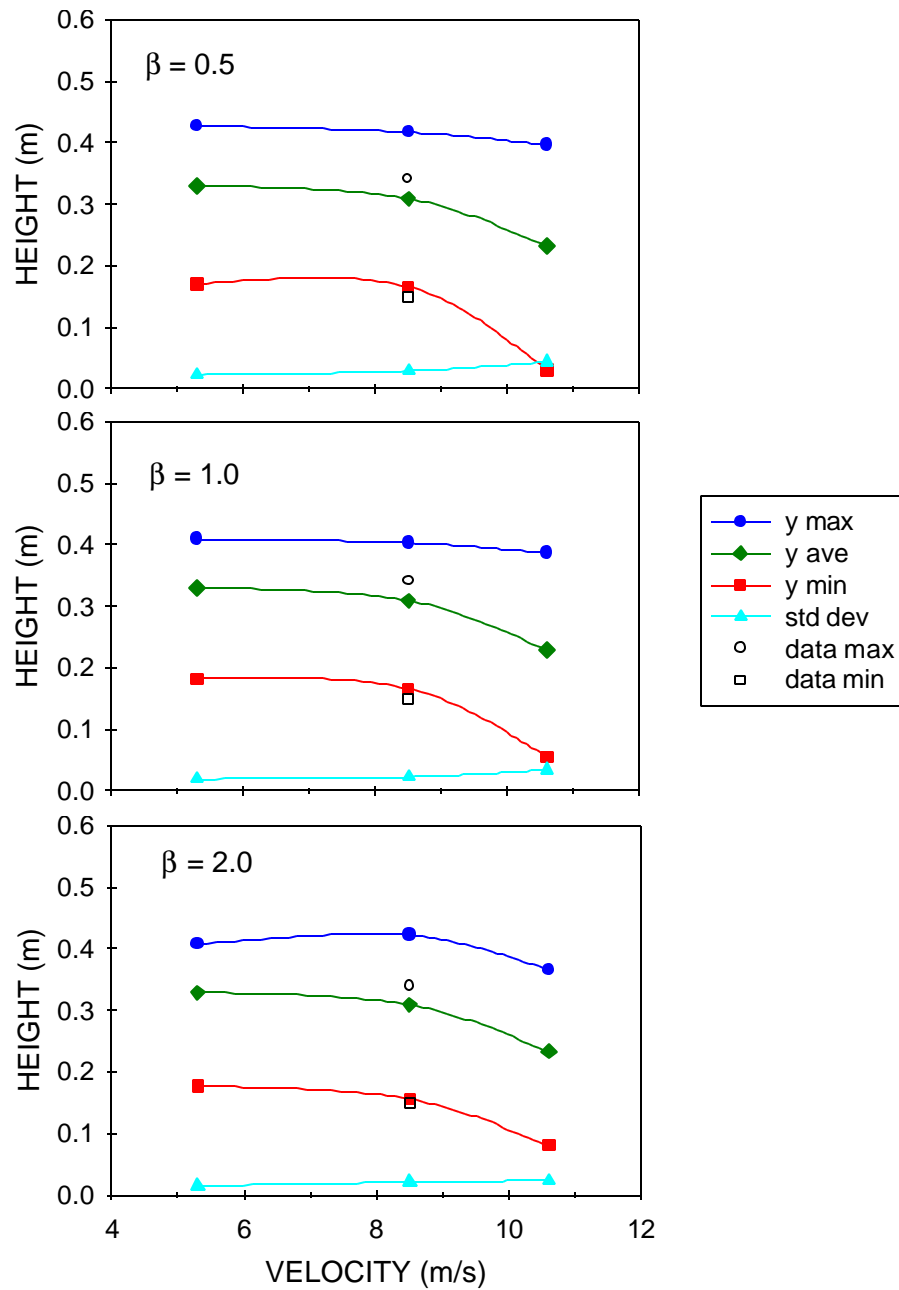
Figure 6.16: Variation in the Y direction as a function of velocity and β. As beta decreases from a value of 1.0 the vertical *y* spread increases. As beta increases from a value of 1.0, the vertical spread decreases. As β decreases, so does the standard deviation. This is especially evident in the 10.5 m/s data.
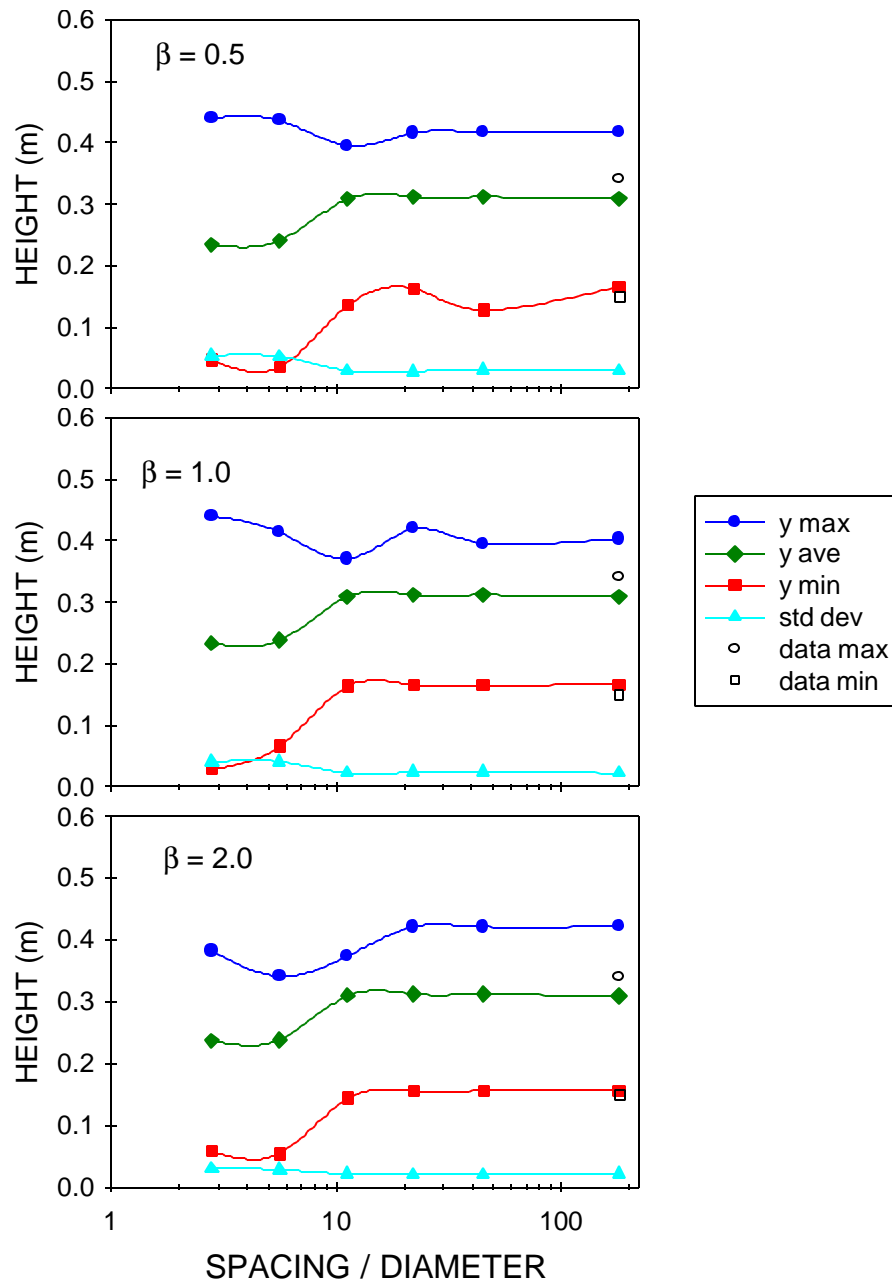
Figure 6.17: Variation in the Y direction as a function of initial interdroplet spacing and β. As beta decreases from a value of 1.0 the vertical *y* spread increases. As beta increases from a value of 1.0, the vertical spread decreases. As β decreases, so does the standard deviation.
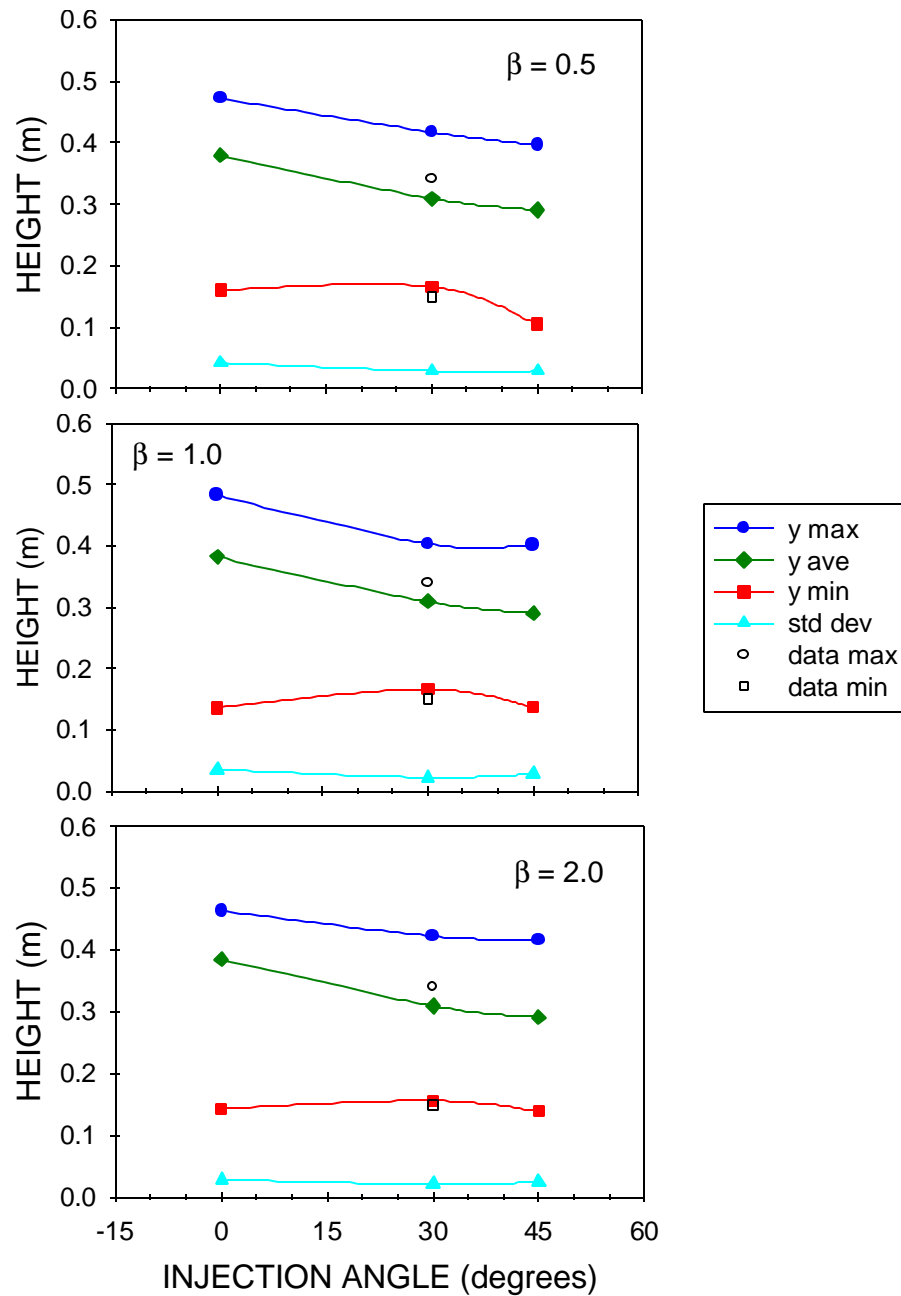
Figure 6.18: Variation in the Y direction as a function of initial injection angle and β. As beta decreases from a value of 1.0 the vertical *y* spread increases. As beta increases from a value of 1.0, the vertical spread decreases.
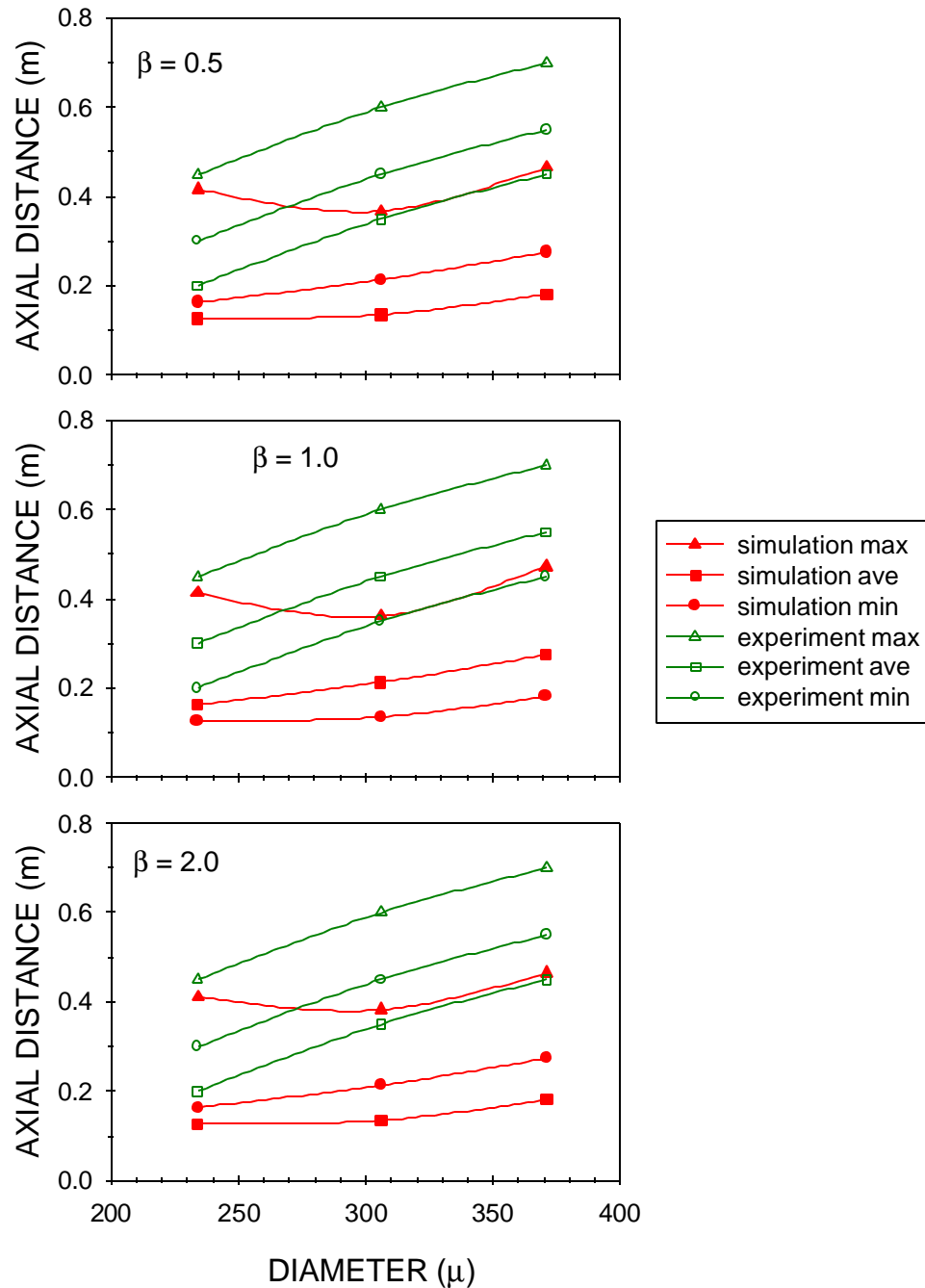
**Figure 6.19:** Variation in the axial direction as a function of initial diameter and β. Comparison of experimental measurements and simulated burning droplets. The closed symbols represent the predicted values. The experimental data are shown in open symbols. An ensenble size of 750 was used. No trend with beta variation was noted.
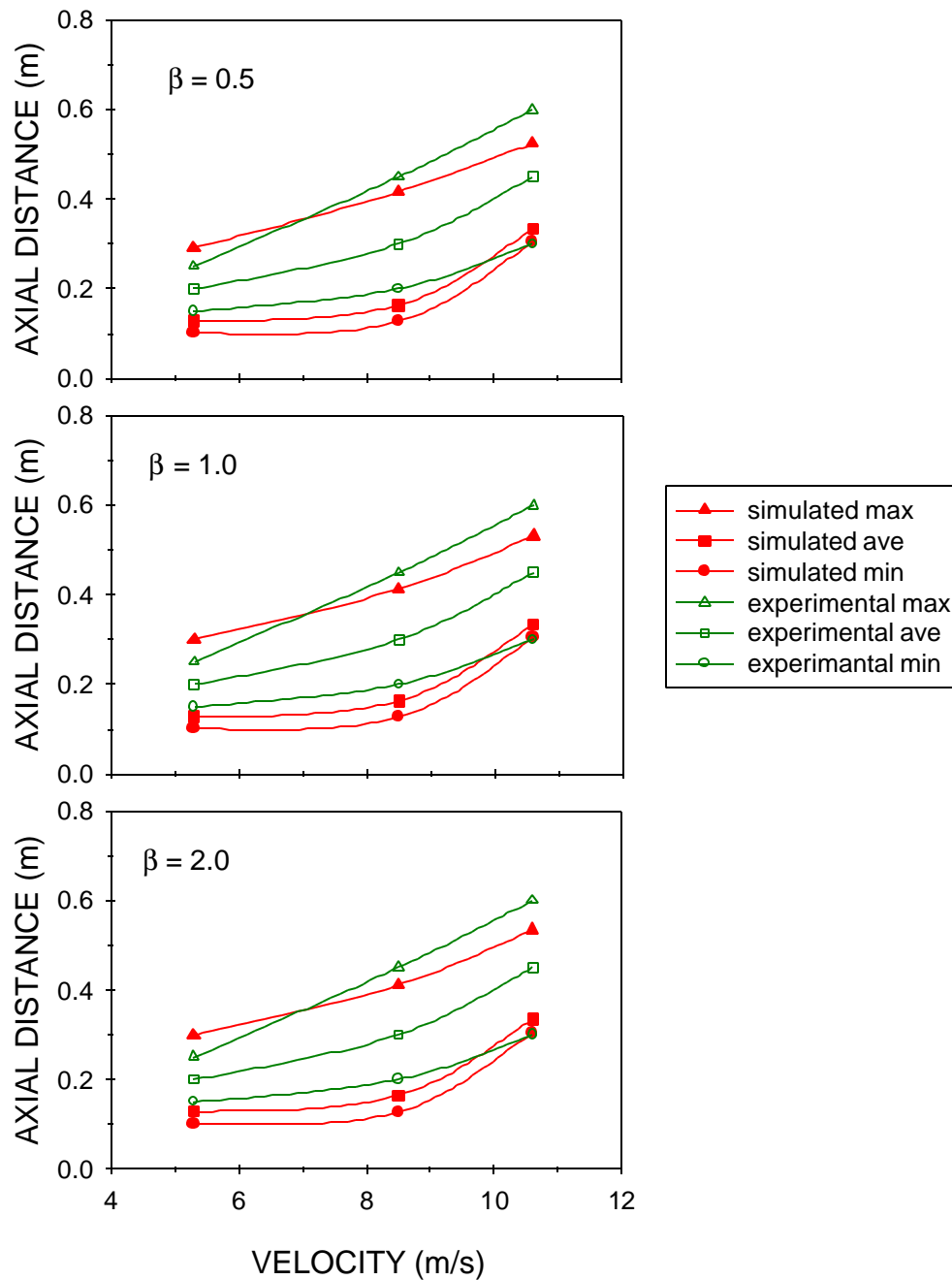
Figure 6.20: Variation in the axial direction as a function of initial velocity and β. Comparison of experimental measurements and simulated burning droplets. The closed symbols represent the predicted values. The experimental data are shown in open symbols. An ensemble size of 750 was used. No trend with beta variation was noted.
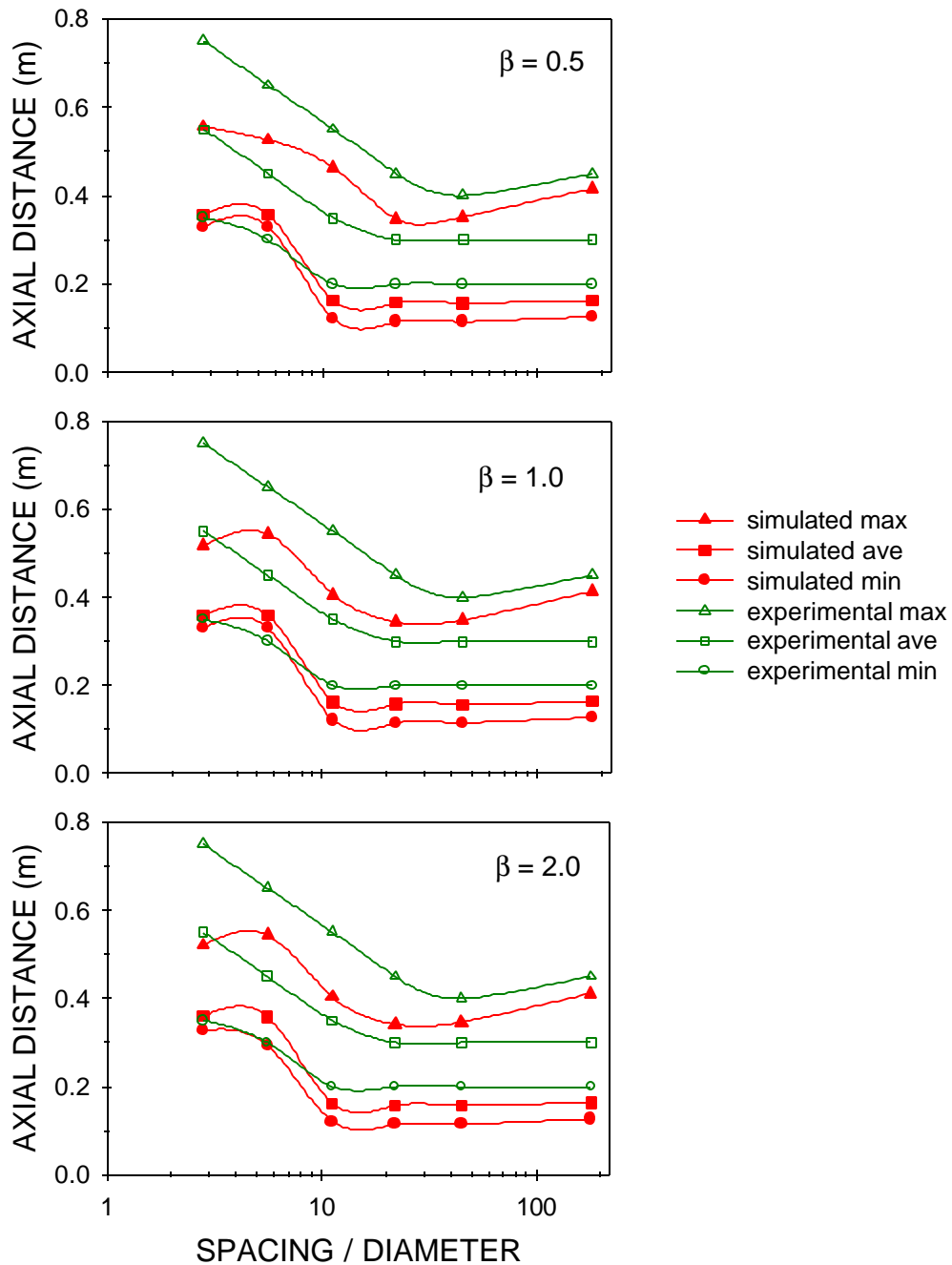
Figure 6.21: Variation in the axial direction as a function of initial droplet spacing and β. Comparison of experimental measurements and simulated burning droplets. The closed symbols represent the predicted values. The experimental data are shown in open symbols. An ensenble size of 750 was used. No trend with beta variation was noted.
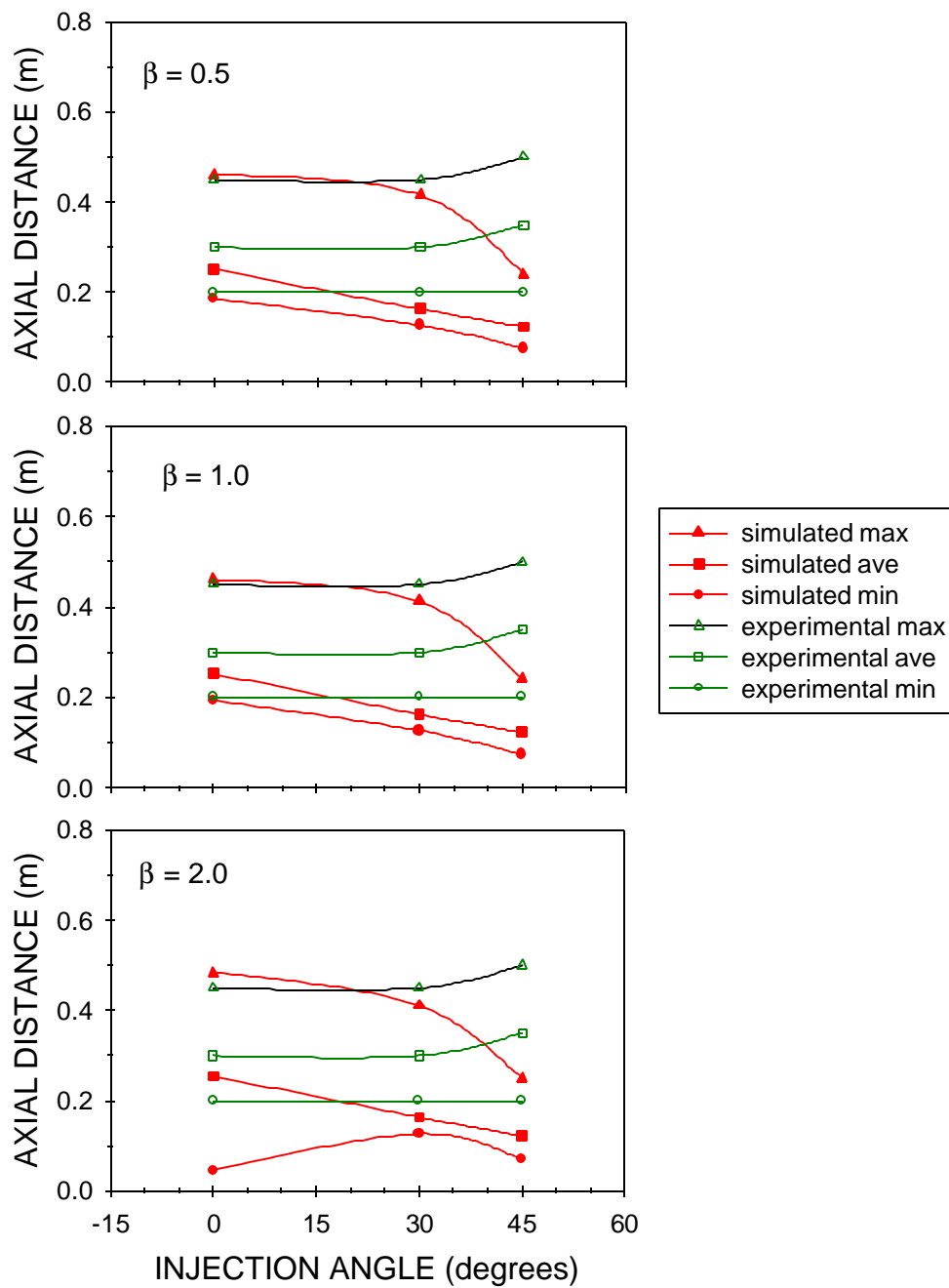
Figure 6.22: Variation in the axial direction as a function of initial injection angle and β. Comparison of experimental measurements and simulated burning droplets. The closed symbols represent the predicted values. The experimental data are shown in open symbols. An ensenble size of 750 was used. No trend with beta variation was noted.

Chapter 7

Conclusions and Future Work

7.1 Conclusions

A One Dimensional Turbulence Model (ODT)-droplet trajectory model was developed to examine the performance and safety of a thermal treatment process for metal containing wastes. Results indicate that one can predict possible failure modes inherent in the incineration process due to rogue droplet penetration past the flame zone and subsequent failure to completely burn out.

The ODT model proper is able to reasonably predict the mean velocity and temperature profiles of a 100 kW combustor using as an initial condition the measured mean profiles (velocity and temperature) at a distance of 5 cm downstream of the burner.

The ODT two-phase flow model can accurately predict the spread of droplet burnout points due to the random variation of the velocity/temperature field (the high turbulence) without the cost of doing a 3-dimensional (DNS) calculation. Excellent agreement (using an ensemble size of 750) was found for predicting the spread due to variations in initial diameter. Good agreement was found for predicting the spread caused by

variations in initial velocity and for the first two cases of droplet stream injection angle. (Those being the zero and thirty degree trials.) This was achieved without the computational burden of attempting a DNS calculation.

The 45 degree angle spread is underpredicted because type-C interactions were not considered in the ODT droplet model. Other important physics may also be missing from the model formulation.

The ODT two-phase flow model did not reproduce the spacing/diameter spread because no s/D effects were included inside the ODT droplet model and the point at which the droplet stream broke up into individual droplets was probably incorrect. Aside from a pure guess, there were no data available from the experiment to choose a droplet break up point other than the one which was presented in this paper.

7.2   Future Work

Future work should include the development and implementation of the type-C interactions. The theoretical groundwork for type-C interactions is mostly done. The implementation of type-C interactions may account for the error in the predicted values for the forty-five degree injection angle (Case 12) along with the error in the trend predicted of the axial spread

decreasing as the angle increases. This error was attributed to the combination of the lack of type-C interactions and the possibility of other forces, such as the Saffmon lift force, causing the droplets to veer from the course predicted by the physics which are included in this model.

Hence an effort should be made to investigate other forces and their effect on the droplet trajectory. This could include thermophoresis.

The assumption of a spherical droplet is used often. However, during the initial part of the trajectory, the particle Re is such that the droplets are not likely to be spherical. Hence improvements in drag coefficients and droplet vaporization models should be investigated.

The failure of this model to predict a trend for the entire range of initial droplet spacing effects on the axial spread indicates that if this model is to be used to predict the droplet spacing variations, it must be modified to somehow include s/D effects. Because of the success the model had for the variations in diameter, velocity, and (to a lesser extent) injection angle a possible avenue of approach would be to design a different model to compute the initial conditions and the position at which the droplet stream breaks up and behaves as if it were a bunch of random, independent droplets. So rather than simply taking the point of stream break up to be the same for

all six trials (Cases 1, 6, 7, 8, 9, 10) the new model would adjust this break up point to allow for variations in s/D. Intuitively the smaller the s/D the farther the stream should travel before breakup.

The ODT formulation proper used in this paper (which is constant density, a single velocity component, and between two parallel plates) has had a number of improvements done to it by Kerstein and co-workers. Formulations now exist which will provide variable density, three gas phase velocity components, and cylindrical geometrys. Implementation of any of these should prove an improvement to the present simulation.

As the ODT formulation stands, adding chemical reactions to the gas phase is straightforward. The major approximations made in the development of the droplet heating/vaporization/burning model were such that the author did not deem the introduction of chemistry, e.g. the depletion of oxygen in the fluid cell by the burning droplet, to be worth the trouble when the multi-component fuel was modeled as a single pure substance. If the model were to be redone with a better approximation of the phenomenon of multi-component droplet heating/vaporization, then also including some basic chemistry into the gas phase would be advantageous.

Appendix A

Source Code

SOURCE CODE FOR THE ODT – TWO-PHASE FLOW PROGRAM

The main program (odtdriv) is listed first. Next comes the subprograms used for the two-phase flow portion of the program. This may be followed by the ODT proper code which was provided at the onset of this project. (See acknowledgements for details.) At this point only the code for the burning droplet submodel is included.

The second section of Appendix A lists the programs used to compute the initial conditions, of the 12 cases of droplets, used as input to the ODT two-phase flow program.

A.1 Source code for ODT and droplet submodel

```
      program odtdriv
C     LAST MODIFIED BY JRS        04/28/00 @ 11:00
C     FOR EVAPORATING DROPS WITH PARAMETER SWITCH, multi drops
!!  used to find droplet eddy interactions
C     MODIFIED TO RUN WITH DP/DX NOT = 0.0
C Program to run the ensemble and time stepping of the iterative odt loop
      implicit none
      integer lout, lt, lmap, nts, nevents
      integer nnsc, nnx, nnfld, nnflx, nnt, nnts
C     ***********************
C     THE DROPLET TIME LINE WAS ADDED, NEVENTS CHANGED FROM 4 TO
5
C     NNX = 4619 IS TOO BIG, 4431 good, 4333 bad
C     MUST ALSO SET NNBIN TO NNX / 3 IN updfop.f AND mpdfop.f
C     ***********************
      parameter (lout = 6, nevents = 5)

c     for octane and flames use nnx = 1775

      parameter (nnsc = 2, nnx = 4431, nnfld = 19)
      parameter (nnflx = 3, nnt = 61, nnts = 8)
      integer nx, nt, it, nens, nfld, nsc, nbin, nsam
      integer ispec(20), minseg, i, j, iens, iskip
      integer il, ke, indx(nnx), nesize(nnx)
      integer neloc(nnx), neleft(nnx), neright(nnx), nopa
      integer kuneu, ktneu
      integer kounteddy

      logical dtsreset, eddy

      character*24 names(nnfld), tnames(nnts)
      character*(24*nnfld+1) wrkn
      character*50 desc

      real scal(nnsc,nnx), fld(nnx,nnfld,nnt), flux(nnx,nnflx,nnt)
      real uvfl(nnx), tvfl(nnx), uuvfl(nnx)
      real esize(nnx,nnt), emsd(nnx), edmid, edsize
      real work(nnx*nnfld*nnt), wrk1(nnx), wrk2(nnx)
      real rspec(30), a_eddy, p_a, refdens
      real visc, tdiff, gbeta, dpdx
C        DPDX IS DP/DX DIVIDED BY DENSITY (UNITS M/(S**2))
C        TDIFF IS THERMAL DIFFUSIVITY UNITS (M**2/S)
```

```
C         VISC IS KINEMATIC VISCOSITY UNITS (M**2/S)
      real x1, xn, v1, vn, t1i, tni, t1f, tnf, t1, tn
      real xsc, usc, vbulk, bulktemp
      real scalinit(nnsc,nnx), rho(nnx), x(nnx), dx(nnx), xdom, elmin
      real time, dtm, dts, dta, t(nnt), tlast(nevents), tnext(nevents)
      real tstat(nnt,nnts), accdts, accpa
      real pa, pamax, etau, beta_eddy
      real soonest
C    VARIABLES FOR DROPLET MODEL:
C    DELTA V  = CHANGE IN VELOCITY OF THE DROPLET
C    DELTA Y  = CHANGE IN THE Y POSITION OF THE DROPLET
C    DELTA X  = CHANGE IN THE X POSITION OF THE DROPLET
C    D Y POSIT = THE Y POSSITION OF THE DROPLET
C    D Y PO I  = INITIAL Y POSSITION OF THE DROPLET
C    D X POS  = DROPLET POSITION IN THE X DIRECTION
C    D X POS I = INTIIAL DROPLET POSITION IN THE X DIRECTION
C    D Y VELOC = THE DROPLET V VELOCITY - VERTICLE
C    D Y VEL I = THE INITIAL DROPLET Y VELOCITY (USED IN ENSEMBLE)
C    D U VEL  = DROPLET U VELOCITY - STREAMWISE
C    D U VEL I = INITIAL DROPLET X VELOCITY
C    UPPLIMIT  = UPPER LIMIT FOR THE TIME INTEGRAL
C    DT DROP   = TIME STEP FOR THE DROP TIME LINE
C    E LHS    = EDDY LEFT HAND SIDE
C    E RHS    = EDDY RIGHT HAND SIDE
C    OVRSHOOT  = DISTANCE OVER SHOOT WHEN DROP TRAVELS IN
PSEUDO TIME
C    PSEUDOY   = POSITON  OF DROPLET AFTER INTEGRATION IN PSEUDO
TIME
C    D PARAM  = THE D PARAMETER DEFINED FOR THE DROPLET MODEL
C    D TAU    = D TIMES E TAU,  THE DROPLET TAU
C    IR      = RIGHT HAND NODE OF THE EDDY
C    I D POS  = INTEGER DROPLET POSITION (NODE) IN Y COORDINATE
C    U BAR    = THE AVERAGE U VELOCITY OF THE EDDY
C    U FLUID  = U VELOCITY OF THE FLUID ELEMENT WHICH HOLD THE
DROPLET
C    V END    = PARTICLE Y VELOCITY AT THE END OF THE INTEGRATION
C    U END    = PARTICLE X VELOCITY AT THE END OF THE INTEGRATION
C    DIA      = PARTICLE DIAMETER
C    DIAI     = INTIAL DROPLET DIAMETER
C    TAU P    = THE DROPLET TIME CONSTANT
C    TAU P I  = THE INITIAL DROPLET TIME CONSTANT
C    BULK VEL  = BULK VELOCITY OF ALL THE FLUID
C    DROP TIME = DROPLET TIME WHICH IS DIFFERENT FROM DROPLET
TIME LINE
```

```
C   N O D   = NUMBER OF DROPS
C***************************************************************************
*****
      INTEGER NOD
      PARAMETER (NOD = 15)
      REAL    AIRNU, ALAMDA, BIRTHT(NOD), BLN, BMAST, BP1, BULKVEL
      REAL    CPFGAS
      REAL    DABZERO, DELTAT, DELTAX, DELTAY, DELTAV
      REAL    DIA(NOD), DIAI(NOD), DIANEW, DIGNIT(NOD), DPARAM,
DPOSROOT
      REAL    DRMASS(NOD)
      REAL    DROPTIME(NOD), DTAU, DTDROP, DTDROPF, DTIMEI(NOD)
      REAL    DUVEL(NOD), DUVELI(NOD)
      REAL    DXPOS(NOD), DXPOSI(NOD)
      REAL    DYPOSIT(NOD), DYPOI(NOD), DYVELOC(NOD), DYVELI(NOD)
      REAL    ELHS, EPS, ERHS, GRAVAC
      REAL    HEATCAP, HEATCOM, HEATVAP, HEFF, HOLD
      INTEGER ICOUNT, IDPOS, IG1, IG2
      INTEGER IR, ISEED, INEW, ITT, J1, LDOUT, KDROP
      INTEGER NODA
      LOGICAL LALLIGN
      LOGICAL LALLST, LDFINSH(NOD), LDROP, LDSTART(NOD),
LDSTARTI(NOD)
      LOGICAL LHEATUP(NOD), LITT, LLAMDA, LLONG, LMDIG(NOD)
      INTEGER LMDOUT(NOD)
      LOGICAL LMDROP(NOD), LMDROPI(NOD)
      INTEGER LMDSOUT(NOD)
      LOGICAL LTEST
      CHARACTER*9 OUTFIL(NOD)
      REAL    OVRSHOOT, PEPS, PI, PSEUDOV, PSEUDOY, RHOGAS, RHOL
      REAL    SCHMIDT, STOICH, TAUP, TAUPI, TDARRAY (NOD,10)
      REAL    TDROP(NOD), TDROPI(NOD), TEMPBP, TEMPZERO
      REAL    TFLAME(NOD), TINFIN
      REAL    TTHIRD, UBAR, UEND, UFLUID, UPPLIMIT, VEND, YOINFIN

      OPEN (LOUT, FILE = 'screen.out')

      call lunext(lt)
      call lunext(lmap)

      open (lt,file = 'timelog')
      open (lmap,file = 'ltmap')

C Read the specs in the input file
```

```
      nsc = nnsc
      call rdkey(lout, nx, nt, nens, nnts, a_eddy, p_a,  minseg,
     1    ispec, rspec, refdens, nnfld, nfld, nts, names, tnames,
     2    desc, iskip, kuneu, ktneu, beta_eddy)

C Memory check

       call memck(lout, nt, nnt, nx, nnx, nfld, nnfld, nts, nnts)

C Set the problem-specific parameters

      if (ispec(3) .eq. 0) then
        call stormspec(lout, rspec, visc, tdiff, gbeta, dpdx,
     1      x1, xn, v1, vn, t1i, tni, t1f, tnf)
      elseif (ispec(3) .eq. 1) then
        call relamspec(lout, rspec, visc, tdiff, gbeta, dpdx,
     1      x1, xn, v1, vn, t1i, tni, t1f, tnf)
      elseif (ispec(3) .eq. 2) then
        call polyakovspec(lout, rspec, visc, tdiff, gbeta, dpdx,
     1      x1, xn, v1, vn, t1i, tni, t1f, tnf)
      elseif (ispec(3) .eq. 3) then
        call channelspec(lout, rspec, visc, tdiff, gbeta, dpdx,
     1      x1, xn, v1, vn, t1i, tni, t1f, tnf)
      elseif (ispec(3) .eq. 4) then
        call couettespec(lout, rspec, visc, tdiff, gbeta, dpdx,
     1      x1, xn, v1, vn, t1i, tni, t1f, tnf)
      elseif (ispec(3) .eq. 5) then
         call tjetspec(lout, rspec, visc, tdiff, gbeta, dpdx,
     1      x1, xn, v1, vn, t1i, tni, t1f, tnf, xsc, vbulk)
      elseif (ispec(3) .eq. 6) then
         call slspec(lout, rspec, visc, tdiff, gbeta, dpdx,
     1      x1, xn, v1, vn, t1i, tni, t1f, tnf)
      elseif (ispec(3) .eq. 7) then
         call blspec(lout, rspec, visc, tdiff, gbeta, dpdx,
     1      x1, xn, v1, vn, t1i, tni, t1f, tnf)
      else
        write(lout,*) 'odtdriv error: bad flow specification'
        write(lout,*) 'stop'
        stop
      endif

C Initialize the grid and specify the initial scalar fields
```

```
      call start(nnsc, nx, minseg,
     1    x1, xn, v1, vn, rspec(16), rspec(17), t1i, tni, refdens,
     2    xdom, x, dx, scalinit, rho, elmin)

C Specialized initial profiles

      if (ispec(3) .eq. 5)
     1      call tjetstart(lout, nnsc, nx, x, dx, xsc, vbulk, scalinit)
      if (ispec(3) .eq. 6)
     1      call slstart(lout, nnsc, nx, x, dx, v1, vn, scalinit)

C     MODIFIED BY JRS FOR MULHOLLAND INITIAL CONDITIONS  ******
      IF (ISPEC(3) .EQ. 3) CALL INPVELOC (LOUT, NNSC, NX,
     2                  SCALINIT)
C     **********************

C If desired, replace the initial scalar field with one that's read in
C from a file

      if (ispec(6) .ge. 2)
     1      call profrestart(lout, nnsc, nsc, nx, x1, xn, xdom,
     2         x, dx, rspec(16), rho, scalinit)

C Other initialization

      call zfield(nnx, nnfld, nt, fld)
      call zfield(nnx-1, nnflx, nt, flux)
      call zorm(nnx, nt, esize)
      call zorm(nnt, nts, tstat)

C     *************************************************************
C     INITIALIZE THE VARIABLES SPECIFIC TO THE DROPLET MODEL
      CALL LUNEXT (LDOUT)
      OPEN (LDOUT, FILE = 'jevap.out')
      CALL LUNEXT (LMDSOUT (1))
      OPEN (LMDSOUT(1), FILE = 'jshort1.out')

      CALL DROPINIT(DX, NENS, NEVENTS, NOD, NNX, NX, ALAMDA, BIRTHT,
     2    BULKVEL, DABZERO, DIAI, DIGNIT, DPARAM, DTIMEI, DYPOI,
     3    DTDROPF, DUVELI, DXPOSI, DYVELI, EPS, GRAVAC, HEATCAP,
     4    HEATCOM, HEATVAP, HOLD, LDOUT, LDROP, LDSTARTI, LLAMDA,
     5    LLONG, LMDROPI, NODA, OUTFIL, PEPS, PI, RHOL,
     6    STOICH, TDROPI, TEMPBP, TEMPZERO, TFLAME, YOINFIN)
```

```
C1    ATY THIS POINT, THE SHORT OUTPUT IS NOT AVAILABLE !! 3/30/00
      DO ICOUNT = 2, NODA,1
C        IF (LLONG) THEN
          CALL LUNEXT (LMDOUT(ICOUNT))
          OPEN (LMDOUT(ICOUNT), FILE = OUTFIL(ICOUNT))
C        END IF
        CALL LUNEXT (LMDSOUT(ICOUNT))
        OPEN (LMDSOUT(ICOUNT), FILE = 's' // OUTFIL(ICOUNT))
      END DO
      LMDOUT(1) = LDOUT
C     CALL LUNEXT (ISEED)
C     OPEN (ISEED, FILE = 'seed.out')
C
C     ****************************************************************

C Begin the ensemble averaging loop

      do iens = 1, nens

C  Initialize the scalars and set the bulk temperature

        call scalstart(nx, nnsc, nsc, scalinit, scal)
        call temprefset(bulktemp, nnsc, nx, scal)

C  Initialize the boundary conditions and time stepping

        t1 = t1i
        tn = tni

        call dtmol(visc, tdiff, dx, dtm, rspec(22))
        call dtstir(lout, nnsc, nx, minseg, scal, x, dx, a_eddy,
     1       elmin, visc, xdom, p_a, dtm, dts)
        call tset(nt, rspec(20), rspec(21), dta, t)

        time = 0.
        tlast(1) = 0.
        tlast(2) = 0.
        tlast(3) = 0.
        tlast(4) = 0.
        tnext(1) = dtm
        tnext(2) = dts
        tnext(3) = rspec(20)
        tnext(4) = rspec(18)
        it = 0
```

```
C     ***************************************************************
C     JRS'S ADDITION FOR DROPLET SCALAR RESET
      CALL DROPSTART (BIRTHT, DIAI, DTDROPF, DTIMEI, DTM, DUVELI,
     2    DXPOSI, DYPOI, DYVELI, HOLD, IENS, LDOUT, LDSTARTI,
     3    LLONG, LMDOUT, LMDROPI, NEVENTS, NOD, NODA, PI, RHOL,
     4    TDROPI, DIA, DRMASS, DROPTIME, DTDROP, DUVEL, DXPOS,
     5    DYPOSIT, DYVELOC, LALLIGN, LALLST, LDFINSH, LDROP, LDSTART,
     6    LHEATUP, LMDIG, LMDROP, TDARRAY, TDROP, TLAST, TNEXT)

!! get trajectories stuff
C     CLOSE (LDOUT)
C     CLOSE (LMDSOUT(1))
C     CALL GETRAJ (IENS, LDOUT, LMDSOUT(1))

C     CALL RNUGET (IG1,IG2)
C     WRITE (ISEED, 137 ) IENS, IG1, IG2
C 137  FORMAT (1X, I6, 1X, I20, 1X, I20)
C     ***************************************************************

C   Time-stepping loop

      do while (it .le. nt)

C     Molecular loop

         dtsreset = .false.
         do while (tnext(1) .eq. soonest(nevents, tnext))

C       On the first pass, update the stirring time step

         if (.not. dtsreset) then
           call dtstir(lout, nnsc, nx, minseg, scal, x, dx, a_eddy,
     1          elmin, visc, xdom, p_a, dtm, dts)
           dtsreset = .true.
         endif

C       Solve the diffusion equation

C     *************************************
C       MODIFIED BY JRS SO THAT IN CHANNEL FLOW (MULHOLLAND DATA)
C       TEMPERATURE ALSO GOES THROUGH DIFFUSION
c          if (ispec(3) .ge. 3) then
           IF (ISPEC(3) .GT. 3) THEN
```

```
C     *****************************************
            call inertdiffuse(nnsc, nx, dx, dtm, visc,
     1            kuneu, v1, vn, dpdx, scal)

         else

C     ***************************************** ttttttttt
c             if (ispec(3) .ge. 1) dpdx
c     1             = ((v1 + vn) - (scal(1,2) + scal(1,nx-1)))
c     2             * visc / (xdom * dx(1))
            DPDX = 0.
C     ***************************************** ttttttttt

            call diffuse(nnsc, nx, dx, dtm, visc, tdiff, bulktemp,
     1            kuneu, ktneu, v1, vn, t1, tn, dpdx, gbeta, scal)

         call temprefset(bulktemp, nnsc, nx, scal)

c             bulktemp = (t1 + tn) / 2.

         endif

C     Update the timing and the time itself

         tlast(1) = tnext(1)
         tnext(1) = tnext(1) + dtm
         time = time + dtm
          enddo    !End the molecular loop

C    Stirring loop

         do while (tnext(2) .eq. soonest(nevents, tnext))

C     Select an eddy

         call scottselodt(lout, visc, dts, nnsc, nx, scal, dx,
     1         a_eddy, beta_eddy, minseg, elmin, x1, xn, xdom,
     2         rspec(24), rspec(25), il, ke, tnext(2), pamax,
     3         eddy, edmid, edsize, pa, etau,IR)

C     Update the eddy-specific statistics

         if ( eddy ) then
```

```
C       Implement the eddy using Vebjorn's routines
            call tripmap(nx, il, ke, indx)

C      *************************************************************
C      JRS'S ADDITION FOR DROPLET MODEL -- TYPE I INTERACTIONS

            IF (LDROP) THEN
              DELTAT   = TNEXT(2)-TLAST(5)
              IF (.NOT. LALLST) THEN
                LTEST = .TRUE.
                DO  KDROP = 1, NODA,1
                  IF (.NOT. LDSTART(KDROP)) THEN
                    LTEST = .FALSE.
                  END IF
                END DO
                IF (LTEST) THEN
                  LALLST = .TRUE.
                END IF
              END IF
              IF (.NOT. LALLIGN) THEN
                LTEST = .TRUE.
                DO  KDROP = 1, NODA,1
                  IF (.NOT. LMDIG(KDROP)) THEN
                    IF (DIGNIT(KDROP) .GE. TNEXT (2)) THEN
                      LTEST = .FALSE.
                    ELSE
                      LMDIG(KDROP) = .TRUE.
                    END IF
                  END IF
                END DO
                IF (LTEST) THEN
                  LALLIGN = .TRUE.
                END IF
              END IF
              DO  KDROP = 1, NODA,1
                IF (.NOT. LALLST) THEN
                  IF ((.NOT. LDSTART(KDROP)) .AND.
     2                 (BIRTHT(KDROP) .LT. TNEXT(2))) THEN
                    LDSTART(KDROP) = .TRUE.
                    LMDROP(KDROP)  = .TRUE.
                    DELTAT        = TNEXT(2) - BIRTHT(KDROP)
                  ELSE
                    DELTAT = TNEXT(2)-TLAST(5)
                  END IF
```

```
                    END IF
                    IF (LMDROP (KDROP)) THEN

                    IDPOS    = (DYPOSIT(KDROP) - X1)/DX(1) + 1.5
                    UFLUID   = SCAL(1,IDPOS)
                    TINFIN   = SCAL(2,IDPOS)
                    IF (LALLIGN) THEN
                      CALL EFLAMET (DIA(KDROP), HEATCOM, KDROP,
     2                  LMDOUT(KDROP), .TRUE., LLONG, LOUT,
     3                  RHOL, STOICH, TDROP(KDROP),
     4                  TFLAME(KDROP), TINFIN, YOINFIN, AIRNU,
     5                  CPFGAS, HEFF, RHOGAS, TAUP, TTHIRD)
                    ELSE
                      CALL EFLAMET (DIA(KDROP), HEATCOM, KDROP,
     2                  LMDOUT(KDROP), LMDIG(KDROP), LLONG,
     3                  LOUT, RHOL, STOICH, TDROP(KDROP),
     4                  TFLAME(KDROP), TINFIN, YOINFIN, AIRNU,
     5                  CPFGAS, HEFF, RHOGAS, TAUP, TTHIRD)
                    END IF

                    UPPLIMIT = DPOSROOT(AIRNU, BULKVEL, DELTAT,
     2                      DIA(KDROP), DUVEL(KDROP),
     3                      LOUT, TAUP, UFLUID)

C                   UPDATE THE POSITION & VELOCITY OF THE PARTICLE
C  ! STOPED HERE FIXING OUTPUT  !!!!
                    IF (LMDIG(KDROP)) THEN
                      CALL DUPDATE (AIRNU, ALAMDA, CPFGAS,
     2                   DABZERO, DIA(KDROP), DRMASS(KDROP),
     3                   UPPLIMIT, GRAVAC, HEATVAP, HEATCAP,
     4                   HEATCOM, HEFF, KDROP, LMDOUT(KDROP),
     5                   LHEATUP(KDROP), LLAMDA, LOUT, NOD, PEPS,
     6                   PI, RHOGAS, RHOL, STOICH, DUVEL(KDROP),
     7                   DYVELOC(KDROP), TAUP,
     8                   TDARRAY, TDROP(KDROP), TEMPZERO,
     9                   TFLAME(KDROP), TINFIN, TTHIRD, UFLUID,
     1                 YOINFIN, DELTAX,DELTAY,DIANEW,UEND,VEND)
                    ELSE
                      CALL DUPDATE (AIRNU, ALAMDA, CPFGAS,
     2                   DABZERO, DIA(KDROP), DRMASS(KDROP),
     3                   UPPLIMIT, GRAVAC, HEATVAP, HEATCAP,
     4                   HEATCOM, HEFF, KDROP, LMDOUT(KDROP),
     5                   LHEATUP(KDROP),.FALSE., LOUT, NOD, PEPS,
     6                   PI, RHOGAS, RHOL, STOICH, DUVEL(KDROP),
```

```
7                DYVELOC(KDROP), TAUP,
8                 TDARRAY, TDROP(KDROP), TEMPZERO,
9                 TFLAME(KDROP), TINFIN, TTHIRD, UFLUID,
1                YOINFIN, DELTAX,DELTAY,DIANEW,UEND,VEND)
              END IF
              DYPOSIT(KDROP)  = DYPOSIT(KDROP) + DELTAY
              DXPOS(KDROP)    = DXPOS(KDROP)  + DELTAX
              DUVEL(KDROP)    = UEND
              DYVELOC(KDROP)  = VEND
              DIA(KDROP)      = DIANEW
              DROPTIME(KDROP) = DROPTIME(KDROP) + UPPLIMIT

              IF ((DIA(KDROP) .EQ. 0.0) .OR.
2                (DYPOSIT(KDROP) .GE. XN) .OR.
3                (DYPOSIT(KDROP) .LE. X1)   ) THEN
C        **************************
C        FOR OUTPUTTING DROPLET POSITION & TIME
              CALL DROPOUT(DROPTIME(KDROP),
2                  DUVEL(KDROP), DYVELOC(KDROP),
3                  DXPOS(KDROP), DYPOSIT(KDROP),
4                  LMDOUT(KDROP), TNEXT(2))
              CALL DROPOUT(DROPTIME(KDROP),
2                  DUVEL(KDROP), DYVELOC(KDROP),
3                  DXPOS(KDROP), DYPOSIT(KDROP),
4                  LMDSOUT(KDROP), TNEXT(2))
C        **************************
              IF (DIA(KDROP) .EQ. 0.) THEN
                WRITE (LMDOUT(KDROP), 8)
8                  FORMAT (' DROPLET EVAPORATED')
              ELSE

                WRITE (LMDOUT(KDROP),10)
10                 FORMAT ( ' DROP HIT THE WALL')
                WRITE (LMDSOUT(KDROP),10)
              END IF
              LDFINSH(KDROP) = .TRUE.
              LMDROP(KDROP) = .FALSE.
            END IF
          END IF
        END DO
        LTEST = .TRUE.
        DO  KDROP = 1, NODA,1
          IF ( .NOT. LDFINSH(KDROP)) THEN
            LTEST =.FALSE.
```

```
                END IF
              END DO
              IF (LTEST) THEN
                LDROP = .FALSE.
                TNEXT(5) = TLAST(5) + T(NT) + .1
              ELSE
                TLAST(5) = TNEXT(2)
                TNEXT(5) = TLAST(5) + DTDROP
              END IF
              UBAR    = 0.
              DO J1 = IL,IR
                UBAR = UBAR + SCAL(1,J1)
              END DO
              UBAR = UBAR/(IR-IL +1)
C            NOTE, IF EVER USE A NON-UNIFORM GRID, MUST CHANGE THIS
              ELHS    = (IL - 1.5) * DX(1)
              ERHS    = (IR - 0.5) * DX(1)
              DO  KDROP = 1, NODA,1
                IF (LMDROP (KDROP)) THEN
                  IF ((DYPOSIT(KDROP) .LE. ERHS) .AND.
     2                (DYPOSIT(KDROP) .GE. ELHS)  )  THEN
C                    PARTICLE IS INSIDE THE EDDY
C                    DTAU SHOULD NOT BE MULTIPLIED BY BULKVEL/DUVEL !
                    DTAU  = DPARAM * ETAU
                    IDPOS = (DYPOSIT(KDROP) - X1)/DX(1)+1.5
                    UFLUID = SCAL(1,IDPOS)
                    LITT = .TRUE.
                    ITT  = 1
C  CHECK INDEX () FOR FIRST & LAST INDEX VALUES - SHOULD BE 1 & NX.
C   SINCE THE WAY INDX IS STORED IS DETERMINED BY THE AUTHOR OF
THE MAIN
C   PROGRAM THIS HAS TO BE REVISITED EACH TIME THE DROPLET
MODEL IS PUT
C   INTO A NEW PROGRAM.
                    DO WHILE (ITT .LE. (IR-IL+1) .AND. LITT)
                      IF (INDX(ITT) .EQ. IDPOS) THEN
                        INEW = ITT
                        LITT = .FALSE.
                      END IF
                      ITT = ITT + 1
                    END DO

C      *********************
C      TEMP DEBUG TERM
```

```
C                        IF((IENS .EQ. DIENS).AND.(IT .EQ.DIT))THEN
C                            DEBUG = IT + 1
C                          END IF
C       *********************
                      PSEUDOV = (IL+ INEW-1 - IDPOS)*DX(1)/DTAU
                      TINFIN   = SCAL(2,IDPOS)

                      CALL EFLAMET (DIA(KDROP), HEATCOM, KDROP,
     2                    LMDOUT(KDROP), LMDIG(KDROP), LLONG,
     3                    LOUT, RHOL, STOICH, TDROP(KDROP),
     4                    TFLAME(KDROP), TINFIN, YOINFIN, AIRNU,
     5                    CPFGAS, HEFF, RHOGAS, TAUP, TTHIRD)
C
!!!   TEMP. ADDITION IN ORDER TO GET MORE DETAIL ON THE DROPLET
TRAJECTORIES
C
C                      CALL TDROPOUT(DROPTIME(KDROP),
C    2                      DUVEL(KDROP), DYVELOC(KDROP),
C    3                      DXPOS(KDROP), DYPOSIT(KDROP),
C    4                      LMDOUT(KDROP), TNEXT(2),
C    5                      DIA(KDROP), TDROP(KDROP),
C    6                      TFLAME(KDROP))
C                      CALL TDROPOUT(DROPTIME(KDROP),
C    2                      DUVEL(KDROP), DYVELOC(KDROP),
C    3                      DXPOS(KDROP), DYPOSIT(KDROP),
C    4                      LMDSOUT(KDROP), TNEXT(2),
C    5                      DIA(KDROP), TDROP(KDROP),
C    6                      TFLAME(KDROP))
C
C
!!!   END TEMP OUTPUT
C
                      CALL DEUPDAT (AIRNU, DIA(KDROP), DTAU,
     2                    ELHS, EPS, ERHS, IT, LMDOUT(KDROP),
     3                    LOUT, DYPOSIT(KDROP), DUVEL(KDROP),
     4                    DYVELOC(KDROP), TAUP, UBAR, UFLUID,
     5                    PSEUDOV,  DELTAY, DELTAV)
C              INSTANTANEOUS ADJUSTMENT TO THE POSITION &
C              VELOCITY HERE.  NOTE THIS EDDY - DROPLET
C              INTERACTION DOES NOT EFFECT THE X VELOCITY OR POS.
                      DYPOSIT(KDROP) = DYPOSIT(KDROP) + DELTAY
                      DYVELOC(KDROP) = DYVELOC(KDROP) + DELTAV

C
```

```
!!!   TEMP. ADDITION IN ORDER TO GET MORE DETAIL ON THE DROPLET
TRAJECTORIES
C
C                     CALL TDROPOUT(DROPTIME(KDROP),
C    2                     DUVEL(KDROP), DYVELOC(KDROP),
C    3                     DXPOS(KDROP), DYPOSIT(KDROP),
C    4                     LMDOUT(KDROP), TNEXT(2),
C    5                     DIA(KDROP), TDROP(KDROP),
C    6                     TFLAME(KDROP))
C                     CALL TDROPOUT(DROPTIME(KDROP),
C    2                     DUVEL(KDROP), DYVELOC(KDROP),
C    3                     DXPOS(KDROP), DYPOSIT(KDROP),
C    4                     LMDSOUT(KDROP), TNEXT(2),
C    5                     DIA(KDROP), TDROP(KDROP),
C    6                     TFLAME(KDROP))
C                     WRITE (LMDOUT(KDROP),9137) DELTAV, DELTAY
C 9137                 FORMAT (2X, 'DELTAV FROM EDDY = ', E12.6,
C    2                      ' DELTAY = ', E12.6)
C
C
!!!   END TEMP OUTPUT


                     IF ((DYPOSIT(KDROP) .GE. XN) .OR.
     3                     (DYPOSIT(KDROP) .LE. X1)   ) THEN
C                FOR OUTPUTTING DROPLET POSITION & TIME
                     CALL DROPOUT (DROPTIME(KDROP),
     2                     DUVEL(KDROP),DYVELOC(KDROP),
     3                     DXPOS(KDROP), DYPOSIT(KDROP),
     4                     LMDOUT(KDROP), TNEXT(2))
                     CALL DROPOUT (DROPTIME(KDROP),
     2                     DUVEL(KDROP),DYVELOC(KDROP),
     3                     DXPOS(KDROP), DYPOSIT(KDROP),
     4                     LMDSOUT(KDROP), TNEXT(2))
C                 DROP HIT THE WALL
                     WRITE (LMDOUT(KDROP),10)
                     WRITE (LMDSOUT(KDROP),10)
                     LDFINSH(KDROP) = .TRUE.
                     LMDROP(KDROP) = .FALSE.
                  END IF
                END IF
              END IF
            END DO

          LTEST = .TRUE.
```

```
        DO  KDROP = 1, NODA,1
          IF ( .NOT. LDFINSH(KDROP)) THEN
            LTEST =.FALSE.
          END IF
        END DO
        IF (LTEST) THEN
          LDROP = .FALSE.
          TNEXT(5) = TLAST(5) + T(NT) + .1
        END IF
       END IF

C2345678901234567892123456789312345678941234567895123456789612345678971
C     *************************************************************

          call stirevent(nnsc, nx, nsc, il, ke, indx, wrk1,
     1          scal)

C     Accumulate eddy-based statistics


          call eddyhist(il, ke, nnsc, nnx, nx, dx, dts,
     1          pa, indx, scal, neloc, nesize, neleft, neright,
     2          emsd, kounteddy, accdts, accpa, nopa,
     3          uvfl, tvfl, uuvfl)


C     Write out eddy map statistics

          if (ispec(10) .eq. 1 .and. iens .eq. 1) then
            write (lmap,103) tnext(2), edmid, edsize / 2.
 103            format(3(1pe12.4))
           endif

         endif

C     Update the timing

       tlast(2) = tnext(2)
       tnext(2) = tnext(2) + dts

       enddo          ! end of the stirring loop
C2345678901234567892123456789312345678941234567895123456789612345678971
2
C     *************************************************************
```

```
C    JRS'S ADDITION OF A DROPLET TIME LINE
        DO WHILE (TNEXT(5) .EQ. SOONEST (NEVENTS,TNEXT))
          DELTAT = TNEXT(5)-TLAST(5)
         IF (.NOT. LALLST) THEN
           LTEST = .TRUE.
           DO  KDROP = 1, NODA,1
             IF (.NOT. LDSTART(KDROP)) THEN
               LTEST = .FALSE.
             END IF
           END DO
           IF (LTEST) THEN
             LALLST = .TRUE.
           END IF
         END IF
         DO  KDROP = 1, NODA,1
           IF (.NOT. LALLST) THEN
             IF ((.NOT. LDSTART(KDROP)) .AND. (BIRTHT(KDROP)
     2                         .LT. TNEXT(5))) THEN
               LDSTART(KDROP) = .TRUE.
               LMDROP(KDROP)  = .TRUE.
               DELTAT        = TNEXT(5) - BIRTHT(KDROP)
             ELSE
               DELTAT = TNEXT(5)-TLAST(5)
             END IF
           END IF
           IF (LMDROP (KDROP)) THEN
             IF (.NOT. LMDIG(KDROP)) THEN
               IF (DIGNIT(KDROP) .LT. TNEXT (5)) THEN
                 LMDIG(KDROP) = .TRUE.
               END IF
             END IF
           IDPOS   = (DYPOSIT(KDROP) - X1) / DX(1) + 1.5
           UFLUID  = SCAL(1,IDPOS)
           TINFIN  = SCAL(2,IDPOS)

           CALL EFLAMET (DIA(KDROP), HEATCOM, KDROP,
     2            LMDOUT(KDROP), LMDIG(KDROP), LLONG,
     3            LOUT, RHOL, STOICH, TDROP(KDROP),
     4            TFLAME(KDROP), TINFIN, YOINFIN, AIRNU,
     5            CPFGAS, HEFF, RHOGAS, TAUP, TTHIRD)

           UPPLIMIT = DPOSROOT(AIRNU, BULKVEL, DELTAT,
     2              DIA(KDROP), DUVEL(KDROP),
     3              LOUT, TAUP, UFLUID)
```

```
C               THE FIRST TIME THIS IS EXECUTED UPPLIMIT = 0.
C   HENCEFORTH UPPLIMIT IS ALWAYS DTDROP - NOT TRUE WITH
MULTIPLE DROPS
            IF (LMDIG(KDROP)) THEN
             CALL DUPDATE (AIRNU, ALAMDA, CPFGAS,
     2               DABZERO, DIA(KDROP), DRMASS(KDROP),
     3               UPPLIMIT, GRAVAC, HEATVAP, HEATCAP,
     4               HEATCOM, HEFF, KDROP, LMDOUT(KDROP),
     5               LHEATUP(KDROP), LLAMDA, LOUT, NOD, PEPS,
     6               PI, RHOGAS, RHOL, STOICH, DUVEL(KDROP),
     7               DYVELOC(KDROP), TAUP,
     8               TDARRAY, TDROP(KDROP), TEMPZERO,
     9               TFLAME(KDROP), TINFIN, TTHIRD, UFLUID,
     1               YOINFIN, DELTAX,DELTAY,DIANEW,UEND,VEND)
            ELSE
             CALL DUPDATE (AIRNU, ALAMDA, CPFGAS,
     2               DABZERO, DIA(KDROP), DRMASS(KDROP),
     3               UPPLIMIT, GRAVAC, HEATVAP, HEATCAP,
     4               HEATCOM, HEFF, KDROP, LMDOUT(KDROP),
     5               LHEATUP(KDROP),.FALSE., LOUT, NOD, PEPS,
     6               PI, RHOGAS, RHOL, STOICH, DUVEL(KDROP),
     7               DYVELOC(KDROP), TAUP,
     8               TDARRAY, TDROP(KDROP), TEMPZERO,
     9               TFLAME(KDROP), TINFIN, TTHIRD, UFLUID,
     1               YOINFIN, DELTAX,DELTAY,DIANEW,UEND,VEND)
            END IF


            DYPOSIT(KDROP)  = DYPOSIT(KDROP) + DELTAY
            DXPOS(KDROP)    = DXPOS(KDROP)  + DELTAX
            DUVEL(KDROP)    = UEND
            DYVELOC(KDROP)  = VEND
            DIA(KDROP)      = DIANEW
            DROPTIME(KDROP) = DROPTIME(KDROP) + UPPLIMIT
            IF ((DIA(KDROP) .EQ. 0.0) .OR. (DYPOSIT(KDROP)
     2        .GE. XN) .OR. (DYPOSIT(KDROP) .LE. X1)) THEN
C              ************************
C              FOR OUTPUTTING DROPLET POSITION & TIME
             CALL DROPOUT (DROPTIME(KDROP),
     2               DUVEL(KDROP), DYVELOC(KDROP),
     3               DXPOS(KDROP), DYPOSIT(KDROP),
     4               LMDOUT(KDROP), TNEXT(5))
             CALL DROPOUT (DROPTIME(KDROP),
     2          DUVEL(KDROP), DYVELOC(KDROP), DXPOS(KDROP),
```

```
    3                DYPOSIT(KDROP), LMDSOUT(KDROP),TNEXT(5))
C             *************************
          IF (DIA(KDROP) .EQ. 0.) THEN
C           DIA WENT TO ZERO
             WRITE (LMDOUT(KDROP), 8)
          ELSE
C           DROP HIT THE WALL
             WRITE (LMDOUT(KDROP),10)
             WRITE (LMDSOUT(KDROP),10)
          END IF
          LDFINSH(KDROP) = .TRUE.
          LMDROP(KDROP) = .FALSE.
        END IF
      END IF
    END DO

    LTEST = .TRUE.
    DO  KDROP = 1, NODA,1
      IF ( .NOT. LDFINSH(KDROP)) THEN
        LTEST =.FALSE.
      END IF
    END DO
    IF (LTEST) THEN
      LDROP = .FALSE.
      TNEXT(5) = TLAST(5) + T(NT) + .1
    ELSE
      TLAST(5) = TNEXT(5)
      TNEXT(5) = TNEXT(5) + DTDROP
      LDROP = .TRUE.
    END IF
  END DO              ! END DRPOLET LOOP
C    *****************************************************************

C   Ensemble averaging

      do while (tnext(3) .eq. soonest(nevents, tnext))

C     On the first call, zero out the eddy accumulation variables

        if (it .eq. 0) then
          call zoiv(nx, neloc)
          call zoiv(nx, neleft)
          call zoiv(nx, neright)
          call zoiv(nx, nesize)
```

```
          call zorv(nx, emsd)
          call zorv(nx-1, uvfl)
          call zorv(nx-1, tvfl)
          call zorv(nx-1, uuvfl)
          accdts = 0.
          accpa = 0.
          kounteddy = 0
          nopa = 0
C     *************************
C   JRS ADJUSTMENT FOR POSSIBLE ERROR
          ELSE IF (IT .GT. NT) THEN
           PRINT *, 'PROBPROBLEM WITH DTA, DTS, DTM'
           PRINT *, 'IN ENSEMBLE AVERAGING'
           STOP
C     *************************

C     Do the ensemble averaging

          else
           call ensav(lout, it, iens, scal, nnx, nnsc, nnfld, nnt,
     1          nt, nx, nnflx, nfld, nts, neloc, neleft, neright,
     2          emsd, names, tnames, dx, gbeta, dpdx, bulktemp,
     3          kounteddy, nesize, esize, accdts, accpa, nopa,
     4          dtm, dta, uvfl, tvfl, uuvfl, flux, fld, tstat)
          endif




C     Update the timing

          it = it + 1
          tlast(3) = tnext(3)
          tnext(3) = tlast(3) + dta


C   ************************* may move this latter
C   JRS ADJUSTMENT FOR OUTPUTTING DROPLET POSITION & TIME
          IF (LDROP) THEN
            DO  KDROP = 1, NODA,1
             IF (LMDROP (KDROP)) THEN
              CALL DROPOUT (DROPTIME(KDROP),
     2           DUVEL(KDROP), DYVELOC(KDROP), DXPOS(KDROP),
     3           DYPOSIT(KDROP), LMDOUT(KDROP),TNEXT(5))

!!!  temp addition to get more accurate data on traj
```

```
C                  CALL TDROPOUT(DROPTIME(KDROP),
C     2                  DUVEL(KDROP), DYVELOC(KDROP),
C     3                  DXPOS(KDROP), DYPOSIT(KDROP),
C     4                  LMDSOUT(KDROP), TNEXT(2),
C     5                  DIA(KDROP), TDROP(KDROP),
C     6                  TFLAME(KDROP))
!!!  end traj


           END IF
         END DO
        END IF
C     **************************


       enddo              ! end of the ensemble averaging loop


C    Ramp in the new boundary condition over time rspec(19)

       do while (tnext(4) .eq. soonest(nevents, tnext))
        if (rspec(19) .gt. 0.) then
         t1 = t1i +
    1          (t1f - t1i) / rspec(19) * (tnext(4) - rspec(18))
         tn = tni +
    1          (tnf - tni) / rspec(19) * (tnext(4) - rspec(18))
        else
          t1 = t1f
          tn = tnf
        endif
        t1 = min(t1,t1f)
        tlast(4) = tnext(4)
        if (t1 .lt. t1f) then
          tnext(4) = tnext(4) + dtm
        else
          tnext(4) = rspec(21) * 1.1
        endif
        enddo


      enddo      !End of the time stepping loop


C    Field and temporal output

       if (mod(iens,iskip) .eq. 0 .or. iens .eq. nens) then
        include 'op.inc'
        endif
```

```
       rewind(lt)
       write(lt,*), 'Realization ', iens, ' of ', nens
       call flush(lt)

       if (iens .eq. 1) close(lmap)

     enddo      !End of the ensemble loop

C Output

     if (mod(ispec(6), 2) .eq. 1)
1        call profsave(nfld, nnx, nx, nsc, rho, x, fld(1,1,nt))

     call esizeop(nnx, nx, xdom, dx, nt, dta, esize)
C    JRS ADDITION
     CLOSE (LDOUT)
     CLOSE (LMDOUT(1))
     DO ICOUNT = 2, NODA,1

       CLOSE (LMDOUT(ICOUNT))
       CLOSE (LMDOUT(ICOUNT))
     END DO
C    CLOSE (ISEED)
C
     stop
     end
```

```
      SUBROUTINE DEUPDAT (AIRNU, DIAP, DTDROP, ELHS, EPS, ERHS, ITOM,
   2          LDOUT, LOUT, STRTPOS, STRTU, STRTVEL, TAUP, UBAR,
   3                    UFLUID, VFLUID, DELTAY, DELTAV)
```

C   **
!! modified by jrs on 5/29 to get rid on deint stuff
C   WRITTEN BY JRS FOR THE DROPLET MODEL. INTEGRATES THE DROPLET-
C   DRAG LAW THE THE AMOUNT OF TIME STORED IN DELTA TIME.
C   LAST UPDATED 04/28/00 AT 15:50
C   LINEAR DROPLET-DRAG LAW WITH A CORRECTION FACTOR F
C   NOTE: THIS SUBPROGRAM IS USED WHEN THE DROPLET IS IN AN EDDY
C   HENCE, THERE IS A V VELOCITY OF THE FLUID, THERE IS GRAVITY
C   SO THE DIFF. EQN. IS
C   DV'/DT = F/TAUP *(VFLUID - V') - GRAV
C   SINCE EDDIES OCCUR INSTANTANEOUS IN TIME STEP, F, VFLUID, & TAUP
C   ARE CONST. THE PARTICLE EXPERIENCES THE FLUID VELOCITY OF THE CELL
C   WHICH CONTAINS IT DURING THE WHOLE TIME OF INTERACTION BETWEEN
C   THE PARTICLE AND THE EDDY

C   SIGNIFICANT VARIABLE DECLARATIONS:
C   STRT POS = THE INITIAL DROPLET POSITION
C   STRT VEL = THE INITIAL DROPLET VELOCITY
C   STRT U   = THE INITIAL DROPLET VELOCITY IN THE X DIRECTION
C   DTDROP   = TIME CHANGE OVER WHICH TO INTEGRATE
C   DELTA V   = CHANGE IN VELOCITY OF THE PATICLE (VEND HERE)
C   DELTA Y   = CHANGE IN THE POSITION OF THE PARTICLE
C   E LHS   = THE LEFT HAND SIDE (OR LOWER) EDDY END POINT
C   E RHS   = THE RIGHT (OR UPPER) EDDY END POINT
C   CONST Y 3 = COEFFICIENT IN THE D.E.Q. MULTIPLYING VELOCIT ON RHS
C   CONST X 3 = THE X DIRECTION EQUIVALENT TO CONSTY3
C   CONST1,5   = CONVENIENT COEFFICIENT TO MAKE CALCULATIONS FASTER
C   F COEF   = CORRECTION FACTOR SO THE LINEAR DRAG LAW FITS BETTER
C   TAU P   = DROPLET TIME CONSTANT, RELAXATION TIME
C   V FLUID   = VELOCITY OF THE FLUID IN THE Y DIRECTION
C   U FLUID   = VELOCITY OF THE FLUID IN THE X DIRECTION
C   U BAR   = AVERAGE VELOCITY OF THE EDDY IN THE X DIRECTION
C   REN   = REYNOLDS NUMBER

```
C    DIA P     = DIAMETER OF THE PARTICLE
C    GRAV      = THE GRAVITATIONAL CONST.  (+9.8 M/SS)
C    T HAT     = THE TIME FOR THE PARTICLE TO REACH THE EXTREMA
C    Y HAT     = THE Y POSITION AT THE EXTREMA TIME (T HAT)
C    X         = A DUMMY VARIABLE REPRESENTING TIME IN THE FUNC.
STATEMENTS
C    EPS       = SMALLEST DISTANCE IN WHICH MATTERS (I.E. ZERO)
C    HALF EDDY  = HALF THE EDDY LENGTH
C    X NEW P   = X POSITION OF THE DROPLET IN THE MOVING CO-
ORDINATE SYSTEM
C    T MIN     = THE MINIMUM INTERACTION TIME BETWEEN THE EDDY 7
DROP

     IMPLICIT NONE
     REAL   AIRNU, BC
     REAL   CON3, CON4, CON7
     REAL   CONST1, CONST2,  CONST4, CONST5
     REAL   CONST6, CONST7, CONSTX3, CONSTY3
     REAL   DELTAT, DELTAY, DELTAV, DIAP
     REAL   DPOSIT, DTDROP, DVELOC
     REAL   ELHS, EPS, EPSDIS, ERHS
     REAL   FXCOEF, FYCOEF, FMID, FXL, FXR, FYL, FYR, GRAV
     REAL   HALFEDDY
     INTEGER  ITOM, ITT
     LOGICAL LABOVE, LITT
     INTEGER LDOUT, LOUT
     REAL   POSITION, RENX, RENY, STRTPOS, STRTU, STRTVEL, TAUP
     REAL   TMID, TMIN, TNEW
     REAL   TXHAT, TXL, TXR, TYHAT, TYL, TYR
     REAL   UBAR, UFLUID
     REAL   VELOCITY, VFL, VFLUID, X
     LOGICAL XEXTREMA
     REAL   XHATP, XNEWP, XPOSITP
     LOGICAL YEXTREMA
     REAL   YHAT, YNEW

!! TEMP ADDITON FOR MORE DETAILED OUTPUT
C    REAL   CY4, CY7
C    INTEGER ITEMP
C    REAL   TDT, TDV, TDY, TTIME, TX, TY
C    LOGICAL XEXTRIN, YEXTRIN
!! END TEMP ADDITON

C    DEFINE FUNCTIONS FOR VELOCITY & POSITION
```

```
      DVELOC(VFL, CON3, X) = VFL * (1. - EXP(-CON3*X))
      DPOSIT(VFL, CON3, X) = VFL*X-VFL/CON3*(1. - EXP(-CON3*X))
      POSITION(BC,CON3,CON4,CON7,X) = BC + CON4 * X + CON7 / CON3 *
     2                   (EXP(-CON3*X) -1)
      XPOSITP(CON3,CON4,CON7,X) = CON4/CON3*(1.-EXP(-CON3*X))-CON7*X
C     USE THE ANALYTIC SOLUTION TO THE CONST. COEFICIENT
C     DIFFERENTIAL EQUATION TO COMPUTE THE END POINT
C     NOTE: GRAVITAIONAL ACCELERATION IN UNITS OF ---
!! TEMP. ADD A FLLAG TO SHOW THAT IT REACHED AN EXTREMA INSIDE
THE EDDY
C         YEXTRIN = .FALSE.
C         XEXTRIN = .FALSE.
!! END TEMP ADDITION



C     SINCE LINEAR, BREAKS DOWN INTO X & Y COMPONENTS:  Re CAN BE
C     DIFFERENT IN THE X & Y DIRECTIONS

      RENY    = DIAP * ABS(STRTVEL - VFLUID) / AIRNU
      IF (RENY .LE. 1.0) THEN
C    STOKES LAW
        FYCOEF = 1.0
      ELSE IF (RENY .LE. 1000) THEN
C    CORRECTION FACTOR
        FYCOEF  =  1.0 + 0.15 * (RENY) ** 0.687
      ELSE
        WRITE (LDOUT,*) ' PARTICLE ReY > 1000'
        WRITE (LDOUT,*) ' STOPPED IN DEUPDAT', RENY
        WRITE (LOUT,*)  ' PARTICLE ReY > 1000'
        WRITE (LOUT,*)  ' STOPPED IN DEUPDAT', RENY
        STOP
      END IF

      RENX    = DIAP * ABS(STRTU - UFLUID) / AIRNU
      IF (RENX .LE. 1.0) THEN
C    STOKES LAW
        FXCOEF = 1.0
      ELSE IF (RENX .LE. 1000) THEN
C    CORRECTION FACTOR
        FXCOEF  =  1.0 + 0.15 * (RENX) ** 0.687
      ELSE
        WRITE (LDOUT,*) ' PARTICLE ReX > 1000'
        WRITE (LDOUT,*) ' STOPPED IN DEUPDAT', RENX
        WRITE (LOUT,*)  ' PARTICLE ReX > 1000'
```

```
      WRITE (LOUT,*)  ' STOPPED IN DEUPDAT', RENX
      STOP
    END IF

    CONSTY3 = FYCOEF / TAUP
    CONSTX3 = FXCOEF / TAUP
C  **********************
C  THIS TAKES INTO ACCOUNT THE POSSIBILITY OF PARTICLES ON
C  THE EDGE OF THE EDDY AND BEING TAKEN OUT BY ITS OWN VELOCITY
C  **********************
    IF ((((ERHS-EPS) .LE. STRTPOS) .AND. (STRTVEL .GT. 0.)) .OR.
   2   (((ELHS+EPS) .GE. STRTPOS) .AND. (STRTVEL .LT. 0.)) .OR.
   3             (VFLUID .EQ. 0.)) THEN
C      IF THE PARTICLE IS EPSILON CLOSE TO THE EDDY BORDER AND
GOING
C      IN THE DIRECTION TO TAKE IT OUT OF THE EDDY THEN THERE IS NO
C      INSTANTANEOUS DROPLET-EDDY INTERATION.  ALSO IF THERE IS NO
C      INITIAL PERTURBATION VELOCITY (I.E. VFLUID) THEN THERE IS NO
C      INTANTANEOUS EDDY EFFECT
    DELTAY = 0.0
    DELTAV = 0.0
C  **********************
C  VELOCITY VARIATION AND POSITION CHANGE IS SET TO ZERO.  RETURN
TO
C  CALLING ROUTINE
C  **********************

    ELSE
C    AT THIS POINT, PARTICLE IS "WELL" INSIDE EDDY.  CHECK FOR
EXTREMA
C   NEW ADDITION TO TAKE CARE OF EXTREMA - ADDED ON 10/4
    YEXTREMA = .FALSE.
    LITT   = .TRUE.
    TMIN   = DTDROP
    CONST4 = VFLUID - GRAV  / CONSTY3
    CONST7 = CONST4 - STRTVEL
C    DO NOT LOOK FOR AN EXTREMA IF THE STARTING PARTICLE
VELOCITY (STRTVEL)
C    IS NEAR ZERO; THE STRTVEL MUST BE OF OPPOSITE SIGN OF CONST4
IN ORDER
C    FOR THERE TO BE AN EXTREEMA IN REAL TIME.  IF CONST4 IS NEAR
ZERO THEN
C    THERE IS VIRTUALLY NO DRIVING FORCE TO CHANGE THE PARTICLE
VELOCITY
```

```
       IF ((ABS(STRTVEL) .GT. EPS/1000.) .AND.
   2      (STRTVEL * CONST4 .LT. 0.)) THEN
        IF (ABS(CONST4) .GT. EPS/1000.) THEN
         CONST6  = ABS(CONST7 / CONST4)
         IF (CONST6 .GT. 1.) THEN            !IS THIS ALWAYS TRUE????
          TYHAT =  ALOG(CONST6) / CONSTY3
          YHAT = POSITION(STRTPOS,CONSTY3,CONST4,CONST7,TYHAT)
          IF (TYHAT .LE. DTDROP) THEN
            YEXTREMA = .TRUE.
C            YEXTREMA IS TRUE IF AND ONLY IF THE EXTREMA FALLS
C            DURING THE LIFE TIME OF THE EDDY
          END IF
        END IF
       END IF
      END IF
       IF (YEXTREMA .AND. (YHAT .GT. (ERHS+EPS))) THEN
C    PARTICLE IS OUTSIDE OF THE EDDY BEFORE IT REACHES ITS
EXTREMA
C    (MAXIMUM POSITION)
C    RE-ADJUST DELTA TIME  FOR THE INTEGRAL USING REGULA FALSI
METHOD
C    NOTE: VELOCITY IS THE DERIVATIVE OF DISTANCE
        LABOVE = .TRUE.
        TYR  = TYHAT
        FYR  = YHAT - ERHS
        TYL  = 0.0
        FYL  = STRTPOS - ERHS
        TMID = -TYHAT * FYL / (FYR - FYL)
       ELSE IF (YEXTREMA .AND. (YHAT .LT. (ELHS-EPS))) THEN
C    PARTICLE IS BELOW THE EDDY BEFORE THE EDDY ENDS

        LABOVE = .FALSE.
        TYR  = TYHAT
        FYR  = YHAT - ELHS
        TYL  = 0.0
        FYL  = STRTPOS - ELHS
        TMID = -TYHAT * FYL / (FYR - FYL)

      ELSE

       YNEW = POSITION(STRTPOS,CONSTY3,CONST4,CONST7,DTDROP)
       IF (((ERHS+EPS) .GE. YNEW).AND.((ELHS-EPS) .LE. YNEW))THEN
```

```
C          PARTICLE ENDS UP IN THE EDDY AT THE END OF THE EDDY
LIFETIME
C     PARTICLE REACHES Y EXTREMA INSIDE THE EDDY, IF IT HAS AN
EXTREMA!
C     ALSO STILL IN THE EDDY AT END OF EDDY LIFETIME (REDUNDANT)
!! TEMP. ADD A FLLAG TO SHOW THAT IT REACHED AN EXTREMA INSIDE
THE EDDY
C          IF (YEXTREMA) THEN
C             IF (ITOM .EQ. 23) THEN
C              WRITE (LDOUT,9157) ELHS, ERHS, STRTPOS, CONSTY3,
C    2             CONST4, CONST7, DTDROP, VFLUID, TYHAT, YHAT
C 9157          FORMAT (1X, 'Y BOT= ', E16.10, ' Y TOP= ',
C    3          E16.10, ' STRTPOS= ', E16.10, ' CY3= ', E16.10,
C    4          /, ' CY4= ', E16.10, ' CY7= ', E16.10,
C    5           ' DTDROP= ', E16.10, ' VFLUID= ', E16.10,/,
C    6           ' TYHAT= ', E16.10, ' YHAT= ', E16.10,
C    7            ' ITOM = 23')
C          CY4 = CONST4
C          CY7 = CONST7

C          END IF
C          YEXTRIN = .TRUE.
CC            YEXTRIN IS TRUE IFF THE EXTREMA FALLS WITH IN THE EDDY
C        END IF
!! END TEMP ADDITION


          DELTAY = DPOSIT(VFLUID, CONSTY3, DTDROP)
          DELTAV = DVELOC(VFLUID, CONSTY3, DTDROP)
         LITT = .FALSE.
       ELSE
         IF ((ERHS+EPS) .LT. YNEW) THEN
           LABOVE = .TRUE.
           IF (YEXTREMA) THEN
             TYR  = DTDROP
             FYR  = YNEW - ERHS
             TYL  = TYHAT
             FYL  = YHAT - ERHS
             TMID = (TYL*FYR-TYR * FYL) / (FYR - FYL)
           ELSE
             TYR  = DTDROP
             FYR  = YNEW - ERHS
             TYL  = 0.0
             FYL  = STRTPOS - ERHS
```

```
        TMID = -TYR * FYL / (FYR - FYL)
      END IF
    ELSE
      LABOVE = .FALSE.
      IF (YEXTREMA) THEN
        TYR  = DTDROP
        FYR  = YNEW - ELHS
        TYL  = TYHAT
        FYL  = YHAT - ELHS
        TMID = (TYL*FYR-TYR * FYL) / (FYR - FYL)
      ELSE
        TYR  = DTDROP
        FYR  = YNEW - ELHS
        TYL  = 0.0
        FYL  = STRTPOS - ELHS
        TMID = -TYR * FYL / (FYR - FYL)
      END IF
    END IF
  END IF
END IF
C      --------------------------
ITT  = 1

DO WHILE ((LITT) .AND. (ITT .LE. 55))
  IF (LABOVE) THEN
    FMID=POSITION(STRTPOS,CONSTY3,CONST4,CONST7,TMID)-ERHS
  ELSE
    FMID=POSITION(STRTPOS,CONSTY3,CONST4,CONST7,TMID)-ELHS
  END IF
  IF (ABS(FMID) .LE. EPS) THEN
    LITT = .FALSE.
    DELTAY = DPOSIT(VFLUID, CONSTY3, TMID)
    DELTAV = DVELOC(VFLUID, CONSTY3, TMID)
    TMIN = TMID
  ELSE
    IF (FMID * FYR .LT. 0.) THEN
      TYL = TMID
      FYL = FMID
    ELSE
      TYR = TMID
      FYR = FMID
    END IF
    TMID = (TYL * FYR - TYR* FYL)/ (FYR-FYL)
  END IF
```

```
      ITT = ITT + 1
     END DO
     IF (LITT) THEN
       WRITE (LDOUT,*) ' REGULA FALSI DID NOT CONVERGE (Y) IN 55 '
       WRITE (LDOUT,*) 'ITTERATIONS, DROPLET IN DEUPDAT'
       WRITE (LDOUT,*) TYL, TMID, TYR
       WRITE (LDOUT,*) FYL, FMID, FYR
       WRITE (LDOUT,*) YEXTREMA, LABOVE, ITOM
       WRITE (LDOUT,*) TYHAT, YHAT, DTDROP, YNEW
       WRITE (LOUT,*)  ' REGULA FALSI DID NOT CONVERGE (Y) IN 55 '
       WRITE (LOUT,*)  'ITTERATIONS, DROPLET IN DEUPDAT'
       DELTAY = DPOSIT(VFLUID, CONSTY3, TMID)
       DELTAV = DVELOC(VFLUID, CONSTY3, TMID)
       TMIN = TMID
     END IF
C********************************************************STOP
HERE
     XEXTREMA = .FALSE.
     LITT    = .TRUE.
     CONST4  = STRTU - UFLUID
     CONST7  = UBAR  - UFLUID
     CONST2  = UBAR - STRTU
     CONST1  = CONST2 * CONST7
C     EDDY IS A DISTANCE L IN EACH DIRECTION (HENCE HALFEDDY IS L)
     HALFEDDY = (ERHS - ELHS)
C     DO NOT LOOK FOR AN EXTREMA IF THE STARTING PARTICLE
VELOCITY (STRTU)
C     RELATIVE TO THE U BAR IS NEAR ZERO OR IF THE U FLUID RELATIVE
TO
C     U BAR IS NEAR ZERO -- THERE IS NO DRIVING FORCE
C     UBAR - STRTU MUST BE OF OPPOSITE SIGN OF UBAR - UFLUID IN
ORDER
C     FOR THERE TO BE AN EXTREEMA IN REAL TIME.

C     !!!!  WHAT TO DO ABOUT EPSILON ????????  EPS IS A DISTANCE
MINIMUM !!

     IF ((CONST1 .LT. 0.) .AND. (ABS(CONST7) .GT. EPS) .AND.
   2    (ABS(CONST2) .GT. EPS) .AND. (ABS(CONST4) .GT. EPS)) THEN
       CONST6  = CONST4 / CONST7
       IF (CONST6 .GT. 1.) THEN              !IS THIS ALWAYS TRUE????
         TXHAT =  ALOG(CONST6) / CONSTX3
         XHATP  = XPOSITP(CONSTX3,CONST4,CONST7,TXHAT)
         IF (TXHAT .LE. TMIN) THEN
```

```
            XEXTREMA = .TRUE.
C            XEXTREMA IS TRUE IFF THE EXTREAMA FALLS BEFORE THE
EDDY ENDS
         END IF
       END IF
     END IF
     IF (XEXTREMA .AND. ((XHATP-HALFEDDY) .GT. (EPS))) THEN
C    PARTICLE IS OUTSIDE OF THE EDDY BEFORE IT REACHES ITS
EXTREMA
C    (MAXIMUM POSITION)
C    RE-ADJUST DELTA TIME  FOR THE INTEGRAL USING REGULA FALSI
METHOD
C    NOTE: VELOCITY IS THE DERIVATIVE OF DISTANCE; ALSO LABOVE
MEANS
C    TO THE RIGHT OF THE EDDY IN THE X DIRECTION
       LABOVE = .TRUE.
       TXR  = TXHAT
       FXR  = XHATP - HALFEDDY
       TXL  = 0.0
       FXL  = - HALFEDDY
       TMID = -TXHAT * FXL / (FXR - FXL)
     ELSE IF (XEXTREMA .AND. ((XHATP+HALFEDDY) .LT. (-EPS))) THEN
       LABOVE = .FALSE.
       TXR  = TXHAT
       FXR  = XHATP + HALFEDDY
       TXL  = 0.0
       FXL  = HALFEDDY
       TMID = -TXHAT * FXL / (FXR - FXL)
     ELSE
C     PARTICLE DOES NOT GO OUT OF THE EDDY IN THE X DIRECTION AT
THE
C     EXTREMA, BUT CAN STILL GO OUT BY THE END OF THE EDDY
LIFETIME

!! TEMP. ADD A FLLAG TO SHOW THAT IT REACHED AN EXTREMA INSIDE
THE EDDY
C        IF (XEXTREMA) THEN
C          XEXTRIN = .TRUE.
CC           XEXTRIN IS TRUE IFF THE X EXTREMA FALLS WITH IN THE EDDY
LIFETIME
C          IF (YEXTRIN) THEN
C            WRITE (LDOUT,9137) STRTU, UBAR, UFLUID, CONSTX3,
C    2          CONST4, CONST7, TXHAT, XHATP, HALFEDDY
C 9137      FORMAT (1X, 'STRTU= ', E16.10, ' UBAR= ', E16.10,
```

```
C    2            ' UFLUID= ', E16.10, ' CX3= ', E16.10,/,
C    3            ' CX4= ', E16.10, ' CX7= ', E16.10,
C    4            ' TXHAT= ', E16.10, ' XHATP= ', E16.10,/,
C    5            ' HALFEDDY= ', E16.10 )
C            WRITE (LDOUT, 9141) 0.0, 0.0, STRTPOS, 0.0, 0.0
C 9141       FORMAT (4X, ' TIME ', 12X, ' X ', 12X, ' Y ', 12X,
C    2            ' DELAT Y ', 7X, ' DELTA V ',/, 1X,
C    3            5(E15.9, 1X))
C            TDT = DTDROP/250.0
C            DO ITEMP = 1, 250, 1
C              TTIME = TDT*FLOAT(ITEMP)
C              TX   = XPOSITP(CONSTX3, CONST4, CONST7, TTIME)
C              TY   = POSITION(STRTPOS, CONSTY3, CY4, CY7,
C    2             TTIME)
C              TDY  = STRTPOS - TY
C              TDV  = DVELOC(VFLUID, CONSTY3, TTIME)
C
C              WRITE (LDOUT,9145) TTIME, TX, TY, TDY, TDV
C 9145          FORMAT (1X, 5(E15.9, 1X))
C            END DO
C          END IF
C        END IF
!! END TEMP ADDITION


        XNEWP = XPOSITP(CONSTX3,CONST4,CONST7,TMIN)
        IF ((XNEWP-HALFEDDY) .GT. EPS) THEN
          LABOVE = .TRUE.
          IF (XEXTREMA) THEN
            TXR  = TMIN
            FXR  = XNEWP - HALFEDDY
            TXL  = TXHAT
            FXL  = XHATP - HALFEDDY
            TMID = (TXL*FXR-TXR * FXL) / (FXR - FXL)
          ELSE
            TXR  = TMIN
            FXR  = XNEWP - HALFEDDY
            TXL  = 0.0
            FXL  = - HALFEDDY
            TMID = -TXR * FXL / (FXR - FXL)
          END IF
        ELSE IF((XNEWP+HALFEDDY) .LT. -EPS) THEN
          LABOVE = .FALSE.
          IF (XEXTREMA) THEN
            TXR  = TMIN      !NEEDS WORK HERE
```

```fortran
      FXR  = XNEWP + HALFEDDY
      TXL  = TXHAT
      FXL  = XHATP + HALFEDDY
      TMID = (TXL*FXR-TXR * FXL) / (FXR - FXL)
    ELSE
      TXR  = TMIN
      FXR  = XNEWP + HALFEDDY
      TXL  = 0.0
      FXL  = HALFEDDY
      TMID = -TXR * FXL / (FXR - FXL)
    END IF
  ELSE
    LITT = .FALSE.
  END IF
END IF
C     ************************
ITT  = 1
DO WHILE ((LITT) .AND. (ITT .LE. 55))
  IF (LABOVE) THEN
    FMID=XPOSITP(CONSTX3,CONST4,CONST7,TMID)-HALFEDDY
  ELSE
    FMID=XPOSITP(CONSTX3,CONST4,CONST7,TMID)+HALFEDDY
  END IF
  IF (ABS(FMID) .LE. EPS) THEN
    LITT = .FALSE.
    DELTAY = DPOSIT(VFLUID, CONSTY3, TMID)
    DELTAV = DVELOC(VFLUID, CONSTY3, TMID)
    TMIN   = TMID
  ELSE
    IF (FMID * FXR .LT. 0.) THEN
      TXL = TMID
      FXL = FMID
    ELSE
      TXR = TMID
      FXR = FMID
    END IF
    TMID = (TXL * FXR - TXR * FXL)/(FXR - FXL)
  END IF
  ITT = ITT + 1
END DO
IF (LITT) THEN
  WRITE (LDOUT,*) ' REGULA FALSI DID NOT CONVERGE (X) IN 55'
  WRITE (LDOUT,*) ' ITTERATIONS DROPLET IN DEUPDAT'
  WRITE (LDOUT,*) TXL, TMID, TXR
```

```
      WRITE (LDOUT,*) FXL, FMID, FXR
      WRITE (LDOUT,*) XEXTREMA, LABOVE, ITOM
      WRITE (LOUT,*)  ' REGULA FALSI DID NOT CONVERGE (X) IN 55 '
      WRITE (LOUT,*)  'ITTERATIONS, DROPLET IN DEUPDAT'
      DELTAY = DPOSIT(VFLUID, CONSTY3, TMID)
      DELTAV = DVELOC(VFLUID, CONSTY3, TMID)
      TMIN  = TMID
    END IF
   END IF
!! TEMP. ADD A FLLAG TO SHOW THAT IT REACHED AN EXTREMA INSIDE
THE EDDY
C       IF (ITOM .EQ. 23) THEN
C         WRITE (LDOUT,9159) TMIN
C 9159      FORMAT (1X, 'TMIN= ', E16.10)
C         TY = POSITION(STRTPOS, CONSTY3, CY4, CY7, TMIN)
C         TX = XPOSITP(CONSTX3, CONST4, CONST7, TMIN)
C         WRITE (LDOUT,9145) TMIN, TX, TY, DELTAY, DELTAV
C       END IF
!! END TEMP ADDITION
   RETURN
C*************************************************************STOP
HERE
   END
```

```
      SUBROUTINE DROPINIT(DX, NENS, NEVENTS, NOD, NNX, NX, ALAMDA,
   2    BIRTHT, BULKVEL, DABZERO, DIA, DIGNIT, DPARAM, DROPTIM,
   3    DPOSIT, DTDROPF, DUVEL, DXPOS, STRTVEL, EPS, GRAVAC,
   4  HEATCAP, HEATCOM, HEATVAP, HOLD, LDOUT, LDROP, LDSTART,
LLAMDA,
   5    LLONG, LMDROP, NODA, OUTFIL, PEPS, PI, RHOL, STOICH, TDROP,
   6    TEMPBP, TEMPZERO, TFLAME, YOINFIN)


C    ***********************************************************
C    LAST UDATED 03/30/00  @ 11:30      for ignit  FOR EVAP CASE, MULTI
DROPS
C  ! SHORT OUTPUT NOT YET AVAILABLE !!
C
C    WRITTEN BY JRS
C    THIS CONTAINS DATA FOR THE TYPE C - NOMINAL DROPLET
CONDITIONS
C    225 MICRON DIAMETER DROPLET
C    6.5 M/S   INJECTION SPEED
C    30 DEGREE INJECTION ANGLE
C    130 DROPLET DIAMETER SPACING
C    USE DENSITY OF AIR AT 1300 K, 1 ATM (KG/M**3)
C    USE VISCOSIITY OF AIR 1300 K, 1 ATM {Pa*S = KG/(M*S)}


C    RE     = REYNOLDS NUMBER
C    AREA P  = AREA OF THE PARTICLE (M**2)
C    A MU    = THE AIR VISCOSITY, MU (Pa*S)
C    A NU    = GAS PHASE (AIR) KINEMATIC VISCOSITY
C    STRT VEL = THE STARTING VELOCITY OF THE PARTICLE
C    GRAV AC  = GRAVITAIONAL ACCELERATION {M/(S**2)}
C    RHO A    = DENSITY OF THE AIR
C    RHO L    = DENSITY OF THE LIQUID DROPS (KG/M**3) FROM REPORT PG
43
C    TAU P   = PARTICLE RELAXATION TIME
C    D PARAM  = DROPLET PARAMETER TO ADJUST THE EDDY TAU
C    BIRTH T  = TIME OF BIRTH OF THE PARTICLE
C    L DROP   = LOGICAL VARIABLE FOR DROPLET
C    BULK VEL = BULK FLUID VELOCITY
C    DROP TIM = TIME AT WHICH THE DROPLET IS BORN INTO ODT,
ASSUMED 0
C    HEAT CAP = MEAN HEAT CAPACITY OF THE LIQUID [J/KG/K]
C    HEAT COM = MEAN HEAT OF COMBUSTION OF THE LIQUID [J/KG]
C    HEAT VAP = MEAN HEAT OF VAPORIZATION OF THE LIQUID [J/KG]
C    TEMP BP  = MEAN BOILING POINT TEMP. OF THE LIQUID  [K]
C    STOICH   = STOICHIOMETRIC FUEL-TO-OXYGEN MASS RATIO
```

```
C    D RATIO  = DENSITY RATIO OF GAS / LIQUID
C    B MAS T  = MASS TRANSFER NO. CALLED B
C    SCHMIDT  = THE SCHMIDT NUMBER FOR THE GAS PHASE
C    Y0 INFIN = MASS FRACTION OF OXYGEN IN THE FLUE GASS
C    T FLAME  = INITIAL GUESS FOR THE FLAME TEMPERATURE AROUND
THE DROP
C    T DROP   = INITIAL DROP TEMPERATURE
C    N O D A  = ACTUAL NUMBER OF DROPS IN THIS SIMULATION

    IMPLICIT NONE
    REAL    ALAMDA, AMU, BIRTHT(NOD)
    REAL    BULKVEL
    REAL    DABZERO, DIA(NOD)
    REAL    DIGNIT(NOD), DPARAM, DPOSIT(NOD)
    REAL    DROPTIM(NOD), DTDROPF, DTM, DUVEL(NOD)
    REAL    DX(NNX), DXPOS(NOD)
    REAL    EPS, EPSF
    REAL    GRAVAC, HEATCAP, HEATCOM, HEATVAP, HOLD
    INTEGER I, IHOLD, ILAMDA, ILONG, INP, LDOUT
    LOGICAL LDROP, LDSTART(NOD), LLAMDA, LLONG, LMDROP(NOD)
    INTEGER NENS, NEVENTS, NOD, NODA, NNX, NX
    CHARACTER*9 OUTFIL(NOD)
    REAL    PEPS, PI
    REAL    RHOA, RHOL
    REAL    STOICH, STRTVEL(NOD)
    REAL    TEMPBP, TEMPZERO, TDROP(NOD), TFLAME(NOD)
    REAL    TLAST(NEVENTS), TNEXT(NEVENTS)
    REAL    VELOCITY, YOINFIN


    CALL LUNEXT(INP)
    OPEN (UNIT=INP,FILE='jevap.inp', STATUS = 'OLD')
    READ (INP,10)
    READ (INP,10)
    READ (INP,10) DPOSIT(1)
 10  FORMAT (1X, F15.5)
    READ (INP,10) STRTVEL(1)
    READ (INP,10) DIA(1)
    READ (INP,10) RHOL
    READ (INP,10) RHOA   ! ?????
    READ (INP,10) AMU    ! ?????
    READ (INP,10) EPSF
    READ (INP,10) DPARAM
    READ (INP,10) DTDROPF
```

```
      READ (INP,10) BIRTHT(1)
      READ (INP,10) DUVEL(1)
      READ (INP,10) DXPOS(1)
      READ (INP,10) BULKVEL
      READ (INP,10) DROPTIM(1)
      READ (INP,10) GRAVAC
      READ (INP,10) TEMPBP
      READ (INP,10) HEATCAP
      READ (INP,10) HEATVAP
      READ (INP,10) HEATCOM
      READ (INP,10) STOICH
      READ (INP,10) ALAMDA
      READ (INP,10) YOINFIN
      READ (INP,10) TFLAME(1)
C     DABZERO IS THE DIFFUSIVITY OF THE REPRESENTATIVE FUEL
C     COMPONENT IN AIR AT THE TEMPERATURE [K] TEMPZERO
      READ (INP,10) DABZERO
      READ (INP,10) TEMPZERO
      READ (INP,10) TDROP(1)
      READ (INP,10) PEPS
      READ (INP,20) NODA
 20   FORMAT (1X, I2)
      READ (INP,22) ILAMDA
 22   FORMAT (1X,I1)
      READ (INP,22) ILONG
      READ (INP,10) DIGNIT(1)


C BULK VELOCITY = 0.8344 M/S  AS COMPUTED FROM MULHOLAND ET. AL.
C    *************************************************************
      WRITE  (LDOUT, 25) DIA(1), DROPTIM(1), BIRTHT(1), BULKVEL,
     2           DUVEL(1), STRTVEL(1)
 25   FORMAT (1X, 'INITIAL DIA = ', E10.4, ' Age of the drop when',
     2    ' it is born into ODT = ', E10.4 ,/,1X, 'Time at which the',
     3    ' droplet appears in the ODT domain = ', E12.6, /, 1X,
     4          'BULK FLUID VELOCITY = ', E12.6, ' U = ', E12.6,
     5               ' V = ', E12.6)
      WRITE  (LDOUT, 30) DXPOS(1), DPOSIT(1)
 30   FORMAT (1X,'INITIAL X POSITION = ',E12.6, ' INITIAL Y = ',E12.6)
      WRITE  (LDOUT, 40) RHOL, RHOA, AMU
 40   FORMAT (1X, 'DENSITY OF LIQUID=',E10.4,' AIR: DENSITY = ',
     2          E10.4, ' VISCOSITY = ',E10.4)
      WRITE  (LDOUT, 50) DPARAM, NENS, EPSF, DTDROPF
 50   FORMAT (1X,'PARAMETER FOR ADJUSTING THE PSEUDO TIME TO
DROPLET',
```

```
    2  ' TIME IS ', E12.6, /, 1X,'No. of ensambles is ', I7, 1X,
    3  'FACTOR FOR EPSILON,', ' SMALLEST DISTANCE IN WHICH' ,/, 1X,
    4  ' THE ODT IS CONCERNED = ', E10.4, /, 1X, 'FACTOR FOR ',
    5  'COMPUTING DROPLET TIME STEP FROM MOLECULAR STEP (dtm) = ',
    6        E10.4)
     WRITE  (LDOUT, 60) GRAVAC, TEMPBP, HEATCAP, HEATCOM, HEATVAP
 60  FORMAT (1X, 'GRAVITATIONAL ACCELERATION = ', E12.6, ' BOILING',
    2   ' PT. = ', E10.4, /, 1X, 'HEAT CAP. = ', E10.4, ' HEAT OF',
    3   ' COMBUST. = ', E10.4, ' HEAT OF VAPOR. = ', E10.4)
     WRITE  (LDOUT, 70) STOICH, ALAMDA, YOINFIN, TFLAME(1)
 70  FORMAT (1X,'FUEL TO OXYGEN MASS RATIO = ', E10.4, ' BURNING ',
    2       'PARAM. = ', E15.8, /,1X, 'MASS FRACTION OF O2 IN FLUE',
    3       ' GAS = ', E10.4, ' GUESS FLAME SHEET ',
    4       'TEMPERATURE ', E11.5)
     WRITE (LDOUT,80) DABZERO, TEMPZERO
 80  FORMAT (1X, 'DIFFUSIVITY OF FUEL INTO AIR IS ', E15.7, ' SQUARE',
    2     ' METERS/SECOND' ,/, '    AT ', E12.6, ' KELVIN' )
     WRITE (LDOUT,90) TDROP(1)
 90  FORMAT (1X, 'STARTING TEMPERATURE OF THE LIQUID DROP = ',
    2         E15.7, ' KELVIN' )
     WRITE (LDOUT,95) NX
 95  FORMAT (1X,' NX= ', I6)
     PI     = ACOS(-1.)
C
     IF (ILAMDA .EQ. 1) THEN
       LLAMDA = .TRUE.
     ELSE
       LLAMDA = .FALSE.
     END IF

C !!  FOR NOW, ONLY USE LONG OUTPUT  !!!
C    IF (ILONG .EQ. 1) THEN
       LLONG = .TRUE.
C    ELSE
C       LLONG = .FALSE.
C    END IF
     LDROP   = .FALSE.

     EPS = EPSF * DX(1)     !ONE-TENTH OF A GRID POINT IS SMALL

C    FOR EACH ADDITIONAL DROP, READ IN THE PERTENANT INFO.

     DO I = 2,NODA,1
       READ (INP,130) OUTFIL(I)
```

244

```fortran
130   FORMAT (1X, A9)
      READ (INP,10) DPOSIT(I)
      READ (INP,10) STRTVEL(I)
      READ (INP,10) DIA(I)
      READ (INP,10) BIRTHT(I)
      READ (INP,10) DUVEL(I)
      READ (INP,10) DXPOS(I)
      READ (INP,10) DROPTIM(I)
      READ (INP,10) TDROP(I)
      READ (INP,10) TFLAME(I)
      READ (INP,10) DIGNIT(I)
    END DO
    HOLD  = BIRTHT(1)
    IHOLD = 1
    DO I=1,NODA,1

      IF (BIRTHT(I) .LT. HOLD) THEN
        HOLD = BIRTHT(I)
        IHOLD = I
      END IF
    END DO
    DO I=1,NODA,1

      IF (BIRTHT(I) .EQ. HOLD) THEN
        LMDROP(I)  = .TRUE.
        LDSTART(I) = .TRUE.
      ELSE
        LMDROP(I)  = .FALSE.
        LDSTART(I) = .FALSE.
      END IF

    END DO
    LMDROP(IHOLD)  = .TRUE.
    LDSTART(IHOLD) = .TRUE.

    RETURN
    END
```

```
      SUBROUTINE DROPSTART (BIRTHT, DIAI, DTDROPF, DTIMEI, DTM,
DUVELI,
   2 DXPOSI, DYPOSITI, DYVELOCI, HOLD, IENS, LDOUT, LDSTARTI, LLONG,
   3    LMDOUT, LMDROPI, NEVENTS, NOD, NODA, PI, RHOL, TDROPI,
   4    DIA, DRMASS, DROPTIME, DTDROP, DUVEL, DXPOS, DYPOSIT,
   5    DYVELOC, LALLIGN, LALLST, LDFINSH, LDROP, LDSTART,
   6    LHEATUP, LMDIG, LMDROP, TDARRAY, TDROP, TLAST, TNEXT)
C    ***************************************************************

C    LAST UPDATED     03/30/00   AT 11:30
C    MODIFIED FOR MULTIPLE DROPS
C    WRITTEN ON 11/16/99
C    JRS'S PROGRAM TO RESET THE DROP VARIABLES FOR EACH
ENSEMBLE
C    THE SUFFIX -I MEANS INITIAL VALUE TO BE RESET TO
     IMPLICIT NONE
     REAL    BIRTHT(NOD), DIA(NOD), DIAI(NOD), DRMASS(NOD)
     REAL    DROPTIME(NOD), DUVEL(NOD)
     REAL    DTDROP, DTDROPF, DTIMEI(NOD), DTM, DUVELI(NOD),
DXPOS(NOD)
     REAL    DXPOSI(NOD), DYPOSIT(NOD), DYPOSITI(NOD), DYVELOC(NOD)
     REAL    DYVELOCI(NOD), HOLD
     INTEGER I, IENS
     LOGICAL LALLIGN, LALLST, LDFINSH(NOD)
     INTEGER LDOUT
     LOGICAL LDROP, LDSTART(NOD), LDSTARTI(NOD), LHEATUP(NOD)
     LOGICAL LLONG, LMDIG(NOD)
     INTEGER LMDOUT(NOD)
     LOGICAL LMDROP(NOD), LMDROPI(NOD)
     INTEGER NEVENTS, NOD, NODA
     REAL    PI, RHOL, TDARRAY (NOD,10)
     REAL    TDROP(NOD), TDROPI(NOD), TLAST(NEVENTS), TNEXT(NEVENTS)

     DO I=1,NODA,1
       DIA(I)      = DIAI(I)
       DYPOSIT(I)  = DYPOSITI(I)
       DYVELOC(I)  = DYVELOCI(I)
       DUVEL(I)    = DUVELI(I)
       DXPOS(I)    = DXPOSI(I)
       DROPTIME(I) = DTIMEI(I)
       TDROP(I)    = TDROPI(I)
       DRMASS(I)   = RHOL * PI * DIA(I)**3 / 6.0
       TDARRAY(I,1) = 240.0
       TDARRAY(I,2) = 245.0
```

```
      TDARRAY(I,3)  = 250.0
      TDARRAY(I,4)  = 255.0
      TDARRAY(I,5)  = 260.0
      TDARRAY(I,6)  = 265.0
      TDARRAY(I,7)  = 270.0
      TDARRAY(I,8)  = 275.0
      TDARRAY(I,9)  = 280.0
      TDARRAY(I,10) = 285.0

    END DO
    LDROP   = .FALSE.
    LALLST  = .FALSE.
    LALLIGN = .FALSE.
    TLAST(5) = HOLD
    TNEXT(5) = HOLD

    DO I=1,NODA,1
      LDFINSH(I) = .FALSE.
      LMDROP(I)  = LMDROPI(I)
      LDSTART(I) = LDSTARTI(I)
      LHEATUP(I) = .TRUE.
      LMDIG(I)   = .FALSE.
    END DO
    DTDROP    = DTDROPF * DTM

    WRITE (LDOUT,5) IENS
  5   FORMAT (1X,'DROPLET NO. ', I7)

C    ************************** ADD TEMP. TO DEBUG !!!
C    WRITE (LDOUT, 20) DIA, DROPTIME, BIRTHT, DUVEL, DYVELOC
C 20  FORMAT (1X, 'INITIAL DIA = ', E10.4, ' Age of the drop when',
C   2   ' it is born into ODT = ', E10.4 ,/,1X, 'Time at which the',
C   3   ' droplet appears in the ODT domain = ', E12.6, /, 1X,
C   4            ' U = ', E12.6, ' V = ', E12.6)
C    WRITE (LDOUT, 30) DXPOS, DYPOSIT
C 30  FORMAT (1X,'INITIAL X POSITION = ',E12.6, ' INITIAL Y = ',E12.6)
C    WRITE (LDOUT, 50) DTDROPF
C 50  FORMAT (1X, 'FACTOR FOR COMPUTING DROPLET TIME STEP FROM',
C   5   ' MOLECULAR STEP (dtm) = ', E10.4)
C    ************************** END OF TEMP DEBUG OUTPUT

    WRITE (LDOUT,10)
 10   FORMAT ( 4X, 'TIME',11X, 'U', 13X, 'V', 13X, 'X', 13X, 'Y',
    2      13X, 'ODT TIME')
```

```
C  !! SHORT OUTPUT NOT YET AVAILABLE !!
C     IF (LLONG) THEN
      DO I = 2, NODA, 1
         WRITE (LMDOUT(I),5) IENS
         WRITE (LMDOUT(I),10)
      END DO
C     END IF
      RETURN
      END
```

```
      SUBROUTINE EFLAMET (DIAP, HEATCOM, KDROP, LDOUT, LIGNIT,
LLONG,
   2          LOUT, RHOL, STOICH, TDROP, TFLAME, TINFIN, YOINFIN,
   3              AIRNU, CPFGAS, HEFF, RHOGAS, TAUP, TTHIRD)
C ****************************************************************
C   LAST UPDATED ON 02/03/00  AT 5:00  PM

C   WRITTEN BY JRSCHMIDT ON 02/02/00

C   T FLAME = FLAME SHEET TEMPERATURE, START WITH A GUESS
C   T DROP  = DROP TEMP.

    IMPLICIT NONE
    REAL   AIRMU, AIRNU, CPGAS, CPFGAS
    REAL   DIAP, HEATCOM, HEFF
    INTEGER ITT, KDROP
    LOGICAL LIGNIT, LITT, LLONG
    INTEGER LDOUT, LOUT
    REAL   RHOGAS, RHOL, STOICH
    REAL   TAUP, TDROP, TFLAME, TFNEW, TINFIN, TTHIRD
    REAL   XFS, YCONST, YFS, YOINFIN

C   CLAUSIUS-CLAPEYRON EQUATION.  PRESSURE IS IN ATMOSPHERES
C   GIVES MOLE FRACTION IN GAS AT THE SURFACE
C   GAS CONSTANT R = 8.314 J/MOL/K
C   FROM EPA REPORT.  AVE. MOLECULAR WEIGHT = 0.136 KG/MOL,
C   BOILING TEMP. = 400 K, HEAT OF VAPORIZATION = 350,000 J/KG

    XFS = EXP(5725.283*(0.0025 - 1./TDROP))
C   30% EXCESS AIR, ASSUMING 79% N2, 21% O2, COMPLETE BURNING.
C   NATURAL GAS IS BETWEEN 95-98 % METHANE (CH4)
    YCONST = 1738.08 * XFS
    YFS   = YCONST / (353.866*(1.-XFS) + YCONST)

C !!!!!  AIRNU MUST BE EVALUATED AT 1/3 RULE   -SIRIGNANO
C       YOINFIN WAS CALCULATED TO BE 5.1465342

    LITT = .TRUE.
    ITT  = 1
    DO WHILE ((LITT) .AND. (ITT .LE. 35))
      TTHIRD = TDROP + (TFLAME - TDROP) / 3.
      CALL ETMPVAR (LDOUT, LLONG, TTHIRD, AIRMU, AIRNU, CPGAS,
   2          CPFGAS, RHOGAS)
      HEFF = (1. - YFS) * (CPGAS*(TINFIN - TDROP)
```

```
2   + YOINFIN * STOICH * HEATCOM) / (YFS + YOINFIN * STOICH)
      IF (LIGNIT) THEN
        TFNEW = (TINFIN + YOINFIN*STOICH*(HEATCOM - HEFF + CPFGAS
2          * TDROP)/CPGAS)/(1. + YOINFIN*STOICH*CPFGAS/CPGAS)
      ELSE
        TFNEW = TINFIN
      END IF
C   !!  CPGAS SHOULD BE AT 1/3 THE DIFFERENCE FROM DROP TO FLAME
TEMP.
      IF (ABS(TFNEW - TFLAME) .LE. 0.1) THEN
        LITT = .FALSE.
      ELSE
        ITT = ITT + 1
      END IF
      TFLAME = TFNEW
C      DEBUG  !!!!!!
C      IF (TDROP .GT. 380.8) THEN
C        WRITE (LDOUT, 15) TFLAME, TDROP
C      END IF
C      END DEBUG
    END DO
    IF (LITT) THEN

C !!  SHORT OUPUT NOT READY YET
C      IF (LLONG) THEN
        WRITE (LDOUT,*) ' FLAME TEMP. DID NOT CONVERGE IN 35 '
        WRITE (LDOUT,*) 'ITTERATIONS, DROPLET IN EFLAMET'
        WRITE (LDOUT,*)
        WRITE (LDOUT,*)
C      END IF
      WRITE (LOUT,*)  ' FLAME TEMP. DID NOT CONVERGE IN 35 '
      WRITE (LOUT,*) 'ITTERATIONS, DROPLET # ', KDROP,' IN EFLAMET'
      STOP
    END IF
C   !!!!!  TAUP IS A VARIABLE   !!!!!!!!!!!!
    TAUP   = RHOL * DIAP**2 / (18.0 * AIRMU)
C   TEMP OUTPUT FLAME TEMP, DROP TEMP   !! DEBUG

C      WRITE (LDOUT, 15)  TFLAME, TDROP
C 15     FORMAT (6X, 'Tf ', E12.6, 'Td ', E12.6)
C   DEBUG   !!!!

    RETURN
    END
```

```
      SUBROUTINE ETMPVAR (LDOUT, LLONG, TEMP, VISC, AIRNU,
   2              CPGAS, CPFGAS, DENSITY)
C *****************************************************************
C    LAST UPDATED 03/30/00    AT   7:30  PM
C  !!!!! TEMPARARILY MODIFIED ON 02/17/00  TO TRY CPF = C10H21

C    CREATED BY JOHN SCHMIDT  ON 01/24/00
C    THIS ROUTINE TAKES A TEMP AND FINDS THE CORESPONDING
VISCOSITY (NU),
C    THE HEAT CAPACITY OF THE GAS PHASE (CPGAS), AND THE HEAT
CAPACITY OF
C    THE GAS PHASE FUEL (CPFGAS) AT THAT TEMPERATURE
C    R GAS = MOLAR GAS CONSTANT UNITS J/G-MOL/K

      IMPLICIT NONE
      REAL    AIRNU, CPFGAS, CPGAS, CP1, CP2, CP3
      REAL    DENSITY, EMW,EXMW, HMW
      INTEGER LDOUT
      LOGICAL LLONG
      REAL    SLOPE, TEMP, TMW, VISC

C    FOR NOW ASSUME CPFGAS = CPGAS
C    FIND TEMP RANGE AND LINEARLY INTERPOLATE

C    IMPORTANT VARIABLES
C      VISCOSITY OF AIR IN KG/S/M
C      DENSITY OF AIR IN KG/M**3
C      HEAT CAPACITY IN J/KG/K

     IF (TEMP .LE. 299.8166) THEN
       VISC    = 0.000018602
       DENSITY = 1.175754964
       CPGAS   = 1004.832
     ELSE IF (TEMP .LE. 533.15) THEN
       SLOPE   = (0.000027696 - 0.000018602) / 233.3333
       VISC    = 0.000018602 + SLOPE * (TEMP - 299.8166)
       SLOPE   = (0.659960552 - 1.175754964) / 233.3333
       DENSITY = 1.175754964 + SLOPE * (TEMP - 299.8166)
       SLOPE   = (1013.2056 - 1004.832) / 233.3333
       CPGAS   = 1004.832 + SLOPE * (TEMP - 299.8166)
     ELSE IF (TEMP .LE. 588.7055) THEN
       SLOPE   = (0.000029763 - 0.000027696) / 55.5555
       VISC    =  0.000027696 + SLOPE * (TEMP - 533.15)
       SLOPE   = (0.597488558 - 0.659960552) / 55.5555
```

```
     DENSITY = 0.659960552 + SLOPE * (TEMP - 533.15)
     CPGAS   = 1013.2056
   ELSE IF (TEMP .LE. 644.2611) THEN
     SLOPE   = (0.000031417 - 0.000029763) / 55.5555
     VISC    = 0.000029763 + SLOPE * (TEMP - 588.7055)
     SLOPE   = (0.546229486 - 0.597488558) / 55.5555
     DENSITY = 0.597488558 + SLOPE * (TEMP - 588.7055)
     SLOPE   = (1017.3924 - 1013.2056) / 55.5555
     CPGAS   = 1013.2056 + SLOPE * (TEMP - 588.7055)
   ELSE IF (TEMP .LE. 699.8166) THEN
     SLOPE   = (0.00003307 - 0.000031417) / 55.5555
     VISC    = 0.000031417 + SLOPE * (TEMP - 644.2611)
     SLOPE   = (0.502979644 - 0.546229486) / 55.5555
     DENSITY = 0.546229486 + SLOPE * (TEMP - 644.2611)
     SLOPE   = (1021.5792 - 1017.3924) / 55.5555
     CPGAS   = 1017.3924 + SLOPE * (TEMP - 644.2611)
   ELSE IF (TEMP .LE. 755.3722) THEN
     SLOPE   = (0.000035137 - 0.00003307) / 55.5555
     VISC    = 0.00003307 + SLOPE * (TEMP - 699.8166)
     SLOPE   = (0.47254457 - 0.502979644) / 55.5555
     DENSITY = 0.502979644 + SLOPE * (TEMP - 699.8166)
     SLOPE   = (1025.766 - 1021.5792) / 55.5555
     CPGAS   = 1021.5792 + SLOPE * (TEMP - 699.8166)
   ELSE IF (TEMP .LE. 810.9277) THEN
     SLOPE   = (0.000036791 - 0.000035137) / 55.5555
     VISC    = 0.000035137 + SLOPE * (TEMP - 755.3722)
     SLOPE   = (0.44050765 - 0.47254457) / 55.5555
     DENSITY = 0.47254457 + SLOPE * (TEMP - 755.3722)
     SLOPE   = (1029.9528 - 1025.766) / 55.5555
     CPGAS   = 1025.766 + SLOPE * (TEMP - 755.3722)
   ELSE IF (TEMP .LE. 922.0388) THEN
     SLOPE   = (0.000040098 - 0.000036791) / 111.1111
     VISC    = 0.000036791 + SLOPE * (TEMP - 810.9277)
     SLOPE   = (0.381239348 - 0.44050765) / 111.1111
     DENSITY = 0.44050765 + SLOPE * (TEMP - 810.9277)
     SLOPE   = (1038.3264 - 1029.9528) / 111.1111
     CPGAS   = 1029.9528 + SLOPE * (TEMP - 810.9277)
   ELSE IF (TEMP .LE. 1033.15) THEN
     SLOPE   = (0.000043405 - 0.000040098) / 111.1111
     VISC    = 0.000040098 + SLOPE * (TEMP - 922.0388)
     SLOPE   = (0.339591352 - 0.381239348) / 111.1111
     DENSITY = 0.381239348 + SLOPE * (TEMP - 922.0388)
     SLOPE   = (1050.8868 - 1038.3264) / 111.1111
     CPGAS   = 1038.3264 + SLOPE * (TEMP - 922.0388)
```

```
      ELSE IF (TEMP .LE. 1144.2611) THEN
        SLOPE   = (0.000046298 - 0.000043405) / 111.1111
        VISC    = 0.000043405 + SLOPE * (TEMP - 1144.2611)
        SLOPE   = (0.307554432 - 0.339591352) / 111.1111
        DENSITY = 0.339591352 + SLOPE * (TEMP - 1144.2611)
        SLOPE   = (1063.4472 - 1050.8868) / 111.1111
        CPGAS   = 1050.8868 + SLOPE * (TEMP - 1144.2611)
      ELSE IF (TEMP .LE. 1255.3722) THEN
        SLOPE   = (0.000049605 - 0.000046298) / 111.1111
        VISC    = 0.000046298 + SLOPE * (TEMP - 1255.3722)
        SLOPE   = (0.28032305 - 0.307554432) / 111.1111
        DENSITY = 0.307554432 + SLOPE * (TEMP - 1255.3722)
        SLOPE   = (1076.0076 - 1063.4472) / 111.1111
        CPGAS   = 1063.4472 + SLOPE * (TEMP - 1255.3722)
      ELSE IF (TEMP .LE. 1366.4833) THEN
        SLOPE   = (0.000052499 - 0.000049605) / 111.1111
        VISC    = 0.000049605 + SLOPE * (TEMP - 1366.4833)
        SLOPE   = (0.257897206 - 0.28032305 ) / 111.1111
        DENSITY = 0.28032305 + SLOPE * (TEMP - 1366.4833)
        SLOPE   = (1088.5680 - 1076.0076) / 111.1111
        CPGAS   = 1076.0076 + SLOPE * (TEMP - 1366.4833)
      ELSE
        VISC    = 0.000052499
        DENSITY = 0.257897206
        CPGAS   = 1088.5680

C  !! SHORT OUTPUT N0T YET INSTALLED
C      IF (LLONG) THEN
         WRITE (LDOUT,*) ' FLAME TEMPERATURE TOO HIGH '
         WRITE (LDOUT,*) ' VISCOSITY IN ETMPVAR'
C      END IF
      END IF

C    VALUES OF DENSITY, VISCOSITY, AND HEAT CAPACITY ARE
C    FROM "AIR POLLUTION CONTROL, A DESIGN APPROACH"
C    BY C.D. COOPER & F.C. ALLEY. PAGE 654
C

C    NU = VISCOSITY/DENSITY [M**2/S]
      AIRNU  = VISC / DENSITY

C     RGAS = 8.3144    ! UNITS J/G-MOL/K
      HMW  = 100.204
      EMW  = 106.1674
```

```
      TMW  = 91.13258
      EXMW = 141.27670

C ****************************************************************
    IF (TEMP .GE. 200.) THEN
      IF (TEMP .LE. 1000.) THEN
C      200 - 1000 K
C        HEPTANE
       CP1 = 11.15325 - 0.009494155*TEMP + 0.0001955712*TEMP**2
   2       - 0.0000002497525 * TEMP**3 + 9.848732D-11 * TEMP**4

C        ETHYLBENZENE
       CP2 = 3.51535 + 0.01781457 * TEMP + 0.000118934*TEMP**2
   2       - 1.756398D-07 * TEMP**3 + 7.320611D-11 * TEMP**4
C        C10H21
       CP3 = 3.089701 + 0.08411795*TEMP + 1.590184D-05*TEMP**2
   2       - 7.238793D-08*TEMP**3 + 3.226693D-11*TEMP**4

      ELSE IF (TEMP .LE. 6000) THEN
C      1000 - 6000 K
C        HEPTANE
       CP1 = 18.53547 + 0.03914205*TEMP - 1.380303D-05*TEMP**2
   2       + 2.224039D-09 * TEMP**3 - 1.334526D-13 * TEMP**4
C        ETHYLBENZENE
       CP2 = 15.57608 + 0.03230646*TEMP - 1.190027D-05*TEMP**2
   2       + 1.967925D-09 * TEMP**3 - 1.199112D-13 * TEMP**4

       CP3 = 21.32213 + 0.06157352*TEMP - 2.384948D-05*TEMP**2
   2       + 4.220912D-09*TEMP**3 - 2.788931D-13*TEMP**4

      ELSE
       PRINT*, '  TEMP. IS OVER 6000 K'
      END IF
     ELSE
       PRINT*, '  TEMP. IS LESS THEN 200 K'
     END IF
C    DONE!!  TEMPARARY TO CHECK OUT USING CP3 AS AN AVERAGE
     CPFGAS = 0.399*CP1/HMW + 0.289*CP2/EMW + 0.312*CP3/EXMW
C         CPFGAS = CP3/EXMW
C    RGAS * CP * 1000
     CPFGAS = 8314.4 * CPFGAS
     RETURN
     END
```

```
      REAL FUNCTION DPOSROOT (AIRNU, BULKVEL, DELTAT, DIAP, DUVEL,
   2                          LOUT, TAUP, UFLUID)

C   ****************************************************************
C   LAST MODIFIED ON  11/19/99  @  11:00

C   WRITTEN BY JRS ON 11/18/99 TO TAKE INTO ACCOUNT THE
DIFFERENCES
C   IN MAPPING THE LAGRANGIAN MODEL FOR THE PARTICL AND THE
EULARIAN
C   CONVERSION FACTOR IN THE ODT MODEL

C   THIS PROGRAM FINDS THE 'POS'ITIVE 'ROOT' OF A QUADRADIC
EQUATION
C   AND RETURNS IT AS A REAL VALUE.  IF THERE ARE TWO POSITIVE
ROOTS,
C   THE SMALLEST IS THE ONE OF INTEREST.  IF THERE ARE NO POSITIVE
C   ROOTS (I.E. ONLY NEGATIVE ROOTS, OR IMAGINARY ROOTS) THEN
CHOOSE
C   DELTAT AS THE CORRECT TIME.
C   AX**2 + BX + C = 0
C   HOWEVER, THIS FUNCTION IS WRITTEN TO SPECIFICALLY SOVLE FOR
THE
C   POSITIVE ROOT OF THIS EQUATION
C   (DUVEL - UFLUID)*FXCOEF*T**2/(2*TAUP) -DUVEL*T + DELTAX = 0.

C   SIGNIFICANT VARIABLES
C   ATTWO  = 'A' 'T'IMES 'TWO' -- USEFUL IN NUMERIC IMPLEMENTATION
C   TERM   = B**2 - 2*ATTWO*C
C   ROOT1  = (-B + SQRT(TERM)) / ATTWO
C   ROOT2  = (-B - SQRT(TERM)) / ATTWO

    IMPLICIT NONE
    REAL    AIRNU, ATTWO, BULKVEL, CONST6
    REAL    DELTAT, DELTAX, DIAP, DUVEL, FXCOEF
    INTEGER LOUT
    REAL    RENX, ROOT1, ROOT2, TAUP, TERM, UFLUID

    IF (DELTAT .GT. 0.0) THEN
C     USE CORRRECTION FACTOR GIVEN BY WANG & STOCK
      CONST6 = DUVEL - UFLUID
      RENX   = DIAP * ABS(CONST6) / AIRNU
      IF (RENX .LE. 1.0) THEN
C       STOKES LAW
```

```
         FXCOEF = 1.0
      ELSE IF (RENX .LE. 1000) THEN
C        CORRECTION FACTOR
         FXCOEF  =  1.0 + 0.15 * (RENX) ** 0.687
      ELSE
        WRITE (LOUT,*) ' PARTICLE Re X > 1000'
        WRITE (LOUT,*) ' STOPPED IN DPOSROOT', RENX
        STOP
      END IF
      ATTWO  = CONST6 * FXCOEF / TAUP
      DELTAX = BULKVEL * DELTAT
      IF (ATTWO .EQ. 0.)THEN
        IF (DUVEL .GT. 0.0) THEN
          DPOSROOT = DELTAX / DUVEL
        ELSE
          DPOSROOT = DELTAT
        END IF
      ELSE
        TERM   = DUVEL**2 - 2.0 * ATTWO *DELTAX
        IF (TERM .GE. 0.) THEN
C          NOT IMAGINARY ROOTS, -- REAL ROOTS
          IF (TERM .EQ. 0.) THEN
C           REAL REPEATED ROOTS
            DPOSROOT = DUVEL / ATTWO
            IF (DPOSROOT .LE. 0.0) THEN
              DPOSROOT = DELTAT
            END IF
          ELSE
            ROOT1 = (DUVEL + SQRT(TERM)) / ATTWO
            ROOT2 = (DUVEL - SQRT(TERM)) / ATTWO
            IF (ROOT1*ROOT2 .LT. 0.0) THEN
C             TWO REAL ROOTS, DIFFERENT SIGNS.  WANT THE POSITIVE
ONE
              IF (ROOT1 .LT. 0.0) THEN
                DPOSROOT = ROOT2
              ELSE
                DPOSROOT = ROOT1
              END IF
            ELSE
C             TWO REAL ROOTS, SAME SIGNS OR ONE IS ZERO
              IF (ROOT1 .LE. 0.0) THEN
                IF (ROOT2 .GT. 0.0) THEN
                  DPOSROOT = ROOT2
                ELSE
```

```
              DPOSROOT = DELTAT
            END IF
          ELSE
            IF (ROOT2 .GT. 0.0) THEN
              IF (ROOT2 .GT. ROOT1) THEN
                DPOSROOT = ROOT1
              ELSE
                DPOSROOT = ROOT2
              END IF
            ELSE
              DPOSROOT = ROOT1
            END IF
          END IF
        END IF
      END IF
    ELSE
C         IMAGINARY ROOTS, CHOOSE DELTA T
      DPOSROOT = DELTAT
    END IF
  END IF
ELSE
  DPOSROOT = 0.0
END IF

RETURN
END
```

```
      SUBROUTINE DUPDATE (AIRNU, ALAMDA, CPFGAS, DABZERO, DIAP,
DRMASS,
   2 DTDROP, GRAVAC, HEATVAP, HEATCAP, HEATCOM, HEFF, KDROP,
LDOUT,
   3 LHEATUP, LLAMDA,  LOUT, NOD, PEPS, PI, RHOGAS, RHOL, STOICH,
   4 STRTU, STRTVEL, TAUP, TDARRAY, TDROP, TEMPZERO, TFLAME,
TINFIN,
   5   TTHIRD, UFLUID, YOINFIN, DELTAX, DELTAY, DIANEW, UEND, VEND)
```

C **
C   WRITTEM BY JRS FOR THE DROPLET MODEL. INTEGRATES THE
DROPLET-
C   DRAG LAW THE THE AMOUNT OF TIME STORED IN DELTA TIME.
C   CALLED FROM MAIN ROUTINE ODTDRIV
C
C   LAST UPDATED ON 03/03/00   AT 20:00
C
C   UPDATED 02/02/00   MODIFIED FOR EVAPORATING DROPLETS
C   LINEAR DROPLET-DRAG LAW WITH A CORRECTION FACTOR F
C   NOTE: THIS SUBPROGRAM IS USED WHEN THE DROPLET IS NOT IN AN
EDDY
C   HENCE, THERE IS NOT A V VELOCITY OF THE FLUID SO THE DIFF. EQN.
IS
C   DV/DT = - FY/TAUP *(V) - G
C   DU/DT = - FX/TAUP*(U-UFLUID)
C   FOR THE SMALLEST TIME STEP, F, VFLUID, & TAUP ARE CONST.
C   SINCE WE ARE USING A LINEAR DROPLET DRAG LAW WITH A
CORRECTION
C   THE CORRECTION IN THE Y DIRECTION IS CONCIDERED INDEPENDENT
OF THE
C   CORRECTION IN THE X DIRECTION. F Y COEFF & F X COEFF ARE
INDEPENDENT
C   STRT VEL = THE INITIAL PARTICLE VELOCITY IN THE Y DIRECTION
C   STRT U   = INITIAL PARTICLE VELOCITY IN THE X DIRECTION
C   DTDROP   = TIME CHANGE OVER WHICH TO INTEGRATE
C   DELTA Y   = CHANGE IN Y POSITION OF THE PARTICLE
C   DELTA X   = CHANGE IN X POSITION OF THE PARTICLE
C   V END   = PARTICLE Y VELOCITY AT THE END OF THE INTEGRAL
C   U END   = PARTICLE X VELOCITY AT END OF INTEGRAL
C   CONST 4   = TERM IN THE D.E.Q. NOT MULTIPLYING VELOCITY
C   CONST 3   = COEFFICIENT IN THE D.E.Q. MULTIPLYING VELOCIT ON
RHS
C   CONST1,8 = CONVENIENT COEFFICIENT TO MAKE CALCULATIONS
FASTER

```
C     F Y COEF   = CORRECTION FACTOR SO THE LINEAR DRAG LAW FITS
BETTER
C     F X COEF   = CORRECTION FACTOR IN THE X DIRECTION
C     TAU P     = DROPLET TIME CONSTANT, RELAXATION TIME
C     U FLUID   = VELOCITY OF THE FLUID IN THE X DIRECTION
C     GRAV AC   = GRAVITATIONAL ACCELERATION [UNITS]  ----
C     AIR NU    = KINEMATIC VISCOSITY OF THE GAS PHASE (AIR)
C     DIA P     = DIAMETER OF THE PARTICLE
C     Y F S     = MASS FRACTION OF THE FUEL AT DROPLET SURFACE
C     X F S     = MOLE FRACTION OF FUEL USING CLAUSIUS-CLAPEYRON
EQN.
C     Y O INFI  = MASS FRACTION OF OXYGEN FAR FROM THE DROP
C     T FLAME   = TEMPERATURE OF THE FLAME SHEET [K]
C     T DROP    = TEMPERATURE OF THE DROP [K]
C     T INFIN   = TEMPERATURE FAR FROM THE DROP BUT IN THE
COMPUTATIONAL CELL
C     B MAS T   = THE SPALDING MASS TRANSFER NUMBER
C     D AB      = GAS DIFFUSIVITY OF A IN B
C     SCHMIDT   = SCHMIDT NUMBER OF GAS
C     RE N T    = TOTAL REYNOLDS NO.
C     F RE      = FUNCTION OF REYNOLDS NO.
C     BASE SH   = SHERWOOD NO. WITHOUT MASS TRANSFER (I.E. BASE)
C     SH STAR   = MODIFIED SHERWOOD NO. FOR CALCULATIONS
C     PSI       = 2*DRATIO*DAB*LN(1+B)
C     HEAT CAP  = THE LIQUID HEAT CAPACITY IN [J/KG/K]
C     CP GAS    = AVERAGE GAS HEAT CAPACITY [J/KG/K]
C     CP F GAS  = AVE. FUEL GAS HEAT CAPACITY [J/KG/K]
C     R GAS     = MOLAR GAS CONSTANT, R  [J/KG/K]
C     H EFF     = THE ENTHALPY, H EFFECTIVE
C     RHO GAS   = DENSITY OF GAS
C     E TMP VAR = SUBROUTINE WHICH COMPUTES VARIATION AT 1/3
TEMPERATURE
C     Y CONST   = VALUE FOR CONVERTING MOLE FRACTION TO MASS
FRAC.
C     DELTA D   = CHANGE IN DIAMETER OF THE DROP FOR DT DROP
C     DELTA M   = CHANGE IN MASS OF THE DROP       "
C     DELTA T D = CHANGE IN TEMPERATURE OF THE DROP "

      IMPLICIT NONE
      REAL    ALAMDA, AIRMU, AIRNU, BASESH, BLN, BMAST, BP1
      REAL    CONST1, CONST2, CONST4, CONST5
      REAL    CONST6, CONST7, CONST8
      REAL    CONSTX3, CONSTY3, CPFGAS, CPGAS
      REAL    DABAVE, DABZERO
```

```
      REAL    DELTAD, DELTAM, DELTATD, DELTAX, DELTAY
      REAL    DIANEW, DIAP, DMNEW, DRMASS, DTDROP
      REAL    FRE, FXCOEF, FYCOEF, GRAVAC
      REAL    HEFF, HEATCAP, HEATCOM, HEATVAP
      INTEGER ITT, KDROP, LDOUT
      LOGICAL LHEATUP, LITT, LLAMDA
      INTEGER LOUT, NOD
      REAL    PEPS, PI, RENT, RENX, RENY, RHOGAS, RHOL
      REAL    SCHMIDT, SHSTAR, STOICH, STRTU, STRTVEL
      REAL    TAUP, TDARRAY(NOD,10), TDNEW, TDROP, TEMPZERO, TFLAME,
     TFNEW
      REAL    TINFIN, TTHIRD, TVEL
      REAL    UEND, UFLUID, VEND
      REAL    XFS, YCONST, YFS, YOINFIN

C    WHEN TIME IS ZERO, SET VELOCITIES AND DELTAS AND RETURN
      IF (DTDROP .EQ. 0.0) THEN
        DELTAY = 0.0
        DELTAX = 0.0
        VEND   = STRTVEL
        UEND   = STRTU
        DIANEW = DIAP
      ELSE
C    USE THE ANALYTIC SOLUTIONS TO THE CONST. COEFICIENT
DIFFERENTIAL
C    EQUATIONS TO APPROZIMATE THE END POINT TO THE INTEGRAL

C      USE CORRRECTION FACTOR GIVEN BY WANG & STOCK
      CONST6 = STRTU - UFLUID

      RENY   = DIAP * ABS(STRTVEL) / AIRNU
      RENX   = DIAP * ABS(CONST6) / AIRNU
      IF (RENY .LE. 1.0) THEN
C      STOKES LAW
        FYCOEF = 1.0
      ELSE IF (RENY .LE. 1000) THEN
C      CORRECTION FACTOR
        FYCOEF  =  1.0 + 0.15 * (RENY) ** 0.687
      ELSE
        WRITE (LOUT,*) ' PARTICLE Re Y > 1000'
        WRITE (LOUT,*) ' STOPPED IN DUPDATE', RENY
        WRITE (LOUT,*) ' PARTICLE Re Y > 1000'
        WRITE (LOUT,*) ' STOPPED IN DUPDATE', RENY
        STOP
```

```
      END IF
      IF (RENX .LE. 1.0) THEN
C     STOKES LAW
         FXCOEF = 1.0
      ELSE IF (RENX .LE. 1000) THEN
C     CORRECTION FACTOR
         FXCOEF  =  1.0 + 0.15 * (RENX) ** 0.687
      ELSE
         WRITE (LOUT,*) ' PARTICLE Re X > 1000'
         WRITE (LOUT,*) ' STOPPED IN DUPDATE', RENX
         WRITE (LOUT,*) ' PARTICLE Re X > 1000'
         WRITE (LOUT,*) ' STOPPED IN DUPDATE', RENX
         STOP
      END IF

C      COMPUTE THE FINAL VELOCITY AND THE CHANGE IN POSITION IN
THE Y
C      DIRECTION OF THE PARTICLE

      CONSTY3 = FYCOEF / TAUP
      CONST4 = GRAVAC / CONSTY3
      CONST1 = STRTVEL + CONST4
      CONST5 = EXP(-CONSTY3*DTDROP)
      VEND   = CONST1 * CONST5 - CONST4
      DELTAY = -CONST4 * DTDROP + (CONST1 / CONSTY3) * (1 - CONST5)


C      COMPUTE THE FINAL VELOCITY AND CHANGE IN POSITION IN THE X
C      DIRECTION OF THE PARTICLE

      CONSTX3 = FXCOEF / TAUP
      CONST8 = EXP(-CONSTX3*DTDROP)
      UEND   = UFLUID + CONST6 * CONST8
      DELTAX = (CONST6/ CONSTX3) * (1 - CONST8) + UFLUID * DTDROP

C      ADJUST DROPLET DIAMETER AFTER MOVEMENT

      TVEL = SQRT((STRTVEL)**2 + (CONST6)**2)

C      AIRNU IS EVALUATED AT 1/3 RULE
      RENT   = DIAP * TVEL / AIRNU
      IF (RENT .LE. 1.0) THEN
C
         FRE = 1.0
```

```
          ELSE IF (RENT .LE. 400) THEN
C     CORRECTION FACTOR
          FRE = (RENT) ** 0.077
          ELSE
            WRITE (LOUT,*) ' PARTICLE Re T > 400'
            WRITE (LOUT,*) ' STOPPED IN DUPDATE', RENT
            WRITE (LOUT,*) ' PARTICLE Re T > 400'
            WRITE (LOUT,*) ' STOPPED IN DUPDATE', RENT
            STOP
          END IF
          BMAST = (CPFGAS * (TINFIN - TDROP) +
     2              YOINFIN * STOICH * HEATCOM) / HEFF
          BP1   = BMAST + 1.
          BLN   = ALOG(BP1)


C   FOR NOW RHOGAS IS THE DENSITY OF AIR AT THE 1/3 RULE TEMP.
          CALL ESCHMIDT(AIRNU, DABZERO, TTHIRD, TEMPZERO,
     2              DABAVE, SCHMIDT)

          BASESH  = 1. + FRE * (1. + RENT * SCHMIDT) ** (1./3.)

          SHSTAR  = 2. + (BASESH - 2.) * BMAST/((BP1)**0.7 * BLN )

          IF (LHEATUP) THEN

            CONST7  =  RHOGAS * DABAVE * SHSTAR * BLN * DTDROP

            DELTAD  = - 2.0 * CONST7 / (RHOL * DIAP)
            DIANEW  = DIAP + DELTAD
            DELTAM  = PI * DIAP * CONST7
            DMNEW   = DRMASS - DELTAM
            DELTATD = (HEFF - HEATVAP) * DELTAM / (HEATCAP * DRMASS)
            TDNEW   = TDROP + DELTATD
            IF (LLAMDA) THEN
              CALL PSWITCH (PEPS, TDARRAY, TDNEW, KDROP, LDOUT,
     2              NOD, LHEATUP)
            END IF
          ELSE
            DELTAD  = - ALAMDA * SHSTAR / (4.0 * DIAP)
            DIANEW  = DIAP + DELTAD
            DELTAM  = PI * RHOL * (DIAP**3 - DIANEW**3) / 6.0
C     ACCORDING TO THE MULHOLLAND MODEL THE QUANTITIES OF
TEMP.
```

```
C      DOES NOT MATTER MUCH HERE BECAUSE IT HAS ACHIEVED THE
C      DEW POINT TEMPERATURE, AND THE MASS DOES NOT MATTER
BECAUSE
C      IT IS THE SAME AS DIAMETER

       DMNEW   = DRMASS - DELTAM
       DELTATD = (HEFF - HEATVAP) * DELTAM / (HEATCAP * DRMASS)
       TDNEW   = TDROP + DELTATD
     END IF

     IF (DIANEW .LE. 0.0 .OR. DMNEW .LE. 0.0) THEN
       DIANEW = 0.0
       DRMASS = 0.0
       TDROP   = TDNEW
     ELSE
       DRMASS = DMNEW
       TDROP  = TDNEW
     END IF

C      ALAMDA = 8. * RHOGAS * DABAVE/RHOL*BLN
C  !!  THIS BURNED TOO FAST SO DO DROPLET HEATING CASE        !!
C      BASESH = 1. + FRE * (1. + RENT * SCHMIDT) ** (1./3.)
C      SHSTAR = 2. + (BASESH - 2.)/((BP1)**0.7 * BLN / BMAST)
C      CONST2 = DIAP**2 - PSI * SHSTAR * DTDROP
C      IF (CONST2 .LE. 0.) THEN
C         DIANEW = 0.
C      ELSE
C         DIANEW = SQRT(CONST2)
C      END IF
     END IF
C ****************************************************************
     RETURN
     END
```

```
      SUBROUTINE ESCHMIDT (AIRNU, DABZERO, TEMP, TEMPZERO,
   2                     DABAVE, SCHMIDT)
C    LAST UPDATED 02/01/00    AT  6:30 PM

C    CREATED BY JOHN SCHMIDT  ON 01/26/00
C    THIS ROUTINE TAKES A TEMP AND FINDS THE CORESPONDING
SCHMIDT NO.
C    BIANARY DIFFUSIVITY, AND GAS PHASE DENSITY AT THAT
TEMPERATURE


   IMPLICIT NONE
   REAL AIRNU, DABAVE, DABZERO, TEMP, TEMPZERO, SCHMIDT

   DABAVE = DABZERO * (TEMP/TEMPZERO)**1.5
   SCHMIDT = AIRNU/DABAVE

   RETURN
   END
```

```
      SUBROUTINE PSWITCH (PEPS, TDARRAY, TDNEW, KDROP, LDOUT,
   2       NOD, LHEATUP)
C    ************************************************************
C    LAST UPDATED ON 2/25   AT  20:30
C    MODIFIED FOR MULTIPLE DROPS
C    WRITTEN BY JR SCHMIDT TO COMPUTE THE TIME TO SWITCH OVER TO
THE
C    PARAMETER LAMDA. WRITTEN ON 02/07/00
C    CALLED FROM SUBROUTINE DUPDATE
C

     IMPLICIT NONE
     REAL    DELTA (10)
     INTEGER ITEST, KDROP, LDOUT
     LOGICAL LHEATUP, LTEST
     INTEGER NOD, NON, NOP
     REAL    PEPS, TDARRAY(NOD,10), TDNEW

     DELTA(1)  = TDARRAY (KDROP,2)  - TDARRAY (KDROP,1)
     DELTA(2)  = TDARRAY (KDROP,3)  - TDARRAY (KDROP,2)
     DELTA(3)  = TDARRAY (KDROP,4)  - TDARRAY (KDROP,3)
     DELTA(4)  = TDARRAY (KDROP,5)  - TDARRAY (KDROP,4)
     DELTA(5)  = TDARRAY (KDROP,6)  - TDARRAY (KDROP,5)
     DELTA(6)  = TDARRAY (KDROP,7)  - TDARRAY (KDROP,6)
     DELTA(7)  = TDARRAY (KDROP,8)  - TDARRAY (KDROP,7)
     DELTA(8)  = TDARRAY (KDROP,9)  - TDARRAY (KDROP,8)
     DELTA(9)  = TDARRAY (KDROP,10) - TDARRAY (KDROP,9)
     DELTA(10) = TDNEW - TDARRAY (KDROP,10)
     NON      = 0
     NOP      = 0
     LTEST    = .TRUE.
     DO ITEST = 1,10,1
       IF (DELTA (ITEST) .LT. 0.0) THEN
         NON = NON + 1
       ELSE
         NOP = NOP + 1
       END IF
       IF (ABS(DELTA(ITEST)) .GT. PEPS) THEN
         LTEST = .FALSE.
       END IF
     END DO
     IF (LTEST .AND. ABS(NON - NOP) .LT.8) THEN
       LHEATUP = .FALSE.
       WRITE (LDOUT,10)
```

```
 10     FORMAT (1X, 'SWITCHED TO LAMDA')
      END IF

C    WHEN DONE, ADD TDNEW TO THE END OF THE LIST
      DO ITEST = 1,9,1
        TDARRAY (KDROP,ITEST) = TDARRAY (KDROP,ITEST+1)
      END DO
      TDARRAY (KDROP,10) = TDNEW

      RETURN
      END
```

```
      SUBROUTINE DROPOUT (DROPTIME, DUVEL, DVVEL0C, DXPOS,
     2                  DYPOSIT, LDOUT, ODTTIME)

C    **************************************************************
C    WRITTEN BY JRS ON 111/8/99 TO WRITE OUT DROPLET TIME,
C    VELOCITY AND POSSITION, DROP TEMPERATURE
C    CALLED BY MAIN ROUTINE ODTDRIV.F

C    LAST MODIFIED ON 03/28/00  AT 12:30

C    DROP TIME = THE DROPLET TIME
C    D U VEL   = DROPLET VELOCITY IN THE X DIRECTION
C    D V VELOC = DROPLET VELOCITY IN THE Y DIRECTION
C    D X POS   = DROPLET X POSITION
C    D Y POSIT = DROPLET Y POSITION
      IMPLICIT NONE
      REAL    DROPTIME, DUVEL, DVVEL0C, DXPOS, DYPOSIT
      INTEGER LDOUT
      REAL    ODTTIME

      WRITE (LDOUT,10) DROPTIME, DUVEL, DVVEL0C, DXPOS, DYPOSIT,
     2            ODTTIME
 10   FORMAT (6(2X,E12.6))

      RETURN
      END
```

```
      SUBROUTINE TDROPOUT (DROPTIME, DUVEL, DVVEL0C, DXPOS,
     2             DYPOSIT, LDOUT, ODTTIME, DIAP, TDROP, TFLAME)

C    ************************************************************
C    WRITTEN BY JRS ON 111/8/99 TO WRITE OUT DROPLET TIME,
C    VELOCITY AND POSSITION, DROP TEMPERATURE
C    CALLED BY MAIN ROUTINE ODTDRIV.F

C    LAST MODIFIED ON 03/28/00  AT 12:30

C    DROP TIME = THE DROPLET TIME
C    D U VEL   = DROPLET VELOCITY IN THE X DIRECTION
C    D V VELOC = DROPLET VELOCITY IN THE Y DIRECTION
C    D X POS   = DROPLET X POSITION
C    D Y POSIT = DROPLET Y POSITION
     IMPLICIT NONE
     REAL    DIAP, DROPTIME, DUVEL, DVVEL0C, DXPOS, DYPOSIT
     INTEGER LDOUT
     REAL    ODTTIME, TDROP, TFLAME

     WRITE (LDOUT,10) DROPTIME, DUVEL, DVVEL0C, DXPOS, DYPOSIT,
     2             ODTTIME, DIAP, TDROP, TFLAME
 10  FORMAT (6(2X,E12.6), 3(1X, E11.5) )

     RETURN
     END
```

```
      SUBROUTINE INPVELOC (LOUT, NNSC, NX, SCALINIT)
C     CREATED ON 6/8/99  BY JRS    LAST UPDATED 6/23/99
C     THIS ROUTINE SETS UP THE VELOCITY INPUT FOR TOM DREEBEN'S
CODE FOR
C        ENSEMBLE AVERAGING ODT.
C     THE FOLLOWING DATA IS THAT GIVEN IN MULHOLLAND'S PAPER 1991
BASED ON
C     EPA/600/7-88/006  PAGE E-4 DATA FOR *4* INCHES IN, AXIAL VELOCITY
C     *** KNOWN MATCHES FOR NX NUMBER OF GRID POINTS ARE
C     ****   795, 897, 1185, 1455, 1775
C     VELOCITIES ARE IN METERS PER SECOND   M/S
C     TEMPERAURES ARE IN KELVIN         K
C     THE 16 VALUES (SYMMETRIC DATA POINTS) ARE FIT TO THE CHANNEL
C     WIDTH ACCORDING TO THE 11 REGIONS GIVEN.  A LINEAR FIT
BETWEEN DATA
C     POINTS IS ASSUMED
C     INPUTS ARE:
C     LOUT = THE DEVICE NUMBER FOR OUTPUT
C     NNSC = SPACE DIMENSIONED FOR THE NO. OF SCALARS (2)
C     NX   = NUMBER OF GRID NODES
C     SCALINIT (,) = THE INITIAL VELOCITY AND TEMP DISTRIBUTION

C     NOG    = ONE HALF OF (THE DOMAIN GRID POINTS -1)
C     REG    = REGION OF INTEREST
C     IREG   = INTEGER VALUE OF THE REGION IN NODE POINTS
C     TREG   = THE REGION OF INTERSET FOR THE TEMPERATURE
C     FREG   = FOLLOWING REGION
C     IFREG  = INTEGER VALUE OF THE FOLLOWING REGION
C     IREGAT = INTEGER REGION AFTER THE FOLLOWING REGION
C     IREGM  = IREG - 1
C     IPOSB  = INTEGER NODE STARTING POSITION, BOTTOM
C     IPOST  = INTEGER NODE STARTING POSITION, TOP
C     TPOSB  = TEMPERARY INTEGER NODE POSITION, BOTTOM
C     TPOSB  = TEMPERARY INTEGER NODE POSITION, TOP
C     VELPOS = VELOCITY AT POSITION OF INTEREST
C     TEMPOS = TEMPERATURE AT POSITION OF INTEREST
C     TEMPTEM= TEMPARARY TEMPERATURE
C     TSLOPE = GRADIANT OF THE TEMPERATURE OVER THE REGION
C     VSLOPE = GRADIANT OF VELOCITY OVER REGION

      IMPLICIT NONE
      REAL   FREG
      INTEGER I, IFREG, IPOSB, IPOST, IREG, IREGAT, IREGM
      INTEGER J, K
```

```
      INTEGER LOUT, NNSC, NOG, NX
      REAL    REG,  SCALINIT(NNSC,NX), TEMPVEL, TEMPOS, TEMPTEM
      INTEGER TPOSB, TPOST
      REAL    TSLOPE
      REAL    VELPOS, VSLOPE

C    THIS DATA MUST HAVE AS AN ABSOLUTE MINIMUM NO. OF GRID
POINTS 103
C    AND IT SHOULD HAVE AN ODD NO. OF GRID POINTS

      IF (NX .LT. 103 .OR. MOD(NX,2) .EQ. 0) THEN
         WRITE (LOUT,*) ' ERROR IN INPUT VELOCITY: MUST HAVE AN ODD'
         WRITE (LOUT,*) ' NUMBER OF GRID POINTS WITH A MINIMUM OF 103'
         WRITE (LOUT,*) ' FOR THE MULHOLLAND DATA.  287 works well'
         STOP
      END IF
      NOG = NX/2

C    DATA EXISTS IN 12 REGIONS IN EACH HALF OF THE DOMAIN. REGION 1
      SCALINIT (1,1)  = 0.0
      SCALINIT (1,NX) = 0.0
      TEMPOS        = 1100.
      SCALINIT (2,1)  = TEMPOS
      SCALINIT (2,NX) = TEMPOS

C    THIS REGION IS .2484 THE HALF DISTANCE OF THE CHANNEL.
C    THE CHANGE IN THE VELOCITY BETWEEN THE WALL AND THE FIRST
DATA POINT
C    IS -3.5 M/S  AND THE CHANGE IN TEMPERATURE IS +50. K .

      REG    = 0.2484 * NOG * 2.
      IREG   = REG + 0.49999
      FREG   = 0.0536 * NOG * 2.
      IFREG  = FREG +0.49999
      VSLOPE = -3.5/IREG
      TSLOPE = 50./(IREG+IFREG)
      DO I = 1, IREG-1, 1
        TEMPVEL        = VSLOPE * I
        TEMPTEM        = TSLOPE * I + TEMPOS
        SCALINIT (1,1+I)  = TEMPVEL
        SCALINIT (1,NX-I) = TEMPVEL
        SCALINIT (2,1+I)  = TEMPTEM
        SCALINIT (2,NX-I) = TEMPTEM
      END DO
```

```
      IPOSB          = 1 + IREG
      IPOST          = NX - IREG
      VELPOS = -3.5
      SCALINIT (1,IPOSB) = VELPOS
      SCALINIT (1,IPOST) = VELPOS
      TEMPOS         = TSLOPE * IREG + TEMPOS
      SCALINIT (2,IPOSB) = TEMPOS
      SCALINIT (2,IPOST) = TEMPOS

C    REGION 2
      IREG   = IFREG
      IREGM  = IREG - 1
      VSLOPE = 3.5/IREG
      DO I = 1, IREGM,1
        TEMPVEL       = VSLOPE * I + VELPOS
        J         = IPOSB+I
        K          = IPOST-I
        SCALINIT (1,J) = TEMPVEL
        SCALINIT (1,K) = TEMPVEL
        TEMPTEM       = TSLOPE * I + TEMPOS
        SCALINIT (2,J) = TEMPTEM
        SCALINIT (2,K) = TEMPTEM
      END DO


C    REGION 3
      VELPOS = 0.
      TEMPOS = 1150.
      IPOSB  = IPOSB + IREG
      IPOST  = IPOST - IREG
      SCALINIT (1,IPOSB) = VELPOS
      SCALINIT (1,IPOST) = VELPOS
      SCALINIT (2,IPOSB) = TEMPOS
      SCALINIT (2,IPOST) = TEMPOS

      REG    = 0.0509 * NOG * 2.
      IREG   = REG + 0.49999
      FREG   = 0.0105 * NOG * 2.
      IFREG  = FREG +0.49999
      IREGAT = 0.00915 * NOG * 2. + 0.49999
      IREGM  = IREG - 1
      VSLOPE = 5./IREG
      TSLOPE = 50./(IREG + IFREG + IREGAT)
```

```
      DO I = 1, IREGM, 1
        TEMPVEL      = VSLOPE * I
        J          = IPOSB+I
        K          = IPOST-I
        SCALINIT (1,J) = TEMPVEL
        SCALINIT (1,K) = TEMPVEL
        TEMPTEM      = TSLOPE * I + TEMPOS
        SCALINIT (2,J) = TEMPTEM
        SCALINIT (2,K) = TEMPTEM
      END DO

C    REGION 4
      IPOSB  = IPOSB + IREG
      IPOST  = IPOST - IREG
      VELPOS = 5.
      TEMPOS =  TSLOPE * IREG + TEMPOS
      IREG   = IFREG
      IFREG  = IREGAT
      IREGM  = IREG - 1
      SCALINIT (1,IPOSB) = VELPOS
      SCALINIT (1,IPOST) = VELPOS
      SCALINIT (2,IPOSB) = TEMPOS
      SCALINIT (2,IPOST) = TEMPOS
      VSLOPE = 15./IREG

      DO I = 1, IREGM, 1
        TEMPVEL      = VSLOPE * I + VELPOS
        J          = IPOSB+I
        K          = IPOST-I
        SCALINIT (1,J) = TEMPVEL
        SCALINIT (1,K) = TEMPVEL
        TEMPTEM      = TSLOPE * I + TEMPOS
        SCALINIT (2,J) = TEMPTEM
        SCALINIT (2,K) = TEMPTEM
      END DO

C    REGION 5
      IPOSB  = IPOSB + IREG
      IPOST  = IPOST - IREG
      VELPOS = 20.
      TEMPOS = TSLOPE * IREG + TEMPOS
      SCALINIT (1,IPOSB) = VELPOS
      SCALINIT (1,IPOST) = VELPOS
```

```
      SCALINIT (2,IPOSB) = TEMPOS
      SCALINIT (2,IPOST) = TEMPOS
      IREG   = IFREG
      IREGM  = IREG - 1
      VSLOPE = 4./IREG

      DO I = 1, IREGM, 1
        TEMPVEL      = VSLOPE * I + VELPOS
        J         = IPOSB+I
        K          = IPOST-I
        SCALINIT (1,J) = TEMPVEL
        SCALINIT (1,K) = TEMPVEL
        TEMPTEM      = TSLOPE * I + TEMPOS
        SCALINIT (2,J) = TEMPTEM
        SCALINIT (2,K) = TEMPTEM
      END DO

C    REGION 6
      IPOSB = IPOSB + IREG
      IPOST = IPOST - IREG
      VELPOS = 24.
      TEMPOS = 1200.
      SCALINIT (1,IPOSB) = VELPOS
      SCALINIT (1,IPOST) = VELPOS
      SCALINIT (2,IPOSB) = TEMPOS
      SCALINIT (2,IPOST) = TEMPOS
      REG    = 0.01307 * NOG * 2.
      IREG   = REG + 0.49999
      FREG   = 0.01706 * NOG * 2.
      IFREG  = FREG +0.49999
      IREGM  = IREG - 1
      VSLOPE = -4./IREG
      TSLOPE = 100./(IREG + IFREG)

      DO I = 1, IREGM, 1
        TEMPVEL      = VSLOPE * I + VELPOS
        J    = IPOSB+I
        K    = IPOST-I
        SCALINIT (1,J) = TEMPVEL
        SCALINIT (1,K) = TEMPVEL
        TEMPTEM      = TSLOPE* I + TEMPOS
        SCALINIT (2,J) = TEMPTEM
        SCALINIT (2,K) = TEMPTEM
      END DO
```

```
C    SUB-REGION  7
     IPOSB = IPOSB + IREG
     IPOST = IPOST - IREG
     VELPOS = 20.
     TEMPOS = TSLOPE * IREG + TEMPOS
     SCALINIT (1,IPOSB) = VELPOS
     SCALINIT (1,IPOST) = VELPOS
     SCALINIT (2,IPOSB) = TEMPOS
     SCALINIT (2,IPOST) = TEMPOS
     IREG   = IFREG
     FREG   = 0.01823 * NOG * 2.
     IFREG  = FREG +0.49999
     IREGM  = IREG - 1
     VSLOPE = -10./(IREG + IFREG)
     DO I = 1, IREGM, 1
       TEMPVEL      = VSLOPE * I + VELPOS
       J         = IPOSB+I
       K         = IPOST-I
       SCALINIT (1,J) = TEMPVEL
       SCALINIT (1,K) = TEMPVEL
       TEMPTEM      = TSLOPE* I + TEMPOS
       SCALINIT (2,J) = TEMPTEM
       SCALINIT (2,K) = TEMPTEM
     END DO

C    REGION 8
     IPOSB  = IPOSB + IREG
     IPOST  = IPOST - IREG
     VELPOS = VSLOPE * IREG + VELPOS
     TEMPOS = 1300.
     SCALINIT (1,IPOSB) = VELPOS
     SCALINIT (1,IPOST) = VELPOS
     SCALINIT (2,IPOSB) = TEMPOS
     SCALINIT (2,IPOST) = TEMPOS
     IREG   = IFREG
     IREGM  = IREG - 1
     TSLOPE = 100./IREG

     DO I = 1, IREGM, 1
       TEMPVEL      = VSLOPE * I + VELPOS
       J    = IPOSB+I
       K    = IPOST-I
       SCALINIT (1,J) = TEMPVEL
```

```
      SCALINIT (1,K) = TEMPVEL
      TEMPTEM      = TSLOPE * I + TEMPOS
      SCALINIT (2,J) = TEMPTEM
      SCALINIT (2,K) = TEMPTEM
   END DO

C    REGION 9
   IPOSB  = IPOSB + IREG
   IPOST  = IPOST - IREG
   VELPOS = 10.
   TEMPOS = 1400.
   SCALINIT (1,IPOSB) = VELPOS
   SCALINIT (1,IPOST) = VELPOS
   SCALINIT (2,IPOSB) = TEMPOS
   SCALINIT (2,IPOST) = TEMPOS
   REG    = 0.03086 * NOG * 2.
   IREG   = REG + 0.49999
   FREG   = 0.01228 * NOG * 2.
   IFREG  = FREG + 0.49999
   IREGM  = IREG - 1
   VSLOPE = -10./(IREG + IFREG)
   TSLOPE = 100./IREG
   DO I = 1, IREGM, 1
      TEMPVEL      = VSLOPE * I + VELPOS
      J    = IPOSB+I
      K    = IPOST-I
      SCALINIT (1,J) = TEMPVEL
      SCALINIT (1,K) = TEMPVEL
      TEMPTEM      = TSLOPE * I + TEMPOS
      SCALINIT (2,J) = TEMPTEM
      SCALINIT (2,K) = TEMPTEM
   END DO

C    REGION 10
   IPOSB  = IPOSB + IREG
   IPOST  = IPOST - IREG
   VELPOS = VSLOPE * IREG + VELPOS
   TEMPOS = 1500.
   SCALINIT (1,IPOSB) = VELPOS
   SCALINIT (1,IPOST) = VELPOS
   SCALINIT (2,IPOSB) = TEMPOS
   SCALINIT (2,IPOST) = TEMPOS
   IREG   = IFREG
   IREGM  = IREG - 1
```

```
      TSLOPE = 100./IREG

      DO I = 1, IREGM, 1
        TEMPVEL      = VSLOPE * I + VELPOS
        J   = IPOSB+I
        K    = IPOST-I
        SCALINIT (1,J) = TEMPVEL
        SCALINIT (1,K) = TEMPVEL
        TEMPTEM      = TSLOPE* I + TEMPOS
        SCALINIT (2,J) = TEMPTEM
        SCALINIT (2,K) = TEMPTEM
      END DO

C    REGION 11
      IPOSB  = IPOSB + IREG
      IPOST  = IPOST - IREG
      VELPOS = 0.0
      TEMPOS = 1600.
      SCALINIT (1,IPOSB) = VELPOS
      SCALINIT (1,IPOST) = VELPOS
      SCALINIT (2,IPOSB) = TEMPOS
      SCALINIT (2,IPOST) = TEMPOS
      REG    = 0.01246 * NOG * 2.
      IREG   = REG + 0.49999
      FREG   = 0.02349 * NOG * 2.
      IFREG  = FREG + 0.49999
      IREGM  = IREG - 1
      VSLOPE = -2.5/(IREG + IFREG)
      TSLOPE = 100./IREG

      DO I = 1, IREGM, 1
        TEMPVEL      = VSLOPE * I
        J   = IPOSB+I
        K    = IPOST-I
        SCALINIT (1,J) = TEMPVEL
        SCALINIT (1,K) = TEMPVEL
        TEMPTEM      = TSLOPE* I + TEMPOS
        SCALINIT (2,J) = TEMPTEM
        SCALINIT (2,K) = TEMPTEM
      END DO

C    REGION 12
      IPOSB  = IPOSB + IREG
      IPOST  = IPOST - IREG
```

```
      VELPOS = VSLOPE * IREG + VELPOS
      TEMPOS = 1700.
      SCALINIT (1,IPOSB) = VELPOS
      SCALINIT (1,IPOST) = VELPOS
      SCALINIT (2,IPOSB) = TEMPOS
      SCALINIT (2,IPOST) = TEMPOS
C    USE IREGAT TO HOLD THE OLD IREG
      IREGAT = IREG
      IREG   = IFREG
      IREGM  = IREG - 1

      TPOSB = IPOSB + IREG
      TPOST = IPOST - IREGM

      IF (TPOST .LE. TPOSB ) THEN
        WRITE (LOUT,*) ' ROUNDOFF ERROR IN INPUT VELOCITY
DISTRIBUTION'
         WRITE (LOUT,*) '   NUMBER OF GRID POINTS MUST BE ADJUSTED.'
         WRITE (LOUT,*) '      SHOULD BE ODD AND 103 OR > .'
         STOP
      END IF
      IF (TPOST - 1 .EQ. TPOSB) THEN

        TSLOPE = 50./IREG
        DO I = 1, IREGM, 1
          TEMPVEL      = VSLOPE * I + VELPOS
          TEMPTEM      = TSLOPE * I + TEMPOS
          J          = IPOSB+I
          K          = IPOST-I
          SCALINIT (1,J) = TEMPVEL
          SCALINIT (1,K) = TEMPVEL
          SCALINIT (2,J) = TEMPTEM
          SCALINIT (2,K) = TEMPTEM
        END DO
      ELSE IF (TPOST - 3 .EQ. TPOSB) THEN
C      NOTE, YOU CAN NEVER HAVE AN ODD NO. OF EXTRA SPACES
C       THIS CASE TAKES CARE OF 2 EXTRA SPACES
      IREG = IREG + 1
      VSLOPE = (-2.5 - VELPOS)/IREG
      TSLOPE = 50./IREG
      DO I = 1, IREG-1, 1
        TEMPVEL      = VSLOPE * I + VELPOS
        TEMPTEM      = TSLOPE * I + TEMPOS
        J          = IPOSB+I
```

```
      K           = IPOST-I
       SCALINIT (1,J) = TEMPVEL
       SCALINIT (1,K) = TEMPVEL
       SCALINIT (2,J) = TEMPTEM
       SCALINIT (2,K) = TEMPTEM
     END DO
    ELSE
C     IF THERE ARE MORE THEN 2 EXTRA SPACES, ABORT
      WRITE (LOUT,*) ' ROUNDOFF ERROR IN INPUT VELOCITY
DISTRIBUTION'
       WRITE (LOUT,*) ' THERE ARE MORE THEN TWO EXTRA SPACES '
       WRITE (LOUT,*) ' NUMBER OF GRID POINTS MUST BE ADJUSTED.'
       WRITE (LOUT,*) '      SHOULD BE ODD AND 103 OR > .'
       STOP
    END IF
    SCALINIT (1,NOG + 1) = -2.5
    SCALINIT (2,NOG + 1) = 1750.
    RETURN
    END
```

A.2 Source code for the initial conditions (Mulholland et al. "like model)

```
PROGRAM INITIALCON
C    ***********************************************************
C    LAST MODIFIED ON   03/18/00   @   10:00
!!!!!    TFLAME = TINFIN  I.E. NO FLAME SHEET, OR NO IGNITION
C    WRITTEN BY JRS ON 02/14/00 TO COMPUTE THE INPUT CONDITIONS TO
C    THE ODT MODEL, USING A MODIFIED VERSION OF THE DROPLET
C    TRAJECTORY MODEL IN MULHOLLAND ET AL. APPENDIX A
     IMPLICIT NONE
     REAL    AIRNU, ANGLE, AREA, ATTWO, BASESH, BMAST
     REAL    BLN, BP1, BULKVEL
     REAL    CDBAS, CDINF, CDO, CDOO, CDSTAR, CONST1
     REAL    CONST2, CONST3, CONST4, CONST5, CONST6
     REAL    CONST7, COSANG, CPFGAS
     REAL    DABAVE, DABZERO, DELTAD, DELTAM, DELTASD
     REAL    DELTAT, DELTATD, DELTAX, DIANEW, DIAP
     REAL    DMASS, DMNEW, DPOS
     REAL    EPSIL, EPSILON, ETAE, FGD, FRE, FXCOEF
     REAL    GAD, GAMMA, HEATCAP, HEATCOM, HEATVAP, HEFF
     INTEGER IDEGRE, IINT
     LOGICAL LCP3
     INTEGER LOUT, NOI
     REAL    PI
     REAL    REN, RHOG, RHOL, ROOT1, ROOT2
     REAL    SCHMIDT, SHSTAR, SINANG, SOD, STOICH, TAUP, TDNEW, TDROP
     REAL    TEMPZERO, TERM, TFLAME, TIME, TINFIN
     REAL    TTHIRD
     REAL    VDNEW, VDROP, VGD
     REAL    XPOS, XVEL, YOINFIN, YPOS, YVEL

C    AX**2 + BX + C = 0


C    SIGNIFICANT VARIABLES
C    ATTWO  = 'A' 'T'IMES 'TWO' -- USEFUL IN NUMERIC IMPLEMENTATION
C    TERM   = B**2 - 2*ATTWO*C
C    ROOT1  = (-B + SQRT(TERM)) / ATTWO
C    ROOT2  = (-B - SQRT(TERM)) / ATTWO
C    V DROP = VELOCITY OF THE DROP IN THE D DIRECTION [=] M/S
C    V G D  = VELOCITY OF THE GAS STREAM IN THE D DIRECTION [=] M/S
C    F G D  = FORCE OF GRAVITY IN THE D DIRECTION = SIN(30)MASS *
GRAVITY
```

```
C    GA D  = GRAVITAIONAL ACCEL.(9.811 M/S**2) TIMES SIN(THETA) IN D
     DIRECT.
C    S O D = S/D THE INTERDROPLET SPACING
C    RE N  = REYNOLDS NUMBER IN THE D DIRECTION
C    CD INF = DRAG COEFF. FOR INFINITELY SPACED DROPS
C    CD BAS = BASE DRAG COEF, WITH OUR MASS TRANSFER
C    ETAE  = MASS TRANSFER CORRECTION TO CD

C    ASSIGN SIGNIFICANT VALUES HERE
     LOUT  = 6
     OPEN (LOUT, FILE = 'noignc10cp3.out')
     IDEGRE  = 30
     DIAP    = 0.000234
     VDROP   = 8.5
     SOD     = 45.0
     TDROP   = 296.15
     LCP3   = .TRUE.
     DPOS    = 0.0
     TFLAME  = 1100.
C     NO FLAME IN THIS ROUTINE !!!!
C     TFLAME  = 1386.8877
     HEATCAP = 2000.0
     HEATCOM = 44000000.0
     HEATVAP = 350000.0
     RHOL    = 813.3
     STOICH  = 0.317
     YOINFIN = 0.0515
     DABZERO = 0.0000088
     TEMPZERO= 303.15
C    GAD = SIN (THETA) * GRAV. ACC.
     GAD    = 0.5 * 9.811
     RHOL   = 813.3   ! [=] KG/M**3
     PI     = ACOS(-1.0)
     ANGLE  = 3./18. * PI
     COSANG = COS(ANGLE)
     SINANG = SIN(ANGLE)
     NOI    = 9000
     TIME   = 0.14 / VDROP / 4000.0
     DMASS  = PI * DIAP**3 * RHOL / 6.0
     WRITE (LOUT,5) DIAP, SOD, TDROP
  5  FORMAT ( 2X, 'INITIAL DIAM = ', E14.7, ' SPACING = ', E14.7,
    2        ' TEMP. =',E14.7, ' K')
     IF (LCP3) THEN
       WRITE (LOUT,10) IDEGRE, TIME, VDROP
```

```
10    FORMAT (3X, I3, ' DEGREES, TIME STEP =', E14.7, ' VEL. =',
   2          E14.7, ' cpf = touluene, heptane, c10h21', /,
   3          ' new corrected background velocity gradient')
   ELSE
     WRITE (LOUT,15) IDEGRE, TIME, VDROP
15    FORMAT (3X, I3, ' DEGREES, TIME STEP =', E14.7, ' VEL. =',
   2          E14.7, ' cpf = c10h21', /,
   3          ' new corrected background velocity gradient')
   END IF
   WRITE (LOUT,20)
20  FORMAT(1X,'     DPOS        XPOS         YPOS',
   2     '       DIAP        TDROP         VDROP')
   DO IINT = 1,NOI,1
     CALL VGDTHIRTY(DPOS, LOUT, TINFIN, VGD)

     CALL EFLAMET (DIAP, HEATCOM, LCP3, LOUT, RHOL,
   2          STOICH, TDROP, TFLAME, TINFIN, YOINFIN,
   3          AIRNU, CPFGAS, HEFF, RHOG, TAUP, TTHIRD)


     AREA  = PI * DIAP**2 / 4.0
     FGD   = GAD*DMASS
     CONST6 = VDROP - VGD
     REN   = DIAP * ABS(CONST6) / AIRNU
     BMAST = (CPFGAS * (TINFIN - TDROP) +
   2      YOINFIN * STOICH * HEATCOM) / HEFF

     IF (CONST6 .GT. 0.0) THEN
C        MULHOLLAND ET AL. MODEL WORKS FOR VDROP > VGD

       CDINF  = 24.0/REN * (1 + 0.11 * REN**0.687)
       CDOO   = 0.755/REN
       CDO    = CDOO + 43.0/REN * (SOD - 1)
       CDBAS  = (CDO**(-0.678) + CDINF**(-0.678))**(-1/0.678)
       ETAE   = 1. / (1.0 + BMAST)
       CDSTAR = ETAE * CDBAS
       CONST1 = CDSTAR * RHOG * AREA
       EPSIL  = CONST1 / DMASS
       IF (FGD .EQ. 0.0) THEN
C        FGD = 0 WHEN INCIDENT ANGLE IS 0.0
         IF (VGD .EQ. 0.0) THEN
C          SIMPLE FORM OF DVD/VD**2 = ACONST * DT
           CONST2 = VDROP * CONST1 * TIME
           VDNEW  = DMASS * VDROP/(CONST2 + DMASS)
```

```
          CONST3 = CONST2 / DMASS + 1.0
          IF (CONST3 .LE. 0.0) THEN
            WRITE (LOUT, 90)

            STOP
          ELSE
            DELTASD = DMASS / CONST1 * LOG (CONST3)
          END IF
        ELSE
          CONST2 = CONST6 * CONST1 * TIME
          VDNEW  = DMASS * CONST6 / (DMASS + CONST2) + VGD
          CONST3 = 1.0 + CONST2 / DMASS
          IF (CONST3 .LE. 0.0) THEN
            WRITE (LOUT, 90)
            STOP
          ELSE
            DELTASD = DMASS / CONST1 * LOG (CONST3)
          END IF
        END IF
      ELSE
        GAMMA   = FGD / CONST1
        EPSILON = CONST1 / DMASS
        CONST2  = SQRT(GAMMA)
        ROOT1   = VGD + CONST2
        ROOT2   = VGD - CONST2
        CONST3  = (VDROP - ROOT2)/(VDROP - ROOT1)
        CONST4  = EXP(EPSILON * 2.0 * CONST2 * TIME)
        CONST5  = CONST3 * CONST4
        CONST7  = 1.0 - CONST5
        VDNEW   = (-ROOT1 * CONST5 + ROOT2) / CONST7

        DELTASD = LOG(CONST7 / (1.0 - CONST3)) / EPSILON
   2            + ROOT2 * TIME
C   ***************************************************************
      END IF
     ELSE IF ((CONST6 .EQ. 0.0) .AND. (FGD .NE. 0.0)) THEN
       VDNEW   = GAD * TIME + VDROP
       DELTASD = GAD * TIME**2 / 2.0 + VDROP * TIME
     ELSE IF (FGD .EQ. 0.0) THEN
C       MUST COMPUTE CD STAR SOMEHOW  !!
       CDINF  = 24.0/REN * (1 + 0.11 * REN**0.687)
       CDOO   = 0.755/REN
       CDO    = CDOO + 43.0/REN * (SOD - 1)
       CDBAS  = (CDO**(-0.678) + CDINF**(-0.678))**(-1/0.678)
```

```
      ETAE   = 1. / (1.0 + BMAST)
      CDSTAR = ETAE * CDBAS
      CONST1  = CDSTAR * RHOG * AREA
      CONST2  = CONST6 * CONST1 * TIME
      VDNEW   = VGD + DMASS * CONST6 / (DMASS + CONST2)
C     !!!  DO I NEED TO CHECK THE SIGN OF LOG ?
      CONST3  = 1.0 + CONST2/DMASS
      IF (CONST3 .LE. 0.0) THEN
        WRITE (LOUT, 90)
 90      FORMAT (1X, 'CONST3 IS NEGATIVE')
       STOP
      END IF
      DELTASD = VGD * TIME + DMASS/CONST1 * LOG(CONST3)
    ELSE
      WRITE (LOUT,95)
 95      FORMAT (1X, 'ALWAYS IMAGINARY ROOTS!!')
      STOP
    END IF
    DPOS = DPOS + DELTASD
C ********************************************************
    IF (REN .LE. 1.0) THEN
C
      FRE = 1.0
    ELSE IF (REN .LE. 400) THEN
C      CORRECTION FACTOR
      FRE = (REN) ** 0.077
    ELSE
      WRITE (LOUT,*) ' PARTICLE Re T > 400'
      WRITE (LOUT,*) ' STOPPED IN DUPDATE', REN
      WRITE (LOUT,*) ' PARTICLE Re T > 400'
      WRITE (LOUT,*) ' STOPPED IN DUPDATE', REN
      STOP
    END IF

    BP1   = BMAST + 1.
    BLN    = ALOG(BP1)


C   FOR NOW RHOGAS IS THE DENSITY OF AIR AT THE 1/3 RULE TEMP.
    CALL ESCHMIDT(AIRNU, DABZERO, TTHIRD, TEMPZERO,
   2            DABAVE, SCHMIDT)

    BASESH  = 1. + FRE * (1. + REN * SCHMIDT) ** (1./3.)
```

```fortran
      SHSTAR  = 2. + (BASESH - 2.) * BMAST/((BP1)**0.7 * BLN )

      CONST7  =  RHOG * DABAVE * SHSTAR * BLN * TIME

      DELTAD  = - 2.0 * CONST7 / (RHOL * DIAP)
      DIANEW  = DIAP + DELTAD
      DELTAM  = PI * DIAP * CONST7
      DMNEW   = DMASS - DELTAM
      DELTATD = (HEFF - HEATVAP) * DELTAM / (HEATCAP * DMASS)
      TDNEW   = TDROP + DELTATD

      IF (DIANEW .LE. 0.0 .OR. DMNEW .LE. 0.0) THEN
        DIANEW = 0.0
        DMASS = 0.0
        TDROP  = TDNEW
      ELSE
        DMASS = DMNEW
        TDROP  = TDNEW
      END IF
      DIAP  = DIANEW
      VDROP = VDNEW
      XPOS  = DPOS * COSANG
      YPOS  = - DPOS * SINANG
      XVEL  = VDROP*COSANG
      YVEL  = -VDROP*SINANG
      WRITE (LOUT,30) IINT, DPOS, XPOS, (0.40005+YPOS), DIAP,
     2          TDROP, VDROP, XVEL, YVEL
  30    FORMAT (1X, I4, 8E17.7)
C *******************************************************************
      END DO
      STOP
      END
```

```
      SUBROUTINE ESCHMIDT (AIRNU, DABZERO, TEMP, TEMPZERO,
   2                    DABAVE, SCHMIDT)
C    LAST UPDATED 02/01/00    AT  6:30 PM

C    CREATED BY JOHN SCHMIDT  ON 01/26/00
C     THIS ROUTINE TAKES A TEMP AND FINDS THE CORESPONDING
SCHMIDT NO.
C     BIANARY DIFFUSIVITY, AND GAS PHASE DENSITY AT THAT
TEMPERATURE


      IMPLICIT NONE
      REAL AIRNU, DABAVE, DABZERO, TEMP, TEMPZERO, SCHMIDT

      DABAVE = DABZERO * (TEMP/TEMPZERO)**1.5
      SCHMIDT = AIRNU/DABAVE

      RETURN
      END
```

```
      SUBROUTINE EFLAMET (DIAP, HEATCOM, LCP3, LOUT, RHOL,
   2              STOICH, TDROP, TFLAME, TINFIN, YOINFIN,
   3              AIRNU, CPFGAS, HEFF, RHOGAS, TAUP, TTHIRD)
C ***************************************************************
C    LAST UPDATED ON 03/18/00  AT 10:00  AM

!!!!!   TFLAME = TINFIN

C    WRITTEN BY JRSCHMIDT ON 02/02/00

C    T FLAME = FLAME SHEET TEMPERATURE, START WITH A GUESS
C    T DROP  = DROP TEMP.

     IMPLICIT NONE
     REAL   AIRMU, AIRNU, CPGAS, CPFGAS
     REAL   DIAP, HEATCOM, HEFF
     INTEGER ITT
     LOGICAL LCP3, LITT
     INTEGER LOUT
     REAL   RHOGAS, RHOL, STOICH
     REAL   TAUP, TDROP, TFLAME, TFNEW, TINFIN, TTHIRD
     REAL   XFS, YCONST, YFS, YOINFIN

C    CLAUSIUS-CLAPEYRON EQUATION.  PRESSURE IS IN ATMOSPHERES
C    GIVES MOLE FRACTION IN GAS AT THE SURFACE
C    GAS CONSTANT R = 8.314 J/MOL/K
C    FROM EPA REPORT.  AVE. MOLECULAR WEIGHT = 0.136 KG/MOL,
C    BOILING TEMP. = 400 K, HEAT OF VAPORIZATION = 350,000 J/KG

     XFS = EXP(5725.283*(0.0025 - 1./TDROP))
C    30% EXCESS AIR, ASSUMING 79% N2, 21% O2, COMPLETE BURNING.
C    NATURAL GAS IS BETWEEN 95-98 % METHANE (CH4)
     YCONST = 1738.08 * XFS
     YFS   = YCONST / (353.866*(1.-XFS) + YCONST)

C !!!!!  AIRNU MUST BE EVALUATED AT 1/3 RULE   -SIRIGNANO
C      YOINFIN WAS CALCULATED TO BE 5.1465342

     LITT = .TRUE.
     ITT  = 1
     DO WHILE ((LITT) .AND. (ITT .LE. 35))
       TTHIRD = TDROP + (TFLAME - TDROP) / 3.
       CALL ETMPVAR (LCP3, LOUT, TTHIRD, AIRMU, AIRNU, CPGAS,
   2           CPFGAS, RHOGAS)
```

```fortran
       HEFF = (1. - YFS) * (CPGAS*(TINFIN - TDROP)
     2   + YOINFIN * STOICH * HEATCOM) / (YFS + YOINFIN * STOICH)

!!!!! TFLAME = TINFIN
       TFNEW = TINFIN
C      TFNEW = (TINFIN + YOINFIN*STOICH*(HEATCOM - HEFF + CPFGAS
C   2         * TDROP)/CPGAS)/(1. + YOINFIN*STOICH*CPFGAS/CPGAS)
C   !!  CPGAS SHOULD BE AT 1/3 THE DIFFERENCE FROM DROP TO FLAME
TEMP.
       IF (ABS(TFNEW - TFLAME) .LE. 0.1) THEN
         LITT = .FALSE.
       ELSE
         ITT = ITT + 1
       END IF
       TFLAME = TFNEW
C      DEBUG  !!!!!!
C      IF (TDROP .GT. 380.8) THEN
C         WRITE (LOUT, 15) TFLAME, TDROP
C      END IF
C      END DEBUG
     END DO
     IF (LITT) THEN
       WRITE (LOUT,*) ' FLAME TEMP. DID NOT CONVERGE IN 35 '
       WRITE (LOUT,*) 'ITTERATIONS, DROPLET IN EFLAMET'
       WRITE (LOUT,*)
       WRITE (LOUT,*)
       WRITE (LOUT,*)  ' FLAME TEMP. DID NOT CONVERGE IN 35 '
       WRITE (LOUT,*)  'ITTERATIONS, DROPLET IN EFLAMET'
       STOP
     END IF
C   !!!!!  TAUP IS A VARIABLE   !!!!!!!!!!!
     TAUP   = RHOL * DIAP**2 / (18.0 * AIRMU)
C   TEMP OUTPUT FLAME TEMP, DROP TEMP   !! DEBUG

C      WRITE (LOUT, 15)  TFLAME, TDROP
C 15     FORMAT (6X, 'Tf ', E12.6, 'Td ', E12.6)
C   DEBUG   !!!!

     RETURN
     END
```

```
      SUBROUTINE ETMPVAR (LCP3, LDOUT, TEMP, VISC, AIRNU, CPGAS, CPFGAS,
   2            DENSITY)
C ******************************************************************
C    LAST UPDATED 02/03/00    AT   7:30  PM
C  !!!!! TEMPARARILY MODIFIED ON 02/17/00  TO TRY CPF = C10H21

C    CREATED BY JOHN SCHMIDT  ON 01/24/00
C    THIS ROUTINE TAKES A TEMP AND FINDS THE CORESPONDING VISCOSITY (NU),
C    THE HEAT CAPACITY OF THE GAS PHASE (CPGAS), AND THE HEAT CAPACITY OF
C    THE GAS PHASE FUEL (CPFGAS) AT THAT TEMPERATURE
C    R GAS = MOLAR GAS CONSTANT UNITS J/G-MOL/K

      IMPLICIT NONE
      REAL    AIRNU, CPFGAS, CPGAS, CP1, CP2, CP3
      REAL    DENSITY, EMW,EXMW, HMW
      LOGICAL LCP3
      INTEGER LDOUT
      REAL    SLOPE, TEMP, TMW, VISC

C    FOR NOW ASSUME CPFGAS = CPGAS
C    FIND TEMP RANGE AND LINEARLY INTERPOLATE

C    IMPORTANT VARIABLES
C      VISCOSITY OF AIR IN KG/S/M
C      DENSITY OF AIR IN KG/M**3
C      HEAT CAPACITY IN J/KG/K

      IF (TEMP .LE. 299.8166) THEN
        VISC    = 0.000018602
        DENSITY = 1.175754964
        CPGAS   = 1004.832
      ELSE IF (TEMP .LE. 533.15) THEN
        SLOPE   = (0.000027696 - 0.000018602) / 233.3333
        VISC    = 0.000018602 + SLOPE * (TEMP - 299.8166)
        SLOPE   = (0.659960552 - 1.175754964) / 233.3333
        DENSITY = 1.175754964 + SLOPE * (TEMP - 299.8166)
        SLOPE   = (1013.2056 - 1004.832) / 233.3333
        CPGAS   = 1004.832 + SLOPE * (TEMP - 299.8166)
      ELSE IF (TEMP .LE. 588.7055) THEN
        SLOPE   = (0.000029763 - 0.000027696) / 55.5555
        VISC    =  0.000027696 + SLOPE * (TEMP - 533.15)
```

```
     SLOPE   = (0.597488558 - 0.659960552) / 55.5555
     DENSITY = 0.659960552 + SLOPE * (TEMP - 533.15)
     CPGAS   = 1013.2056
   ELSE IF (TEMP .LE. 644.2611) THEN
     SLOPE   = (0.000031417 - 0.000029763) / 55.5555
     VISC    = 0.000029763 + SLOPE * (TEMP - 588.7055)
     SLOPE   = (0.546229486 - 0.597488558) / 55.5555
     DENSITY = 0.597488558 + SLOPE * (TEMP - 588.7055)
     SLOPE   = (1017.3924 - 1013.2056) / 55.5555
     CPGAS   = 1013.2056 + SLOPE * (TEMP - 588.7055)
   ELSE IF (TEMP .LE. 699.8166) THEN
     SLOPE   = (0.00003307 - 0.000031417) / 55.5555
     VISC    = 0.000031417 + SLOPE * (TEMP - 644.2611)
     SLOPE   = (0.502979644 - 0.546229486) / 55.5555
     DENSITY = 0.546229486 + SLOPE * (TEMP - 644.2611)
     SLOPE   = (1021.5792 - 1017.3924) / 55.5555
     CPGAS   = 1017.3924 + SLOPE * (TEMP - 644.2611)
   ELSE IF (TEMP .LE. 755.3722) THEN
     SLOPE   = (0.000035137 - 0.00003307) / 55.5555
     VISC    = 0.00003307 + SLOPE * (TEMP - 699.8166)
     SLOPE   = (0.47254457 - 0.502979644) / 55.5555
     DENSITY = 0.502979644 + SLOPE * (TEMP - 699.8166)
     SLOPE   = (1025.766 - 1021.5792) / 55.5555
     CPGAS   = 1021.5792 + SLOPE * (TEMP - 699.8166)
   ELSE IF (TEMP .LE. 810.9277) THEN
     SLOPE   = (0.000036791 - 0.000035137) / 55.5555
     VISC    = 0.000035137 + SLOPE * (TEMP - 755.3722)
     SLOPE   = (0.44050765 - 0.47254457) / 55.5555
     DENSITY = 0.47254457 + SLOPE * (TEMP - 755.3722)
     SLOPE   = (1029.9528 - 1025.766) / 55.5555
     CPGAS   = 1025.766 + SLOPE * (TEMP - 755.3722)
   ELSE IF (TEMP .LE. 922.0388) THEN
     SLOPE   = (0.000040098 - 0.000036791) / 111.1111
     VISC    = 0.000036791 + SLOPE * (TEMP - 810.9277)
     SLOPE   = (0.381239348 - 0.44050765) / 111.1111
     DENSITY = 0.44050765 + SLOPE * (TEMP - 810.9277)
     SLOPE   = (1038.3264 - 1029.9528) / 111.1111
     CPGAS   = 1029.9528 + SLOPE * (TEMP - 810.9277)
   ELSE IF (TEMP .LE. 1033.15) THEN
     SLOPE   = (0.000043405 - 0.000040098) / 111.1111
     VISC    = 0.000040098 + SLOPE * (TEMP - 922.0388)
     SLOPE   = (0.339591352 - 0.381239348) / 111.1111
     DENSITY = 0.381239348 + SLOPE * (TEMP - 922.0388)
     SLOPE   = (1050.8868 - 1038.3264) / 111.1111
```

```
         CPGAS   = 1038.3264 + SLOPE * (TEMP - 922.0388)
      ELSE IF (TEMP .LE. 1144.2611) THEN
        SLOPE   = (0.000046298 - 0.000043405) / 111.1111
        VISC    = 0.000043405 + SLOPE * (TEMP - 1144.2611)
        SLOPE   = (0.307554432 - 0.339591352) / 111.1111
        DENSITY = 0.339591352 + SLOPE * (TEMP - 1144.2611)
        SLOPE   = (1063.4472 - 1050.8868) / 111.1111
        CPGAS   = 1050.8868 + SLOPE * (TEMP - 1144.2611)
      ELSE IF (TEMP .LE. 1255.3722) THEN
        SLOPE   = (0.000049605 - 0.000046298) / 111.1111
        VISC    = 0.000046298 + SLOPE * (TEMP - 1255.3722)
        SLOPE   = (0.28032305 - 0.307554432) / 111.1111
        DENSITY = 0.307554432 + SLOPE * (TEMP - 1255.3722)
        SLOPE   = (1076.0076 - 1063.4472) / 111.1111
        CPGAS   = 1063.4472 + SLOPE * (TEMP - 1255.3722)
      ELSE IF (TEMP .LE. 1366.4833) THEN
        SLOPE   = (0.000052499 - 0.000049605) / 111.1111
        VISC    = 0.000049605 + SLOPE * (TEMP - 1366.4833)
        SLOPE   = (0.257897206 - 0.28032305 ) / 111.1111
        DENSITY = 0.28032305 + SLOPE * (TEMP - 1366.4833)
        SLOPE   = (1088.5680 - 1076.0076) / 111.1111
        CPGAS   = 1076.0076 + SLOPE * (TEMP - 1366.4833)
      ELSE
        VISC    = 0.000052499
        DENSITY = 0.257897206
        CPGAS   = 1088.5680
        WRITE (LDOUT,*) ' FLAME TEMPERATURE TOO HIGH '
        WRITE (LDOUT,*) ' VISCOSITY IN ETMPVAR'
      END IF

C    VALUES OF DENSITY, VISCOSITY, AND HEAT CAPACITY ARE
C    FROM "AIR POLLUTION CONTROL, A DESIGN APPROACH"
C    BY C.D. COOPER & F.C. ALLEY. PAGE 654
C

C    NU = VISCOSITY/DENSITY [M**2/S]
      AIRNU  = VISC / DENSITY

C     RGAS = 8.3144    ! UNITS J/G-MOL/K
      HMW  = 100.204
      EMW  = 106.1674
      TMW  = 91.13258
      EXMW = 141.27670
```

```
C ****************************************************************
    IF (TEMP .GE. 200.) THEN
      IF (TEMP .LE. 1000.) THEN
C      200 - 1000 K
C        HEPTANE
        CP1 = 11.15325 - 0.009494155*TEMP + 0.0001955712*TEMP**2
     2      - 0.0000002497525 * TEMP**3 + 9.848732D-11 * TEMP**4

C        ETHYLBENZENE
        CP2 = 3.51535 + 0.01781457 * TEMP + 0.000118934*TEMP**2
     2      - 1.756398D-07 * TEMP**3 + 7.320611D-11 * TEMP**4
C        C10H21
        CP3 = 3.089701 + 0.08411795*TEMP + 1.590184D-05*TEMP**2
     2      - 7.238793D-08*TEMP**3 + 3.226693D-11*TEMP**4
C  TEMPARARY TO CHECK OUT USING CP3 AS AN AVERAGE
C        CPFGAS = 0.399*CP1/HMW + 0.289*CP2/EMW + 0.312*CP3/EXMW
C        CPFGAS = CP3/EXMW

      ELSE IF (TEMP .LE. 6000) THEN
C      1000 - 6000 K
C        HEPTANE
        CP1 = 18.53547 + 0.03914205*TEMP - 1.380303D-05*TEMP**2
     2      + 2.224039D-09 * TEMP**3 - 1.334526D-13 * TEMP**4
C        ETHYLBENZENE
        CP2 = 15.57608 + 0.03230646*TEMP - 1.190027D-05*TEMP**2
     2      + 1.967925D-09 * TEMP**3 - 1.199112D-13 * TEMP**4

        CP3 = 21.32213 + 0.06157352*TEMP - 2.384948D-05*TEMP**2
     2      + 4.220912D-09*TEMP**3 - 2.788931D-13*TEMP**4

C  TEMPARARY MODIFICATION TO CHECK OUT USING CP3 AS AN
AVERAGE
C        CPFGAS = 0.399*CP1/HMW + 0.289*CP2/EMW + 0.312*CP3/EXMW
C        CPFGAS = CP3/EXMW

      ELSE
        PRINT*, '  TEMP. IS OVER 6000 K'
      END IF
    ELSE
      PRINT*, '  TEMP. IS LESS THEN 200 K'
    END IF
C  TEMPARARY TO CHECK OUT USING CP3 AS AN AVERAGE
    IF (LCP3) THEN
      CPFGAS = 0.399*CP1/HMW + 0.289*CP2/EMW + 0.312*CP3/EXMW
```

```
      ELSE
         CPFGAS = CP3/EXMW
      END IF
C     RGAS * CP * 1000
      CPFGAS = 8314.4 * CPFGAS
      RETURN
      END
```

```
      SUBROUTINE VGDTHIRTY (DPOS, LOUT, TINFIN, VGD)

C   SPECIFIC FOR THE 30 DEGREE DROPS
C   UNIT NORMAL IN D DIRECTION IS (-2.88675i + 0j + 5k)/5.773502692

    IMPLICIT NONE
    REAL    DPOS
    INTEGER LOUT
    REAL    RUN, SLOPE, TINFIN, VGD

    RUN = 0.05773502692
C   5 CM POSITION  DPOS = 0.05773502692  EQ. TO 5 CM IN Z DIRECTION

    IF (DPOS .LE. RUN) THEN
      SLOPE = -1.116378713 / RUN
      VGD   = SLOPE * DPOS
      SLOPE = (1128.2 - 1090.0)/ RUN
      TINFIN= 1090.0 + SLOPE * DPOS
    ELSE IF (DPOS .LE. 2.0 * RUN) THEN
      SLOPE = (1.174872261 + 1.116378713) / RUN
      VGD   = -1.116378713 + SLOPE * (DPOS - RUN)
      SLOPE = (1170.0 - 1128.2)/ RUN
      TINFIN= 1128.2 + SLOPE * (DPOS - RUN)
    ELSE IF (DPOS .LE. 0.162) THEN
      SLOPE = (8.4 - 1.174872261) / (0.162 - 2.0 * RUN)
      VGD   = 1.174872261 + SLOPE * (DPOS - 2.0 * RUN)
      SLOPE = (1250 - 1170.0)/ (0.162 - 2.0 * RUN)
      TINFIN= 1170.0 + SLOPE * (DPOS - 2.0 * RUN)
    ELSE
      WRITE (LOUT,10)
 10     FORMAT (1X, ' WENT BEYOND 14 cm IN THE Z DIRECTION')
      STOP
    END IF
    RETURN
    END
```

```
      SUBROUTINE VGDZERO (DPOS, LOUT, TINFIN, VGD)

C   SPECIFIC FOR THE 0 DEGREE DROPS
C   UNIT NORMAL IN D DIRECTION IS (2.88675i + 0j + 5k)/5.773502692

      IMPLICIT NONE
      REAL    DPOS
      INTEGER LOUT
      REAL    RUN, SLOPE, TINFIN, VGD

      RUN = 0.05
C   5 CM POSITION  DPOS = 5.773502692  EQ. TO 5 CM IN Z DIRECTION

      IF (DPOS .LE. RUN) THEN
        SLOPE = -3.149489357 / RUN
        VGD   = SLOPE * DPOS
        SLOPE = (1125.4 - 1090.)/ RUN
        TINFIN= 1090 + SLOPE * DPOS
      ELSE IF (DPOS .LE. 2.0 * RUN) THEN
        SLOPE = (-5.267692907 + 3.149489357) / RUN
        VGD   = -3.149489357 + SLOPE * (DPOS - RUN)
        SLOPE = (1130.4 - 1125.4)/ RUN
        TINFIN= 1125.4 + SLOPE * (DPOS - RUN)
      ELSE
        WRITE (LOUT,10)
10      FORMAT (1X, ' WENT BEYOND 10 cm IN THE Z DIRECTION')
        STOP
      END IF
      RETURN
      END
```

```fortran
      SUBROUTINE VGDFORTYFIVE (DPOS, LOUT, TINFIN, VGD)
C     SPECIFIC FOR THE 45 DEGREE DROPS
C     UNIT NORMAL IN D DIRECTION IS (2.88675i + 0j + 5k)/5.773502692

      IMPLICIT NONE
      REAL   DPOS
      INTEGER LOUT
      REAL   RUN, SLOPE, TINFIN, VGD

      RUN = 0.03535533906
C     5 CM POSITION  DPOS = 5.773502692  EQ. TO 5 CM IN Z DIRECTION

      IF (DPOS .LE. RUN) THEN
        SLOPE  = -2.866005 / RUN
        VGD    = SLOPE * DPOS
        SLOPE  = (1120. - 1090.0)/ RUN
        TINFIN = 1090.0 + SLOPE * DPOS
      ELSE IF (DPOS .LE. 2.0 * RUN) THEN
        SLOPE  = (4.330129 + 2.866005) / RUN
        VGD    = -2.866005 + SLOPE * (DPOS - RUN)
        SLOPE  = (1155.0 - 1120.0)/ RUN
        TINFIN = 1120.0 + SLOPE * (DPOS - RUN)
      ELSE IF (DPOS .LE. 2.5 * RUN) THEN
        SLOPE  = (24.150619 - 4.330129) / (RUN/2.0)
        VGD    = 4.330129 + SLOPE * (DPOS - 2.0 * RUN)
        SLOPE  = (1200.0 - 1155.0)/ (RUN/2.0)
        TINFIN = 1155.0 + SLOPE * (DPOS - 2.0 * RUN)
      ELSE IF (DPOS .LE. 3.0 * RUN) THEN
        SLOPE  = (11.16023209 - 24.150619) / (RUN/2.0)
        VGD    = 24.150619 + SLOPE * (DPOS - 2.5 * RUN)
        SLOPE  = (1400.0 - 1200.0)/ (RUN/2.0)
        TINFIN = 1200.0 + SLOPE * (DPOS - 2.5 * RUN)
      ELSE IF (DPOS .LE. 4.0 * RUN) THEN
        SLOPE  = (-3.46401323 - 11.16023209) / RUN   note: vz = 17 m/s
        VGD    = 11.16023209 + SLOPE * (DPOS - 3.0 * RUN)  vr = 5 m/s
        SLOPE  = (1750.0 - 1400.0)/ RUN
        TINFIN = 1400.0 + SLOPE * (DPOS - 3.0 * RUN)
      ELSE
        WRITE (LOUT,10)
 10     FORMAT (1X, ' WENT BEYOND 10 cm IN THE Z DIRECTION')
        STOP
      END IF
      RETURN
      END
```

Appendix B

List of Random Number Seeds

A complete list of all the initial values of the random number generator seeds is provided for all 2000 realizations. Any ensemble realization can be generated in any order by simply inputting the random number pair subsequent to the subroutine call DROPLINIT.

The realization number is listed first. The next two numbers on the same line are the random number seeds which were used to start that particular ensemble.

1	12345	67890	50	1074312419	973785132
2	1186279957	69005677	51	1352358419	1866928629
3	1690624489	211101369	52	1161849866	1848858644
4	1795846609	1456147840	53	258763620	1420724382
5	868835522	1002735207	54	1589846737	553980043
6	1749268059	2101811192	55	781044615	2048819304
7	834384517	561404391	56	1401027045	666635467
8	1305514941	728648880	57	520783586	601713317
9	792686244	765654447	58	1230177439	693112874
10	347183723	226715027	59	571499690	193053836
11	1668624725	1879801423	60	2074082037	1059719827
12	163682225	1663712837	61	484389688	1475716536
13	1017370303	1162812113	62	1792330786	1218693923
14	767732798	1025633173	63	1304128765	1571625624
15	1027662748	1009212420	64	608921086	1680671271
16	1912163172	780109556	65	231124642	488616410
17	1377783800	1920041416	66	811240934	38371122
18	1378625952	969054343	67	2143912096	1578998139
19	1845178641	908365528	68	1580560513	1230095510
20	1593358618	1298840694	69	127643294	479959950
21	112840350	2050693735	70	910459273	204478471
22	537145081	2003939625	71	1712130301	713880291
23	1940986384	1592407989	72	1138982360	406132529
24	978291229	274351680	73	1724368929	1128109168
25	688766542	834298067	74	236064501	142341261
26	872317613	41335488	75	1146520950	66430823
27	1443058074	1743631118	76	448997168	1518677961
28	209917579	1843240682	77	317971091	1424366250
29	1054574241	896994182	78	147076255	973730810
30	1929434401	964193217	79	2080901098	573600355
31	151269297	1232499654	80	1278264254	1683255589
32	850760451	1253440098	81	396599059	939800107
33	1665953462	123270931	82	1007419940	159327419
34	529469208	1603084778	83	1274622524	2046320806
35	1735167252	1467960639	84	841789059	1530640285
36	752369616	1666067347	85	2020013400	322719301
37	371162873	1408293313	86	1146258361	482829452
38	1729251049	545886262	87	554133148	1298393944
39	2004147156	1308833762	88	620488237	2009709776
40	1256550714	2027121577	89	1038115902	1125642409
41	520326295	180485227	90	1573361580	568873943
42	523361037	112185635	91	2103335868	370564251
43	303061974	1613251527	92	1332799398	440259673
44	1829406235	483678039	93	174263239	1691150618
45	2132986265	1606122815	94	1400518741	1576932835
46	1263111895	915201664	95	1202142930	257492718
47	549605900	1551385008	96	2091923457	1727583184
48	1826782150	613338377	97	2066878349	1454862013
49	1235913031	101860716	98	2037982505	81592728

99	1534364503	681484694	152	399995428	1033245690
100	1353505990	139281425	153	335577628	1884165922
101	316379665	692645865	154	772281295	1771293824
102	1422911596	1741027341	155	441688430	12318293
103	1617028093	1829046090	156	73914492	1946787956
104	1966322753	207031741	157	1339330664	127576599
105	53734522	2037336266	158	516180202	1171799564
106	88769184	81586106	159	1930013724	367768973
107	1395653044	2039121254	160	1273049744	418710975
108	1632373712	1142068965	161	996299189	1021557839
109	1236202080	1532557227	162	1344004690	202249753
110	1545390256	774071936	163	1156017218	1658756808
111	1254291175	1098568345	164	790232100	423933585
112	352860717	1396712198	165	192790345	1689739541
113	456785419	776943970	166	1012187731	39989808
114	1864286288	1451667994	167	303299331	1596314286
115	792936520	1004288999	168	1684373187	884488773
116	1123236698	946461362	169	596442472	235922311
117	524359377	1227551022	170	372273911	1435804340
118	2073931531	1087975091	171	1188363758	1087559656
119	1565281358	1793670829	172	452239311	348247400
120	899460129	1870790834	173	1978041431	2051348194
121	1295715191	1685490796	174	2013668233	1377576452
122	671990602	2114634167	175	1171951946	1153887003
123	871619689	1310564649	176	128965577	1405234734
124	1562528074	999706816	177	534164264	650825098
125	1187179865	1436748136	178	1334634475	308715443
126	948841502	1603541180	179	1699993048	1438193574
127	584867317	1363710252	180	10730975	1364719394
128	959414535	2029311870	181	776808177	1670425591
129	1064108851	1273179556	182	1128669691	971388479
130	2052490821	45183121	183	23959463	656730208
131	1792503598	944769387	184	464634325	38449253
132	2000346834	1958982655	185	577209206	588259153
133	1116973781	1089595402	186	75664259	813127169
134	176212546	1489154479	187	1236337863	1528500151
135	149088988	1002114439	188	986945543	220659907
136	532627125	1416866238	189	1392159857	896950143
137	1328588014	1109935707	190	1162693271	1915425509
138	1760100544	1441532886	191	1926942905	2011323288
139	986701072	1540828410	192	716339850	351856912
140	2028151563	1114816938	193	2048812503	1526686547
141	1203944694	255992726	194	139912267	166848355
142	1601584413	402916159	195	774183112	1603613346
143	1608768230	820162894	196	40314461	1760945339
144	1272212662	1302061686	197	1862375087	1547467728
145	539630487	1783425599	198	922931048	2138231185
146	1680993430	643328599	199	1700016462	1612700865
147	736799359	692751124	200	1503895733	1734490578
148	1998268385	867881526	201	335518060	1139189603
149	344773061	1787059558	202	475031609	2063342745
150	1245899065	347316868	203	653670677	1274118940
151	530817802	1175506073	204	2112262468	2107575910

205	1388897175	887646311	258	1312050776	584330139
206	886197835	1775987183	259	2141418935	1398863571
207	2006041520	1824202878	260	1245332147	428275452
208	1846114640	1839752023	261	77248785	1625464370
209	371991841	1004869923	262	257281739	1504607338
210	256628332	2059976090	263	795698235	1384183848
211	577656443	290848225	264	1410756273	616749127
212	1365552684	1217853554	265	890523787	1182825539
213	607713362	1342318006	266	1089934493	439981218
214	1397905833	337706462	267	464975597	1056165456
215	143774410	409414900	268	1061469282	784067942
216	630149976	1712888800	269	1153064820	407439828
217	1583053866	1593364008	270	1792871357	1204555552
218	1774160020	509281924	271	1831981870	1357224187
219	1734859660	1451198654	272	739784997	1036309182
220	585981359	1864951180	273	2093605854	404570353
221	1705182038	1690070250	274	1412483300	1602066603
222	957493071	159922051	275	391868626	1084343251
223	738594063	980700862	276	402704287	2115655586
224	174901762	404177469	277	1826026332	811650417
225	166210468	2060540112	278	160925558	186631783
226	861134986	488164062	279	794586115	1396457137
227	312739712	1964185534	280	1224132106	676928970
228	813244032	1203996675	281	1709409215	1743151030
229	1880141482	1693463447	282	711319873	2030582758
230	362715101	71119974	283	873195913	1757582611
231	32149084	971940061	284	1897770831	1965090892
232	1663458951	969846069	285	1992952803	1767653300
233	1191365238	340512777	286	1109382742	1921344734
234	1885115048	890899598	287	1310298138	1116155526
235	1087553149	489297179	288	1884079626	1509816114
236	1956380645	1928957525	289	1937854990	1299229875
237	99061688	386125290	290	632510679	1318644629
238	758455947	701689653	291	2112788786	275193112
239	1512184138	1024141839	292	1668150123	1684866830
240	1079550676	1837141807	293	572478429	1608740710
241	1369084569	787698450	294	1576714825	861953555
242	1253859466	2100861590	295	1211724637	438833654
243	260937365	1436882719	296	1755010733	1260701146
244	2019058373	557806386	297	737310543	1536793247
245	2145843711	965209034	298	22833584	1652960674
246	93541056	33960827	299	571289681	1003187391
247	164196467	967178080	300	1147652666	550064331
248	1313894758	2119569182	301	1678854998	1999054875
249	2005656967	677078626	302	1141305352	164483214
250	1195268110	591293112	303	302982268	752151102
251	1172126242	1290875013	304	76792022	836895694
252	1832417435	625671069	305	2008528172	314418418
253	602873955	1232365359	306	1963340227	1970360475
254	1899092396	1348621896	307	438441826	2016903336
255	653180388	1549822722	308	1071097714	661776208
256	643956001	662759856	309	423018578	1886988651
257	1666152564	176649168	310	1467243631	1960091671

311	1260314185	1141813464	364	1289309791	1332978770
312	1781629685	1574814653	365	1716568058	90638482
313	74134126	1559308155	366	588541615	107437509
314	1341521548	1235505970	367	931730704	836539238
315	199829188	1498587635	368	1628898897	1544899367
316	968663515	1172596928	369	12272696	1944202921
317	579330971	1376214753	370	295831688	463979418
318	2103306756	1074232198	371	1840992523	78581409
319	1263334214	639802697	372	1141199566	264976046
320	861802515	490656795	373	1923283252	751905082
321	1205740578	2054658401	374	1661121380	9390369
322	2042445825	838066546	375	1385885036	809635876
323	1155418198	30581044	376	293949725	1115675222
324	1790888635	761425294	377	430075440	795328467
325	646682360	97650985	378	1729348402	1794485016
326	1190011586	656509781	379	1672717171	809390695
327	1266053413	946719240	380	1510143305	1094020983
328	1070040516	11444575	381	184679140	421739853
329	1172797462	1408911572	382	1623747814	680327039
330	1866270297	434108840	383	2140264317	417130778
331	811899425	1883559192	384	987539049	1313470759
332	206399276	1347342406	385	36863841	1007246464
333	33669685	687877178	386	65210880	1222349785
334	1264504465	1023809338	387	1007202930	1356605371
335	2091923581	1260295466	388	1340426627	83304061
336	1141209719	161513616	389	981583416	94758727
337	2117289644	796907663	390	1780429097	1307408932
338	1804403569	1296707796	391	1312155787	1248679280
339	286600807	1016685880	392	1035884489	619508063
340	1989726528	1560102813	393	125135950	642719154
341	127062184	1251712400	394	742740429	1693890731
342	1347058183	832210430	395	288825255	1955118230
343	1409340522	1996018650	396	2014156709	1254279496
344	1189227405	2104331372	397	1214307410	1018694086
345	1899480715	426715196	398	641148392	822438719
346	1711723894	1694565484	399	325387496	54414209
347	753680565	1239192032	400	2055056277	613449976
348	1032991156	1717081230	401	776442765	2076486058
349	1324267489	1234983203	402	885102022	1149796441
350	1228710464	1146948653	403	927275849	752844039
351	1018802434	21813410	404	1334327393	917679585
352	1911244789	337532525	405	1675453773	1281629760
353	1983157251	2074171422	406	555294696	2133108384
354	1539339023	1829805786	407	800783442	1587803903
355	1060082626	1972231738	408	1740720889	1731544993
356	276201572	1097008267	409	1730609842	1096128219
357	149880558	934481177	410	1058241085	1846766848
358	714121826	298183567	411	1785146475	1531785678
359	1843325261	1610219570	412	740357912	1787941284
360	631523153	1248389806	413	1147500	670262593
361	391848137	1371569011	414	575200385	896487560
362	551329533	1212483377	415	1471808410	1736230883
363	938989005	2073840280	416	1941068257	824995758

417	1160856161	1475446798	470	1514213203	313779669
418	921806729	2018804778	471	1920775260	102539627
419	1788098369	574313877	472	64724571	994457135
420	133789132	721445202	473	1329349426	128968179
421	285803709	2032694861	474	704512771	1362969883
422	1864846469	1255385842	475	716389172	359259411
423	1394368802	1770979060	476	1350390463	898274290
424	428096424	717390469	477	994640427	820580723
425	1530011961	1810685406	478	1990487275	168796960
426	87720417	1487356173	479	2016449080	1385624087
427	1688620286	570471055	480	406198312	501737421
428	1772635608	1720849654	481	1291306112	349413705
429	305629937	171137503	482	1936895553	1081844744
430	2019319262	1003907006	483	804007878	360746069
431	1245837848	455090054	484	1216908435	949843423
432	1723936450	2004813525	485	1149783014	1314830419
433	1254214291	21663349	486	525669499	1204688427
434	988806309	1762791285	487	1451733570	115820452
435	1486257176	1938951816	488	2057456263	1729063416
436	528722329	265523341	489	1589818680	1016661611
437	1615987471	97000370	490	1172308231	767976867
438	1968848052	1095217691	491	173470663	1408412475
439	1762887491	1448510334	492	2030571242	548906642
440	1746948900	1585256823	493	2099487725	1429979261
441	561257488	674453006	494	100802875	777346498
442	1998544889	1241774042	495	465831687	1369568087
443	1713155272	805169418	496	1213006582	1820983059
444	412354136	835982966	497	377599565	211694992
445	259673874	319769302	498	2113968442	1861292489
446	1343565228	488852680	499	1511528650	3552113
447	259687812	154668440	500	825573620	123790919
448	434487406	579378249	501	1347209343	1617019942
449	673432385	712056863	502	1903684402	354805716
450	1891005503	1597995846	503	1950131213	1712557288
451	373288012	2104548073	504	341162418	613338376
452	399213769	582725001	505	2079196026	1900108003
453	1570447985	703904093	506	1518743748	1011881568
454	519758726	1897977421	507	1573726427	1149059810
455	1190907461	1910726428	508	1837760687	378753279
456	1532578229	850986986	509	1267943539	610960024
457	1277169775	589096147	510	487332958	1125294995
458	2139137135	1701648196	511	1481239760	1672399164
459	2124965063	1199338723	512	2017502195	2100767980
460	1901408148	2136019460	513	1611145466	974135938
461	1422303415	851151583	514	1037537336	1145478759
462	1643821410	659871253	515	2060906356	696408018
463	27764346	723946608	516	468250002	734552037
464	1541873143	1762908967	517	849754097	1306150353
465	788749927	170784860	518	128249084	1745004428
466	940612682	1982347087	519	1047323917	263322818
467	1766382927	822715884	520	1599611436	1908238055
468	1164806076	1529267999	521	1661573927	1346063841
469	1303892614	1206018921	522	1273082375	403707125

523	1161870917	798157817		576	1339606827	726148332
524	1028014402	2040008576		577	192757058	190237815
525	965692614	1123093686		578	2139692563	983684706
526	1301831077	1961133565		579	610527028	129719695
527	599559324	1207646506		580	2145025782	1503214604
528	1992628552	947715100		581	1064988541	1382331839
529	1080469780	703778413		582	950519526	363563736
530	1695439219	2112417841		583	891672657	1198966942
531	1865232798	1708678058		584	365479037	1387126662
532	793907253	1523254806		585	840933783	915419050
533	287507413	485785884		586	1000880066	291922389
534	1307090439	1872828210		587	1914633538	221919535
535	94153252	1112253058		588	2053263396	1778512038
536	248329167	1047300490		589	1662710058	1406062067
537	1255891655	352462819		590	869750392	567102530
538	1342578140	200436258		591	219651550	1465116750
539	1128811393	342371565		592	1561773292	1099916667
540	684059411	157196518		593	1338666098	1421016852
541	192843790	1806905158		594	817153290	355010092
542	757911484	909088767		595	1936112939	41303893
543	2094877972	2076198489		596	840070149	116194216
544	1521617173	2015626315		597	1937918451	1430041003
545	1690423289	1191445148		598	469772241	81175569
546	123475452	1180625450		599	378877641	393179972
547	1739410881	1067896		600	626982170	110597988
548	1971415905	1999500895		601	1876933435	1013399843
549	1570584314	604058701		602	979590664	2139972938
550	616688930	481652737		603	417997964	1022364432
551	1452964214	1322152946		604	1142674231	1585582419
552	1648154184	2020474349		605	1344799876	2132203958
553	536179518	518029535		606	1175283465	939327522
554	210413213	107832165		607	918845489	810255574
555	1316873234	309834618		608	384410385	1421795304
556	1239237104	64705243		609	1172884838	1741183620
557	1408572747	2132748931		610	1785355789	251750292
558	1105206813	540136846		611	1351351695	1469998520
559	1296675788	1633953662		612	1194887870	183384099
560	311157571	1270892397		613	1021117843	878963463
561	1913180375	579551341		614	1192134034	1951724719
562	361965394	2086164853		615	606079214	560163047
563	678733435	1909407061		616	1228009572	934018601
564	1900749209	717500834		617	1304360428	903678870
565	473353117	1008284359		618	532618540	384910313
566	502618513	1096527811		619	763194726	1083662416
567	1111210760	353441376		620	2005129761	2012245814
568	1073204170	152385830		621	1051824616	1787130897
569	139114258	2062720897		622	1342290614	1273077750
570	665212036	573523094		623	1767308920	151459158
571	78958400	2140940992		624	2137393023	1292664392
572	1340026313	2015106063		625	1563910114	1782904264
573	1070741205	639731493		626	315984262	1266144854
574	1359904212	1553901877		627	799137468	683057050
575	1976633724	1246559812		628	322897380	1465603872

629	879858557	1413396637	682	569281496	734547835
630	1971649187	590308456	683	1735141825	1157136743
631	1389296742	73619211	684	1708392198	1019516856
632	2038977772	398365551	685	1656370257	2052569863
633	1296434108	575532750	686	1172510227	1089671946
634	1904958378	265434147	687	1590082616	1518321161
635	1296663931	314956556	688	1995076949	1599008707
636	406016541	855648898	689	1866960302	1222045472
637	1341667012	1348502326	690	539799296	568133759
638	509163858	441630926	691	214609086	1905441655
639	295920320	1423921723	692	467034919	405874259
640	228147726	1988516544	693	1454904655	13325141
641	246819730	1860030987	694	2061774327	1837628716
642	805798880	1097770896	695	245517089	1727188799
643	1887353965	469122319	696	651610502	2067230783
644	1601281967	1489735074	697	2055813165	2038309543
645	184005517	2122041340	698	299770526	457119092
646	2000714164	1224644294	699	1265885164	1460272465
647	1050614131	1843543104	700	390285975	183594145
648	18450969	1359449769	701	614863030	983652313
649	2037301791	1649015603	702	1352039806	14472227
650	1257762843	387605029	703	1688912960	309400019
651	270012966	1918109143	704	1475277001	905212637
652	856282854	337120581	705	623059165	1211174887
653	1199135876	925971046	706	677060625	1103838023
654	590401654	667177332	707	1304767863	723211517
655	2050507837	1597371560	708	1494313604	1727687760
656	1792561151	1671581440	709	655143619	1557309125
657	1473180888	48801129	710	999643726	453822693
658	695488413	325196499	711	103913624	1234437237
659	2034065102	2005216717	712	214456222	1255338286
660	321163104	1612979587	713	183974463	410297043
661	2033109981	390164981	714	1425324918	1904058094
662	1810705409	1441368155	715	576041230	1088409460
663	1297300985	1100855845	716	1854564475	2040310744
664	1313524075	82105216	717	537212291	674819486
665	23690604	1630506869	718	44896068	1357067059
666	860521510	10517671	719	285218316	547710224
667	427163761	900411361	720	1888222388	907621948
668	699930254	254299936	721	1844541679	62768446
669	770467990	1891744976	722	714996056	1444344573
670	316108179	1146877270	723	2024396968	465597618
671	105445804	899337523	724	1476443427	1349425341
672	1723634978	821249886	725	269167998	563222022
673	2050168568	1427817043	726	2073651537	1464025231
674	882768091	746760020	727	1552624594	643051815
675	328033928	1211952506	728	904200976	1767094852
676	362468427	129311401	729	591911588	408395929
677	1337265389	1286281020	730	193603012	104309716
678	1083793641	1669994540	731	1635276234	2118616635
679	30744239	1361978712	732	269534072	586413346
680	838457806	883335016	733	495111194	2031149907
681	386833515	847860458	734	652104434	1861053426

735	1549621890	606932006	788	603260299	1016609620
736	568973961	2137667037	789	1942866583	1450131526
737	813132436	502816034	790	1966881205	1194334402
738	1336017158	1139558464	791	98940130	1834786196
739	2071596236	657046668	792	938591094	1501288250
740	779393390	903207919	793	1788669	548906223
741	1804773814	2124651837	794	818078991	550709219
742	708944123	2140742153	795	831741665	470953378
743	1358121740	1578318555	796	678750261	930639951
744	416587614	1428486717	797	1214630979	867876881
745	1862714134	2079535032	798	706969436	683791455
746	1904973701	744502297	799	1665822559	1469770788
747	753773950	729850485	800	1636359045	1101520784
748	1362418469	51398739	801	1245658947	728733088
749	1791080455	355894745	802	770895483	1562862259
750	668747570	1493311534	803	1081488056	1189116736
751	717405743	788579588	804	1788263704	1226936635
752	1194224249	844393016	805	2091086118	234809488
753	1524471741	1283354336	806	465814633	2117571834
754	1645308077	480110849	807	1202601672	90141784
755	1554335652	1172575103	808	1163546797	176308674
756	1372719286	1478188318	809	8265669	536367546
757	1598828487	310507642	810	2991910	97011034
758	987406440	429478546	811	286259077	777332244
759	985929029	823824422	812	957041779	339752025
760	335700720	2113853784	813	1676807412	1748657593
761	376527438	1730824654	814	492236217	755848555
762	242664657	1021906877	815	841182624	665732276
763	2121735020	1354728910	816	1536190781	1813340910
764	1327897940	889006596	817	1333552019	440861906
765	1970662657	1666245602	818	379388092	1954600911
766	1920201445	963733081	819	1261210682	246599731
767	422442582	1453461343	820	1665503721	1180613087
768	2003863729	1087830245	821	1229258734	393611108
769	858447002	401645133	822	253932038	1306172048
770	971578456	1117501101	823	1350335177	1287498924
771	1466895876	77309022	824	196617278	790302179
772	602919921	1283663176	825	1056505297	203703749
773	1509114735	987869867	826	805750730	1225116269
774	129801316	118904973	827	138628040	1204408318
775	1842398258	677888047	828	388136030	1730164170
776	1217344316	254015901	829	2132211527	1362304872
777	1049631999	1369824110	830	1523763470	1139975127
778	1688162090	1130079100	831	429024224	634610725
779	360492337	1870281605	832	448141959	1156182458
780	2125255252	1244503369	833	1544434358	2003315747
781	1800605788	501136467	834	412055400	1898528373
782	806777465	876529528	835	1796085439	1961689965
783	833746762	1609891137	836	2130378651	1507702451
784	1512511171	937635328	837	621144941	1924077274
785	772547761	1355321984	838	576013353	168345174
786	1994543238	1163413333	839	278474290	1558910692
787	1502625202	1862705312	840	1007588450	297873961

841	189659492	1426282628	894	569580565	2063797248
842	1549386342	1063133883	895	145860577	557743849
843	1464432368	2134358053	896	1749343170	595182200
844	1622360294	1730282467	897	1742151508	2098281232
845	1216360874	1069569045	898	1986870148	168627864
846	2085590591	1905369354	899	1240381461	1591418276
847	100518245	609923737	900	1443411677	2065876470
848	1041681347	1844072131	901	358853212	738999234
849	1154855117	205597261	902	1792679753	1799807991
850	1952228254	520852702	903	781577791	153018955
851	1868904127	1597836043	904	557896040	865359883
852	1805018889	1347893542	905	720342174	1578966858
853	730595367	14939763	906	1258784072	480563479
854	2081787660	2129063590	907	1795507439	28300839
855	24613594	842975978	908	958276197	1935246820
856	1550320980	1134481207	909	1573576131	1667150276
857	1554010854	2023196023	910	245836596	715750058
858	1338021463	1503531824	911	507875401	1137066463
859	834930214	1518739221	912	1468637288	1808826700
860	4980078	1613109128	913	1369369289	617022592
861	978701636	1401488204	914	505211999	1854850944
862	925310659	1868170601	915	1076179717	1826618842
863	2018606654	62991103	916	79430661	1842071310
864	784361996	1801737675	917	914700893	974260565
865	2129457043	83500459	918	1270092358	1038533406
866	187564438	1432183519	919	387115672	320042913
867	1435766986	1853684108	920	424082943	526976964
868	1977391683	339192316	921	1959930884	1091249810
869	1739709675	496353298	922	1657875177	2004252113
870	1990149958	444868210	923	894408965	583144855
871	736848787	1586686049	924	1712552436	1362601167
872	93756849	1103683426	925	122317987	1586944482
873	94732634	2136275555	926	1722724504	711966500
874	1920896178	992018922	927	1535475814	84120780
875	692906723	807012742	928	1128584846	1342600984
876	778618281	74445502	929	1442293122	1152685195
877	2070573599	656993496	930	105545458	1707021128
878	101702110	1075047423	931	1253655175	1350852019
879	306370154	2027947707	932	627925321	244115220
880	123744277	1288720685	933	1649426210	1923757599
881	569137163	914593389	934	371040301	1999879482
882	1741957404	730510090	935	139792537	1862953037
883	1935580948	2103553901	936	39621123	2083634411
884	1221799271	1118323098	937	1911007337	863097028
885	1765428079	1387127800	938	1057580664	824001308
886	593719119	1702251275	939	1672122228	215559997
887	2023344700	825202023	940	1407765945	293020814
888	995099800	1819831391	941	924687022	400463614
889	1032466845	1409798426	942	262059125	260626
890	1425425981	1521001800	943	1202250847	1727287195
891	1470116259	311496099	944	1807707702	987766565
892	1224198037	905630039	945	416008863	778290102
893	1980939658	2006556013	946	1212716291	62468831

947	1550540293	2131980504	1000	2098403047	1795647722
948	690231262	1624073243	1001	582087394	1547430139
949	1859824510	1682450350	1002	1500319924	1942832978
950	466562081	1309247970	1003	268274790	63396443
951	1117866127	484114791	1004	1984269740	1483307004
952	350981795	1664953465	1005	620974345	521298334
953	328681929	1472610359	1006	1694340223	1648875271
954	1154065668	931914891	1007	417069438	2129744694
955	389671481	717419913	1008	1631261200	1070044228
956	1557342903	1380380811	1009	1869621444	1973064398
957	929715374	1143982011	1010	978049678	1211821264
958	632080275	2085128401	1011	302621674	574139566
959	196989854	1127122649	1012	643989471	373799674
960	257630756	126142490	1013	2119762287	876550333
961	1481731973	932681075	1014	936815450	630510843
962	1131443818	352190985	1015	740092235	2039312854
963	2076472275	1431371651	1016	754191525	1361151262
964	306579967	1481130136	1017	2081853691	210297209
965	873292095	1591482248	1018	397319817	64288361
966	1241167652	965114288	1019	1391778438	1955714290
967	652734589	231120903	1020	281532932	947865039
968	1962764836	981921390	1021	550322248	723713558
969	1452097313	824435113	1022	764706808	2082865872
970	262778656	1384069562	1023	348668959	1514432369
971	636552735	2124099112	1024	168889412	1689678414
972	1947705943	1634584048	1025	256252265	1691896028
973	1298751990	202254118	1026	1479544459	280147193
974	1227483540	1565701938	1027	205174393	1209896060
975	1953350015	2044981894	1028	2095041788	116415974
976	692120442	12482561	1029	1572481731	1015057200
977	842407569	249165249	1030	463816515	321718374
978	1429529937	1045438384	1031	626894492	2122868719
979	481923120	549681535	1032	1898401020	186100333
980	1816585128	1121120383	1033	591768014	337928454
981	915499934	1551347515	1034	1812087409	709107099
982	1489811660	1651059116	1035	1844629067	1113482128
983	2131870244	186713544	1036	130120520	1208402300
984	486435599	1728204306	1037	1046217973	1518664124
985	1906099470	960011795	1038	1435979737	1774595890
986	1004313051	2104941270	1039	1543805024	241798858
987	1409786269	673315085	1040	1224658984	1275132934
988	1280745264	399403599	1041	1832984530	385336709
989	421301336	1450703063	1042	1701341982	1717570761
990	2109527744	848504545	1043	1207370730	1179292286
991	1762301116	638250731	1044	1501895721	578363805
992	900403581	325744433	1045	474919743	1158489530
993	558590037	1936112959	1046	1867392781	853045475
994	1044612017	1604227016	1047	967204169	825374626
995	2011860500	752824607	1048	154003684	912327532
996	1337852760	2118038800	1049	1427953300	187906156
997	872199193	633659178	1050	1054901256	1047785038
998	763627693	1371335136	1051	636401898	166767561
999	1170365	111278425	1052	214993172	1583558954

1053	868299589	1197536786	1106	1561561886	1467155860
1054	1792740545	2120208810	1107	897755166	970145126
1055	1685382318	2041318244	1108	1902784514	1231126019
1056	1009035642	2081498441	1109	836749758	1443874738
1057	207560370	558817466	1110	1281129768	1965782274
1058	321214659	1177611750	1111	1117983213	1075080572
1059	2127076312	1181311227	1112	643620225	1026663782
1060	767089852	1085142492	1113	1987965234	1676398385
1061	529383580	356082840	1114	2055191896	793256707
1062	406885819	1175277902	1115	877649402	1009877247
1063	1155844352	925874004	1116	1616648970	2052475573
1064	2144600136	561830683	1117	862683430	510397079
1065	1929871872	28234600	1118	962970537	115316105
1066	136788723	1604508149	1119	1867496430	2383432
1067	896624785	1636078253	1120	1835236572	2135629675
1068	1207508341	1579436594	1121	1785647116	430054039
1069	96769002	1050595949	1122	1013462286	272517198
1070	1614190925	660439219	1123	843454157	1324766538
1071	1767888610	1834768326	1124	429879478	1262795367
1072	915865899	370252052	1125	1891042870	119117564
1073	1421475999	1839307170	1126	1231462285	476267077
1074	1702587975	2057459659	1127	450060242	1339256504
1075	1832407942	1517842216	1128	185193432	428064020
1076	747775129	1759294109	1129	1878518777	993819015
1077	1416956813	78600056	1130	241727672	250208465
1078	527465959	2032796221	1131	1204768748	1020145378
1079	1928054640	1630502065	1132	1669864168	1535573382
1080	285220964	1476468977	1133	1885989678	371896841
1081	76865213	1649608038	1134	980271600	2016005578
1082	1265594525	1136301041	1135	1664705284	1000388424
1083	658254486	624707655	1136	1541882087	1078641602
1084	376202886	92021559	1137	477031320	1898387598
1085	474421297	751786175	1138	1855602349	2084505716
1086	1038018472	34053094	1139	1425499653	893801664
1087	1944134447	957761032	1140	981643853	1280626221
1088	1595252131	930056987	1141	530512249	2135530807
1089	713615469	1116571139	1142	785201287	918354651
1090	1270616884	1957639212	1143	239962919	22905477
1091	1267504172	1266172043	1144	1596997586	2080505082
1092	741784997	1083525613	1145	169756353	362178019
1093	1537921804	1297915386	1146	1070838109	808584087
1094	19884794	1460730661	1147	328731231	1760225818
1095	2005357805	1579081866	1148	1546726314	1570685433
1096	284527880	1851720820	1149	1850764169	1186517317
1097	838870868	1909169784	1150	349979449	241728099
1098	1023337363	523691363	1151	1373662011	1723517284
1099	1868958795	213510211	1152	327078266	31420573
1100	651454838	1167380421	1153	1757786491	1343095587
1101	1007757679	1079181010	1154	1697327676	1337094674
1102	341236870	762552158	1155	2133924836	720818544
1103	1629149734	955104776	1156	641581381	696728336
1104	1364868264	1778291437	1157	1998340175	770440155
1105	1861171722	2086044347	1158	1398921164	2046415629

1159	1910209335	1505205457	1212	1777979964	2038985312
1160	1458107992	1160312546	1213	2003691470	2031886042
1161	1797064346	723104862	1214	269222088	126881735
1162	2092569710	1223769806	1215	1101827210	1788596132
1163	1882208369	1978041597	1216	708024830	1480249642
1164	1929900211	1601063895	1217	1737691587	1909144722
1165	1275769318	355889868	1218	386535782	296082022
1166	1751858318	1665589870	1219	358082626	408825339
1167	245864857	680582327	1220	758382098	723008060
1168	1138034801	2112164428	1221	388579217	414116955
1169	1100529193	1979094441	1222	800185491	847998358
1170	2076307694	1887361948	1223	844976677	1617721815
1171	1448510299	1438071286	1224	242023418	896925141
1172	51226700	392405371	1225	1875625375	1686990085
1173	737831467	379824665	1226	2014545064	1469623711
1174	2019806740	603473755	1227	99167929	365069460
1175	856869603	1958580050	1228	1733908232	466453227
1176	1788521570	627443410	1229	463755464	1244759281
1177	1836297514	2069130506	1230	985599674	1401301252
1178	568894273	1592358924	1231	1073113567	783229836
1179	318125386	1405194149	1232	1036534905	379424021
1180	1197370120	1621462708	1233	631908101	1254274978
1181	1613036358	1290440049	1234	729715207	329385847
1182	575873955	1982734674	1235	1962317503	1765240913
1183	288949564	1424425693	1236	318391149	2106637806
1184	691674655	243987534	1237	1602996274	1865597943
1185	412549865	1172275184	1238	554667495	520199028
1186	193191117	413290620	1239	1039163916	1887722665
1187	643447277	781536306	1240	1419238370	483889898
1188	463154112	1717494035	1241	2018128348	191003587
1189	2084021046	251342995	1242	1608020696	713625003
1190	420714434	1519442349	1243	1375627361	1783593992
1191	949526110	1732454167	1244	513853217	772038322
1192	1443723058	2029295492	1245	100646437	1905103025
1193	1610704389	599166942	1246	260861899	268667561
1194	1262757904	354155117	1247	409854814	498358450
1195	1709132089	239929171	1248	706010569	1610830423
1196	1447940720	627850537	1249	351796218	1037696108
1197	1623966753	1642262311	1250	279082267	1708735884
1198	1459711516	1647957567	1251	1727732814	65550379
1199	83596129	650714782	1252	1515247632	620173792
1200	1534938822	734389925	1253	1250524944	2098005990
1201	2082738379	1947067720	1254	101045652	443427211
1202	751566322	1448540044	1255	525137331	753403639
1203	1848191948	2052764727	1256	1308556452	978817008
1204	466634813	1576263232	1257	1284562083	1715945392
1205	1740827153	2004046254	1258	1755041538	845239706
1206	1137742734	802626584	1259	2042811342	328784258
1207	2118319632	1275112694	1260	1729499957	1910275969
1208	445848475	1329945404	1261	954953258	1047142760
1209	1463429558	1098286280	1262	1180370541	1850980086
1210	1893399196	1269490369	1263	2056881194	223107510
1211	1715024497	1714302367	1264	1805543824	2033209369

1265	1938420262	1353309264	1318	1409758929	158944681
1266	992085298	396881058	1319	1742350937	1504621840
1267	917421339	579488859	1320	1420213232	300328550
1268	1865858060	1335578259	1321	524176726	2009218748
1269	1612663492	746542618	1322	2049490509	2003651343
1270	1320979724	218517710	1323	783339800	1351019393
1271	1019997975	152312250	1324	513801280	1696251248
1272	1711467638	1909481400	1325	1546144252	317151514
1273	206663354	946263647	1326	49945446	735914629
1274	2012822912	1551154535	1327	1568635971	1477914470
1275	1164835489	915717049	1328	1467909965	1560013729
1276	248049990	187518163	1329	1614756973	1730712168
1277	1870462824	2039279628	1330	1154453372	1637989555
1278	1331306566	914770495	1331	403821014	1948856752
1279	1052508853	1730208258	1332	831616594	681514890
1280	2066698122	77438511	1333	1910353614	1713440227
1281	150707201	1914185964	1334	1948268146	787042904
1282	1858517078	1732585568	1335	1273461904	1160853984
1283	1714770060	1918441435	1336	398986595	328835073
1284	874756506	1047935655	1337	1036146182	1545178118
1285	379518346	112644302	1338	394370164	276168173
1286	697433801	1361816681	1339	201954031	613529063
1287	747229901	1862478658	1340	1515125425	1670623429
1288	227586173	1087724606	1341	1223203885	90664017
1289	1491757751	162010870	1342	664756321	1188828699
1290	123660261	540621925	1343	493355737	374254737
1291	1950536909	1331979740	1344	226233839	1303404582
1292	884866464	1003591253	1345	1791898414	994572529
1293	1840691834	1272803288	1346	1039547237	1977611774
1294	328045984	1876571130	1347	1368204898	1554691372
1295	730102723	1235725791	1348	1664667114	562343187
1296	222370351	254616855	1349	18110846	1445818558
1297	2061557340	1819999707	1350	573551901	1745451631
1298	8236789	1801386295	1351	1400203875	1593437271
1299	425048583	1535308230	1352	663143260	2001230900
1300	1387267976	1951319841	1353	98374216	1536292839
1301	122959405	641157948	1354	1674499003	1081831757
1302	897537819	1465546170	1355	662597223	1213846375
1303	1277934398	185692243	1356	218370875	1123281894
1304	2016032852	889670571	1357	682675452	275757716
1305	521559394	34453155	1358	2005337826	2077728728
1306	1971838314	1417844088	1359	727574283	1816934445
1307	109850650	1060392380	1360	2083622008	1759843933
1308	840148479	465104748	1361	1384264739	443649799
1309	651072117	1244315140	1362	482744912	394778212
1310	1723158873	577170208	1363	790114098	2062532151
1311	263747052	518409543	1364	78132923	1091552367
1312	2019672293	1272035079	1365	603369153	307000647
1313	131727661	1877031666	1366	1853133011	189527760
1314	1891476783	90756051	1367	438936344	1094627271
1315	1192721542	694344656	1368	1562891840	1925163520
1316	626632324	718714699	1369	712906628	1034108105
1317	588763863	1304712452	1370	1696786231	2130030696

1371	1067511231	226896065	1424	1849369336	58062118
1372	1238154454	245686256	1425	692487155	69868631
1373	839106473	1907725508	1426	1467030854	1105802823
1374	579689833	1467282874	1427	1052313225	1394551129
1375	1156352128	1310295605	1428	203490181	1231248510
1376	1320418956	1798118060	1429	531567489	1203246554
1377	188439104	890865388	1430	1420937752	1395727772
1378	1002760163	2072421549	1431	162295878	1161748477
1379	1020005900	1794453552	1432	1953669060	1087152115
1380	1813268603	1653350832	1433	1116364788	1137459873
1381	144169749	1612111171	1434	552094929	1244967974
1382	155925237	502245907	1435	461450751	1067675964
1383	162701019	261155961	1436	1772590148	787969626
1384	267275303	1966520850	1437	680261088	2070430548
1385	1900441308	112169760	1438	1325863534	893670744
1386	1471085755	1297723388	1439	927711703	289464282
1387	216940708	1696666429	1440	723702204	2072787405
1388	678289762	1497494576	1441	1758918253	1340483054
1389	970789776	344212284	1442	621602094	1459523535
1390	1601503619	789939178	1443	50585949	1904810577
1391	710516028	381045994	1444	1746929508	1150747983
1392	685156785	1568705281	1445	1219685187	1410569582
1393	231899923	1908179612	1446	1979807033	1852667180
1394	703532568	774637291	1447	913429892	299566379
1395	1941131970	906731478	1448	419233867	1474911437
1396	1316626595	138684760	1449	1906222988	838793779
1397	1189942080	1618769979	1450	1613546433	700746733
1398	1609158362	381558212	1451	206421920	1044304267
1399	1384155542	1099935013	1452	2126492072	13385301
1400	2106301267	992131321	1453	658442822	1279336558
1401	1205706960	1800168458	1454	1895790595	234219571
1402	1185544025	1082162728	1455	957070019	437265791
1403	2063245365	457804331	1456	477802472	1742854176
1404	752054893	1549344061	1457	540573705	1395810474
1405	1840414573	911709329	1458	1222456720	1159307918
1406	907026916	1316189492	1459	642212302	1187444713
1407	1679467553	870090934	1460	157249813	1643935894
1408	78918077	146756508	1461	912436216	1804357297
1409	602835818	1359573699	1462	262265168	1439690367
1410	548931161	1071337716	1463	1044296175	1638592786
1411	811711139	758856869	1464	1056080294	1056395500
1412	2018260759	736538496	1465	434377688	2053846014
1413	1293406275	2067445579	1466	1954761827	212747978
1414	882763618	894721600	1467	48939873	1606014656
1415	806404968	511911620	1468	1134632940	801715833
1416	805173488	1949725221	1469	1578047672	1535095181
1417	215661273	1183123899	1470	1553808636	481206529
1418	249849771	181012435	1471	34987215	733976264
1419	1660825868	763056551	1472	2034620008	937190206
1420	883970330	439122188	1473	2067918340	953829687
1421	618128196	1570885109	1474	1254150854	973846264
1422	807595585	748936122	1475	1123453543	1635536669
1423	2070558645	1008522829	1476	230060182	43308004

1477	2038451632	1821339121	1530	215084298	761446539
1478	2001538745	1833325638	1531	613287687	614022234
1479	789860655	286519379	1532	357214632	165309066
1480	1144262327	1679685550	1533	296969099	1850176102
1481	694329156	1939116468	1534	1312192863	1964111157
1482	1467572802	1633476986	1535	1286658066	278207145
1483	1876958166	1733044426	1536	136306110	949965210
1484	80379517	7465051	1537	1812180549	780142846
1485	1123461358	1448126634	1538	26802958	489973314
1486	208876641	432782878	1539	2093294327	865547657
1487	2070858618	406033976	1540	850009775	921800402
1488	134782047	24844577	1541	1948064373	1332757460
1489	578409241	982412049	1542	540065011	838725039
1490	644446952	412115337	1543	717505060	895563349
1491	1402094809	1639941069	1544	2071390318	1748775424
1492	539450474	1493590652	1545	1555366360	1474235196
1493	1697100524	1036300414	1546	406005288	261313525
1494	2091765856	1878499749	1547	1884722367	1721255051
1495	1616272849	1026328813	1548	701961458	1224076944
1496	105994637	1004116799	1549	740592677	718041110
1497	632417914	1684159183	1550	1777317446	1804810357
1498	1349000038	1708628918	1551	875964821	1275106976
1499	1857809104	731644258	1552	882622926	1733120309
1500	1837156669	1783980821	1553	1462038295	1850367188
1501	300221221	1445121866	1554	1321385785	1294639395
1502	376427501	1082636036	1555	267353760	2067125010
1503	2006019893	480365275	1556	1000680096	1743847497
1504	370254759	1859875442	1557	2062022113	330984932
1505	1804628901	1347652249	1558	59970792	1317742791
1506	30179183	1215765289	1559	393380620	1648349736
1507	2044062195	701773181	1560	285139178	1234805632
1508	926799341	972507671	1561	1390937816	779053924
1509	1979323469	1002285173	1562	125859822	2135637575
1510	1886446254	245600128	1563	560526994	479508850
1511	503778972	1681082037	1564	794377064	710355063
1512	207051730	490603596	1565	1701992626	70796908
1513	809099143	1743936585	1566	1853615649	38719006
1514	1308729369	1070395219	1567	1445723797	1211216627
1515	2039882896	1365513389	1568	1289126292	545000793
1516	1435787582	1719722837	1569	2056573209	236028951
1517	1118625911	1293181155	1570	500909741	1281059857
1518	732480930	211701878	1571	737907886	2120490974
1519	640178312	997636023	1572	491250120	970242986
1520	665498762	1865688627	1573	720278375	1329974003
1521	1596749307	2139722124	1574	94690695	1052550732
1522	899473051	4311708	1575	539829466	1762201433
1523	1823191685	953848203	1576	479228934	823556077
1524	2139989761	63455522	1577	1881792273	420415878
1525	1634279271	529695388	1578	429329182	1826572568
1526	407136064	1481663439	1579	1939722379	1377901483
1527	1416530455	463571879	1580	688828388	1005763337
1528	925748605	1823382493	1581	212077881	1196395858
1529	961756782	1073019998	1582	1014836323	512048876

1583	876546126	180481797	1636	431249618	1999197914
1584	1347711917	953915981	1637	2034741426	1484298447
1585	1508302185	151428300	1638	591554363	858740665
1586	1341445146	703329600	1639	1465324057	645300975
1587	1021246035	1967486497	1640	173688363	919744327
1588	1486023329	1418491603	1641	1229835371	1487254812
1589	1953436940	1213453256	1642	730687194	1228185712
1590	688203245	374496755	1643	1687800117	1723246803
1591	25111392	1756809754	1644	1113793410	1869628761
1592	1472794911	777560974	1645	2059331170	1990061307
1593	2023133413	520672388	1646	1164491572	1837936299
1594	262584983	1878988298	1647	617642233	1886033992
1595	1060140512	614949004	1648	862515667	64605081
1596	148935871	56123734	1649	606568484	2138574144
1597	489011080	92660441	1650	1833473262	1649473292
1598	1561740635	65845048	1651	2113463498	1997247777
1599	178795131	648794187	1652	349186629	1329869530
1600	534502028	1754059675	1653	199649172	970072799
1601	586626106	370529866	1654	19941015	52963773
1602	1658081567	1515874044	1655	1602108658	42007318
1603	1561834458	1560572233	1656	523106489	622263426
1604	345924407	1478694919	1657	647290792	170505568
1605	1380899969	1688678767	1658	118366782	1676828944
1606	416569953	339695298	1659	483719292	591899398
1607	1751888137	426464758	1660	670038979	1981353544
1608	1043666171	364806681	1661	1108311707	782309292
1609	2075929142	702238355	1662	628613195	1356700627
1610	1848413938	1838866018	1663	361471736	1015794886
1611	1481589063	1547185298	1664	775384055	306221215
1612	2147055959	1369782442	1665	643724611	469529059
1613	868263797	1741354369	1666	1308373560	754130153
1614	2052673799	115459505	1667	1681302748	1293117910
1615	262337902	663377826	1668	714330361	738708789
1616	1006557838	1884609916	1669	1441704947	1729777674
1617	1742006109	2008844677	1670	1986699746	1645471638
1618	537970539	1892665765	1671	1643224930	924651135
1619	666868866	150713997	1672	1190531046	68311585
1620	1125492241	956617360	1673	1577701080	1391503172
1621	678424091	132891748	1674	1689023741	849337610
1622	2104667231	1452904458	1675	327935493	955608125
1623	2113533278	1249797962	1676	297549730	682500623
1624	145303559	1678325091	1677	1317725153	122646372
1625	32231760	1593379386	1678	976700194	1124109085
1626	1298134466	515704021	1679	1047816379	666357786
1627	1019377240	268776521	1680	1983780330	836141739
1628	638845910	2012179580	1681	1869612473	1712256322
1629	1057271239	1857391397	1682	1618615231	1740346183
1630	1024534661	1981472284	1683	1868572158	1880344442
1631	1976467142	1864534694	1684	1595404837	1713205510
1632	1540428786	1971352703	1685	2026124789	477717677
1633	1007660759	1892353733	1686	1741026337	909038600
1634	1368173572	1036670937	1687	1205304617	1236008235
1635	1167548847	1773055044	1688	987574256	2075208950

1689	1308372518	119812629	1742	1069554470	1596355049
1690	600082453	566210255	1743	1224361565	953681367
1691	1327566783	1811607522	1744	711158030	841827724
1692	638837957	1202199922	1745	1943024177	1272366815
1693	1508035404	263010759	1746	185559277	2061643304
1694	494243902	1866801315	1747	1991866447	431670308
1695	1043376571	2044667111	1748	1296265770	1398000555
1696	833394966	1811836133	1749	776578403	1561326163
1697	217151736	524850152	1750	1049895568	1226670373
1698	1847733097	1451436386	1751	1156001895	806803418
1699	469152080	755002090	1752	131653770	1997055620
1700	46659778	1763572191	1753	652853715	1506316316
1701	998358201	244005516	1754	478502904	620838913
1702	2059588343	1015245243	1755	976405729	1231323247
1703	476839069	1028111798	1756	5581098	3857214
1704	479419698	464550976	1757	204426267	581687364
1705	631698586	531428033	1758	498811960	1766253627
1706	569351231	1818758233	1759	1283381396	76633146
1707	1187678750	113512002	1760	2132069321	1779530873
1708	714924146	789178792	1761	1943877497	1921584764
1709	1599282007	1259162467	1762	1179798154	1870830937
1710	1639512118	1368051774	1763	1535666351	1680444210
1711	808573750	1122272718	1764	2128350095	1464511570
1712	15222873	1589951453	1765	495109181	939836606
1713	310033629	368568250	1766	292476398	18467322
1714	1452841860	1469531810	1767	1445382233	107880247
1715	1633688596	1254810525	1768	1682739627	1574423200
1716	1849831264	951151408	1769	736273846	2102893710
1717	1188844048	301389076	1770	660968201	1583311375
1718	367362955	2076356397	1771	1687774859	1034509246
1719	1611662750	2095211713	1772	231939627	2098962667
1720	1796840336	763278883	1773	495628219	770901675
1721	366530119	1426794320	1774	2078114357	1361205016
1722	1243723756	1077422424	1775	1614463772	992179705
1723	1582043817	1326527113	1776	1876608745	1959912108
1724	852668531	1784821442	1777	1038355199	1437863995
1725	878451286	713999956	1778	173240155	2008957222
1726	1412916504	355051082	1779	562860926	1021743557
1727	1542482620	1529313314	1780	601111396	1080956922
1728	380052281	1998229824	1781	97355608	646222892
1729	687714529	1388382474	1782	1799633484	398834182
1730	1218217807	1053051419	1783	735281137	296082598
1731	1867816589	1740975576	1784	1269870696	22823250
1732	1056942787	1266963980	1785	786456593	1340278066
1733	1082397513	682832675	1786	99699564	1131321837
1734	1666624772	175079248	1787	731937277	52482941
1735	727631750	1598682675	1788	713056018	332140384
1736	1002090237	1854017388	1789	255970098	1060017487
1737	974272299	1063793268	1790	1744802495	475100729
1738	1027422326	216908857	1791	652768377	1147364499
1739	329945564	1949216527	1792	1452958587	1790416718
1740	1561618442	1270266368	1793	1248051164	103711286
1741	1785110679	156859614	1794	967132713	558877578

1795	1306723441	53613073	1848	22875089	750582650
1796	1824370691	364856635	1849	916285985	80209179
1797	193389047	822831030	1850	1823417359	668492830
1798	1183964759	1383732981	1851	1895272191	247505247
1799	1357209985	329083192	1852	702850088	1354531240
1800	97688038	1964857607	1853	1065515611	987568694
1801	468563867	1250859951	1854	614868891	1493171569
1802	775618139	1605135118	1855	2004136650	2060745992
1803	40300458	1876517308	1856	368873961	859157737
1804	989792430	684964759	1857	106694018	567520440
1805	1548277381	2101161528	1858	2115488155	81666276
1806	1369011552	585602020	1859	1048067272	1277134316
1807	1979359990	126987723	1860	1678132177	821415899
1808	1097240894	1699017927	1861	993061920	1111379418
1809	689957244	494513606	1862	1236549662	1766505289
1810	1016424683	433027950	1863	1360986454	1860156407
1811	116823138	1124548150	1864	882849355	2119253056
1812	568035283	2069955488	1865	1889052503	1987079071
1813	471609569	247115020	1866	522478249	577538295
1814	2029709465	1553955346	1867	40829668	1127593261
1815	1968216015	1350704733	1868	1968503125	1095241294
1816	1208274464	439697573	1869	1802301951	228588316
1817	1901972673	555741699	1870	1463393179	1554145933
1818	1816727530	1670623207	1871	1077137170	211533566
1819	518548484	433153365	1872	1376815498	1355369237
1820	986043052	1946171399	1873	253774360	1314379716
1821	1200097012	451633799	1874	1078287226	73919883
1822	1262315631	1885573059	1875	2015641867	1511940540
1823	153815567	471766143	1876	1358707656	1298703212
1824	929924988	305319460	1877	153797305	1639810980
1825	1277650126	1255170019	1878	1421623873	1728240283
1826	1357710116	2027388581	1879	2001283298	115165003
1827	489903484	1746813429	1880	1929625549	373615754
1828	1937016308	1248733964	1881	1396319972	2070959700
1829	877135982	71060835	1882	1059778787	1807494755
1830	1854833774	1984997339	1883	933622833	1984623817
1831	638067527	829649896	1884	800907079	1284537236
1832	395385216	1693046344	1885	480099620	893384183
1833	1503529189	809566997	1886	427703704	204927730
1834	1909253905	741370905	1887	246294888	53753414
1835	1026216765	855241168	1888	1873144346	828677657
1836	1109326659	1199651300	1889	1214617885	28756969
1837	1299417248	968818299	1890	1290481608	164626048
1838	1190572028	746266402	1891	1085574712	1179233327
1839	460925618	914987152	1892	65068031	180386129
1840	1257883161	730366766	1893	538662057	1990219634
1841	987217691	972608212	1894	1814075886	730916329
1842	1562141661	908216238	1895	1066522421	53129262
1843	899928330	2061039746	1896	1284743177	1687060144
1844	10038845	896438726	1897	1246021432	1439224317
1845	1504412052	2124415431	1898	1512534271	1938646287
1846	771393248	472153032	1899	284453307	2117151015
1847	843854766	1781802093	1900	742551961	1613045003

Year			Year		
1901	1194723552	730655350	1951	1979418008	2113983876
1902	1911211132	848511829	1952	1676503446	578429934
1903	72901757	528406025	1953	625690974	907413121
1904	1590905915	1401525345	1954	410439111	1498304138
1905	1267201976	1638438269	1955	166384413	200339130
1906	1962579703	524047714	1956	394390800	439199991
1907	24017781	789232588	1957	1919635857	914381559
1908	983890213	1060899747	1958	82501826	1503851715
1909	628398522	229771721	1959	1836984381	1699855878
1910	1324515708	435278737	1960	1733004326	734767138
1911	1302537823	1476102526	1961	1130638008	1803595063
1912	983250281	519841596	1962	1817423469	2075266448
1913	1611826098	1065243024	1963	532432583	960219862
1914	120234928	1141880034	1964	462939494	1092363026
1915	738873800	1174823969	1965	236555855	1302673698
1916	156089648	1284220406	1966	222600077	513825655
1917	781596009	1274559486	1967	1259149155	1206068277
1918	90799661	1669380083	1968	1508868801	222250655
1919	582770292	5978831	1969	286237667	1932387185
1920	1675624057	1141470142	1970	810619978	84221489
1921	2087058689	1982098128	1971	1968789342	3406300
1922	1448244551	1399798419	1972	7143772	1624831848
1923	985715519	836519657	1973	380876987	595910
1924	2005542815	124097475	1974	806679797	532613858
1925	1787481873	1015838230	1975	587829473	447324038
1926	1962649666	457993605	1976	796580056	2092594215
1927	574256785	5205523	1977	2017071437	345120951
1928	1245341641	499807671	1978	993480643	297355686
1929	959148918	1443054722	1979	2100308972	1130726449
1930	93795773	861053684	1980	8559413	1933712031
1931	477787846	936058506	1981	1815133990	743580341
1932	1275479146	897987006	1982	778653742	608531008
1933	1638044142	594515675	1983	1274600195	1836593135
1934	305894613	1663580191	1984	270136916	1531912299
1935	1643160383	2066966886	1985	1924921264	1022748
1936	894207793	2047774362	1986	1028900827	216879682
1937	1227921742	2019167879	1987	1792365310	2066941187
1938	2121984515	270316059	1988	485292584	2117943793
1939	574227789	1838241605	1989	2008367322	1901506479
1940	1858561831	2137389464	1990	1986537433	764832
1941	793322184	1514473341	1991	271885611	2138290558
1942	1307712985	1527646462	1992	858517359	447504486
1943	1508682543	1013356194	1993	1728487375	773684721
1944	217022716	368548386	1994	1100561290	933912958
1945	1401466633	713855090	1995	2129602216	447794448
1946	707230345	685309479	1996	1132652774	1612006369
1947	178991308	275064400	1997	459973107	652194731
1948	170847806	1736248075	1998	1508472885	733305425
1949	1794177750	378487995	1999	1776229888	1204581758
1950	811317412	1654125795	2000	765822650	97111410

Appendix C

Sample Run Sheets

First is given the input file required for the droplet portion of the ODT program. The file given is that used to generate all the $\beta = 1$ data given in this thesis. This file should be in a file called "jevap.inp".

Second is given the input data required for the ODT proper. The input file here was used to generate all the data given in this thesis. This file should be called "input.data".

Third is given a sample long output for the base case (case number 1) for one realization. This data comes out in a file called "jevap.out". There is also a series of output files (for all the cases being run) called "scase#.out". This stands for short output for case number __. The short output contains only the burn out point. Hence one line per realization. A sample of this output is not shown.

C.1   Sample input sheet for 12 cases two-phase flow submodel

itial cond. first 11 cases at 10cm, for a= .169, bv=.6833 no ignition in BC
delayed ignition, cp3 = heptane, toluene, c10h21, case 12 at 5.24 cm

```
0.3423097        ! y possition of droplet
-3.232294        ! y velocity of droplet
0.0002137292     ! shpherical diameter of drop (standard 0.000234)
813.3            ! Density of the liquid drop [kg/m3]
0.2715           ! density of the gas phase
0.0000493        ! viscosity of the gas phase
0.1              ! epsilon factor; fraction of a grid step
1.0              ! D parameter
1.5              ! drop time step factor
0.07318          ! birth time of droplet into the combustor
5.598498         ! u velocity of the drop
0.1000091        ! x position of the drop
0.6833           ! bulk velocity of fluid
0.14635          ! age of the drop when it appears in ODT domain
9.81             ! gravitational acc.  [m/s2]
400.0            ! mean boiling point of liquid [K]
2000.0           ! mean heat capacity (Cp) of liquid [J/kg/K]
350000.0         ! heat of vap. [J/kg]
44000000.0       ! heat of combustion [J/kg]
0.317            ! stoichiometric fluel-to-oxygen mass ratio  (f)
0.00000066       ! burning rate param. asymptotic value of lamda [m2/s]
0.0515           ! mass frac. of O2 in the flue gas (EPAreportpgE-30)
1100.            ! initial guess of the flame temp [K]
0.0000088        ! Diffusivity (toluene at 30 C) [m2/sec] (Perry's)
303.15           ! temp. at which Schmidt number for the gas [K]
378.9214         ! starting temp. of the liquid drop  [K]
0.0025           ! epsilon for determining when to switch to lamda
13               ! number of drops in this simulation.  Max 15
1                ! switch to lamda?  1 for yes, 2 for no
1                ! long output? 1 for yes, 2 for no - not working yet
0.112688         ! ignition time of drop 1, must be >= birth time (5 in)
case2.out        ! start a new drop, OUTPPUT FILE HAS THIS NAME
0.3423157        ! y possition of droplet for drop #2
-3.382890        ! y velocity of droplet for drop #2
0.0002939429     ! shpherical diameter of drop #2 (standard 0.000234)
0.07318          ! birth time of droplet into the combustor
5.859337         ! u velocity of the drop for drop #2
0.09999877       ! x position of the drop for drop #2
0.14635          ! age of drop #2 when it appears in ODT domain
374.6468         ! starting temp. of the liquid drop #2  [K]
1100.            ! initial guess of the flame sheet temperature [K] for drop #2
```

0.094102 ! ignition time of drop 2, must be >= birth time (4.5 in)
case3.out ! start a new drop, OUTPPUT FILE HAS THIS NAME
0.3423163 ! y possition of droplet for drop #3
-3.482738 ! y velocity of droplet for drop #3
0.0003632376 ! shpherical diameter of drop #3 (standard 0.000234)
0.07318 ! birth time of droplet into the combustor
6.032278 ! u velocity of the drop for drop #3
0.09999777 ! x position of the drop for drop #3
0.14635 ! age of drop #3 when it appears in ODT domain
367.6673 ! starting temp. of the liquid drop #3 [K]
1100. ! initial guess of the flame sheet temperature [K] for drop #3
0.112688 ! ignition time of drop 3, must be >= birth time (5 in)
case4.out ! start a new drop, OUTPPUT FILE HAS THIS NAME
0.3423116 ! y possition of droplet for drop #4
-1.902991 ! y velocity of droplet for drop #4
0.0001778522 ! shpherical diameter of drop #4 (standard 0.000234)
0.07318 ! birth time of droplet into the combustor
3.296077 ! u velocity of the drop for drop #4
0.1000059 ! x position of the drop for drop #4
0.14635 ! age of drop #4 when it appears in ODT domain
379.5895 ! starting temp. of the liquid drop #4 [K]
1100. ! initial guess of the flame sheet temperature [K] for drop #4
0.075516 ! ignition time of drop 4, >= birth time (4 in)-no data
case5.out ! start a new drop, OUTPPUT FILE HAS THIS NAME
0.3423158 ! y possition of droplet for drop #5
-4.119725 ! y velocity of droplet for drop #5
0.0002360611 ! shpherical diameter of drop #5 (standard 0.000234)
0.07318 ! birth time of droplet into the combustor
7.135573 ! u velocity of the drop for drop #5
0.09999865 ! x position of the drop for drop #5
0.14635 ! age of drop #5 when it appears in ODT domain
377.1597 ! starting temp. of the liquid drop #5 [K]
1100. ! initial guess of the flame sheet temperature [K] for drop #5
0.37290 ! ignition time of drop 5, must be >= birth time (12 in)
case6.out ! start a new drop, OUTPPUT FILE HAS THIS NAME
0.3423099 ! y possition of droplet for drop #6
-3.795005 ! y velocity of droplet for drop #6
0.0002160238 ! shpherical diameter of drop #6 (standard 0.000234)
0.07318 ! birth time of droplet into the combustor
6.573141 ! u velocity of the drop for drop #6
0.1000088 ! x position of the drop for drop #6
0.14635 ! age of drop #6 when it appears in ODT domain
378.5820 ! starting temp. of the liquid drop #6 [K]
1100. ! initial guess of the flame sheet temperature [K] for drop #6

0.410069   ! ignition time of drop 6, must be >= birth time (13 in)
case7.out   ! start a new drop, OUTPPUT FILE HAS THIS NAME
0.3423162   ! y possition of droplet for drop #7
-3.603644   ! y velocity of droplet for drop #7
0.0002153167   ! shpherical diameter of drop #7 (standard 0.000234)
0.07318   ! birth time of droplet into the combustor
6.241694   ! u velocity of the drop for drop #7
0.09999793   ! x position of the drop for drop #7
0.14635   ! age of drop #7 when it appears in ODT domain
378.7016   ! starting temp. of the liquid drop #7 [K]
1100.   ! initial guess of the flame sheet temperature [K] for drop #7
0.410069   ! ignition time of drop 7, must be >= birth time (13 in)
case8.out   ! start a new drop, OUTPPUT FILE HAS THIS NAME
0.3423081   ! y possition of droplet for drop #8
-3.466336   ! y velocity of droplet for drop #8
0.0002147615   ! shpherical diameter of drop #8 (standard 0.000234)
0.07318   ! birth time of droplet into the combustor
6.003870   ! u velocity of the drop for drop #8
0.1000119   ! x position of the drop for drop #8
0.14635   ! age of drop #8 when it appears in ODT domain
378.7857   ! starting temp. of the liquid drop #8 [K]
1100.   ! initial guess of the flame sheet temperature [K] for drop #8
0.103395   ! ignition time of drop 8, must be >= birth time (4.75 in)
case9.out   ! start a new drop, OUTPPUT FILE HAS THIS NAME
0.3423185   ! y possition of droplet for drop #9
-3.372172   ! y velocity of droplet for drop #9
0.0002143662   ! shpherical diameter of drop #9 (standard 0.000234)
0.07318   ! birth time of droplet into the combustor
5.840773   ! u velocity of the drop for drop #9
0.09999395   ! x position of the drop for drop #9
0.14635   ! age of drop #9 when it appears in ODT domain
378.8405   ! starting temp. of the liquid drop #9 [K]
1100.   ! initial guess of the flame sheet temperature [K] for drop #9
0.094102   ! ignition time of drop 9, must be >= birth time (4.5 in)
case10.ot   ! start a new drop, OUTPPUT FILE HAS THIS NAME
0.3423103   ! y possition of droplet for drop #10
-3.304122   ! y velocity of droplet for drop #10
0.0002140602   ! shpherical diameter of drop #10 (standard 0.000234)
0.07318   ! birth time of droplet into the combustor
5.722907   ! u velocity of the drop for drop #10
0.1000080   ! x position of the drop for drop #10
0.14635   ! age of drop #10 when it appears in ODT domain
378.8805   ! starting temp. of the liquid drop #10 [K]
1100.   ! initial guess of the flame sheet temperature [K] for drop #10

0.094102   ! ignition time of drop 10, must be >= birth time (4.5 in)
case11.ot   ! start a new drop, OUTPPUT FILE HAS THIS NAME
0.40005   ! y possition of droplet for drop #11
0.0   ! y velocity of droplet for drop #11
0.0002185826   ! shpherical diameter of drop #11 (standard 0.000234)
0.07318   ! birth time of droplet into the combustor
6.612148   ! u velocity of the drop for drop #11
0.09999882   ! x position of the drop for drop #11
0.14635   ! age of drop #11 when it appears in ODT domain
377.7420   ! starting temp. of the liquid drop #11 [K]
1100.   ! initial guess of the flame sheet temperature [K] for drop #11
0.242792   ! ignition time of drop 11, must be >= birth time (8.5 in)
case12.ot   ! start a new drop, OUTPPUT FILE HAS THIS NAME
0.3476813   ! y possition of droplet for drop #12
-5.046695   ! y velocity of droplet for drop #12
0.0002267722   ! shpherical diameter of drop #12 (standard 0.000234)
0.003466   ! birth time of droplet into the combustor
5.046695   ! u velocity of the drop for drop #12
0.05236865   ! x position of the drop for drop #12
0.07664   ! age of drop #12 when it appears in ODT domain
372.1740   ! starting temp. of the liquid drop #12 [K]
1100.   ! initial guess of the flame sheet temperature [K] for drop #12
0.003466   ! ignition time of drop 12, must be >= birth time (2.06in)
case13.ot   ! start a new drop, OUTPPUT FILE HAS THIS NAME same as d11
0.39909   ! y possition of droplet for drop #13   but y pos &
-0.13699   ! y velocity of droplet for drop #13   y vel is adjusted
0.0002185826   ! shpherical diameter of drop #13 (standard 0.000234)
0.07318   ! birth time of droplet into the combustor
6.612148   ! u velocity of the drop for drop #13
0.09999882   ! x position of the drop for drop #13
0.14635   ! age of drop #13 when it appears in ODT domain
377.7420   ! starting temp. of the liquid drop #13 [K]
1100.0   ! initial guess of the flame sheet temperature [K] for drop #13
0.242792   ! ignition time of drop 13, must be >= birth time (8.5 in)
case14.ot   ! start a new drop, OUTPPUT FILE HAS THIS NAME
0.40035   ! y possition of droplet for drop #14
-4.25   ! y velocity of droplet for drop #14
0.000234   ! shpherical diameter of drop #14 (standard 0.000234)
0.016   ! birth time of droplet into the combustor
7.3612   ! u velocity of the drop for drop #14
0.05   ! x position of the drop for drop #14
0.016   ! age of drop #14 when it appears in ODT domain
296.15   ! starting temp. of the liquid drop #14 [K]
1901.7034   ! initial guess of the flame sheet temperature [K] for drop #14

0.048846   ! ignition time of drop 14, must be >= birth time (5 in)
case15.ot   ! start a new drop, OUTPPUT FILE HAS THIS NAME
0.40035   ! y possition of droplet for drop #15
-4.25   ! y velocity of droplet for drop #15
0.000234   ! shpherical diameter of drop #15 (standard 0.000234)
0.016   ! birth time of droplet into the combustor
7.3612   ! u velocity of the drop for drop #15
0.05   ! x position of the drop for drop #15
0.016   ! age of drop #15 when it appears in ODT domain
296.15   ! starting temp. of the liquid drop #15 [K]
1901.7034   ! initial guess of the flame sheet temperature [K] for drop #15
0.048846   ! ignition time of drop 15, must be >= birth time (5 in)
0.01

C.2 Sample input sheet for ODT program proper

Input file: Each parameter is preceeded by its index in the line above
'channel search'
DISCRETE SPECIFICATIONS: ispec
1 - Number of iterations
 61
2 - Number of cells
 4431
3 - Flow config: 0 - storm, 1 - relam, 2 - Polyakov, 3 - channel, 4 - Couette, 5 - jet
 3
4 - Number of ensembles
 2000
5 - Diffusion scheme: 0 for explicit, 1 for implicit
 0
6 - Profile restart: 0 none; 1 just write; 2 just read; 3 read and write
 0
7 - Rough number of intermediate field updates to output
 1
8 - Boundary conditions on velocity: 0 for Dirichlet; 1 for Neumann (+flux in)
 0
9 - Boundary conditions on temperature: 0 for Dirichlet; 1 for Neumann
 0
10 - Tarek's eddy map
 1
-1

CONTINUOUS SPECIFICATIONS: rspec
1 - Lower / left endpoint
 0.
2 - Upper / right endpoint
 0.5207
3 - Speed of lower / left wall condition
 0.
4 - Speed of upper / right wall condition
 0.
5 - Initial lower / left temperature condition
 1100.
6 - Initial upper / right temperature condition
 1100.
7 - Final lower / left temperature condition
 1100.
8 - Final upper / right temperature condition
 1100.

9 - Eddy distribution parameter A
 .169
10 - Eddy acceptance probability for the time step calculation
 0.0014
11 - pressure gradient divided by rho(M/(S*S))
 -2.759e-5
12 - kinematic viscosity (M*M/S air at 1300 K)
 18.2e-5
13 - thermal diffusivity {M*M/S air at 1300 K}
 2.5798e-4
14 - reference density; default = 1.
 1.
15 - Boussinesq coefficient g beta
 0.
16 - Initial bulk velocity
 0.
17 - Initial temperature
 0.
18 - Time to impose a new condition
 0.
19 - Time scale over which to ramp in the new boundary condition
 0.
20 - Time at which to begin taking data
 0.005
21 - Total run time
 .95
22 - diffusion time step coefficient
 .45
23 - beta for eddies
 0.
24 - size of the most frequent eddy, as a fraction of the whole domain
 0.005
25 - Eddy cutoff parameter
 16.
-1

C.3 Sample long output sheet for one case, one realization

INITIAL DIA = 0.2137E-03 Age of the drop when it is born into ODT = 0.1464E+00
 Time at which the droplet appears in the ODT domain = 0.731800E-01
 BULK FLUID VELOCITY = 0.683300E+00 U = 0.559850E+01 V = -.323229E+01
 INITIAL X POSITION = 0.100009E+00 INITIAL Y = 0.342310E+00
 DENSITY OF LIQUID=0.8133E+03 AIR: DENSITY = 0.2715E+00 VISCOSITY =
0.4930E-04
 PARAMETER FOR ADJUSTING THE PSEUDO TIME TO DROPLET TIME IS
0.100000E+01
 No. of ensambles is   2000 FACTOR FOR EPSILON, SMALLEST DISTANCE IN
WHICH
  THE ODT IS CONCERNED = 0.1000E+00
 FACTOR FOR COMPUTING DROPLET TIME STEP FROM MOLECULAR STEP
(dtm) = 0.1500E+01
 GRAVITATIONAL ACCELERATION = 0.981000E+01 BOILING PT. = 0.4000E+03
 HEAT CAP. = 0.2000E+04 HEAT OF COMBUST. = 0.4400E+08 HEAT OF VAPOR.
= 0.3500E+06
 FUEL TO OXYGEN MASS RATIO = 0.3170E+00 BURNING PARAM. =
0.66000000E-06
 MASS FRACTION OF O2 IN FLUE GAS = 0.5150E-01 GUESS FLAME SHEET
TEMPERATURE 0.11000E+04
 DIFFUSIVITY OF FUEL INTO AIR IS   0.8800000E-05 SQUARE
METERS/SECOND
   AT 0.303150E+03 KELVIN
 STARTING TEMPERATURE OF THE LIQUID DROP =   0.3789214E+03 KELVIN
 NX=   4431
 DROPLET NO.   1
    TIME   U   V   X   Y   ODT TIME
 0.147477E+00 0.561863E+01 -.313522E+01 0.106332E+00 0.338728E+00
0.824699E-01
 0.149355E+00 0.566447E+01 -.299195E+01 0.116915E+00 0.332975E+00
0.979578E-01
 0.151213E+00 0.572269E+01 -.284016E+01 0.127504E+00 0.327629E+00
0.113454E+00
 0.153076E+00 0.562871E+01 -.298997E+01 0.138090E+00 0.313538E+00
0.128947E+00
 SWITCHED TO LAMDA
 0.153751E+00 0.557510E+01 -.224963E+01 0.141873E+00 0.403125E+00
0.134447E+00
 DROPLET EVAPORATED

Appendix D

Nomenclature

a   acceleration

A   free parameter in ODT proper

B   Spalding mass transfer number

c_p specific heat capacity

C_D^∞ *drag coefficient for isolated droplet*

C_D^0 drag coeffiecint for closely spaced droplets

C_D^{00} skin friction drag coefficient of an infinite rod

D   droplet diameter

D_{AB} gas diffusivity

f stoichiometric fuel-to-oxygen mass ratio or the empirical nonlinear drag law

F   force

F_G gravitational force

g   gravitational acceleration

H   total heat transfer to the drop

ΔH_c heat of combustion

ΔH_v heat of vaporization

k   thermal conductivity

l length of an eddy

m   mass of the droplet

P   probability of an eddy occurrence

Pr   Prandtl number

r   droplet radius

Re   Reynolds number

s   interdroplet spacing

Sc   Schmidt number

Sh   Sherwood number

t   time

T   temperature

u   x component of the fluid velocity

U   x component of the droplet velocity

v   y component of the fluid velocity

V   y component of the particle velocity

x, y, z   Cartesian coordinates

X   gas phase mole fraction

Y   gas phase mass fraction

$Y_{O\infty}$ *oxygen mass fraction in the gas free stream*

Y_{Fs} fuel mass fraction at the droplet surface

Greek Symbols

α   stability coefficient for forward Euler differencing

β   free parameter in the two-phase flow submodel

λ   burning rate constant

μ   viscosity

η_e evaporation factor on drag

η_s droplet interaction factor on vaporization rate

κ diffusion coefficient

ρ density

θ injection angle or any advected scalar

τ eddy time scale

τ_p particle aerodynamic response time

υ kinematic viscosity

Subscripts/Superscripts

c   using continuous time for computations

d   droplet

e   using pseudotime for computations

f   flame

ODT   belonging to the ODT domain

p   particle

x, y, z   Cartesian coordinates

1   droplet stream coordinate

0   initial condition

*   with mass transfer or using the moving coordinate system

Overbar

$^{-}$ mean quantity, in the droplet film layer

$^{\sim}$ a vector quantity

References

Abromzon, B., Sirignano, W.A., **Approximate Theory of a Single Droplet Vaporization in a Convective Field: Effects of Variable Properties, Stefan Flow and Transient Liquid Heating**, in 1987 ASME/JSME Thermal Engineering Conference – Volume one (P.J. Martor and I. Tanasawa, Eds.), Book No. 10219A, American Society of Mechanical Engineers, New York, p. 11 – 18, (1987)

Ayers, W.H., Boysan, F., and Swithenbank, J., **Droplet Trajectories in Three-Dimensional Gas Turbine Flow Fields**, Air Force Report AFOSR-TR-81-0543, September 1980.

Carnahan, B., Luther, H.A., Wilkes, J.O., **Applied Numerical Methods**. John Wiley & Sons, New York (1969).

Clift, R., Grace, J.R., and Weber, M.E., **Bubbles, Drops, and Particles**, Academic Press, New York, p. 111 (1978)

Eisenklam, P., Arunachalam, S.A., and Weston, J.A., **Evaporation Rates and Drag Resistance of Burning Drops**, Eleventh Symposium (International) on Combustion, The Combustion Institute, Pittsburgh, pp. 715 – 728, (1967)

Elghobashi, S., **Particle-Laden Turbulent Flows: Direct Simulation and Closure Models**, Appl. Sci. Res. **48**, 301-314, (1991)

Elghobashi, S., **On Predicting Particle-Laden Turbulent Flows**, Appl. Sci. Res. **52**, 309-329, (1994)

Hubbard, G.L., Denny. V.E., and Mills, A.F., **Droplet Evaporation: Effects of Transients and Variable Properties**, Int. J. Heat Mass Transf. **18**: 1003 – 1008 (1975)

Kerstein, Alan R., *A Linear-eddy model of turbulent scalar transport and mixing*, Combust. Sci. and Tech. **60**: 391-421 (1988)

Kerstein, Alan R., *Linear-eddy modelling of turbulent transport. Part V: Geometry of scalar interfaces*, Physics of Fluids A3: 1110-1114 (1991).

Kerstein, Alan R., *One-dimensional turbulence: model formulation and application to homogeneous turbulence, shear flows, and buoyant stratified flows*, J. Fluid Mech. 392: 277-334 (1999).

Kerstein, A.R., Ashurst, W.T., Nilsen, V. and Wunsch, S.E., manuscript in preparation, (2000).

Kerstein, A.R., and Dreeben, T.D., **Prediction of turbulent free shear flow statistics using a simple stochastic model**, Phys. Fluids **12**: 418 – 424 (2000)

Kramlich, J.C., Heap, M.P., Seeker, W.R., and Samuelsen, G.S., **Flame-Mode Destruction of Hazardous Waste Compounds**, Twentieth Symposium (International) on Combustion**,** p. 1991, The Combustion Institute, 1984.

Labowsky, M., **Calculation of the Burning Rates of Interacting Fuel Droplets**, Combust. Sci. Technol. **22**: 217-226 (1980)

Law, C.K., **Unsteady Droplet Combustion with Droplet Heating**, Combust. Flame . **26**: 17 – 22 (1976)

Monin, A.S. and Yaglom, A.M. **Statistical Fluid Mechanics,** vol. 1. MIT Press (1971).

Mulholland, J.A., Srivasta, R.K., Ryan, J.V., and Wendt, J.O.L., **Influence of Droplet Spacing on Drag Coefficient in Nonevaporating, Monodisperse Streams**, AIAA J. **26**: 1231 – 1237 (1988)

Mulholland, J.A., Srivasta, R.K., Wendt, J.O.L., Agrawal, S.R., and Lanier, W.S., *Trajectory and Incineration of Rogue Droplets in a Turbulent Diffusion Flame*, Combust. Flame, 86: 297-310 (1991).

Mulholland, J.A., Private conversation. March 2000.

Papoulis, Athanasios, **Probability, Random Variables, and Stochastic Processes**. McGraw-Hill Inc. (1991).

Sirignano, W.A., **Fluid Dynamiccs and Transport of Droplets and Sprays**, Cambridge University Press, United Kingdom (1999)

Srivastava, R.K., Ryan, J.V., Van Roy, J., **The Role of Rogue Droplet Combustion in Hazardous Waste Incineration**, Environmental Protection Agency Report EPA/600/7-88/006, April 1988.

Stock, D.E., **Particle Dispersion in Flowing Gases – 1994 Freeman Scholar Lecture**, Transactions of the ASME, **118**: 4 – 17 (1996)

Wang, Lian-Ping, and Stock, D.E., *Dispersion of Heavy Particles by Turbulent Motion*, J. Atmos. Sci., **50**: 1897-1913 (1993).

Wendt, J.O.L., **Combustion Science for Incineration Technology**, Twentieth-Fifth Symposium (International) on Combustion**,** p. 277, The Combustion Institute, 1994.

Appendix C

**"Trajectories of Evaporating Droplets in a Turbulent
Combustor Using the One Dimensional Turbulence Model"**

J. R. Schmidt, J.O.L. Wendt, and A.R. Kerstein

unpublished manuscript

(Self paginated)

Trajectories of Evaporating Droplets in a Turbulent Combustor Using the One Dimensional Turbulence Model

J. R. Schmidt, J. O. L. Wendt*,
Department of Chemical and Environmental Engineering
University of Arizona,
Tucson, Arizona 85721
wendt@u.arizona.edu

and A. R. Kerstein
Combustion Research Facility, Sandia National Laboratories,
Livermore, California 94550-0969

A full length article with the running title of

Droplet Trajectories using ODT

Corresponding author:
Jost O. L. Wendt
Department of Chemical and Environmental Engineering
University of Arizona,
P. O. Box 210011, Rm 108
Tucson, Arizona 85721-0011
(520) 621-2591
(520) 621-6048   FAX
wendt@u.arizona.edu

ABSTRACT

During the incineration of liquid hazardous wastes there may exist "rogue" droplets (>300 μm diameter) which penetrate past the flame zone and burn as isolated droplets in the postflame gases. The ability to predict individual, as distinct from average, droplet burnout points would enable establishment of a guarantee that no drops can exit past a certain point. This would facilitate the design of incinerators that are able to achieve destruction efficiency in excess of the 99.99% as required by law. Previous work has shown that there is a large spread of droplet burnout endpoints in a combustor. This is due to turbulence and cannot be predicted from knowledge of the mean flow field alone.

In this paper the spread in trajectory endpoints of individual evaporating droplet streams injected into a turbulent combustor is investigated numerically. Correlations between the spread in the burnout points and initial droplet size, droplet velocity, interdroplet spacing, and droplet injection angle are examined. The numerical investigation utilizes the novel One Dimensional Turbulence Model (ODT) by Kerstein for the time-developing fluid velocity and temperature fields, and adds a new two-phase-flow model (one-way coupling) for predicting particle trajectories. The numerical investigation also includes a droplet heating/burning model. Results are in good agreement with the measurements available in the literature.

NOMENCLATURE

A   free parameter in ODT proper
C_p heat capacity per unit mass
C_D drag coefficient
D   diameter
f empirical nonlinear drag law
F_G gravitational force
h   distance traveled by a fluid cell during a triplet map rearrangement
k   thermal conductivity
l length of an eddy
m   mass of the droplet
p   pressure
r   droplet radius
Re   Reynolds number
s   interdroplet spacing
t   time
t_e eddy lifetime
T_p particle time
u   x component of the fluid velocity
U   x component of the droplet velocity
v   y component of the fluid velocity
V   y component of the particle velocity
x, y   position in the respective Cartesian coordinate

Greek Symbols
β free parameter in the two-phase flow submodel
λ eddy rate distribution
μ dynamic viscosity
κ diffusion coefficient
ρ density
θ injection angle or any advected scalar
τ ODT eddy time scale
τ_p particle aerodynamic response time
υ kinematic viscosity

Subscripts/Superscripts
b   bulk
c   using ODT time for computations
e   using particle time for computations
g   gas phase
ODT   belonging to the ODT domain
p   particle
x, y   Cartesian coordinates
0   initial condition

Overbar

_

     mean quantity

INTRODUCTION

There exists a large volume of liquid hazardous waste in virtually perpetual storage by the Department of Energy (DOE). This has motivated the DOE to look at other ways to handle, perhaps dispose of, these liquid hazardous wastes. A good method of disposing of these wastes is thermal reaction or incineration. The US regulations on emissions in many cases require a 99.99% destruction of the organic hazardous material as demonstrated during test burns. In some cases (e.g. polychlorobiphenyls and dioxins) a destruction level of 99.9999% is required [1] during test burns. Studies of liquid injection incineration systems have shown the existence of large "rogue" droplets which penetrate the flame zone and burn as individual droplets [1]. Mulholland et al. [2] have shown that turbulence causes a surprisingly large spread (maximum axial distance traveled before complete burning minus the minimum axial distance traveled before complete burning) in the burnout points of droplet streams introduced into a combustor. These large spreads occurred even with streams of identical droplets injected with identical initial diameters, velocities, inter-droplet spacings, and injection angles into a 100 kW turbulent combustor. In twelve cases studied they varied each of these initial parameters (see Table 1) and measured the ensuing effect on the spread of the droplet burnout points. A fuel oil was used as the hazardous waste surrogate. The droplets passed through the flame zone and subsequently ignited and burned out and the locations of ignition and burnout were noted. The nominal droplet stream conditions, Case 1, consisted of 234 µm initial droplet diameter, 8.5 m/s initial droplet velocity, 180 diameter initial droplet spacing, and 30 degree stream injection angle.

4

Mulholland et al. found that models predicting mean behavior were clearly inadequate in predicting the spread. Figure 1 shows the observed range of trajectory endpoints (location at which burnout was completed) for the nominal case (Case 1). The diagram represents a cylindrical combustor. The 100 kW burner is located on the centerline (radius = 0) on the left hand side just outside the view of the diagram. The mean measured gas phase axial velocity is superimposed on the diagram. The experiments were done with a high swirl number (1.3) which caused the swirling turbulent jet diffusion flame to stabilize close to the burner. The large measured burnout spread was attributed solely to the highly turbulent nature of the flow inside the combustor. The purpose of the research described here was to predict quantitatively the spread in burnout points (in contrast to the average location). Prediction of maximum possible penetration of droplets in turbulent flow constitutes a step towards a procedure that helps establish a guarantee that each droplet is completely destroyed.

In turbulent flows, different fragments of waste that are introduced in an identical manner have different histories. A description of the mean time/temperature/environment history does not capture this. Rather it is necessary to employ a modeling method which captures the relevant physics of the turbulent fluid flow and the two-phase flow, in as simple a formulation as possible. Simplicity is required in order to reach an answer for a specific practical problem. This approach is in contrast to Direct Numerical Simulation (DNS) where all the turbulent fluctuations are modeled in detail. The state-of-the-art DNS modeling of turbulent flows is restricted by the maximum Reynolds number (Re) allowable, due to the memory and speed of the fastest computers available. The memory requirement for DNS goes as the cube of the number of grid points needed to resolve fully the smallest (Kolmogorov) turbulent scale. Since ODT keeps track of only one dimension, the required memory of ODT scales directly with the

number of grid points needed to resolve the Kolmogorov scale. Though progress to bring DNS to the high Re regime continues, it has a way to go before it can be used for practical industrial applications such as the one considered here. Since the ODT model capitalizes on the symmetry of the flow and utilizes innovative methods to model three-dimensional turbulent behavior on a one-dimensional domain, it is the model of choice for this highly turbulent flow configuration.

Other methods such as Large Eddy Simulation (LES) might also be applied successfully to solve this problem. However, unlike LES, ODT is able to resolve the scales necessary to capture the smallest eddies, albeit only in the one dimension (transverse to the flow). LES requires a subgrid model to account for energy losses due to such things as viscosity. Since ODT keeps track of the smallest eddy scales, the standard viscous dissipation equation handles this requirement. An additional consideration is that the LES method would need a subgrid model to account properly for the two-phase flow portion of the model. Because ODT captures the smallest scales, no additional assumptions are needed for two-phase flow implementation into ODT.

RANS based models have also been used to predict two-phase-flow problems. Call and Kennedy [3, 4] have shown that stochastic separated RANS models do a poor job in capturing the behavior of evaporating droplets in turbulent flow. They suggest that the treatment of droplet vaporization may be problematic. The multi-physics involved (the coupling between the droplet evaporation, the drag, and the turbulent eddies on the droplet trajectory) indicates that the instantaneous gas temperature profile is also of primary importance when droplets are undergoing vaporization since the variations in the gas phase temperature directly corresponds to variations in the droplet temperature profile. Since ODT keeps track of the instantaneous

6

velocity and temperature profiles, it has a distinct advantage, for the present problem, over RANS which does not correlate the velocity and temperature fluctuations.

The existing ODT model framework had to be adapted to incorporate 1) a two-phase-flow model and 2) a model for predicting the droplet heating and evaporation.

ODT MODEL

The ODT model is well suited to address this problem. It has been applied to several different flows including decaying turbulence and wall bounded shear flows [5]. In essence, ODT is a one-dimensional Monte Carlo modeling technique to describe turbulent mixing of velocity and scalar fields. The ODT approach represents turbulent advection by a random sequence of "eddy" maps (or triplet maps) applied to a one-dimensional computational domain. Profiles of the advected velocity component (u) and the advected scalars evolve on this domain. Equations for the turbulent flow field are thus not solved explicitly.

The viscous and diffusive equations are solved,

$$\frac{\partial u}{\partial t} = \boldsymbol{u}\frac{\partial^2 u}{\partial y^2} - \frac{1}{\boldsymbol{r}_g}\frac{\partial p}{\partial x} \tag{1}$$

$$\frac{\partial \boldsymbol{q}}{\partial t} = \boldsymbol{k}\frac{\partial^2 \boldsymbol{q}}{\partial y^2} \quad , \tag{2}$$

where υ is the kinematic viscosity, θ is here taken to be any number of advected scalars, in this case temperature, and κ is the corresponding molecular diffusion coefficient, in this case the molecular thermal diffusion coefficient {$k/(\rho_g\,C_p)$ }. Kerstein [5] also developed a spatially developing version of ODT, but only the time-developing model was used.

In order for ODT to be used there must be a minimum of one homogeneous direction and there should be a predominantly streamwise direction. The single dimension in the ODT model is transverse to the mean flow. The ODT model implements triplet maps, or eddies, as

instantaneous rearrange-ments of the velocity field $u(y,t)$. (See Fig. 2.) The triplet map has a starting point y_o and a length l which are sampled randomly from a rate distribution. For this purpose, Kerstein develops an eddy rate distribution $\lambda(l; y, t)$, where $\lambda(l)$ dl dy is the frequency of events per unit distance along the y coordinate in the size range [l, l+dl] with y_o in the range [y, y+dy], which gives λ units of (length^2 x time)$^{-1}$. An event is taken to be the occurrence of a triplet map. It describes the idealization of an eddy on the ODT domain. By dimensional arguments,

$$\boldsymbol{l}(l) = \frac{1}{l^2 \boldsymbol{t}(l)} \qquad (3)$$

where $\tau(l)$ is an eddy time scale. Kerstein [5] treats $\tau(l)$ as a local instantaneous time scale denoted $\tau(l;y,t)$ whose evaluation is based on $u(y,t)$,

$$\boldsymbol{t}(l; y_o, t) = \frac{l}{A \Delta u(y_o, l)} \qquad (4)$$

where $\Delta u(y_o, l)$ is a measure of velocity variation along the interval [y_o, y_o+l] and A is a free parameter. Specifically

$$\Delta u(y_o, l) = 2 \left| u_l\left(y_o + \frac{l}{2}, t \right) - u_l(y_o, t) \right| \qquad (5)$$

where

$$u_l(y, t) = \frac{2}{l} \int_{y}^{y + \frac{l}{2}} u(y', t) dy' \quad . \qquad (6)$$

8

Hence Δu in Eq. 5 is based on the mixing-cup average velocity of each half of the eddy. If these averages are shown to differ greatly (hence there is a large strain rate across the eddy) then $\tau(l;y_o,t)$ is small and $\lambda(l; y_o, t)$ is large. Equations 3 – 5 give

$$\boldsymbol{l}\left(l;y_o,t\right) = \frac{2A\left|u_l\left(y_o,t\right) - u_l\left(y_o + \frac{l}{2},t\right)\right|}{l^3} \quad .$$ (7)

The free parameter A is the only free parameter in the ODT model proper. The free parameter A was introduced to compensate for the fact that $\Delta u(y_o, l)$ was chosen as a matter of preference. This arbitrary choice of Eq. 6 may in turn affect the numerical results, hence A allows fine adjustments to the eddy rate distribution. The upshot is that A becomes a turbulence intensity knob. Decreasing A decreases the level of turbulent intensity, and increasing A increases the turbulent intensity.

A pictorial rendering of the triplet maps is given in Fig. 3. In this diagram the vertical spatial axis is the ODT y domain and the abscissa is time. At each instant in time (each vertical line) there exist a complete (instantaneous) velocity profile and complete profiles for all the passive scalars, none of which are shown in the diagram. Whenever a triplet map is implemented at a certain point in time, the domain of the eddy event $[y_o, y_o+l]$ is recorded by placing a darkened line segment over said domain. Therefore the figure gives an overview of the eddy event history. One can see the time evolution of eddy events, including the clustering of eddies that emulates the turbulent cascade. The pictorial in Fig. 3 is an actual space-time history diagram from a member of the ensemble used to generate the data presented in this paper.

For the implementation of this cylindrical turbulent diffusion flame combustor the geometry was idealized as turbulent channel flow. The center of the channel corresponds to the zero radius

9

position in Figs. 1 and 4. The bottom of the channel ($y = 0$ on the ODT domain) corresponds to the bottom (maximum radius) of Fig. 1. The axial bulk mean flow velocity of 0.6 m/s used in the simulation corresponds to the outflow bulk velocity as measured in the experiment [8].

The time development of the velocity and temperature fields is numerically computed for individual realizations, and statistics are extracted from an ensemble of realizations. To convert ODT time development to distance traveled downstream, we simply multiply the elapsed time by the bulk mean velocity. In order to have ODT generate the time developing fluid velocity and temperature fields, the mean measured velocity and temperature profiles at 5 cm downstream (as reported in [2]) were input as initial conditions. With these initial conditions, ODT was able to match trends in the published mean velocity and mean temperature profiles of [2], which are reproduced in Fig. 4. The simulated results for mean velocity and temperature profiles are shown in Fig. 5 A and B. The results presented in this paper were computed from 350 realizations, which roughly correspond to the order of the number of experimental observations used to compile Fig. 1 [7]. It is clear that the velocities predicted by ODT decay too rapidly for this flow. This reflects the combined effect of neglecting swirl, recirculation, and thermal expansion in this application. Computations were done using decaying turbulence (dp/dx set equal to zero) and repeated for dp/dx nonzero. There was no discernable difference in the results between the two. This is due to the short downstream distance of interest, approximately one channel height.

A recent ODT model improvement [8] includes three velocity components. This would allow the capture of swirl (in cylindrical coordinates). Consequently it might improve the comparison, though there are other ODT simplifications that also affect the comparison. Variations of the one ODT parameter A showed that both velocity and temperature profiles could not be matched

10

simultaneously.   Temperature has a more pronounced influence over vaporization, so temperature was chosen to calibrate the value of *A* and therefore the bulk mean fluid velocity. Another consideration for choosing temperature over velocity was that there is no reported value of the measured velocity fluctuations [6], hence no way to measure the accuracy of the ODT prediction of velocity fluctuations for this flow, which matters more than the mean velocity for droplet dispersion (endpoint variability).   Examples of the predicted mean and instantaneous velocity and temperature as shown in Fig. 6 A and B.

The existing ODT formulations were limited to single-phase flow. Consequently a two-phase-flow submodel compatible with ODT is introduced here.

TWO-PHASE-FLOW MODEL

To derive the equation of motion of a particle of mass m_p, a force balance is performed on the particle. For this application, the only forces on the particle are gravity and the drag force. The *y* and *x* components of the assumed particle drag law are given in Eqs. 8 and 9 with *U* being the particle velocity in the *x* direction and *V* being the particle velocity in the *y* direction.

$$\frac{dV}{dt} = -\left(V\right)\frac{f}{t_p} + F_G \quad , \tag{8}$$

$$\frac{dU}{dt} = \frac{-\left(U-u\right)f}{t_p} \quad . \tag{9}$$

A complete derivation of these equations can be found in [9]. Note that ODT idealizes the gas *y* velocity, *v*, by setting it equal to zero outside eddy events. Triplet maps do mimic a *v* velocity within eddies during their implementation, as explained later. The aerodynamic response time,

τ_p, the empirical nonlinear drag correction factor, f, of Rowe [10] and the particle Reynolds number components are given by:

$$t_p = \frac{r_p C_D D_p^2}{18 m_g} \tag{10}$$

$$f = \begin{cases} 1 & \text{Re} \leq 1 \\ 1 + 0.15 \text{Re}^{0.687} & 1 \leq \text{Re} \leq 1000 \end{cases} \tag{11}$$

$$\text{Re}_x = \frac{r_g r_d |U - u_g|}{m_g} \tag{12}$$

$$\text{Re}_y = \frac{r_g r_d |V - v|}{m_g} \quad . \tag{13}$$

ODT evolves in time, with the time coordinate (here denoted t_{ODT}) interpreted as streamwise (x) development based on the mean bulk velocity of the fluid, denoted $\overline{u}_b$. However, each particle proceeds with its own x velocity, U. The particle is subject to time-varying gas velocity, u, both because u evolves in time, t_{ODT}, and because particle motion in the y direction induces variation of u in the particle reference frame. Due to the finite inertia of the particle, U generally differs from u at the particle location, and both these quantities differ from $\overline{u}_b$. Thus, there is typically a difference between the speed at which the particle traverses the x direction and that at which the bulk mean velocity $\overline{u}_b$ traverses the x direction. The time Δt_p required for a particle to traverse the x distance that the mean bulk flow traverses in a given time Δt_{ODT} is

$$\Delta t_p = \frac{\overline{u}_b \Delta t_{ODT}}{U(t_p)} \quad . \tag{14}$$

Integration of Eq. 14 operationally defines a particle time coordinate t_p whose dependence on ODT (gas-phase) time t_{ODT} is distinct for each particle trajectory. The dependence of t_p on t_{ODT} is complicated because U is a function of t_p due to the equation of motion. Integration of Eqs. 8 and 9, with t_p substituted for t, concurrently with Eq. 1, in which t corresponds to t_{ODT}, and Eq.

14, which relates the two time coordinates, determines particle streamwise trajectory evolution except when a particle interacts with an instantaneous eddy event (triplet map). A full discussion can be found in [9].

Particle interaction with a triplet map requires a novel approach. This interaction occurs when the particle and triplet map occupy the same space-time. Before discussing in detail particle-eddy interactions, there is a problem which arises due to the ODT formulation of eddies as instantaneous in time. Particles with finite inertia will generally have a finite, nonzero, y velocity. Figure 7 depicts an eddy event history diagram which includes four possible particle trajectories with various initial y velocities (V). Particle trajectory 1 has no initial y velocity component. Trajectories 2, 3, and 4 have increasing (in magnitude) negative y velocity components. In the scenario set forth in Fig. 7 both particle trajectories 1 and 2 eventually intersect an eddy event. At the intersection points the particle positions and velocities are changed instantaneously. However the larger (in magnitude) the y velocity becomes, the less likely a particle is to intersect an eddy event. In the limit (Fig. 7, path 4) as the y velocity component becomes infinite, the probability of an eddy interaction becomes zero because both the triplet maps and the particle trajectories are vertical lines. This phenomenon is an artifact of the ODT formulation since particles with large y velocities should be allowed to interact with eddies. This artifact becomes important when the particle y velocity becomes large, for example as the initial injection angle deviates more from zero incidence.

The particle drag law as written is not applicable to ODT particle-eddy interactions because triplet maps are instantaneous in time yet the particle-drag law requires an interaction time to cause a change in the particle velocity or position. The logical solution to this difficulty is to assign an interaction time to the particle-eddy interaction. For now, we will denote the

interaction time coordinate as T_p, and the duration of the interaction as T_1. The interaction time coordinate t_p, distinct from the simulation time coordinate t_{ODT}, is a device to enable particle-eddy interactions. The quantity T_1 will be developed and defined later in the discussion. Particle evolution during this interaction is governed by the y and x components of the particle drag law Eqs. 8 and 9 adapted for the interaction time coordinate,

$$\frac{dV}{dT_p} = -\frac{(V - v)}{t_p} f + F_G \tag{15}$$

$$\frac{dU}{dT_p} = -\frac{(U - u)f}{t_p} \quad , \tag{16}$$

where v (defined later) is the fluid y-component velocity induced by the triplet map, T_p is the interaction time coordinate, u is the velocity of the fluid cell which contains the particle, and all other terms are as previously defined. In this formulation tracer particles behave correctly, that is, they remain within the fluid cells that contain them initially [9].

Determination of the particle-eddy interaction time, T_1, requires a definition of the lifetime t_e of an ODT eddy. The ODT local instantaneous time scale $\tau(l; y_o, t)$ (see [5]) is best interpreted as the characteristic time of the eddy event if it were to happen over a time period and not instantaneously. $\tau(l; y_o, t)$ is however an artifact of the ODT model development and not an actual or physical time. Even though parameter dependencies of $\tau(l; y_o, t)$ are based on solid reasoning there is no compelling reason to believe that it necessarily corresponds to the eddy lifetime. Therefore it is justifiable to introduce a particle-model free parameter denoted β. The eddy lifetime is then

$$t_e = \boldsymbol{b}\,\boldsymbol{t}(l; y_o, t) \quad . \tag{17}$$

14

Ideally β is a number close to unity since τ(*l*; y_o, *t*) was based on good reasoning and logically should not be too far off. β = 1 was used for all runs reported in this paper. A set of sensitivity runs designed to investigate the model's response to changes in β were made for β = 0.5 and β = 2.0. Results can be found in [9]. Decreasing β causes increasing deviation of the particle trajectory in the *y* direction from its original path due to the particle-eddy interaction. Increasing β causes less deviation. This may seem counterintuitive, but the free parameter β has two important and somewhat competing effects on the particle-eddy interaction. The first effect is that it adjusts the maximum allowable end time of the particle-eddy interaction, Eq. 17, which either lengthens or shortens the amount of time during which the particle relaxes to the fluid velocity. The second is that it adjusts the fluid phase *y* velocity, Eq. 18 below. A value β < 1 increases *v*, while a value β > 1 decreases *v*. The burden of the drag law (Eq. 15) is to relax the particle to the surrounding gas flow *v*. With β > 1, the maximum relaxation time t_e increases, but the velocity *v* to which the particle relaxes decreases. A detailed discussion on the subject can be found in [9], along with the results from the sensitivity runs on burning droplets.

As noted, the eddy lifetime is used to determine *v* during the eddy event. The gas phase *y* velocity is computed by dividing *h*, the *y* distance traveled by the fluid element containing the particle just prior to the eddy event, by the eddy lifetime:

$$v = h \big/ t_e \quad .\tag{18}$$

A problem arises when comparing the integration done in the interaction time coordinate over a time period T_1 and the conventional continuous-time integration of the drag law subsequent to the particle-eddy interaction, over comparable time intervals $\Delta T_p = T_1$ and $\Delta t_p = T_1$. Comparison

of Eqs. 8 and 15 indicates that the equations contain similar terms and therefore the resultant actions of integrating them over the same time period are in fact double-counting the effect of the gravitational force, once during the interaction time integration from $T_\mathrm{p} = 0$ to $T_\mathrm{p} = T_1$ and once during the particle time, t_p, time integration from the birth time of the eddy to a time increment of T_1. In other words the particle experiences the gravitational force first for a period of T_1 in interaction time, T_p, and again for a period of T_1 in particle time, t_p. To overcome this problem, which occurs when the particle and the triplet map occupy the same space-time, the particle trajectories with and without the effect of the eddy are computed. This is achieved by integrating (first to get velocity and then again to get position) both Eqs. 8 and 15 concurrently over the period T_1, and determining the difference in the ending y_p position (defined in Eq. 19). Similarly, the difference in the ending V velocities (defined in Eq. 20) is also computed. These computations define the instantaneous perturbations felt by the particle due to the particle-eddy interaction,

$$\Delta y_p = y_p^e(T_1) - y_p^c(T_1) \tag{19}$$

$$\Delta V = V^e(T_1) - V^c(T_1) \quad , \tag{20}$$

where the superscript e (for eddy) denotes the results based on Eq. 15 and the superscript c (for continuous) denotes using Eq. 8. Fig. 8 shows this procedure graphically. Figure 9 shows additional examples with varying particle inertia.

No adjustments are made to the x position, x_p, or the x velocity, U, of the particle due to a particle-eddy interaction. The nature of the time developing ODT model does not lend itself readily to sudden jumps in the x domain, which is related to the ODT time. No reasonable method to account for instantaneous movement backward or forward in time could be developed.

A real-life eddy would exist in a defined space (three-dimensional) and exist for a defined (measurable) lifetime. Particle-eddy interactions would occur while the particle occupies the same space-time (x, y, z, t). Hence this two-phase-flow model must assure that the particle-eddy interaction ceases the first time the particle leaves the ODT space time (x, y, t) which the eddy is idealized to occupy. A complete definition of idealized eddy is in order. The y dimension of the eddy is defined in the ODT model proper and those dimensions are also used in the two-phase-flow submodel. The eddy is bounded in the y direction by: $y_o \le y_e \le y_o + l$. The x dimension of the idealized eddy is taken to be the centered around the x position of the particle with an assigned length l in each direction. Test runs were completed to determine the effect of using an assigned length of $l/2$ in each direction. There was no discernable difference in the spread due to this change. Particle-eddy interactions are more complicated in the x direction because the fluid parcels usually have a u velocity. This velocity would usually be carrying the eddy at a different rate then the particle. The particle would see an eddy moving in time in the x direction at a rate of the average u velocity. A logical definition for the average u velocity of an eddy event is the average of the u velocities of the individual cells in the domain of the triplet map, [y_o, y_o+l], at the time of the eddy event. Hence the eddy is defined in the x direction as:

$$x_o + u_{eddy} T_p - l \le x_e \le x_o + u_{eddy} T_p + l \quad . \tag{21}$$

With the x, y, and t_e of the idealized eddy completely defined, it is merely a matter of bookkeeping to keep track of the first time T_1 that the particle leaves the idealized eddy. This time is then plugged into Eqs. 19 and 20 to compute the instantaneous effect of the particle-eddy interaction.

17

DROPLET HEATING/BURNING MODEL

A modified version of the burning model used by Mulholland et al. was used to predict droplet lifetimes. A brief summary of the droplet transient heating/burning model follows. (The reader is referred to [2] for more details of the burning model and to [9] for details on this specific application.) The liquid droplet is assumed to be spherically symmetric with infinite heat diffusivity ("rapid mixing limit"). Therefore the droplet temperature is allowed to change with time, but there is no need to solve any of the fluid-flow equations inside the droplet since the temperature is assumed constant in the droplet. The liquid-phase properties (e.g. density and heat capacity) are constant. The heating time of the droplet is slow compared to the gas diffusion time. Mulholland et al. idealize the droplet fuel mixture to be one representative (unnamed) chemical component. The concentration of this component in the gas phase (assuming equilibrium) is determined by the Clausius-Clapeyron equation. The gas phase is assumed to be in a quasi-steady state, with heat and mass diffusion rate controlling. With the assumption of unity Lewis number, the Sherwood number is equal to the Nusselt number. Ambient gas-phase conditions are subcritical and the gas-phase mixture is assumed to behave as an ideal-gas mixture. Infinitely fast kinetics are assumed, so the flame sheet surrounds the burning droplet. (In other words, the reaction time is shorter than the diffusion time and a flame surrounds the droplet after it has ignited.) This was experimentally verified by Mulholland et al.. The droplets would ignite (glow) a short time before they would completely burn out.

The ODT formulation used in this work utilizes a constant kinematic viscosity (1.82×10^{-5} m^2/s) for air at 1300 K [11] in the gas-flow calculations. However, when computing the mean gas phase properties in the droplet film layer, for evaluation of the pertinent drag and heat and mass transfer rates, the "one-third rule" [12] for evaluating the temperature was utilized.

Hubbard et al. [12] demonstrate that proper temperature choice is essential to obtain the correct heat and mass transfer rates. These temperatures were used to estimate values of viscosity, density and heat capacity of the fuel-air mixture in the resistance film surrounding the drop as needed (e.g. Eqs. 10 – 13).

In contrast, the values of υ and κ used to compute the fluid phase flow (in ODT proper) only affect the details of the fine-scale structure of the velocity and temperature fields. Hence temperature variations in and of themselves are not crucial, but accurate temperature dependencies of the physical properties (υ, ρ, C_p) are essential to compute heat and mass transfer correctly and are therefore central to the aforementioned coupling between droplet evaporation and drag.

A distinguishing feature of ODT is that it fully captures these unsteady couplings and therefore provides higher fidelity representation of the multi-physics involved than conventional methods [3,4].

IMPLEMENTATION AND RESULTS

Simulations were done to mimic the 12 published cases [2] in which the initial diameter, initial velocity, initial droplet spacing and the injection angle of a stream of droplets into a 100 kW combustor were varied. Experimental observation [2] revealed that the droplets traveled along a straight-line trajectory until they reached the high-fluid-shear layer. After this point the droplet stream appeared to disperse. This point is taken to be the point at which the individual droplets are born into the ODT simulation since the ODT model does not lend itself to modeling streams of droplets [9, p. 120]. In order to properly account for droplet heating and vaporization from the point of droplet injection to the point at which the droplets are born into ODT, the droplet drag law and droplet heating/vaporization scheme put forth in [2] were calculated for

each case to determine the best possible estimate of the droplet diameter and temperature. Consistent with Mulholland et al. [2] the average measured ignition points, as reported in [6], were used in the simulation to initiate droplet flame sheet. Mulholland also alludes to the difficulties in predicting ignition points of droplets [2]. The burnout point is taken to be the point at which the last amount of liquid is vaporized. This occurs after the droplet has been ignited, so the vapor is assumed combusted in the surrounding flame sheet.

The two-phase-flow model allows instantaneous jumps in the y position of the droplet to account for eddy-particle interactions. Fig. 10 shows trajectories from the nominal case (Case 1) which exemplify the extremes in the spread (x and y) in the burnout points. The random nature of the submodel can be seen by examining the different trajectories. Individual trajectories can jump up and down randomly.

To provide a clearer understanding of the simulated effects of the different varied parameters, scatter plots of the burnout points for the first three cases are grouped together in Fig. 11. Scatter plots are x-y plots where x is the axial distance penetrated by the droplet and y is the height. The $y = 0$ datum plane is defined as a quarter of a meter below the burner. The burner is on the central axis of the tubular combustor.

A major objective of this paper is to try to predict the spread in the burnout points due to the turbulent fluctuations. Fig. 12 shows, for an ensemble size of 350, the predicted axial spread for the four variations of initial stream conditions, namely diameter, velocity, droplet spacing, and injection angle. An ensemble size of 350 was used because it roughly corresponds to the order of the number of experimental observations used in [2]. Analysis shows excellent agreement of the predicted spread with the measured spread for the variation in initial *diameter*. Table 1 shows that in the experiments for size variation (Cases 1-3) the droplet spacing was also varied

20

$(180 \geq s/D_o \geq 115)$. These values of s/D_o are in the range where one would expect the droplets in the stream to behave independently of each other.

The agreement with the variation in initial *velocity* is reasonable, with both the simulated and experimental data bending downward as the initial velocity increases. As can be seen in Table 1, the runs for velocity variations (Cases 4,1,5) not only included variations in the initial velocity, but also in the initial spacing ($120 \leq s/D_o \leq 210$) and in initial diameter ($216 \leq D_o \leq 250$ μm). The s/D_o values were large enough so that there should be a negligible effect on the observed results.

The model shows a marked change in behavior of the spread as the initial *spacing/diameter* (s/D_o) changes. Above a value of s/D_o of 10, the particles behave independently. There is very good agreement in the second grouping (the last three cases) of the spread as compared to the measured data. The first grouping (of three) is not a good match. The lack of s/D_o parameterization in the ODT droplet submodel is probably the cause of this discrepancy.

The agreement for the zero and thirty degree *injection angles* is good. The trend of the simulated data is significantly different from the measured data. This is probably due to the artifact created in ODT by the assumption that eddies are instantaneous in time. As the injection angle increases the *y*-component of the particle velocity increases and the error due to this artifact becomes more pronounced.

An additional objective of this paper is try and develop a guarantee that each droplet is completely destroyed. The results quoted so far were with a sample size of 350 iterations, a number chosen to be of the same order as the number of samples taken in the experiments of [2, 8]. To verify that the ODT two-phase-flow model is able to predict a maximum possible spread of burnout points, runs were made for much larger ensemble size, approximately 1400 iterations, and analyzed to determine spread for all the cases. Further analysis of a run of approximately

2000 iterations was completed with no increase in the spread of droplet endpoints. This indicates that the spread in burnout points seems to peak at approximately 1400 iterations then stay stable from then on.

CONCLUSIONS

1)   An ODT-droplet-trajectory model was developed to simulate incinerator performance attributes. Results indicate that one can predict possible failure modes inherent in the incineration process due to rogue droplet penetration past the flame zone and subsequent failure to completely burn out.

2)   The ODT model proper is able to reasonably predict trends in the mean velocity and temperature profiles of a 100 kW combustor using as an initial condition the measured mean profiles (velocity and temperature) at a distance of 5 cm downstream of the burner. However, matching both velocity and temperature was not possible due to simplifications in the model. The choice of fitting temperature over velocity provided good results.

3)   The ODT two-phase-flow model can accurately predict the spread of droplet burnout points due to the random variation of the velocity/temperature field. Excellent agreement (using an ensemble size of 350) was found for predicting the spread due to variations in initial diameter. Good agreement was found for predicting the spread caused by variations in initial velocity and for the first two cases of droplet stream injection angle.

4)   The spread is underpredicted for the 45-degree-angle injection because of the artifact that results from assuming instantaneous eddy events.

5)   The ODT two-phase-flow model did not reproduce the trends for variation in the spacing/diameter spread because no *s/D* effects were included inside the ODT droplet model.

22

6) Decreasing the eddy-lifetime coefficient β causes the particle trajectory to deviate in the *y* direction more from its original path due to the particle-eddy interaction. Increasing β causes less of a disturbance.

7) The model demonstrated a maximum in spread for an ensemble size of approximately 1400.

FUTURE WORK

Rather than using the experimentally measured mean profiles as an initial condition (IC) for the ODT flow simulation, an alternative tested method either in ODT itself or using a CFD package could be used to obtain a better IC for this simulation which would include temperatures and velocities above the mean at the IC. Also since the experiments were done on a combustor with high swirl a method to implement swirl into ODT may help.

ACKNOWLEDGEMENTS

References

1. Wendt, J. O. L., *Twentieth-Fifth Symposium (International) on Combustion*, The Combustion Institute, 1994, pp. 277-289.

2. Mulholland, J. A., Srivasta, R. K., Wendt, J. O. L., Agrawal, S. R., and Lanier, W. S., *Combust. Flame*, 86:297-310 (1991).

3. Call, C. J., Kennedy, I. M., *Droplet dispersion, Velocity and Vaporization in Heated and Unheated Jets,* AIAA 93-0904, 31st Aerospace Sciences Meeting and Exhibit, Reno, NV (1993).

4. Call, C. J., Kennedy, I. M., *AIAA Journal*, 32:874-875 (1994).

5. Kerstein, A. R., *J. Fluid Mech*, 392:277-334 (1999).

6. Srivastava, R. K., Ryan, J.V., and Van Roy, J., *The Role of Rogue Droplet Combustion in Hazardous Waste Incineration*, Environmental Protection Agency Report EPA/600/7-88/006, April 1988.

7. Mulholland, J. A., Private conversation. March 2000

8. Kerstein, A. R., Ashurst, Wm. T., Wunsch, S., and Nilsen, V., *One-dimensional turbulence: vector formulation and application to free shear flows*, *J. Fluid Mech*, in press (2001).

9. Schmidt, J. R., *Trajectories of Evaporating Droplets in a Turbulent Combustor Using the One Dimensional Trubulence Model,* Masters Thesis, University of Arizona, 2000.

10. Rowe, P. N., *Trans. Inst. Chem. Eng*, 39:175-181 (1961).

11. *Perry's Chemical Engineers' Handbook* (R. H. Perry, D. W. Green, and J. O. Maloney, Eds.) McGraw Hill, New York, 1997.

12. Hubbard, G. L., Denny, V. E., and Mills, A. F., *Int. J. Heat Mass Transf*. 18:1003-1008 (1975).

TABLE 1
Droplet Stream Test Conditions[a]

Title	Parameter Varied	D^0 (μm)	V_d^0 (m/s)	s^0/D^0	q^0 (deg)
Case 1	Nominal	234	8.5	180	30
Case 2	Size	306	8.5	140	30
Case 3		371	8.5	115	30
Case 4	Velocity	216	5.3	120	30
Case 5		250	10.6	210	30
Case 6	Spacing	234	8.5	2.8	30
Case 7		234	8.5	5.6	30
Case 8		234	8.5	11.2	30
Case 9		234	8.5	22	30
Case 10		234	8.5	45	30
Case 11	Angle	234	8.5	180	0
Case 12		234	8.5	180	45

[a] redrawn from Mulholland et al. by permission of the authors.

List of Figures

Fig. 11:Burnout points for variation in initial diameter, D. Various scatter plots of the burn out points for different initial diameter are shown in increasing order. An ensemble size of 350 was used to generate these plots. Larger droplets travel further downstream and are less dispersed in the y direction (height).

Fig. 12:Comparison between the experimentally measured spread in burnout endpoints and the spread predicted by the simulation. This simulated data comes from an ensemble size of 350.
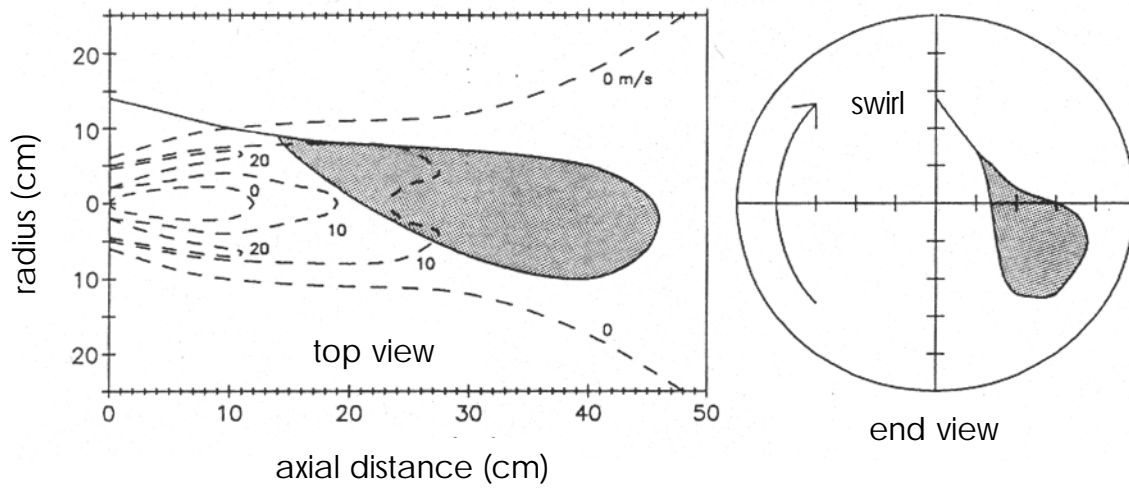
Fig. 1. Measured trajectories for the nominal droplet stream condition (Case 1) in a turbulent flame. The shaded area represents the range of trajectory endpoints. The gas phase axial velocity profile is superimposed on the top view (dashed lines). Taken from Ref. [2] with permission of the authors.
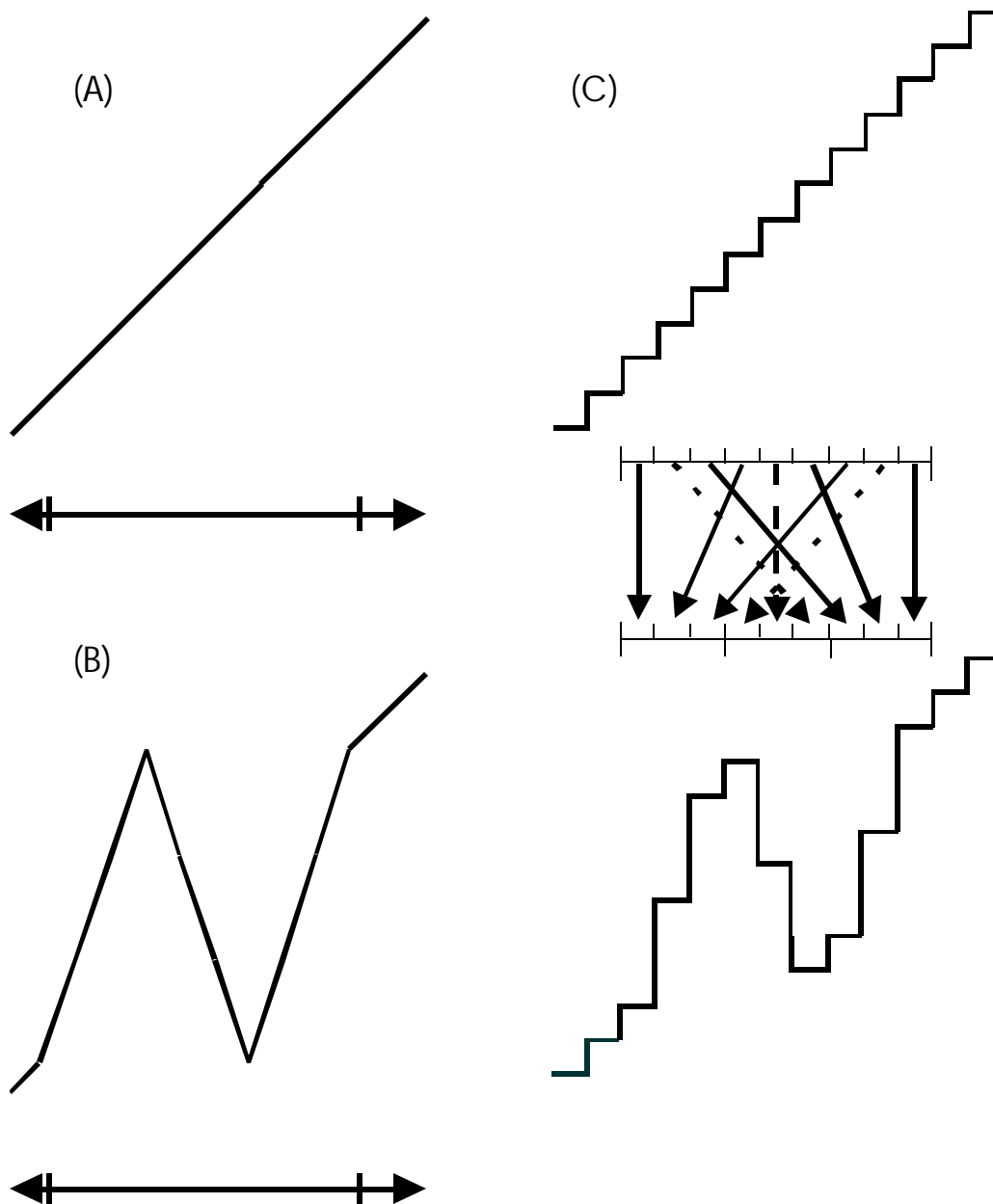
Fig. 2. Effect of the triplet map on an initially linear velocity profile $u(y,t)$. (A) Initial profile. (B) Velocity profile after applying the triplet map to the interval denoted by ticks. (C) Discrete representation of the initial profile and illustration of the effect of a triplet map on an interval consisting of nine cells. For clarity, arrows indicating formation of the central of the three images of the original interval are dashed. Redrawn from Ref. [5] with permission of the author.
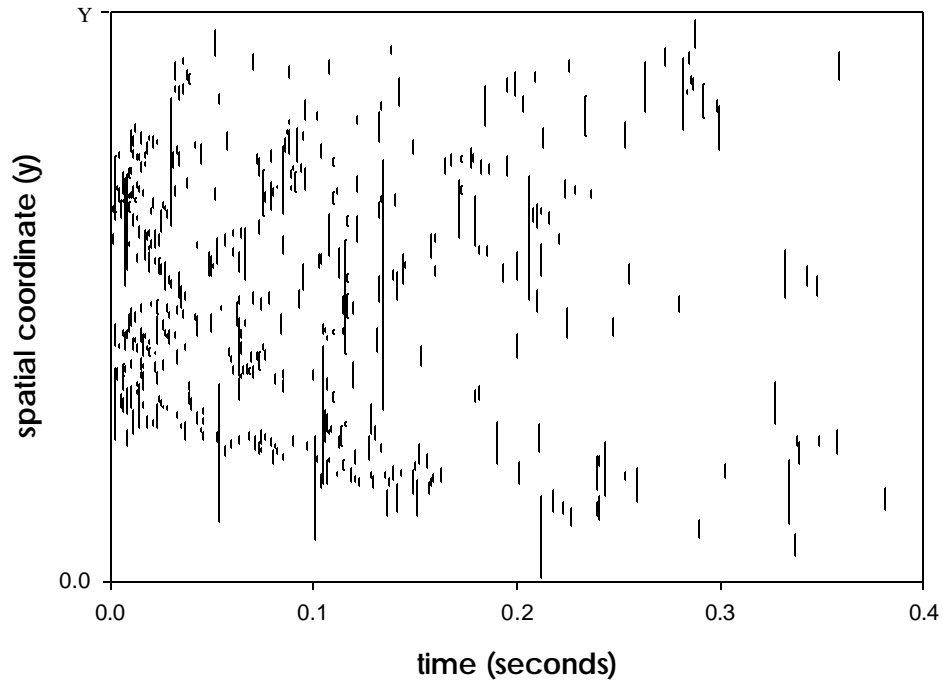
Fig. 3. Pictorial representing the eddy events in space-time coordinates. Vertical lines represent spatial ranges and times of occurrence of eddies. Presented here is the space-time history of an actual realization used in this paper.
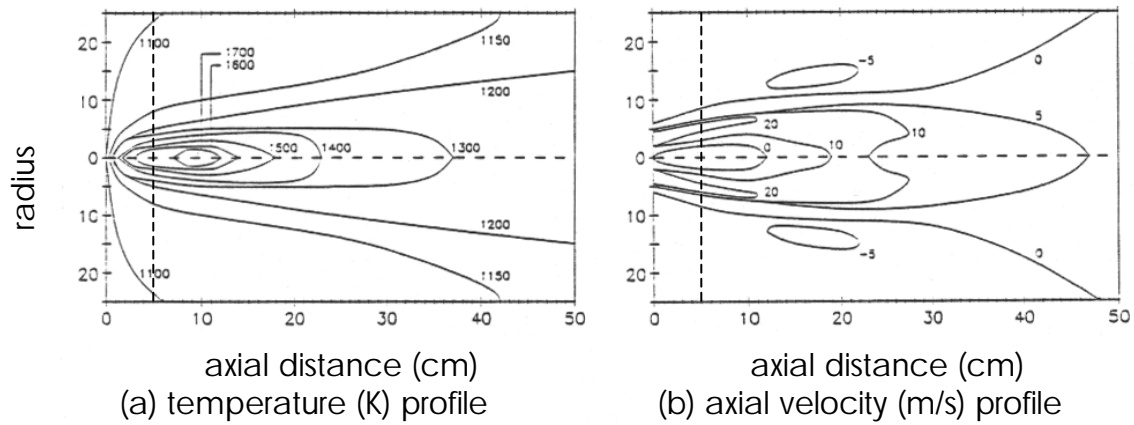
Fig. 4. Measured mean temperature (a) and axial velocity (b) profiles. These are the measured near-burner profiles. The dashed vertical lines were added to facilitate comparison with the simulated profiles shown in Fig. 5. Taken from Ref. [2] with permission of authors.

(a) temperature (K) profile

(b) axial velocity (m/s) profile
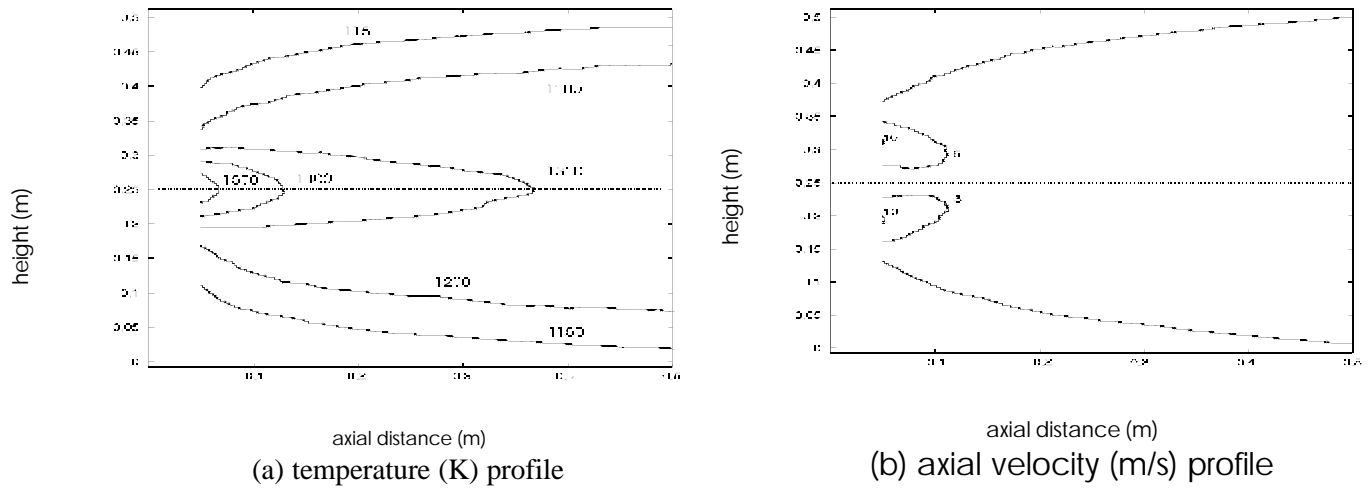
Fig. 5. Simulated mean temperature and axial velocity profiles, based on an ensemble size of 750. From here on measurements made by Mulholland et al. [2] are transformed into the ODT y coordinate as explained in the text. The ODT gas-phase simulation starts at 0.05 m into the reactor as explained in the text.
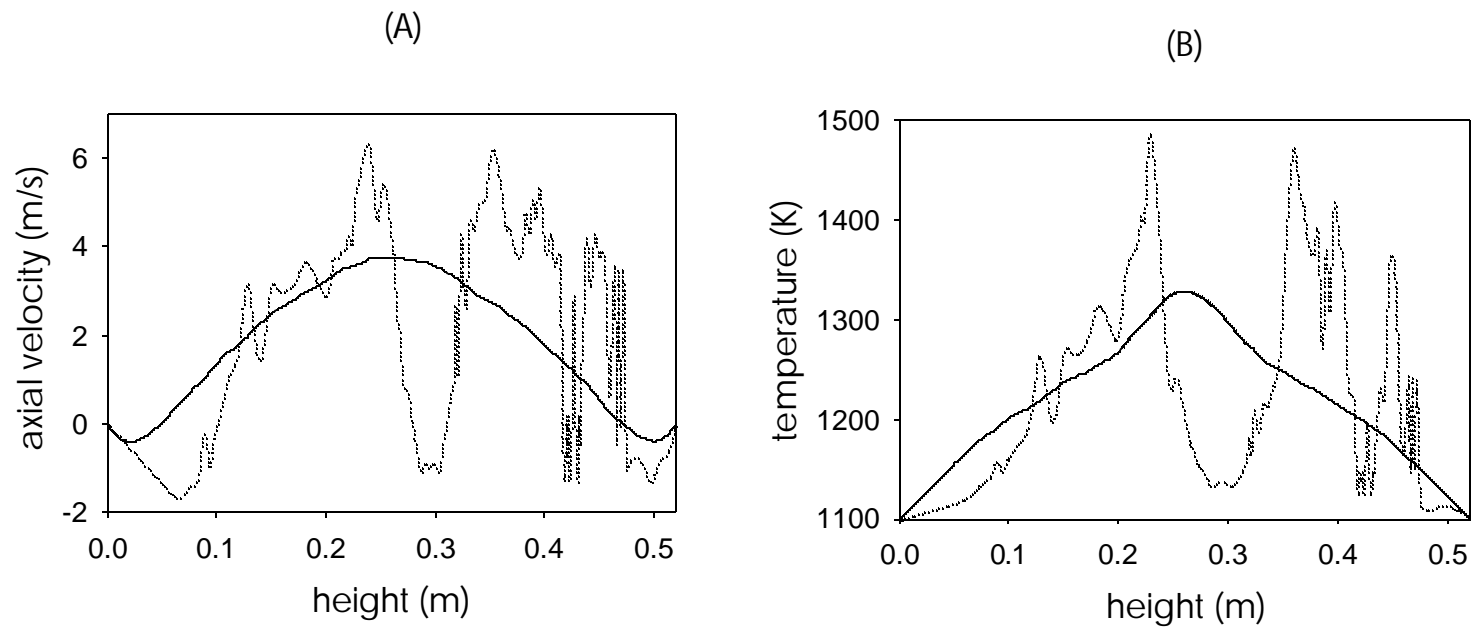
Fig. 6. Mean (solid curves) and instantaneous (dashed curves) velocity (A) and temperature (B) profiles at an axial distance of about 0.19 m. The mean profiles are based on 2000 simulated realizations.
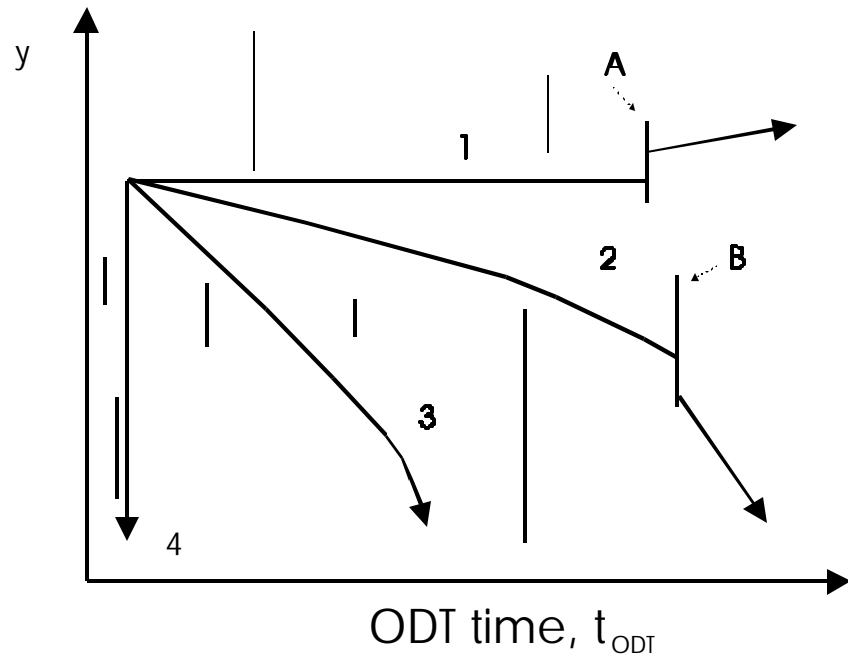
Fig. 7. Particles with high initial *y* velocity are more likely to traverse the ODT space-time domain without interacting with an instantaneous eddy event.
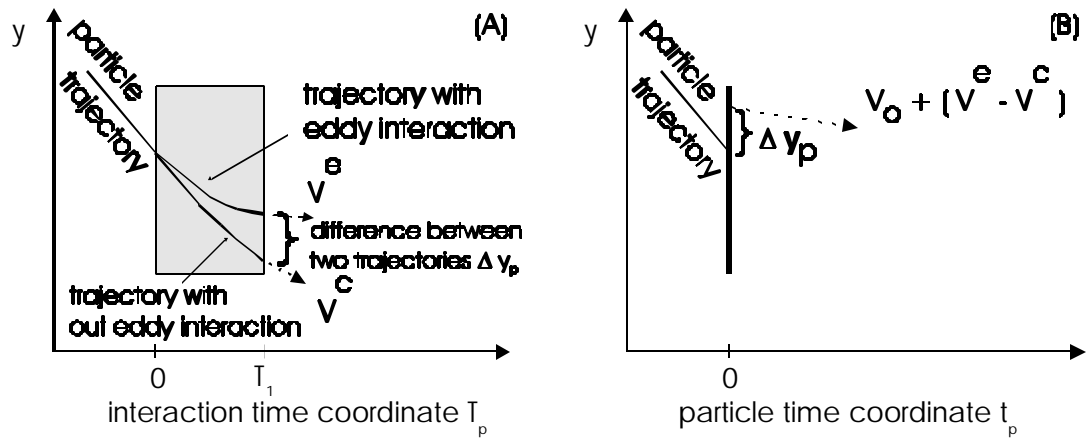
Fig. 8. The procedure for implementing particle-eddy interactions which avoids double counting. Find Δy_p and ΔV by integrating the drag law with and without eddy interaction (A) then add them to the original position and velocity (evaluated when the particle-eddy interaction begins). The resultant position and velocity based on the original velocity V_o, are shown in (B).
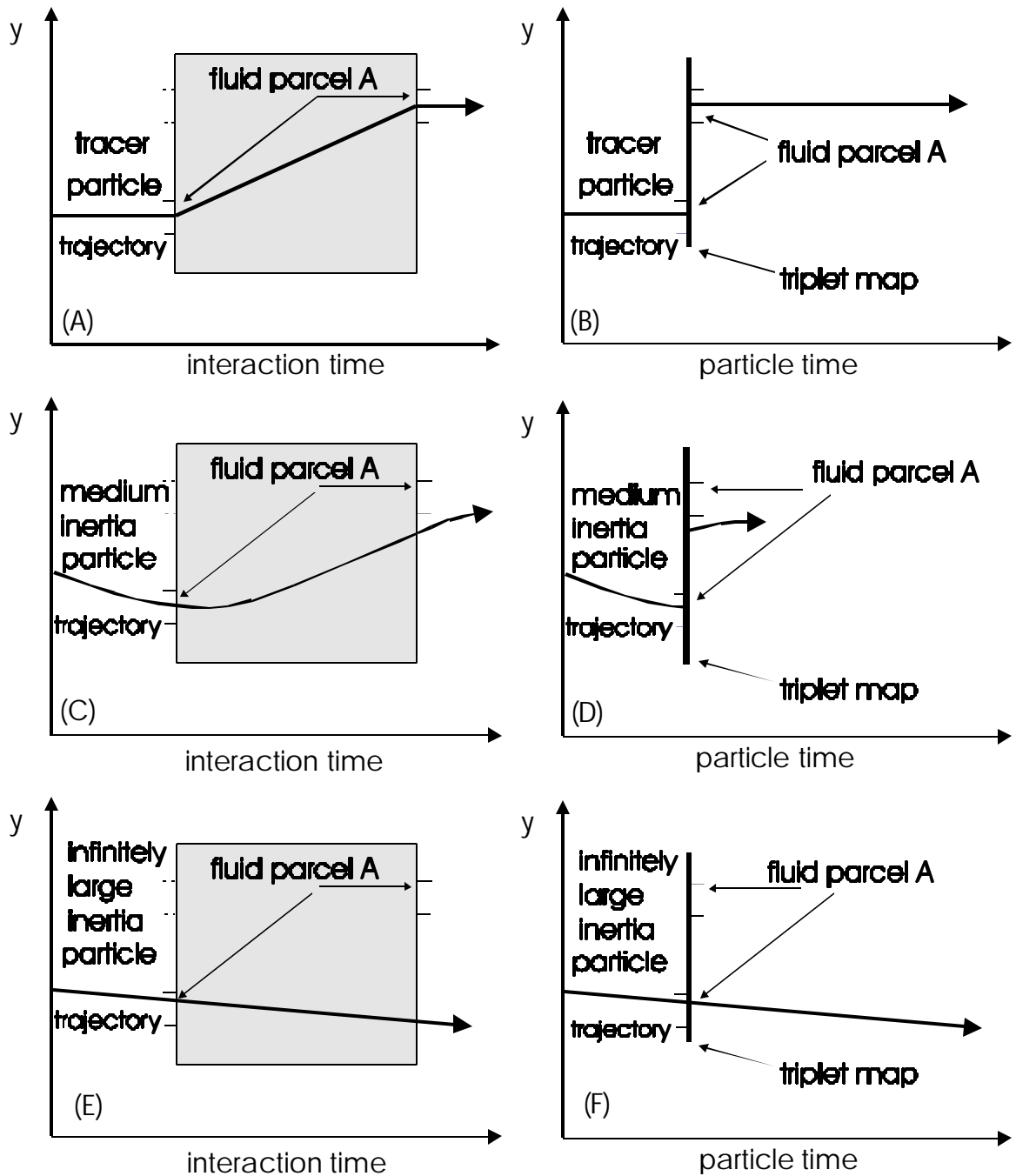
Fig. 9. The trajectories of particles with varying inertia (low to high) are shown in interaction time during particle-eddy interactions (A), (C), and (E). The paths in particle time are shown for comparison, paths (B), (D), and (F) respectively.
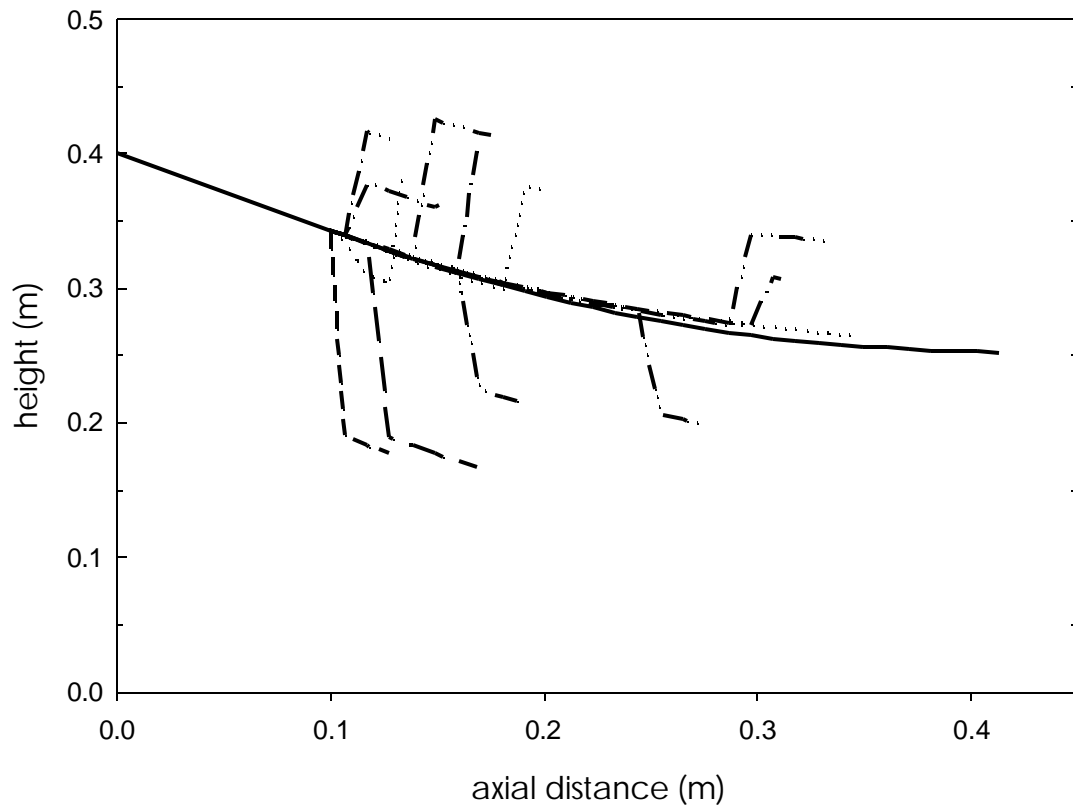
Fig. 10. Trajectories from Case 1 chosen to exemplify the extremes of spread in the *x* and *y* directions of the burnout points.
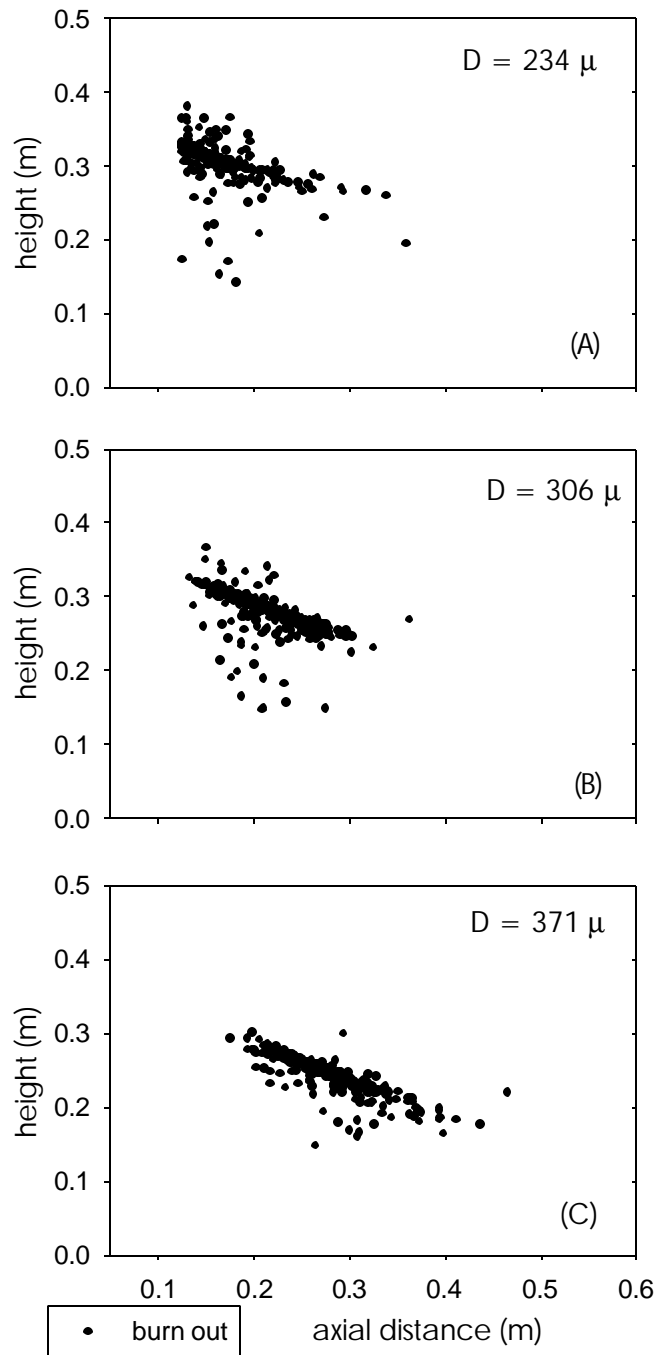
Fig. 11. Burnout points for variation in initial diameter, D. Various scatter plots of the burn out points for different initial diameter are shown in increasing order. An ensemble size of 350 was used to generate these plots. Larger droplets travel further down stream and resist being jostled around as much in the y direction (height).
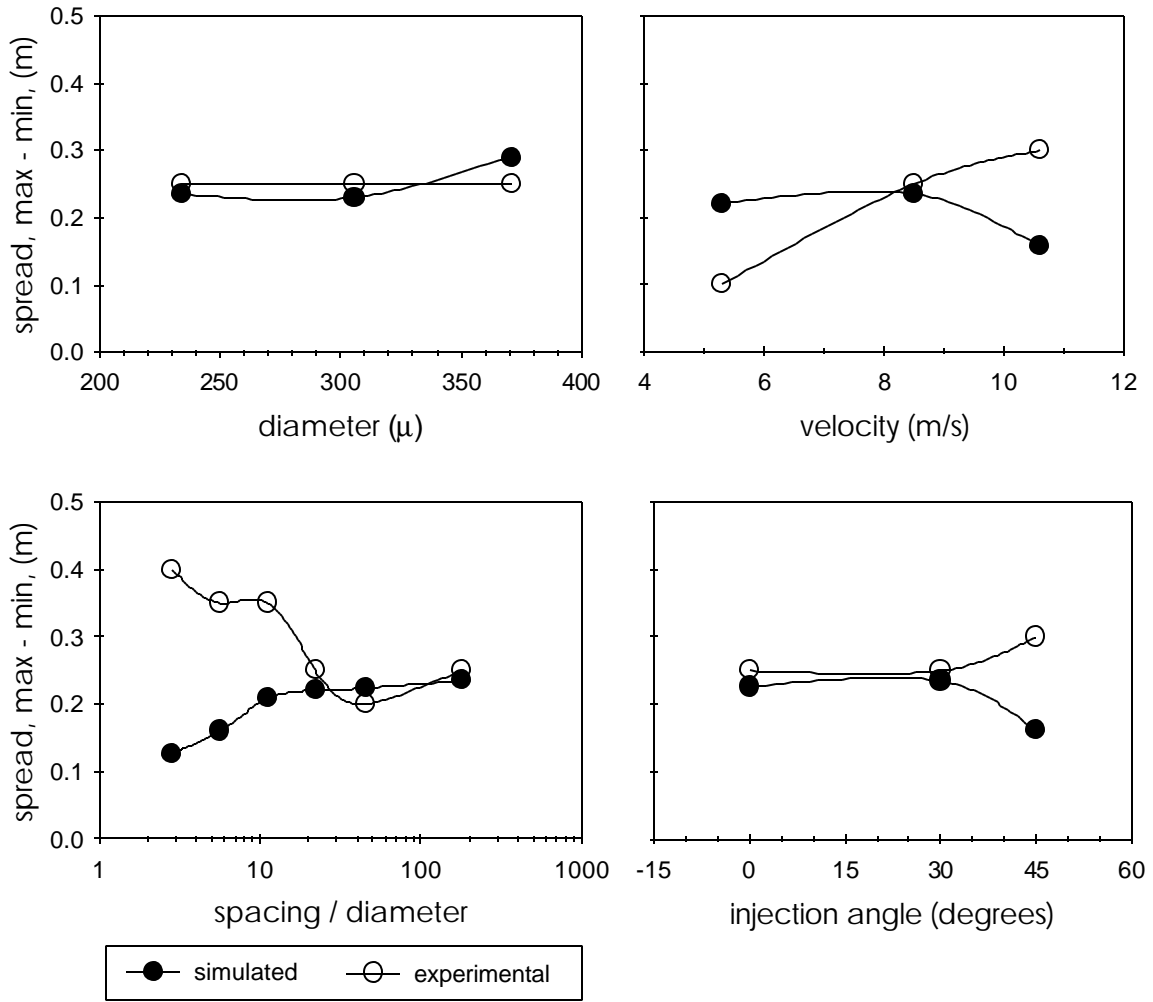
Fig. 12. Comparison between the experimentally measured spread in burnout endpoints and the spread predicted by the simulation. This simulated data comes from an ensemble size of 350.